Assessing Micro-Scale Carbon Dioxide (CO_2) Emission on UK Road Networks using a Coupled Traffic Simulation and Vehicle Emission Model

David William Wyatt

Submitted in accordance with the requirements for the degree of Doctor of Philosophy as part of the Integrated Degree of PhD and MSc (Low Carbon Technologies)

University of Leeds

The School of Chemical and Process Engineering,
Doctoral Training Centre in Low Carbon Technologies

October 2017

The candidate confirms that the work submitted is his own, except where work which has formed part of jointly authored publications has been included. The contribution of the candidate and the other authors to this work has been explicitly indicated below. The candidate confirms that appropriate credit has been given within the thesis where reference has been made to the work of others.

Parts of Chapters 3, 4, 5 and 6 in this thesis are based on work as follows, which has either been published in academic journals or was presented as part of conference proceedings:

WYATT, D.W., KIES, A. & TATE, J.E. (2012). The Influence of Road Grade on Carbon Dioxide Emission for a Hybrid Bus under Real-World Urban and Extra Urban Driving Conditions. *Conference Paper: 19th Transport and Air Pollution (TAP) Conference. 26-27 November 2012, Thessaloniki, Greece.*

WYATT, D.W., LI, H. & TATE, J. (2013). Examining the Influence of Road Grade on Vehicle Specific Power (VSP) and Carbon Dioxide (CO_2) Emission over a Real-World Driving Cycle. SAE International.

WYATT, D.W., LI, H. & TATE, J.E. (2014). The impact of road grade on carbon dioxide (CO_2) emission of a passenger vehicle in real-world driving. *Transportation Research Part D-Transport and Environment,* 32**,** 160-170.

WYATT, D.W., LI, H. & TATE, J.E. (2014). Modelling the Effect of Road Grade on the CO_2 and NO_x Emissions of a Passenger Car through a Real-World Urban Traffic Network. *Conference Paper: 20th Transport and Air Pollution (TAP) Conference. 18-19 September 2014, Graz, Austria.*

WYATT, D., LI, H. & TATE, J. (2016). Analysis of Diurnal Trends in Vehicle Fleet Composition and their Emission Contribution on an Urban Arterial Road in Leeds, UK. *Conference Paper: 21st Transport and Air Pollution (TAP) Conference. 24-26 May 2016, Lyon, France.*

In each of the jointly authored publications the candidate was the lead author and responsible for all data processing, analysis and evaluation. The co-authors in each of the publications were responsible for supervisory support.

ACKNOWLEDGEMENTS

The work in this thesis was funded by the Engineering and Physical Sciences Research Council through the Doctoral Training Centre (DTC) in Low Carbon Technologies at the University of Leeds. Their support and vision in establishing the Doctoral Training Centre have enabled this research. The opportunities made available through the DTC such as the funding for a two month placement with the Technische Universität Graz (TU-Graz) in Austria and the financial backing to attend both academic and industry conferences has given the author the chance to engage with experts involved in all aspects of vehicle emission and to gain a fantastic grounding in the field.

Many thanks to Prof. Paul Williams, Director of the DTC, to James McKay, to David Haynes and to all the other DTC staff, for their help over the past five years. A big thank you to all my colleagues at the DTC. Thank you especially to Holly Edwards and Jo Robinson.

I would like to thank my supervisors, Dr James Tate and Dr Hu Li, for their invaluable support and guidance through the duration of my research. At the TU-Graz I would like to thank Prof. Stefan Hausberger, Dr Martin Rexeis and Antonius Kies, along with the team at the Institute of Internal Combustion Engines and Thermodynamics, for extending such a warm welcome whilst in the department and for giving me access to the instantaneous emission model, PHEM.

Most importantly, the biggest thank you must go to my family in England and Austria. I don't have the right words to express the depth of my gratitude for everything you have done, Sue, David, Roswitha and Flori, and, of course, Liz, Andrew and Will.

And to Alexandra; thank you for sharing the six most stressful, exhausting and wonderful years; thank you for all the laughter that makes the difficult times worth it and thank you for all the things that you do for me, which you regard as inconsequential but that actually allow me to function. Whilst you may not have written a word of this PhD, it is as much of a testament to your hard work as it is to mine.

Finally, to our daughters Skye and Charlotte, thank you. This work is for you.

ABSTRACT

With an increasing divergence between test certified vehicle emission and on-road vehicle emission, the accurate appraisal of real-world vehicle emission has arguably never been more important. This research advances the development, calibration and validation of a coupled traffic micro-simulation and instantaneous emission model.

A portable emission measurement system (PEMS) data set was used to quantify the real-world CO_2 emission of a passenger car through an urban traffic network, in Leeds (UK), over the diurnal range of traffic flow conditions. Utilising these data, analysis was conducted to assess the accuracy of CO_2 micro-scale emission estimates by four emissions models; the Emissions Factors Toolkit (EFT), the Handbook Emission Factors for Road Transport (HBEFA); the Motor Vehicle Emission Simulator (MOVES); and the Passenger car and Heavy duty Emission Model (PHEM). The results demonstrated the strength of power based models over average speed based methods. The study identified the influence that road grade can have on the micro-scale modelling of exhaust CO_2 emission and developed a novel methodology to incorporate grade into the modelling.

A coupled traffic simulation and instantaneous emission model was developed for the study area, using the simulation tool AIMSUN and the emission model PHEM. The model was separately calibrated and validated for five time periods. Parameters within the coupled model, such as the vehicle fleet and vehicle dynamics were customised for the specific study area and time period. The research demonstrated the ability of the AIMSUN-PHEM model to deliver an accurate appraisal of on-road CO_2 emission for each time period and its capacity to generate a range of emission factors from those of a single vehicle to those of the entire fleet. This work confirms that a properly calibrated traffic simulation emission model can provide an effective method for conducting high resolution analysis of vehicle emission in a network.

CONTENTS

LIST OF FIGURES

LIST OF TABLES

LIST OF ABBREVIATIONS

AADF	Annual Average Daily Flow
ACEA	Association of European Automobile Manufacturers
AIMSUN	Advanced Interactive Microscopic Simulator for Urban and non-urban Networks
ANPR	Automatic Number Plate Recognition
API	Advanced Programming Interface
AR5	Intergovernmental Panel on Climate Change's Fifth Assessment Report
ATC	Automatic Traffic Count
CAN	Controller Area Network
CCC	Committee on Climate Change
CCT	Company Car Tax
CEM	Comprehensive Emission Model
CEP	Circular Error Probability
CO	Carbon Monoxide
CO_2	Carbon Dioxide
COP	Conference of the Parties
COPERT	COmputer Programme to calculate Emissions from Road Transport
CV	Coefficient of Variance
CVS	Constant Volume Sampling
DECC	Department of Energy and Climate Change
DEFRA	Department for Environment, Food and Rural Affairs
DEM	Digital Elevation Model
DfT	The Department for Transport
DIU	Data Integration Unit
DT	Delay Time
DTM	Digital Terrain Model
DVLA	Driver and Vehicle Licensing Agency
EC	European Commission
ECE15	ECE15 Urban Driving Cycle
EEA	European Environment Agency
EFT	Emissions Factors Toolkit (EFT v6.0.2)
EGR	Exhaust Gas Recirculation
EPA	United States (US) Environmental Protection Agency
EPSRC	Engineering and Physical Sciences Research Council
ERRI	Energy and Resources Research Institute
EU	European Union
FC	Fuel Consumption
GHG	Greenhouse Gas
GIS	Geographic Information System
GPS	Global Positioning System
GVW	Gross Vehicle Weight
HBEFA	HandBook on Emission FActors for road transport (HBEFA v3.1)
HDV	Heavy Duty Vehicle
HGV	Heavy Goods Vehicle
ICCT	The International Council on Clean Transportation

IEA	International Energy Agency
IPCC	International Panel on Climate Change
IQR	Interquartile range
ITS	Institute for Transport Studies, University of Leeds
JAMA	Japan Automobile Manufacturers Association
JISC	Joint Information Systems Committee
KAMA	Korean Automobile Manufacturers Association
km/h	kilometres per hour
LANTERN	Leeds health Air quality, Noise, Traffic, Emissions Research Network
LCC	Leeds City Council
LCV	Light Commercial Vehicle
LDV	Light Duty Vehicle
LiDAR	Light Detection And Ranging
LOS	Level of Service
MAE	Mean Absolute Error
MAPE	Mean Absolute Percentage Error
MCC	Manual Classified Counts
MIMAS	Manchester Information & Associated Services
MOVES	MOtor Vehicle Emission Simulator (MOVES v2010b)
mpg	miles per gallon
mph	miles per hour
NAEI	National Atmospheric Emission Inventory
NDIR	Nondispersive Infrared Sensor
NEDC	New European Driving Cycle
NGT	New Generation Transport
NO_x	Nitrogen Oxides including Nitrogen Monoxide (NO) and Nitrogen Dioxide(NO_2)
OBS	Horiba On Board emission measurement System (OBS-1300)
ONS	Office of National Statistics
PEMS	Portable Emission Measurement System
PHEM	Passenger car and Heavy duty Emission Model (v11.7.5)
PM	Particulate Matter
PN	Particulate Number
RCP	Representative Concentration Pathway
RDE	Real Driving Emissions
RETEMM	Real-world Traffic Emissions Measurement and Modelling
rpm	revolutions per minute
SCR	Selective Catalytic Reduction
SMMT	Society of Motor Manufacturers and Traders
SOES	Sheffield Omnibus Enthusiast Society
TAG	Transport Analysis Guidelines
TfL	Transport for London
TNO	Netherlands Organisation for Applied Scientific Research
TSS	Transport Simulation Systems
TU-Graz	Technical University of Graz
TWC	Three Way Catalyst
UCF	Unit Conversion Factors
UK	United Kingdom
UNFCCC	United Nations Framework Convention on Climate Change
UoL	University of Leeds
US	United States
VED	Vehicle Excise Duty
VKM	Vehicle Kilometres Travelled
VRM	Vehicle Registration Mark
VSP	Vehicle Specific Power

CHAPTER 1: INTRODUCTION

1.1 BACKGROUND

The Intergovernmental Panel on Climate Change's (IPCC) Fifth Assessment Report (AR5), published in 2014 (Pachauri et al., 2014), building on nearly 30 years of research by climate scientists around the world has established the clear influence of humanity on the Earth's climate, with anthropogenic greenhouse gas (GHG) emissions extremely likely to have been the dominant cause of observed warming at the Earth's surface and in the oceans since the mid-20th century. Carbon Dioxide (CO_2) has been identified as imparting the greatest impact of these GHGs. Continued GHG emission, at the current rate, will result in a level of warming that is very likely to induce substantial and potentially irreversible changes in the Earth's climate system. The projected climatic changes are likely to have a detrimental influence on many of the world's physical, biological and human systems, affecting food production, human health, and economic growth, with dire consequences for the most vulnerable communities and ecosystems around the world (Bernstein et al., 2007b). In response to this threat, the recent 21st meeting of the United Nations Framework Convention on Climate Change (UNFCCC) saw 195 countries commit to reducing their GHG emissions (EC, 2015a). The UK Government, for its part, signed into law the Climate Change Act 2008, committing the UK to an ambitious target of lowering its GHG emissions to 80% of the 1990 baseline by 2050 (Legislation.gov.uk, 2008).

If this target is to be met, the road transport sector, with 35.6 million vehicles in use on UK roads in 2014 (DfT, 2015i), contributing 22% of the UK's total domestic CO_2 emission (DfT, 2015h), is clearly a segment that will need to deliver a vast reduction in CO_2 emission. The UK Government's 'Carbon Plan' published in December 2011 suggests that in order to meet this obligation the vehicle fleet will need to be almost completely decarbonised by 2040 due to the rate of fleet turnover (DECC, 2011).

In combination with reducing the fossil fuel dependence of the vehicle fleet through the introduction of new alternative fuel vehicles, environmental road traffic management schemes can also deliver substantial CO_2 emission reductions. Mechanisms such as better traffic control systems, which reduce the number of aggressive braking and acceleration events through a network; training that teaches drivers how to drive their vehicles in the most fuel-efficient manner; policies which reward multiple-occupancy of cars or the use of public transport to

reduce both the number of vehicle trips and traffic congestion; and improved road geometry design to reduce the impact of road grade could all be used to reduce CO_2 emission from the road transport sector.

In order to provide a detailed assessment of the impact of such strategies, emission estimation models are required that can project emissions of vehicles in real-world conditions with sufficient accuracy and resolution to quantify their environmental benefit, to inform the policy decision making process. Current 'average speed' models do not predict vehicle emission sufficiently accurately because many factors are not adequately considered, e.g. road grade, local speed profiles, driver behaviour and the benefits of smoothing traffic flow by environmental traffic management strategies.

A coupled traffic micro-simulation with an instantaneous emission model has the potential to deliver improved assessments of the environmental impact of traffic networks. Such models utilise traffic micro-simulation software to generate simulated speed profiles for an entire vehicle fleet travelling in a network. These simulated second by second transient data are used to populate an instantaneous emission model, enabling the calculation of emission estimates on a second by second basis, for all vehicles, which can be aggregated from the micro-scale level to provide a high resolution estimation of vehicle fleet emission. The development of a properly calibrated traffic simulation model allows for large volumes of second-by-second data to be generated for each individual simulated vehicle. Collecting a similar volume of real-world data, for a large number of drivers under a full range of conditions, is both impractical and prohibitively expensive (Jackson and Aultman-Hall, 2010). A coupled micro-simulation and instantaneous emission model should provide a cost effective way of conducting high resolution emission estimation.

1.2 OBJECTIVES AND SCOPE OF THE RESEARCH WORK

The main objective of this work is to improve the estimation of real-world CO_2 emission from the UK vehicle fleet in an urban network by developing and demonstrating a coupled traffic micro-simulation instantaneous emission model.

This study attempts to answer the following questions:

1. Can the New European Driving Cycle (NEDC) vehicle type-approval CO_2 emission factors be considered good indicators of vehicle CO_2 emission in real-world driving?

2. How does micro-scale CO_2 emission vary in on-road driving conditions?

3. How good are current emission models at estimating real-world micro-scale vehicle CO_2 emission?

4. To what degree does road grade influence vehicle CO_2 emission estimation at a micro-scale?

5. Can simulated vehicle activity generate CO_2 emission estimates comparable to the CO_2 emission recorded in real-world testing?

6. To what degree are there diurnal variations in CO_2 emission factors for different vehicle types in an urban traffic network?

Answers to these research questions have been developed through:

1. Reviewing literature relevant to CO_2 emission from the UK road transport fleet and the growing gap between type-approval test-cycle generated CO_2 emission estimates and real-world driving emission.

2. Micro-scale analysis of a large Portable Emission Measurement System (PEMS) data set for a Euro 4 compliant passenger car, with measurement through an urban traffic network, over a week-long testing period.

3. Analysis of four popular emission models to assess their capability to replicate the PEMS recorded real-world emission of a test vehicle through an urban network, over a range of traffic conditions. Each of the emission models investigated uses a different approach to modelling on-road vehicle emission.

4. Development of a Light Detection and Ranging (LiDAR) – Global Information System (GIS) methodology for 1 Hz estimation of road grade for PEMS recorded vehicle trips.

5. Creation of a traffic simulation model for an urban traffic network, capable of integrating accurate road design (and road grade), signal timings, accurate 24-hour vehicle fleet composition, Manual Classified Count (MCC) and Automatic Traffic Count (ATC) data, and bus scheduling, coupled with an instantaneous emission model to generate emission estimates from simulated vehicle activity.

The objectives of this study are to:

i. To provide an accurate quantification of real-world micro-scale CO_2 emission factors from a passenger car over a full range of traffic conditions in an urban traffic network

ii. To assess the ability of different emission model methodologies to estimate real-world on-road exhaust CO_2 emission factors over the spectrum of traffic conditions likely in an urban network.

iii. To evaluate the importance of road grade in the accurate appraisal of real-world CO_2 emission and establish a practical method for incorporating road grade into the second-by-second modelling of on-road CO_2 emission.

iv. To create a calibrated and validated, coupled traffic simulation and vehicle emission model and demonstrate the ability of the model to produce high resolution CO_2 emission factor estimates for a UK network, identifying the relative contribution of different vehicle types and sub-categories.

Whilst there are a number of vehicle exhaust emission species which are more concerning from an air quality perspective, the focus of this research is CO_2 emission because:

- The on-road vehicle fleet makes a significant contribution to the total UK national emission of CO_2, which needs to be addressed in order to meet commitments to legally binding emission targets by 2020 and 2050.

- There is an increasing disparity between real-world vehicle CO_2 emission and test cycle type-approval emission factors, which necessitates the development of simulation tools that provide realistic vehicle emission factors that are not reliant on test procedure generated emission factors.

- There is a need for accurate micro-simulation emission tools for transport planning purposes both in the development of the transport network (e.g. optimised traffic signals, junction design and bus lane evaluation) and in providing an instrument for policymakers which enables more detailed appraisal of measures to lower vehicle emission (e.g. the uptake of low emission vehicles, increased car sharing and limiting certain vehicle types).

1.3 THESIS STRUCTURE

The research in this thesis is presented as follows:

Chapter One is an introduction to the work in this thesis, which discusses the background and rationale behind the study and presents the research questions, scope and objectives that underpin the research.

Chapter Two discusses the current consensus of the climate science community regarding observed global warming and the potential consequences of continued substantial emission of GHGs (including CO_2) from anthropogenic sources. The chapter looks at the contribution to GHG emissions from the UK vehicle fleet and discusses an observed increase in the discrepancy between the CO_2 emission rate estimates generated for vehicles during type-approval testing and the real-world CO_2 emission rates once those vehicles are driven on-road.

Chapter Three details a new analysis of a PEMS data set which was collected between the 26th February 2007 and the 5th of March 2007 by the University of Leeds (UoL) Energy and Resources Research Institute (ERRI) and the UoL Institute for Transport Studies (ITS). This was part of an Engineering a Physical Sciences Research Council (EPSRC) funded Real-world Traffic Emissions Measurement and Modelling (RETEMM) research project and was part of the Leeds health Air quality, Noise, Traffic, Emissions Research Network (LANTERN) research programme. The aim of the RETEMM project was to investigate vehicle emissions characteristics under real-world driving conditions, in peak and non-peak traffic conditions, to examine the influence of traffic in an urban road network. As a busy urban road network, the A660 and Headingley area of Leeds were chosen as a suitable study area for this project. The data set is a record of the real-world CO_2 emission of a passenger car through an urban traffic network, over a week-long testing period. The survey encompassed the typical range of traffic conditions for the network from heavily congested to free flowing traffic.

Although the on-road emission analysis within this chapter makes use of the RETEMM database, the data collection was not conducted as part of the work in this thesis (i.e. the author was not involved in collection of the data). This database comprises 20 excel files, a total of 63,941 seconds of PEMS data, processed (as part of the RETEMM project) into a second-by-second format. The presented analysis of the database in Chapter 2 is original to this thesis. This includes the data quality control checks, the adjustment for an identified exhaust idle emission rate error and the definition of the test lap and segments within the test area, to enable analysis of vehicle emission at a micro-scale.

Chapter Four presents an assessment of the capability of four popular emission models to replicate the real-world micro-scale emissions of a test vehicle in an urban network. Each of the emission models investigated in this chapter uses a different approach to modelling on-road vehicle emission. Using the on-road vehicle trajectory data from the database analysed in Chapter 3 and specific description of the test vehicle, the work undertaken in Chapter 4 appraises the ability of current tools to model on-road vehicle CO_2 emission over short road sections. The chapter presents a comparison between CO_2 emission estimates derived from each of the four emission models and the real-world CO_2 emission recorded by the PEMS test vehicle.

Chapter Five records the analysis of the influence of road grade on CO_2 emission, beginning with a sensitivity analysis of CO_2 emission to road grade. A new Light Detection And Ranging (LiDAR) – Geographic Information System (GIS) road grade estimation methodology is presented, which was devised as part of the research in this thesis, in order to facilitate the incorporation of road grade into emission estimation methodologies that require second-by-second data.

Chapter Six describes the development of a coupled traffic simulation model and instantaneous emission model, which includes road grade. The research utilises the Advanced Interactive Microscopic Simulator for Urban and non-urban Networks (AIMSUN) (Barceló et al., 2005) and the Passenger car and Heavy duty Emission Model (PHEM) (Hausberger, 2003). The coupled model constructed for this study, built upon work conducted at the University of Leeds (in which the author was not involved), which had previously developed an AIMSUN 'beta' model that described the main road through the test area. Development of the model in this thesis involved; completely redrawing and expanding the Headingley network in AIMSUN with the addition of road grade; calibrating and validating the model using the up-to-date traffic flow data, junction control signal timings and turning movements data from Leeds City Council; incorporating vehicle dynamics data from real-world measurement; and the addition of a detailed vehicle fleet through analysis of a 24-hour Automatic Number Plate Recognition (ANPR) survey conducted in the test area. The AIMSUN beta model was referenced only for some global and local parameters, and to corroborate traffic control signal data and junction turning movements. The AIMSUN model in this thesis was separately calibrated and validated for five time periods to enabled diurnal trends in vehicle emission to be analysed.

The final chapter, **Chapter Seven**, is a discussion and summary of the findings and conclusions from this work. Recommendations for areas of future research are also presented.

CHAPTER 2: ROAD TRANSPORT AND CO_2 EMISSION

2.1 INTRODUCTION

Research conducted by climate scientists around the world, synthesised in the Intergovernmental Panel on Climate Change's Fifth Assessment Report (AR5) has established that anthropogenic greenhouse gas (GHG) emissions are responsible for the period of global warming observed over the past few decades, CO_2 imparting the largest impact of these GHGs (Pachauri et al., 2014). If the volume of GHG emissions from human activity is maintained at its current level or continues to grow, greater warming is likely to induce substantial changes to the Earth's climate system with potentially dire consequences for the most vulnerable communities and ecosystems around the world (Bernstein et al., 2007b). In response to this threat, many countries around the world have made commitments towards reducing their GHG emissions.

UK transport contributes approximately 22% of the total UK domestic GHG emissions (CCC, 2015), of which road transport accounts for 92.4% (DfT, 2015h). As the UK has committed itself to lowering its GHG emissions to 80% of the 1990 baseline by 2050 (Legislation.gov.uk, 2008) an almost complete decarbonisation of the vehicle fleet will be necessary.

This aim of this chapter is to review the current contribution of the UK vehicle fleet to GHG emissions and assess the drivers, trends and progress toward reducing CO_2 emission from the road transport sector, primarily focusing on the passenger car fleet, as it forms the majority of the overall fleet.

In order to establish the emission rate for a particular new vehicle, the European Union (EU) employs the New European Driving Cycle (NEDC) to calculate a type-approval gCO_2/km value. This chapter will finish by investigating how well the NEDC type-approval represents real-world vehicle exhaust CO_2 emission. A universal method for type-approval testing should facilitate reproducibility and enable like-for-like comparison between vehicles, however, to achieve real-world CO_2 emission improvement, laboratory recorded emission reductions also need to be reflected by decreases in CO_2 emission in on-road driving conditions (Mock et al., 2015). For later chapters in this thesis, it is important to have representative real-world CO_2 emission values to assess the accuracy of modelled CO_2 emission estimates.

2.2 THE SCIENCE AND IMPACT OF CLIMATE CHANGE

The Fifth Assessment Report compiled by the Intergovernmental Panel on Climate Change (IPCC) published in 2014 concludes with near certainty that anthropogenic GHG emissions are driving global warming (Pachauri et al., 2014). CO_2 is the most important of these anthropogenic GHGs, due to its impact on the Earth's radiative balance (see Figure 2.1).

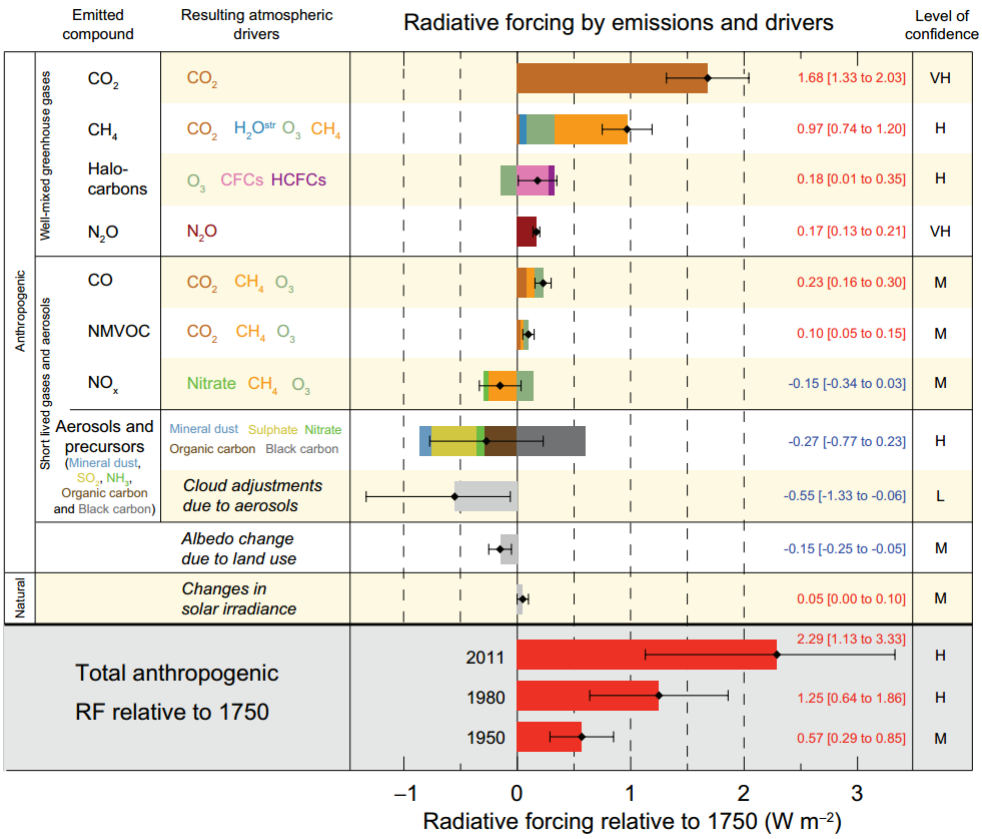

Figure 2.1: Radiative Forcing Estimates in 2011 Relative to 1750 and Aggregated Uncertainties for the Main Drivers of Climate Change (Pachauri et al., 2014)

GHGs trap a portion of the Earth's outgoing infrared radiation, preventing it from escaping into space. Positive radiative forcing induces warming, whilst negative forcing cools the system. At natural levels, GHGs have a necessary warming effect on the planet. Atmospheric GHG concentrations, however, have been rising over the past century (Figure 2.2a) due to increased levels of anthropogenic GHG emissions, primarily from the burning of fossil fuels (Figure 2.2b). This has resulted in an uncharacteristically rapid period of warming in the past few decades (Figure 2.2c). If anthropogenic GHG emissions are left unabated and their concentrations in the atmosphere continue to rise to well above the natural range, there is potential for a dangerous level of climatic interference within the next century.

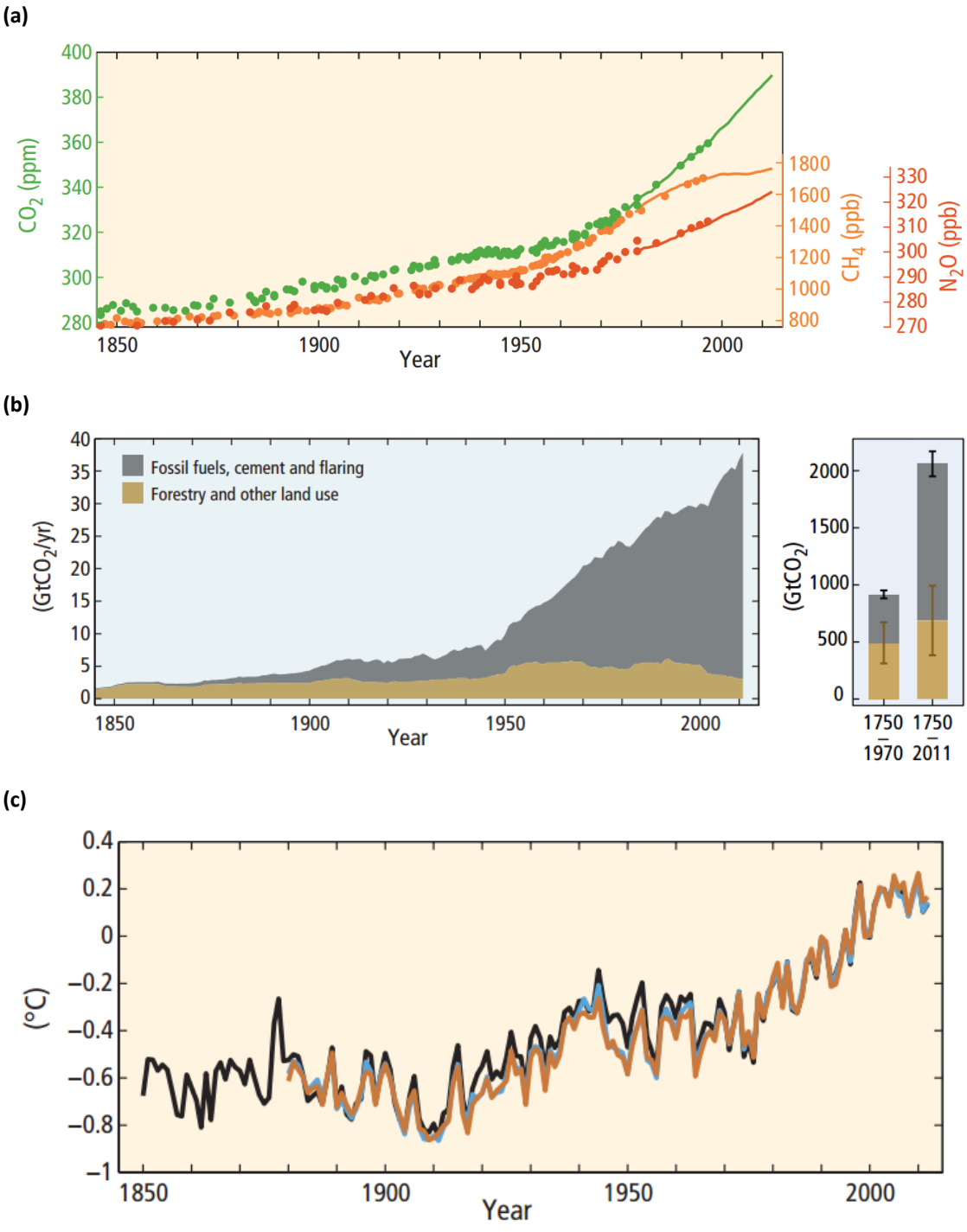

Figure 2.2: (a) Globally Averaged Greenhouse Gas Concentrations (b) Global Anthropogenic CO_2 Emissions (c) Globally Averaged Combined Land and Ocean Surface Temperature Anomaly (Relative to the Average from 1986 to 2005 – Colours Indicate Different Datasets) (Pachauri et al., 2014)

As part of the IPCC AR5, Representative Concentration Pathways (RCPs) were developed, which describe four potential trajectories for 21st century GHG concentrations. The RCPs detail a range of GHG emissions projections from RCP2.6, under which stringent GHG mitigation policies limit GHG concentrations to a radiative forcing of 2.6 W/m^2 relative to pre-industrial levels by 2100, to RCP8.5 which suggests increasing GHG concentration over the next century. There are two intermediate scenarios RCP4.5 and RCP6 which describe stabilisation of GHG concentrations at

radiative forcing values of 4.5 W/m^2 and 6 W/m^2 respectively (Meinshausen et al., 2011; Moss et al., 2008; Collins et al., 2013).

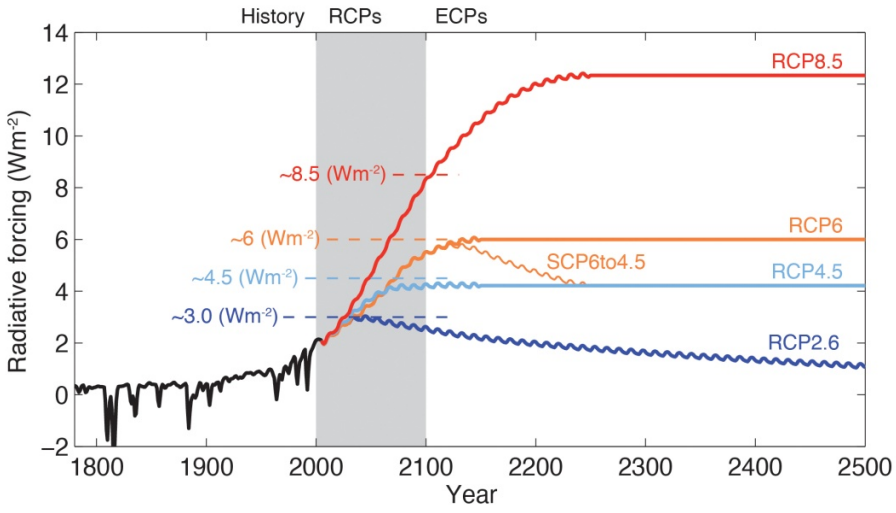

Figure 2.3: Total Radiative Forcing for AR5 RCPs (Meinshausen et al., 2011)

These scenarios were devised through the creation of several future projections that attempt to quantify how forces affecting GHG emissions (population, economy, technology, energy and land use) will develop under differing assumptions about global economic growth, population growth and international policy. The RCPs suggest that GHG emissions could lead to a global average surface temperature rise of between 0.4°C - 2.6°C within fifty years and more than 4.8°C by the end of the century (Collins et al., 2013; Stocker et al., 2013b). The projected change in global annual mean surface temperature for each of the RCP scenarios is presented in Figure 2.4 and Table 2.1. Figure 2.4 also presents the mean and minimum-maximum range for the average temperature change over 2081-2100, in comparison to the 1986-2005 base period.

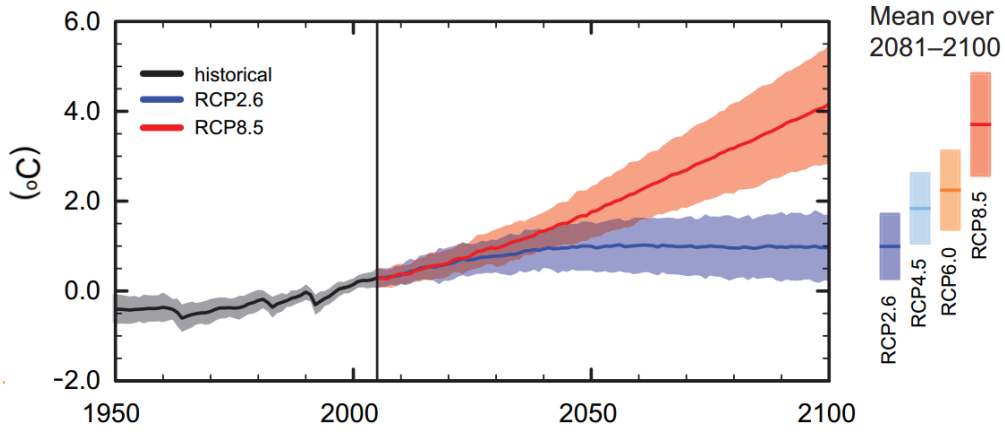

Figure 2.4: Change in Global Annual Mean Temperature Relative to 1986 -2005 (Stocker et al., 2013b)

Table 2.1: Projected Change in Global Mean Surface Air Temperature Relative to the Reference Period 1986 – 2005 (Adapted from (Stocker et al., 2013b))

		2046-2065		2081-2100	
	Scenario	Mean	Likely Range	Mean	Likely Range
Global Mean Surface Temperature Change (°C)	RCP2.6	1.0	0.4 to 1.6	1.0	0.3 to 1.7
	RCP4.5	1.4	0.9 to 2.0	1.8	1.1 to 2.6
	RCP6.0	1.3	0.8 to 1.8	2.2	1.4 to 3.1
	RCP8.5	2.0	1.4 to 2.6	3.7	2.6 to 4.8

The projected temperature rise is not spread evenly but will be greater at higher latitudes and in continental regions. This pattern is clear from Figure 2.5, which displays the average annual surface temperature change for RCP8.5, the scenario with the greatest level of GHG emissions. However, under all scenarios, the projected temperature rise is unevenly dispersed over the world, with some regions exposed to a much greater potential increase in surface temperature than indicated by the global average.

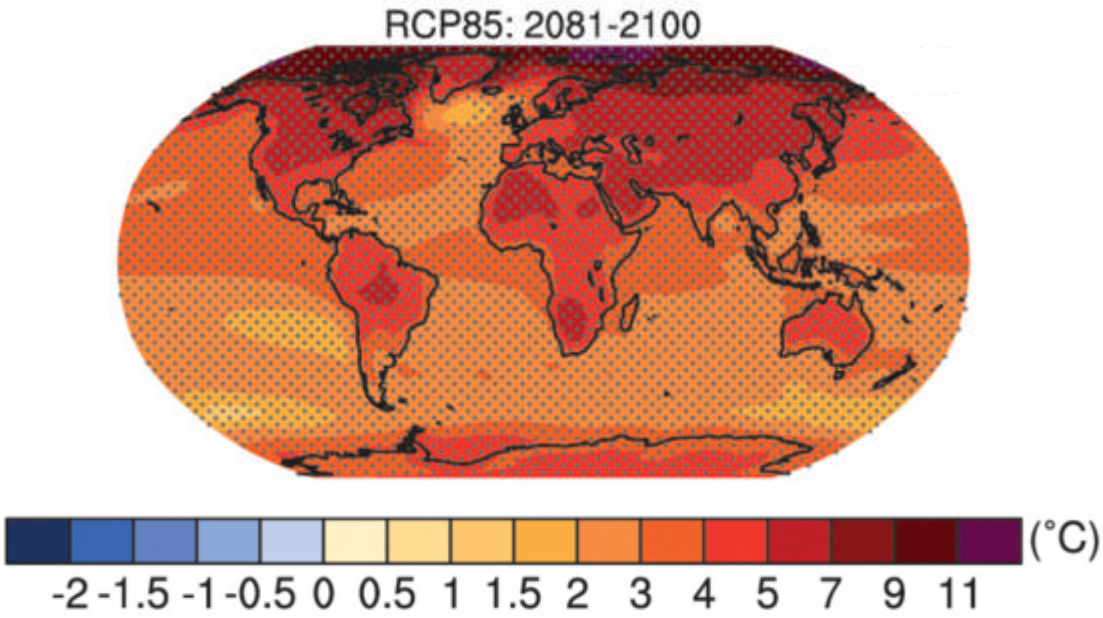

Figure 2.5: Average Annual Surface Temperature Change for RCP8.5 for 2081-2100 Compared to the 1986-2005 Base Period (Stocker et al., 2013a)

The potential effects of climate change are many and varied. At a regional level, climate change is likely to reduce Arctic sea ice; increase the frequency of heat waves; alter precipitation patterns; increase tropical cyclone intensity and threaten low-lying coastal systems due to sea level rise (Bernstein et al., 2007a; Field and Van Aalst, 2014). Greater levels of induced climate warming inflict increasingly detrimental consequences for ecosystems, agriculture, health and water provision. Figure 2.6 gives an indication of the impacts that are the likely result of differing rates of global warming.

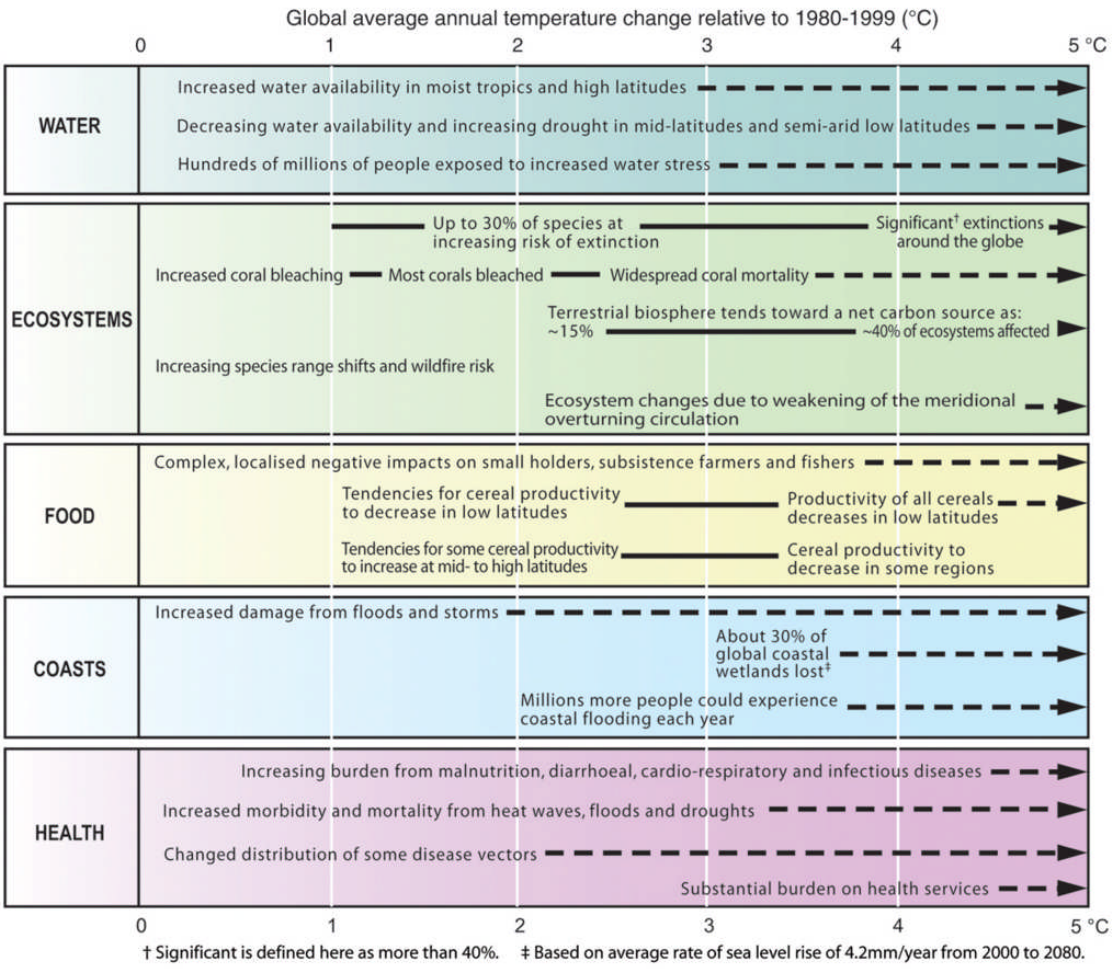

Figure 2.6: Examples of Impacts Associated with Global Average Temperature Change (Bernstein et al., 2007a)

At a human level, the impacts will be felt most by developing nations, where there is a lack of adaptive capacity to meet the challenges of climate change, such as, increased water stress, the effect of changing precipitation patterns on agriculture and heightened flood risk in river delta regions. As a result, climate change puts at risk some of the most vulnerable populations in the world and threatens to undermine development efforts being made in those regions today. These are the regions that will not have the resources to build flood defences against rising sea levels or to install expensive irrigation networks to water their crops. The impacts of climate change could force large scale migration and resultant resource shortages could contribute to the causes of future conflicts.

Climate change also threatens to move some large scale components of the Earth system past critical thresholds, or “tipping points”, when a small rise in temperature could cause an abrupt non-linear impact and result in self-perpetuating feedbacks that have serious consequences for the state of the global climate. For example, the possible shut-down of the Atlantic

Thermohaline Circulation, the rapid disintegration of the West Antarctic Ice Sheet or dieback of the Amazon Rainforest (Lenton et al., 2008).

The Stern Review on the Economics of Climate Change (Stern, 2006), investigated the financial implications that climate change could have on the world's economy. It reached the conclusion that if a Business As Usual (BAU) approach were followed and there was no attempt to limit GHG emissions, the cost would be somewhere in the order of 5% to 20% of the global Gross Domestic Product (GDP). The report also calculated the cost of near immediate investment in a low-carbon economy. It estimated this would reduce the expected annual global GDP growth rate of 2.8% by only 0.19% up to 2030. By comparing the cost of a BAU approach to immediate investment, the report concluded that the *"the benefits of strong, early action on climate change outweigh the costs".*

2.3 GLOBAL TRANSPORT GREENHOUSE GAS EMISSION

In 2010, globally the transport sector was responsible for 7.0 $GtCO_2e$ of direct GHG emissions (IEA, 2012), which equates to 14% of the total 2010 global anthropomorphic GHG emission. As illustrated in Figure 2.7 GHG emissions from transport has more than doubled since 1970, with approximately 80% of the increase from road transport (Sims et al., 2014).

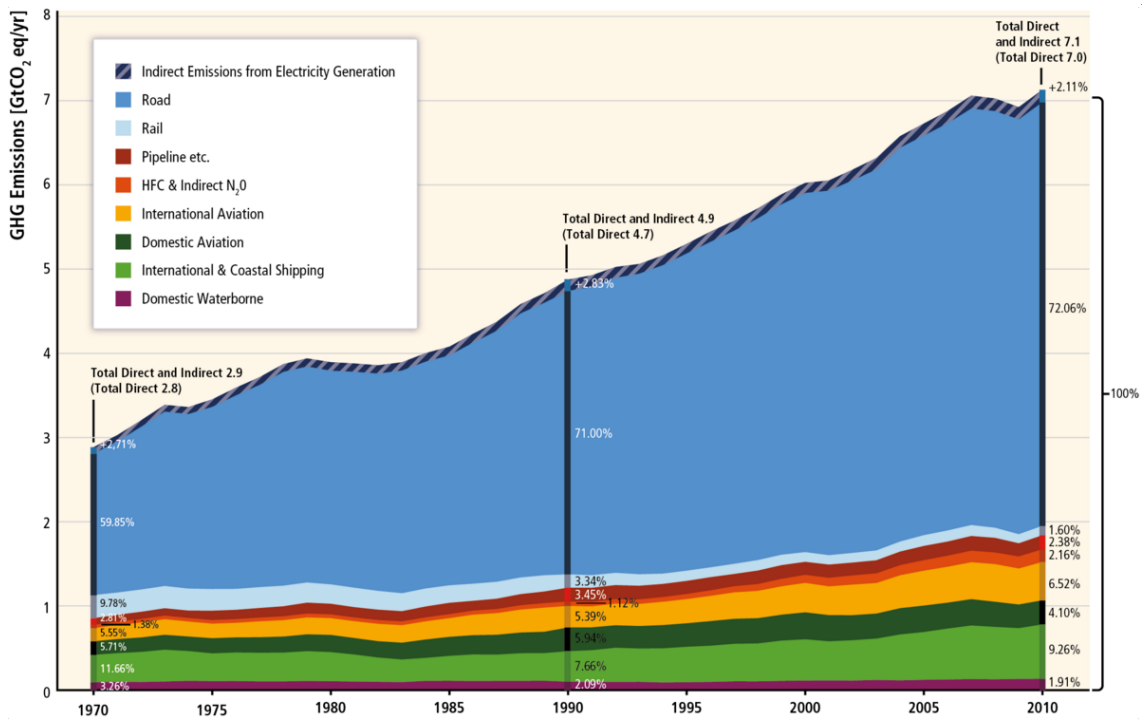

Figure 2.7: Global Direct GHG Emissions from the Transport Sector (Sims et al., 2014)

The International Energy Agency (IEA) reports that global freight and passenger movements have increased by 4% a year since the year 2000, and it is expected that global passenger and freight travel will double between 2010 and 2050, resulting in a 70% increase in global GHG emissions from the road transport sector (IEA, 2014).

2.4 THE UK TRANSPORT SECTOR AND GREENHOUSE GAS EMISSION

The 21st United Nations Framework Convention on Climate Change (UNFCCC) Conference of the Parties (COP) meeting held in Paris in December 2015, resulted in the signing of the 'Paris Agreement' by 195 countries, putting into place *"the first-ever universal, legally binding global climate deal"* (EC, 2015a). The goal of the agreement is to see global GHG emission peak *"as soon as possible"* in order to meet a long established target of limiting global warming to less than two degrees Celsius (UNFCCC, 2010). As part of the agreement, many countries around the world have made strong commitments towards reducing their GHG emissions through formally submitted Intended Nationally Determined Contributions (INDCs) (EC, 2015a).

The UK has led the way on legislated national GHG reduction. In 2008 'The Climate Change Act' was signed into law, committing the UK to an ambitious target of lowering its GHG emissions to 80% of the 1990 baseline by 2050 (Legislation.gov.uk, 2008). As UK transport contributes approximately 22% of the UK domestic GHG emission (Figure 2.8), decarbonising this sector will be essential in meeting the UK's GHG reduction targets.

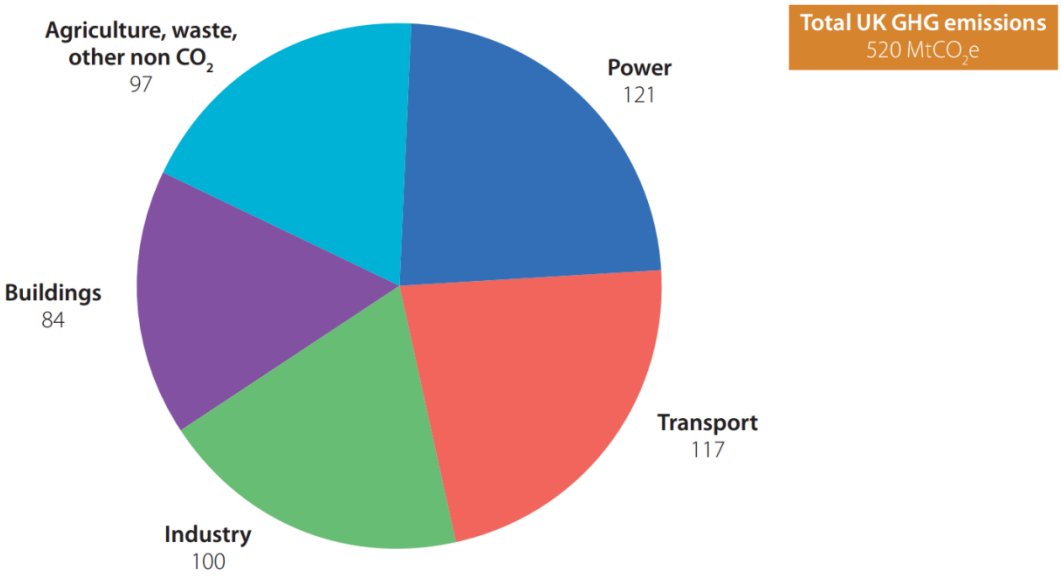

Figure 2.8: UK Domestic $MtCO_2e$ GHG Emission by Sector in 2014 (CCC, 2015)

In the Department for Transport's (DfT) 2009 Low Carbon Transport Plan (DfT, 2009b), the UK Government set out its transport carbon reduction strategy. The report suggests the delivery of GHG emission reductions in the transport sector, through three strategy areas:

- Using Market Mechanisms to Encourage a Shift to Lower Carbon Transport
- Supporting a Shift to New Technologies and Fuels
- Promoting Lower Carbon Choices

At the end of 2014, there were 35.6 million vehicles registered for use on UK roads, with 2.97 million new vehicles registered during 2014 (DfT, 2015i). As illustrated in Figure 2.9, the DfT estimated that in 2013 road transport accounted for 92.4% of total domestic transport's GHG emissions; emitting 107.9 $MtCO_2e$ of the total GHG emission of 116.8 $MtCO_2e$.

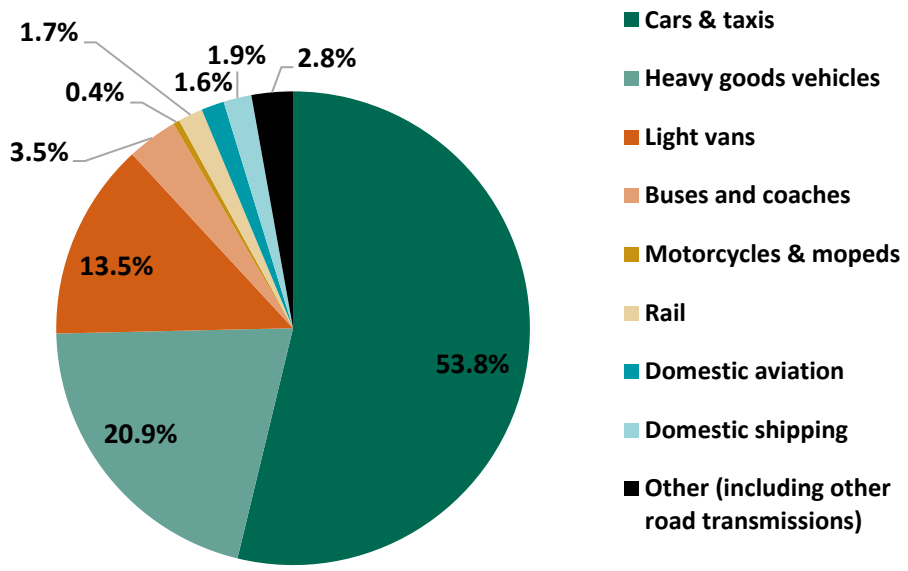

Figure 2.9: UK Transport GHG Emission by Sector (DfT, 2015h)

Reducing the GHG emission contribution from road travel will be critical to meeting the 2050 80% reduction target, with some suggestion that to meet the overall UK target there will need to be an almost complete decarbonisation of the transport sector (DECC, 2011; DfT, 2010b). The European Commission's (EC) 'Roadmap for Moving to a Low Carbon Economy in 2050' (EC, 2011) suggests that to meet an 80% reduction target, depending on the scenario, transport emissions will need to be reduced by 54% to 67% by 2050 across the EU.

The UK 2013 road transport GHG emissions of 107.9 $MtCO_2e$ are only 2.1% lower than the 1990 baseline emission of 110.3 $MtCO_2e$, however, this is a decrease of 10.9% from the maximum emission estimate of 121.1 $MtCO_2e$ calculated for 2007 (DfT, 2015h).

2.5 UK ROAD TRANSPORT CO_2 EMISSION

Focusing purely on CO_2 emission, between 2007 and 2013 the total CO_2 emission from road transport reduced from 120.0 $MtCO_2$ to 107.0 $MtCO_2$ a decrease of 10.9%, but this level of emission is only 1.3% below that of 1990 (DfT, 2015g). The passenger car fleet, the main contributor to the overall vehicle fleet emission (58.2% in 2013), has seen a 12.6% reduction in its CO_2 emission between 1990 and 2013 (71.2 $MtCO_2$ to 62.3 $MtCO_2$) despite a 40.3% increase in licensed private cars in the same period from 19.7 million to 27.7 million (DfT, 2015f) and a 15.0% increase in total driven distance for cars and taxis from 335.9 billion km to 386.2 billion km (DfT, 2015c). This decrease in CO_2 emission from the car fleet has mostly been offset by increased CO_2 emission from buses and coaches, Light Commercial Vehicles (LCV – four wheeled vehicles for the carriage of goods with a gross vehicle weight less than 3.5 tonnes) and Heavy Goods Vehicles (HGV – vehicles with a gross vehicle weight greater than 3.5 tonnes). The LCV category shows the greatest rise, where a considerable increase in licensed LCV vehicles, from 2.1 million in 1994 to 3.4 million in 2013 (DfT, 2015b) and an increase of 71.7% in total distance driven from 39.9 billion km in 1990 to 68.5 billion km in 2013 (DfT, 2015c), have contributed to a growth in LCV emission from 9.3 $MtCO_2$ in 1990 to 15.6 $MtCO_2$ in 2013 (DfT, 2015g).

There are several factors that have driven the improvement in passenger car fleet emission. One of these factors was the increasing price of fuel, which saw a premium unleaded pump price rise of around 67.8% from 79.9 pence per litre in 2000 to 134.1 pence per litre in 2013 (DECC, 2015). Over the corresponding period the pump price for diesel rose from 81.3 pence per litre to 140.4 pence per litre (DECC, 2015). This was the result of the combination of a rise in the cost of crude oil and an increased level of government tax on fuel. The fuel duty rate is currently 57.95 pence per litre for both petrol and diesel (GOV.UK, 2015c). The rising cost of fuel encouraged consumers to look for more fuel-efficient vehicles and/or to drive less, both of which contribute to lower CO_2 emission. In the last two years the price of fuel has fallen, with average prices between October to December 2015 of 106.7 pence per litre and 109.6 pence per litre for petrol and diesel respectively (DECC, 2015). In 2014, the UK fleet total vehicle km driven increased by 2.4%, with total driven distance up from 488.8 billion km in 2013 to 500.4 billion km; the largest annual increase since 1996 (DfT, 2015c). The lower fuel price may explain the rise, however as data for the 2014 UK fleet emission have not been published, it is yet to be established whether this has resulted in an increase in the fleet CO_2 emission estimate.

The UK Government is also incentivising a shift toward lower CO_2 emission vehicles through its car tax policy. Vehicle Excise Duty (VED) and Company Car Tax (CCT) both use bands of CO_2

emission to define the rate of tax for each vehicle. For example, VED applies a zero rate of tax for newly registered petrol and diesel cars emitting less than 130 gCO_2/km, which rises to £1,100 for first registration of a petrol or diesel car emitting over 255 gCO_2/km (SMMT, 2012). The rate of vehicle tax for subsequent years after first registration is also scaled by CO_2 emission, from £0 per year for petrol and diesel cars with a rated CO_2 emission less than 100 gCO_2/km to £505 per year for cars with a rated CO_2 emission greater than 255 gCO_2/km (GOV.UK, 2015b).

Arguably the greatest factor driving the reduction of CO_2 emission in the car fleet is the introduction of the EU's New Car CO_2 Regulation. Initial efforts to reduce CO_2 emission from passenger cars within the EU took the form of voluntary agreements between the EC and associations representing vehicle manufacturers. In 1998 the EC signed voluntary agreements with the Association of European Automobile Manufacturers (ACEA), the Japan Automobile Manufacturers Association (JAMA) and the Korean Automobile Manufacturers Association (KAMA) which at the time accounted for over 95% of annual new car registrations within the EU. Under the terms of the voluntary agreements, the manufacturers agreed to reduce average new car CO_2 emission to 140 gCO_2/km, as measured over the NEDC (detailed in Chapter 2.6). This target was to be met by 2008 for ACEA members and by 2009 for members of JAMA and KAMA, with the goal of reducing the average EU new car CO_2 emission from a 1995 reference value of 186 gCO_2/km. In 2007, despite some progress toward meeting the voluntary targets, the EC reached the conclusion that without additional action the emission reduction targets would not be achieved (EC, 2008). As a result of the failure of vehicle manufacturers to meet voluntary targets, the EC found it necessary to introduce compulsory targets for future vehicle CO_2 emission reduction. In 2009, the EU put in place New Car CO_2 Regulation (EC) No 443/2009 (EC, 2009b) which specified mandatory CO_2 emission performance standards for new passenger cars sold within the EU. This legislation set an average fleet emission target for all new cars in the EU of 130 gCO_2/km starting in 2012, with full compliance by 2015, which will then be reduced to a target of 95 gCO_2/km for 2021 (DfT, 2009b). For LCVs the EC legislature has also been put into place which targets a fleet average for all new LCVs of 175 gCO_2/km from 2014 phased-in to 2016 and a target of 135 gCO_2/km in 2020 (EC, 2009a). Under this regulation, individual vehicle manufacturers have been set reduction targets based on the weight of their vehicles, with failure to reach their target resulting in a penalty of up to €95 for each gCO_2/km that the manufacturer is over their target applied to each registered new vehicle.

A combination of legislation and increased customer demand for more fuel-efficient lower emission vehicles has driven significant innovation from vehicle manufacturers to reduce CO_2 emission. Table 2.2 describes measures that have either been developed or are in development,

which manufacturers are employing to produce lower CO_2 emitting vehicles to meet current and future EU CO_2 emission legislation.

Table 2.2: Technological Innovations for Lower CO_2 Emitting Vehicles (Adapted from (SMMT, 2012))

Alternative Fuels	Improvements	Engine Changes	Others
Biofuels	Aerodynamics	Direct injection	Gear shift indicators
Diesel-electric hybrids	Energy recovery braking	Downsizing of engine capacity, with turbocharging	Smart satellite navigation systems
Petrol-electric hybrids	Lightweighting		
Plug-in hybrids	Low rolling resistance tyres		
Range extenders	Low viscosity lubricants	Stop-start systems	
Hydrogen vehicles	More efficient ancillary devices	Variable valve lift	
Electric vehicles	More efficient cooling and heating systems		
	Optimised transmissions		

A key reason for the marked improvement in average car CO_2 emission over the last decade can be attributed to the increased proportion of diesel vehicles in the UK fleet. As shown in Figure 2.10, new diesel car sales have risen from 17.8% of the market in 2000 to 49.8% in 2014, whilst petrol new car sales have decreased from 82.1% in 2000 to 48.1% in 2014. For the first time in 2011 diesel overtook petrol as the most popular fuel for new car sales (GOV.UK, 2015a). The proportion of hybrid electric new car sales has doubled since 2009, from 0.7% to 1.6% of the market. The contribution of this vehicle type to overall car fleet emission is becoming increasingly significant.

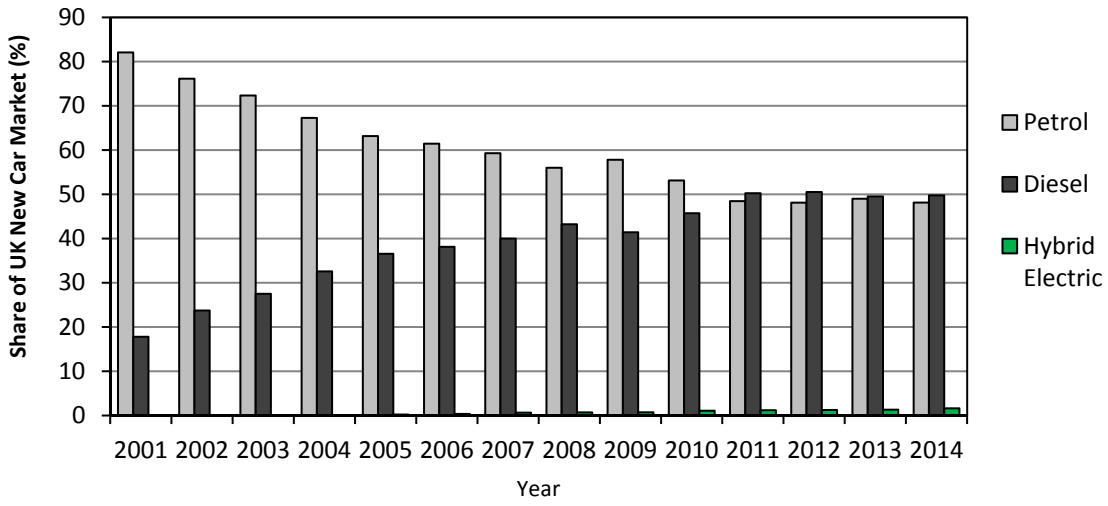

Figure 2.10: Diesel and Petrol Share of the UK New Car Market. Data from (GOV.UK, 2015a)

The diesel engine combustion process is more efficient than that of spark ignition petrol vehicles, resulting in lower fuel consumption and lower CO_2 emission for similar power engines. However, analysis of the Society of Motor Manufacturers and Traders (SMMT) new UK car registration data from 2010 to July 2015, shows that, on a UK sales-weighted average, the CO_2 emission rates of new petrol and diesel vehicles are broadly the same (see Figure 2.11), meaning that the average new car sold in the UK in 2014 had a similar level of CO_2 emission whether it was petrol (126.4 gCO_2/km) or diesel (124.9 gCO_2/km) (SMMT, 2015a).

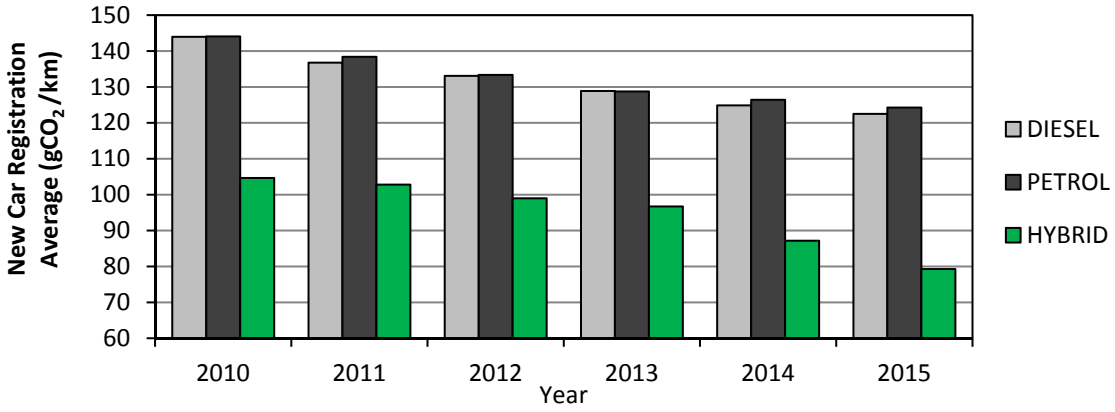

Figure 2.11: Average New Car CO_2 Emission by Fuel Type (HYBRID = both petrol and diesel hybrids) (SMMT, 2015a)

The CO_2 emission values are similar because, on average, diesel passenger cars have a much greater mass and a larger rated engine power than petrol cars. In 2014 the average new diesel passenger car had a kerbweight of 1,512 kg and an average engine power of 106.3 kW (142.6 bhp). In comparison, the average new petrol passenger car had a considerably smaller kerbweight of 1,150 kg and an average engine power of 82.4 kW (110.5 bhp) (SMMT, 2015a).

It should be noted that although an increase in the percentage of diesel vehicles has had a positive impact in reducing the average CO_2 emission of the vehicle fleet, under current emission standards, compression ignition (diesel) engines are permitted a greater level of Nitrogen Oxide (NO_x) emission compared with spark ignition (petrol) engines (because combustion in diesel engines occurs at higher pressure and temperature, generating more NO_x). In 1993, the EU adopted Euro Emission Standards for Passenger Cars (Euro 1) that set limits on the exhaust emission of the air pollutants carbon monoxide (CO); un-burnt hydrocarbons (HC); NO_x; and particulate matter (PM), with emissions tested on a chassis dynamometer over the NEDC. Since its inception the acceptable limit for these pollutants in exhaust emission has been reduced through updated EU directives, from Euro 1 to the current Euro 6 standards introduced in September 2014. In addition to NO_x, diesel engines have also historically been permitted a greater mass of particulate matter (PM) emission (Delphi, 2013). The emission of NO_x species

and PM can have negative consequences for local air quality with resulting detrimental impacts on human health. An inadvertent side effect from EU policies to reduce CO_2 exhaust emission (which have incentivised the production and uptake of diesel vehicles within the EU) has been to increase emissions of NO_x and PM from the vehicle fleet, with dangerous implications for air quality especially in congested urban networks (Skeete, 2017; Harrison et al., 2014; Font and Fuller, 2016).

The combination of low CO_2 technological innovation, increased dieselisation, economic incentives and disincentives through government policy and legislation, and increased public awareness of the issues around climate change have seen the average rated CO_2 emission of new cars bought in the UK fall over the last 15 years, but most substantially in the last 5 years. Figure 2.12 shows the decrease, from an average 177.8 gCO_2/km in 2001 to 124.8 gCO_2/km in 2014 (GOV.UK, 2015d). The 2014 UK new car average is therefore currently below the 2015 EU target of 130 gCO_2/km by 5.2 gCO_2/km (or 4%), but further progress will have to be made to meet the 2021 target of 95 gCO_2/km.

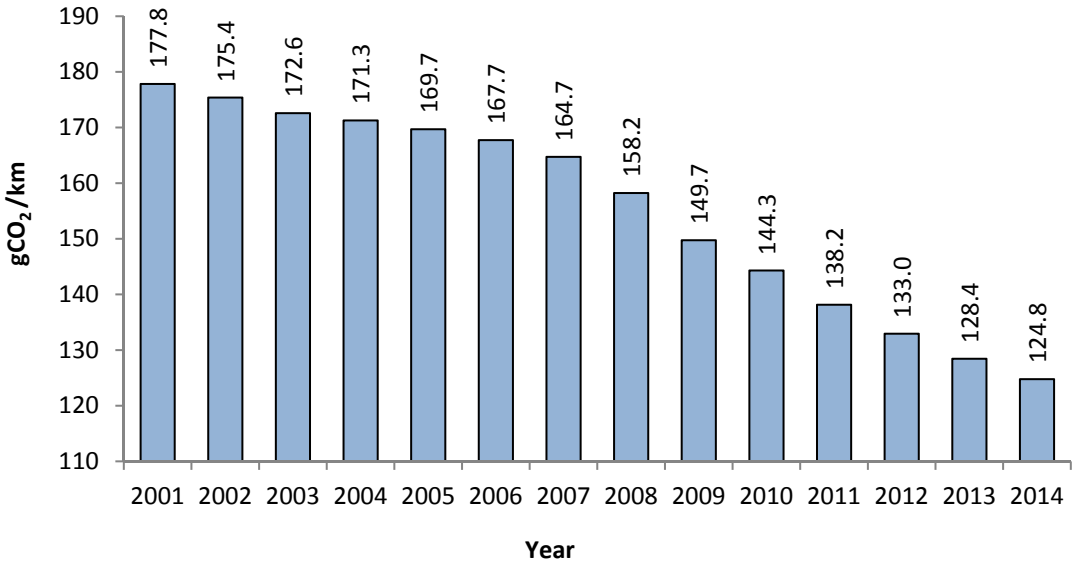

Figure 2.12: UK Average New Car CO_2 Emission 2001-2014
Data from (GOV.UK, 2015d)

The SMMT New Car CO_2 Report 2015 (SMMT, 2015b), details an SMMT measured active vehicle fleet of 32.61 million cars in circulation on UK roads, of which 95% have a CO_2 type-approval emission rate. The SMMT calculate the average rated emission of a car in the UK fleet as 156.6 gCO_2/km in 2014, which suggests that the average new car bought in 2014 should emit approximately 20.3% (or 31.8 gCO_2/km) less CO_2 per km than the average in-use car in the UK.

2.6 TEST CYCLE MEASUREMENT FOR CO_2 EMISSION CERTIFICATION

In order to establish the gCO_2/km emission for a particular vehicle, the EU employs the New European Driving Cycle (NEDC) which is described in Figure 2.13. The NEDC was originally developed for the measurement of air pollutant emissions, but from 2009 it has acted as the benchmark test for vehicle CO_2 type-approval emission as part of the EU mandatory CO_2 regulations (EC, 2009b; Mock et al., 2012; ICCT, 2015). The NEDC specifies a standardised cycle of acceleration, constant speed and deceleration, and prescribed test conditions, to generate repeatable emissions measurements (Pelkmans and Debal, 2006; Weiss et al., 2011a). This cycle is made up of a phase of urban driving (called the ECE15 urban drive cycle) and a phase of Extra-Urban Driving (EUDC representing high speed driving). These cycles are measured on a chassis dynamometer with Constant Volume Sampling (CVS) technique used to analyse each of the monitored exhaust emission species.

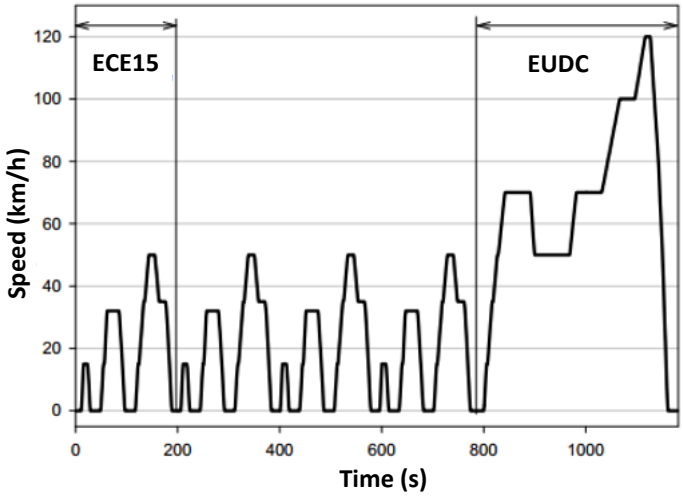

Figure 2.13: Speed Profile of the New European Driving Cycle (Els, 2015)

The method is designed to represent real-world driving conditions and quantify vehicle emission in a way that is reproducible so that the data recorded are comparable between vehicles. However, the NEDC has a very smooth profile of acceleration and deceleration, on a flat test platform, using only a small portion of a vehicle's operating range and it begins with the vehicle soaked at 20-30°C (Pelkmans and Debal, 2006). Real-world conditions are likely to be very different to the standard test cycle. Parameters such as traffic congestion, ambient temperatures, topography, driver behaviour and road geometry, will all have an influence on emissions that are not reflected in the test cycle. The NEDC takes no account of how traffic flow is affected by street layout or how people drive in congested or free flowing traffic (Li et al., 2008b). Research has established that the NEDC fails to represent *"low speed high torque operation"*, *"dynamic transient velocities"*, and *"very high speed driving"* (Pelkmans and Debal,

2006; Weiss et al., 2011a). As a result, the NEDC is considered a poor representation of real-world driving conditions (Dings, 2013).

2.7 DISCREPANCY BETWEEN TEST CYCLE AND REAL-WORLD EMISSION

A study by Weiss *et al.* for the European Commission Institute for Energy tested a total of 12 Euro 3 to Euro 5 Light-Duty Vehicles (LDVs – which comprises passenger cars and LCVs) over real-world drive cycles with vehicle emission measurements recorded using a Portable Emission Measurement System (PEMS). As shown in Figure 2.14, the CO_2 emission values recorded over the real-world test cycles were larger than those measured in the NEDC testing. The NEDC measured CO_2 emission values were exceeded on average by 21% ± 9%. Similar differences were found for the other pollutants, for example, the NO_x emission values for the Euro 3-5 diesel vehicles were found to exceed emission limits substantially, whereas the NEDC cycle had found them to comply with the legislation (Weiss et al., 2011a).

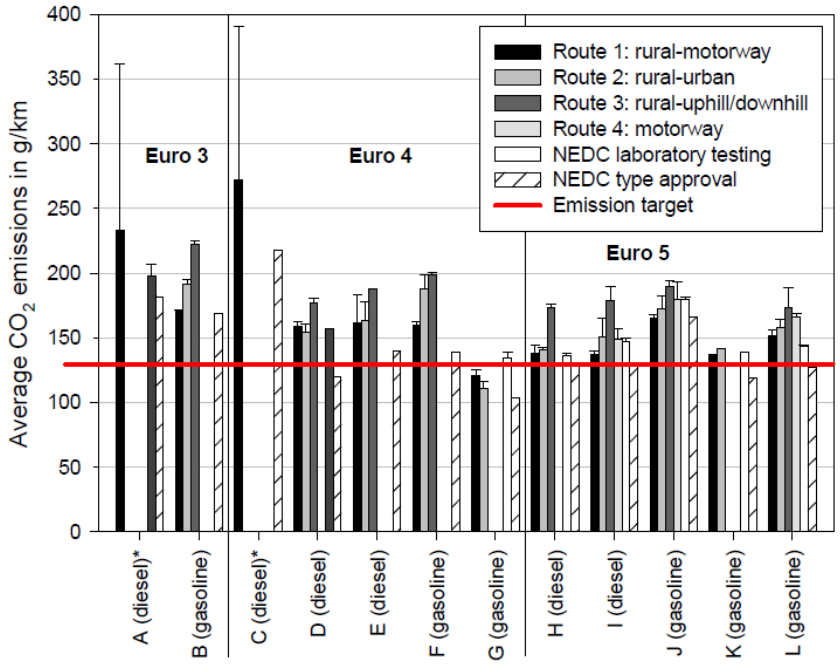

Figure 2.14: Average CO_2 Emission on PEMS Test Routes and During NEDC Laboratory Testing (Weiss et al., 2011a)

A number of recent reports have investigated the reasons why, despite great reductions in the NEDC type-approval test CO_2 emission values of new cars, when these new vehicles are tested on-road, neither the fuel consumption nor the CO_2 emission reflect the same improvement as the certified measurements (Dings, 2013; ICCT, 2015; Mock et al., 2015). Figure 2.15 is taken from a report by the International Council on Clean Transportation (ICCT) which analysed the

gap between type-approval CO_2 emission and real-world CO_2 emission, utilising eleven data sets covering 600,000 vehicles from six countries (Mock et al., 2015). These findings illustrate a clear trend of increasing divergence between real-world and test cycle measured CO_2 emission, with the gap widening from approximately 8% in 2001 to 40% in 2014.

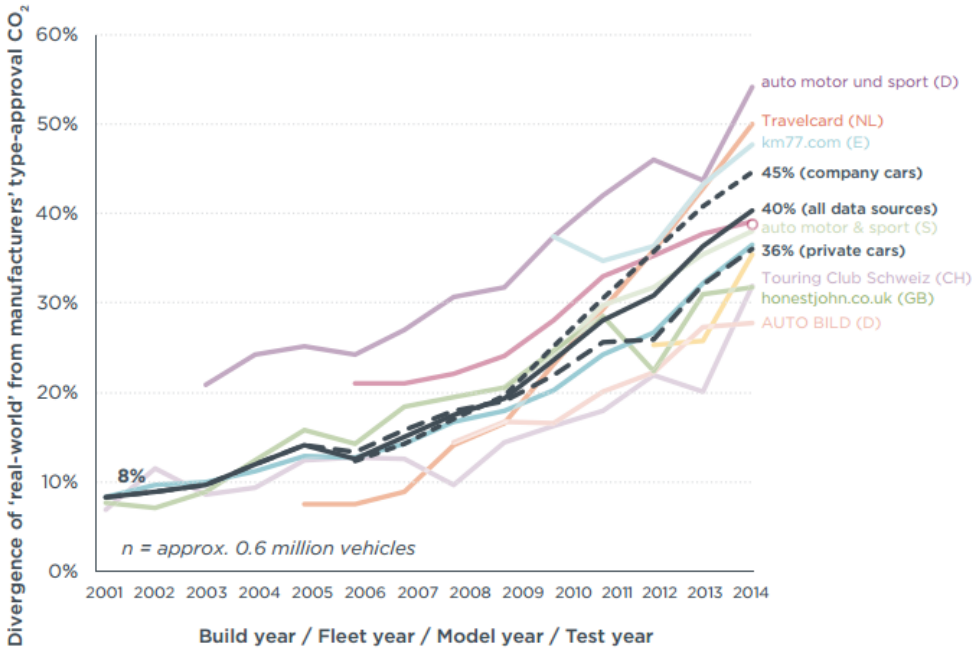

Figure 2.15: Divergence Between Real-World and Manufacturer's Type-Approval CO_2 Emission for Various Real-World Data Sources (Mock et al., 2015)

Detailed analysis of the factors responsible for the increasing gap between real-world and type-approval CO_2 emission revealed three main elements (Dings, 2013; ICCT, 2015).

1. The NEDC being unrepresentative of typical driving conditions
2. Loopholes in the test procedure:
   - Determination of aerodynamic drag and rolling resistance during the road-load test
   - Loopholes in the testbed procedure for measuring CO_2 emission
3. Technologies that reduce CO_2 emission to a greater extent during the certification test than in real-world driving.

Although it is widely accepted that the NEDC is not a good indicator of real-world driving patterns, the test cycle hasn't changed since the inception of the EU regulations whilst the gap has continued to widen. Mock et al. (2012) conclude that the rising divergence can be attributed to the increasing exploitation of flexibilities and loopholes within the road-load determination and type-approval testing, suggesting that "*reducing type-approval CO_2 emission values by exploiting existing flexibilities in the test procedures is cheaper than applying technical measures*

to reduce CO_2 emissions, so that these "soft" measures are likely to be used before any technical changes to the vehicles". This conclusion is reflected in the illustration of influencing parameters in Figure 2.16, which highlights ways in which manufacturers are able to manipulate the test procedure to minimise CO_2 emission during the certification (Mock et al., 2015). These include; reducing the weight of the test vehicle; adjusting the brakes to avoid frictional losses; ensuring the battery is fully charged; testing the car at high temperature and improving the aerodynamics. A full discussion of these methods is available in the reports of Mock et al. (2015) and Dings (2013).

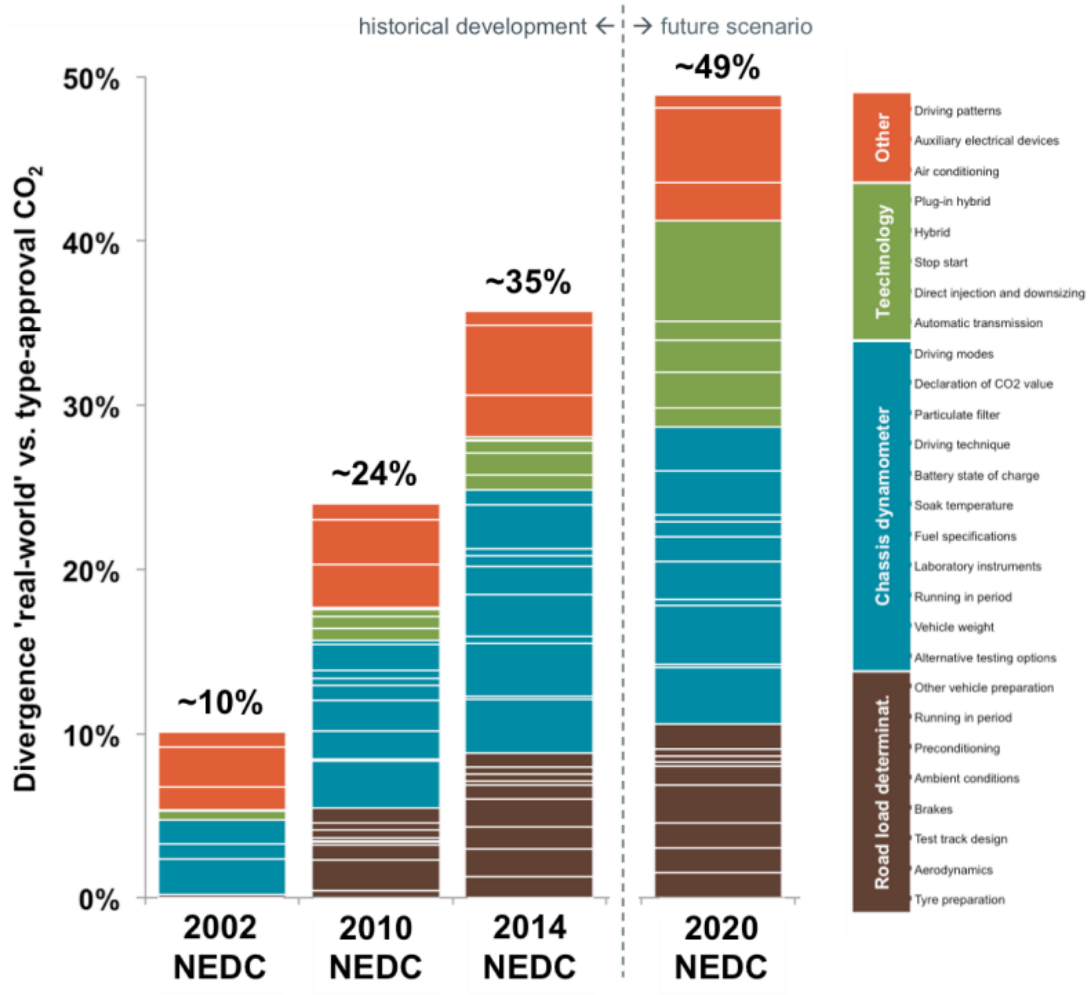

Figure 2.16: Estimate of the Emission Gap between Type-Approval and Real-World CO_2 Emissions, Divided into Individual Influencing Parameters (Mock et al., 2015)

Whilst the year-on-year new car CO_2 reductions for the UK vehicle fleet reported in Figure 2.12, on the face of it, seem promising, in reality, it is likely that the real-world reduction in CO_2 emission from these new vehicles will be considerably less than suggested by the reduction in type-approval CO_2 emission values. The motor manufacturers have, to a large extent, met the EU mandatory emission targets by improving their ability to deliver low emission during testing, rather than by deploying more effective real-world CO_2 and exhaust pollutant emission

reduction technologies. This issue was highlighted by the recent emission scandal at the Volkswagen group (Holder, 2015). As Figure 2.15 illustrates, NEDC test certified CO_2 emission values are becoming increasingly unrepresentative of real-world CO_2 emission.

Given the contribution of road transport to the UK's GHG emission, a significant underestimation of real-world CO_2 emission from the transport sector could result if the gap between NEDC type-approval and real-world emission is not adequately accounted for by models which utilise certified NEDC CO_2 emission values to calculate emission inventories.

2.8 ON-ROAD CO_2 EMISSION TESTING

The ICCT (2015) report *"Quantifying the impact of real-world driving on total CO_2 emissions from UK cars and vans"* suggests that by introducing comprehensive in-use conformity testing that would allow the EU to test mass-production vehicles and complementing it with on-road CO_2 emission testing, through Portable Emission Measurement System (PEMS), the gap between real-world and certified CO_2 emission could be reduced to around 5%. The testing of mass-production vehicles in real-world driving conditions through PEMS could provide results that would give a much more accurate assessment of expected fuel consumption and CO_2 emission for vehicle owners. On-road PEMS analysis is being developed as Real Driving Emissions (RDE) for regulated pollutants, which is to be introduced for Euro 6c type-approval from 2017 (EC, 2015c). However, there are currently no plans to introduce RDE for CO_2 emission (ICCT, 2015).

PEMS are on-board analysis systems which enable second-by-second measurement of exhaust emission under real-world in-use conditions. Typically a PEMS consists of an exhaust pipe attachment to direct a fraction of the exhaust gas through heated lines to gas analysers, which rapidly analyse the exhaust gas concentrations of the regulated pollutants CO, HC and NO_x as well as CO_2; a Pitot tube to record the exhaust flow rate, which enables g/s emission to be calculated from the analysed emission species; a Global Positioning System (GPS) to log vehicle latitude, longitude and speed at 1-10 Hz; a data recorder connected to the vehicle Controller Area Network (CAN) to access the vehicle's factory installed sensors and record, for example, engine speed, vehicle speed and coolant temperature; humidity and ambient temperature sensors; a laptop to record all test data and batteries to power all the equipment.

PEMS studies have become an increasingly popular method of real-world vehicle emission estimation and there is a wealth of evidence in the literature to demonstrate that PEMS can be

employed to provide accurate measurement of on-road vehicle exhaust emission (Liu et al., 2010; Frey et al., 2003; Ropkins et al., 2007; Andersson et al., 2014; May et al., 2014).

2.9 SUMMARY

The UK Government signed into law The Climate Change Act in 2008, committing the UK to an ambitious target of lowering its GHG emissions to 80% of the 1990 baseline by 2050 (Legislation.gov.uk, 2008). If this target is to be met the road transport sector, with 35.6 million vehicles in use on UK road in 2014, contributing 22% of the UK's total domestic CO_2 emission (CCC, 2015), will clearly need to deliver a vast reduction in CO_2 emission. The UK Government's 'Carbon Plan' published in December 2011 suggests that, in order to meet this target, the vehicle fleet will need to be almost completely decarbonised by 2040 due to the rate of fleet turnover (DECC, 2011).

Between 2007 and 2013 the total CO_2 emission from road transport decreased from 120.0 $MtCO_2$ to 107.0 $MtCO_2$, a reduction of 10.9%, but this is only 1.3% below that of 1990 CO_2 emission (DfT, 2015g). The passenger car fleet, has seen a 12.6% reduction in its CO_2 emission between 1990 and 2013 (71.2 $MtCO_2$ to 62.3 $MtCO_2$) despite a 40.3% increase in licensed private cars in from 19.7 million to 27.7 million (DfT, 2015f) and a 15.0% increase in total driven distance for cars and taxis from 335.9 billion km to 386.2 billion km (DfT, 2015c). However, this decrease in CO_2 emission from the car fleet has mostly been offset by the increased CO_2 emission from buses and coaches, LCVs and HGVs.

An important factor driving the reduction of CO_2 emission in the car fleet has been the introduction of the EU's New Car CO_2 Regulation (EC) No 443/2009 (EC, 2009b). This legislation set an average fleet emission target for all new cars in the EU of 130 gCO_2/km starting in 2012, with full compliance by 2015, which will then be reduced to an average of 95 gCO_2/km by 2021 (DfT, 2009b). The UK Government is also incentivising a shift toward lower CO_2 emission vehicles through its car tax policy. Along with these mechanisms, the steep rise in the price of fuel between 2000 and 2013, led a shift in the passenger car fleet towards more fuel-efficient vehicles with lower CO_2 emission.

Diesel engines are more efficient than petrol and therefore have lower fuel consumption and lower CO_2 emission for similar power engines. The cheaper running cost of diesel vehicles has caused a rapid dieselisation of the passenger car fleet over the past 15 years, with diesel

overtaking petrol as the most popular fuel for new cars sales since 2011 (GOV.UK, 2015a). However, analysis of the SMMT new UK car registration data from 2010 to July 2015 shows that on a UK sales-weighted average, the CO_2 emission of petrol and diesel vehicles are now broadly the same (see Figure 2.11).

A combination of low CO_2 technological innovation, increased dieselisation, economic incentives and disincentives, through government policy and legislation, along with increased public awareness of the issues around climate change, have seen the average type-approval CO_2 emission of new cars bought in the UK fall dramatically, from an average 177.8 gCO_2/km in 2001 to 124.8 gCO_2/km in 2014 (GOV.UK, 2015d). The 2014 UK new car average is therefore currently below the 2015 EU target of 130 gCO_2/km by 4%.

The EU employs the NEDC as the benchmark test for vehicle type-approval CO_2 emission, as part of the EU mandatory CO_2 regulations (EC, 2009b; ICCT, 2015). However, several studies have revealed that real-world vehicle emission substantially exceeds the NEDC measured emission. These reports demonstrate an increasing divergence between real-world and test cycle measured CO_2 emission, with the gap widening from approximately 8% in 2001 to 40% in 2014. The NEDC has been found to be a poor representation of real-world driving conditions (Dings, 2013) with a very smooth profile of acceleration and deceleration utilising only a small portion of a vehicles operating range.

The greatest reason for the increasing gap in real-world and NEDC can be attributed to the increasing exploitation of flexibilities and loopholes within the road-load determination and type-approval testing, with manufacturers manipulating the test procedure to minimise CO_2 emission during the certification (Mock et al., 2015). So whilst the year-on-year reduction in new car CO_2 emission values would seem to be reducing the UK vehicle fleet's GHG emission, in reality, it is likely that the real-world reductions in exhaust CO_2 emission will be considerably smaller. The NEDC type-approval CO_2 emissions are becoming increasingly unrepresentative of real-world CO_2 emission.

In order to test the accuracy of emission model estimates of real-world CO_2 emission in later chapters of this research, the next chapter analyses the results of a Portable Emission Measurement System survey. The PEMS survey is required to provide an accurate appraisal of on-road CO_2 emission as the summary presented in this chapter has shown that the type-approval NEDC vehicle CO_2 emission values provide poor real-world estimates.

CHAPTER 3: REAL-WORLD VEHICLE EMISSION

3.1 INTRODUCTION

As discussed in Chapter 2, vehicle emission measurements have historically been primarily conducted over standardised driving cycles through laboratory based dynamometer testing (Coelho et al., 2009). This form of testing may not adequately reflect the real-world variations in engine power demand that result from factors such as driver input, traffic conditions, road management and road topography (Frey et al., 2008) and therefore fails to represent Real Driving Emissions (RDE) adequately (Weiss et al., 2011b; Weiss et al., 2012; Chen and Borken-Kleefeld, 2014). In order to measure on-road emission under real-world conditions Portable Emission Measurement Systems (PEMS) can be employed to record vehicle parameter data and exhaust emission. These data can then be used to investigate the effect of real-world influences on vehicle emission and facilitate the development of improved models for the estimation of RDE.

Research has demonstrated that on-board vehicle PEMS can be utilised to provide accurate measurement of vehicle exhaust emissions in real-world driving (Liu et al., 2010; Frey et al., 2003; Ropkins et al., 2007). PEMS instrumentation in such studies are deployed to record the motion, geographical position and exhaust emission of a vehicle driven over a real-world test route, most commonly measured on a second-by-second basis.

The purpose of this chapter is to quantify the real-world CO_2 emission of a petrol Euro 4 passenger car travelling through an urban traffic network, in a range of differing traffic conditions. The analysis undertaken in this chapter acts as a resource for later chapters, in which the second-by-second and aggregate vehicle trajectory data are used to generate emission estimates from different emission models. The measured real-world CO_2 emission factors are used as validation data to assess the accuracy of the modelled micro-scale emission estimates. The work presented in this chapter makes use of an existing PEMS data set, collected in 2007 (prior to the start of this research) by the University of Leeds (UoL) Energy and Resources Research Institute (ERRI) and the Institute for Transport Studies (ITS). All analysis of the PEMS database is original to the thesis.

3.2 PEMS MEASUREMENT OF ON-ROAD EXHAUST CO_2 EMISSION

3.2.1 Study Design

The 2007 instrumented vehicle study was conducted in Headingley, a suburb of Leeds, approximately three kilometres (km) northeast of the city centre. The test lap used in this research, plotted in Figure 3.1**,** comprises a 4.6 km route on the A660 (Otley Road and Headingley Lane) and the B6157 (North Lane), on mainly single lane urban commuter roads. The route features three major signalised junctions, four speed cameras, five signalled pedestrian crossings and a number of non-signalised junctions with smaller adjoining side roads. The speed limit throughout the lap is 30 mph (48 km/h).

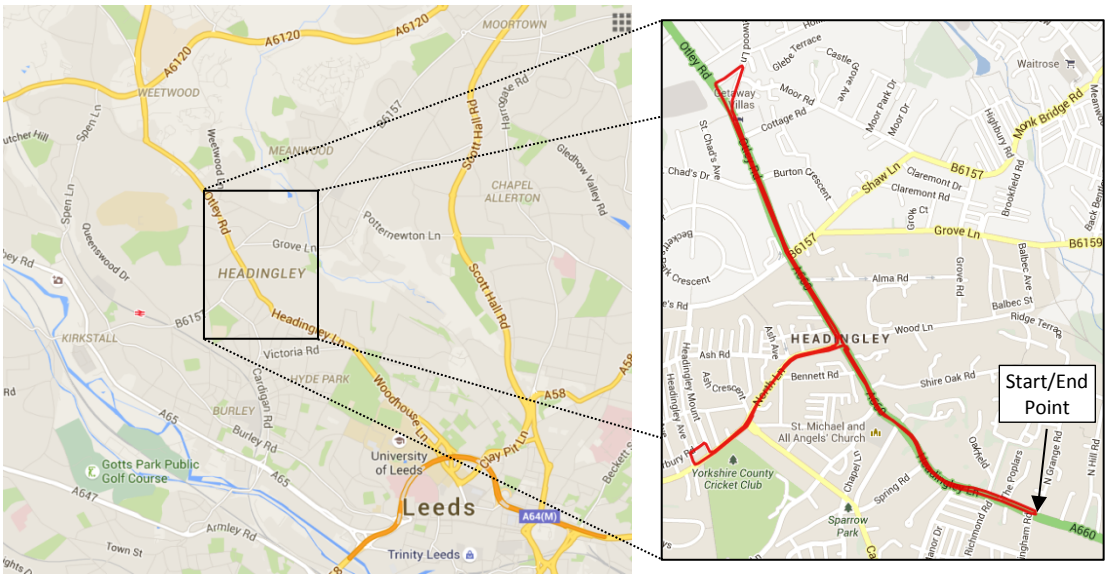

Figure 3.1: **Headingley Test Lap**
***(*Source: GPSVisualizer.com and *©Copyright GoogleTM 2015*)**

The Headingley test lap driven by the test vehicle is not flat. Figure 3.2 shows the elevation profile for the lap, along with an indication of road grade throughout the route, and the position of signalised road junctions and pedestrian crossings. The lap has a maximum absolute elevation of 98.1 m above sea level and a minimum of 76.6 m. Summed over the lap, the route ascends and descends by approximately 49 metres. However, as the lap is a loop, the start and finish elevations are roughly the same (with small disparities a result of differences in the measured GPS position of the lap start and end points) and the average road gradient over the lap is therefore zero. Greater detail on the topography of the test lap and the influence of road grade on the test vehicle emission is provided in Chapter 5.

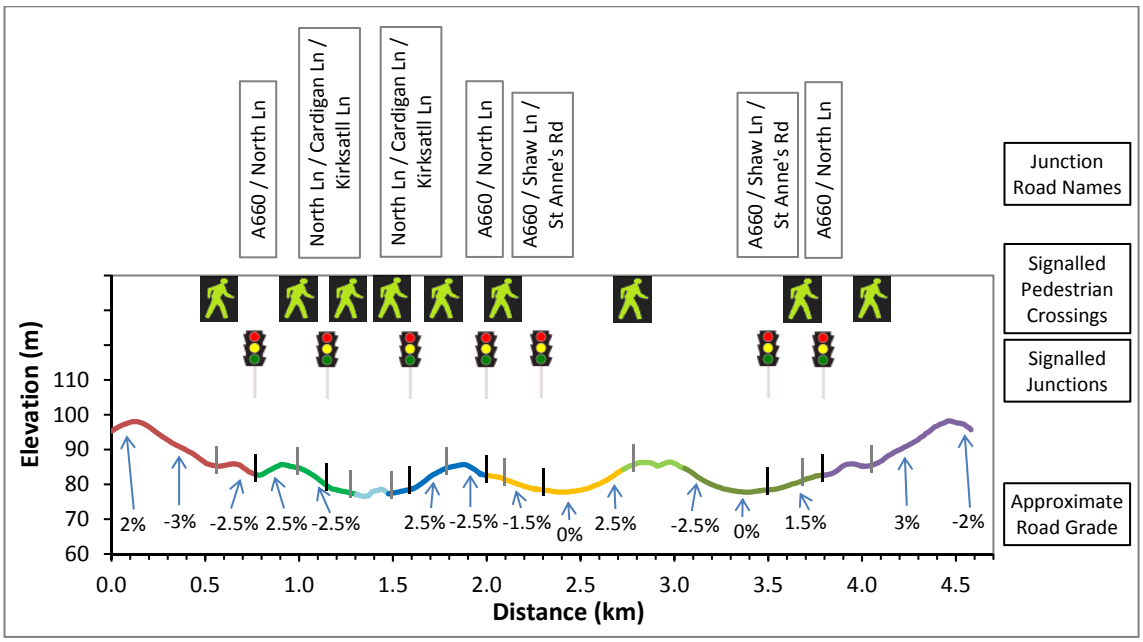

Figure 3.2: Headingley Test Lap Elevation Profile

The A660, on which a majority of the test was conducted, is one of the main arterial corridors into and out of Leeds, the third largest city in the UK, with a population of approximately 751,500 (ONS, 2012). The Department for Transport (DfT) Annual Average Daily Flow (AADF) recorded in 2014, for both directions of travel on the A660 (excluding motorbikes) was 19,169 vehicles (DfT, 2015e). It is the busiest and most crowded bus corridor into and out of Leeds (S.D.G., 2014a), covering routes from the city centre to the northern suburbs. This corridor features bus stops at regular intervals and a number of high frequency bus services, which contribute approximately 50 buses per hour to the combined traffic flow during peak hours. As such, the A660 has been identified as one of the most congested routes in Leeds, with high levels of congestion during both the morning and afternoon peak hours. A 2015 Leeds City Council (LCC) survey using 2011-2012 data revealed that the three signalised junctions on the Headingley test lap sit 3rd (A660 / B6157 North Lane), 9th (A660 / B6157 Shaw Lane) and 62nd (B6157 North Lane / Cardigan Road), respectively, on the list of Leeds' congestion hotspots (LCC, 2015). The study area provides a wide range of traffic flow conditions as the journey times in the peak periods have been found to be more than double the average of those recorded under uncongested conditions. (NGT, 2014).

The test lap was covered 48 times by the same driver in an instrumented vehicle during a week-long testing period between the 26th February 2007 and the 5th March 2007, with runs conducted between the hours of 07:30 and 21:00 to capture the full range of traffic conditions for this road network. The test lap was completed following two routes, A and B. Following route A the vehicle began on the A660 at the southern most point of the test route, proceeded to the northern most point of the test route before returning on the A660, to make a right-hand

turn at the signalised junction with the B6157. The vehicle then completed the B6157 part of the lap returning to the signalled junction with the A660, where it makes a right turn to finish the lap opposite the initial starting point. The vehicle started route B at the same place as route A, but when it reached the signalised junction with the B6157 it makes a left-hand turn. The vehicle completed the B6157 part of the lap and at the signalised junction with the A660 it made a left-hand turn and proceeded to the most northern point of the test route. The test vehicle then returned on the A660 to the point opposite the initial starting point. The test lap was completed 25 times with route A and 23 times with route B. The laps were completed in a variety of weather conditions, with sunny, dry, overcast and rainy test laps, in temperatures ranging from 1°C to 15°C.

3.2.2 Test Vehicle

The instrumented vehicle used in this study was a 2005 Euro 4 emission compliant petrol Ford Mondeo with a 5-speed manual gearbox and a port fuel-injected 1.8 litre, 4 cylinder, 16 valve spark ignition engine with a maximum power of 92 kW (123 bhp) at 6,000 rpm. The vehicle was equipped with a Three Way Catalyst (TWC). The vehicle specifications adopted are a kerbweight of 1,374 kg including 90% fuel levels, full fluid levels and a 75 kg driver (Li et al., 2008a), a rolling resistance coefficient of 0.013 (Ehsani et al., 2009), an aerodynamic drag coefficient of 0.32 (Doucette and McCulloch, 2011), a frontal area of 2.3 m^2 (Doucette and McCulloch, 2011) and an idle engine speed of 850 rpm. A loading value of up to 150 kg was included to account for the weight of the PEMS equipment.

In 2015 the average engine capacity for licensed UK petrol cars was 1,571 cc (1.571 L) with 23.1% of all such cars on UK roads having a petrol engine of between 1,551 cc and 2,000 cc (GOV.UK, 2016a). As of April 2016 there were 127,460 licensed petrol Ford Mondeo's with an engine size between 1,500 and 2,000 cc in Great Britain and the Ford Mondeo was the 12th most popular car model (GOV.UK, 2016d). Whilst the age of the test vehicle means that the current UK vehicle fleet contains a majority of cars which are newer than this, 33.1% of all cars registered in the UK were registered in or before 2005 (GOV.UK, 2016b). As the test vehicle was a popular car model, of a common engine size and of an age not unusual on UK roads, the PEMS recorded CO_2 figures can be considered relevant to current on-road emission (N.B. the PEMS test was conducted when the car was only two years of age, so the recorded figures are not that of an 'old' vehicle).

3.2.3 Test Vehicle Instrumentation

An Horiba On Board emission measurement system (OBS-1300) was used to measure the exhaust flow rate and air/fuel ratio, enabling calculation of CO_2 mass emission from the volumetric measurements. The OBS System comprises a Data Integration Unit (DIU); a global positioning system (GPS), a Heated Non-Dispersive Infra-Red Analyser (HNDIR), an air/fuel ratio sensor, an Annubar flow meter for measuring exhaust gas volumetric flow rate; a peripheral sensor for ambient air temperature; a data logger (laptop) and software; and a power supply unit and batteries. Exhaust monitoring was carried out by a purpose built attachment fitted to the end of the vehicle exhaust pipe, with the sample line and analyser cells operated at 120° ± 2°C and 87° ± 2°C, respectively. Speed, acceleration and geographical position data were measured and recorded by a RaceLogic VBOX II, a GPS data logging device for automotive applications. The VBOX was also used to collect engine and vehicle speed through connection to the vehicles Controller Area Network (CAN) which accesses the vehicle's factory installed sensors. All data were recorded at 1 Hz.

The data from the OBS and VBOX were time aligned using the separate vehicle velocity data measured by each instrument. Exhaust flow measurement drift was corrected, where required, using a standard on-road correction method utilised in other University of Leeds studies, measuring 'zero flow' values before and after each test run and recalibrating the zero-points, assuming a linear drift over the test (Ropkins et al., 2007).

A documented OBS-1300 'pulse effect' overestimation of idle exhaust flow (Ropkins et al., 2008; Nakamura et al., 2002; Daham et al., 2005) was observed in the data and corrected based on the work of Ropkins et al. (2008), which demonstrated an OBS overestimation in the order of 1.85 to 2.25 times the actual idle exhaust flow rate when using the standard OBS-1300 exhaust attachment. To correct for the erroneous exhaust flow rates measured at all points of engine idle during the Headingley PEMS survey, the OBS measured exhaust flow values were halved for each second of data when the engine speed was recorded to be less than engine idle speed of 850 rpm.

The capacity of the PEMS design employed in this research to provide reliable CO_2 emission measurement over a wide range of engine operating conditions and drive cycles has been validated in previous work (Ropkins et al., 2008). The Ropkins *et al.* study found good agreement (coefficient of determination $\{R^2\} \approx 0.95$, sensitivity 0.98 ± 0.05 at 95% confidence limit) between the OBS-1300 HNDIR 1 Hz transient CO_2 emission measurements and the measurements of a

static Horiba MEXA-7400 gas analyser (NDIR), which is part of the Powertrain and Vehicle Research Centre Chassis Dynamometer Facility at the University of Bath. Therefore, the PEMS employed in the Headingley study can be considered to give reliable CO_2 measurements.

3.2.4 Carbon Dioxide Mass Emission Calculation

The exhaust CO_2 emissions, as measured by use of the OBS-1300, were captured on a volumetric basis. The CO_2 mass emission for each second was calculated from the measured exhaust gas volumetric flow rate, the density of CO_2 and the wet gas concentration of CO_2 (Ropkins et al., 2007), using the following equation:

Equation 3.1:

$$CO_{2\ MASS} = [CO_2]_{t=t+DT} \times MWT_{CO_2} \times [Q_{EX}]_{t=t} \times \frac{273.15}{293.15} \times UCF$$

Where,

- $CO_{2\ MASS}$ is the CO_2 mass emission rate in g/s, standardised to 20°C and 1 Atm (293.15 K and 101.3 kPa);
- $[Q_{EX}]_{t=t}$ is the exhaust flow rate in m^3/min at time t;
- $[CO_2]_{t=t+DT}$ is the percentage concentration of CO_2 associated with $[Q_{EX}]_{t=t}$ which is read after a measurement Delay Time (DT), as the exhaust concentration measurement is typically slower to register on the data logger than the exhaust flow rate measurement because of gas analyser sample line length (N.B. It is very important that the exhaust flow rate and the exhaust gas concentrations are accurately time aligned to compute the mass emission rate);
- MWT_{CO_2} is the molecular weight of CO_2 (44.01 g/mol);
- UCF are the required Unit Conversion Factors. These Factors are a multiplication by 1/100 to correct the units of $[CO_2]_{t=t+DT}$ from a percentage volume to volume; a multiplication of 1/60 to change the units of $[Q_{EX}]_{t=t}$ from m^3/min to m^3/s; a multiplication of 1/22.415 to convert MWT_{CO_2} from g/mol to CO_2 density using the ideal gas volume of 1 mole at Standard Temperature and Pressure, with 273.15/293.15 amending the density of CO_2 to that at 20°C and 1 bar (making the assumption that CO_2 is an ideal gas and the change in density is directly related to the change in temperature).

The CO_2 emission rate for each lap was calculated in g/km using Equation 3.2:

Equation 3.2:

$$CO_{2\ TOTAL/km} = \left(\sum_{t=1}^{t_x} CO_{2\ MASS}\right) \Big/ x$$

Where,

- $CO_{2\ MASS}$ is the CO_2 mass emission rate in g/s;
- x is the distance travelled during the test lap in km;
- Time t=1 to t_x is the time taken to complete the test lap in seconds.

3.3 ANALYSIS OF PEMS MEASUREMENTS: HEADINGLEY LAP

The processed PEMS data set comprises 56,986 seconds of data recorded over 48 laps of the Headingley test route, covering a total distance of 219.8 km. For each lap there is a second-by-second (1 Hz) log of all parameters recorded by the OBS and VBOX time aligned by velocity (which was recorded by both instruments). A summary table of all 48 recorded test laps is presented in Appendix 1. Figure 3.3 plots the 1 Hz vehicle speed; engine speed and CO_2 emission data recorded over a test lap as a time series.

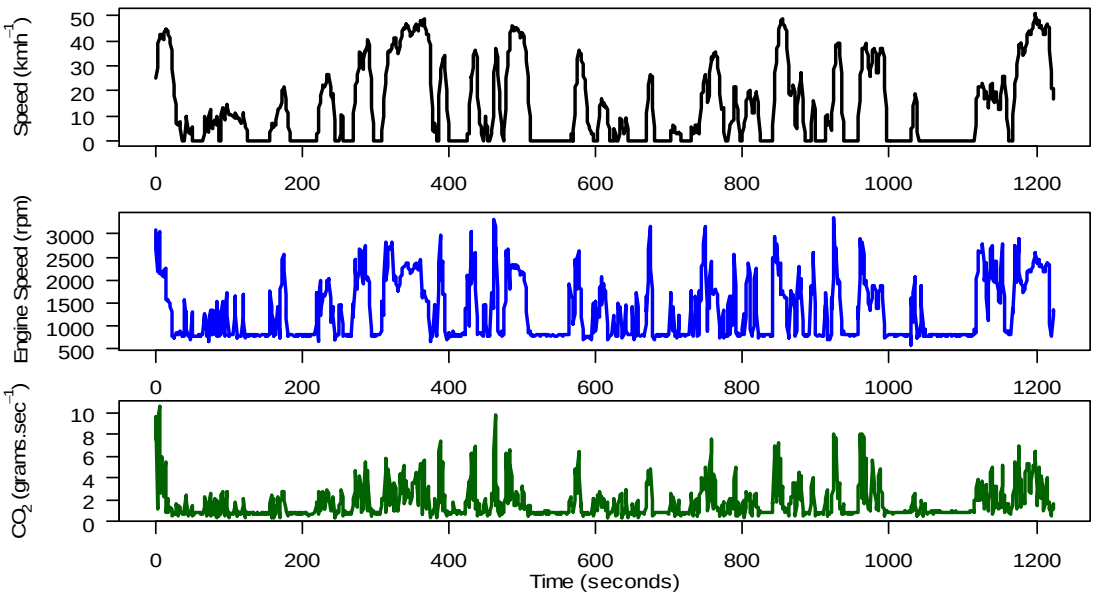

Figure 3.3: Illustrative time series plot of PEMS recorded on-road measurements for Headingley Test Lap 1.1 driven by a Euro 4 passenger car (a) speed; (b) engine speed; (c) CO_2 Emission

The median time to complete the test route over the 48 test laps was 1,170 s, however, the lap times ranged from 614 s in free flowing conditions to 1,717 s in congested traffic. The distribution of lap times in Figure 3.4 indicates that a spectrum of different traffic flow conditions was recorded. The box plots show the median emission value; the 25th (Q_1) and 75th (Q_3) percentiles (i.e. the middle 50% of the data); dots show 'outliers', which are classified as any point less than Q_1 minus 1.5 times the interquartile range (IQR = Q_3 - Q_1) or greater than Q_3 plus 1.5 times the IQR; and the whiskers detail the range of the values which are not considered outliers.

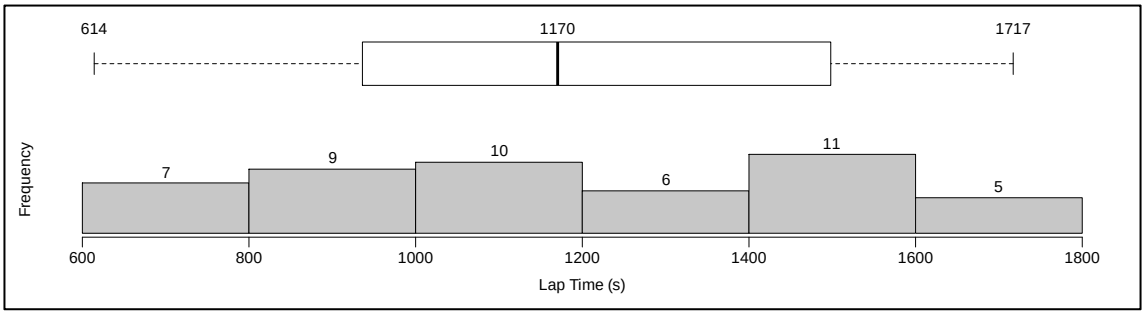

Figure 3.4: Headingley Test Lap Completion Time (seconds)

Figure 3.5 presents the lap times converted to the lap average speed for each of the test runs. The average lap speed was 14.2 km/h (8.8 mph), with a range from 9.6 km/h (6 mph) to 27 km/h (16.8 mph).

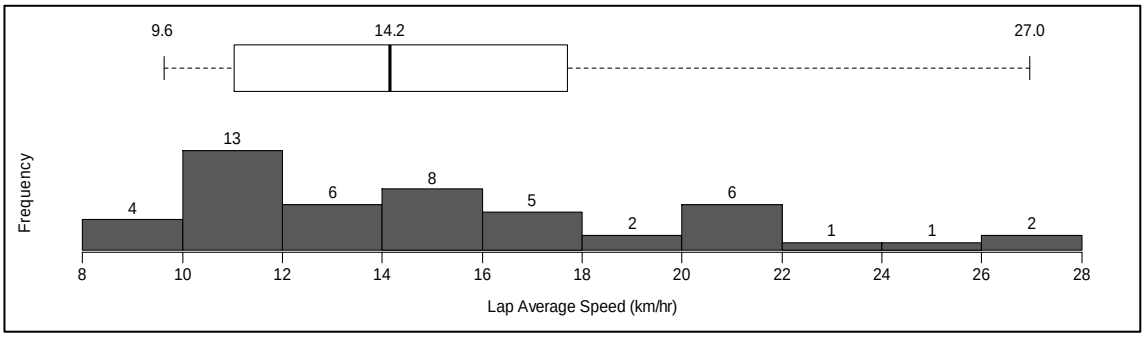

Figure 3.5: Average Lap Speed (km/h)

Plotting the distance - speed profile for the slowest lap, recorded at 08:20 during peak morning traffic against the fastest lap, recorded at 20:36 in free flowing traffic conditions, highlights the variation in vehicle performance which can occur over the same lap.

The speed profile for the congested lap, marked in red on Figure 3.6, displays recurrent periods of very low speed, during which the vehicle frequently stopped and started. Even outside these

periods, congestion hindered the vehicle from achieving the 48 km/h speed limit for the road. The distance - speed profile for the fastest lap, marked in blue, shows that whilst there were points at which the vehicle was stationary (at traffic lights, pedestrian crossings, junctions, etc.), there were noticeably fewer stationary points than during the slowest lap, and, upon restarting, the vehicle was able to accelerate rapidly up to the speed limit of the road.

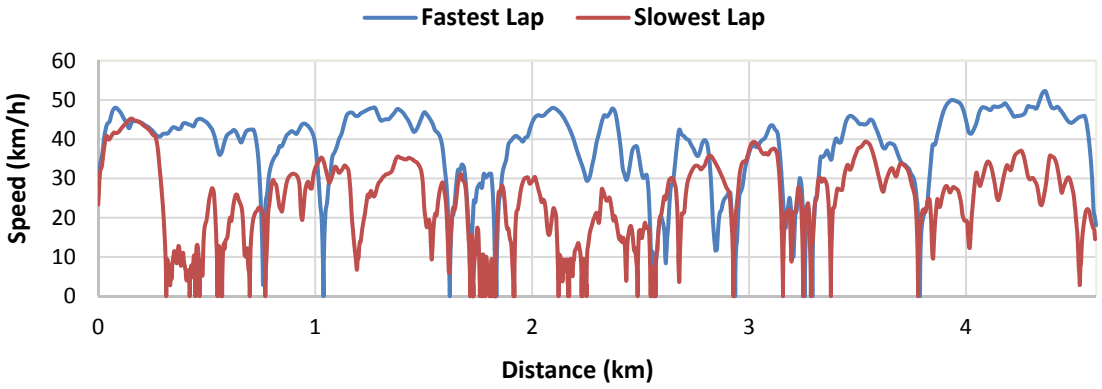

Figure 3.6: Vehicle Speed Profiles for the Fastest and Slowest Recorded Headingley Laps

The specific traffic conditions experienced during each of the real-world test runs influenced both the driver input (and as a result engine load) and the total time to complete the lap. The run-to-run differences in traffic conditions resulted in substantial variation between the recorded PEMS total CO_2 emission over the 48 test lap runs (see Figure 3.7). The maximum CO_2 emission measured by the PEMS over a test lap was 2,692 g which was almost double the minimum recorded emission of 1,440 g. The median value recorded for total CO_2 emission over the lap was 2011 g, with 83% of the recorded lap values between 1,606 g and 2,376 g.

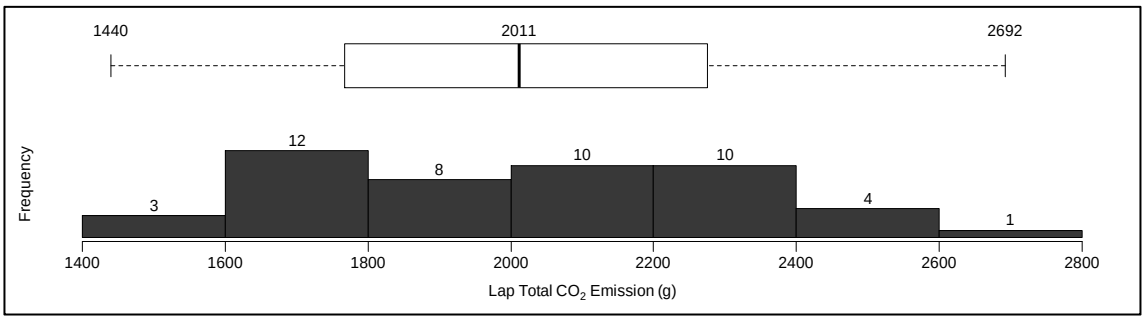

Figure 3.7: Total Lap CO_2 Emission (g)

Figure 3.8 shows the total CO_2 emission converted into gCO_2/km over the lap. The range, 313 gCO_2/km to 586 gCO_2/km, corresponds to a fuel economy of between 20.8 mpg (13.58 L/100km) and 11.1 mpg (25.45 L/100km) over the Headingley lap, when using the DECC $kgCO_2$ per litre petrol conversion factor of 2.305 (DECC, 2012). The median emission over the 48 laps was 438

gCO_2/km, which is more than twice the rated CO_2 emission for the vehicle of 182 gCO_2/km (Ford, 2005).

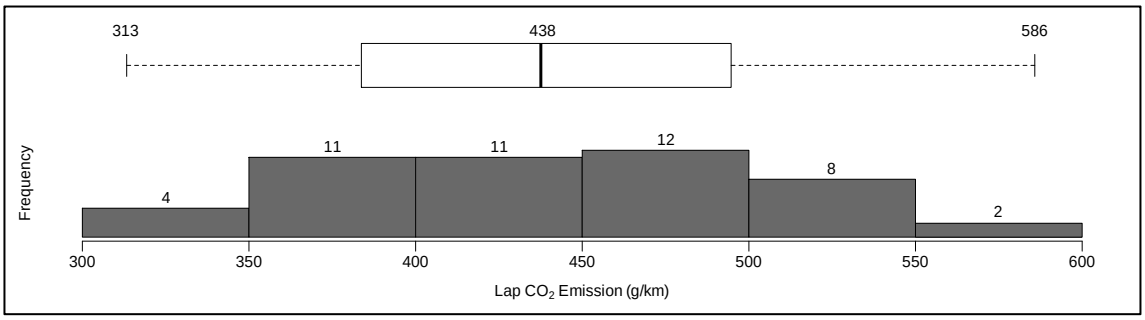

Figure 3.8: Lap CO_2 Emission (g/km)

The fuel consumption for the median lap of 14.9 mpg (18.96 L/100km) is considerably poorer than the reported consumption for this vehicle as measured under the testing procedure required by EEC Directive 1999/100/EC, under which a combined urban and extra-urban fuel consumption of 37.2 mpg (7.59 L/100km or 175 gCO_2/km) has been recorded (Ford, 2005). As the test lap was conducted entirely on urban roads (defined as *"major or minor roads within an urban area with a population of 10,000 or more" (DfT, 2015e)*) the results are best compared against the fuel consumption measured over solely the urban portion of the test cycle, which for this test vehicle is 25.7 mpg (10.99 L/100km) or approximately 253 gCO_2/km (Ford, 2005).

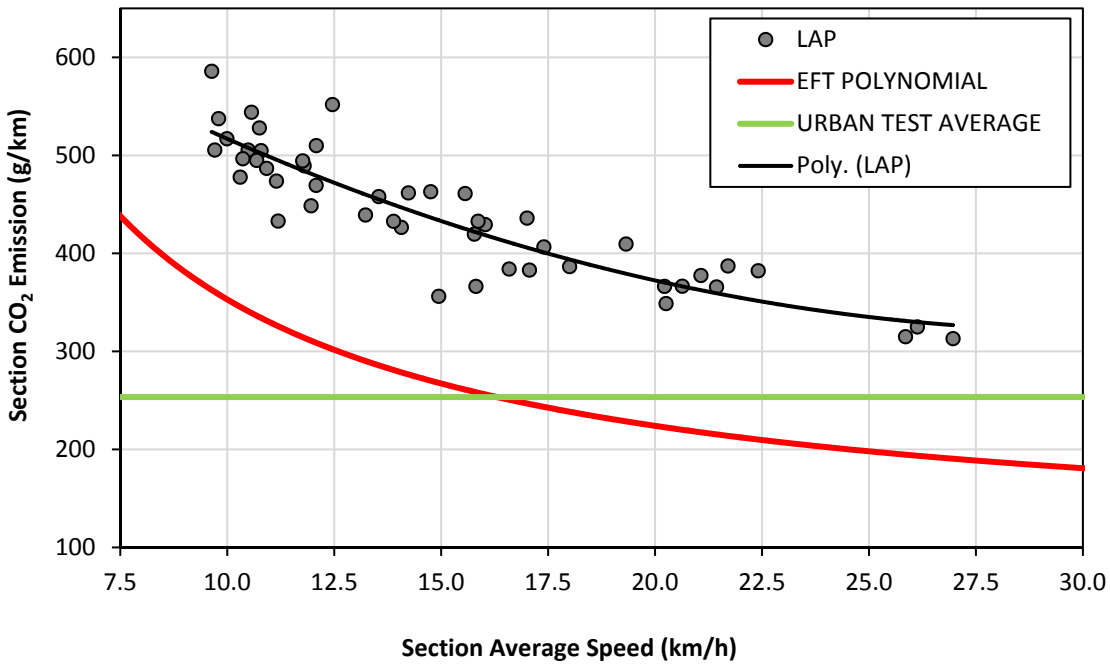

Figure 3.9: PEMS Measured Lap CO_2 Emission versus Lap Average Speed (n=48)

Figure 3.9 is a plot of the measured gCO_2/km for each lap against the average speed for that lap and the green line marks the certified ECE15 urban fuel consumption for the test vehicle. Each PEMS measured lap CO_2/km emission value is clearly greater than the certified urban emission. Use of the Mean Absolute Percentage Error (MAPE) statistic (Equation 3.3) to assess the accuracy of the ECE15 urban test cycle in prediction of the observed CO_2 g/km emission value for this test vehicle, gives an average percentage error between the observed PEMS value and the urban test cycle certified emission of 41.38%. On average, the emission from the test vehicle was 74.60% greater than predicted by the urban test cycle. Clearly, the EU urban test cycle certification provides a poor indicator for the average CO_2 g/km emission for this test vehicle over the real-world Headingley lap.

Equation 3.3:

$$\text{Mean Average Percentage Error} = \frac{1}{N} \sum_{i=1}^{N} \frac{|x_i - y_i|}{y_i}$$

Where,

- x is the simulated measurement
- y is the observed measurement
- $i = 1, 2, \ldots, N$ is the number of measurements

The red line in Figure 3.9 plots the fourth order polynomial equation which describes the average speed emission function for the test vehicle type (Car <2.5 t, Petrol, 1,400-2,000 cc, Euro 4) (GOV.UK, 2009) used in DEFRA's Emissions Factors Toolkit (DEFRA, 2009). A MAPE value of 36.80% suggests that although the polynomial is a better estimate of the test vehicle's CO_2 emission than the certified EU urban-cycle value, it still yielded a significant underestimate of the real-world emission of the test vehicle. Whilst there may be some difference between the test vehicle used in this study and an 'average' Euro 4 petrol vehicle, represented by the polynomial, an increase in emissions of approximately 60% is unlikely to be purely attributable to this difference.

The black line in Figure 3.9 describes a second order polynomial trend line through the data ($y = 0.4661x^2 - 28.436x + 754.69$). The speed emission points in the figure show a degree of scatter from the trend line calculated from the 48 data points (MAPE = 5.02%), indicating that CO_2 emission assessment through an average speed function may not provide a reasonable estimate of real-world CO_2 emission in all cases, even when the emission factor equation is specifically tailored to the data.

3.4 ANALYSIS OF PEMS MEASUREMENTS: HEADINGLEY SECTIONS

In order to facilitate analysis at a micro-scale level the Headingley lap was divided into 8 test sections as described in Figure 3.10.

Figure 3.10: Headingley Test Sections
(*Source: GPSVisualizer.com*)

These sections were determined by classifying points of latitude and longitude to mark the beginning and end of each section and finding the closest measured GPS points from each run to those selected start and end points. Variation in the measured section length (for the same section) occurs primarily due to differences between the position of the measured GPS start and end points relative to the classifying latitude-longitude point. For example, if the vehicle was travelling at 11 ms^{-1} (39.6 km/h) and travelled through the classifying mark in the middle of a recorded second, then the distance of the measured GPS latitude-longitude point from the classifying mark would be approximately 5.5 m. Each measured section start and end point will have a slight distance discrepancy relative to the classifying mark (unless a 1 Hz measurement occurred exactly at the classifying mark), which is a function of the vehicle position at the recorded 1 Hz time increment. This causes some variance in the overall section length measurements. The section length also depends on the path travelled by the vehicle with lane position and lane switching both having an impact on distance travelled within the section. The overall maximum variability in section length was found to be between approximately ±10 m of the median section length.

By sub-dividing each lap into 8 sections, the 48 test laps give a total of 384 section emission measurements. Sections 1 and 8 cover the same segment of road but with opposite directions of traffic flow (i.e. Section 1 is the road lane into Headingley and Section 8 is the road lane out of Headingley). Likewise, Sections 2 and 4, and Sections 5 and 7 describe opposing traffic flow directions over the same segment of road. Section 3 and Section 6 are separate short turning sections.

3.4.1 Section 1 and Section 8: PEMS Data Analysis

Section 1 and 8 are on the A660. Section 1 starts on Headingley Lane (A660) at the junction with North Grange Road and culminates at the signalised junction at the intersection of Otley Road (A660) and North Lane (B6157), in the centre of Headingley. Section 8 describes the opposite traffic flow over the same road section, heading out of Headingley towards Leeds.

The median length of Sections 1 and 8 over the 48 test runs were 781 m and 777 m respectively. Figure 3.12 presents Google Street View images at various points on the route represented in Figure 3.11 by letters (A, B and C) and the orientation of each image is indicated by the arrows attached to each letter.

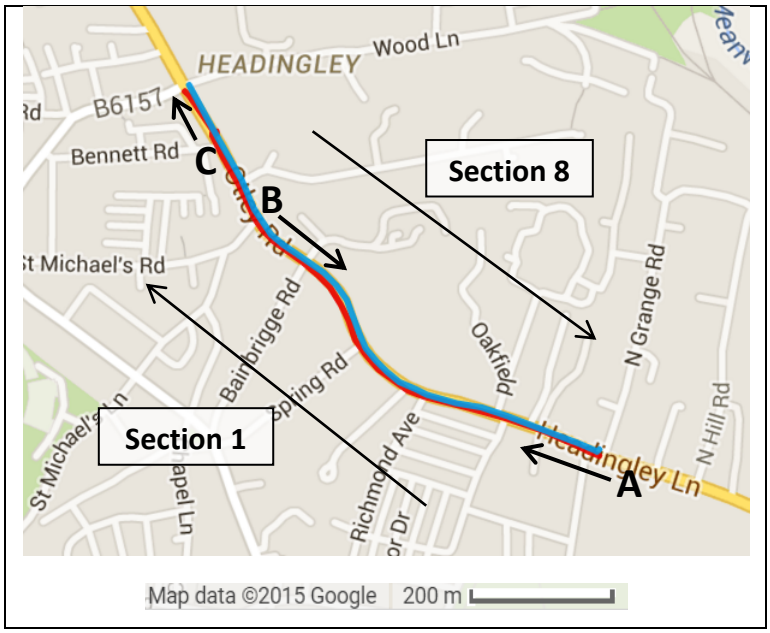

Figure 3.11: Headingley Section 1 and Section 8
***(Source: GPSVisualizer.com and* ©Copyright GoogleTM 2015)**

Starting from the beginning of Section 1 (point A) there is a short uphill section after which the road reaches its maximum elevation and then descends into Headingley with the road curving

slightly to the right. As the road flattens out, the road name on the A660 changes from Headingley Lane to Otley Road and there is a push button operated pedestrian pelican crossing (point B). The road then rises slightly over the next 100 m before descending through the main high street in Headingley, with shops and pubs on either side of the road, toward the signalled junction with North lane that ends the section.

A) Starting point of Section 1. Headingley Lane Junction with North Grange Road (end point for Section 8)

B) Pedestrian Crossing on Otley Road at the Junction with St. Michael's Road

C) End of Section 1. Junction of Otley Road and North Lane (starting point for Section 8)

Figure 3.12: Images for Section 1 and Section 8
(©Copyright GoogleTM 2015)

Figure 3.13 highlights the congestion experienced in Section 1, as the average travel time through Section 1 (276.5 s) was almost three times as long as for Section 8 (94.5 s). The longest recorded time taken to complete Section 1 of 756 s was more than ten times the length of the quickest time through the section. The signalised junction at the end of Section 1 in conjunction with the pedestrian crossing beforehand and two right turns onto residential streets, can cause significant delay at peak travel times. At times of greatest congestion the queue from the A660 / North Lane junction can stretch back to the start point of Section 1. In Section 8 the only traffic management measure which obstructs traffic flow is the pedestrian crossing. The pedestrian crossing is in frequent use, especially during the morning (07:30 - 09:30) and afternoon (16:00 - 18:00) rush hours, but otherwise Section 8 remains relatively free flowing throughout the day as the nearest large traffic light controlled junction is a further 500 m past the end of the section so that, even during peak traffic, the queue from these lights does not reach the section.

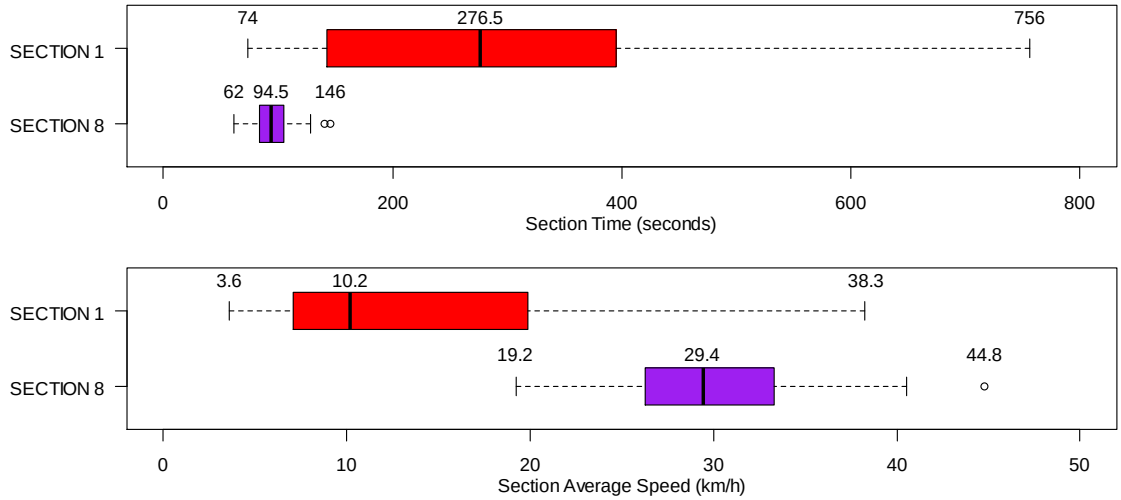

Figure 3.13: Section 1 and Section 8: Section Time (s) and Average Speed (km/h)

The average section speed highlights the wide range of traffic flow conditions experienced over Section 1; the slowest average section speed of 3.6 km/h was recorded at 17:35 at the peak of the afternoon rush hour with traffic leaving Leeds and passing through Headingley. The fastest average speed through Section 1 was 38.3 km/h, which was measured at 20:36 in the evening in free flowing traffic conditions. The Section 8 average speeds were consistently high, indicating relatively free flowing conditions at all times throughout the day.

The CO_2 emission data for Section 1 are presented as a box plot in Figure 3.14. These data show the wide range of CO_2 emission values for the same vehicle, over the same section, which results from different traffic flow conditions. The highest measured emission over Section 1 was 1,082 gCO_2/km, recorded on the test run with the slowest average speed. During that test run the section was completed in 756 s, during which the vehicle was stationary for 406 s (54% of the total time). Whilst idle CO_2 emission is relatively low, 321 gCO_2 of the total measured 822 gCO_2 (39% of total CO_2 emission) was emitted whilst the vehicle was not moving. Stationary emissions can have a large impact on the calculated value of gCO_2/km as the total CO_2 emission increases even though no distance is covered. Congestion during peak hours (where the traffic demand is greater than the capacity of the road) results in queuing which hinders traffic flow. This congestion increases total CO_2 emission (and therefore CO_2/km) from the vehicle, but as the rate of idle exhaust emission is relatively low compared with the rate of exhaust emission whilst the vehicle is in motion, it reduces the average gCO_2/s rate of emission over a section. The lowest measured CO_2 emission over Section 1 was 226 gCO_2/km, for the test with the highest average speed (38.3 km/h) during which the vehicle did not have to stop. On average the vehicle was stationary 40% of the measurement time in Section 1, by comparison for Section 8 the average was just 4%. In contrast, for the Section 8 test run with the highest measured emission (395

gCO_2/km), the vehicle was stationary for 13% of the measurement time and only 5% of the total CO_2 emitted in the section was produced whilst the vehicle was stationary. The total stationary time in Section 1 ranged from 0 s to 406 s, with only 2 of the 48 test runs being non-stop. In Section 8, the total stationary time range was 0 s to 22 s, with 18 of the 48 test being non-stop. As the run times in Section 8 were quicker and much more consistent than in Section 1, with a relatively high average vehicle speed, the Section 8 measured CO_2 emission were in general much lower than in Section 1 and overall much less variable. The median emission in Section 1 was 510 gCO_2/km compared with 326 gCO_2/km in Section 8.

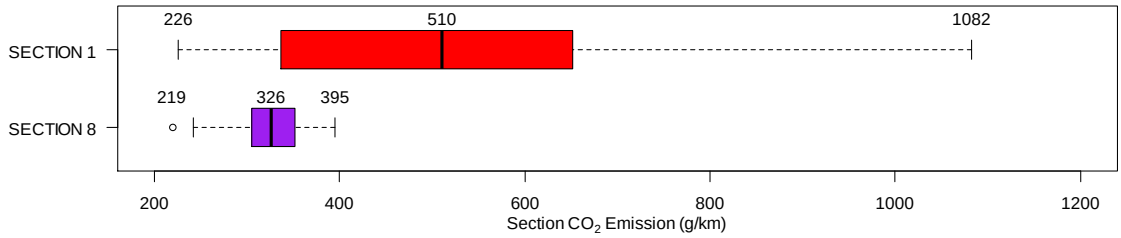

Figure 3.14: Section 1 and Section 8: CO_2 Emission (g/km)

3.4.2 Section 2 and Section 4: PEMS Data Analysis

Section 2 and Section 4 are also located on the A660. Section 2 starts at the junction between North Grange Road and the Otley Road, at a point past the traffic lights which mark the end of Section 1. This is shown as point C in Figure 3.15.

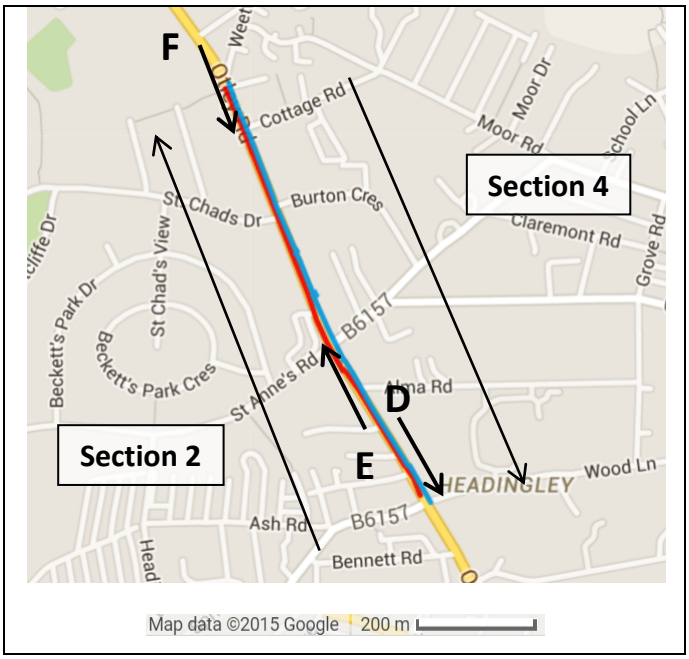

Figure 3.15. Headingley Section 2 and Section 4
***(Source: GPSVisualizer.com and* ©Copyright GoogleTM 2015)**

The end of the section is on the Otley Road opposite the junction of Weetwood Lane. Section 4 is the opposite traffic flow over the same road segment, travelling from the direction of the ring road (A6120) into Headingley. The median measured lengths of Section 2 and Section 4, over 48 test runs, were 739 m and 744 m respectively.

Figure 3.16 presents Google Street View images captured along the road segment. The position of the images is shown in Figure 3.15 as points D, E and F, with adjacent arrows indicating the orientation of the photograph.

D) Pedestrian crossing Otley Road and view to North Lane Junction (start point of Section 2, end point for Section 4)

E) Signalled junction of Otley Road and Shaw Lane.

F) End of Section 2. Junction of Otley Road and Weetwood Lane (starting point for Section 4)

Figure 3.16. Images for Section 2 and Section 4 ***(©Copyright GoogleTM 2015)***

Beginning at the start of Section 2, Otley Road descends for the first 300 m of the section. This part of the A660 passes the Headingley Arndale Centre, a large shopping complex, shown on the left of image D in Figure 3.16. There is a busy pedestrian pelican crossing 100 m from the start of Section 1, shown in image D, which allows people to cross from the main bus stop in central Headingley to the Arndale Centre. After 300 m the road briefly flattens out at the traffic light controlled junction of Otley Road and Shaw Lane. This junction has a separate right-hand turn as shown in image E. After the junction the road remains relatively flat for 150 m before ascending for the final 300 m to the end of the section.

In Section 2, the traffic flow is only likely to be hindered at the traffic light controlled junction with Shaw Lane and at the pedestrian crossing near the Arndale Centre. Figure 3.17 shows that Section 2 had a fairly consistent section time in all traffic conditions, with 47 of the 48 section

times between 65 s and 155 s, suggesting that, although traffic conditions could slow the section time, it was not a section that frequently experienced major delays in peak traffic. The outlier at 249 s was recorded at 18:02 late in the afternoon rush hour. The average speed through Section 2 was consistently high, with 47 of the 48 section measurements between 17.3 and 40.9 km/h (10.7 km/h average speed for the outlier).

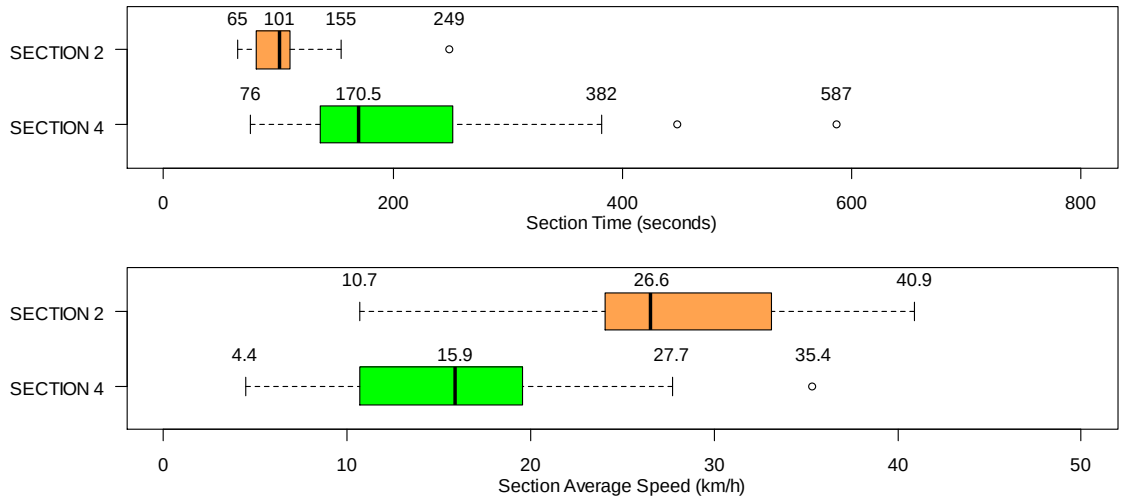

Figure 3.17: Section 2 and Section 4: Section Time (s) and Average Speed (km/h)

Section 4, as a result of the two signalled junctions, had a higher average and a wider spread of section times than Section 2. The combined waiting time for the lights at both the A660/Shaw Lane junction and the A660/North Lane junction led to a longer average section time in comparison with Section 2, which only experienced delay from the Shaw Lane junction. During peak traffic the queuing time at both junctions increases and vehicles are less likely to be able to pass through in a single cycle; this effect widened the variance of the Section 4 times. The average time to complete Section 4 was 170 s which translates to an average section speed of 15.9 km/h. This is much slower than the Section 2 average speed of 26.6 km/h. The fastest section time through Section 4 was 76 s which was recorded at 20:23 in free flowing traffic conditions. The slowest time of 587 s was recorded at 8:19 during the peak morning rush hour, as traffic heads into Leeds.

Figure 3.18 presents the measured gCO_2/km emission for the test vehicle over both sections, showing the range of CO_2 emission in all traffic conditions. Section 2, as with Section 8 had a relatively narrow range of CO_2 emission across each of the 48 laps, from 222 gCO_2/km to 468 gCO_2/km. For the test run that recorded the lowest value, the vehicle was stationary for only 3% of the time; for the highest recorded value, the vehicle was stationary for 26% of the time. On average for Section 2, the vehicle was stationary for 11% of the time over the 48 test runs.

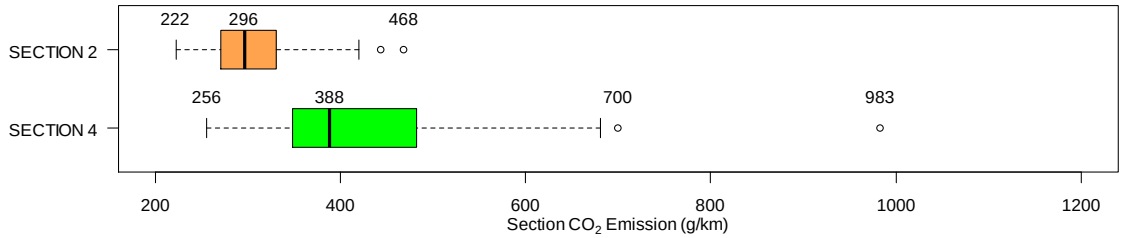

Figure 3.18: Section 2 and Section 4: CO_2 Emission (g/km)

The vehicle's transit through Section 4 was hindered to a much greater degree by congestion during peak traffic and the wide range of completed run times is reflected in a large spread of gCO_2/km measurements. The fastest recorded Section 4 test run (76 s) had the lowest measured CO_2 emission of 256 gCO_2/km, during which the vehicle was stationary only for 1 s. The highest rate of CO_2 emission (983 gCO_2/km) was measured for the slowest test run through the section when the vehicle was stationary for 375 s of the run time of 587 s; 64% of the time in the section. On average the vehicle was stationary for 38% of the time for the 48 test runs in the section.

The total stationary time in Section 2 ranged from 0 s to 66 s, with the vehicle not having to stop in 13 of the 48 test runs. In Section 4 the total stationary time ranged from 1 to 375 s, with none of the test runs being non-stop.

3.4.3 Section 5 and Section 7: PEMS Data Analysis

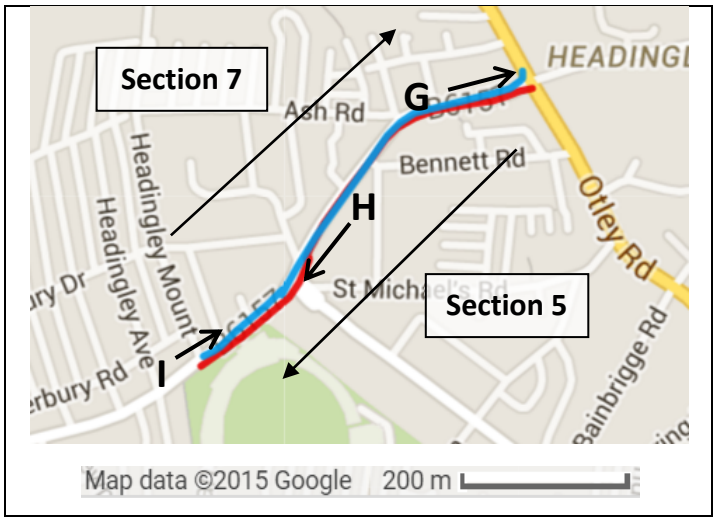

Figure 3.19: Headingley Section 5 and Section 7
***(Source: GPSVisualizer.com and* ©Copyright GoogleTM 2015)**

As shown in Figure 3.19 above, Sections 5 and Section 7 are on the B6157. Section 5 starts on North Lane (B6157) at the junction with Otley Road (A660) and finishes on Kirkstall Lane (B6157) opposite the entry of Headingley Mount. Section 7 describes the opposite traffic flow over the

same road section, heading into Headingley from Kirkstall. The average length of both Sections 5 and 7 over the 48 test runs was 523 m.

The letters in Figure 3.20 (G, H, and I) correspond to those in Figure 3.19. The arrows describe the orientation of the images. The start of Section 5 (image G) is at the signalled junction of North Lane and Otley Road and begins with a 120 m long uphill section. The road reaches its maximum elevation and then starts to descend. There is a pelican crossing 200 m into the section, operated by a pedestrian push button system, after which the road continues to descend to the signalled junction of three roads, North Lane, Kirkstall Lane and Cardigan Road (image H).

G) Start point of Section 5 (end point for Section 7). Junction of North Lane and the A660

H) Signalled junction of North Lane, Kirkstall Lane (straight on) and Cardigan Road (left turn).

I) End of Section 5 (starting point for Section 7). Junction of Kirkstall Lane and Headingley Mount (before the crossing)

Figure 3.20: Images for Section 5 and Section 7 ***(©Copyright GoogleTM 2015)***

The section continues heading straight over the traffic lights, following the B6157, which becomes Kirkstall Lane. The final 130 m of the section descend more gradually. There is a second pelican pedestrian crossing 10 m before the end of the section. The section ends on Kirkstall Lane opposite the junction with Headingley Mount (Figure 3.20, Image I).

The box plot of total section time through Section 5, shown in Figure 3.21, indicates that in a majority of the runs the vehicle experienced only small delay and the section was completed relatively quickly. In 41 of the 48 test runs the section was completed in between 51 s and 182 s, corresponding to an average speed range of between 36.6 km/h and 10.3 km/h. However, in

a few of the test runs very significant delay occurred, with the longest time to complete the test section being 657 s, which equates to an average speed of 2.8 km/h through the section.

As Section 7 contains two major junctions controlled by traffic lights, which have the potential to hold up the vehicle, whereas Section 5 only has one, the average time to complete Section 7 was slower than Section 5. The average time to complete Section 5 was 94 s whilst the average time through Section 7 was 167.5 s.

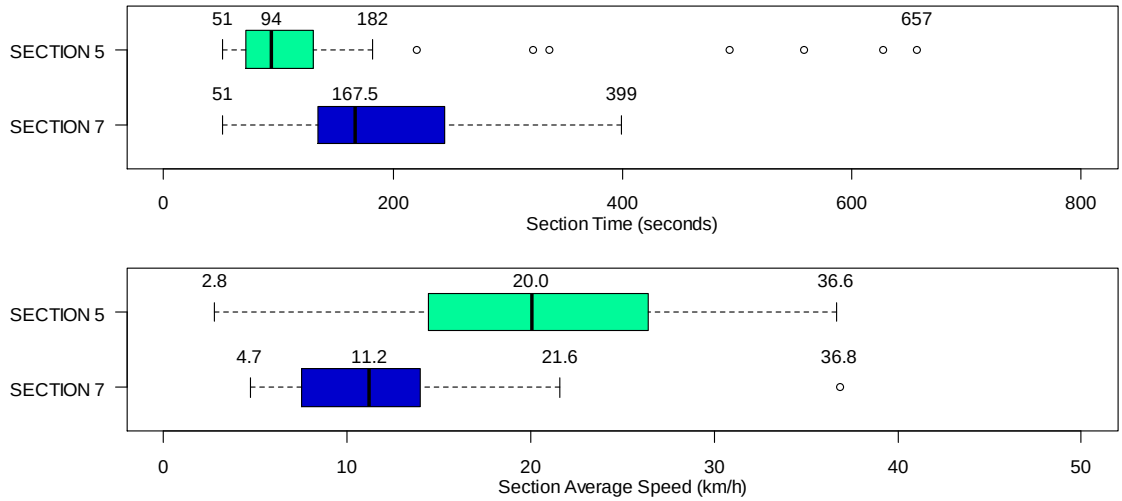

Figure 3.21: Section 5 and Section 7: Section Time (s) and Average Speed (km/h)

The gCO_2/km box plots for Sections 5 and 7 in Figure 3.22 show a wide range of gCO_2/km values which clearly relate to the section times presented in Figure 3.21. In Section 5, 41 of the 48 test runs through the section had a section emission of between 232 and 536 gCO_2/km, with the average emission 361 gCO_2/km. The stationary time over these 41 test runs had a range from 0 s to 108 s with a median value of 23 s. For the 7 test runs with the highest emissions over Section 5, the stationary time range was from 131 s to 526 s, with a median value of 399 s. In the case of the greatest emission over Section 5, which was 1,358 gCO_2/km, the vehicle was stationary for 526 s of the total 657 s it took to complete the section, which is 80% of the measurement time. The average percentage stationary time for the section was 31%. In the majority of test runs through Section 5, there was little traffic congestion to impede the transit of the vehicle, but in cases where the vehicle was hindered by traffic conditions the queuing time formed the majority of the total time over the run.

As a result of the two junctions contained in Section 7, the highest average percentage stationary time of all the sections was recorded here; on average the vehicle was stationary during 53% of the transit time, with a range from 0% to 74% over all test runs. The median CO_2 emission for

Section 7 was the highest of all the longer sections (excluding turning Sections 3 and 6) at 529 gCO_2/km. The fastest average speed recorded for a test run through Section 7 was 36.8 km/h. This run was the only trip through Section 7 which had no stationary time and the run recorded a CO_2 emission of 371 gCO_2/km. There were 9 test runs through Section 5 which had no stationary points. The average speed of these 9 runs was 32.6 km/h and the average emission 268 gCO_2/km, with a range from 232 gCO_2/km to 314 gCO_2/km. Whilst not statistically sound to compare one measured section with nine, it perhaps gives an indication of the influence that road grade has on the emissions of the vehicle. Comparing only free moving traffic sections, on the predominantly uphill Section 7, CO_2 measurement is greater than for each of the 9 predominantly downhill Section 5 measurements.

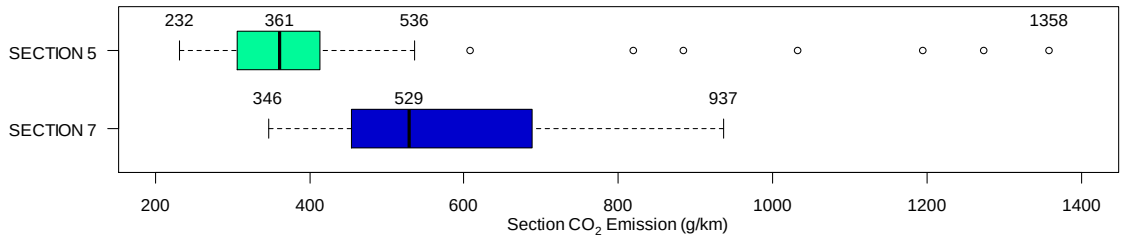

Figure 3.22: Section 5 and Section 7: CO_2 Emission (g/km)

3.4.4 Section 3 and Section 6: PEMS Data Analysis

Between Sections 2 and 4 and Sections 5 and 7 there are two short 'turning' sections which form loops back to the end point of the proceeding section. These sections can be seen in Figure 3.23 and Figure 3.25.

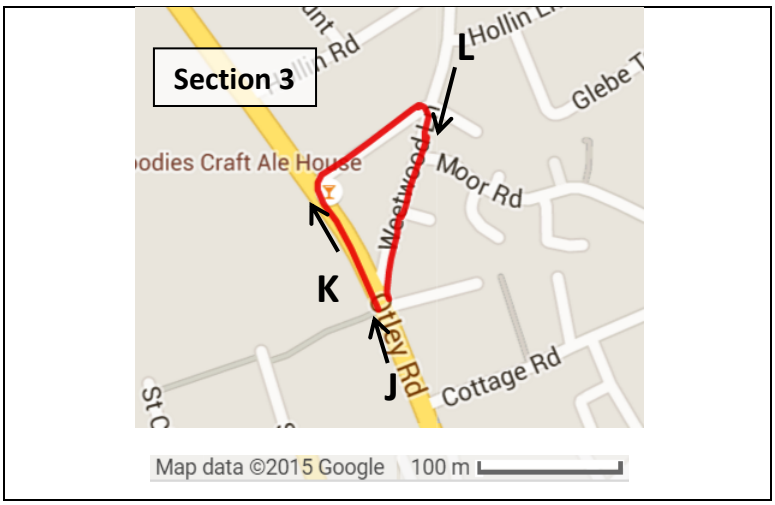

Figure 3.23: Headingley Section 3
***(Source: GPSVisualizer.com and* ©Copyright GoogleTM 2015)**

The Section 3 turning loop starts on the A660 Otley Road, at the end of Section 2, opposite the junction of Weetwood Lane. This is shown in image J in Figure 3.24. The section continues on Otley Road and after 30 m there is a pelican pedestrian crossing. A further 60 m down Otley Road, the section takes a right-hand turn, crossing the oncoming traffic to join St Chad's Lane (image K in Figure 3.24). The route continues 80 m to the end of St Chad's Lane and turns right at the give way junction at the end of the road to join Weetwood Lane (image L Figure 3.24). The section follows Weetwood Lane for 130 m to a give way junction where it re-joins Otley Road and the section ends (junction on the right-hand side of image J Figure 3.24). The average length of Section 3 over the 48 test runs was 325 m.

J) Start and end points of Section 3. Section continues on Otley Road (left-hand side of image).

K) Right turn from Otley Road onto St Chad's Lane.

L) Right turn from St Chad's Lane onto Weetwood Lane and junction in picture A.

Figure 3.24: Images for Section 3 ***(©Copyright GoogleTM 2015)***

Similar to Section 3, Section 6 is a short turning loop. The average length of Section 6 over all 48 test runs was 175 m.

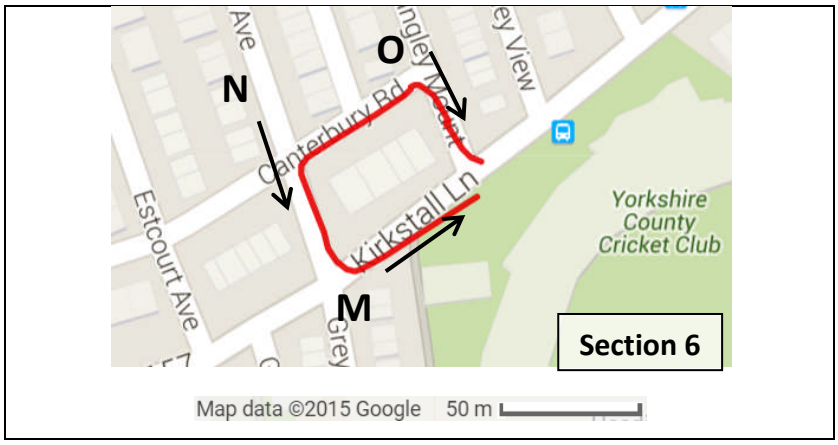

Figure 3.25: Headingley Section 6
(Source: GPSVisualizer.com and **©Copyright GoogleTM 2015)**

The Section 6 loop starts at the end of Section 5 on Kirkstall Lane (B6157) opposite the entry of Headingley Mount (image I in Figure 3.20). The route travels along Kirkstall Lane for 50 m before making a right-hand turn over the opposite lane into Headingley Avenue (image M in Figure). It continues 35 m along Headingley Avenue before making a right-hand turn into Canterbury Road (image N in Figure 3.26) and after 50 m turns right at the give way junction onto Headingley Mount (image O in Figure 3.26). The section follows Headingley Mount for 35 m before turning left at a give way junction to re-join Kirkstall Lane, where the section ends.

M) In the distance is the start point of Section 6 on Kirkstall lane (by the lights seen in image I). On the left is the right-hand turn onto Headingley Avenue.

N) Headingley Avenue right-hand turn into Canterbury Road (on left-hand side of image)

O) From Canterbury Road, right-hand turn onto Headingley Mount. The route returns to the Kirkstall Road (turning left) at the end of Section 6.

Figure 3.26: Images for Section 6 ***(©Copyright GoogleTM 2015)***

Both Section 3 and Section 6 are short turning loops completed predominantly on smaller side roads that have relatively low traffic volumes. Figure 3.27 presents box plots of the section time and average speed for each of the 48 test runs. As these are short turning sections, the average speeds are low as they include multiple give way junctions at which the vehicle was required to slow and therefore the test vehicle had few opportunities to reach the speed limit of the road. The average time through Section 3 was 76.5 s, which represents an average speed of 15.6 km/h, with 43 of the 48 sections completed in 42 s to 130 s. There was one section run significantly slower than the others, taking 273 s, recorded at 8:19 during the morning rush hour; for 163 s (59% of the section time) the vehicle was stationary.

The average speed for the vehicle through Section 6 was slower than through Section 3, with a median value of 11.7 km/h, this is most likely due to Section 6 having one more turn (as the loop is rectangular, rather than triangular) and having shorter segments of road between turns. The

spread of the Section 6 run times is narrower than the spread of the times through Section 3, indicating that rush hour congestion in the area has less impact on delays in Section 6.

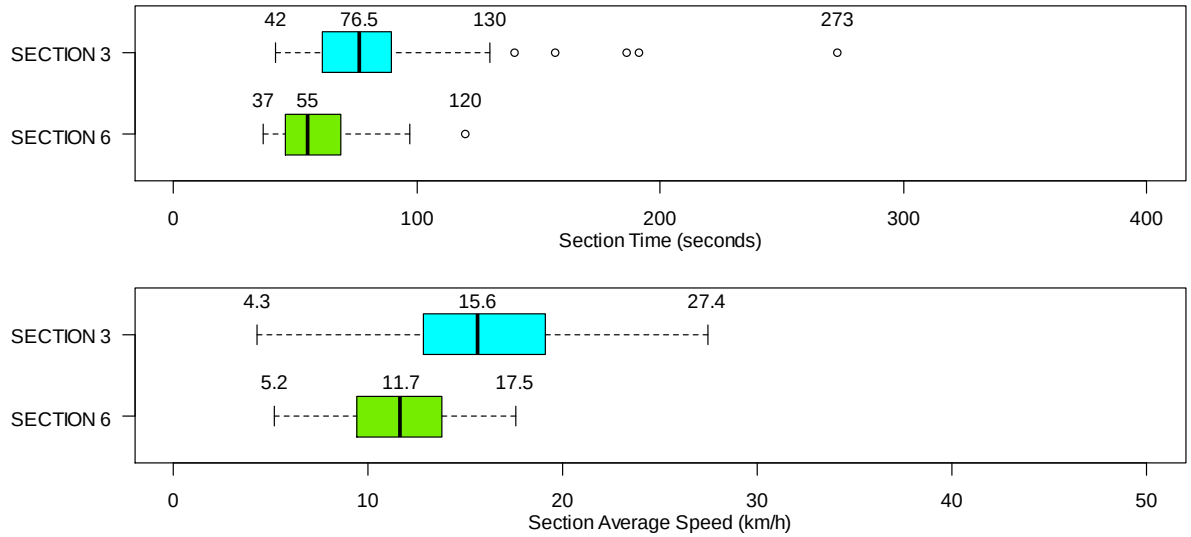

Figure 3.27: Section 3 and Section 6: Section Time (s) and Average Speed (km/h).

The CO_2 emission in these short sections, as shown in Figure 3.28 was comparatively high compared to that of many of the longer sections, with Section 6 having the highest median CO_2 emission of all the sections at 624 gCO_2/km. These high rates of emission are likely to be due to the stop-start nature of the sections, where the vehicle was frequently accelerating up to the speed of the road, braking shortly after for the next turn and then stationary whilst waiting to turn. This profile of acceleration and braking is very fuel inefficient and, combined with periods of idle emissions, during which the vehicle was stationary, resulted in very high rates of CO_2 emission.

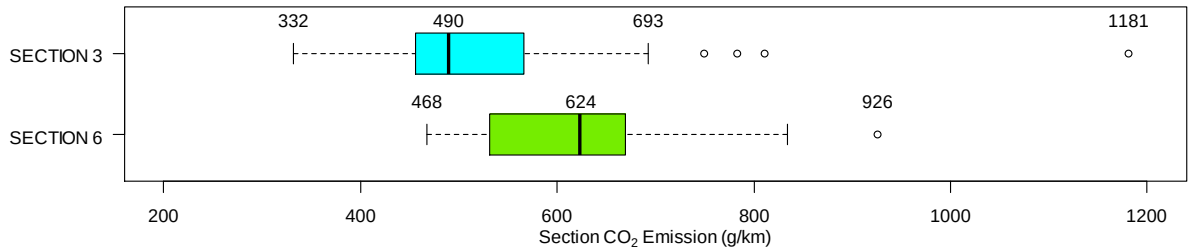

Figure 3.28: Section 3 and Section 6: CO_2 Emission (g/km)

The total stationary time in Section 3 ranged from 0 s to 163 s, with the vehicle not having to stop in only 3 of the 48 test runs. In Section 6 the total stationary time range was 0 s to 64 s, with 2 of the 48 test runs having no stationary time. The average rate of CO_2 emission in Section 3 for the 3 test runs that had no stationary time was 395 gCO_2/km and in Section 6 for the 2 test runs where the vehicle did not have to stop, the average rate was 476 gCO_2/km. Comparing

these emission rates against the rates for the other sections reveals the two turning sections to have the highest average rate of emission for test runs with no stationary time (Section 1, 228 gCO_2/km; Section 2, 262 gCO_2/km; Section 5, 268 gCO_2/km; Section 7, 371 gCO_2/km; Section 8, 299 gCO_2/km).

3.4.5 PEMS Section Emission Comparison to Test Certified Emission.

Figure 3.29 presents box plots of the gCO_2/km emission rate, the average gCO_2/s emissions, the average speed and coefficient of variance (CV) for the lap and sections from each of the 48 test runs. The CV is the ratio of the standard deviation to the mean, is a measure of the relative dispersion of vehicle speeds from the average speed and describes the consistency of the vehicle speed through a lap or section. A low CV indicates a relatively constant speed and a high CV shows a wide dispersion of vehicle speeds. The sections in Figure 3.10 are presented by location, with opposite traffic flows over the same road section grouped together. It is clear from the plots that Sections 2 and 8 had the lowest recorded rate of CO_2/km emission and also the narrowest spread of emission values. As discussed in the sections analysis (and shown in the summary Table 3.1), these were the sections with consistently high average speeds, relatively consistent vehicle speed and the least amount of time during which the vehicle was stationary. In these sections even during peak traffic periods, traffic flow was not greatly hindered by increased traffic density in the network.

Conversely, the data for Sections 1 and 7 present a wide spread of CO_2 emission values. During free flowing conditions, these sections could be completed relatively quickly, at relatively low gCO_2/km emission rates. However, during rush hour periods, the queuing times over these sections increased, raising the vehicles gCO_2/km emission rate substantially because the stationary vehicle's idle CO_2 emission adds to the total CO_2 emission. The average g/s rate of CO_2 emission seems to broadly follow the pattern of the plots for average speed. Sections with a low average speed tended to have the lowest average gCO_2/s emission rates, as the gCO_2/s exhaust emissions when a vehicle was moving are significantly greater than the stationary idle exhaust rate. Sections with considerable stationary idle time (e.g. as a result of congestion) therefore have very low average emission rate. The pattern between congestion and g/s CO_2 emission is not clear, however, as low gCO_2/s emission values could also reflect quick journeys through road sections where the vehicles speed was relatively constant, with little acceleration and declaration required. A low average gCO_2/s emission rate can reflect both congested journeys and journeys in free-flow conditions. As a result, g/s emission can be difficult to interpret and is a poor indicator of the variability of traffic conditions in a network.

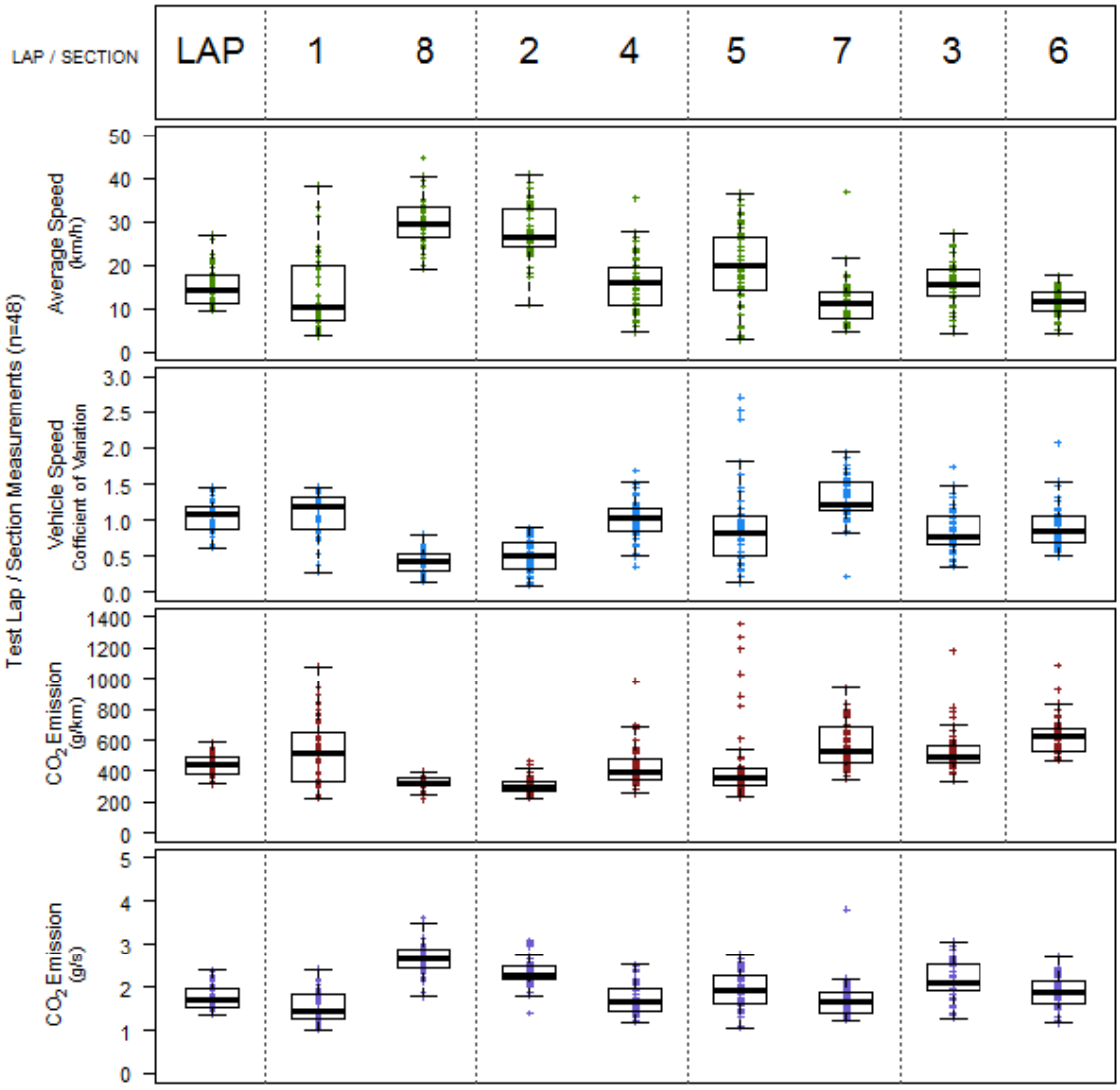

Figure 3.29: Box Plots of the Test Lap and Sections gCO_2/km, gCO_2/s, Average Speed and Vehicle Speed Coefficient of Variation Measurements, over the 48 Test Runs

Table 3.1: Summary Table for the PEMS Measured Headingley Data

Section			Vehicle Speed		Percentage of the Run Time during which Vehicle was Stationary		CO_2 Emission		Percentage of the Total CO_2 Emission whilst Stationary	
Number	Test Runs (#)	Length (m)	Ave. km/h	Range (km/h)	Ave. (%)	Range (%)	Ave. g/km	Range (g/km)	Ave. (%)	Range (%)
1	48	781	10.2	3.6 – 38. 3	40.4	0 – 54	510	226 - 1082	23.4	0 – 40
2	48	739	26.5	10.7 - 40.9	11.2	0 – 37	296	222 - 468	4.8	0 – 16
3	48	325	15.6	4.3 – 27.4	23.8	0 – 59	490	332 - 1181	10.7	0 – 40
4	48	744	15.9	4.5 – 35.4	41.0	1 – 64	388	256 – 983	21.7	1 – 49
5	48	523	20.0	2.8 – 36.6	28.4	0 – 81	361	232 -1359	12.8	0 – 65
6	48	175	11.6	4.3 – 17.5	26.2	0 – 72	624	468 - 926	13.6	0 – 49
7	48	523	11.2	4.7 – 36.8	52.7	0 – 74	529	346 – 937	27.2	0- 52
8	48	777	29.4	19.2 – 44.8	3.6	0 – 19	326	219 – 395	1.6	0 – 6
LAP	48	4592	14.1	9.6 – 27.0	38.1	17 - 56	438	313 - 586	20.1	7 - 34

Figure 3.30 is similar to Figure 3.9 but instead of average lap emission, the measured gCO_2/km for each of the 384 sections is plotted against the average speed for that section. As discussed earlier in the chapter, the reported ECE15 urban test cycle fuel consumption for the test vehicle is 25.7 mpg (10.99 L/100km) (Ford, 2005), with a corresponding average CO_2 emission rate of 253 gCO_2/km. Over the 384 test section runs recorded in this study only 16 runs (4.2%) were at less than or equal to that emission rate. As 12 of the 384 average speed values were below 5 km/h, they are not within the valid range of speeds for EFT calculation. Calculating the MAPE for the valid 372 measurements reveals that the average absolute percentage error between the observed PEMS value and the certified urban test cycle gCO_2/km was 66.09%, with the recorded PEMS emission on average 77.93% greater than the certified urban emission.

The red line in Figure 3.9 represents the EFT average speed emission function for the vehicle type (Car <2.5 t, Petrol, 1,400-2,000 cc, Euro 4). Although the section emission estimates roughly follow the curve of the EFT function for this vehicle, the function underestimates the emission generated in every section, with a MAPE of 38.52% between the EFT function and the real-world values. It is also clear from the graph that at each speed the real-world measurements show a wide spread of possible emission rates. Calculating a best fit trendline through the 372 valid sections (a fourth order polynomial equation) and evaluating the best fit values against the PEMS measured values gives a MAPE of 10.55%. This suggests that CO_2 emission assessment through an average speed function may not provide a reasonable estimate for real-world CO_2 emission as each average speed could cover a broad spread of emission values. This is especially clear in Figure 3.30 at average speeds between 5 km/h and 25 km/h.

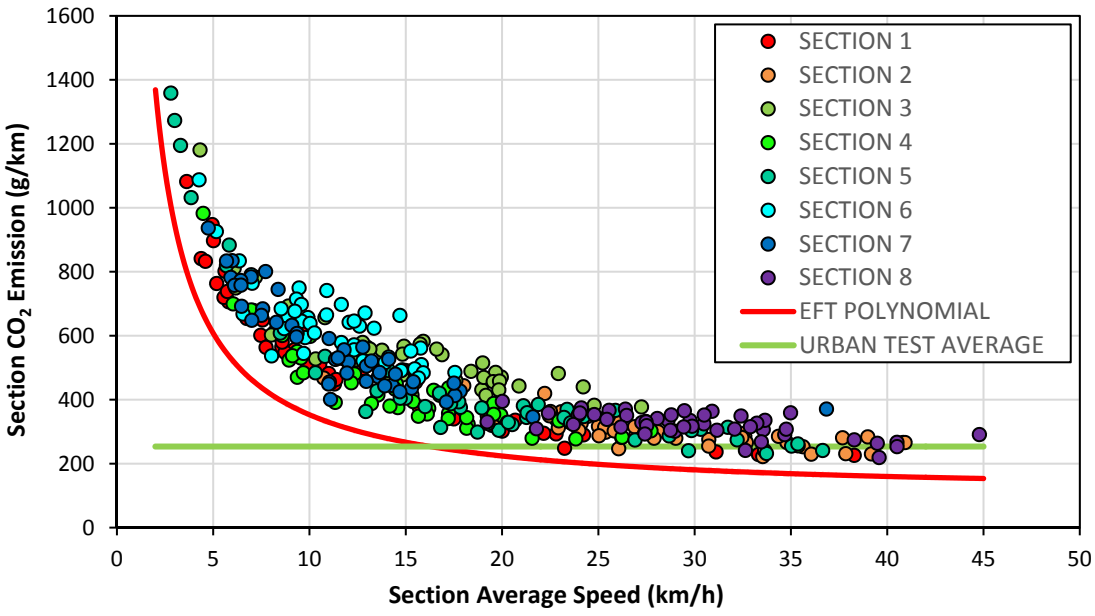

Figure 3.30: Section CO_2 Emission versus Section Average Speed for All Section (n=384)

The results from this PEMS research are in agreement with other studies that have found significant discrepancy between test cycle and real-world CO_2 emission (ICCT, 2015; Weiss et al., 2011b; Chen and Borken-Kleefeld, 2014; Mock et al., 2015). The disparity is especially clear at lower average speeds, i.e. in congested traffic. The stop-start conditions, with long stationary idle periods, which were encountered in the Headingley study are extremely inefficient for fuel consumption and therefore result in high CO_2 emission factors. The NEDC ECE15 urban test cycle is evidently unrepresentative of the urban conditions encountered in the Headingley network.

The disparity between the EFT average speed emission function and the PEMS measurements can be partly accounted for by the fact that the EFT function is an aggregate for all Euro 4, Petrol Cars under 2.5 tonnes, with a capacity between 1.4 and 2 L and as the test vehicle had a 1.8 L engine, the resultant emission is likely to be higher than an aggregate average. However, the magnitude of the difference (≈78% greater average real-world CO_2 emission than predicted by the EFT model) is considerably larger than can be explained by this factor. The wide range of emission values recorded for sections with the same average speed also indicates that average speed emission functions are liable to be inaccurate especially in congested traffic with low average speeds.

This research demonstrates that the NEDC test cycle certification values and EFT average speed emission functions are likely to lead to significant underestimates of real-world emissions over micro-scale sections in urban road networks.

3.5 DIURNAL VARIATION IN CO_2 EMISSION

Analysis of the CO_2 emission in the network revealed a wide range of CO_2 emission factors for the same test vehicle over the same road sections dependent on the time taken to complete the sections. In order to demonstrate the diurnal variation of congestion in the network, and the resultant impact on CO_2 emission, analysis of the 'northbound' and 'southbound' sections of the A660 was conducted. The northbound section is a combination of Sections 1 and 2 and the southbound section the combination of Sections 4 and 8 (see Figure 3.31). The northbound and southbound sections are approximately 1.5 km in length. The test runs over these sections were separated into four periods: AM peak (between 07:00 and 09:30); Inter-Peak (between 12:30 and 15:00); PM peak (between 15:30 and 18:00) and Evening (between 19:30 and 22:00). Of the 48 test runs, 15 were classed AM peak, 14 as Inter-Peak, 11 as PM peak and 6 as Evening.

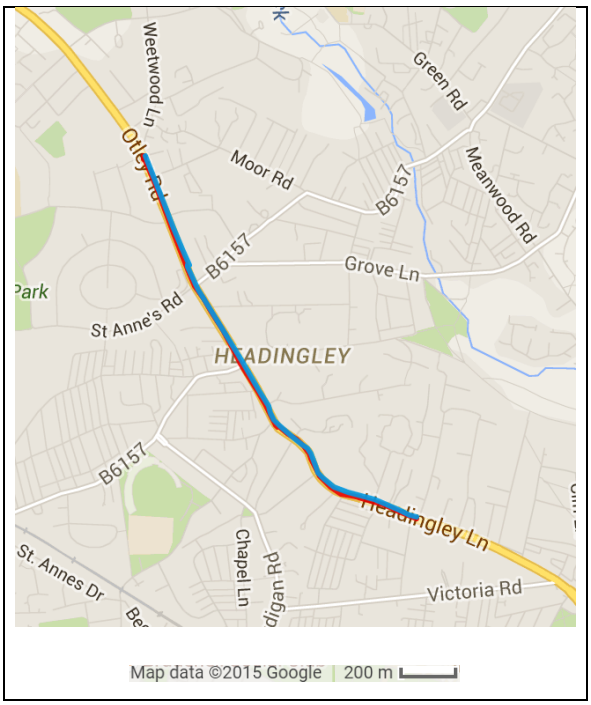

Figure 3.31: Headingley A660 Northbound (Red) and Southbound (Blue) Sections
***(Source: GPSVisualizer.com and* ©Copyright GoogleTM 2015)**

Figure 3.32 presents box plots of the CO_2 emission and the average speed through the completed sections, by time period, for the northbound and southbound sections. Northbound sections show the greatest variation in CO_2 emission with relation to time period. The northbound evening test runs were completed in an average time of 199 s which equates to 27.6 km/h, with a narrow range of completion times from 153 s (36.3 km/h) to 231 s (24.0 km/h). This is reflected in the CO_2 emission values which vary from 255 gCO_2/km to 301 gCO_2/km, with an average of 280 gCO_2/km. In free flow conditions in the network, the emissions of the test vehicle are therefore relatively close to the NEDC urban test cycle certified emission of 253 gCO_2/km. The PM peak northbound section times indicate severe congestion throughout the PM rush hour as traffic heads out of Leeds at the end of the working day. This is consistent with observed behaviour in the network, where the signalled junction of the B6157 (North Lane) and A660 lead to significant delays. The average time to complete the northbound section during the PM peak was 627 s (8.7 km/h), over three times longer than during free flow evening conditions. The average CO_2 emission in the PM peak was 519 g CO_2/km with a range from 401 gCO_2/km to 692 gCO_2/km. The AM peak displays the widest range of average speeds (4.9 km/h – 20.0 km/h), suggesting that, although there were times of severe congestion, this was not experienced throughout the entirety of the designated 07:00 to 09:30 AM peak. Serious congestion during the AM rush hour may be only experienced for a short period within the designated hours, with the remainder of the time relatively free flowing. The Inter-Peak average speed on the northbound section is only marginally quicker than the AM peak (16.8 km/h versus 14.7 km/h for the AM peak), indicating similar traffic conditions in the AM peak and Inter-Peak.

The inter-quartile range shows that there were fewer slow test runs in the Inter-Peak, suggesting less congestion than in the morning rush hour. This is reflected in smaller variance in CO_2 emission.

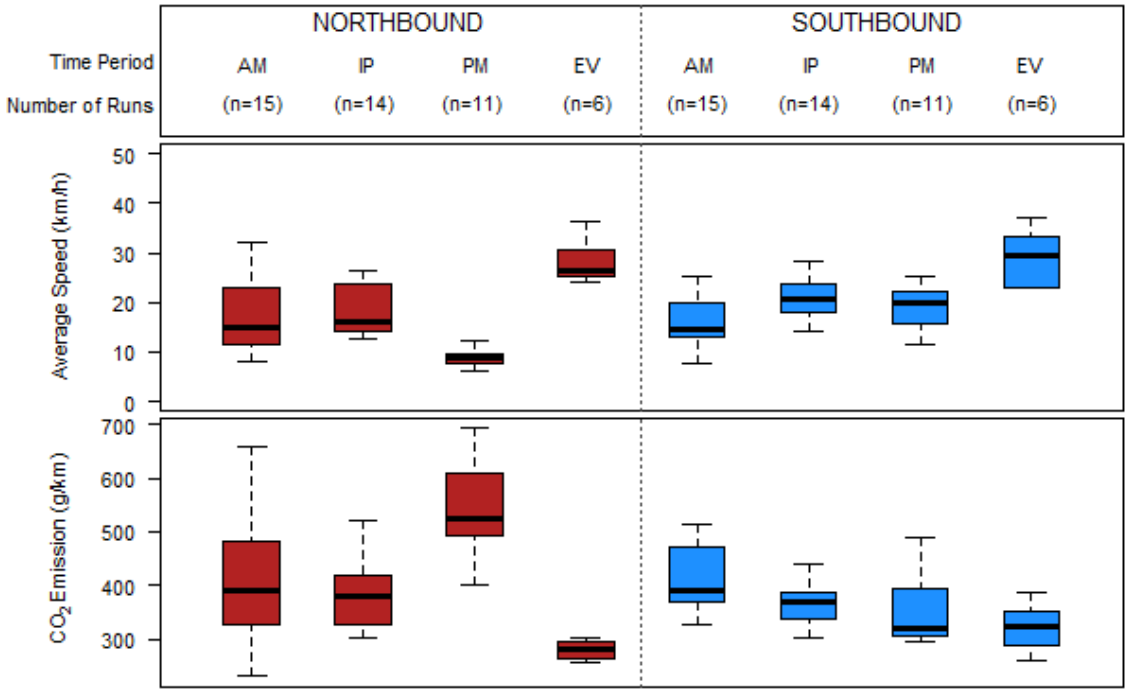

Figure 3.32: A660 Northbound and Southbound Sections: Average Speed and CO_2 Emission

Like the northbound section, the evening period for the southbound section shows by far the highest average speed (28.3 km/h) and the lowest average CO_2 emission (321 gCO_2). Despite similar average speeds through the northbound and southbound sections in the evening period (27.6 km/h and 28.3 km/h respectively), the southbound section shows a consistently greater average CO_2 emission (321 gCO_2/km versus 280 gCO_2/km). This is likely explained by the topography of the road, with the southbound section being primarily uphill and the northbound section downhill. This relationship between grade and emissions is investigated in later chapters. The PM peak for the southbound section does not show the severe congestion of the northbound PM peak. This is to be expected, as the PM peak mainly concerns vehicles leaving the centre of Leeds and travelling out to the northern suburbs, there is much less of an increase in southbound traffic flow associated with the afternoon rush hour. The PM peak has an only marginally slower average speed than the Inter-Peak period (18.1 km/h compared to 20.4 km/h). The southbound AM peak has the slowest average speed (14.5 km/h) and highest average CO_2 emission (426 gCO_2/km) of all the southbound time periods, indicating increased congestion in the morning rush hour as traffic heads towards Leeds city centre from the north. The average AM peak southbound journey time of 378 s is almost double that during the free flow conditions of the evening period (193 s), however, the inter-quartile ranges of the southbound AM peak, Inter-Peak and PM peak overlap, which would suggest the traffic conditions in these three

periods are not wildly dissimilar, and that any AM peak severe congestion is likely found over a shorter duration than the two and a half hour period it has been defined by (07:00 – 09:30) in this study.

The recorded PEMS data demonstrates the diurnal variability of CO_2 emission factors, depending on the level of congestion throughout the day. The results from the Headingley survey correspond with field observations of the A660 which show considerable variation in traffic conditions, with frequent severe congestion, over a prolonged period, on the northbound A660 during PM peak traffic and congestion over the southbound section of the A660 during AM peak traffic.

3.6 SUMMARY

Due to recognised deficiencies in the laboratory based certification process for vehicle emission, the type-approval emission values for passenger cars fail to represent real-world pollutant emission once the vehicle is driven in on-road conditions. In order to quantify the variation in CO_2 emission associated with real-world driving, the work contained in this chapter presented a micro-scale analysis of a PEMS data set recording of real-world CO_2 emission in an urban traffic network. The research identified large spatial and temporal variability in CO_2 emission within the network. Analysis was conducted over a 4.6 km route and found a range of CO_2 emission factors from 313 gCO_2/km to 586 gCO_2/km. The division of the test route into 8 shorter micro-scale sections from 175 m to 781 m in length, revealed a range of section CO_2 emissions from 219 g/km to 1,359 g/km. The majority of the recorded emission rates were found to be substantially greater than the certified ECE15 urban test cycle emission for the test vehicle (253 gCO_2/km). Both the NEDC urban test cycle and the EFT average speed polynomial for the test vehicle were demonstrated to yield significant underestimates of the on-road CO_2 emission of the vehicle. Whilst the gCO_2/km emission factors calculated from the PEMS survey are specific to the Headingley test area in which the research was conducted, the test area can be considered representative of an urban traffic network in any UK city, with no atypical road features or traffic management strategies. Whilst other urban areas may suffer less congestion than the Headingley network, the fact that even during free flowing traffic conditions, the Headingley PEMS survey recorded gCO_2/km emission rates greater than the NEDC measured urban test cycle gCO_2/km rate for the vehicle type, suggests that PEMS studies in other urban areas would find similarly high on-road CO_2 emission rates for this vehicle. The analysis of the PEMS data presented in this chapter will be used in subsequent chapters to assess the accuracy of modelled micro-scale emission estimates of real-world CO_2 emission.

CHAPTER 4: MODELLED VEHICLE EMISSION

4.1 INTRODUCTION

Utilising the real-world PEMS data set analysed in Chapter 3, the work reported in this chapter is an assessment of the ability of four popular emission models to replicate the real-world emission of the test vehicle through the Headingley network. Each of the emission models investigated in this chapter uses a different approach to modelling on-road vehicle emission. The emission models employed in this study are:

- DEFRA's Emissions Factors Toolkit (EFT v6.0.2) (DEFRA, 2009), discussed in Chapter 3, an average speed model, in which the vehicle emission is calculated as a function of the average speed of the vehicle over a link section.

- The HandBook on Emission FActors for road transport (HBEFA v3.1), a 'traffic situation' model, in which emission factors are determined on the basis of road type and traffic conditions, including link average speed.

- The United States (US) Environmental Protection Agency's MOtor Vehicle Emission Simulator (MOVES v2010b) (EPA, 2012a), a 'modal' model in which a 'binning' methodology is employed, that groups each second of engine operation from a drive cycle, by Vehicle Specific Power (VSP) and vehicle speed, into mutually exclusive 'bins'. Each bin has an emission factor defined by the average emission at that point of engine operation. The vehicle emissions are calculated by multiplying the emission factor for each bin by the length of time spent in each bin.

- The Technical University of Graz's (TU-Graz) Passenger car and Heavy duty Emission Model (PHEM v11.7.5) (Hausberger, 2003) is an instantaneous emission model, assigning an emission rate for each second of data. PHEM employs a 'modal' methodology but utilises a higher resolution engine emission map rather than operating mode bins. For each second of a test cycle, the combination of calculated engine power output and simulated engine speed is used to interpolate, from engine maps specific to the test vehicle type, a rate of pollutant emission.

In light of increasing air quality issues in urban areas (Borge et al., 2012) and the need to reduce the vehicle fleet CO_2 emission to meet GHG reduction targets, estimation of the on-road vehicle fleet emission has become increasingly important (Smit et al., 2010). Previous studies (Elkafoury et al., 2015; Colberg et al., 2005; Xue et al., 2013; Wyatt et al., 2014) have identified numerous factors that influence the on-road vehicle exhaust emission:

- Vehicle specification (including vehicle type, engine characteristics, aerodynamic design and vehicle condition)
- Fuel consumption factors (vehicle weight, loading, road surface and the type of fuel)
- Traffic conditions (traffic speed, acceleration and braking, traffic situation and idling time)
- Road geometry (road gradient)

A wide variety of emission models have been developed, under a variety of methodologies, which attempt to distinguish the most important parameters that influence the emission of various pollutant species from vehicle exhausts on different spatial and temporal scales. Emission models can be broadly classified as either macro-scale or micro-scale (Wang and McGlinchy, 2009; Zachariadis and Samaras, 1997). Macro-scale models are primarily designed to estimate vehicle fleet emission at an urban or national network level, whereas micro-scale models are designed to perform more detailed assessments at a road section level.

Emission models at the macro-scale are necessary to calculate emission inventories and project emissions at a regional or national level. The US EPA's MOBILE6 (NRC, 2000) and Europe's COmputer Programme to calculate Emissions from Road Transport (COPERT) (Cloke et al., 1998) are the most commonly used macro-scale emission factor models but lack the resolution for micro-scale emission calculation (Frey et al., 2010). These models estimate the mass of emission based on the average measured g/km emission rate for a vehicle at each speed. They are constructed for each vehicle category by devising an average speed emission function (for each pollutant) from which an estimate of the vehicle emission for a particular trip can be made from the average speed and the distance travelled.

Emission estimates at the micro-scale can be generated by establishing the relationship between vehicle speed, acceleration (vehicle dynamics), road grade (road topography) and emission, on a second-by-second basis for each for each type of vehicle. These models are based on the assumption that the emission from a vehicle will be broadly similar for similar modes of engine operation. This method establishes an average rate of emission, derived from second-by-second PEMS and chassis dynamometer testing, for a set of discrete engine modes. This is required for

each vehicle type to construct a database of emission values. These emission rates for each vehicle activity engine mode are then used to provide emission estimates on a second-by-second basis for any vehicle type over any driving cycle during which second-by-second vehicle activity can be calculated. Micro-scale models offer the ability to analyse very short road sections and journey times, e.g. emission at a specific junction or traffic control measure. If properly calibrated, these models could have the potential to generate emission estimates in a dynamic traffic network at a detailed enough resolution to greatly enhance environmental assessments of traffic networks, to evaluate the emission impact of different road control strategies and to analyse the effect of vehicle technology developments in real-world driving conditions (Zallinger et al., 2009). The use of such models could strengthen the traffic management decision making processes for policies designed to reduce fuel consumption and vehicle emission (Wang and Fu, 2010). With enough data, micro-scale emission estimates could be aggregated to form macro-scale estimates. Such a development could produce a highly flexible system for emission estimation (Frey et al., 2010).

Macro-scale models, based on average speed, have been the traditional method for estimating vehicle emission. However, there are a number of limitations to the average speed emission function methodology, which include:

- Trips through a link with the same average speed may have had a diverse range of transient speed and acceleration profiles, with very different engine operation characteristics and therefore different levels of emission (Panis et al., 2006). As a result vehicle emission cannot be adequately covered by a single emission factor without ignoring other important explanatory variables such as acceleration and road grade (Barlow and Boulter, 2009; Vallamsundar and Lin, 2011).

- The shape of the derived average speed emission function is dependent on the test cycle over which it was generated. The expected level of emission is related to the specific cycle over which the vehicle was tested which may not represent all real-world conditions (Barlow and Boulter, 2009).

- Because the average speed emission functions are calculated from an average speed over a certain link length, the emission estimates may not be representative of real-world emission at a more detailed spatial resolution (Wang and Fu, 2010). As such, they are not applicable at the micro-scale (Frey et al., 2010).

- In the case of traffic situation models, the characteristics which describe each of the traffic situations are likely to vary significantly between different locations (Boulter et al., 2007). As a result of this, using predefined traffic situations in areas other than those described in the initial model calibration may lead to unrepresentative emission estimates.

The latest generation of instantaneous emission models have been designed to address some of the average speed model limitations. By relating the emission rate to vehicle behaviour on a second-by-second basis, the new methods have removed the errors associated with averaging emission over longer time periods and facilitated emission estimation at a micro-scale level. Instantaneous emission models, however, require detailed vehicle information to describe operation and location, which is not always available and can be prohibitively expensive to obtain (Wang and McGlinchy, 2009).

4.2 MODEL EVALUATION CRITERIA

There are a number of background modelling criteria which are common to each of the four emission models:

- Hot exhaust emission is defined as the vehicle exhaust emissions once the engine has completed a warm-up phase after which the engine and exhaust after treatment system are at operational temperature (Barlow and Boulter, 2009). The performance of an engine before it has warmed up can have a considerable impact on the total level of emission of certain exhaust emission species (Khalfan et al., 2015; Li et al., 2008a). As the Headingley PEMS survey was conducted with the vehicle engine warm before the start of each test run, cold start effects are excluded from each of the emission models.

- Vehicle speed was recorded by multiple means (i) the PEMS system, (ii) the GPS unit, (iii) the OBS unit and (iv) the vehicle CAN, but the vehicle speeds referenced in the modelling process relate to the velocities measured only by the GPS as this instrument had the greatest measurement precision, at ± 0.2 km/h (Racelogic, 2008).

- The recorded GPS altitude measurements were found to be insufficiently accurate to generate estimates of road grade, so all models in this chapter assume that the test area is flat, with a road grade of 0. Road grade is investigated further in Chapter 5.

4.3 EFT AVERAGE SPEED EMISSION MODEL

4.3.1 EFT Background

The Department for Environment Food and Rural Affairs (DEFRA) Emissions Factors Toolkit (EFT) is an average speed emission model designed to help UK local authorities assess the impact that vehicle transit in their area has on local emissions as part of their duties under the Environmental Act 1995 (DEFRA, 2009). Emissions are calculated at a road link level by the input of vehicle fleet composition, average traffic speed and road type. The latest version of EFT (v6.0.2), released in November 2014, employs Nitrogen Oxides (NO_x), Particulate Matter (PM) and Hydrocarbons (HC) emission factors from the European Environment Agency's (EEA) COPERT IV model and the CO_2 emission factors published by the DfT (DfT, 2009a).

In order to develop the average speed emission function, measurements of emission versus average speed are plotted from either a chassis dynamometer or a PEMS setup. A polynomial function is derived from these data from which CO_2 emission can be estimated for an average running speed. Figure 4.1 is an example of this from a paper by Barth *et al.* (Barth and Boriboonsomsin, 2008), in which the blue line represents the emission function and the red dashed line the approximate lower bound.

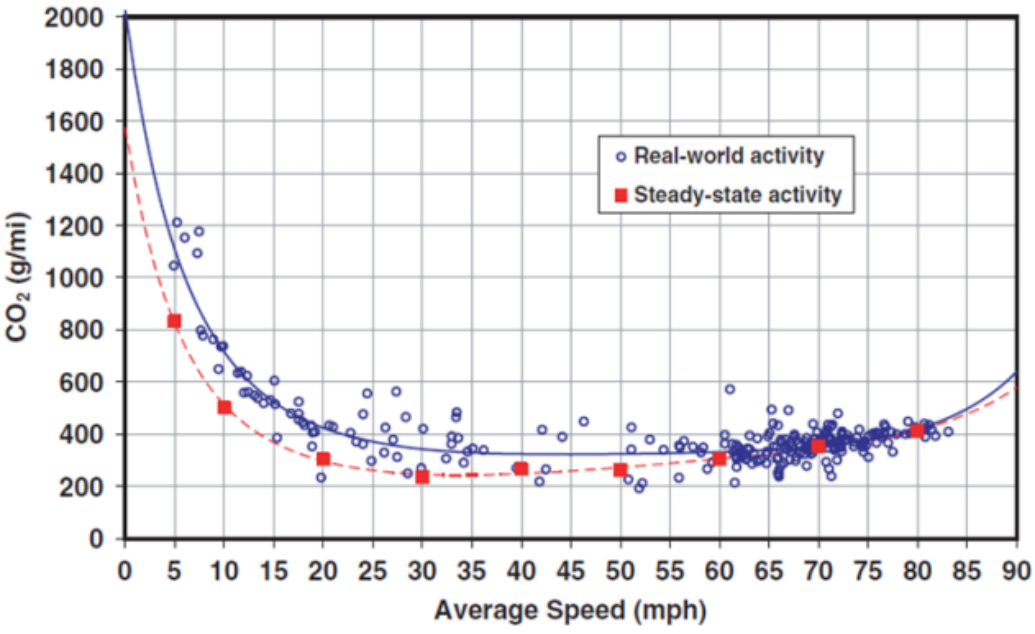

Figure 4.1: CO_2 Emission as a Function of Average Trip Speed (Barth and Boriboonsomsin, 2008)

Although the EEA's COPERT average speed model is more widely used to estimate road transport emissions (Smit et al., 2010; Frey et al., 2010) and its hot exhaust average speed emission functions are derived in a similar way to the EFT, the EFT was chosen for this study due to its ability to model emissions at low average speeds. The valid average speed range for the COPERT IV petrol passenger car fuel consumption function (from which the amount of CO_2 is derived) is between 10 km/h and 130 km/h (Ntziachristos and Samaras, 2014), whereas the EFT's CO_2 emission function is valid between 5 km/h and 140 km/h (DEFRA, 2009). Although 23.18% of the Headingley PEMS survey sections (89 of 384) had a measured average speed below 10 km/h, only 3.13% (12) recorded an average speed below 5 km/h. For this reason, the EFT was selected to generate emission estimates. Both models stipulate that the emission factors should only be applied within the recommended speed ranges, ranges set on the basis of the available input data. Extrapolation of the functions to higher or lower speeds than those defined by the range cannot be justified. In the EFT model, average speed emission functions have been described for Cars, LCVs, HGVs, Buses and Motorcycles, and each vehicle type is further segregated, as appropriate: by Euro emission standard, fuel, weight, and engine capacity. In total, the EFT model contains 265 emission functions.

Figure 4.2 presents the EFT emission functions for petrol cars with a weight of less than 2.5 t and an engine capacity between 1.4 – 2.0 L (DfT, 2009a). The function table (Table 4.1) lists the coefficients for the fourth order polynomial that describes the emission factors. The curves demonstrate the expected trend of improving engine efficiency with each Euro emission standard category.

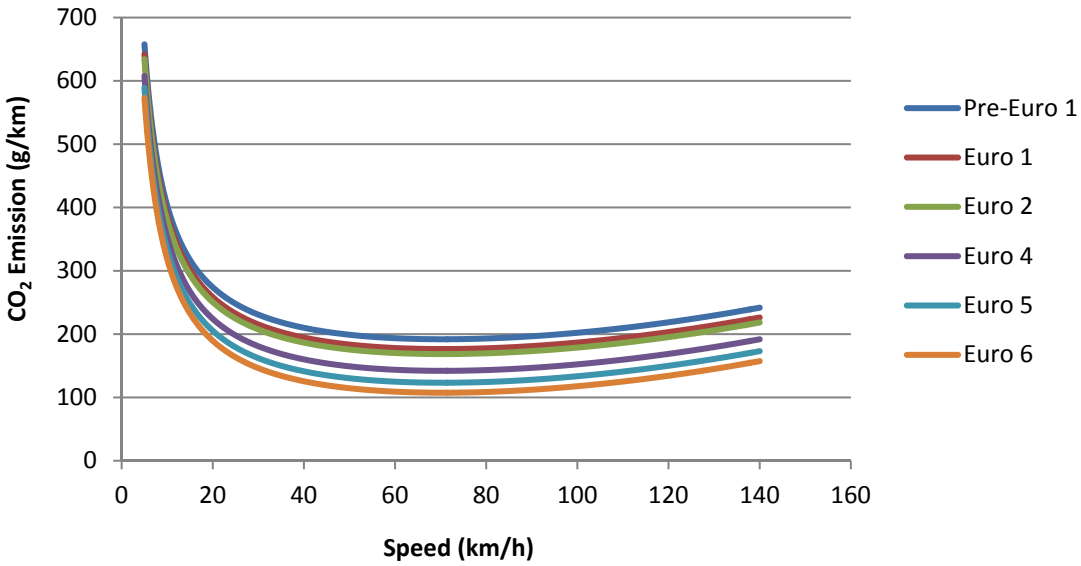

Figure 4.2: EFT CO_2 Average Speed Emission Functions for Petrol Cars < 2.5 t, 1.4 – 2.0 L (DfT, 2009a)

Table 4.1: EFT CO_2 Average Speed Emission Functions for Petrol Cars < 2.5 t, 1.4 – 2.0 L (DfT, 2009a)

Emission Standard	Function		Coefficients				Valid Speed Range	
	Type	Formula (y=EF in g/km; x=speed in km/h)	a	b	c	d	Min (km/h)	Max (km/h)
Pre-Euro 1	Polynomial	$y=k*(a+bx+cx^2+dx^3)/x$	2532.358	153.2843	-0.43167	0.006678	5	140
Euro 1	Polynomial	$y=k*(a+bx+cx^2+dx^3)/x$	2532.358	137.794	-0.43167	0.006678	5	140
Euro 2	Polynomial	$y=k*(a+bx+cx^2+dx^3)/x$	2532.358	129.8751	-0.43167	0.006678	5	140
Euro 3	Polynomial	$y=k*(a+bx+cx^2+dx^3)/x$	2532.358	118.3377	-0.43167	0.006678	5	140
Euro 4	Polynomial	$y=k*(a+bx+cx^2+dx^3)/x$	2532.358	103.3972	-0.43167	0.006678	5	140
Euro 5	Polynomial	$y=k*(a+bx+cx^2+dx^3)/x$	2532.358	84.59543	-0.43167	0.006678	5	140
Euro 6	Polynomial	$y=k*(a+bx+cx^2+dx^3)/x$	2532.358	68.84183	-0.43167	0.006678	5	140

By entering the average link speed, the vehicle fleet composition, the length of the link and the total vehicle flow through the link (over a certain time period) into the model, the total emission for that link can be estimated. The model references the average speed to the emission function curves for each vehicle type, generating an expected emission factor in g/km for each emission vehicle type. These values are then multiplied by the number of vehicles of each respective type through the link and the length of the link so that the total link emission for each vehicle type is calculated. Summing these values gives the total fleet emission through the link over the desired time period. Generating link estimates and summing these calculations for all roads in a test area can generate network, regional and national emission estimates.

4.3.2 EFT Real-World Emission Factor Estimation

The EFT lap emission factors were calculated directly from the Euro 4 EFT polynomial equation that best represents the test vehicle (i.e. Euro 4, Petrol, Car < 2.5 t, engine capacity 1.4 - 2.0 L), which is described in the table in Figure 4.2. The average speed recorded for each of the PEMS measured test laps was entered into the EFT emission function to generate 48 test lap EFT gCO_2/km emission factors. Figure 4.3 is a plot of the distribution by count of each of the 48 EFT emission factors in comparison to the distribution of the 48 PEMS measured CO_2 emission factors. It is clear from the two distributions that the EFT estimates are considerably lower than those recorded during the real-world testing. The average emission estimate by the EFT is 281 gCO_2/km whilst the PEMS measured an average emission factor of 442 gCO_2/km. The mean absolute percentage error (MAPE) between the EFT and PEMS factors is 37.7%, with percentage errors ranging from 24.4% to 45.3%.

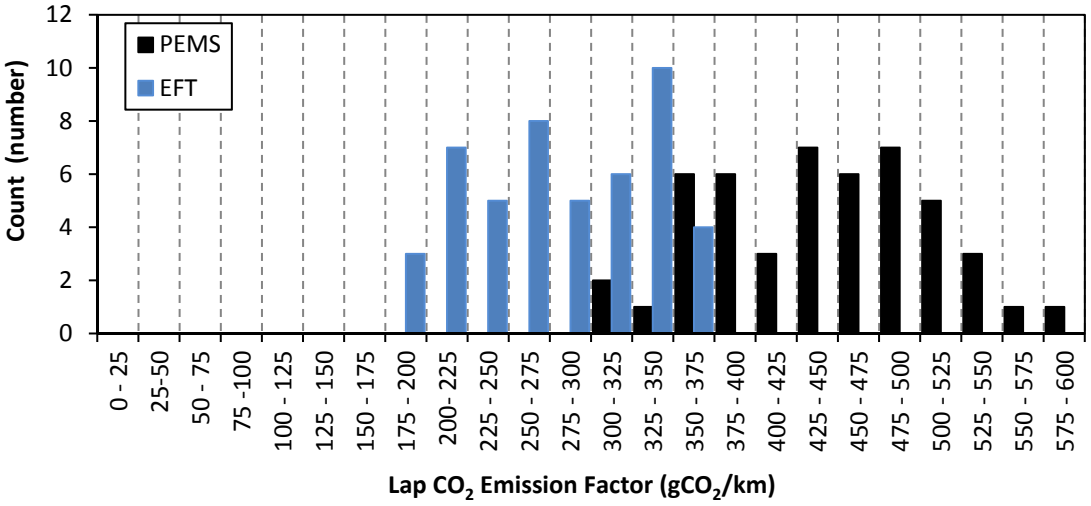

Figure 4.3: Distribution of Headingley Lap CO_2 Emission Factors from the PEMS Real-World Measurement and the EFT Modelled Estimate (n=48).

The same pattern of underestimation of emission through the average speed methodology is displayed at the section level, with the emission factors for the 372 sections, those with valid vehicle speeds (12 sections with the average speed ≤ 5 km/h have been excluded) distributed toward lower emission factors than the PEMS on-road factors. As Figure 4.4 highlights, 69.9% of the EFT estimated emission factors are between 150 gCO_2/km and 300 gCO_2/km, compared with only 14.0% of the PEMS measured emission factors in this range. The PEMS survey recorded 33.9% of sections with emission rates ≥ 500 gCO_2/km whilst the EFT estimates that only 4.8% of sections had an emission factor ≥ 500 gCO_2/km. The underestimation is reflected in the means, with the average EFT section emission estimate being 276 gCO_2/km and the PEMS average measured section emission 451 gCO_2/km.

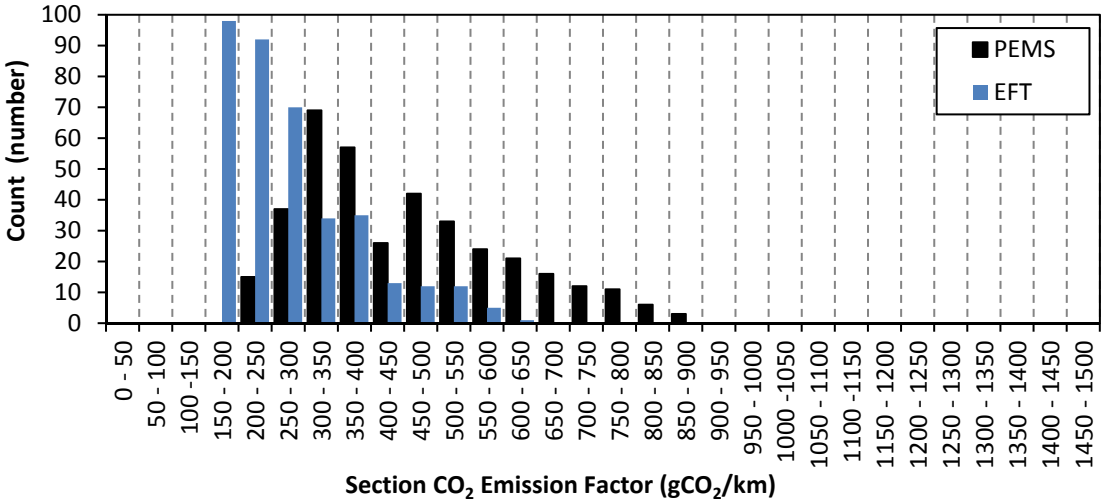

Figure 4.4: Distribution of Headingley Section CO_2 Emission Factors from the PEMS Real-World Measurement and the EFT Modelled Estimate (n=372).

Figure 4.5 displays box plots of the EFT estimated emission as a percentage of the PEMS measured emission, for each of the individual 48 test runs over the test sections and the lap. For example, for Lap 1.1, where the PEMS measured emission factor was 515 gCO_2/km and the EFT average speed calculated emission was 357 gCO_2/km, the EFT percentage estimate is 69.2% of the PEMS measured emission. Figure 4.5 presents these calculated values, for all valid runs, by lap and by section, with sections grouped by geographic proximity (see Figure 3.9).

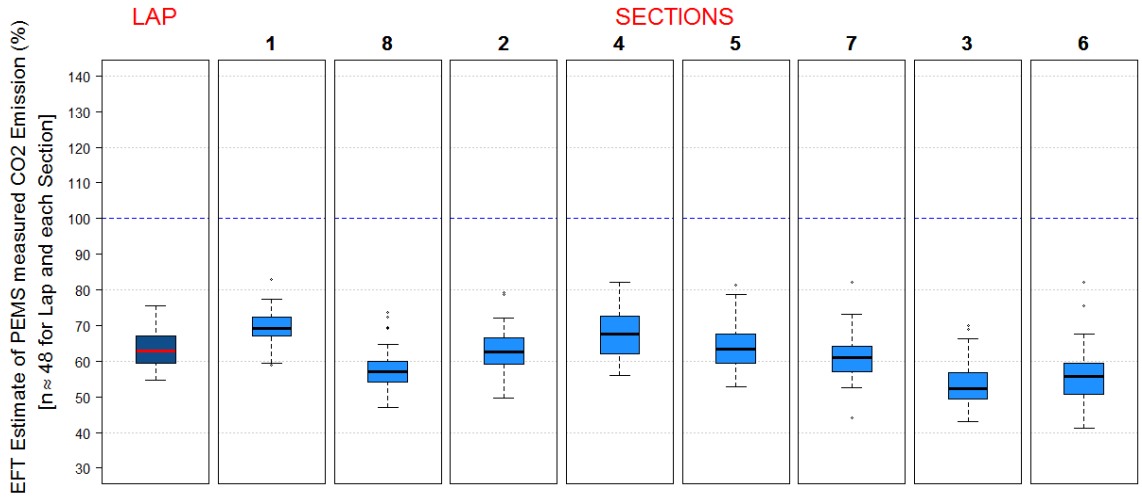

Figure 4.5: EFT Estimate of PEMS Measured gCO_2/km Emission, by Lap and Section.

For the test lap, where the median EFT percentage estimate of the PEMS real-world emission was 62.9%, the IQR was 7.6%. At the section level, the box plots show some section-to-section variation in median EFT percentage estimate of the PEMS values, with a range from 69.2% for Section 1 to 52.4% for Section 3. The average IQR for the sections was 7.6% with a range from 5.4% to 10.6%. The relatively narrow IQR indicates that the estimates, although underestimates, were relatively consistent. Sections 3 and 6 showed the greatest level of underestimation, but as these are shorter turning sections, the stop-start nature of these sections is likely to lead to atypically high emission levels. Section 1 and 8 are the opposing traffic flows over the same stretch of road. The Section 1 EFT estimates are the most accurate of the sections, whilst the Section 8 estimates are among the least accurate. This disparity is likely due to the effect of road grade since Section 1 is primarily downhill and Section 8 uphill. As road grade is not accounted for in this modelling, the Section 8 emissions, which in the real-world would have increased due to the opposing force of gravity, are underestimated, and the Section 1 emissions, which in real-world driving would be less due to the accelerating force of gravity, are overestimated by the EFT model. In this case, the overestimation in Section 1 appears to improve the Section 1 estimate, due to the overall tendency of the model to underestimate CO_2 emission levels.

In this instance, the error associated with employing the EFT average speed emission function to estimate micro-scale CO_2 emission, for this Euro 4 test vehicle, is an underestimation in the order of 25% - 52.5% of the real-world CO_2 emission. The definition of the CO_2 emission polynomial function for the test vehicle in the EFT (Passenger Car; Petrol; 1.4 – 2.0 L; Euro 4) possibly describes too wide a spectrum of vehicles to enable accurate calculation for micro-scale analysis of individual vehicles, and the model lacks the capability to disaggregate the category further e.g. by vehicle mass; specific engine capacity; engine rated power. As the engine capacity of the test vehicle was 1.8 L, a proportion of the underestimate is likely due to the vehicle emitting greater CO_2 than a typical vehicle in the defined category. It is also possible that the test cycles from which the Euro 4 average speed emission polynomial was defined were unrepresentative of the real-world driving conditions encountered during the Headingley test.

4.4 HBEFA TRAFFIC SITUATION EMISSION MODEL

4.4.1 HBEFA Background

The HBEFA is an emission factor database developed on behalf of Germany, Switzerland, Austria, Sweden, Norway and France. It provides hot, cold and evaporation emission factors for all regulated air pollutants, important non-regulated air pollutants along with fuel consumption and CO_2 emission (Schmied, 2014).

The HBEFA model supplies g/km emission estimates based on defined traffic situations and vehicle type (Borge et al., 2012). Traffic situations for each road section are characterised in the HBEFA by:

- The “Area” (urban / rural)
- The “Road Type” (10 types including: Motorway; Trunk; Distributor; Local and Residential)
- The “Speed Limit” (14 categories: from 10, 20, 30,... , 130, >130 km/h)
- Level of Service (LOS):
    - **Freeflow**: Free flowing traffic conditions, with low and steady traffic flow. Indicative speeds of 45-60 km/h on a road with a 50 km/h speed limit.

- **Heavy**: Free flow conditions with heavy traffic conditions, fairly constant speed. Indicative speeds of 30-45 km/h on a road with a 50 km/h speed limit.
- **Saturated**: Saturated traffic, unsteady flow, variable intermediate speeds, with possible stops. Indicative speed of 15-30 km/h within a 50 km/h speed limit.
- **Stop + Go**: Heavily congested flow, stop and go traffic flow or gridlock. Variable slow speed and stops. Indicative speeds of 5-15 km/h on a road with a 50 km/h speed limit.

In total, 276 different traffic situations are included in the model, 152 Rural and 124 Urban. Each of the traffic situations is represented by a real-world speed-time driving pattern, from which the emission factor is calculated for each vehicle type (Car; LCV; HGV; Coach; Bus; Motorcycle). Each of the vehicle types is further categorised, as appropriate, by vehicle size; fuel type; emission standard; and emission reduction technology. Figure 4.6 shows a breakdown of the methodology, displaying the representative test cycles for the four LOS categories on an urban trunk road with a speed limit of 50 km/h. These four test cycles can then be processed through PHEM (Hausberger et al., 2009) for a Euro 3 emission standard, diesel passenger car, with an engine capacity between 1.4 and 2.0 L, to generate a g/km hot exhaust emission function for each of the four traffic situations.

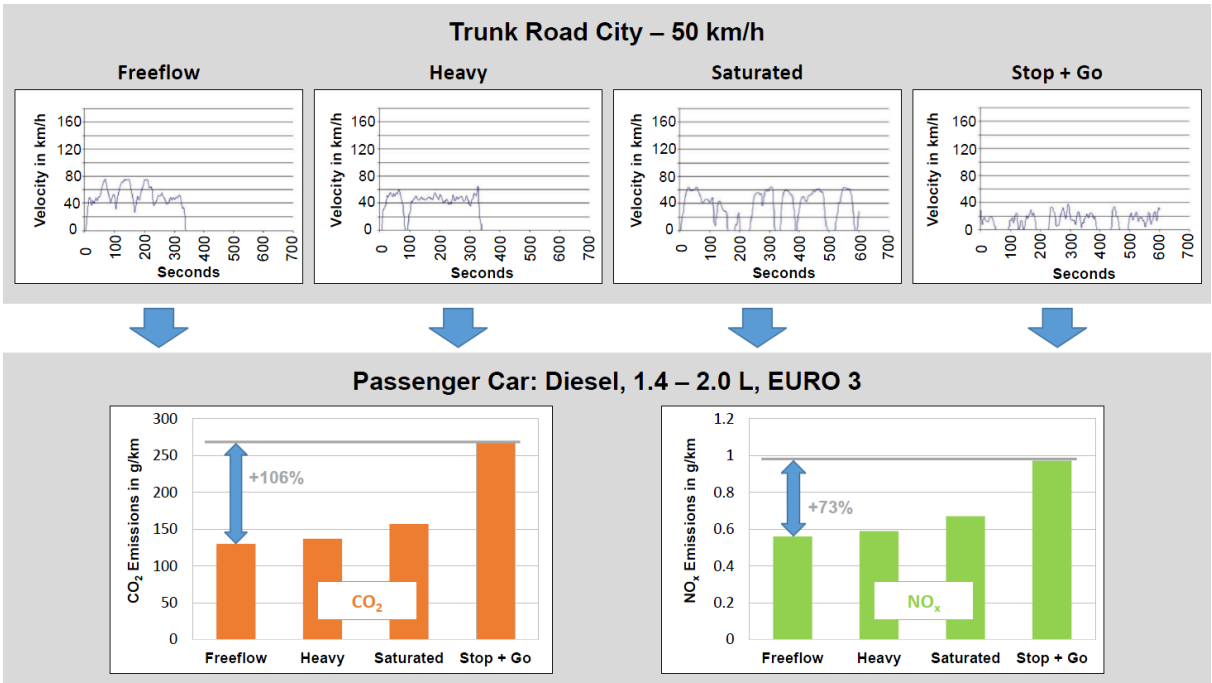

Figure 4.6: HBEFA Methodology for Traffic Situation Based Emission Estimation (Schmied, 2014)

Each of the emission factors in the HBEFA was computed using the PHEM instantaneous emission model. For example, for passenger cars, PHEM was used to provide a total of 142,800 emission factors, covering each of the traffic situations for each vehicle type and vehicle sub-category, over seven road gradient categories (-6%, -4%, -2%, 0%, 2%, 4%, 6%) for seven exhaust gas species and fuel consumption (Hausberger et al., 2009).

Emissions for a vehicle or fleet are calculated by multiplying the distance covered by each vehicle type subcategory (e.g. Euro 3, Diesel, 1.4 - 2.0 L, Passenger Car), by the emission factors specific to the vehicle subcategory and identified traffic situation (Schmied, 2014). This method is intended to be more representative of on-road traffic emissions (Hausberger et al., 2009; Borge et al., 2012), and applicable at finer spatial scales (Fontaras et al., 2014) than average speed based methods.

4.4.2 HBEFA Real-World Emission Factor Estimation

To estimate the Lap and Section emission using the HBEFA requires specification of the vehicle type and the given traffic situation, defined by road type, speed limit and LOS. The categories in Table 4.2 were identified to correspond to the test vehicle and survey area in this study:

Table 4.2: HBEFA Vehicle and Traffic Situation Definitions for the Headingley Test

Test Vehicle	Traffic Situation
• Passenger Car • 1.4 - 2.0 L • Petrol • Euro 4	• Urban • Speed Limit 50 km/h (closest to 30 mph 48.28 km/h) • Road type: Distributor for Sections 1, 2, 4, 5, 7 and 8, Local / Collector for Sections 3 and 6.

For these described vehicle and network conditions, CO_2 emission factors from the HBEFA could be identified for each road type by the LOS (free flow, heavy traffic, saturated and stop and go). These are detailed in Table 4.3 below:

Table 4.3: HBEFA Emission Factors for the Headingley Test

Vehicle Sub-Segment	Traffic Situation	Component	Emission Factor (g/km)	V (km/h)
PC petrol 1.4 – 2.0 L Euro-4	URB/**Distr**/50/**Freeflow**	CO_2	164.95	45 - 60
PC petrol 1.4 – 2.0 L Euro-4	URB/**Distr**/50/**Heavy**	CO_2	187.32	30 - 45
PC petrol 1.4 – 2.0 L Euro-4	URB/**Distr**/50/**Satur.**	CO_2	188.20	15 - 30
PC petrol 1.4 – 2.0 L Euro-4	URB/**Distr**/50/**St+Go**	CO_2	317.42	5 - 15
PC petrol 1.4 – 2.0 L Euro-4	URB/**Local**/50/**Freeflow**	CO_2	158.43	45 - 60
PC petrol 1.4 – 2.0 L Euro-4	URB/**Local**/50/**Heavy**	CO_2	194.00	30 - 45
PC petrol 1.4 – 2.0 L Euro-4	URB/**Local**/50/**Satur.**	CO_2	206.01	15 - 30
PC petrol 1.4 – 2.0 L Euro-4	URB/**Local**/50/**St+Go**	CO_2	340.73	5 - 15

The LOS is determined by the average speed of the traffic through the road section. The velocity relevant to each LOS is listed under column heading V (km/h) in Table 4.3 which are given by the "Indicative Speeds" from the HBEFA LOS definition. For example, the urban distributor road with a speed limit of 50 km/h is defined as having Stop and Go conditions when the average speed of the section is between 5 and 15 km/h, with an emission factor of 317.42 gCO2/km, and the total CO_2 emission is calculated by multiplying the emission factor by the length of the section.

The HBEFA CO_2 emission estimates (gCO_2/km) for each of the road sections were calculated from the average speed for each section recorded during the PEMS survey. The results are presented in Figure 4.7 alongside the distribution of section CO_2 emission values (gCO_2/km) measured during the Headingley PEMS survey.

Clearly, having only four discrete HBEFA CO_2 emission values for each road type, over a range of observed average speeds, does not lend itself well to the calculation of micro-scale emission estimates. The maximum HBEFA emission factors of 317.42 gCO_2/km (Distributor road type) and 340.73 gCO_2/km (Local road type) are lower than 78.6% of the measured PEMS section CO_2 estimates for their respective road types, suggesting that, at least for the Headingley network, congestion causes significantly higher emission of CO_2 than would be predicted by the HBEFA factors. The lowest recorded PEMS CO_2 emission factor for a section in the real-world survey was 216 gCO_2/km. As shown in Table 4.3, this real-world factor is greater than each of the six HBEFA emission factors for the vehicle type in free flow, heavy or saturated traffic.

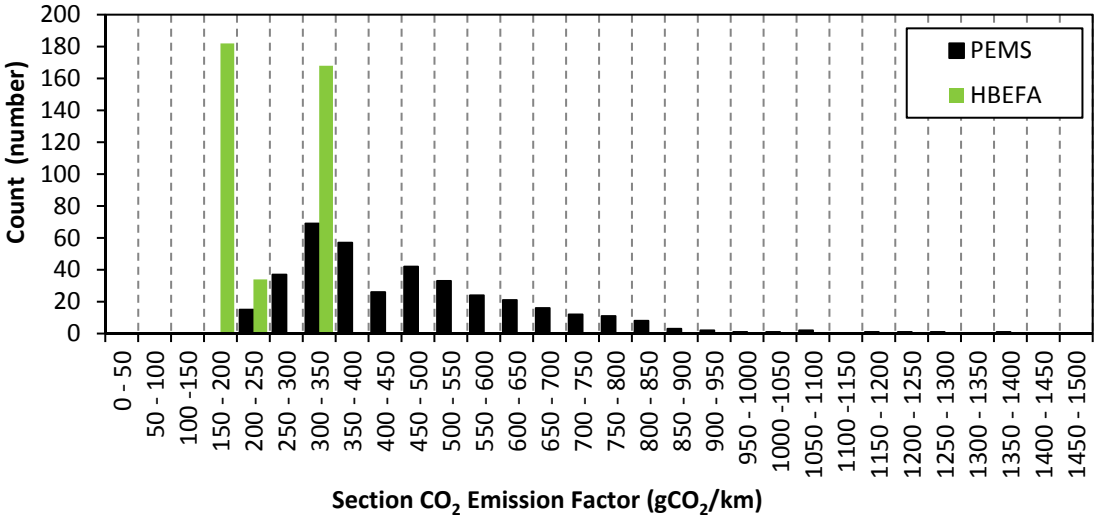

Figure 4.7: Distribution of Headingley Section CO_2 Emission Factors from the PEMS Real-World Measurement and the HBEFA Modelled Estimate (n=384)

The Headingley lap HBEFA CO_2 emission factor estimates in Figure 4.8 are a sum of the HBEFA section CO_2 total emission values for each lap, divided by the lap length (rather than estimates generated from the average speed of the lap, which would have produced a similar pattern to that shown in Figure 4.7, merely reporting the discrete HBEFA emission factors for the vehicle type and traffic situation). The HBEFA CO_2 emission factor estimates are all lower than the real-world values measured by the PEMS survey with a MAPE of 42.7%.

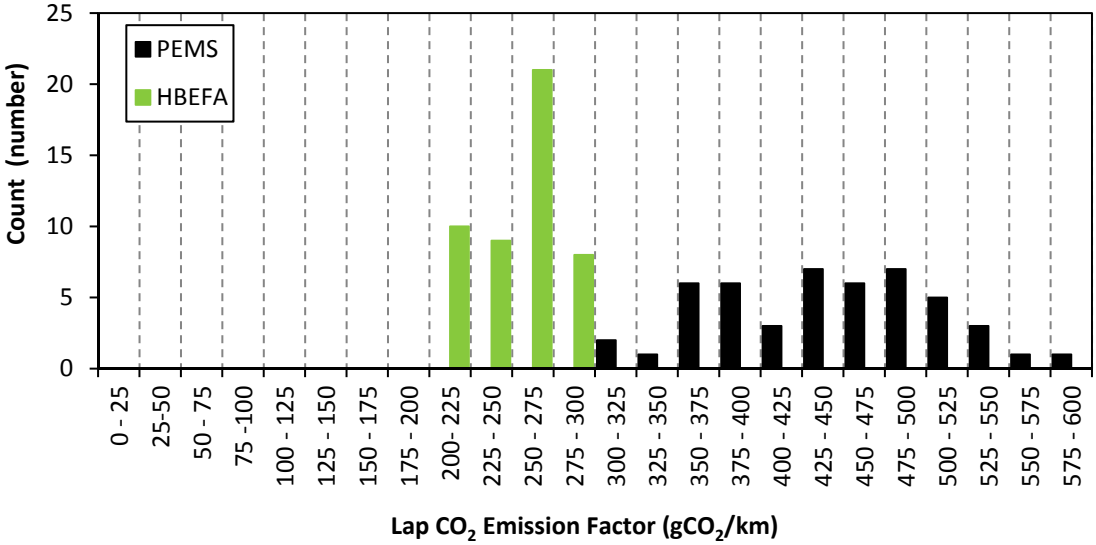

Figure 4.8: Distribution of Headingley Lap CO_2 Emission Factors from the PEMS Real-World Measurement and the HBEFA Modelled Estimate (n=48)

Figure 4.9 presents box plots of the HBEFA estimate of the PEMS measured emission as a percentage, for each of the 48 test runs over the test sections and the lap. The average HBEFA lap CO_2 emission estimate was 251 gCO_2/km, which is only 56.6% of the average PEMS lap (442 gCO_2/km). On average, the HBEFA lap estimate is 42.7% less than the PEMS measured emission with a range of underestimation from 24.8% to 52.9%. The IQR range for the lap estimates is between 52.9% and 61.7%. The box plots for each of the sections reveal a very wide range in the accuracy of the micro-scale estimates of real-world emission using the HBEFA model, with an average IQR of 15.3%. Section 5 for example, has an overall range of estimates between 25% and 93.5% of the PEMS recorded emission.

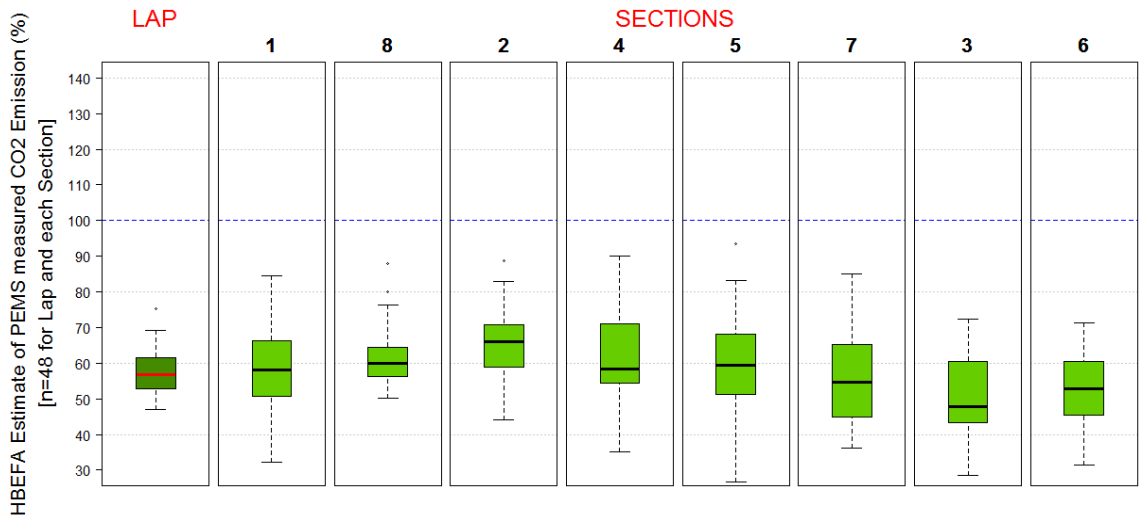

Figure 4.9: HBEFA Estimate of PEMS Measured gCO_2/km Emission, by Lap and Section

Comparing the PEMS measured values to the HBEFA estimates for the Headingley sections, reveals an underestimate of the real-world emission of approximately 20% - 60%. Whilst the HBEFA was primarily designed to provide emission factors for city, regional and national scales (Schmied, 2014), the HBEFA emission factors are used to inform link level analysis especially in combination with air quality microscopic dispersion models (Hülsmann et al., 2014; Borge et al., 2012). Although it is possible that the four discrete traffic situation emission functions may provide a reasonable overview of network emission at an aggregate level, the results of this analysis confirm that it is a poor tool for specific micro-scale emission estimation as it is unable to predict the very high rates of CO_2 emission observed in the stop-start and at times congested real-world study. The lack of a continuous emission function causes large variance in the emission estimates from the HBEFA at the section level, as the estimate on any road is limited to one of four discrete values associated with prevalent traffic situation, whilst the real-world emission could take any value.

Like the EFT model, the definition of the test vehicle in the HBEFA (Passenger Car; Petrol 1.4 - 2.0 L; Euro 4) may be too broad to enable accurate calculation of an individual vehicle. It is also possible that the drive cycles used to generate the emission factors for each of the traffic situations in HBEFA are unrepresentative of the real-world traffic in Leeds, having been primarily developed from German, Swiss and Austrian data (Borge et al., 2012).

4.5 MOVES MODAL EMISSION MODEL

4.5.1 MOVES Background

The US EPA's MOtor Vehicle Emission Simulator (MOVES) (EPA, 2012a) is its latest generation emission estimation model and replaced the average speed emission estimation model MOBILE 6 with a modal-based emission model. MOVES primary purpose is to produce inventories of energy consumption and emission at the national and regional scale (Kwon et al., 2007), however, it has also been designed with the capacity to generate micro-scale emission estimates (Vallamsundar and Lin, 2011) and with the ability to evaluate the effect of local transportation projects (Coelho et al., 2009).

The model utilises a binning methodology, which groups second-by-second transient vehicle data into 23 distinct engine operating modes (or "bins") by Vehicle Specific Power (VSP) and by vehicle speed. Operating on the assumption that a vehicle's emissions will be broadly the same for similar modes of engine operation, for each vehicle type and age, an average modal emission is calculated for the 23 bins. The emission data for model calibration are based on second-by-second data from laboratory based chassis dynamometer testing as well as real-world measurements (Coelho et al., 2009)

4.5.2 Vehicle Specific Power

VSP is defined as the instantaneous power per unit mass of the vehicle, with units of kilowatts per tonne (kW/t) (Jimenez-Palacios, 1999). In order for a vehicle to move, the power from the engine must overcome the aerodynamic drag, rolling resistance and the road grade effect acting against the vehicle motion, whilst additional power to that offset by these opposing forces is required for the vehicle to accelerate (Heisler, 2002). These factors are accounted for in the calculation of VSP. The VSP equation derived by Jimenez is shown below in Equation 4.1 (Jimenez-Palacios, 1999).

Equation 4.1:

$$\text{Vehicle Specific Power} = \frac{\frac{d}{dt}(KE + PE) + F_{rolling} \cdot v + F_{aerodynamic} \cdot v}{m}$$

$$= \frac{\frac{d}{dt}\left(\frac{1}{2} m \cdot (1 + \varepsilon_i) \cdot v^2 + mgh\right) + C_R mg \cdot v + \frac{1}{2}\rho_a C_D A (v + v_w)^2 \cdot v}{m}$$

$$= v \cdot (a \cdot (1 + \varepsilon_i) + g \cdot grade + g \cdot C_R) + \frac{1}{2}\rho_a \frac{C_D \cdot A}{m}(v + v_w)^2 \cdot v$$

Where,

- m : vehicle mass
- v : vehicle speed
- a : vehicle acceleration
- ε_i : "Mass factor", which is the equivalent translational mass of the rotating components (wheels, gears, shafts, etc.) of the power-train. The suffix i indicates that ε_i is gear-dependent[1]
- h : altitude of the vehicle
- $grade$: vertical rise/slope length[2]
- g : acceleration of gravity (9.81 m/s^2)
- C_R: coefficient of rolling resistance (dimensionless)[3] – the power that has to be expended to overcome the restraining forces caused by the deformation of tyres and road surfaces and the interaction of frictional scrub when tractive force is applied (Heisler, 2002).
- C_D: drag coefficient (dimensionless) – a measure of the effectiveness of the vehicle's body shape in reducing the air resistance to the forward motion of the vehicle.
- A : frontal area of the vehicle
- ρ_a : ambient air density (1.207 kg/m^3 at 20 °C)[4]
- v_w : velocity of headwind into the vehicle

Employing typical values for LCVs describing rolling resistance, aerodynamic drag (C_D*A/m) and air density at 20°C, Jimenez simplified the equation as below (with v and v_w in m/s and a in m/s^2). The VSP equation will vary for different vehicle types as the rolling resistance coefficient and the calculation of aerodynamic drag values are vehicle specific.

[1] The term m*v*a*ε_i is called the "acceleration resistance". Typical values of ε_i for a manual transmission are 0.25 in 1st gear, 0.15 in 2nd gear, 0.10 in 3rd gear, 0.075 in 4th gear.

[2] Rigorously sin(atan(grade)) should be used instead of grade, but the error of this approximation is small (less than 1% relative error for grades below 14%).

[3] The value of C_R depends on the road surface and tyre type and pressure, with a small dependence on vehicle speed. Typical values range from 0.0085 to 0.016. A value of 0.0135 has been used here for all vehicles.

[4] The ideal gas law, can be used to correct to other temperature and pressure conditions. The formula is $\rho = \rho_0 * (P/P_0) * (T_0/T) = 1.207 * (P/101.33) * (293.16/T)$, with ρ(kg/m^3), P (kPa), and T (K). This correction may be important, e.g. if the measurements are performed at -10°C (-14°F) and 1 atmosphere the air density will be 10% higher than at 20°C.

Equation 4.2:

$$\mathrm{VSP} = \mathrm{v} \cdot (1.1 \cdot \mathrm{a} + 9.81 \cdot \mathrm{grade} + 9.81 \cdot 0.0135) + \frac{1}{2} \cdot 1.207 \cdot 0.0005 \cdot (\mathrm{v} + \mathrm{v_w})^2 \cdot \mathrm{v}$$

$$= \mathrm{v} \cdot (1.1 \cdot \mathrm{a} + 9.81 \cdot \mathrm{grade}(\%) + 0.132) + 0.000302 \cdot (\mathrm{v} + \mathrm{v_w})^2 \cdot \mathrm{v}$$

Jimenez's research showed that VSP is proportional to engine power, with the inverse of the vehicle mass as the constant of proportionality. Hence there is a strong relationship between VSP and fuel consumption and correspondingly vehicle emission (Jimenez-Palacios, 1999).

Equation 4.3 is Equation 4.2, with the rolling resistance term coefficient ($g \cdot C_R$) of 0.128 and aerodynamic drag term coefficient ($0.5\rho_a(C_D \cdot A)/m$) of 0.000318 calculated to correspond to the specific Euro 4 passenger car employed in this study.

Equation 4.3:

$$\mathrm{VSP_{EURO4}} = \mathrm{v} \times ((1.1\mathrm{a}) + (9.81 \times \sin(\mathrm{atan}(\mathrm{grade})) + 0.128) + (0.000318\mathrm{v}^3)$$

Where,

- VSP is vehicle specific power (kW/t);
- v is vehicle speed (m/s);
- a is vehicle acceleration (m/s^2);
- grade is road grade (dimensionless).
- The rolling resistance term coefficient is the rolling resistance coefficient of the test vehicle of 0.013 (Ehsani et al., 2009) multiplied by the acceleration due to gravity which is 9.81 m/s^2.
- The drag term coefficient is half of the aerodynamic drag coefficient of the test vehicle (0.32) (Doucette and McCulloch, 2011) multiplied by the frontal area of the vehicle (2.3 m^2) (Doucette and McCulloch, 2011) and the ambient air density (1.207 kg/m^3) (Jimenez-Palacios, 1999), divided by the mass of the test vehicle (1,374 kg) (Li et al., 2008a).

Errors from the VSP calculation may arise due to the fact that there are a number of vehicle variables which affect vehicle emission that are not captured by VSP. These include engine speed, engine friction losses, transmission losses, the power consumption of auxiliary systems (such as air-conditioning) and vehicle loading (Jimenez-Palacios, 1999).

Nevertheless, a number of subsequent studies have shown VSP to be a very useful proxy variable for CO_2 emission estimation (Xu et al., 2010; Song and Yu, 2009; Coelho et al., 2009), and the VSP-based emission modelling approach is an increasingly accepted methodology (Xu et al., 2010).

The VSP for each second of data recorded during the 48 PEMS Headingley laps was calculated using Equation 4.3. Figure 4.10 plots the average PEMS measured CO_2 emission in g/s at each VSP value (where the calculated VSP has been rounded to the nearest integer). When VSP is less than zero the average emission rates are consistently low, as the vehicle is decelerating. For positive VSP, the average CO_2 emission rate rises nearly linearly as the engine power demand increases.

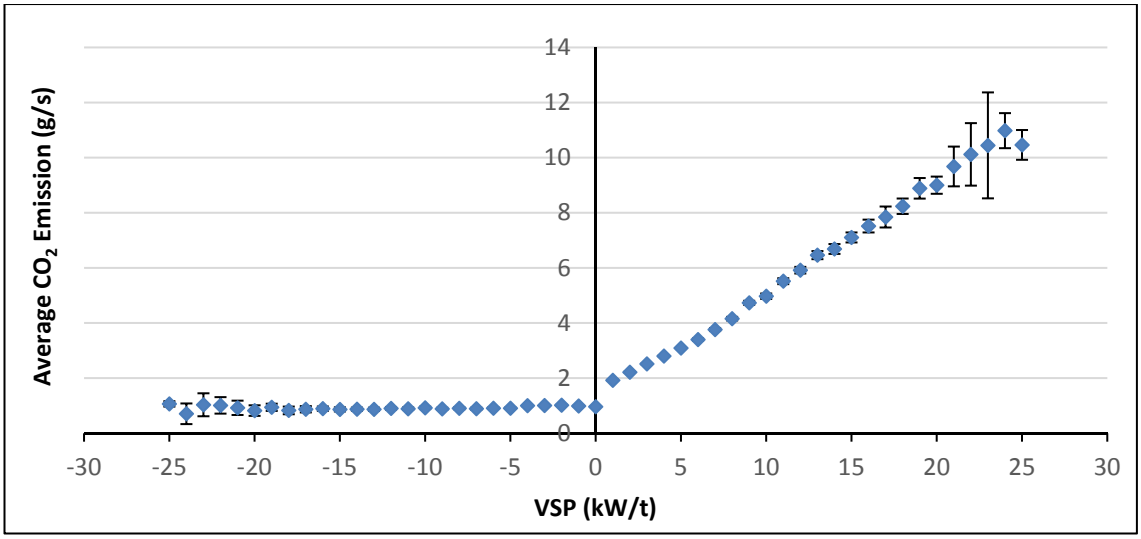

Figure 4.10: Average CO_2 Emission at Each VSP (Euro 4 Passenger Car: 56,986 Seconds of Data)

Figure 4.11 demonstrates why VSP (as a proxy of for instantaneous engine power output) is the primary variable used in modal emission models, rather than vehicle speed. The graphs show plots of VSP and vehicle speed against CO_2 emission for each second of a 760 s test run through Headingley. Clearly, the relationship between VSP and CO_2 emission allows VSP to be used as a much better indicator of CO_2 emission than vehicle speed.

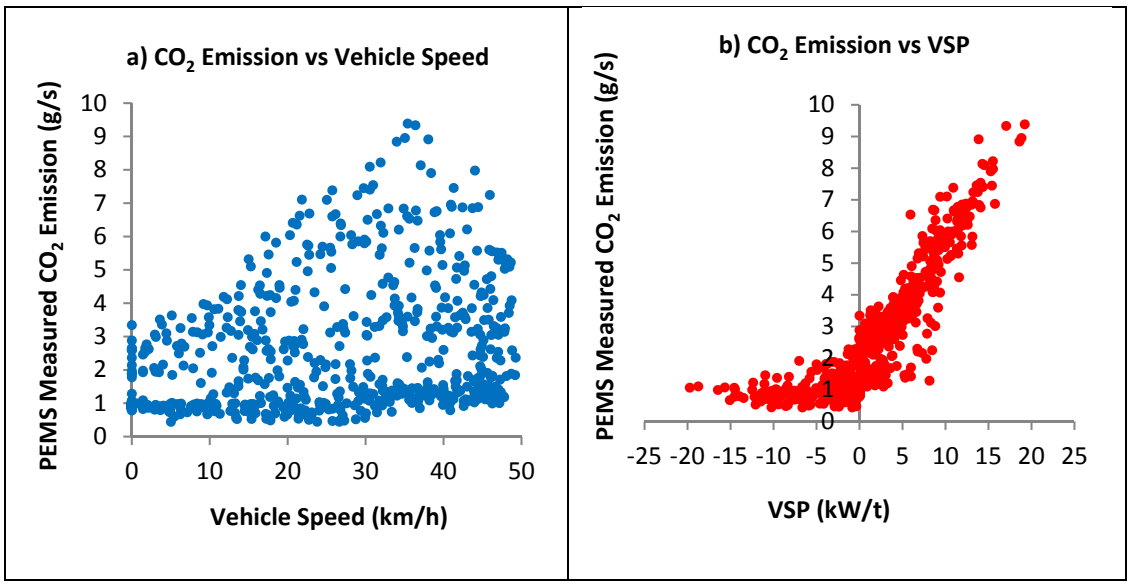

Figure 4.11: Plot of a) Vehicle Speed and b) VSP against PEMS gCO_2/s

4.5.3 MOVES Modal Binning Methodology

Modal methodologies group VSP values into discrete operating mode bins rather than analysing each VSP value individually (as in Figure 4.10). The MOVES emission model further sub-divides the VSP groups by three vehicle speed categories (1-25 mph; 25-50 mph; and 50+ mph) and also has one bin for 'Braking' and one for 'Idling' (Liu and Frey, 2012). In total MOVES has 23 bins, these are described in Table 4.4.

Table 4.4: MOVES Operating Mode Bins by Speed and VSP Range (Liu and Frey, 2012)

VSP Class	Speed Class (mph)		
	$1 < v_t \leq 25$	$25 < v_t \leq 50$	$v_t > 50+$
30 ≤ VSP	BIN 16	BIN 30	BIN 40
27 ≤ VSP < 30		BIN 29	BIN 39
24 ≤ VSP < 27			
21 ≤ VSP < 24		BIN 28	BIN 38
18 ≤ VSP < 21			
15 ≤ VSP < 18		BIN 27	BIN 37
12 ≤ VSP < 15			
9 ≤ VSP < 12	BIN 15	BIN 25	BIN 35
6 ≤ VSP < 9	BIN 14	BIN 24	
3 ≤ VSP < 6	BIN 13	BIN 23	BIN 33
0 ≤ VSP < 3	BIN 12	BIN 22	
VSP < 0	BIN 11	BIN 21	

Other	
Braking	BIN 0
Idling	BIN 1

Braking = $a_t \leq -2$ OR ($a_t \leq -1.0$ AND $a_{t-1} \leq -1.0$ AND $a_{t-2} \leq -1.0$)
Idling = $-1.0 \leq v_t < 1.0$

Where,
a_t = acceleration at the t^{th} second (mph/s)
v_t: instantaneous speed at the t^{th} second (mph)

For each operational mode bin, an average emission rate is calculated, for each emission species. Specific emission factors are available in MOVES for each vehicle type, defined by fuel type and age. The estimated total trip emission for each vehicle is calculated from the sum of the bin average emission rate (g/s), multiplied by the time (seconds) spent in that VSP bin throughout the test (Zhai et al., 2008), as described in Equation 4.4 below.

Equation 4.4:

$$TE = \sum_{i}^{I} TVSP_i \cdot ER_i$$

Where,

- i : VSP Bin, 1, 2, …., I
- TE : total trip emission (g)
- $TVSP_i$: test time spent in VSP Bin *i* (s)
- ER_i : average emission rate for VSP Bin i (g/s)

4.5.4 MOVES Real-World Emission Factor Estimation

The calculation of micro-scale emission estimates in MOVES involves creating scenarios through a "Run Specification" interface, which allows the user to specify the scale of the scenario (National, County or Project), the time period for the emission simulation, the geographical location to be modelled, the vehicle types within the test area, the types of road to be modelled and the required pollutants in the modelling. Depending on the scale of the project, further pre-processing tools enable the user to input detail on other factors such as the vehicle population and age distribution, vehicle miles travelled, average speed distribution, fuel type fraction and road type distribution (EPA, 2012b).

For micro-scale modelling, the project data manager facilitates the input of link drive schedules, which enable the second-by-second transient vehicle speed (mph), road grade (%) and link ID to be entered into the model, from which emission estimates can be calculated. In this study, the 1 Hz velocity data for each of the 48 test runs recorded during the Headingley PEMS survey were entered into the link drive schedule, the test network road type was categorised as "urban unrestricted access" and the test vehicle was described in the model as a two year old 2005 petrol passenger car.

The distribution of MOVES lap estimated emission factors against the PEMS measured gCO_2/km real-world factors is displayed in Figure 4.12. The MOVES lap average emission of 425 gCO_2/km is only slightly lower than the PEMS average of 442 gCO_2/km. The range of emission estimates from MOVES, 281 gCO_2/km to 549 gCO_2/km, is also similar to the on-road measurement range of 315 gCO_2/km to 587 gCO_2/km. The good fit of the MOVES estimates to the real-world emission is reflected in a MAPE value of only 7.9% for the 48 test laps. On average the MOVES estimate was slightly lower than the real-world emission with 36 of the 48 estimates underestimating the CO_2 emission, with a maximum underestimate of 17.7%. The maximum overestimate was 16.6%, for the 12 laps where the model predicted CO_2 emission greater than PEMS measurement. The analysis suggests that, on the whole, MOVES performs very well in estimating real-world emission over the length of the 4.8 km test lap.

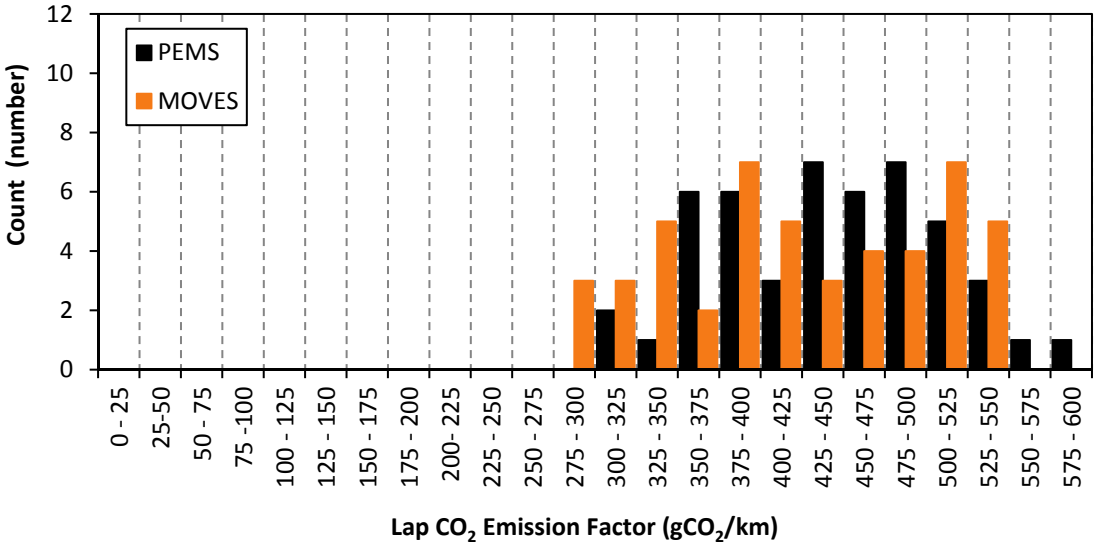

Figure 4.12: Distribution of Headingley Lap CO_2 Emission Factors from the PEMS Real-World Measurement and the MOVES Modelled Estimate (n=48)

The distribution of MOVES estimated section estimates shows good agreement with the PEMS measured section gCO_2/km (Figure 4.13). The average section CO_2 emission from MOVES of 446 gCO_2/km is close to the average measured section emission of 471 gCO_2/km, with a range from 196 gCO_2/km to 1,445 gCO_2/km for the MOVES section estimates compared with 216 gCO_2/km to 1,364 gCO_2/km recorded by PEMS. The maximum difference between the MOVES section estimate and the real-world value was an overestimation by 33.9%; the minimum underestimation for a section was 33.4%. The MAPE statistic calculates an average absolute difference of 10.9% over each of the 384 sections and 10.8% when the shorter turning Sections 3 and 6 are excluded.

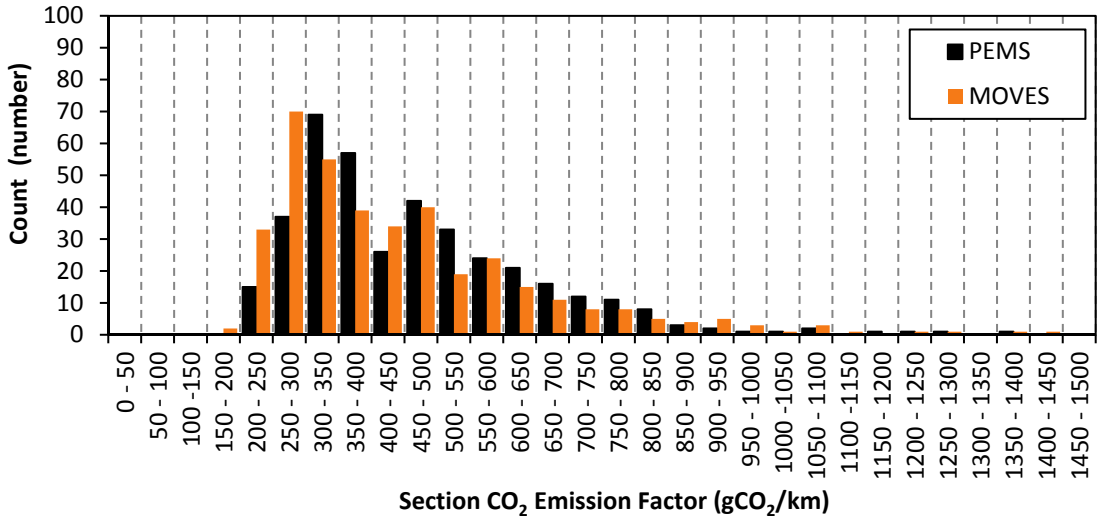

Figure 4.13: Distribution of Headingley Section CO_2 Emission Factors from the PEMS Real-World Measurement and the MOVES Modelled Estimate (n=384)

Figure 4.14 presents box plots of the MOVES estimate of the PEMS measured CO_2 emission as a percentage, by lap and broken down into individual sections. The blue dashed line at 100% marks where the MOVES estimate is equal to the PEMS measured emission.

For the test lap, the median MOVES percentage estimate of the PEMS real-world CO_2 emission was 95.9% with an IQR between 89.1 and 100.3 (11.1%). At the section level there is some variation in accuracy, with a range in median estimate from 107.6% for Section 1 to 80.5% for Section 8, and an overall average of 93.1%. The average IQR for a section was 10.7%, with a range from 7.4% to 14.6%. As noted earlier in the chapter, Section 1 and Section 8 are the sections with the steepest road grade; in Section 8 the traffic flow is uphill and in Section 1 downhill. Without road grade in the MOVES calculation of VSP, the second-by-second analysis likely assigned incorrect output operation modes and therefore incorrect CO_2 emission rates for these sections; underestimating CO_2 emission in Section 8, where the calculated VSP will be lower than the on-road engine power output (due to the decelerating force of gravity uphill) and overestimating Section 1 emissions where the modelled VSP will be higher than the on-road engine power output (due to the accelerating force of gravity downhill). The effect of road grade is addressed in Chapter 5. From the IQR values across all the sections, the error associated with using the MOVES model, without road grade, for micro-scale estimation of CO_2 emission is demonstrated to be in the range of an underestimation of 22.5% to an overestimation of 15% (90% of section estimates are between these values).

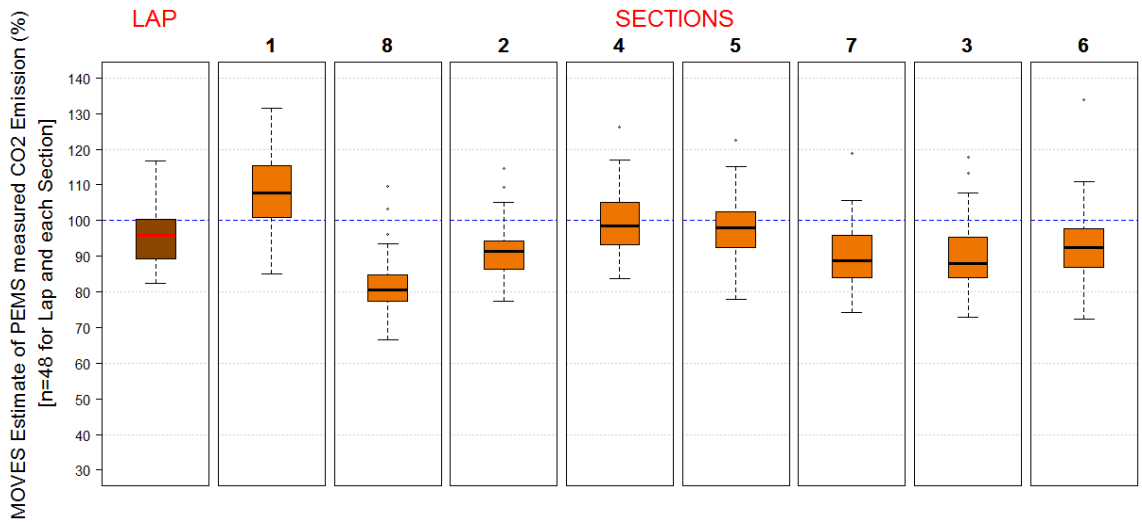

Figure 4.14: MOVES Estimate of PEMS Measured gCO_2/km Emission, by Lap and Section

The MOVES estimates of the test vehicle CO_2 emission are clearly superior to the estimates made by either the HBEFA or EFT. However, it should be noted that part of the accuracy of the model must be related to how well the test vehicle used in the PEMS study represents an average 2005 petrol passenger car, which is two years old in MOVES, as apart from this information, the MOVES model allows no further calibration to describe the test vehicle (i.e. by engine size, vehicle weight, loading, emission standard). As MOVES is an American model, the average vehicles described for each vehicle type and their respective emission outputs are unlikely to be in such good agreement with a typical European vehicle fleet.

4.6 PHEM INSTANTANEOUS EMISSION MODEL

4.6.1 PHEM Background

Since 2000, the Institute for Internal Combustion Engines and Thermodynamics at the Technical University of Graz (TU-Graz) has been developing a Passenger car and Heavy duty Emission Model (PHEM) (Hausberger, 2003). PHEM has been developed utilising both Heavy Duty Vehicle (HDV - which comprises HGVs, buses and coaches) engine test-bed analysis and chassis dynamometer measurement of passenger cars and LCVs, to establish engine emission maps. These engine maps detail the expected fuel consumption and exhaust emission of the emission species Nitrogen Oxides (NO_x), Carbon Monoxide (CO), Hydrocarbons (HC), Particulate Mass (PM), and Nitrogen Monoxide (NO), for each combination of engine power output and engine speed over the operating range of the engine.

The creation of engine maps requires the second-by-second measurement of vehicle power output and engine speed over dynamic test cycles, with simultaneous analysis of the exhaust emission. The measurements are then rendered into a three dimensional (3D) vector space depicting engine power, engine speed and the mean value of emission as shown in Figure 4.15 (Luz and Hausberger, 2015).

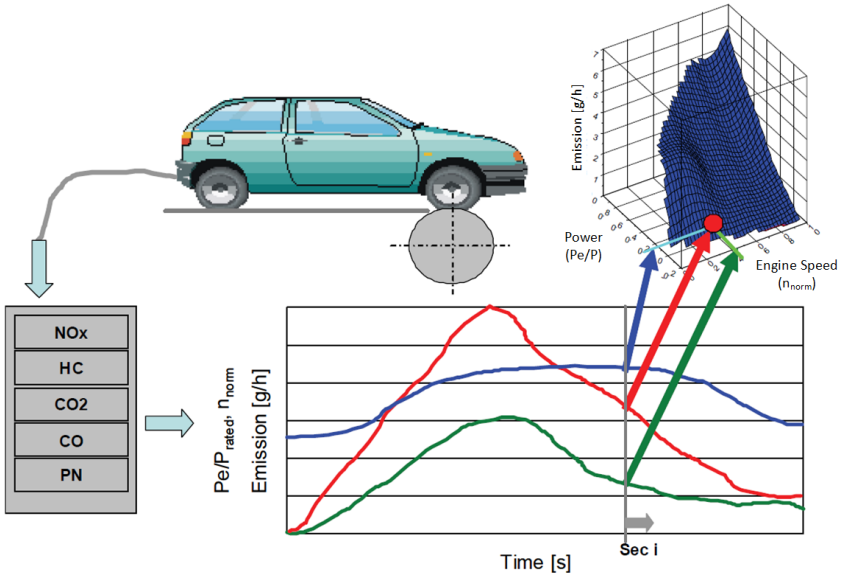

Figure 4.15: Diagram for Creating Engine Maps From Dynamic Test Cycles (Luz and Hausberger, 2015)

This engine mapping analysis has been performed on a wide range of vehicles, and average engine maps have been created for passenger, LCVs and HDVs, with petrol (Otto) or diesel engines, from Euro 0 to Euro 6 EU emission standards. Figure 4.16 shows the extent of the engine mapping that has taken place in PHEM. The TU-Graz reports that *"in comparison to other detailed models, PHEM has the largest database for individual vehicle emission models by far"* (Luz and Hausberger, 2015).

	PASSENGER VEHICLES		LIGHT DUTY VEHICLES		HEAVY DUTY VEHICLES
	Petrol	Diesel	Petrol	Diesel	Diesel
EURO 0	2	(2)	(3)	(3)	41
EURO 1	(2)	(2)	(3)	(3)	13
EURO 2	(2)	4	(3)	(3)	22
EURO 3	9	8	(3)	(3)	26
EURO 4	23	24	(3)	(3)	6 with EGR 3 with SCR (1)
EURO 5	(2)	1 (2)	(3)	(3)	7 with SCR
EURO 6	(2)	(2)	(2)	(2)	(2)

(1) The Euro 4 emission map is a weighted average of heavy duty vehicles with Exhaust Gas Recirculation (EGR) and those with Selective Catalytic Reduction (SCR).
(2) Maps derived from previous emission classes by reduction factors and calibrated by available measured values due to a lack of measured data.
(3) Maps derived from passenger vehicle data and calibrated by light duty vehicle measured values.

Figure 4.16: Filled Engine Maps (measured vehicles / engines per category) (Luz and Hausberger, 2015)

In conjunction with the engine maps, each vehicle category has a default database of average vehicle parameters which are required for calculating the engine power output and engine speed. These parameters include the weight and load of the vehicle, the drag coefficient, the rolling resistance coefficient, the cross-sectional area, and the final drive and transmission ratios (Luz and Hausberger, 2015).

As further data becomes available, the PHEM model is being continuously improved and the base data updated. In addition, the TU-Graz is continuing to increase the functionality of the model to include new vehicle types.

4.6.2 PHEM Engine Load Calculation

The PHEM modelling process requires input of a drive cycle. This consists of data detailing the second-by-second vehicle speed (km/h) and longitudinal road gradient (%) for a test vehicle over a given test cycle.

Utilising second-by-second transient speed and road grade inputs and the vehicle parameters described in the PHEM database (i.e. vehicle weight, cross sectional area, rolling resistance, etc.) the PHEM model calculates the instantaneous engine power output required at each second over the driving cycle using Equation 4.5 below, which describes the vehicles' driving resistances and transmission losses (Luz and Hausberger, 2015).

Equation 4.5: PHEM Instantaneous Power Output

$$P_{output} = P_{rolling\ resistance} + P_{air\ resistance} + P_{acceleration} + P_{road\ gradient} + P_{slip} + P_{transmission} + P_{auxilliaries}$$

Together with engine power output, engine speed is also simulated in PHEM. This is calculated from the transmission ratios described for each vehicle type in the PHEM database and a driver gear shift model.

From the calculated engine power output and the engine's speed, the instantaneous fuel consumption and vehicle emission are interpolated from the measured engine map for the type of test vehicle and reported for each second (Luz and Hausberger, 2015).

PHEM also contains a number of other sub-models to enhance the emission simulation. These include the cold start module that corrects for vehicle operation below the usual operating temperature and time alignment functions that correct for time delays between instantaneous engine power output and analysis of the resultant emissions during the chassis dynamometer testing. A schematic diagram of the PHEM Model is presented below.

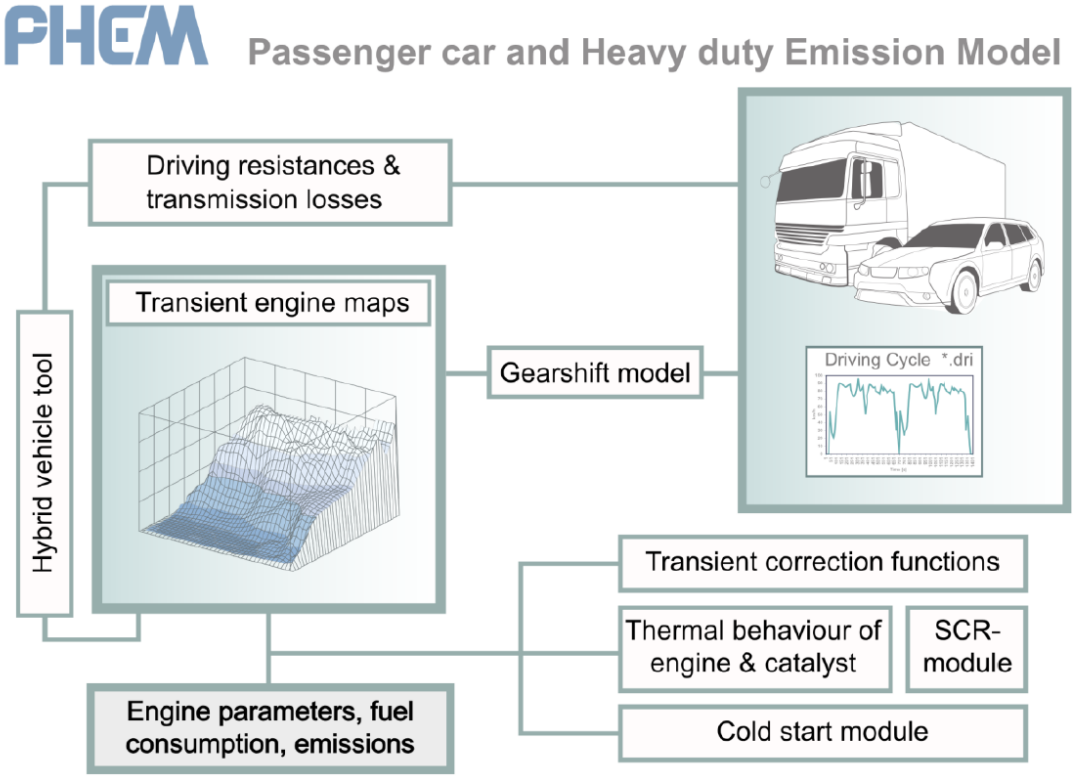

Figure 4.17: Schematic Picture of PHEM (Luz and Hausberger, 2015)

The PHEM approach means that, for any drive cycle, the instantaneous fuel consumption and vehicle exhaust emission can be estimated from a vehicle's second-by-second speed curve and road gradient data (Zallinger et al., 2009; Luz and Hausberger, 2015).

The major advantage of PHEM over modal emission modelling techniques is that the emission estimates in PHEM utilise an engine map of averaged emission values which define very narrow engine operating regions (engine power output and engine speed). MOVES utilises 23 discrete VSP-speed bins, whereas the most basic engine maps in PHEM contain 45 engine power output and engine speed categories, with respective average fuel consumption and emission values. The most detailed engine maps in PHEM have more than 350 bins.

Figure 4.18 shows the PHEM fuel consumption engine map for a Euro 4 Gasoline Passenger Car. This engine map has 345 engine power output / engine speed categories with a measured average fuel consumption value.

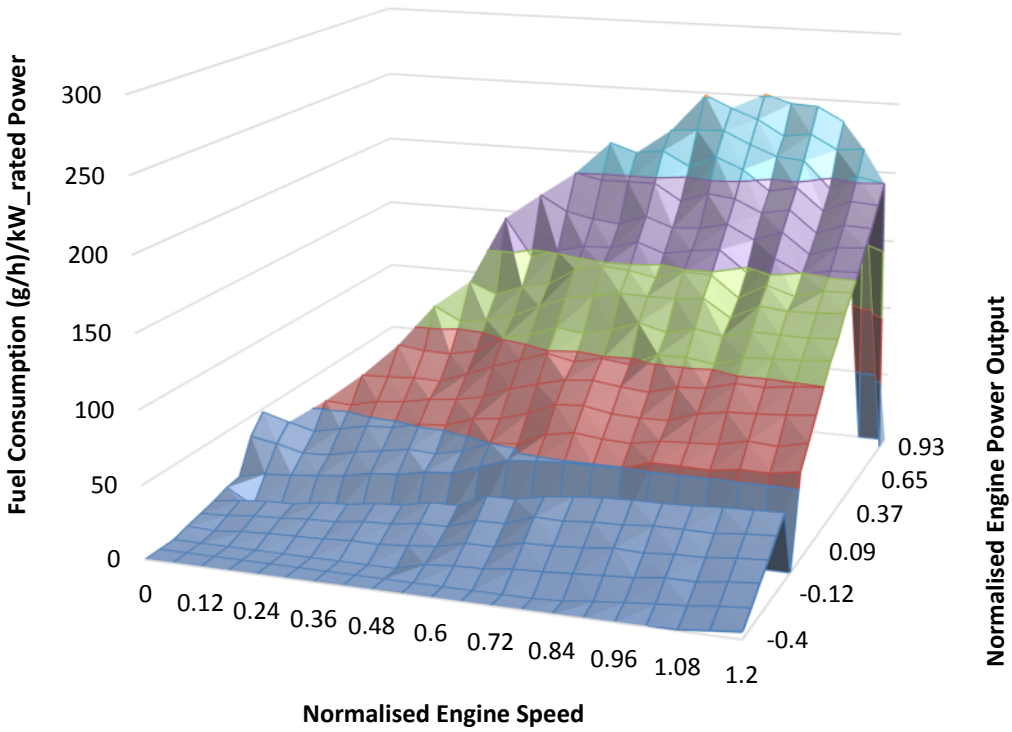

Figure 4.18: **PHEM Fuel Consumption Engine Map: Euro 4 Gasoline Passenger Car**

Measuring the average fuel consumption / emission over a greater number of narrower operating zones should result in a greater accuracy to the PHEM model when compared with modal emission models since the errors caused by averaging are reduced.

4.6.3 Vehicle Fleet Modelling in PHEM

PHEM additionally has the functionality to model vehicle fleets through the PHEM Advanced User Interface (PHEM Advance). Fleet emission can be estimated by measuring a large number of drive cycles (speed profile and road grade) across all vehicle types (bus, car, etc.) through a road network.

In PHEM Advance each recorded drive cycle (.FZP file in PHEM) must be labelled with a vehicle type ID to distinguish the category of the recorded vehicle. These categories are described in Table 4.5.

Table 4.5: PHEM Default Vehicle ID Numbers

100 – Passenger Car: Size II, Diesel and Petrol, Euro 0 – Euro 6
200 – Rigid Truck HGV N_2/N_3: Size I & II, Diesel, Euro 0 – Euro 6, Euro 4 and Euro 5 distinguished by Exhaust Gas Recirculation (EGR) and Selective Catalytic Reduction (SCR)
300 – Light Commercial Vehicles N_1: Size N_1 I-III, Diesel and Petrol, Euro 0 – Euro 6
400 – Truck & Trailer / Semitrailer HGV N_2/N_3: Size N_2/N_3 II average, Diesel, Euro 0 – Euro 6, Euro 4 and Euro 5 distinguished by EGR and SCR
500 – City Bus M_2/M_3: Size M_2/M_3 II average, Diesel, Euro 0 – Euro 6, Euro 4 and Euro 5 distinguished by EGR and SCR
600 – Bus M_2/M_3: Size M_2/M_3 II average, Diesel, Euro 0 – Euro 6, Euro 4 and Euro 5 distinguished by EGR and SCR
700 – Motorcycle & 800 – Moped: Not Available

The composition of the vehicle fleet is determined by the fleet data file (.FLT). This tabulates each of the categories (100, 200, 300, 400, 500 and 600) and designates the distribution (%) of vehicle types in that category, with vehicle type described by fuel type (diesel / petrol); vehicle size (which corresponds to the vehicle weight); and Euro emission standard (Euro 0 to 6). An example of the distribution for the vehicle category 'passenger cars ID 100' is shown in Figure 4.19.

c Passenger Car		Gasoline			Diesel		
c ID 100		Size I	Size II	Size III	Size I	Size II	Size III
c			average			average	
EURO 0	5%	0	0.04369	0	0	0.00949	0
EURO 1	2%	0	0.01211	0	0	0.00726	0
EURO 2	8%	0	0.04324	0	0	0.03848	0
EURO 3	28%	0	0.08731	0	0	0.19194	0
EURO 4	14%	0	0.06851	0	0	0.06847	0
EURO 5	43%	0	0.15418	0	0	0.27532	0
EURO 6	0%	0	0	0	0	0	0
EURO 7	0%	0	0	0	0	0	0
EURO 8	0%	0	0	0	0	0	0
EURO 9	0%	0	0	0	0	0	0
c total	100%	0%	41%	0%	0%	59%	0%

Figure 4.19: Example of FLT Template for Passenger Cars ID 100

In this example, 41% of the passenger cars are driven on petrol and 59% are on diesel. The Euro 5 category comprises 43% of the passenger car fleet and is sub-divided as approximately 15.4% Petrol and 27.5% Diesel. The grey boxes represent vehicle types that are not yet available in the latest PHEM release. The .FLT files can be amended by adjusting the percentages to reflect the composition of the vehicle fleet for each vehicle category on the analysed road network. Each vehicle category is described by a .GEN file that organises the model input files for that specific

vehicle type. The input files include the vehicle specification parameters (average weight, loading etc.); the engine map; and the catalyst map, all of which are required in the calculation of the vehicle's instantaneous exhaust emission.

The ID number representing the vehicle types (i.e. 100, 200, 300... see Table 4.5) is defined in the drive cycle file (.FZP) file, but the vehicle Euro standard, size and fuel type are assigned by a random number generator in PHEM, such that the overall composition of the modelled fleet is the same as the composition specified in the .FLT file for each vehicle type ID (Luz and Hausberger, 2015).

4.6.4 PHEM Real-World Emission Factor Estimation

Producing vehicle emission estimates from PHEM requires the preparation of three primary input file types; a drive cycle file (.FZP); a fleet data file (.FLT) and route section files (.STR). Importing these files into the ADVANCE mode editor creates an .ADV job file which when run by PHEM processes the input data and calculates output files which contain detailed emission and power results for each vehicle (.mod) along with average values per vehicle (.vehicle.sum) and average per segment (.segment.sum).

4.6.4.1 Drive Cycle (.FZP)

In order to provide Headingley lap and section CO_2 emission estimates, separate drive cycle (.FZP) files were populated with the second-by-second transient vehicle data for each of the 48 test runs. The drive cycle required by PHEM comprises continuous second-by-second data for Time; Latitude; Longitude; Velocity; Vehicle ID, Road Grade; Vehicle Type ID and Section.

- The time, latitude, longitude and velocity for each lap recorded during the Headingley PEMS survey were inputs for each drive cycle, with the latitude and longitude provided by the GPS system and the velocity from the vehicle CAN.
- As the PEMS GPS measurement of altitude and therefore road gradient was found to contain significant errors, the grade was set to zero for each second of data, essentially modelling the route as flat.
- Vehicle ID was set to 1 because there was only one test lap per .FZP file.
- The vehicle type was set to 100, which is the numerical abbreviation for passenger cars in PHEM and references the drive cycle to the correct engine emission maps for the vehicle type.

- The Section ID was set 1 as the emissions were calculated on a lap-by-lap basis and the section emission calculated from the generated lap files.

4.6.4.2 Fleet Data File (.FLT)

To select the correct engine map and parameters for a vehicle in PHEM, each vehicle category has a numerical abbreviation (listed in Table 4.5). Every drive cycle is given a vehicle type ID which acts as a reference to the vehicle category in the fleet data file (.FLT). The vehicle type ID number assigns each drive cycle to the correct vehicle category in the .FLT file, and the .FLT file then distributes the drive cycles to sub-categories (segregated by Euro standard, weight and fuel type) which match the percentage composition described in the .FLT file. This ensures that the vehicle fleet in the model is representative of the real-world fleet.

Calculating the emission factor for an individual vehicle in PHEM requires amendment of the fleet data file (.FLT). Instead of representing a fleet of vehicles of varying Euro standard, fuel type and weight, the .FLT template was amended to represent the specific vehicle, in this case by specifying the entire passenger car vehicle fleet as Euro 4 petrol vehicles.

The FLT file ensures the correct .GEN files for the vehicle are used in proportion to the described fleet. The .GEN files dictate the engine map (.MEP and .MAP), full load curve (.FLD) and vehicle specifications (.VEH) applied to the emission calculations for the drive cycle.

The .VEH files contain average parameters for that vehicle category, including: vehicle mass; cross sectional area; rated engine power; rated engine speed and engine idling speed. Prior to running the model, the parameters within the Euro 4 petrol passenger car .VEH file were adjusted to give a better representation of the Ford Mondeo. The parameters amended were kerbweight to 1,374 kg (Li et al., 2008a), loading to 150 kg (PEMS equipment weight), rated power to of 92 kW (123 bhp) at 6,000 rpm (Ford, 2005), an idle engine speed of 850 rpm, an aerodynamic drag coefficient of 0.32 (Doucette and McCulloch, 2011) and a frontal area of 2.3 m^2 (Doucette and McCulloch, 2011).

The results also contain the emission estimates calculated with the Euro 4 petrol passenger car .VEH default values as comparison. These defaults are a kerbweight of 1,198 kg; loading 50 kg; rated power 76 kW (102 bhp); rated engine speed 5,752 rpm; engine idle speed 798 rpm; aerodynamic drag coefficient 0.3113 and frontal area 2.2 m^2.

4.6.4.3 Route Section File (.STR)

For the model to run at least one .STR file needs to be created. This file assigns an identification number to each road section, which corresponds to the Section ID in the .FZP files. The .STR can also be used to describe the start and end points of any specified route sections in the modelling.

For each of the 48 test runs, the test route was added as one complete section, so the start and end GPS latitude and longitude points from the .FZP file were used, and the Section ID was set to 1. The .STR files enable calculation of separate section specific total emission estimates, for a range of exhaust pollutants, if the input .FZP file is coded with more than one Section ID.

4.6.4.4 Analysis of PHEM Emission Estimates for the Headingley Test Data

The emission model PHEM was employed to calculate estimates of the CO_2 emission for each test run from the Headingley PEMS survey. The transient vehicle data were combined in PHEM with data specific to the test vehicle's specifications to generate a CO_2 emission value for each second of recorded data. CO_2 emission data are not calculated directly in PHEM but are derived from the fuel consumption (kg/hr) value generated for each second. The fuel consumption is converted to CO_2 (g/s) using the Department of Energy and Climate Change's (DECC) GHG conversion factor of 3,135 $kgCO_2$ emission per tonne of combusted petrol (DECC, 2012). The second-by-second CO_2 emission estimates are aggregated to calculate CO_2 emission factors for each lap and section.

The distribution of PHEM estimates (with the .VEH file specifications for the test vehicle) for the modelled Headingley lap CO_2 emission factors are presented in Figure 4.20 alongside the PEMS measured lap emission. The average PHEM lap emission rate was 402 gCO_2/km compared to 442 gCO_2/km for the average PEMS recorded lap emission rate. The range for the PHEM modelled lap emission rate is from 268 gCO_2/km to 515 gCO_2/km compared with 315 gCO_2/km to 587 gCO_2/km for the PEMS measured lap emission. Whilst the MAPE of 10.0% is relatively low, the model consistently underestimates the real-world emission, with 45 of the 48 PHEM lap estimates below the measured PEMS lap values. The lap CO_2 emission underestimation is clear from the distribution, with 22.9% of the PHEM laps recorded emission factors being ≤ 350 gCO_2/km compared to 6.3% of PEMS recorded laps. Likewise, only 6.3% of PHEM laps had an emission factor ≥ 500 gCO_2/km, whereas in 20.8% of PEMS recorded laps the emission factor was greater than this value.

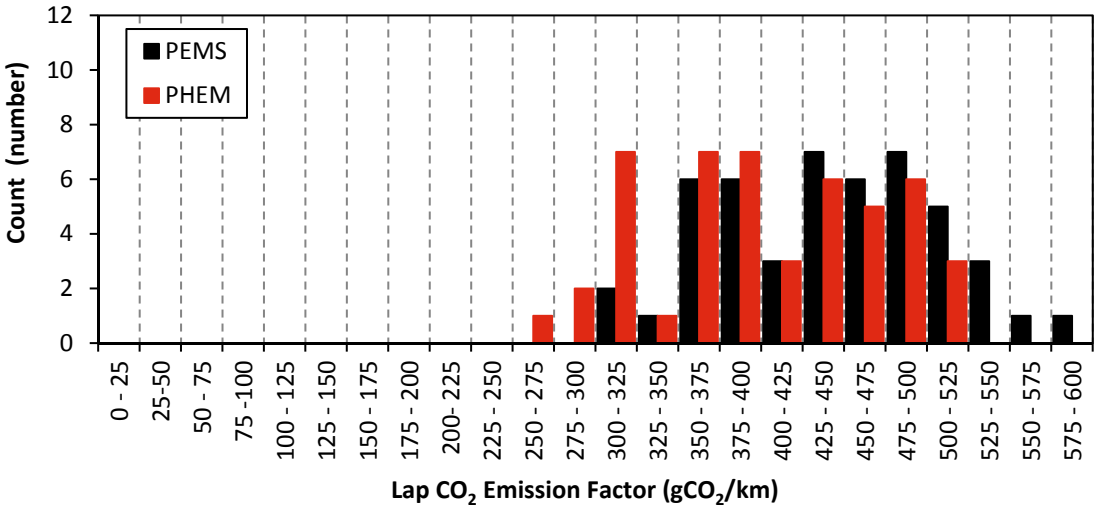

Figure 4.20: Distribution of Headingley Lap CO_2 Emission Factors from the PEMS Real-World Measurement and the PHEM Modelled Estimate (n=48)

The data in Figure 4.21 show a similar slight underestimation of the PEMS emission rate, in the PHEM model. The PHEM average section CO_2 emission factor over the 384 sections was 420 gCO_2/km with a range from 169 gCO_2/km to 1,326 gCO_2/km whereas the PEMS value was 471 gCO_2/km with a range from 216 gCO_2/km to 1,364 gCO_2/km. The MAPE over the 384 sections between the PEMS emission and the PHEM modelled emission was 12.3%, which is slightly greater than the MOVES MAPE value. Again the distributions reveal a greater number of 'low' emission factors from the PHEM model than recorded in the real-world; with 28.1% of PHEM section emission rates ≤ 300 gCO_2/km compared to only 13.5% ≤ 300 gCO_2/km as measured by the PEMS.

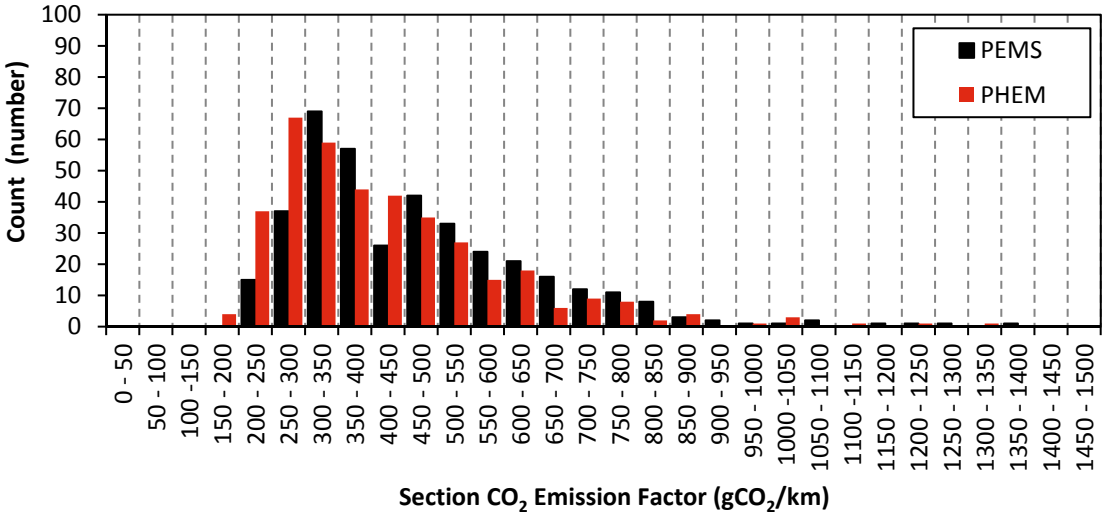

Figure 4.21: Distribution of Headingley Section CO_2 Emission Factors from the PEMS Real-World Measurement and the PHEM Modelled Estimate (n=384)

The PHEM estimate of the PEMS measured gCO_2/km is presented in Figure 4.22, by lap and by each individual section. For the test lap, the median PHEM percentage estimate of the PEMS measured CO_2 emission was 90.1% with an IQR of 9.6% (95.4% - 85.8%). At the micro-scale section level, there is a degree of section-to-section variability in the ability of PHEM to estimate real-world emission, with a range in median estimate from 97.8% in Section 5 to 78.5% through Section 8. The overall average PHEM percentage estimate of the PEMS measured emission over the 384 sections was 89.6%, with an average section IQR of 9.3%, ranging from 6.0% to 11.6%.

As with MOVES, Section 8 has the lowest median percentage estimate of the real-world emission whilst Section 1 has the second highest; these findings strengthen the hypothesis that road grade could play a significant role in micro-scale estimation. The Section 3 and Section 6 percentage estimates using PHEM are noticeably lower than for all other sections excluding Section 8. Section 3 and Section 6 are the shorter turning sections and it is possible that the gear shift model used to identify the likely engine speed, and hence the position on the engine emission map, may be somewhat compromised over these sections, which are probably atypical of usual transient vehicle real-world drive cycles.

The likely error associated with using the PHEM model, without road grade, for the micro-scale estimation of CO_2 emission is in the range of an underestimate of 25% to an overestimate of 7.5% (90% of section estimates are within these values).

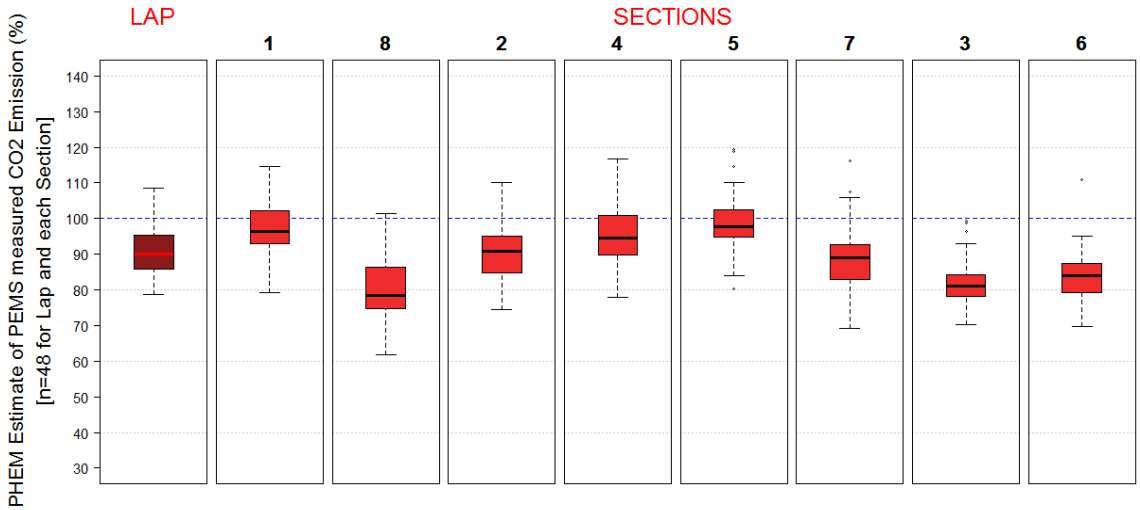

Figure 4.22: PHEM Estimate of PEMS Measured gCO_2/km Emission, by Lap and Section

PHEM estimates of the PEMS measure lap emission rates were also made using the default Euro 4, petrol, passenger car settings discussed in Chapter 4.6.4.2 (i.e. PHEM modelling was conducted without update of the .VEH file to reflect the test vehicle). Figure 4.23 presents the distribution of PHEM estimates of the lap average CO_2 emission rate for each of the 48 test lap,

against the distribution of the PEMS measured lap emission. The PHEM lap average emission is 334 gCO_2/km (range 225 gCO_2/km to 426 gCO_2/km) compared with an average of 442 gCO_2/km (range 315 gCO_2/km to 587 gCO_2/km) for the PEMS measurement. The MAPE of 24.6% shows a substantial difference between the modelled and real-world CO_2 emission values, as the model consistently underestimates the real-world emission, with all of the 48 PHEM lap estimates below the measured PEMS lap values. Of the lap emission factor estimates calculated from PHEM, 58.3% of the values were ≤ 350 gCO_2/km, while the PEMS survey recorded only 6.3% of the 48 laps with emission factors below 350 gCO_2/km.

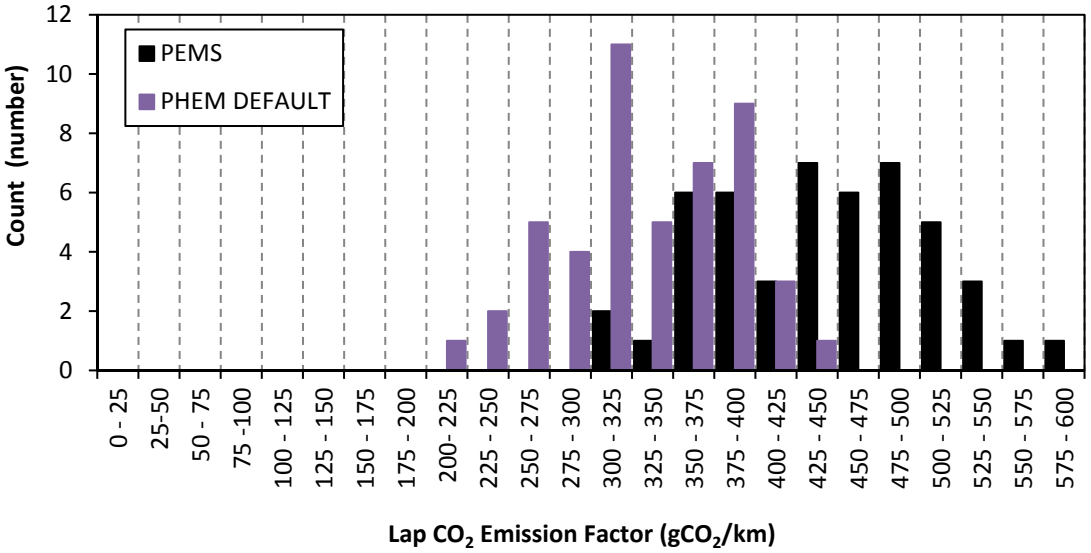

Figure 4.23: Distribution of Headingley Lap CO_2 Emission Factors from the PEMS Real-World Measurement and the PHEM Modelled Estimate with Default Euro 4 .VEH Parameters (n=48)

At the section level, the PHEM average gCO_2/km (with the default .VEH settings) over the 384 test runs was 347.9 gCO_2/km, with a range from 163 gCO_2/km to 1,036 gCO_2/km. The PEMS average emission factor was 471 gCO_2/km with a range from 216 gCO_2/km to 1,326 gCO_2/km. The average difference between the section PHEM estimated emission and the PEMS measured values was an underestimation of the on-road measured emission by 25.3%.

The error range from the default vehicle PHEM model in the micro-scale estimation of CO_2 emission is an underestimate of between 37.5% and 12.5% (≈ 90% of section estimates are within those values).

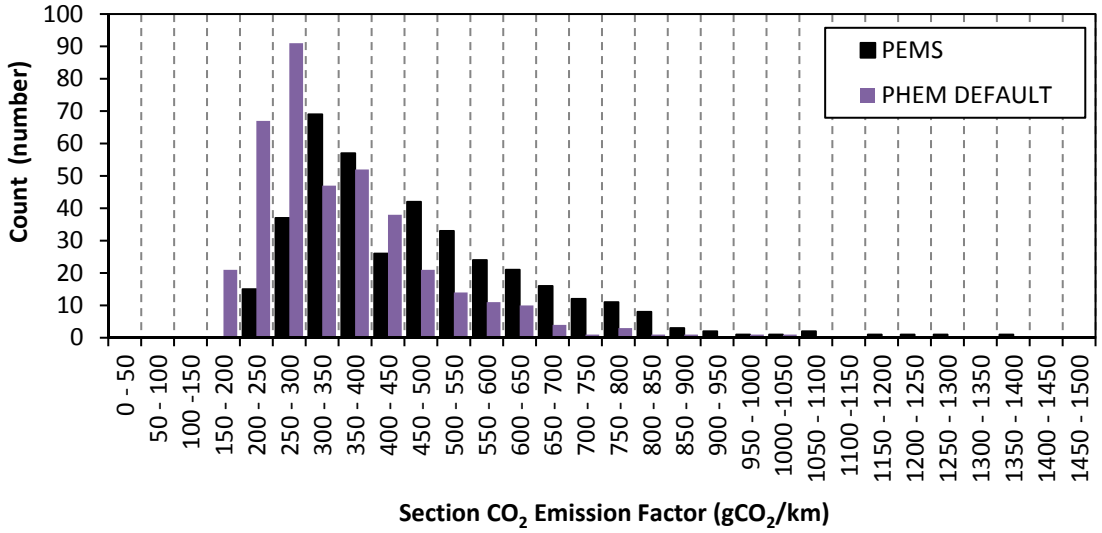

Figure 4.24: Distribution of Headingley Section CO_2 Emission Factors from the PEMS Real-World Measurement and the PHEM Modelled Estimate with Default Euro 4 .VEH Parameters (n=384)

Calibrating the .VEH file in PHEM to match the test vehicle made a significant difference to the accuracy of the PHEM model in predicting the real-world PEMS recorded gCO_2/km values. This is demonstrated by the difference in the MAPE values calculated between the PEMS real-world emission and the two PHEM models. For the PHEM model with the default Euro 4 setting the MAPE was 25.3% compared to 12.3% for the PHEM model entered with the test vehicle specification data. The average estimate of the PEMS measured micro-section data was 74.6% (over the 384 test sections) for the default PHEM model, whereas for the PHEM model with the test vehicle specific data the average estimate was 89.6%. This analysis suggests that, in order to represent specific vehicles or vehicle fleets in PHEM, it is important to ensure that the PHEM vehicle data in the .VEH files are populated with values that accurately describe the average vehicle for each vehicle category in the modelled fleet.

4.7 MODEL COMPARISON

Figure 4.25 displays the frequency distributions of the modelled estimate of the PEMS measured real-world CO_2 emission during each of 384 the micro-scale sections, for each of the four models. Each of the x-axis categories spans the value stated ± 2.5%.

The distributions from the four models demonstrate the superior accuracy of the methodologies which use second by second-by-second data to estimate micro-scale emission over the modelling methods that use aggregate average speed data to discern emission estimates. The HBEFA and EFT models clearly significantly underestimate a majority of micro-scale section real-

world CO_2 emissions recorded during the Headingley PEMS survey. In contrast, whilst both MOVES and PHEM slightly underestimate the CO_2 emission factors recorded by the PEMS survey, they provide a good approximation of the on-road emission of the test vehicle. The standard deviation of the MOVES estimates is 11.63% compared to 10.45% in PHEM as the estimates are marginally more tightly dispersed around the mean in the latter. An ideal model would be both accurate (close to 100% estimation) and precise (all lap / section estimates give a similar percentage estimate). For the Headingley data, the average emission estimate and the MAPE calculations show the MOVES model provides a more accurate appraisal of the real-world CO_2 emission in this instance, whilst the standard deviation and the IQR show that the precision of the PHEM model is better albeit around a slightly lower mean.

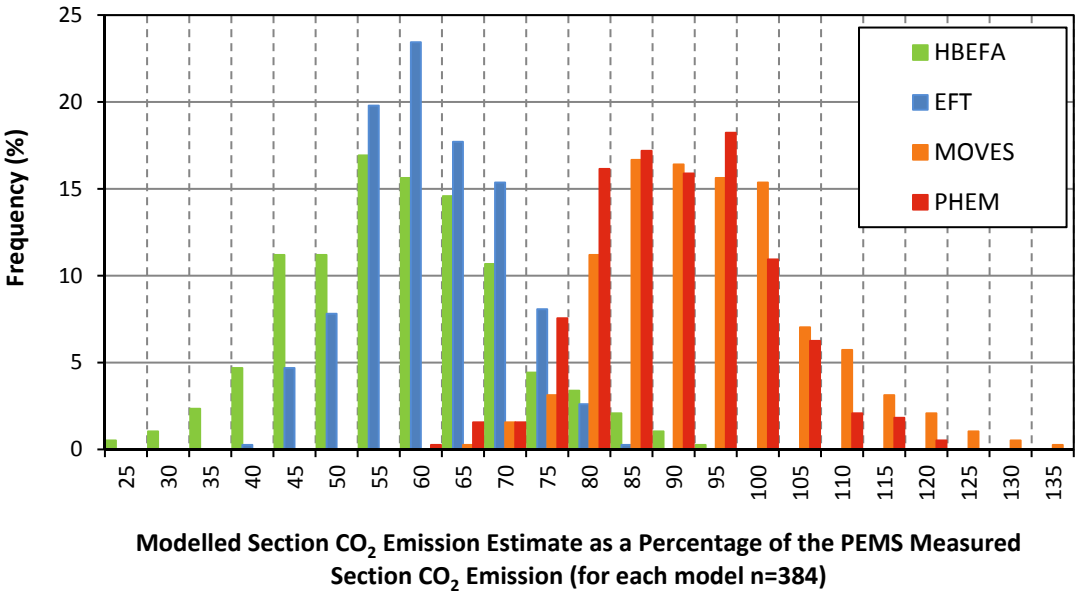

Figure 4.25: Emission Model Frequency Distributions: Modelled Lap Estimate of PEMS Measured Section CO_2 Emission (n=384)

Figure 4.26 presents a scatter plot of the PHEM estimate versus MOVES estimate of PEMS measured CO_2 emission, for each of the 384 recorded micro-scale sections. As shown in Figure 4.25 the majority of estimates from both models lie in the range from 80% to 100% of the PEMS measured CO_2 emission. The trend revealed in the graph shows the two models generate similar estimates of the PEMS measured emission, with an overestimate of section emission in PHEM likely to correspond to an overestimate in MOVES and an underestimate of section emission in PHEM likely to correspond to an underestimate in MOVES, however, the spread of the points demonstrate some clear differences in the section emission estimates of the two models. The dashed black line in Figure 4.26 shows the points at which PHEM generates the same section CO_2 emission estimates as the MOVES model. The greater number of points above the dashed line highlights that the MOVES model frequently generated greater section CO_2 emission

estimates than the PHEM model. This is especially clear for the shorter turning sections (Section 3 and Section 6).

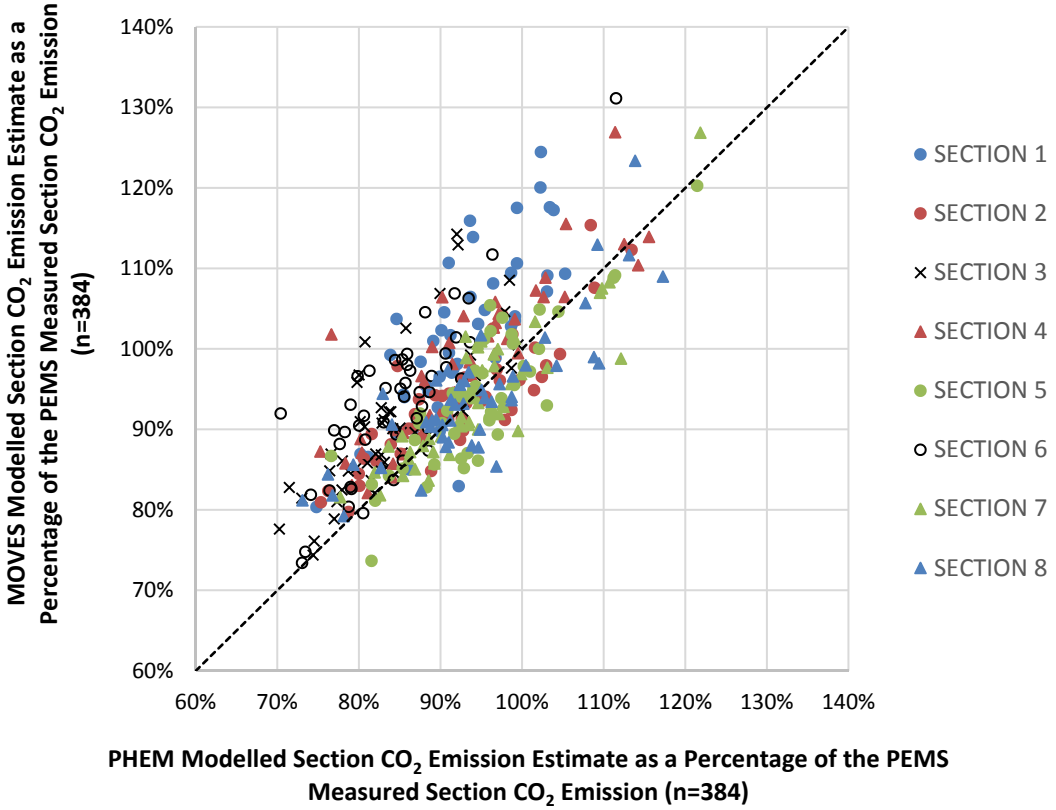

Figure 4.26: MOVES Estimate vs PHEM Estimate of PEMS Measured Section CO_2 Emission (n=384)

Although both the MOVES and PHEM models tend to underestimate the real-world vehicle CO_2 emission for the Headingley test vehicle (and there is a degree of variability in the accuracy of the estimates) there are a number of factors which make some discrepancy between the modelled emission and real-world emission inevitable. Neither the PHEM engine map nor the MOVES operation mode bins provide vehicle specific emission factors. This is because, the level of detail would require a vast number of emission tests, which would make the development of each model unfeasibly time consuming and expensive.

The development of the emission factors is the result of the analysis of a limited number of similar vehicles which are merged to represent an average vehicle. As such there will always be a difference between a test vehicle and the model category representing that vehicle. The PHEM model also relies upon a simulated gear shift model to calculate a second by second engine speed to act as a variable in defining the vehicles position on the engine emission map. Discrepancy between the timing of the modelled and real-world gear changes will result in some inaccuracy in the PHEM estimate.

Much of the observed discrepancy is likely to be caused by factors which have not been accounted for in the modelling; factors such as day-to-day variation in ambient temperature, starter battery state of charge and use of the vehicle's air-conditioning and heating systems, each of which can have a significant effect on vehicle fuel consumption (Mock et al., 2012). Inaccuracy of the simulated vehicle weight may also have had an influence on the PHEM modelled rate of CO_2 emission. Although the test vehicle's kerbweight is recorded in the vehicle's specification and the vehicle loading was estimated, the actual weight of the test vehicle was not directly measured. Future modelling would be improved by an accurate measure of the test vehicle weight, since misestimation may result in lower or higher modelled CO_2 emission than measured in reality. Road grade was also not accurately accounted for in the modelling. The observed difference in the accuracy of the Section 1 and Section 8 modelling from the EFT, MOVES and PHEM, highlights that this may be a very important factor for micro-scale simulation.

Table 4.6 provides a summary of the modelled Headingley lap CO_2 emission estimates for each of the four models. There are obvious discrepancies in the accuracy of the EFT and HBEFA CO_2 emission estimates for the 4.8 km test lap when compared to the MOVES and PHEM modelled CO_2 emission.

The EFT average speed emission model and the HBEFA traffic situation model are unable to replicate the CO_2 emission of the test lap with sufficient accuracy to make either of them a useful tool in estimating the real-world emission of the specific test vehicle. The CO_2 emission factors from these two models, for a Euro 4, petrol, 1.4 – 2.0 L, passenger car, are much lower than measured in the on-road PEMS survey. The EFT CO_2 emission factors are based on NEDC type-approval data (Boulter et al., 2009), which have been shown to be unrepresentative of real-world driving and therefore real-world emission (Weiss et al., 2011b; Chen and Borken-Kleefeld, 2014; Mock et al., 2012). This is despite the fact that the EFT includes a (DEFRA and DfT agreed) "uplift factor" of +15% on the NEDC-based emission factors (Boulter et al., 2009). This research indicates that the EFT average speed emission functions cannot be used to estimate CO_2 emission for an individual vehicle over distances of less than 5 km, let alone at a micro-scale link level. Whilst it is possible that the test vehicle was atypical of a petrol, Euro 4, 1.4 – 2.0 L, passenger car, the average ≈40% underestimation of the real-world CO_2 emission in this study, would suggest that the EFT emission function generates emission factors which are unrepresentative of the average vehicle in the category.

Likewise, the size of the disparity between the HBEFA traffic situation methodology estimates of CO_2 emission and the PEMS measured CO_2 emission (≈40% underestimation) suggests that the HBEFA lacks the resolution to have the capability for accurate micro-scale emission estimation. The four discrete traffic situations for each road type, (Stop + Go, Saturated, Heavy and Freeflow) with their respective emission factors, are used to define too broad a range of conditions to be useful where accurate modelling of CO_2 emission for an individual vehicle is required. As the maximum accuracy achieved on any lap was only 75.6%, even under conditions for which the average speed of the lap should be a good fit for one of the described traffic situations, the HBEFA model underestimated the vehicle CO_2 emission. This suggests that the test cycles used to generate the expected emission estimates for each LOS are not representative of the real-world traffic conditions found in Headingley, although they may better represent traffic conditions in the locations where the model was developed (Germany, Switzerland and Austria).

Table 4.6: Summary Table for the Headingley Lap Modelled CO_2 Emission

	EFT	HBEFA	MOVES	PHEM
Mean Model % Estimate of PEMS CO_2 Emission: **LAP** (n =48)	63.3%	57.3%	95.7%	90.7%
Range of Model % Estimate of PEMS CO_2 Emission: **LAP** (n =48)	54.7% - 75.6%	47.1% - 75.2%	82.3% - 116.6%	78.8% - 108.5%
LAP Emission Estimate IQR	7.6%	8.8%	11.1%	9.6%
LAP Emission Estimate MAPE (n=48)	37.7%	42.7%	7.9%	10.0%

At the section level, the same pattern of real-world CO_2 emission underestimation by the EFT and HBEFA models is observed; whilst the MOVES and PHEM models both delivered relatively good predictions of the PEMS measured emission. Table 4.7 is a summary table for the modelled Headingley section CO_2 emission estimates for each of the four models. The section-by-section variability in emission estimation for both the MOVES and PHEM models, presented in Figure 4.14 and Figure 4.22, result in a broader range of model percentage estimates of the real-world measured CO_2 emission. The marked difference in Section 1 and Section 8 emission estimates

in both models indicate an underlying factor that may be influencing the estimation in those sections. The hypothesis that this is due to road gradient is investigated in the next chapter.

Table 4.7: Summary Table for the Headingley Section Modelled CO_2 Emission

	EFT	HBEFA	MOVES	PHEM
Mean Model % Estimate of PEMS CO_2 Emission: **SECTION** (n =384)	61.6%	58.4%	93.8%	89.6%
Range of Model % Estimate of PEMS CO_2 Emission: **SECTION** (n =384)	41.1% - 82.8%	25.0 - 93.5%	66.6% - 133.9%	61.9% - 119.3%
Average **SECTION** Emission Estimate IQR (n=8)	7.6%	15.3%	10.7%	9.3%
SECTION Emission Estimate MAPE (n=384)	38.2%	41.6%	10.9%	12.3%
Likely Error Range From Model in Estimating PEMS CO_2 (90% of estimate values in this range)	-52.5% to -25%	-60% to -20%	-22.5% to +15%	-25% to +7.5%

It was noted in the analysis of the PHEM emission model that the Section 3 and Section 6 emission estimates (Figure 4.22) were relatively poor compared to other sections. As described in Chapter 3 these are short turning sections. Table 4.8 provides a summary table for the modelled CO_2 emission estimates of the PEMS measured emission excluding Section 3 and Section 6. Without the short turning sections both the MOVES and PHEM average estimate of the PEMS measured CO_2 emission improve, however, the biggest change is seen in the decrease in the PHEM MAPE from 12.3% to 10.7%. For the longer micro-scale sections, the average absolute percentage error for the MOVES and PHEM CO_2 estimates of the real-world CO_2 emission are approximately equal, with the MOVES estimates slightly more accurate and the PHEM estimates marginally more precise. Both models seem suitable for micro-scale CO_2 emission estimation.

Table 4.8: Summary Table for the Headingley Section Modelled CO_2 Emission – Non-Turning Sections

	EFT	HBEFA	MOVES	PHEM
Mean Model % Estimate of PEMS CO_2 Emission: **SECTION** (n =288)	64.1%	60.6%	94.7%	91.8%
Range of Model % Estimate of PEMS CO_2 Emission: **SECTION** (n =288)	44.0% - 82.8%	25.0 -93.5%	66.6% - 131.6%	61.9% - 119.3%
Average **SECTION** Emission IQR (n=6)	7.4%	14.9%	10.6%	9.9%
SECTION MAPE (n=288)	35.9%	39.4%	10.8%	10.7%

Whilst PHEM and MOVES were able to produce relatively accurate estimates of the on-road emission measured for the test vehicle, there is one important distinction between the modelling processes. Whilst the PHEM estimate accurately represents the test vehicle's emission through specifying the test vehicle parameters within PHEM, the MOVES estimate is accurate only through the chance that the average 2005 petrol passenger car emission factors are a good approximation for the test vehicle. Had the test vehicle been a smaller 2005 passenger car, with a lower kerbweight and a smaller rated engine power, MOVES would have generated the same emission estimate for the test vehicle, whilst PHEM could be calibrated to the specifications of the lighter passenger car.

Whether the MOVES modal model or the PHEM instantaneous model is more appropriate for micro-scale emission measurement will be related to the location of the test study. The default PHEM settings reflect a typical European vehicle fleet and the MOVES model has been created from an American vehicle fleet. The advantage of PHEM is that it does possess the functionality to adjust the specific vehicle parameters to best reflect the vehicle or fleet being modelled.

4.8 SUMMARY

Utilising the Headingley PEMS survey data from Chapter 3, the recorded second-by-second transient speed profiles over the 48 Headingley test laps were used as input to four emission models, which employ different methodologies to generate emission estimates. The four models used in the study were; DEFRA's Emissions Factors Toolkit, an average speed emission model; the HandBook on Emission FActors for road transport, a 'traffic situation' model; the US EPAs Motor Vehicle Emission Simulator, a 'modal' emission model; and the TU-Graz's Passenger car and Heavy duty Emission Model, an instantaneous emission model. The chapter included discussion on the background to each model.

From the PEMS recorded vehicle speed data, the four models were employed to calculate CO_2 emission factor estimates for each of the 48 test lap runs and 384 micro-scale road sections. This facilitated comparison of the lap and section CO_2 emission estimates for each model against the PEMS on-road measurement of the real-world CO_2 emission from the test vehicle.

Both the EFT and HBEFA models were found to substantially underestimate the real-world CO_2 emission at both the lap and section scale. The models were found to predict CO_2 emission factors around 40% lower on average than the PEMS measured CO_2 emission. Therefore neither the average speed emission factor methodology nor the traffic situation technique was found to be appropriate for micro-scale emission estimation in this instance. These models are likely to be more appropriately applied where detailed transient vehicle data are unavailable and at a larger geographical scale than the micro-scale estimates presented in this chapter. The main inputs for these model types, namely link based average speed data is more easily measured and therefore more widely available than the 1 Hz GPS data required for models which produce emission estimates on a per second basis. Analysis on a link-by-link rather than second-by-second basis also significantly reduces the volume of data for analysis, enabling emission estimates to be made over larger geographical areas for the entire vehicle fleet. Potentially what such models lack in emission estimation accuracy is counterbalanced by the ease with which they can be applied. As these models require more limited input data, once average speed emission values have been calculated for each vehicle type, the emission modelling process can be performed relatively quickly. Therefore, despite acknowledged deficiencies, there continues to be widespread use of average speed based calculation methods for the estimation of on-road vehicle emission (Barlow and Boulter, 2009).

The MOVES and PHEM models, however, were both shown to generate good estimates of the real-world CO_2 emission recorded during the PEMS testing. The mean model percentage estimate of the PEMS measured CO_2 emission was found to be between 90% to 95% for both MOVES and PHEM. The MAPE for both models was calculated to be around 10%. In general, MOVES was found to be slightly the more accurate of the two models, but PHEM was found to have the greater precision.

A decision on which of the two models is most appropriate for a particular study is likely to come down to the location of that research, as PHEM was developed for the European vehicle fleet, whilst MOVES was calibrated using American vehicle fleet data. Whilst both models provided good estimates of the on-road emission of the test vehicle the accuracy of the MOVES output was largely due to the fact that the emission from the test vehicle employed in the PEMS survey happened to be a good match with the average 2005 petrol passenger car emission factors in the MOVES model (as no specification of the vehicle was possible other than its age and year of manufacture). The PHEM estimates were accurate because the vehicle parameters for the model could be specified. The importance of accurately describing the vehicle specification in PHEM was demonstrated through comparison of the PHEM modelled CO_2 emission estimates with the test vehicle parameters against the PHEM estimates with the default Euro 4 petrol passenger car specification.

As described in Chapter 3, the PEMS data used in this study were collected from a single vehicle, using one driver. The findings from this chapter would be strengthened by an appraisal of further vehicle types as the accuracy of the modelled estimate of real-world CO_2 emission may vary for vehicles of different engine size, fuel type and weight. Further work could also investigate whether variation in driving style has an impact on the accuracy of the modelled estimate of real-world CO_2 emission, by repeating the PEMS data collection with a number of different drivers. However, as the Headingley PEMS testing was conducted in a variety of traffic conditions (from heavily congested to free flowing), it is likely that a range of driving styles were captured in the analysis in this chapter, as the driver was required to adapt the rate of acceleration and braking along with gear choice to suit the traffic conditions amid varying levels of congestion.

Analysis of the type found in this chapter is restricted by the availability of on-road vehicle emission data as the significant cost of large scale PEMS projects limits the collection of such comprehensive data sets. Both the MOVES and PHEM models have been built by collating a large number of vehicle emission data sets from national and international research projects,

and have been developed at a scale only possible for organisations of the magnitude of the US EPA and the European Commission. The work presented in this chapter confirmed that the MOVES and PHEM models can be used to produce reliable real-world CO_2 emission estimates for the test vehicle driven over the Headingley test lap. Further comparison of PEMS recorded and modelled CO_2 emission data is needed to be able to assess if the different methodologies employed in the two models are able to generate similarly accurate real-world estimates for other vehicle types in other locations, especially given that MOVES was developed for the US vehicle fleet and PHEM for the EU fleet.

The analysis of the model estimates of section CO_2 emission, in this chapter, has revealed significant section-by-section variance in the accuracy of estimates of real-world emission. This was especially marked in Section 1 and Section 8, which are the opposite traffic flows over the same road link. It was hypothesised that this discrepancy was due to the impact of road gradient on exhaust emission as Section 1 is primarily downhill and Section 8 uphill. As mentioned earlier, the impact of road grade on the micro-scale estimation of CO_2 emission is investigated in the next chapter.

CHAPTER 5: ROAD GRADE AND MICRO-SCALE EMISSION MODELLING

5.1 INTRODUCTION

The work reported in Chapter 4 demonstrated the capability of the MOVES and PHEM emission models to derive estimates of real-world CO_2 emission values over micro-scale sections. Whilst both models produced good estimates of the PEMS measured on-road CO_2 emission, the analysis revealed some section-to-section variability in the accuracy of the CO_2 estimates, which was hypothesised to be the result of the influence of road grade. Both MOVES and PHEM have the capability to include a second-by-second road grade had it been available, which in combination with the transient vehicle speed data could have been used to generate estimates of engine power output and then referenced to a rate of CO_2 emission. However, a limitation for the modelled estimates in Chapter 4 was the lack of accurate road grade values as the GPS recorded altitude values were found to be too inexact for the required 1 Hz gradient profile to be calculated.

This chapter presents an investigation of the influence of road grade on CO_2 emission, initially through a CO_2 emission sensitivity analysis, which involves setting the road grade within the VSP equation (for the Euro 4 test vehicle) at a range of values to generate VSP estimates at each selected road grade. The rate of CO_2 emission at each road grade is then assessed by referencing the generated VSPs to the average rate of CO_2 emission at that VSP recorded during the PEMS Headingley survey. The difference between the emission rates over a flat profile and at each grade is analysed.

The research introduces a novel Light Detection And Ranging (LiDAR) – Geographic Information System (GIS) road grade estimation methodology, using GIS software to interpolate the elevation for each second of data from a Digital Terrain Model (DTM). The MOVES and PHEM models from Chapter 4 are rerun with the LiDAR-GIS road grade included, to assess whether the addition of road grade improves the modelled estimates of the PEMS measured real-world CO_2 lap and section emission. The sensitivity of the PHEM modelled CO_2 emission estimates to road grade is also evaluated by lessening and exaggerating the LiDAR-GIS gradient profiles. CO_2 emission estimates are generated from PHEM with the PEMS recorded vehicle speed data and the range of gradient profiles.

5.2 BACKGROUND TO ROAD GRADE AND CO_2 EMISSION MODELLING

It has been established in a number of papers that road grade can have a significant effect on vehicle exhaust emission (Jackson and Aultman-Hall, 2010; Frey et al., 2008; Zhang and Frey, 2006; Boriboonsomsin and Barth, 2009). As road gradient increases so does the force opposing the motion of the vehicle due to gravity. The power demand to propel a vehicle is proportional to its weight and the magnitude of the road grade (Heisler, 2002). Hence, as road grade increases, to keep the vehicle at a constant speed, the engine has to provide greater power, requiring greater combustion of fuel, which results in a larger mass emission of combustion products and, therefore, pollutants. For a vehicle travelling on a road with negative gradient, the force of gravity, in contrast, acts to accelerate the vehicle, reducing the power demand on the engine, requiring lower levels of fuel consumption and reducing pollutant emission (Boriboonsomsin and Barth, 2009). For these reasons, the inclusion of road grade in the emission modelling process is very important. Incorrectly assigning the road grade could result in significant estimation errors in sections in which there are fluctuations in grade.

Exploiting the relationship between engine power and exhaust emission, the latest generation of emission models such as the US EPA's MOtor Vehicle Emission Simulator (MOVES) (Koupal et al., 2004), the Netherlands Organisation for Applied Scientific Research's (TNO) VERSIT+ model (Smit et al., 2007) and the Technical University of Graz's (TU-Graz) Passenger car and Heavy duty Emission Model (PHEM) (Hausberger, 2003) generate predictions of vehicle exhaust emission by referencing the calculated engine power output for each second of data to a calibrated mass of exhaust emission at that power, for each emission species.

Derivation of instantaneous engine power output requires a second-by-second measure of vehicle speed, acceleration and road gradient. PEMS can reliably capture vehicle speed, and hence acceleration, during real-world driving, but road grade is very difficult to measure accurately from an instrumented vehicle (Zhang and Frey, 2006). As a result of this difficulty, it appears there has been a tendency for studies to utilise test areas that are flat enough to set the road grade to 0, often without quantification of what "relatively flat" means (Yu et al., 2016; Song et al., 2012a; Anya et al., 2014)

A number of studies have highlighted the significant influence road grade can have on real-world fuel consumption and exhaust emission (Zhang and Frey, 2006; Boriboonsomsin and Barth, 2009; Boroujeni and Frey, 2014). Zhang and Frey (2006) recorded an increase in CO_2 emission

of 40-90% for three petrol light duty vehicles over sections of road with gradient ≥ 5% when compared to sections with gradient ≤ 0%, whilst Boriboonsomsin and Barth (2009) measured a 15-20% rise in fuel consumption for a petrol passenger car between a flat route and a hilly route (driving up and down the same hill, with start and end points at the same elevation).

Given the potential effect of road grade on engine power output and corresponding vehicle emission, it is important for micro-scale emission modelling that instantaneous engine power output is calculated accurately. To achieve this it is necessary to have a representative road grade value for each second of test data. There are a number of methods for quantifying road grade proposed in the literature, including; calculation from design drawings; direct land survey measurement; on-board measurement by GPS, accelerometers, barometric altimeters and inclinometers; and mathematical derivation from Digital Terrain Model (DTM) or Digital Elevation Model (DEM). Each of these methods has different characteristics with respect to accuracy, precision, scale and price (Zhang and Frey, 2006; Boroujeni et al., 2013; Sahlholm and Johansson, 2010). Zhang and Frey (2006) proposed a LiDAR based methodology, concluding that the LiDAR method is advantageous; having relatively few practical and logistical limitations compared with other methods, and can be considered sufficiently accurate for emission estimation.

LiDAR is a mapping technique which quantifies terrain elevation using laser measurement from aircraft. These measurements can be processed to construct a highly accurate DTM, which renders a three dimensional representation of the surface topography, describing elevation and position. The availability and cost of LiDAR data has been cited as the main limitation in its use for road grade estimation (Boroujeni et al., 2013), however, a comprehensive LiDAR 5m resolution DTM data set for the U.K. is available free of charge to academics and students at U.K. institutions, previously through the Landmap Kaia Service hosted at MIMAS based at the University of Manchester (Millin-Chalabi et al., 2011), and now available via the Joint Information Systems Committee (JISC) funded EDINA service (digimap.edina.ac.uk). The advantage of the simple LiDAR-GIS method proposed in this study is that by referencing the measured GPS position to a DTM elevation, a representative 1 Hz road grade profile can be quickly generated for a test area without the multiple runs required by GPS measured altitude methodologies (Sahlholm and Johansson, 2010; Boroujeni et al., 2013) and without the detailed roadway analysis and segmentation required in the LiDAR methodology described by Zhang and Frey (2006). The Zhang and Frey method produces a gradient profile (the road gradient at each distance along a test route) by first generating an elevation profile of the test road. This is done by mapping the location of the centre line of a test road and then identifying all LiDAR elevation

points that lie within a "buffer zone" of the roadway centre line. "Segmentation" of the road profile is conducted by detecting local extrema within the elevation profile, which split the elevation profile into sections. Division of these sections into segments of comparable road grade is undertaken through analysis of the change of road grade within each section. The start and end points for each segment are calculated by ensuring that the difference between the average road grade over the segment and the average road grade through the first half of the segment is not greater than 0.1%. This calculation is initiated at the section level (i.e. between consecutive elevation extrema) and, where the 0.1% difference criteria is exceeded, the section is further subdivided into shorter subsections and the process is repeated. This method produces a gradient profile of road segments with an allotted gradient at each distance along the test road. A road grade can, therefore, be assigned to each second of transient vehicle data by identifying how far along the test road the test vehicle is at each second.

A novel LiDAR-GIS methodology has been developed in this study and is described in Chapter 5.4 after the sensitivity analysis.

5.3 SENSITIVITY OF EXHAUST CO_2 EMISSION TO ROAD GRADE

As discussed in Chapter 4, the latest generation of emission models such as the EPA's MOVES (Koupal et al., 2004) and the TU-Graz's PHEM (Hausberger, 2003) generate emission estimates by referencing a calculated engine power output to a calibrated mass emission for each second of data. In both these emission models, an estimate of second-by-second engine power output is determined from a 1 Hz record of vehicle speed and road grade, combined with specification data for the test vehicle.

Figure 5.1 shows the longitudinal forces that define the vehicle motion in the Vehicle Specific Power (VSP) equation (Equation 5.1), which is used as the measure of engine power output at each second in MOVES. The acceleration of the vehicle is defined by the net effect of the forces acting on it (N.B. when all the forces in the diagram are balanced the resultant force, and therefore acceleration, is zero. In this case, the vehicle is either stationary or moving at a constant speed in the same direction). PHEM employs a similar equation to determine engine power (Chapter 4.6.2), however, this section demonstrates the sensitivity of exhaust CO_2 emission to road grade using the VSP equation employed by MOVES.

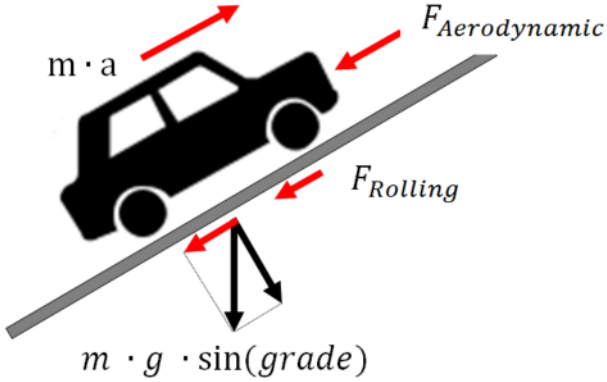

Figure 5.1: Vehicle Longitudinal Dynamics Relating to VSP

As explained in Chapter 4.5.2, the VSP equation described in Equation 5.1, derived by Jimenez-Palacios (1999), can be simplified into a form specific to the Euro 4 test vehicle used in this research, where the coefficient of rolling resistance and the drag coefficient describe a 2005 Ford Mondeo (Equation 5.2).

Equation 5.1:

$$\text{Vehicle Specific Power} = \frac{\frac{d}{dt}(KE + PE) + F_{rolling} \cdot v + F_{aerodynamic} \cdot v}{m}$$

Equation 5.2:

$$VSP_{EURO4} = v \times ((1.1a) + (9.81 \times \sin(\text{atan}(grade)) + 0.128) + (0.000318v^3)$$

Where,

- VSP : is vehicle specific power (kW/t);
- KE : is kinetic energy (J)
- PE : is potential energy (J)
- $F_{rolling}$: is rolling resistance (N)
- $F_{aerodynamic}$: is aerodynamic drag (N)
- v : is vehicle speed (m/s);
- a : is vehicle acceleration (m/s^2);
- grade : is road grade (dimensionless).

Using Equation 5.2 and setting the acceleration and road grade to fixed test values, the VSP at each velocity can be calculated. Figure 5.2 shows the calculated VSP values over a range of positive and negative road grades from –6% to 6%, with vehicle speed varied between 0 km/h and 50 km/h and acceleration set to 0 (i.e. cruising at a constant speed). At each vehicle speed, greater positive road grade causes an increase in VSP, whilst larger negative road grade leads to a decrease in VSP.

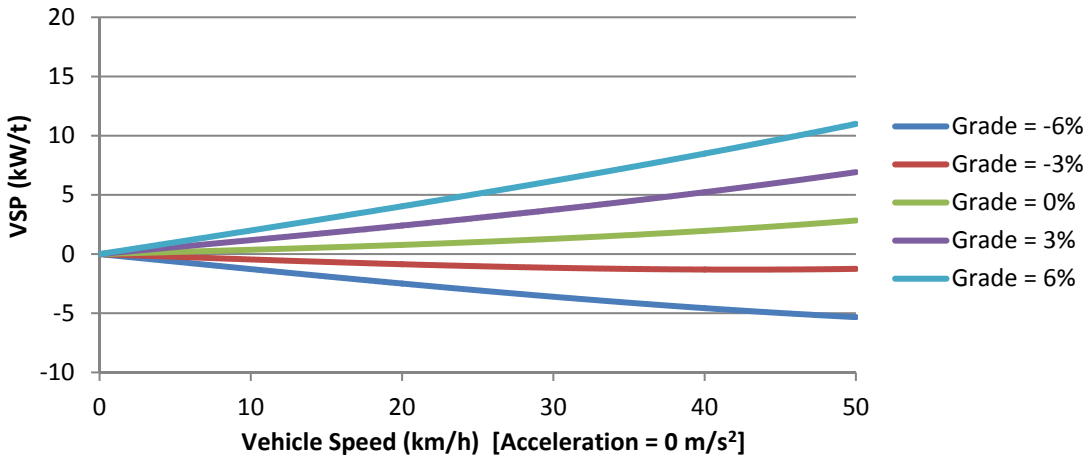

Figure 5.2: Sensitivity of VSP to Vehicle Speed and Road Grade (Acceleration = 0 m/s²)

Using a binning methodology, the average CO_2 emission for each integer increase in VSP (up to 21 kW/t) was calculated from the all of the Headingley PEMS recorded data (56,986 s). All VSP values ≤ 0 kW/t were collated as one bin, as the average emission rates for each negative VSP are similar (see Figure 4.10).

Table 5.1: VSP Bin Average CO_2 Emission from the Headingley PEMS Survey, 1.8 L Euro 4 Petrol Passenger Car (56,986 s)

VSP Bin	Bin Range (kW/t)	Bin Average CO_2 Emission (g/s)	Number of Data Points
-	<=0	0.92	35929
0	>0 - 1	1.69	4126
1	>1 - 2	2.08	2628
2	>2 - 3	2.37	2300
3	>3 - 4	2.67	2154
4	>4 - 5	2.93	1998
5	>4 - 6	3.26	1680
6	>6 - 7	3.57	1426
7	>7 - 8	3.99	1147
8	>8 - 9	4.42	922
9	>9 - 10	4.88	678
10	>10 - 11	5.25	532
11	>11 - 12	5.62	407
12	>12 - 13	6.22	302
13	>13 - 14	6.61	214
14	>14 - 15	6.95	175
15	>15 - 16	7.24	108
16	>16- 17	7.90	71
17	>17 - 18	8.01	54
18	>18 - 19	8.46	42
19	>19 - 20	8.96	29
20	>20 - 21	9.50	39

The PEMS VSP values used in the calculation of each of the bin average CO_2 emission rates included road grades which were calculated by the LiDAR-GIS method outlined later in Chapter 5.4.

From the bin emission rates listed in Table 5.1, each VSP value from Figure 5.2 can be assigned a rate of CO_2 emission. These rates are presented in Figure 5.3 which demonstrates how the average rate of CO_2 emission varies with respect to road grade and vehicle speed whilst the acceleration is fixed at 0 m/s^2, meaning that the vehicle maintains a constant speed. The VSP values at the -6% and -3% gradients are negative for all speeds, which means that the test vehicle would have to be braking in order for the vehicle not to be accelerated by to the force of gravity. As no engine power is required to maintain speed under these conditions, the rate of emission is simply the idle rate of 0.92 gCO_2/s between 0 km/h and 50 km/h. For the road grades between 0% and 6%, the vehicle requires engine power output to maintain a constant speed. The steps in the emission rate profile, shown in Figure 5.3, mark transitions from one VSP bin to the next. The steeper the positive road grade, the greater the increase in VSP with speed and therefore the higher the rate of CO_2 emission.

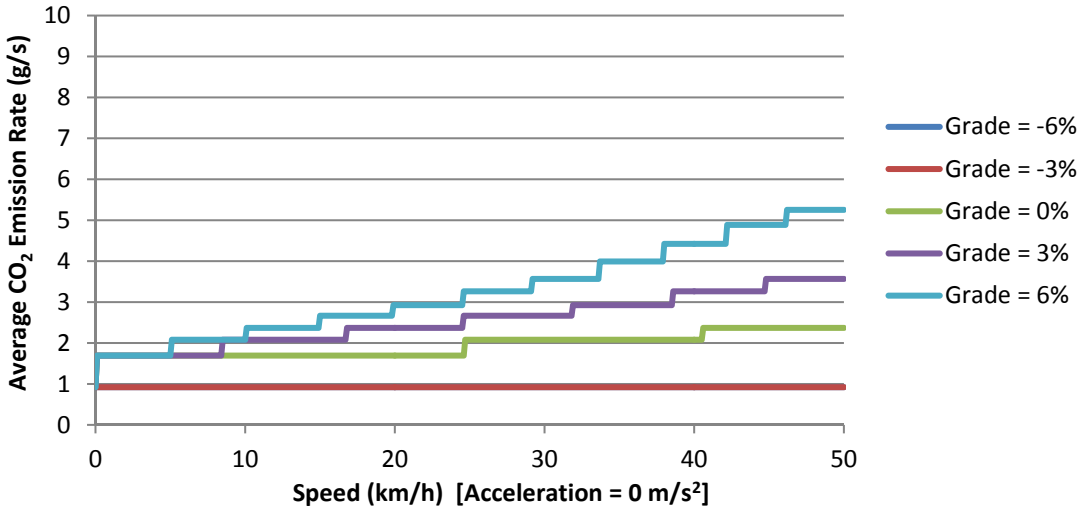

Figure 5.3: Sensitivity of CO_2 Emission Rates to Vehicle Speed and Road Grade For a 1.8 L Euro 4 Petrol Passenger Car (Acceleration = 0 m/s^2)

Figure 5.4 compares the CO_2 emission rate at -6%, -3%, +3% and +6% to the emission rate at 0%, displaying the ratio of the gCO_2/s values between 0 km/h and 50 km/h, with the acceleration set at 0. As the emission rate for -6% and -3% is the same over all speeds (due to the entirely negative VSP for both) the ratio of the CO_2 emission is the same for both (which is why the -6% grade line does not appear in Figure 5.4). The negative grades are demonstrated to have a CO_2 emission rate approximately half that for the flat road grade (0%). The positive grades both have a higher average CO_2 emission rate than the 0% grade and the difference increases as the speed increases. At 50 km/h, the estimated average CO_2 emission rates for the road grades of +3% and +6% are respectively 1.5 and 2.2 times greater than those for the 0% road grade.

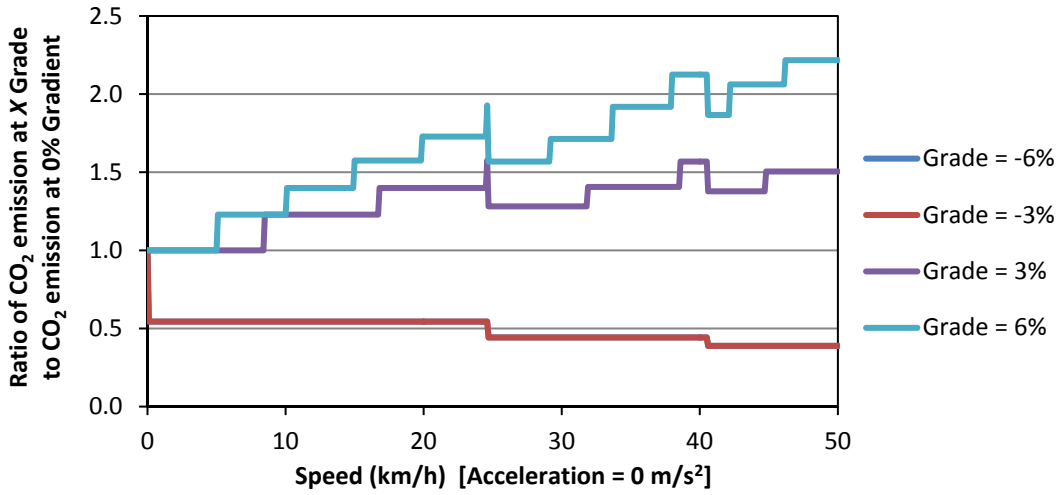

Figure 5.4: Ratio of the CO_2 Emission at Each Road Grade to the CO_2 Emission at -6% Road Grade by Vehicle Speed (Acceleration = 0 m/s²)

Figure 5.5 is a plot of the calculated VSP values over the range of road grades from -6% to +6%, with a vehicle speed range of 0 km/h to 50 km/h, however, the VSP in this example is calculated with an acceleration of 0.5 m/s². The VSP values are greater than those calculated with an acceleration of 0 m/s² (Figure 5.2). To be able to accelerate at 0.5 m/s², power from the engine is required at all road grades as an acceleration of this magnitude cannot be provided by gravity alone.

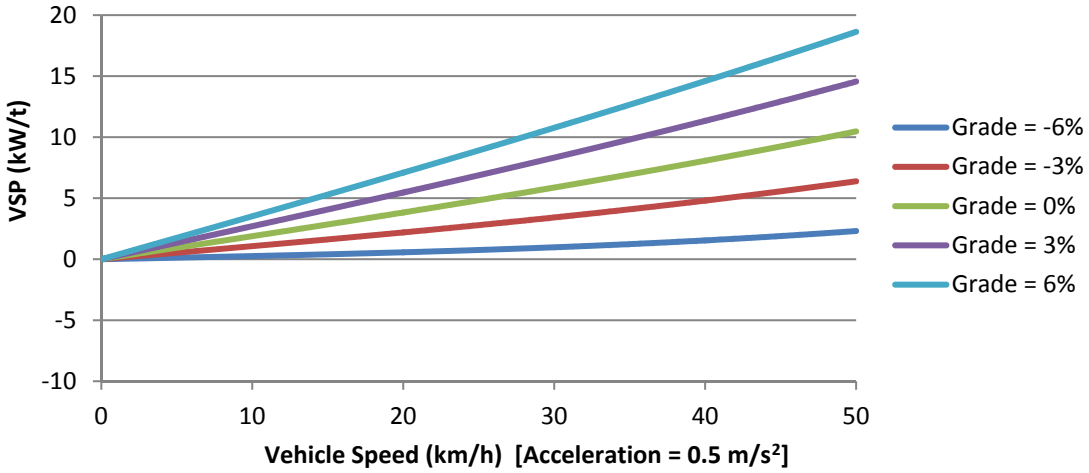

Figure 5.5: Sensitivity of VSP to Vehicle Speed and Road Grade (Acceleration = 0.5 m/s²)

The increase in VSP values is reflected in a greater rate of CO_2 emission at each speed compared to the emission rates with acceleration at 0 (Figure 5.6). For instance, the rate of CO_2 emission at 50 km/h for a road grade of +6% was 5.25 gCO_2/s (Bin 10) with no acceleration, but, with 0.5 m/s² acceleration, the rate of CO_2 emission with the same grade is 8.46 gCO_2/s (Bin 18). It should also be noted, that as the negative grade sections have positive VSP values, their CO_2 emission rates are greater than the idle rate.

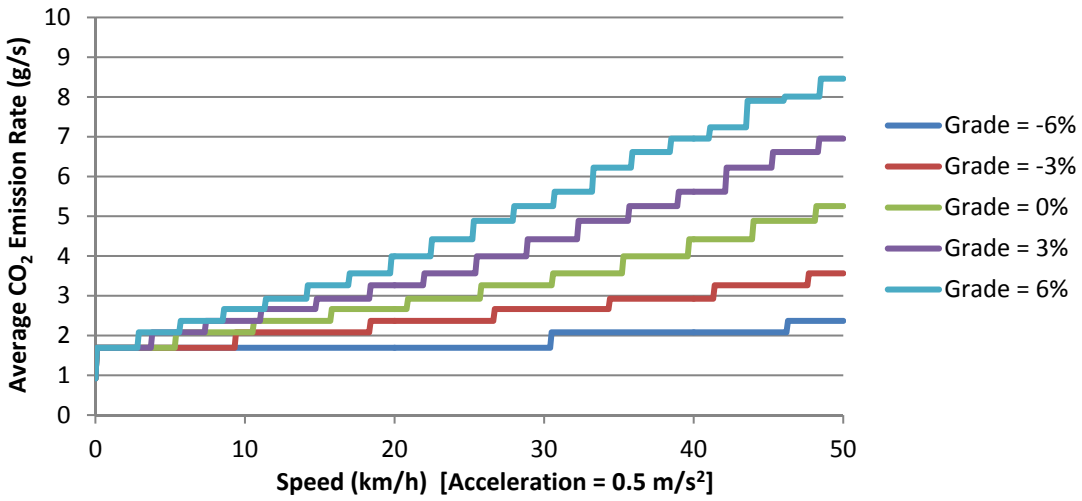

Figure 5.6: Sensitivity of CO_2 Emission Rates to Vehicle Speed and Road Grade For a 1.8 L Euro 4 Petrol Passenger Car (Acceleration = 0.5 m/s²)

Figure 5.7 demonstrates that although the absolute rate of CO_2 emission is greater for the VSP values calculated with acceleration, the relative difference between the CO_2 emission rates for each of the road grades and the CO_2 emission rate at 0% grade are actually smaller with the acceleration than without.

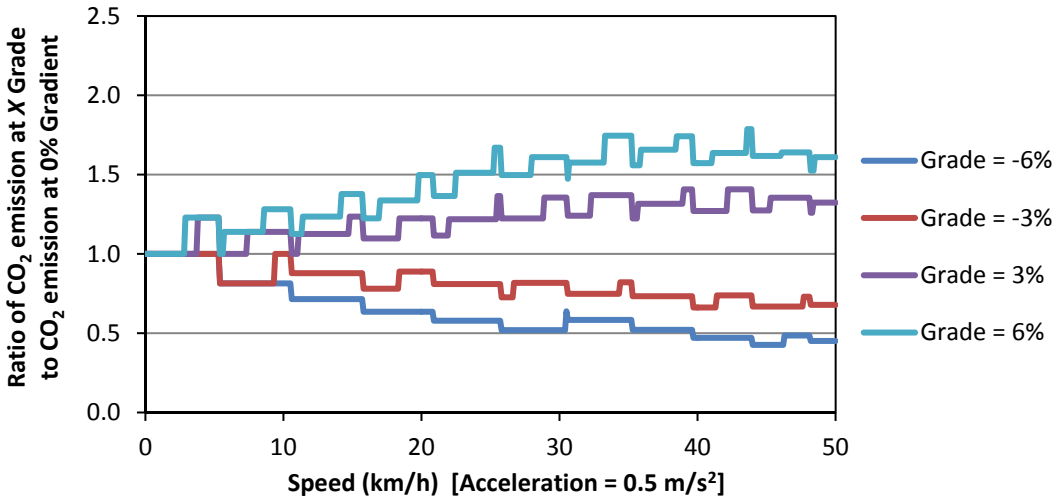

Figure 5.7: Ratio of the CO_2 Emission at Each Road Grade to the CO_2 Emission at -6% Road Grade by Vehicle Speed (Acceleration = 0.5 m/s²)

For each of the test road grades, the ratio between its CO_2 emission rate and the rate at 0% gradient is relatively consistent at speeds between 20 km/h and 50 km/h. For the road grades of +6%, +3%, -3% and -6%, the average rates of CO_2 emission are respectively, 1.6, 1.3, 0.75 and 0.5 times the estimated average CO_2 emission at 0% road grade, between 20 km/h and 50 km/h with an acceleration of 0.5 m/s².

Figure 5.8 shows the calculated VSP values over the range of road grades from -6% to +6%, with vehicle speed varied between 0 km/h and 50 km/h and a deceleration of 0.5 m/s^2. With a deceleration of this magnitude, only the steepest positive test road grade value of +6% has positive VSP values, as only at +6% gradient does the vehicle still require some power from the engine to prevent the force of gravity from slowing the vehicle at a rate faster than 0.5 m/s^2. For all other road grades braking is required to decelerate the vehicle at that rate.

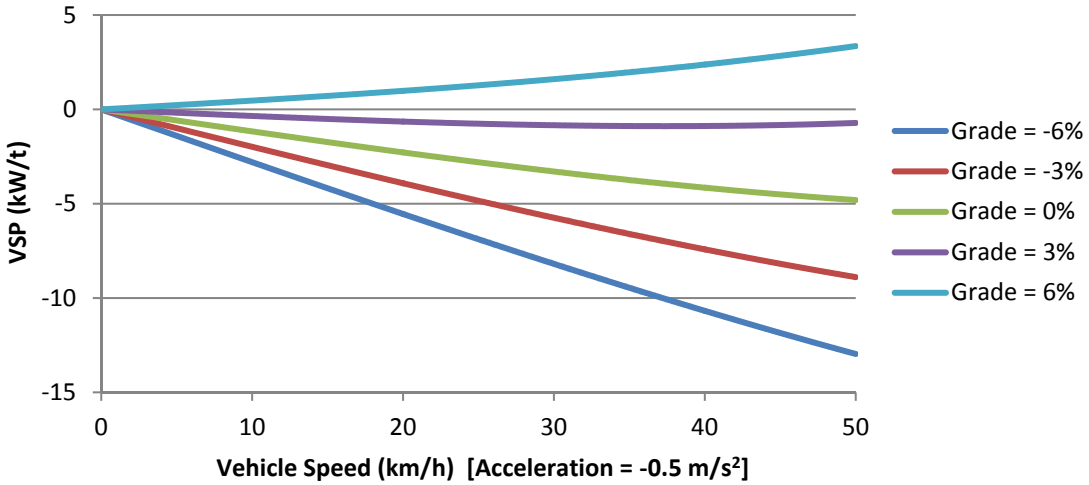

Figure 5.8: Sensitivity of VSP to Vehicle Speed and Road Grade (Acceleration = -0.5 m/s^2)

The average rate of CO_2 emission for the decelerating test vehicle is shown in Figure 5.9. As all the calculated VSP values for -6%, -3%, 0% and +3% are negative, the rate of emission is constant at all speeds at the idle rate of 0.92 gCO_2/s. Only with a road grade of +6% do the calculated VSP values indicate a rate of CO_2 emission greater than the idle emission rate.

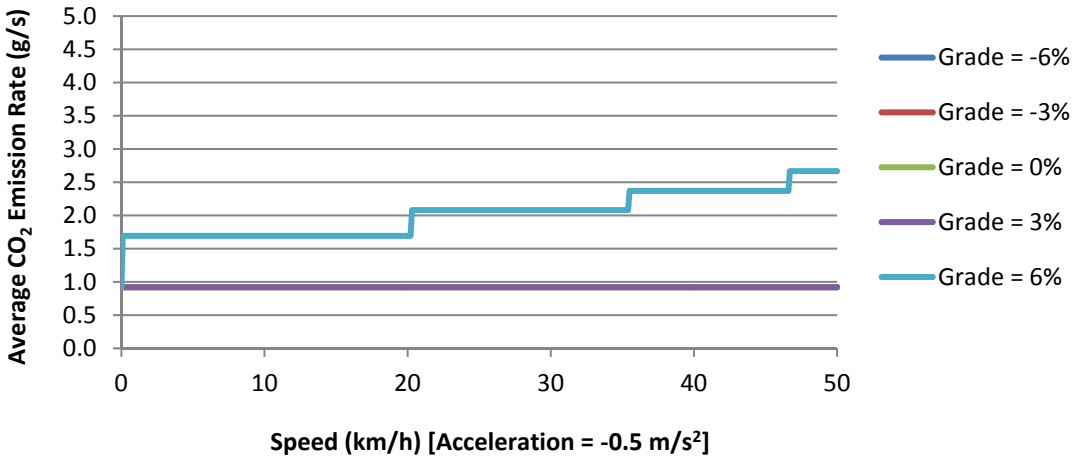

Figure 5.9: Sensitivity of CO_2 Emission Rates to Vehicle Speed and Road Grade For a 1.8 L Euro 4 Petrol Passenger Car (Acceleration = -0.5 m/s^2)

As the rate of CO_2 emission is the same for the VSP values calculated with -6%, -3% and +3% road grade and the VSP values calculated with 0% road grade, the ratio between the rates is 1.

However, for the VSP values calculated with +6% road grade, Figure 5.10 shows that the CO_2 emission rate over this range of speeds can approach almost 3 times the rate of the estimated emission at 0% road grade.

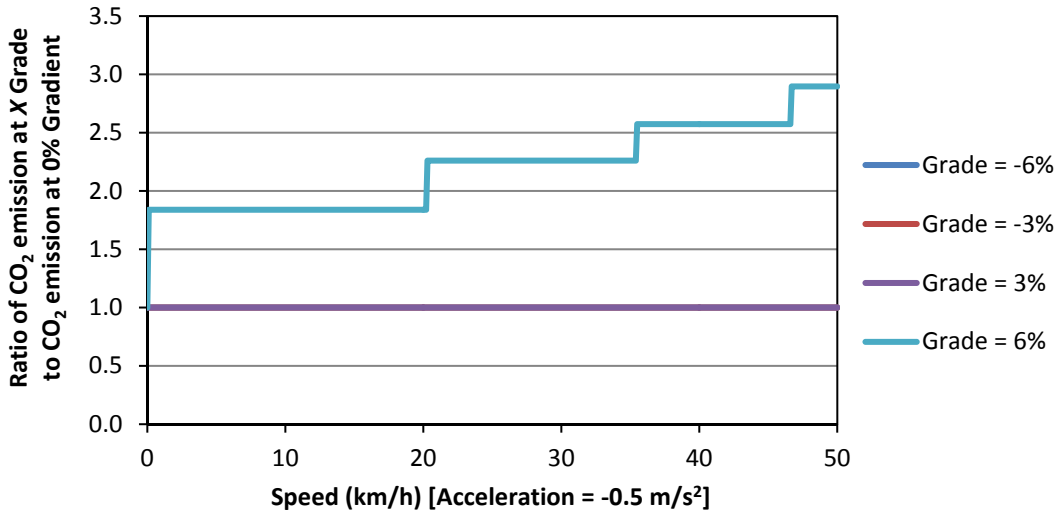

Figure 5.10: Ratio of the CO_2 Emission at Each Road Grade to the CO_2 Emission at -6% Road Grade by Vehicle Speed (Acceleration = -0.5 m/s^2)

Although this analysis shows only three scenarios, one for acceleration, one deceleration and one for constant speed 'cruising', whereas there is a wide spectrum of possible speed and acceleration combinations that would result in different calculated values of VSP, it has demonstrated that under each of these scenarios, failure to account for road grade could lead to significant error in the estimate of CO_2 emission. Even at the relatively modest road grades presented in this section, it has been shown that modelling a road as flat could lead to an underestimation of the CO_2 emission rate by >50% on uphill sections and an overestimation of CO_2 emission rate by up to 60% on downhill sections.

Definition of road grade in the second-by-second power equations is likely to be of particular importance for micro-scale section modelling, where relatively steep average road grades are possible and there is less of an error offsetting influence as a result of uphill and downhill portions within the same section. The next section of this chapter reports work conducted to develop a methodology to improve characterisation of road grade for second-by-second engine power calculation.

5.4 LIDAR-GIS METHOD

The PEMS instrumented test vehicle used for the Headingley survey included a VBOX II GPS system (Racelogic, 2008) employed by this study to measure second-by-second GPS position. This GPS system also recorded an altitude reading for each second of the test runs but errors within the GPS altitude measurement, uncovered in this research, were found to cause inaccuracies in the recorded elevation profile which made it unfeasible to calculate the representative second-by-second road grade required for instantaneous engine power calculation from these data.

The VBOX II has a 95% Circular Error Probability (CEP) of 10 m for its recorded altitude (Racelogic, 2008). This means that the measured height is within 10 m of the true position 95% of the time. The possible error range resulting from this instrument imprecision, in combination with measurement errors during vehicle transit caused, for example, by GPS signal interference from buildings in urban streets make the raw GPS height measurements recorded by the instrumented vehicle too unreliable for generation of an accurate elevation profile for the test lap and insufficiently precise to calculate road grade for each second of data. Figure 5.11 is a plot of the GPS recorded altitude for four different test runs over the 4.6 km the Headingley test lap. The run-to-run variability is clear and, although the four laps have a roughly similar profile, there are significant differences between each record and several instances where the GPS unit has erroneously recorded large changes in altitude over very short distances. Using an erroneous road grade would cause an error in the calculated power output and therefore assign an incorrect emission estimate. This inaccuracy increases with the scale of the input road grade error, so it is very important to ensure a reliable road grade estimate is used.

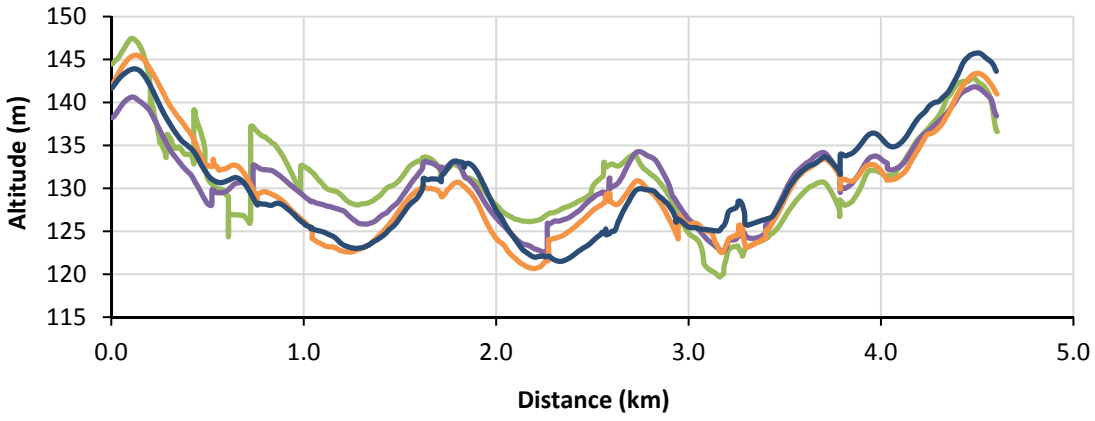

Figure 5.11: GPS Measured Altitude for Four Runs of the Headingley Test Lap

As a consequence of this measurement variability, the test lap elevation profile was instead generated by an alternative technique using a 5 m resolution DTM generated from the LiDAR

elevation data provided by Bluesky International Limited (obtained from http://landmap.mimas.ac.uk). The DTM and the VBOX measured GPS positions (latitude and longitude) for each test run were imported into the Geographic Information System (GIS) software ArcGIS enabling the height at each recorded GPS latitude and longitude point to be extracted from the DTM. Figure 5.12 shows the DTM for the Headingley test area, with topography represented by a black to white spectrum; where black represents the lowest elevation and white the highest. The second-by-second positions from a test lap run, coloured by their respective extracted altitudes, overlay the DTM.

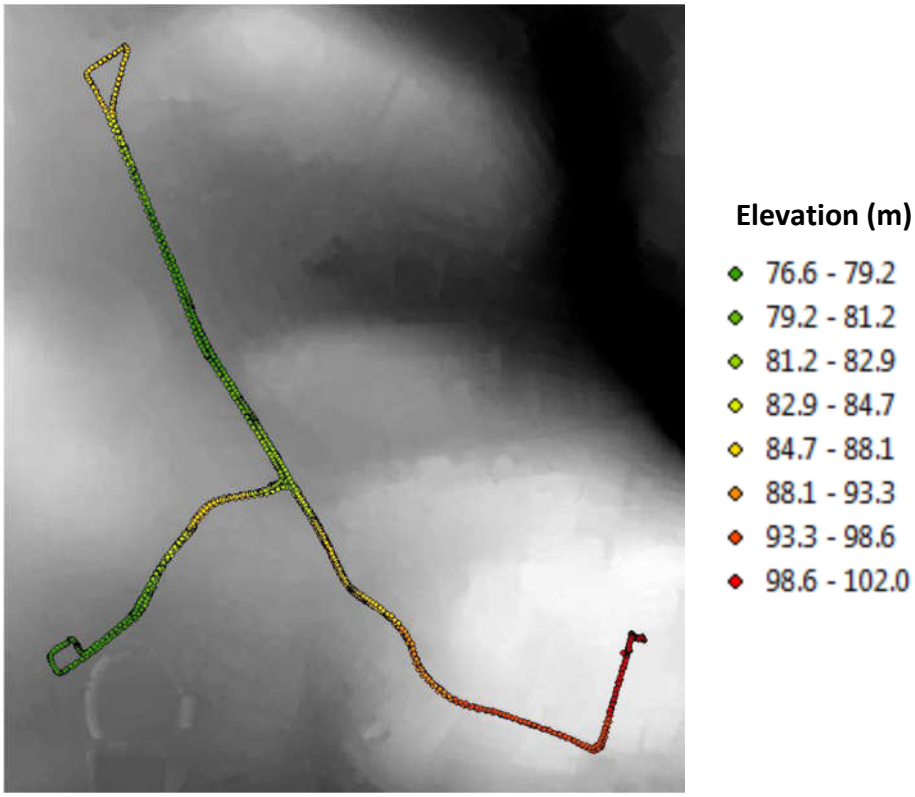

Figure 5.12: ArcGIS Image of DTM and GPS Positions with Extracted Elevations

Figure 5.13 presents the GPS measured altitudes from four test runs through the Headingley network and also plots the LiDAR-GIS generated altitude profiles for the same four test runs. The 1 Hz PEMS latitude and longitude data, for each of the four runs, were processed in GIS along with the 5 m resolution DTM and the altitude at each latitude and longitude were interpolated from the LiDAR DTM data and extracted as a new data set of latitude, longitude and elevation. The elevation profiles generated from the LiDAR-GIS methodology are so similar for each test run that at the scale presented they overlap each other and appear as one line. The LiDAR-GIS approach calculates a consistent profile over multiple runs, displaying none of the measurement errors that afflict the GPS measurements, with no large step changes in elevation. In addition, the elevation measurements in the LiDAR-GIS profile are consistent with expected elevations checked against ordnance survey data. The approximate 45 m difference between

the GPS measurements and the LiDAR-GIS profile is due to instrument calibration error in the initial setup of the GPS unit, whilst the variability in the GPS measurement is due to instrument error.

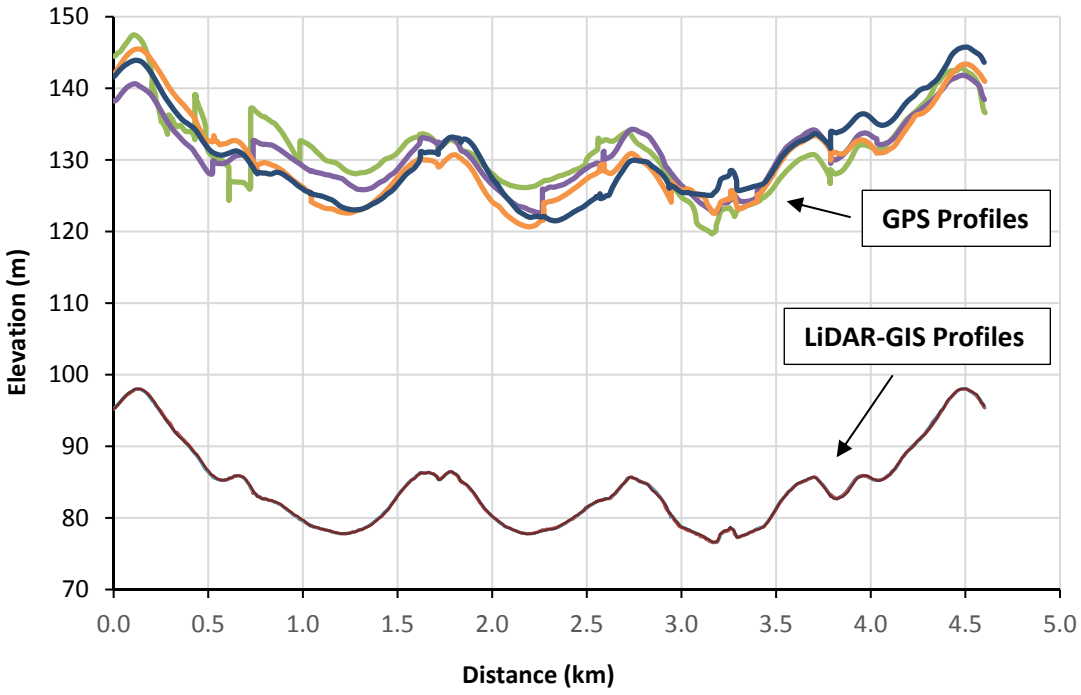

Figure 5.13: GPS and LiDAR-GIS Measured Altitude Over Four Runs of the Headingley Test Lap

The road grade for each second of recorded data were calculated by applying an algorithm to reduce the effect of errors associated with inaccuracies in the measured GPS latitude and longitude position. The VBOX has a 95% CEP for absolute position of 3 m. The errors resulting from GPS absolute position measurement accuracy are especially apparent at points where the vehicle was either moving slowly or stationary, as the GPS position appears to shift whilst the vehicle is not moving. As the GPS position changes, so does the elevation estimate extracted from the 5 m DTM and relatively small changes in GPS position can result in significant changes in elevation estimate. This is especially the case when the measured GPS position shifts from the centre of the road to a position to the side of the road, where the immediate area to the side of the road has a substantial change in elevation (either rise or fall, due to features such as steep banking, walled rises or pedestrian walkway underpasses). In such stationary or low speed situations implausible erroneous gradients may be calculated due to GPS accuracy error shifts perpendicular to the direction of travel along the road, where the vehicle travels only a short distance along the test route but due to GPS measurement error, there is a significant change in the DTM extracted elevation.

In order to determine a representative gradient on a second-by-second basis an algorithm was developed for this study and applied to smooth out the errors resulting from GPS absolute position measurement imprecision. For each second of data, when the vehicle was travelling at greater than 10 m/s the gradient was calculated by dividing the distance travelled in the measured second by the change in height in that measured second. When the vehicle was travelling at less than 10 m/s, rather than calculating the gradient over 1 second, the gradient was calculated from where the vehicle was at least 5 m before the start of that measured second to the point where the vehicle was at least 5 m past the end of the measured second. This ensured that the minimum length of road section over which the gradient was calculated was 10 metres.

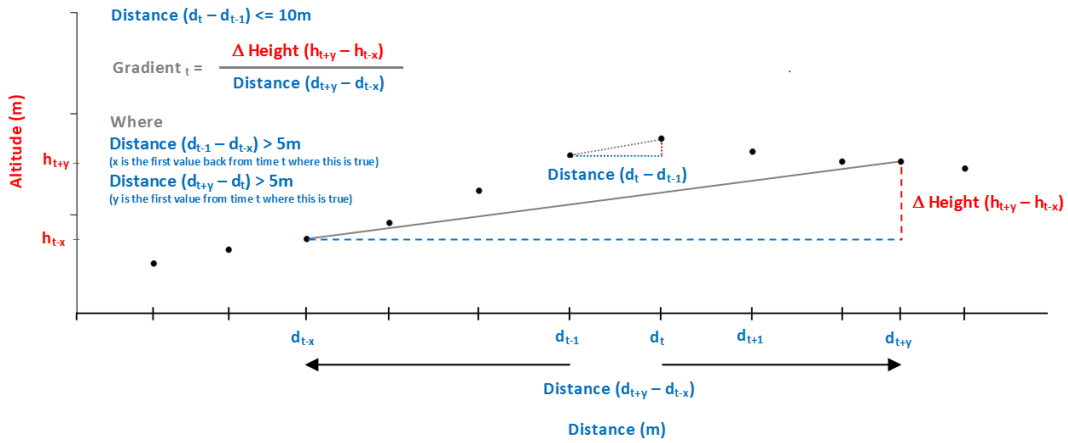

Figure 5.14: Gradient Calculation Methodology

The Bluesky LiDAR height data utilised in this study have an accuracy of up to ±10 cm (Bluesky, 2013), however, the resolution of the DTM does have an influence on the accuracy of LIDAR based elevation estimates. In this study, the 5 m resolution DTM presents a map of LiDAR calculated elevations at the intersection points on a horizontal 5 m grid covering the test area. The height of any GPS point within that grid is calculated by the GIS software by linearly interpolating between the nearest grid intersection points. However, as a result of interpolation surface features such as bridges, underpasses and steep road side banking (where there is an abrupt non-linear change in surface elevation within a 5 m grid square) can cause errors in the altitude estimate. In these cases, the modelled linear change in surface elevation does not reflect the sudden real-world change. Also, due to the nature of the measurement, LiDAR based elevation estimation cannot directly measure road surface height where the test route passes under another section of road. In such cases, the height estimation using LiDAR data will present the height of the road section above rather than the underlying test route.

Errors arising from this LiDAR-GIS methodology are likely to be manifest within a calculated road grade profile as gradients which are physically impossible for a road section, where the surface height has changed markedly over a short distance. Further identification, enabling manual correction of these errors, can be undertaken utilising geo-referenced photographic images from software such as Google Street View, by inputting the GPS coordinates of erroneous data points into the software and analysing the image. In this study no manual adjustments of the estimate road grade were necessary, as the Headingley test lap contained no surface features which would require such correction.

The advantage of this simple LiDAR-GIS method is that by using the GPS position measurements recorded by the PEMS, to reference a DTM elevation, a representative 1 Hz road grade profile can be quickly generated for a test area without the multiple runs required by GPS measured altitude methodologies (Sahlholm and Johansson, 2010; Boroujeni et al., 2013) and without the detailed roadway analysis and segmentation required in the LiDAR methodology described by Zhang and Frey (2006). Generating second-by-second road grade directly from the GPS positions enables quick analysis of transient vehicle data sets where the PEMS data are collected of over multiple test routes.

If significant errors are found in the measured GPS latitude and longitude from the PEMS survey then Zhang and Frey (2006) method is likely more appropriate for road grade calculation. This is because the segmentation methodology does not rely to the same degree on the accuracy of the measured GPS position. Sections where this error is significant can be identified by plotting the measured test route in GIS against a reference road map of the test area.

5.5 ANALYSIS OF THE HEADINGLEY LAP AND SECTIONS ROAD GRADE

5.5.1 Headingley Lap: Road Grade Analysis

Figure 5.15 shows the elevation profile for the Headingley lap, highlighting the elevation profile for each of the road sections, estimated using the LiDAR-GIS method. The profile shows the route descending from a maximum elevation of 98.1 m to a minimum of 76.6 m and then returning back to the initial elevation. Summed over the lap, the route ascends and descends by approximately 49 metres. However, as the Headingley lap is a loop, the start and finish elevations are roughly the same (with small disparities as a result of differences in the measured GPS position of the lap start and end points) and the average road gradient over the lap is therefore zero.

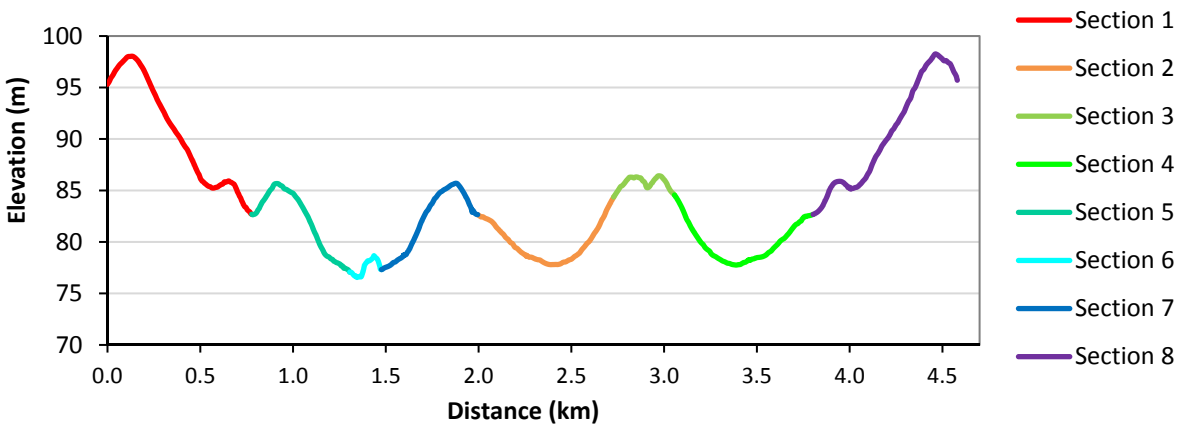

Figure 5.15: Headingley Test Lap and Sections Elevation Profile

Whilst the lap average grade is zero, the profile shows relatively few flat sections of road. Figure 5.16 presents the average road grade frequency distribution for the Headingley test lap, calculated from the GIS 1 Hz road grade estimation data. As the recorded 1 Hz GPS positions are different in each test run (differing as a result of the specific traffic conditions and driver input during each lap measurement) the road grade frequency distributions for each recorded lap may vary considerably. For example, for test runs with substantial congestion and long stationary periods, the road grade at those stationary points will consequently provide a greater fraction of that laps frequency distribution. The results in Figure 5.16 are therefore an average of the 48 individual test lap road grade frequency distributions. As such, it is a representative road grade frequency distribution for the Headingley lap and indicates the range of road grades in the test area. For the Headingley lap, 99.46% of the 1 Hz road grade estimates are between ±6% and 94.4% are within the range of ±4%.

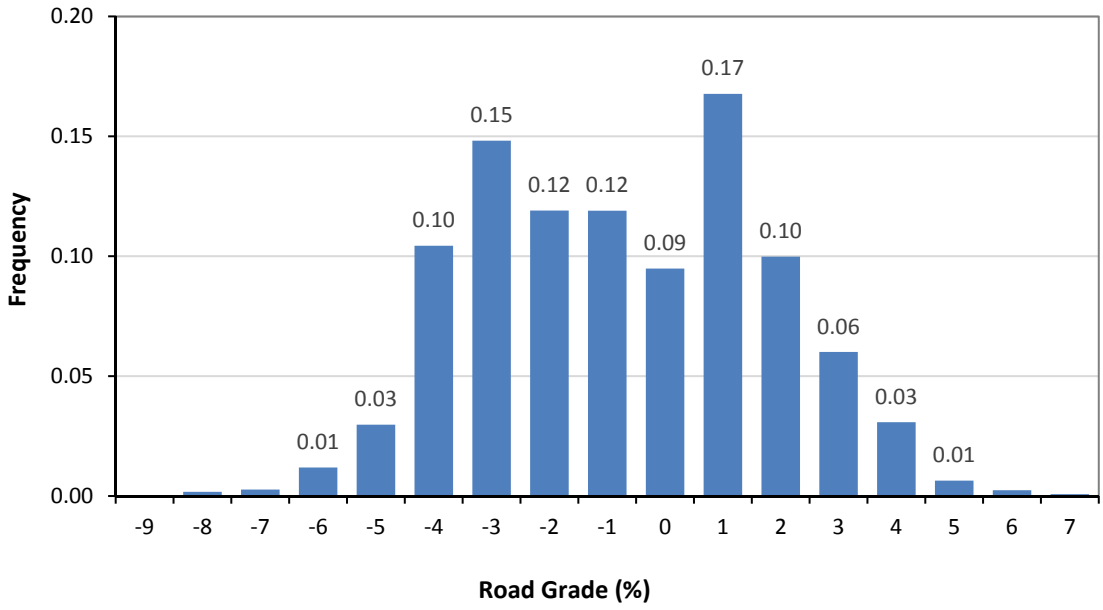

Figure 5.16: Headingley Test Lap Road Grade Distribution

5.5.2 Section 1 and Section 8: Road Grade Analysis

The median length of Sections 1 and 8 over the 48 test runs were 781 m and 777 m respectively, with a 12.5 m change in elevation along the road segment they cover. The maximum elevation of the sections is 98 m with a minimum of 82.7 m. Summed over Section 1, the road in total ascends by 3.9 m and descends by -16.4 m, with approximately the opposite increase in elevation for Section 8. Figure 5.18 presents the elevation profile for Section 1 and Section 8, the letters A, B and C correspond to the images in Figure 3.11.

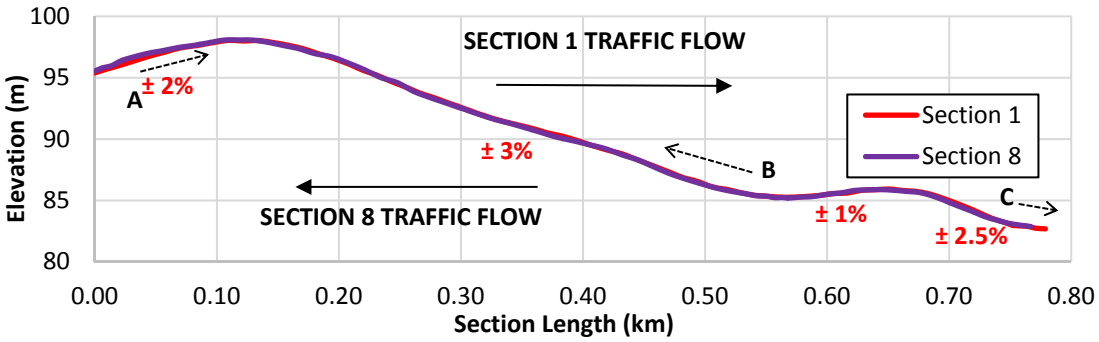

Figure 5.17: Headingley Section 1 and Section 8 Elevation Profiles

Sections 1 and 8 are the steepest sections within the test lap, with average road grades over the entire section of -1.60% and 1.66% respectively. Figure 5.18 shows the representative road grade frequency distributions for Section 1 and Section 8.

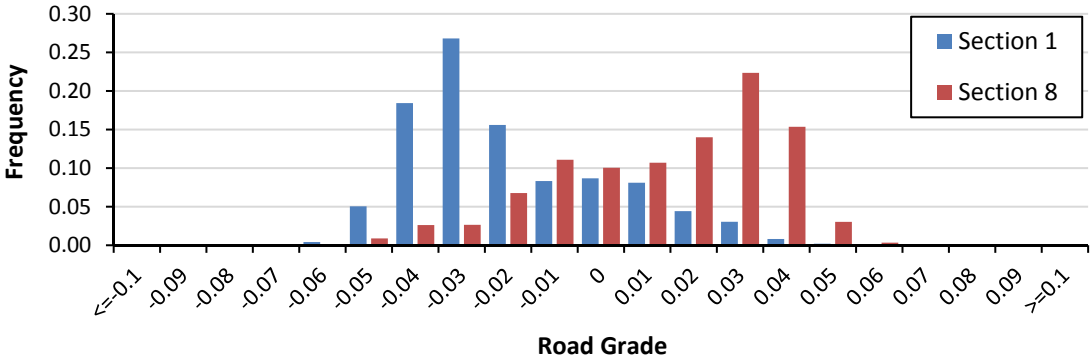

Figure 5.18: Section 1 and Section 8 Average Road Grade Distribution

In Section 1 the average road grade distribution shows 61% of the recorded 1 Hz measurements occurred where the road grade was between -1.5% and -4.5%, whilst for Section 8 52% of the data were recorded where the road grade was between 1.5% and 4.5%. The reason for this difference is most likely greater congestion in Section 1, especially near point C, where the traffic is likely to be held up by the traffic lights on a part of the road with a relatively steep gradient. There is less chance of delay in Section 8, as the only traffic management measure in this section which can stop the flow of traffic is the pedestrian crossing at point B.

5.5.3 Section 2 and Section 4: Road Grade Analysis

The median measured lengths of Section 2 and Section 4, over the 48 test runs, were 739 m and 744 m, respectively, and the average change in elevation from the start of Section 2 to the end was 1.8 m. Over Section 4 the average change in elevation was -1.9 m. The average road grades over Sections 2 and 4 were therefore 0.24% and -0.25%, respectively. Summed over Section 2 the road in total ascends by 6.8 m and descends by -5 m, with approximately the opposite true for Section 4. Figure 5.19 shows the elevation profile for both sections, with the letters D, E and F corresponding to the images in Figure 3.15.

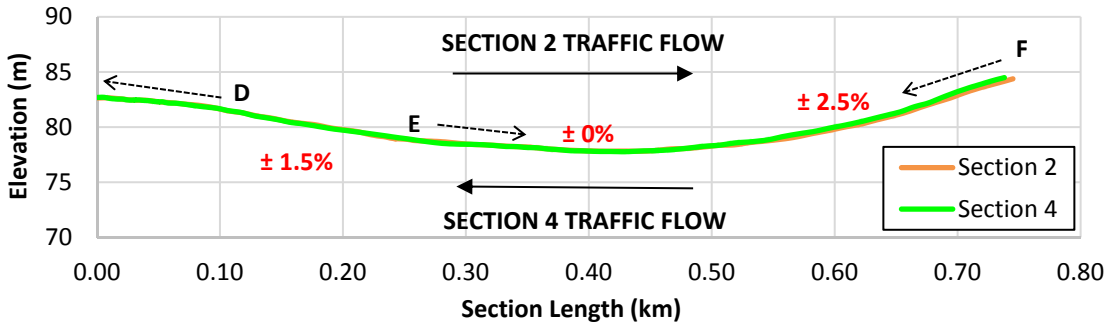

Figure 5.19: Headingley Section 2 and Section 4 Elevation Profiles

Although the average road grade for the sections is almost flat (±0.24%) the average road grade distribution elevation profile (Figure 5.20) reveals that these are not, in fact, flat sections. In Section 2, 60% of the recorded 1 Hz measurements were on sections of road with road grade between -0.5% and -2.5%, as a result of a high proportion of the section's transit time spent queuing near point E, at the traffic lights at the junction of Otley Road and Shaw Lane. Likewise in Section 4, 61% of the 1 Hz measurements were recorded at road grades between 0.5 % and 2.5%, because of the proportion of section time spent queuing at the junction of Otley Road and North Lane (seen in image D, Figure 3.15).

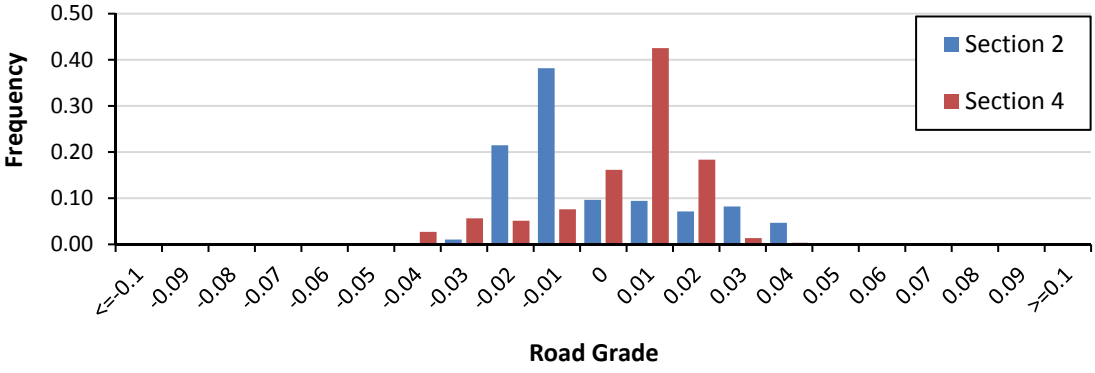

Figure 5.20: Section 2 and Section 4 Average Road Grade Distribution

5.5.4 Section 5 and Section 7: Road Grade Analysis

The average length of both Sections 5 and 7 over the 48 test runs was 523 m and the average change in elevation along the road segment is -5.5 m in Section 5 and 5.3 m in Section 7. As shown in Figure 5.21, the elevation profile for Sections 5 and 7, the road section reaches a maximum elevation of 85.7 m and falls to a minimum of 77.3 m. Summing the ascents and descents in Section 5 separately the road rises by a total of 3.2 m and descends by -8.7 m. In Section 7 approximately the opposite is true, with the road ascending by a total 8.6 m and descending by -3.3 m. The average road grade is -1.06% for Section 5 and 1.01% over Section 7. The letters in Figure 5.21 (G, H, and I) correspond to the images in Figure 3.19.

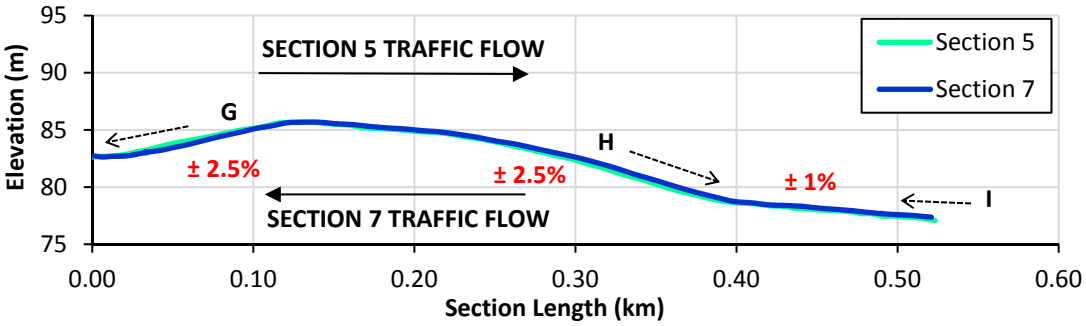

Figure 5.21: Headingley Section 5 and Section 7 Elevation Profiles

Figure 5.22 shows the average road grade distribution for Section 5 and Section 7. This distribution is different to those of Sections 1 and 8 and Sections 2 and 4, where the first section distribution was almost the opposite of the second. In this instance whilst 45% of Section 7's 1 Hz measurements were recorded on road grades between -1.5% and -4.5%, only 12% of Section 5's measurements were recorded between 1.5% and 4.5%. This is because in Section 7 a large percentage of the sections total time is spent queuing at the junction of North Lane and Otley Road, on the steep downhill section (point G). In Section 5 this part of the section is driven in free flowing conditions. The queuing time for Section 5 occurs at the junction between North Lane, Kirkstall Lane and Cardigan Road (point H).

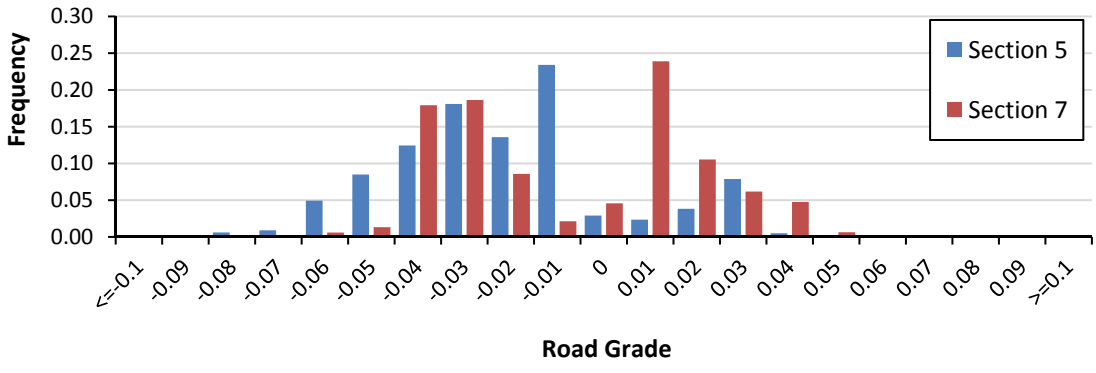

Figure 5.22: Section 5 and Section 7 Average Road Grade Distribution

5.5.5 Section 3 and Section 6: Road Grade Analysis

Section 3 and Section 6 are the two short turning loops between Sections 2 and 4 and Sections 5 and 7 respectively. Figure 5.23 shows the LiDAR-GIS generated elevation profile for Section 3.

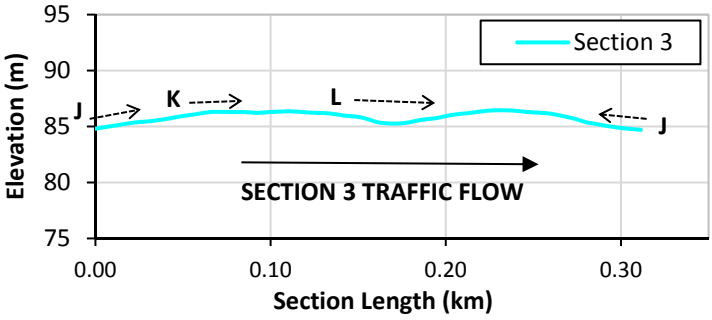

Figure 5.23: Headingley Section 3 Elevation Profile

As Section 3 (≈325 m in length) begins and ends at approximately the same point, but in opposite lanes, the average road grade is zero. However, the section is not flat, as shown by the distribution profile in Figure 5.24. Summing the ascents and descents in Section 3 separately, the road rises by 3.1 m and descends by -3 m, reaching a maximum elevation of 86.4 m and a minimum of 84.4 m. The letters (J, K, L) in Figure 5.23 correspond to the images in Figure 3.23.

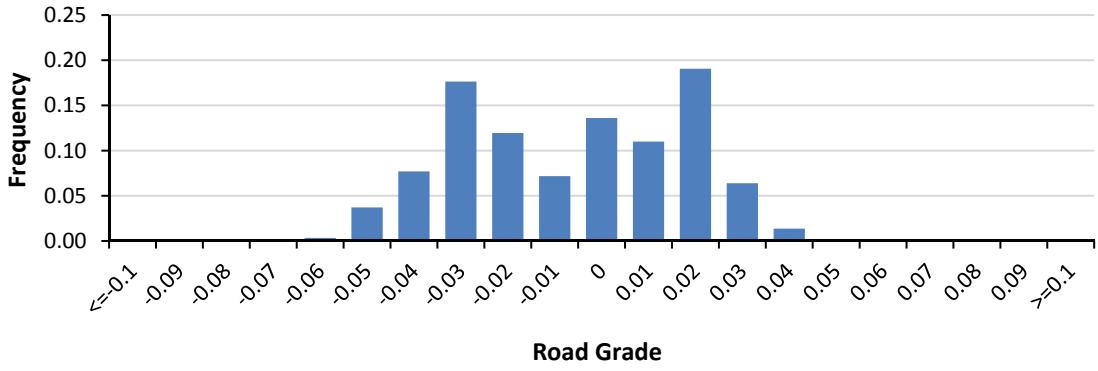

Figure 5.24: Section 3 Average Road Grade Distribution

Figure 5.25 presents the elevation profile for Section 6 (≈175 m in length), points M, N and O correspond to the images in Figure 3.25. The section's maximum altitude is 78.7 m and the minimum 76.6 m. In common with Section 3, Section 6 starts and finishes at roughly the same point but in opposite road lanes, so the average road grade over the section is about zero (0.11%). Summing the ascents and descents in Section 6, the road section rises by an average over the 48 test laps of 2.1 m and descends by -2.0 m.

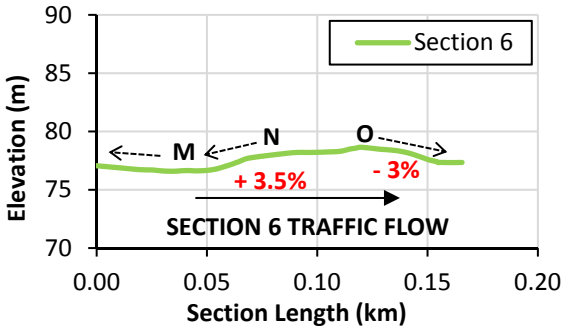

Figure 5.25: Headingley Section 6 Elevation Profile

Within Section 6 there are some relatively steep road grades as shown in the average road grade distribution for Section 6 in Figure 5.26. As this represents the distribution of road grade for each second of data, over short sections, like Section 3 and Section 6, the gradients at stationary points, such as give way junctions, are likely to form a significant fraction of the overall distribution.

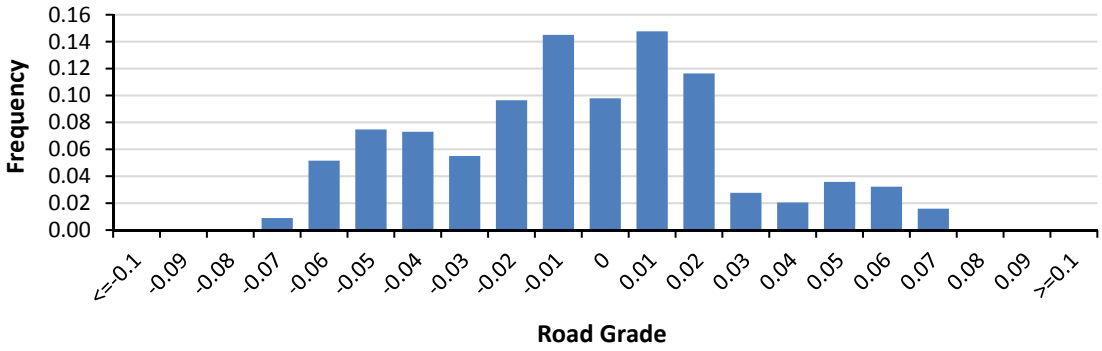

Figure 5.26: Section 6 Average Road Grade Distribution

5.6 EVALUATION OF LIDAR-GIS ROAD GRADE ESTIMATION

To ascertain if the LiDAR-GIS generated road grade improves the modelling of CO_2 emission through derived VSP, an analysis was conducted to assess the strength of the linear association between VSP and CO_2 for both VSP calculated with the LiDAR-GIS road grade (VSP_G) and also for VSP calculated with the road grade set to zero (VSP_0).

As demonstrated in other studies (Coelho et al., 2009; Song and Yu, 2009; Zhai et al., 2008) and shown in Figure 4.10 for the test vehicle used in this study, CO_2 emission increases approximately monotonically with positive VSP, as the relationship between engine power output and fuel consumption is approximately linear. Negative VSP is primarily associated with points of deceleration, where the accelerator pedal is not engaged; the CO_2 emission at negative VSP

values is therefore consistently low and approximately equal to the rate of the engine idle CO_2 emission.

To evaluate whether the LiDAR-GIS road grade values enhanced the association between positive VSP and CO_2 emission, and therefore improved the calculation of VSP, coefficient of determination values (R^2) were calculated for each of the individual 48 test laps for both VSP_0 and for VSP_G. In both cases, VSP values less than or equal to zero were excluded from the analysis, as at these values, the CO_2 emission is relatively constant.

For example, Figure 5.27 shows a scatter plot from one test lap through Headingley, displaying each second where a positive VSP was calculated against the PEMS measured CO_2 emission for that second. The VSP values were generated under the two scenarios VSP_0 and VSP_G. The linear regression lines through both sets of data are described by similar equations, but it is clear that, by adding road grade to the VSP equation, the correlation between positive VSP and CO_2 emission is improved; the position of the VSP_G values are on average closer to the trendline. This is reflected in the R^2 values for the two scenarios, with an improvement in the linear association between positive VSP and CO_2 emission from 0.63 without road grade to 0.77 with road grade.

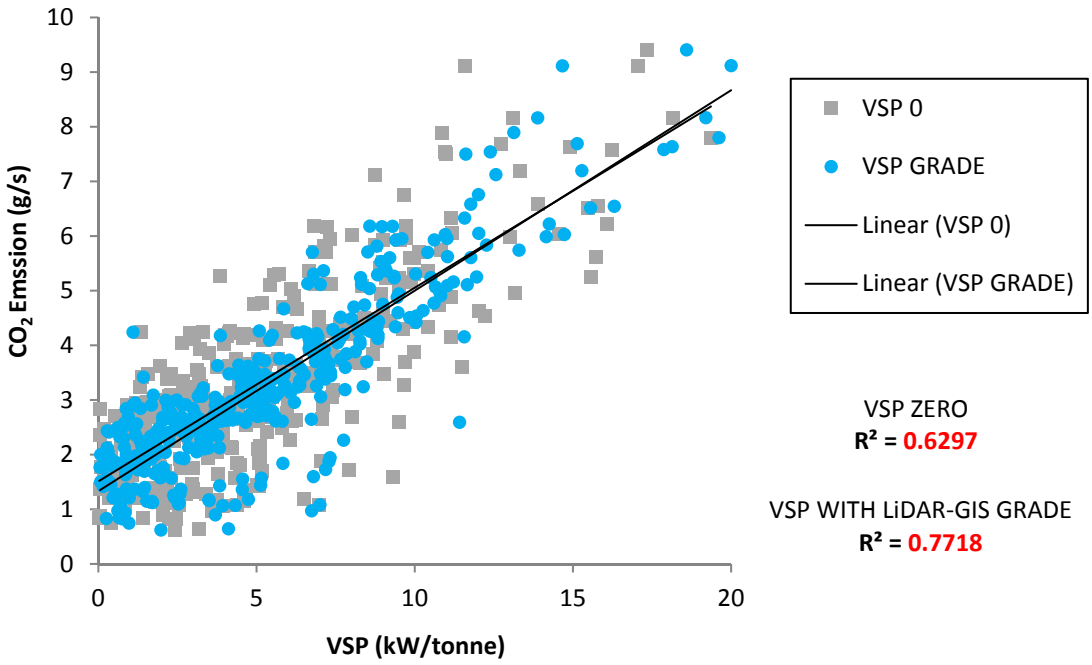

Figure 5.27: Linear Association between Positive VSP and CO_2 Emission, for VSP_0 and VSP_G, over One Headingley Test Lap

Over each of the separate 48 test laps the linear relationship between VSP and CO_2 emission improved with the addition of the LiDAR-GIS road grade. Although both VSP calculation

methods displayed a strong correlation between VSP and CO_2 emission, including road grade in the VSP calculation increased the median R^2 value from 0.65 with VSP_0 to 0.73 with VSP_G. The findings are summarised in Table 5.2. The Coefficient of Variation (CV) for the two sets of test results, which is the ratio of the standard deviation to the mean, shows the dispersion of R^2 values for each of the 48 laps calculated under VSP_0 and VSP_G to be similar.

Table 5.2: Summary of the Coefficient of Determination (R^2) Values for VSP and PEMS Measured CO_2 Emission for a Euro 4 Test Vehicle over the Headingley Test Lap, for Positive Values of VSP

		Positive VSP Values					
		VSP_0			VSP_G		
Test Section	Number of Runs	R^2 Median	R^2 Range	CV	R^2 Median	R^2 Range	CV
Headingley	48	0.65	0.53 – 0.71	0.069	0.73	0.62 – 0.82	0.064

Without a detailed land survey elevation profile for the test route, which would be required to robustly assess the road grade values generated by the LiDAR-GIS method, the substantial improvement in the correlation between calculated VSP and measured CO_2 emission with the addition of the LiDAR-GIS road grades for all test laps, suggests that the method provides a reliable representative 1 Hz gradient.

5.7 COMPARISON OF CO_2 EMISSION MODELLING WITH AND WITHOUT LIDAR-GIS GENERATED ROAD GRADE

Using the same process described in Chapter 4.6, the instantaneous emission model PHEM was used to calculate CO_2 emission estimates for the Euro 4 test vehicle through the Headingley test lap and over the shorter micro-scale test sections. To test the LiDAR-GIS road grade methodology, CO_2 emission estimates from PHEM were generated with the drive cycle .FZP file updated to include a calculated LiDAR-GIS elevation value for each second of data (designated $PHEM_G$). These $PHEM_G$ emission estimates could then be evaluated against the PHEM CO_2 estimates generated in Chapter 4, which were calculated with the test area modelled as flat, with all road grade values set as zero (designated $PHEM_0$). The vehicle specification data for the Euro 4 Mondeo test vehicle (as described in Chapter 3.2.2) was entered into PHEM and CO_2 emission estimates were calculated for this vehicle for each second of test data.

Figure 5.28 shows a time series of the PEMS measured CO_2 for one test run over a 246 s time period to complete Section 4 and Section 8. The calculated $PHEM_0$ and $PHEM_G$ CO_2 emission estimates for the same period are plotted for comparison, along with the test period elevation and speed profiles for reference. The PHEM CO_2 estimates show good agreement to the PEMS measured CO_2 emission recorded by the instrumented vehicle, with peaks and troughs of CO_2 emission resulting from periods of acceleration and deceleration displaying a good fit.

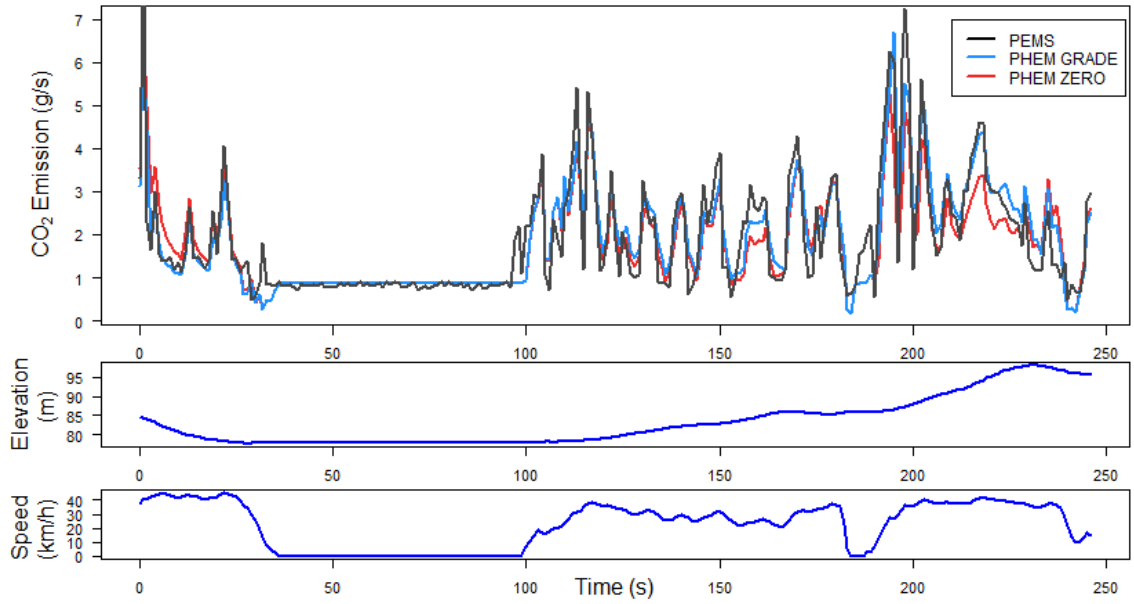

Figure 5.28: Comparison of PEMS Measured CO_2 Emission to PHEM Predicted CO_2 Emission with Road Grade set to Zero ($PHEM_0$) and the LiDAR-GIS Road Grade Values ($PHEM_G$), for One Test Run through Section 4 and Section 8. Referenced to the Test Run Elevation and Vehicle Speed Profile

The vehicle PHEM modelled idle CO_2 rate of emission is in good agreement with the pulse flow adjusted PEMS measured CO_2 emission during the period between 36 s and 98 s when the vehicle was stationary. This is important for the modelling of micro-scale congested traffic networks where a majority of the time taken to complete the section can be queuing time.

It is clear from Figure 5.28 that the inclusion of the LiDAR-GIS road grade improves the accuracy of the PHEM CO_2 emission estimates in this test run. Over the first 14 s of this test period, the elevation on the test run decreased from 84.5 m to 79.5 m in 0.17 km, with an average road grade of -3%. The $PHEM_0$ estimate, shown in red, overestimates the rate of CO_2 emission, whereas the $PHEM_G$ estimate with road grade provides a good approximation for the measured emission. Conversely between seconds 191 and 232, when the elevation height rose from 86 m to 98 m in 0.41 km at an average road grade of +3%, $PHEM_0$ clearly underestimates the CO_2 emission rate, whilst the $PHEM_G$ estimate is closer to the PEMS measurement.

5.7.1 Analysis of the PHEM$_G$ CO_2 Emission Estimates for the Headingley Test Lap and Sections

For each of the 48 test laps, the PHEM$_G$ modelled CO_2 aggregate emission estimates were calculated and compared to the corresponding PHEM$_0$ estimates and the PEMS measured CO_2 emission over the same test lap (Chapter 4.6.4.4). Figure 5.29 describes the results for each of the test laps. The median estimate of the PEMS total CO_2 lap emission by PHEM$_G$ was 91% with a range from 81% to 110% (with 50% of the PHEM$_G$ estimates between 87.4% and 96.1%). These results, for the test lap, are similar to those attained with PHEM$_0$, with only a slight improvement in PHEM CO_2 emission estimation over the test lap using the LiDAR-GIS road grade. The average PHEM$_0$ estimate (without road grade) of the lap total CO_2 emission was 90% of the PEMS recorded valued, with a range from 79% to 108% (with 50% of the values between 85.8% and 95.3%). The results for the PHEM$_G$ test lap are similar to those attained with PHEM$_0$, with only a slight improvement in PHEM CO_2 emission estimation over the test lap using the LiDAR-GIS road grade. The Headingley test lap starts and ends at the same point, therefore the average road grade over the lap is approximately zero. As a result, PHEM$_0$ overestimates of CO_2 emission on downhill road segments are partially offset underestimation on uphill road segments.

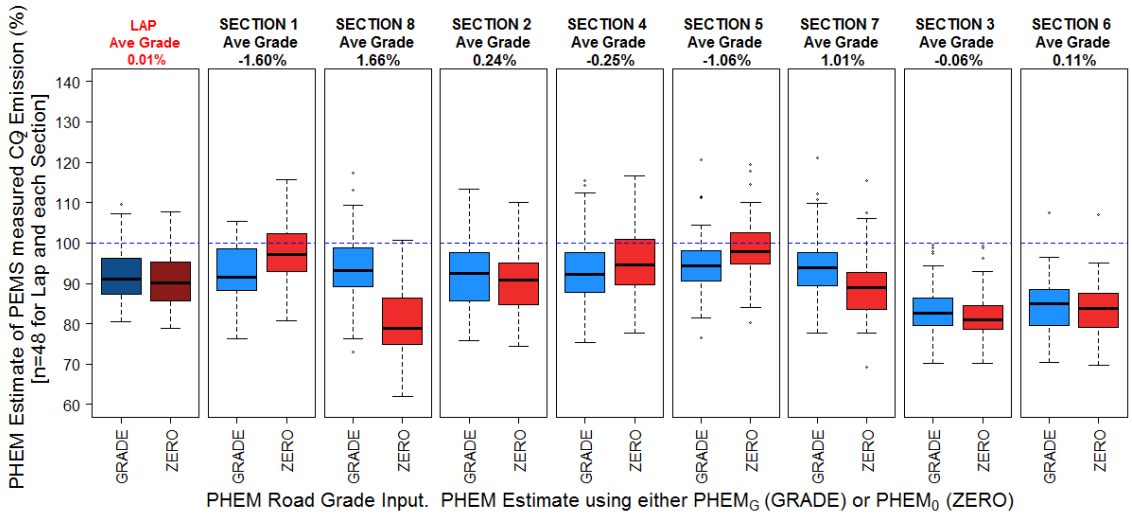

Figure 5.29: PHEM Modelled CO_2 Emission as a Percentage of the PEMS Measured Emission for Each of the 48 Test Laps and Sections, under the Two Road Grade Scenarios PHEM$_0$ and PHEM$_G$

The addition of road grade did not generate a large improvement in the accuracy of the PHEM model over the 4.6 km test lap, as the PHEM$_G$ results also underestimate the real-world vehicle CO_2 emission of the test vehicle. The Mean Absolute Percentage Error (MAPE), over the 48 test laps, of the PHEM estimate of the PEMS measured CO_2 emission decreased only a small amount from 10.0% without grade to 9.1% with grade. However as discussed in Chapter 4, this discrepancy could be the result of factors not included in the modelling for this study. Variation

in ambient temperature; starter battery state of charge and use of the vehicle's air-conditioning and heating systems have been shown to have a substantial effect on vehicle fuel consumption (Mock et al., 2012). Although a best estimate of vehicle weight was used in the modelling, it is possible that an underestimation of the simulated vehicle weight and loading, which were not measured directly during the testing, may also have caused a lower modelled rate of CO_2 emission than measured on-road.

Figure 5.29 does, however, show that the addition of road grade to the PHEM led to an improvement in the estimation of section CO_2 emission, especially for in Section 1 and Section 8 which have the steepest average road grade. Whilst the average $PHEM_G$ estimate of the PEMS CO_2 emission in Sections 1, 2, 4, 5, 7 and 8 (excluding the turning sections) range between 91% and 94%, the $PHEM_0$ estimates of PEMS CO_2 emission were greatly influenced by the road grade in the section and vary from 79% to 98%. For example, over Section 1, a primarily downhill section with an average road grade of -1.6%, the average $PHEM_G$ and $PHEM_0$ estimates of the section total CO_2 emission were 91% and 97% of the PEMS measured emission respectively. In this instance, the $PHEM_0$ appears to provide the most accurate estimates of the real-world CO_2 emission. However, over Section 8, the corresponding uphill section (the opposite traffic flow to Section 1) the average total section CO_2 emission estimate from $PHEM_0$ is 79% of the PEMS measured value, whereas for $PHEM_G$ it is 93%. Whilst the calculated $PHEM_0$ CO_2 emission rates for the downhill sections (1, 4 and 5) are closer to the PEMS measured emission, the stability of the $PHEM_G$ estimates over all sections irrespective of average road grade demonstrates that the addition of the LiDAR-GIS data in PHEM delivers consistently reliable micro-simulation CO_2 emission estimates.

The PHEM CO_2 estimation of the real-world emission through the short 'turning' Section 3 and Section 6 are perceptibly less accurate than for the longer test sections, with $PHEM_0$ median PEMS emission estimates of 81% and 84% and $PHEM_G$ estimates of 83% and 85% respectively. The decrease in the accuracy of the PHEM estimate for these sections is possibly to be due to the driver gear selections in these short stop-start sections not being characteristic of the gear shift patterns in more typical driving conditions and hence not being so adequately represented by the PHEM gear shift model.

The stability and accuracy of the $PHEM_G$ estimates when compared to the measured PEMS CO_2 emission at this micro-scale section level suggest both that the LiDAR-GIS method for generating road grade provides a representative 1 Hz gradient profile and that reliable micro-scale simulation of CO_2 emission over real-world networks is possible utilising PHEM. Excluding the

turning sections, the average CO_2 emission estimate from $PHEM_G$ was 93.4% of the PEMS measured value. The scatter plot of the PEMS measured CO_2 emission factors for each section versus the $PHEM_G$ CO_2 emission estimates (Figure 5.30) demonstrates the strength of the $PHEM_G$ model in estimating the real-world vehicle CO_2 emission over the Headingley test sections.

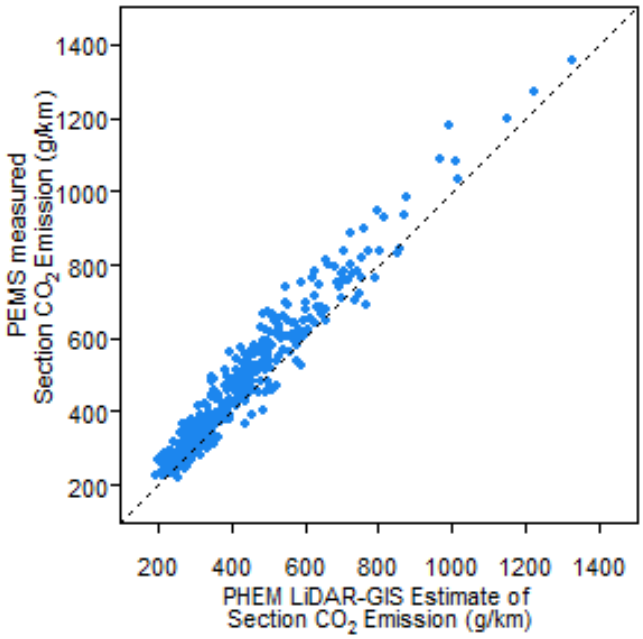

Figure 5.30: PEMS Measured CO_2 Emission Factors versus $PHEM_G$ Estimated CO_2 Emission Factors for the Headingley Test Sections (n=348)

5.7.2 Analysis of the $MOVES_G$ CO_2 Emission Estimates for the Headingley Test Lap and Sections

The modal emission model MOVES allows input of road grade along with transient vehicle speed in second-by-second link drive schedules (Chapter 4.5.4) to calculate vehicle emission values at a micro-scale. To assess whether the road grade estimates improve the micro-scale CO_2 emission modelling in MOVES, the CO_2 emission over each of the 48 laps was calculated from the PEMS recorded vehicle speed data and the LiDAR-GIS generated 1 Hz road grade ($MOVES_G$). The laps were again sub-divided into the eight micro-scale sections described in Figure 3.9. Figure 5.31 presents the $MOVES_G$ CO_2 emission estimates as a percentage of the PEMS measured CO_2 emission for the test lap and sections, in comparison to the MOVES calculated CO_2 emission without road grade ($MOVES_0$) estimates of the real-world emission calculated in Chapter 4.5.

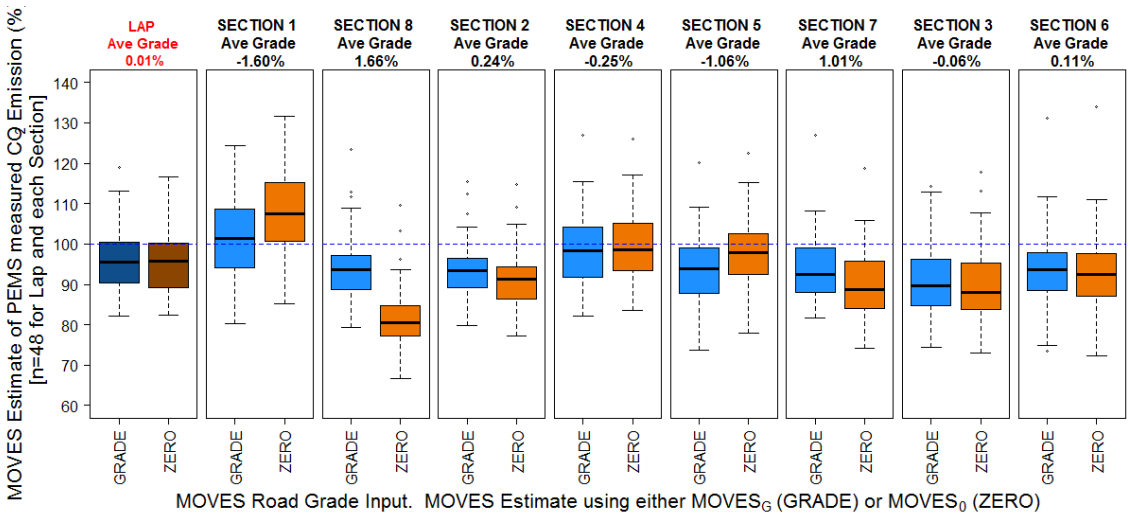

Figure 5.31: MOVES Modelled CO_2 Emission as a Percentage of the PEMS Measured Emission for Each of the 48 Test Laps and Sections, under the Two Road Grade Scenarios MOVES$_G$ and MOVES$_0$

In similar fashion to the PHEM model, the addition of the LiDAR-GIS road grade into the MOVES CO_2 emission estimation had little impact on the accuracy of the modelled lap emission when judged against the MOVES$_0$ estimates. The median estimate of the PEMS total CO_2 lap emission by MOVES$_G$ was 95% with a range from 82% to 119% (with 50% of the MOVES$_G$ estimates between 90.3% and 100.4%). The MOVES$_0$ lap estimates are almost identical to those generated under MOVES$_G$. The average MOVES$_0$ estimate of lap total CO_2 emission was 96%, with a range from 82% to 116% (with 50% of the MOVES$_0$ estimates between 89.1% and 100.3%). As for the PHEM model, because the average grade of the Headingley lap is approximately equal to zero, the overestimation of CO_2 emission downhill and the underestimation of emission uphill under MOVES$_0$ offset each other to a large extent, negating the possibility of any substantial difference between the estimates of MOVES$_0$ and MOVES$_G$. The MAPE between the MOVES estimate of lap emission and the PEMS real-world observed CO_2 emission decreased only slightly with the addition of gradient, from 7.9% to 7.3%.

The addition of the LiDAR-GIS road grade did improve the precision of the MOVES CO_2 emission estimates at the micro-scale section level. As shown in Figure 5.31, under MOVES$_0$ there is significant variance in the accuracy of CO_2 emission estimates between sections, with a range in median estimate from 107.6% for Section 1 to 80.5% for Section 8 and an overall average of 93.1%. The addition of road grade to the MOVES model helped improve the accuracy of the VSP estimate on uphill sections increasing the VSP, leading to higher estimates CO_2 emission, and on downhill sections decreasing the VSP, resulting in lower estimates of CO_2 emission. Under MOVES$_G$ this has led to a more uniform average estimate of CO_2 emission across all sections, with the average MOVES$_G$ estimate of section CO_2 emission (excluding the turning Sections 3 and 6) being 95.5% of the PEMS measured emission, ranging from 92% to 101%. The average

$MOVES_0$ estimate of the real-world observation was 94%, with a range from 80% to 108%. The improvement is especially clear for Section 1 and Section 8, the two steepest sections in the Headingley test.

The Section 3 and Section 6 modelled estimates are considerably less accurate in PHEM, whilst in MOVES the accuracy of the estimated CO_2 emission over these shorter turning sections is on a par with the other sections. This may be one advantage of the MOVES methodology over the PHEM approach. As MOVES does not rely on a gear-shift model to determine engine power output, emissions over short sections with atypical speed profiles may be better accounted for by the modal methodology.

As for PHEM, the results for MOVES demonstrate that for micro-scale sections of even modest road grade, accurate estimation of real-world exhaust emission will be dependent on accurately quantifying the road gradient. For example, Section 8 when modelled in MOVES without road grade had an average percentage estimate of the PEMS measured values of only 80.5%; with road grade the MOVES average section percentage estimate improved to 93.5%.

Both PHEM and MOVES with the LiDAR-GIS road grade provided a close approximation of the on-road emission of the test vehicle over the micro-scale sections. Excluding turning Sections 3 and 6, the section average $PHEM_G$ percentage estimate of the PEMS measured CO_2 emission is 93.4% with an interquartile range from 88.2% to 98.0%. For $MOVES_G$ the average over the same sections was 95.8% with an interquartile range from 89.4% to 101.2%.

Table 5.3 presents a summary of the analysis for the models with and without road grade. The MOVES and PHEM models with the LiDAR-GIS road grade show the same pattern displayed in the Chapter 4 analysis without road grade, in that the $MOVES_G$ estimates of real-world emission tend to be the more accurate, whilst the $PHEM_G$ estimates are marginally more precise, as shown by the calculated IQRs. Again, both models seem suitable for micro-scale emission evaluations. However, because PHEM is more flexible in its ability to model specific vehicles and the fact that it has been developed for a European rather than an American fleet, it the most suitable model for this research.

Table 5.3: Summary Table for the Headingley Sections PHEM and MOVES Modelled CO_2 Emission

	$MOVES_0$	**$MOVES_G$**	**$PHEM_0$**	**$PHEM_G$**
Mean Model % Estimate of PEMS CO_2 Emission: **SECTION** (n =288)	94.7%	95.8%	91.8%	93.4%
Range of Model % Estimate of PEMS CO_2 Emission: **SECTION** (n =288)	66.6% - 131.6%	73.7% - 126.9%	61.9% - 119.3%	73.1% - 121.8%
SECTION Emission IQR (n=288)	16.3%	11.8%	13.4%	9.7%
SECTION MAPE (n=288)	10.8%	8.4%	10.7%	9.0%

5.8 PHEM MODELLED CO_2 EMISSION SENSITIVITY TO ROAD GRADE

Having demonstrated the ability of PHEM to model micro-scale CO_2 emission factors over the Headingley test lap and sections as well as the improved accuracy of those estimates with the addition of the LiDAR-GIS road grade, this section uses the PHEM model to estimate CO_2 emission at a range of road grades. PHEM CO_2 emission estimates for the test vehicle were calculated using the real-world PEMS measured speed profiles under five road grade scenarios, where coefficients of 0, 0.5, 1, 2 and 3 were applied respectively to each second of LiDAR-GIS road grade, both lessening and exaggerating the gradient profiles.

Figure 5.32 is a plot of the frequency distribution for the Headingley lap road grades under each of the road grade scenarios. The zero road grade coefficient ($PHEM_0$) models the test area as totally flat. With the 0.5 coefficient ($PHEM_{0.5G}$), the model uses half of the calculated LiDAR-GIS value at each second. For $PHEM_{0.5G}$ 96.8% of the 1 Hz road grade estimates are between ±2% with 99.6% between ±3%. For $PHEM_G$ as reported earlier in the study, 99.5% of the 1 Hz road grade estimates were between ±6% and 94.4% were within the range of ±4%. Doubling the road grade at each section with the road grade coefficient of 2 ($PHEM_{2G}$), 76.2% of the 1 Hz road grade estimates were between ±6% and 97.5% were within the range of ±10%. With a road grade coefficient set to 3 ($PHEM_{3G}$) 80.9% of the 1 Hz road grade estimates were between ±10% and 96.3% were within the range of ±14%.

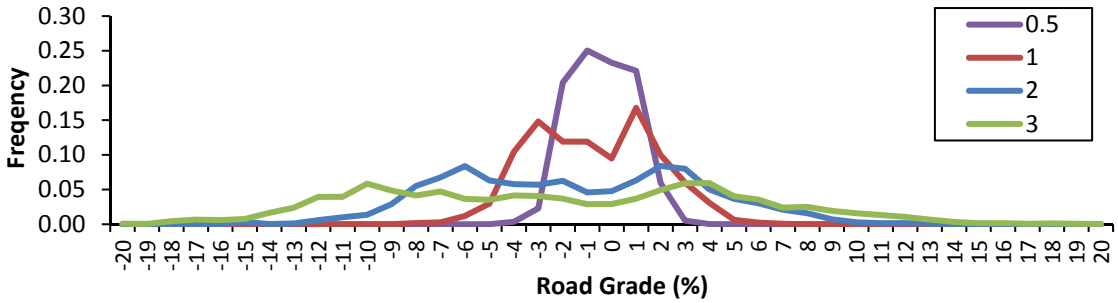

Figure 5.32: Headingley Lap Representative Road Grade Distribution for Each Road Grade Coefficient

Whilst it is likely that in real-world driving the steeper road grades would have an impact on the speed profile of the vehicle, to enable comparison, the modelling in this section of the study assumes the same speed profiles (as measured by the PEMS system) for the vehicle at every road grade coefficient. It should also be noted that the use of a coefficient of 3 produces a very steep gradient profile, however, the road grades employed in the $PHEM_{3G}$ scenario are within the bounds of reality. Whilst there is no database available with reliable statistics for the relative steepness of roads in UK urban areas, there are certainly a number of UK cities such as Sheffield, Bristol and Bradford which feature significant hills in urban areas. An example is Jenkin Road in Sheffield, which is 0.8 km in length and has an average grade of 11.2% with a maximum gradient of 33.3% (Veloviewer, 2013). Such road grade scenario testing is limited by PHEM. The PHEM model produces error warnings when an instantaneous engine power output that is out of the scope of the engine map for the vehicle is calculated. As a result, unrealistic road grades (e.g. in scenarios with large test coefficients) would cause the PHEM modelling process to fail.

It is unlikely that there are real-world urban networks with road grades that precisely correspond to those used the steeper PHEM scenarios and as higher road grades would certainly have implications for the vehicle speed profile, the results from this scenario testing should be treated as providing indicative, rather than definitive, values for the influence of road grade on vehicle emission modelling. Future PEMS testing over urban road networks that feature significant road grades would clearly help to clarify the degree to which the modelling of on-road vehicle emission is dependent on establishing an accurate description of second-by-second road grade.

Table 5.4 details the PHEM modelled CO_2 emission results for the 48 test runs over each lap and section for the 5 road grade scenarios. The average lap CO_2 emission under $PHEM_0$ is 402 gCO_2/km with a range over the 48 test runs from 268 – 515 gCO_2/km. Comparing the $PHEM_G$ results to $PHEM_0$ shows that the average lap CO_2 emission increases by 1.4% with the addition of the LiDAR-GIS road grade, with the CO_2 emission change for each lap ranging from a 0.3% decrease to a 3.9% increase in CO_2 emission. For $PHEM_{2G}$, the average CO_2 emission change over

the lap compared to $PHEM_0$ is 4.0%, ranging from an increase of 1.4% to 8.9%, and for $PHEM_{3G}$ the average change is 7.6% with a range of 3.2% to 15.8%.

Table 5.4: PHEM CO_2 Emission Calculation under Five Road Grade Scenarios. Comparing PHEM Calculated CO_2 Emission at Zero Road Grade to the PHEM Calculated CO_2 Emission with LiDAR-GIS Road Grade and Coefficients of 0.5, 1, 2 and 3, for Each Headingley Test Lap and Section

Section		CO_2 Emission Comparison at Modelled Road Grade Coefficients									
		$PHEM_0$		$PHEM_{0.5G}$		$PHEM_G$		$PHEM_{2G}$		$PHEM_{3G}$	
#	Ave. Grade (%)	Ave. (g/km)	Range (g/km)	Ave. (% Change from $PHEM_0$)	Range (% Change from $PHEM_0$)	Ave. (% Change from $PHEM_0$)	Range (% Change from $PHEM_0$)	Ave. (% Change from $PHEM_0$)	Range (% Change from $PHEM_0$)	Ave. (% Change from $PHEM_0$)	Range (% Change from $PHEM_0$)
1	-1.60	509	210 - 1037	-2.7	-9.3 – 0.3	-4.8	-11.7 – -3.9	-8.0	-17.5 – -3.9	-9.9	-22.2 – -4.5
8	1.66	258	170 - 336	8.5	4.0 – 32.0	17.2	8.5 – 43.2	37.1	18.5 – 67.7	57.1	32.3 – 102.1
2	0.24	274	203 - 503	0.5	-4.7 – 3.7	2.0	-3.8 – 11.0	4.8	-1.7 – 13.9	8.7	1.0 – 17.5
4	-0.25	409	236 - 876	-1.4	-6.3 – 2.7	-2.0	-6.7 – 5.3	-2.3	-7.1 – 7.6	-1.5	-6.7 – 8.3
5	-1.06	434	246 - 1322	-2.4	-7.5 – 1.1	-4.1	-9.7 – 2.3	-7.4	-17.8 – 0.7	-9.1	-20.7 – 3.3
7	1.01	515	257 - 856	3.2	0.9 – 12.9	6.0	2.0 – 17.2	12.1	5.1 – 28.2	20.1	8.3 – 41.0
3	0.06	436	273 - 986	0.7	-1.1 – 2.6	1.7	-0.5 – 6.3	3.9	0.0 – 8.9	7.0	0.5 – 14.3
6	0.11	524	344 - 957	0.4	-3.5 – 3.9	0.9	-3.3 – 2.0	2.4	-2.3 – 6.5	4.4	-0.4 – 9.4
LAP	0.01	402	268 - 515	0.5	-0.8 – 2.3	1.4	-0.3 – 3.9	4.0	1.4 – 8.9	7.6	3.2 – 15.8

As the test lap starts and ends at approximately the same point, the average lap road grade is zero. This modelling suggests that it is incorrect to assume over a test cycle with an average flat road grade but which experiences change in elevation over the length of its profile, that the increase in CO_2 emission in uphill sections will be offset by the decrease in CO_2 emission in downhill sections. The PHEM modelling indicates that for such test cycles CO_2 emission increases with increasing steepness of road grade.

Analysing the PHEM calculations at the section micro-scale level suggests that road grade is a very important factor in establishing CO_2 emission over short road sections. Over Section 8, a relatively fast free flowing uphill section (with an average road grade of +1.66% from the LiDAR-GIS elevation profile), the average increase in CO_2 emission from $PHEM_0$ to $PHEM_G$ is 17.2% with a range in CO_2 emission increase for the section of between 8.5% and 43.2%. Over the same section under $PHEM_{3G}$, with a hypothetical tripling of 1 Hz road grade, the CO_2 emission increase range is from 32.3% to 102.1%. For each of the sections there is a significant difference in CO_2 emission estimates modelled under the flat scenario ($PHEM_0$) and the sections modelled with road grade, with the difference increasing as the road grade increases. This suggests that conducting micro-scale modelling without establishing accurate road grade would cause the CO_2 emission estimates to vary considerably from the real-world CO_2 emissions.

In order to assess how the magnitude of CO_2 emission varies with road grade over a road segment with two-way traffic flow, the total CO_2 emissions over paired sections 1 and 8, 5 and 7, 2 and 4 were calculated. The total CO_2 emission was calculated over each pair of the combined sections for each of the 48 test runs under the five road grade scenarios. As these section pairs cover the same road segment there is no net change in elevation, so the average grade of each of the combined sections is zero. In Figure 5.33, the combined sections' aggregate CO_2 emission for each of the road grade coefficients (0.5, 1, 2 and 3) are referenced against the aggregate CO_2 emission over the same combined section with $PHEM_0$. The results indicate that higher CO_2 emission on uphill sections is not offset by lower emission on downhill sections. The discrepancy over the combined sections tends to rise as the road grade coefficient applied in the PHEM modelling increases. The magnitude of the increase in emission is greatest where the average road grades of the two sections of opposing traffic flow are steepest.

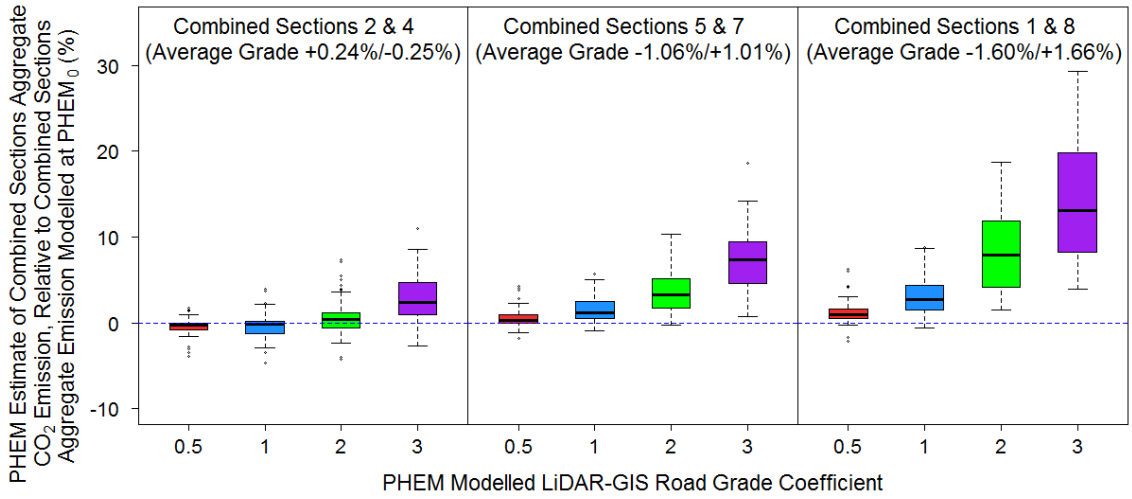

Figure 5.33: Percentage Change in the PHEM Aggregate Total CO_2 Emission between $PHEM_0$ and $PHEM_G$ Modelled with Each Road Grade Coefficient, over the Combined Sections

The largest increase in CO_2 emission was found over the combined Sections 1 and 8, which are the sections with the steepest real-world average gradient (-1.60% and 1.66% respectively). Over the 48 test runs, multiplying the LiDAR-GIS 1 Hz road grade calculations by a coefficient of 3 increased the total CO_2 emission over these combined sections by between 3.9% and 29.3% compared to the calculated CO_2 emission under $PHEM_0$. The difference between the calculated total CO_2 emission for the combined Sections 1 and 8 under $PHEM_G$ and $PHEM_0$ for each of the 48 test runs ranged between -0.6% and 8.8%. It should be noted that the traffic conditions in the road sections that make up the combined pairs can be quite different for each direction of traffic flow, as traffic control measures and traffic volume can cause different levels of congestion, resulting in a wide range of CO_2 emission values in each section. However the results in Figure 5.33 present the calculated emission from real-world speed profiles recorded

throughout the day, so these combined emissions should reflect the likely range of CO_2 emission rates for the test vehicle on these real-world road segments.

The results indicate that road grade can have a significant impact on the modelled vehicle emission and that for road segments where the average road grade is zero but where there is a change in elevation over the segment profile, it is incorrect to assume that the increase in emission in uphill sections will be counter-balanced by the decrease in emission in downhill sections. The PHEM modelling suggests that for such test cycles, total CO_2 emission rises with steeper gradient in the sections.

5.9 PHEM MODELLED NO_X EMISSION SENSITIVITY TO ROAD GRADE

As reported Chapter 4.6.1, PHEM can generate emission estimates for a number of emission species. As a demonstration of this capacity, analysis of the emission sensitivity of PHEM generated Nitrogen Oxides (NO_x) emission estimates under the five road grade scenarios was also performed. Table 5.5 details the PHEM modelled NO_x emission results for the 48 test runs over each lap and section.

The average lap NO_X emission under $PHEM_0$ is 0.082 gNO_X/km with a range over the 48 test runs from 0.066 – 0.096 gNO_X/km. Comparing the $PHEM_G$ results to $PHEM_0$ shows that the average lap NO_x emission estimate increased by 3.0% with the addition of the LiDAR-GIS road grade, with a range from a 0.4% decrease to a 6.9% increase in NO_X emission. For $PHEM_{2G}$ the average NO_X emission change over the lap compared to $PHEM_0$ is 9.8%, ranging from an increase of 4.7% to an increase of 17.3%, and for $PHEM_{3G}$ the average change is 21.3% with a range of increase from 12.3% to 37.9%.

The modelling reveals NO_X emission to be more sensitive to road grade than CO_2 emission, with a greater percentage increase in emission at the larger road grade coefficients. Like the modelled CO_2 emission, it cannot be assumed that over a loop test cycle higher NO_X emission in uphill sections is offset by lower NO_X emission in downhill sections. This modelling suggests that over the Headingley test lap such an assumption would cause an average underestimation of NO_X emission by 3.0%.

Table 5.5: PHEM NO_x Emission Calculation under Five Road Grade Scenarios. Comparing PHEM Calculated NO_x Emission at Zero Road Grade to the PHEM Calculated NO_x Emission with LiDAR-GIS Road Grade and Coefficients of 0.5, 1, 2 and 3, for Each Headingley Test Lap and Section

Section		NO_x Emission Comparison at Modelled Road Grade Coefficients									
		$PHEM_0$		$PHEM_{0.5G}$		$PHEM_G$		$PHEM_{2G}$		$PHEM_{3G}$	
#	Ave. Grade (%)	Ave. (g/km)	Range (g/km)	Ave. (% Change from $PHEM_0$)	Range (% Change from $PHEM_0$)	Ave. (% Change from $PHEM_0$)	Range (% Change from $PHEM_0$)	Ave. (% Change from $PHEM_0$)	Range (% Change from $PHEM_0$)	Ave. (% Change from $PHEM_0$)	Range (% Change from $PHEM_0$)
1	-1.60	0.091	0.062 – 0.120	-1.8	-9.0 – 2.7	-3.2	-10.5 – 5.2	-3.4	-12.8 – 14.3	-0.8	-19.1 – 17.0
8	1.66	0.059	0.038 – 0.083	10.4	3.7 – 20.9	22.3	9.5 – 41.2	54.3	29.0 – 97.0	102.9	61.3 – 186.4
2	0.24	0.062	0.042 – 0.094	0.8	-2.9 – 6.8	2.2	-5.1 – 15.2	9.0	-4.7 – 33.2	20.7	0.5 – 69.0
4	-0.25	0.082	0.058 – 0.122	-1.6	-6.8 – 3.4	-2.6	-7.6 – 3.6	-3.3	-19.4 – 6.0	-1.5	-19.3 – 10.7
5	-1.06	0.089	0.052 – 0.161	-2.6	-5.7 – 1.5	-4.4	-10.9 – 3.3	-5.4	-15.0 – 9.1	-1.6	-14.4 – 34.4
7	1.01	0.098	0.071 – 0.131	4.1	-2.2 – 12.2	9.4	1.7 – 21.6	24.0	11.6 – 54.5	41.4	18.3 – 84.5
3	0.06	0.116	0.083 – 0.154	0.9	-5.7 – 6.5	2.4	-11.0 – 9.6	5.9	-10.4 – 20.2	12.4	-9.5 – 28.1
6	0.11	0.109	0.080 – 0.149	1.3	-4.9 – 4.3	3.1	-8.8 – 11.7	7.5	-8.1 – 17.7	14.7	-4.8 – 29.1
LAP	0.01	0.082	0.066 – 0.096	1.1	-0.4 – 3.3	3.0	0.4 – 6.9	9.8	4.7 – 17.3	21.3	12.3 – 37.9

At the micro-scale section level, road grade is shown to be very important to accurate estimation of NO_X emission, especially for steep uphill sections. Over the steepest sections in the Headingley test lap, Sections 7 and Section 8, the average percentage changes in total NO_x emission from $PHEM_0$ to $PHEM_G$ are 9.4% and 22.3% respectively. At the steepest road grade coefficient, this average percentage change in total NO_X emission (from $PHEM_0$ to $PHEM_{3G}$) for these sections increases to 41.4% and 102.9%, respectively. This modelling indicates that neglecting road grade in the estimation would lead to a significant underestimation of total NO_X emission.

Following the same methodology used in the CO_2 analysis, comparing the total NO_x emission over the combined sections (where those section pairs describe the opposing traffic flows over the same road segment) reveals a considerable increase in total NO_x emission at steeper road grades. Again the steepest segment, Sections 1 and Section 8, show the greatest increase in total emission. The average increases in NO_x emission from $PHEM_0$ to $PHEM_{0.5G}$, $PHEM_G$, $PHEM_{2G}$ and $PHEM_{3G}$, over the combined Sections 1 and 8 are 2.9%, 7.0%, 20.4% and 41.7% respectively. This further highlights the importance of including road grade estimates in micro-scale emission modelling even in instances where the average road grade is flat.

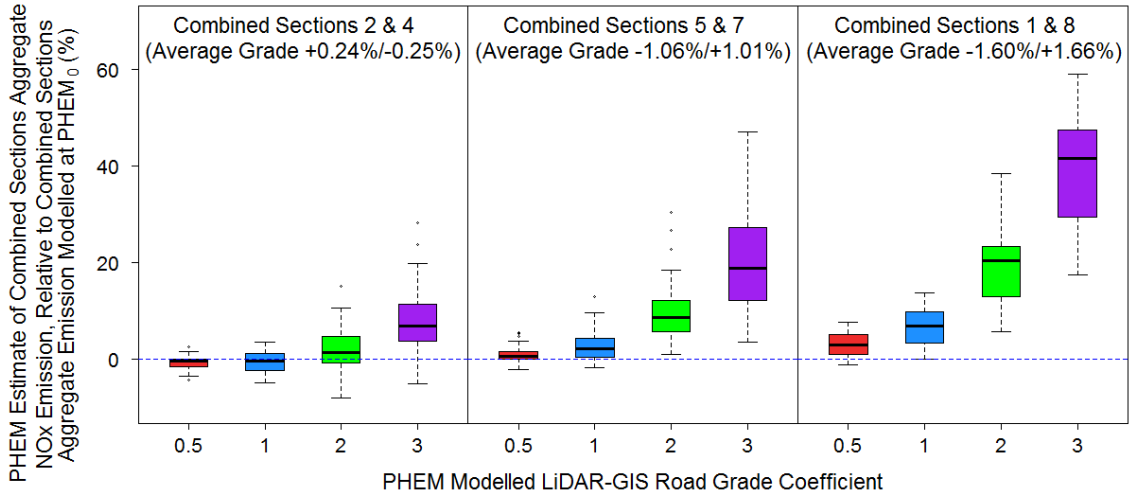

Figure 5.34: Percentage Change in the PHEM Aggregate Total NO_x Emission between $PHEM_0$ and $PHEM_G$ Modelled with Each Road Grade Coefficient, over the Combined Sections

5.10 SUMMARY

In this chapter a sensitivity analysis of CO_2 emission is presented, generated from the VSP equation for the Euro 4 test vehicle at road grades of -6%, -3%, 0%, 3% and 6%, over a the likely range of speeds in the Headingley network from 0 km/h to 50 km/h under three scenarios acceleration (0.5 m/s^2), cruise (0 m/s^2) and deceleration (-0.5 m/s^2). It was demonstrated that in all three scenarios failure to account for road grade could lead to a substantial error in the estimation of CO_2 emission. Even at the relatively modest road grades in this study, when travelling at 30 mph (48 km/h) the inclusion of positive road grade resulted in gCO_2/s exhaust emission rates between 1.3 and 2.9 times greater than on a flat road. Likewise on downhill sections, at 30 mph where the vehicle was accelerating (0.5 m/s^2) or cruising (0 m/s^2) the inclusion of negative road grade led to a gCO_2/s emission rate 40% to 70% of that on a flat road.

Utilising the real-world PEMS measured speed, location and CO_2 emission data this study presented a novel and straightforward LiDAR-GIS based methodology for calculating a 1 Hz road grade. The addition of the LiDAR-GIS road grade values was shown to significantly improve the linearity of the relationship between positive VSP and CO_2 emission, when compared to VSP calculated without road grade, increasing the average R^2 value from 0.65 to 0.73.

Although adding the LiDAR-GIS data to the PHEM instantaneous emission modelling did not significantly improve the Headingley lap CO_2 emission estimates compared to those without grade, it was shown to improve the stability of the PHEM estimate of the measured micro-scale section CO_2 emission. With $PHEM_G$ median total CO_2 emission estimates of between 91% and

94% for the lap and sections (excluding the short turning sections) compared to a range between 79% and 98% for $PHEM_0$. Using the PHEM model with LiDAR-GIS road grade has been demonstrated as a useful technique for estimating real-world CO_2 emission at a micro-scale for an individual test vehicle. The range of the $PHEM_G$ modelled CO_2 estimates, with 90% of section estimates between 79.5% and 109.7% of the PEMS measured CO_2 value and a MAPE from the real-world CO_2 emission of 9.0%, seems reasonable given the wide variety of traffic conditions encountered in the Headingley survey. Other factors that could have caused variability in the model accuracy include the 'pulse effect' exhaust flow adjustment; factors affecting vehicle fuel consumption which were not included in the modelling such as day-to-day variation in ambient temperature, starter battery state of charge and use of the vehicle's air-conditioning and heating systems; and the possible inaccuracy of the vehicle weight estimate.

The LiDAR-GIS 1 Hz data were also shown to improve the MOVES section estimates of the PEMS measured CO_2 emission. The inclusion of road grade removed some of the section-to-section variability in estimate accuracy which was found under $PHEM_0$. The improvement was clearest in Sections 1 and Section 8, which had the steepest average gradient of the sections in the Headingley survey (≈ ±1.6%). The on-road micro-scale CO_2 emission prediction ability of the $MOVES_G$ and $PHEM_G$ were shown to be remarkably similar, given the two different methodologies, with $MOVES_G$ marginally more accurate in its average section CO_2 emission estimate, 95.8% versus 93.4% for $PHEM_G$, and $PHEM_G$ slightly more precise in its emission estimates, with an IQR of 9.7% compared to 11.8% for $MOVES_G$. Both models could be considered appropriate for the micro-scale CO_2 emission modelling of this test vehicle, however the flexibility of PHEM in allowing adjustment to represent other test vehicles (of different mass, engine power, etc.) and the fact that its default settings were developed for the European vehicle fleet (whilst MOVES is an American model) make PHEM most suitable for this research.

An assessment of the effect of road grade on CO_2 emission was conducted using the PHEM model under five road grade scenarios. The scenarios were formed by multiplying the LiDAR-GIS calculated road grade for each second of data by five coefficients 0, 0.5, 1, 2 and 3. The results indicate that road grade can have a significant impact on the modelled vehicle emission. The assessment was also conducted for NO_x emission which was found to be more sensitive to road grade than CO_2 emission, with a greater percentage increase in emission at the larger road grade coefficients. For road segments over which the average road grade is zero, but where there is a change in elevation over the segment profile, it was shown to be erroneous to assume that the increase in emissions in uphill sections will be offset by the decrease in emissions in

downhill sections. The PHEM modelling suggests that for such test cycles, total emissions increase with increasing steepness of road grade in the sections.

This chapter demonstrates that in order to make accurate vehicle exhaust emission estimates at a micro-scale in real-world conditions, establishing a representative road grade profile for each second of the test data is vital. The LiDAR-GIS method proposed in this study provides a simple methodology for calculating 1 Hz road grade and has been shown to improve the modelling of CO_2 emission for this data set. This research suggests that using the PHEM instantaneous emission model with a LiDAR-GIS calculated road grade estimates is a viable method for generating accurate real-world micro-scale emission estimates. The CO_2 emission estimates in this chapter were generated from transient speed profiles recorded by PEMS survey. Whilst this provides an accurate measure of emission for one specific vehicle driving through a network, the next chapter evaluates whether it is possible to use a simulated network (including road grade) to generate 1 Hz vehicle speed data from vehicles in the network, which are sufficiently similar to the real-world vehicle second-by-second speed data, to allow accurate estimates of real-world CO_2 emission to be made from coupled traffic simulation and instantaneous emission models.

CHAPTER 6: EMISSION MODELLING USING A COUPLED TRAFFIC SIMULATION (AIMSUN) AND INSTANTANEOUS EMISSION MODEL (PHEM)

6.1 INTRODUCTION

Whilst PEMS surveys can provide a detailed evaluation of on-road driving emissions, they are limited in that they provide assessment of the emissions from only the individual vehicle being tested and the emission levels recorded are specific to the network and the conditions experienced during the test run. The amount of data which can be collected via PEMS testing is severely limited by the time required to run such detailed surveys and the cost involved in purchasing, running field tests and processing the data from PEMS units. As such the PEMS analysis is mostly restricted to appraisals of single vehicles over repeated test runs following the same route and can provide only a general indication of how network emissions may vary with congestion and diurnal traffic variation.

Even when utilising GPS speed data and road grade to estimate instantaneous power and then using emission estimation tools such as MOVES and PHEM to predict real-world emission (rather than employing a full PEMS setup) there is a limit to the number of vehicles which can be equipped with GPS recording equipment at any one time (i.e. over the AM peak), which prevents a representative sample of vehicles being recorded for emission analysis at a network scale.

Over the last decade the increase in computing power and improved data capture for model validation and calibration, have allowed the development of sophisticated microscopic traffic simulation models such as AIMSUN (TSS, 2013a), VISSIM (PTV, 2004) and PARAMICS (Quadstone, 2005). These models can be used to simulate the movement and interactions of all vehicles, over a defined time period, in a well specified road network (i.e. a simulated network where the real-world traffic signal control timings, speed limits and road geometry are accurately described). If the model is well calibrated, then the modelled second-by-second speed profiles of the simulated vehicles should be representative of the on-road speed profiles for such vehicles in real-world driving (Kraschl-Hirschmann et al., 2011).

As demonstrated in Chapter 5, vehicle emission estimates can be calculated using 1 Hz speed profiles as input to PHEM. Microscopic traffic simulation tools offer the possibility of generating 1 Hz, speed trajectories for all vehicles in a modelled network, which, once processed through an instantaneous emission model, can be aggregated to form high resolution network emission estimates. With detail for each individual vehicle, the output emission data can be analysed at any level of aggregation required. Emissions can be evaluated by the contribution from defined segments of the vehicle fleet in the network (e.g. by vehicle type and Euro emission category).

This study used the Advanced Interactive Microscopic Simulator for Urban and non-urban Networks (AIMSUN), developed by Universidad Politecnica Catalunya and Transport Simulation Systems (TSS) (Barceló et al., 2005), to simulate traffic movements along a 3.8 km section of the A660, passing through the Leeds, UK suburb of Headingley . The AIMSUN model encompasses the Headingley test lap and sections described in Chapter 3.2.1 and Chapter 3.4. AIMSUN is a versatile and powerful microscopic-mesoscopic hybrid traffic simulator, which has been developed to realistically simulate the behaviour of vehicles being driven within a road network. A study by Panwai and Dia (2005) demonstrated that the Gipps model (Gipps, 1981) which informs the car-following behaviour in AIMSUN performed better than the psychophysical spacing models used by PARAMICS and VISSIM in estimating the desired following distance between two moving vehicles. The car-following and lane-changing models are considered the two most critical components in determining the accuracy of traffic-simulation models (Panwai and Dia, 2005). AIMSUN also has fewer modelling parameters for calibration than PARAMICS and VISSIM, which is recommended for delivering accurate results for multiple simulations (Anya et al., 2014; TSS, 2013a).

AIMSUN has a very user-friendly graphic interface which supports relatively straightforward input of the road network. AIMSUN also has the capability to display a continuous animated graphical representation of the network during simulation runs, which is an invaluable tool when evaluating traffic flow in the network and identifying points of error within the model. In order to access the AIMSUN software an annual licence must be purchased. However, as the Institute for Transport Studies (ITS) University of Leeds (UoL) had some experience of modelling with the software and had an available academic licence, AIMSUN was selected as the micro-simulation package for this research.

Each vehicle category within the AIMSUN simulation (e.g. Car, Bus, LCV, etc.) is defined by physical parameters such as vehicle dimension and performance, as well as by behavioural characteristics which model influences like driver awareness, aggression and reaction time (Dia et al., 2006). The transit of an individual vehicle through the network is simulated through behavioural models that control vehicle longitudinal (e.g. acceleration; deceleration) and lateral response (e.g. overtaking; lane-changing) to stimuli within the system. These reactions are driven by operational algorithms which describe behaviours such as car-following, lane-changing and gap-acceptance (Dia et al., 2006; Anya et al., 2014; TSS, 2013a).

The operational algorithms and therefore the speed profiles of vehicles within the model are influenced by controllable parameters at three scales:

1. Vehicle attributes, which are specific to each vehicle type in the model e.g. maximum desired speed, maximum acceleration, normal deceleration, maximum deceleration;
2. Local parameters, e.g. road section speed limit;
3. Global parameters, which are universal across the network e.g. simulation step, reaction time, reaction time at stop.

The algorithms which control the movement of vehicles within the simulated network are calculated at fixed time iterations (simulation steps) and the position and speed for each vehicle are updated at each simulation step. The data for every individual vehicle can be exported from the model, detailing the position and speed at each iteration. A full description of the AIMSUN methodology is available in the AIMSUN User Guide (TSS, 2013a) and the Dynamic Simulators Users' Manual (TSS, 2013b).

Figure 6.1 describes the coupled traffic simulation and instantaneous emission model modelling approach used in this research. The modelling framework was originally developed and evaluated by Tate (ITS, UoL) in collaboration with the Institute of Internal Combustion Engines and Thermodynamics at the Technical University of Graz (TU-Graz), Austria (Zallinger et al., 2008)

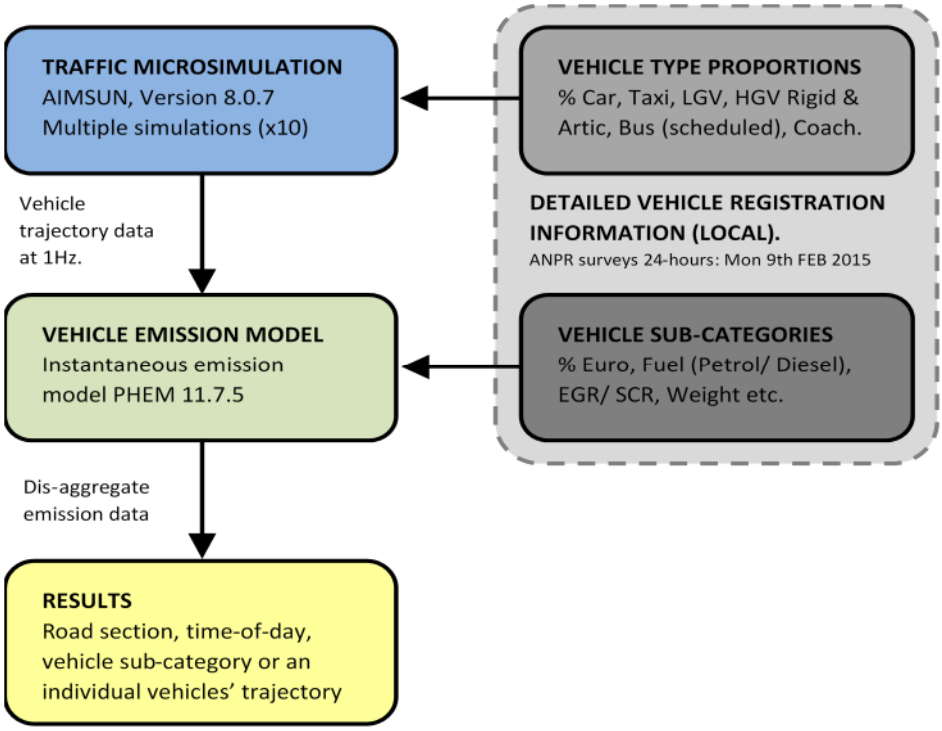

Figure 6.1: AIMSUN-PHEM Coupled Traffic-Emission Modelling Framework (Tate, 2015)

The AIMSUN simulated Headingley network developed in this research was constructed using data from multiple sources. It built on previous work from a study at ITS, which had developed a smaller scale AIMSUN 'beta' model for the A660 through Headingley (Tate, 2011). The beta model simulated a simplified version of the Headingley network, including only the A660 and its major junctions. It modelled vehicle movement in the study area for two time periods "weekday morning" (8:00 – 9:00 hrs) and an "off-peak period" (11:00 – 12:00 hrs). The vehicle fleet was described in AIMSUN by four vehicle types, "Car", "LCV", "HGV" and "Bus". A detailed breakdown of the vehicle fleet, by Euro emission standard for each vehicle type, was not available for Leeds at that time, so the beta model relied on recent fleet data from an Automatic Number Plate Recognition (ANPR) survey conducted in York (Tate, 2011).

The AIMSUN Headingley network, developed in this research, completely redrew the beta model network layout and increased the extent of the simulation to include all roads in the Headingley network, by utilising geo-referenced aerial photography which was downloaded from Landmap Kaia (Millin-Chalabi et al., 2011). Network topography, which was not included in the beta model, was incorporated into the network model by assigning a road grade to each simulated road section. Updated traffic flow input data were provided by way of Automatic Traffic Count (ATC) Manual Classified Count (MCC) data supplied by the Highways and Transportation Department of Leeds City Council (LCC), whose Urban Traffic Management and Control team also made available traffic control signal timing data for junctions not described in

the beta model. To ensure the AIMSUN simulated traffic flows were characteristic of observed flows in the real-world, 26 calibration points were included in the new Headingley model, increased from only 4 calibration points in the beta model. The traffic simulation period in the new model was extended from one hour in the beta model to two hours, with the addition of a 30 minute network warm-up period. An ANPR survey commissioned within the Headingley network (see Chapter 6.3.1) was used to provide an accurate description of the composition of the local vehicle fleet. Detailed metadata (i.e. model, make, vehicle length and width) for each vehicle recorded by the ANPR survey were also acquired, which was used to specify the average vehicle parameters for each vehicle type. To better represent the specific on-road conditions in the network, a number of the parameters in AIMSUN which influence vehicle dynamics, such as maximum acceleration and deceleration, were adjusted to reflect the real-world values recorded by an instrumented vehicle in the network.

Some data from the Headingley beta model was integrated into the new AIMSUN model. A number of adjustments made to the AIMSUN local and global parameter default values, during calibration of the beta model (so that the behaviour of vehicles in the simulation better represented the behaviour of vehicles in the real network) were adopted into the new Headingley AIMSUN model. The Headingley model also incorporated traffic signal control timing data from four junctions in the beta model. Initial set-up of the new model made use of the beta model traffic flow turning proportions at each junction. However, due to the alteration of the network layout and the update of all input flows, the junction turning percentages needed considerable adjustment (from the beta model values) in order to calibrate the new model traffic flows in each simulated time period. Other than describing the same section of the A660, the Headingley network model devised for this research and the Headingley beta model bear little resemblance to each other.

In order to extract the simulated vehicle data from the AIMSUN network model whilst the traffic simulation is in operation, an Advanced Programming Interface (API) written by the ITS, records vehicle ID, road section / junction number, vehicle type ID, vehicle speed, position and road grade, for each vehicle in the network, at every 0.5 second simulation step. The open source software 'R' (R-CoreTeam, 2014) is used to process the AIMSUN output data into a 1 Hz drive cycle .FZP file format for use in PHEM (N.B. drive cycle .FZP file formats are discussed in Chapter 4.6.4.1).

In order to produce vehicle emission estimates from PHEM, an .ADV job file must be prepared that incorporates three primary input files. As discussed in Chapter 4.6 these are the .FZP drive cycle file, the .FLT fleet data file and the route section .STR files.

- The .FZP drive cycle file details the second-by-second activity for each vehicle in the network and is generated from the AIMSUN API and an R script as described above.
- The .FLT fleet data file specifies the fleet composition for each vehicle type by fuel (petrol / diesel), Euro emission standard category (Euro 0 – 6) and, for the LCV and HGV categories, also by vehicle weight. The .FLT files are created from analysis of the detailed vehicle information gathered from the ANPR survey.
- The route section .STR files describe each road section and junction from the simulation. Each object in AIMSUN is automatically assigned a number during creation of the model. To create the necessary .STR files, the numbers from each road section and junction are exported from AIMSUN and a further R script is employed to generate individually numbered .STR files that correspond to the AIMSUN assigned numbers.

For modelling the emission estimates of the individual car in Chapter 4, the vehicle specifications were amended in PHEM to better reflect those of the test vehicle (.VEH file in Chapter 4.6.4.2). The same amendment to the .VEH file was made for each vehicle type in PHEM for modelling the fleet emission. Rather than for an individual vehicle, the specifications were adjusted to reflect the average values (vehicle weight, engine power, etc.) for each category calculated from the vehicle metadata derived from the ANPR survey. Where insufficient data were available from the ANPR survey, data default PHEM values were used. By adjusting the .VEH files, the vehicle specifications within the model better reflect the Headingley fleet, which should improve emission estimates in comparison with simply calculating emission factors using the generic European fleet vehicle specification data which are the default values in PHEM.

A comprehensive fleet description for the test network is vital, as it informs not only the vehicle type proportions of the simulated vehicle fleet in AIMSUN but also provides the detailed resolution necessary for PHEM to further segregate the AIMSUN vehicle type fleet into its constituent vehicle sub-categories (fuel type, Euro emission class and weight class) reflecting the real-world fleet. The fleet detailed vehicle specification data provided by the ANPR survey also allow calibration of the vehicle parameters in PHEM, which should make the fleet more representative of vehicles in the real-world network, compared with the default PHEM vehicle specifications.

From the constituent elements for the .ADV file, PHEM is able to process 1 Hz hot exhaust emission estimates for each vehicle in the model. There are three output file types:

- .mod files are created for each vehicle type category. These contain the second-by-second emission estimates of each vehicle for Fuel Consumption (FC), Nitrogen Oxides (NO_x), Carbon Monoxide (CO), Hydrocarbons (HC), Particulate Mass (PM), and Nitrogen Monoxide (NO) given in grams per hour (g/h), along with speed, acceleration, road grade, and power estimates.
- .vehicle.sum files present the aggregated total emission estimate for each simulated vehicle (g/h), along with time in the simulation (s), distance travelled (km) and average speed (km/h).
- .segment.sum show data for each specific road section in the network, describing the average g/km emission for each pollutant and the g/km fuel consumption , the number of vehicles to drive through the section, the total distance covered in the section (km) and the total time spent by vehicles on the section (hours). The .segment.sum file also presents the same information aggregated for each vehicle category.

Five AIMSUN simulations have been developed to represent five time periods with different traffic flow conditions observed during diurnal analysis of the ANPR vehicle fleet data. These time periods are the morning peak (AM) traffic (07:30 – 09:30); an inter-peak (IP) period (13:00 – 15:00); the afternoon peak (PM) traffic (16:00 – 18:00); the evening (EV) period (20:00 – 22:00) and the night (NI) period (01:00 – 03:00). Each of the AIMSUN time periods was individually calibrated and validated. To account for the stochastic nature of the AIMSUN micro-simulation process, ten simulations were conducted for each time period and the results are presented as an average of those ten simulations.

The high resolution nature of the coupled traffic micro-simulation and vehicle emission model inherently necessitates a substantial amount of detailed specification input data. Throughout the modelling process, every effort was made to identify, obtain and utilise the highest quality and most appropriate data sources available.

A number of recent studies have demonstrated methods of using second-by-second vehicle trajectory data from microscopic traffic simulation as input to an emission model to estimate real-world emission. Kraschl-Hirschmann et al. (2011) linked the traffic simulation model VISSIM and the emission model PHEM to compare PHEM estimates of emission from PEMS recorded

transient vehicle speed to PHEM estimates using VISSIM simulated speed profiles. Zallinger et al. (2009) used AIMSUN to generate 50 virtual drive cycles through a simulated network and recorded 50 on-road drive cycles through the network using an instrumented vehicle. The emission estimates from the on-road and simulated drive cycles were generated both using PHEM and a roller test-bed for comparison. Swidan (2011) employed AIMSUN and a PEMS based VSP modal method for emission estimation, evaluating the difference between PEMS vehicle field data and simulated AIMSUN vehicle trajectories. Similarly, Anya et al. (2014) used AIMSUN and MOVES to compare simulated vehicle emission and activity to on-road PEMS data. Song et al. (2012b), employed VISSIM for traffic simulation and compared real-world PEMS data to VISSIM simulated data using a VSP bin MOVES methodology to estimate emission from both data sets. Ahn et al. (2009) used microscopic traffic simulation models INTEGRATION and VISSIM to replicate driver behaviour at a roundabout, at a signalised intersection and at a stop sign, and then used emission model VT-Micro and the comprehensive emission model (CEM) to estimate fuel consumption and emission level for each traffic control form.

The difference between previous studies and the work in this thesis is predominantly one of scale and definition. Previous research using coupled traffic simulation and emission models have either investigated small geographical areas, such as a single junction, to demonstrate the impact of varying traffic control measures or has focused on the comparison of a small number of simulated vehicles and evaluated the estimated emission against real-world measurements. This research, in contrast, describes a relatively large and detailed network and generates emission estimates using the movement of all simulated vehicles in the network recorded at 0.5 second intervals for two-hour simulation periods. The detailed measurement of the vehicle fleet through an ANPR survey ensures with high confidence that the simulated fleet is representative of the real-world fleet. This enables estimation of real-world vehicle fleet emission factors; allows relative contributions to total emission from each vehicle category to be identified and also allows calculation of diurnal changes in vehicle fleet composition. In previous studies the vehicle fleets, on the whole, are poorly defined, relying on average vehicle fleet data or model default settings which are unlikely to reflect the real-world emission within the specific simulation area.

A further factor that has been almost universally ignored in previous studies is road grade. In the vast majority of the simulations used for such research there has been a tendency for studies to suggest that the test area is flat enough to set the road grade to zero (Yu et al., 2016; Song et al., 2012a; Anya et al., 2014). As demonstrated in Chapter 5, even shallow road gradients can have a substantial effect on emission estimation. To improve the modelling of emission in this

study, each road section in the AIMSUN simulation has an associated road grade calculated from the DTM (described in Chapter 6.3.2).

The development of a properly calibrated traffic simulation model allows for large volumes of second-by-second data for individual vehicles to be generated. Collecting a similar volume of real-world data, for a large number of drivers under a full range of conditions, is both impractical and prohibitively expensive (Jackson and Aultman-Hall, 2010). In contrast, a coupled micro-simulation and instantaneous emission model could provide a very cost effective way of conducting high resolution emission estimation.

6.2 VEHICLE FLEET DATA

A detailed understanding of the vehicle fleet within the Headingley test area is an integral element of both the traffic simulation and emission estimation elements of this research. A typical vehicle fleet is a combination of different types of vehicle, of varying ages, covering a wide range of engine sizes and technologies. There is substantial variation in the emission of vehicles both between different vehicle categories (primarily due to average engine size and vehicle weight) and within categories (due to technology change over time). Vehicle fleet distributions vary both by location and time and these variations in the on-road fleet composition can cause a significant difference in overall fleet emission (Malcolm et al., 2003; Liu et al., 2011; Granell et al., 2002).

The AIMSUN model developed in this research for the Headingley network incorporates nine discreet vehicle categories comprising Passenger Car; Taxi; Rigid Heavy Goods Vehicle (HGV); Light Commercial Vehicle (LCV); Tractor Trailer (Articulated HGV); Articulated Bus; Double-deck Bus; Single-deck Bus and Extra Bus (consisting of coaches and buses which are not part of the scheduled bus fleet service) which correspond to defined vehicle categories within PHEM. In order to simulate the vehicle fleet emission specific to the research network, it is necessary to quantify the composition of the traffic in the test area by vehicle category (as outlined above) and then further differentiate within those categories at the individual vehicle level by Euro standard, fuel type and vehicle weight. As detailed in Chapter 4 each of these sub-categories has a dedicated engine power-emission map within PHEM, which are referenced to provide the average pollutant emission for the vehicle type with the specified fuel, Euro standard and weight over a given second-by-second speed and road grade trajectory. The calculated estimates for

each individual vehicle can then be aggregated to provide estimates of the emission from each vehicle category and the overall network emission.

It is important that the vehicle fleet is correctly described within the simulation not only because it defines the proportion of vehicles assigned to each PHEM power-emission map, and thus the rate of emission, but also because the dynamic characteristics of each vehicle type influence the overall behaviour of the traffic flows within the AIMSUN model. The parameters controlling the dynamic behaviour of each vehicle type in AIMSUN can be adjusted from default values to correspond to the observed behaviour of the vehicle type in the real-world conditions that are being modelled by the simulation. To represent real-world vehicle dynamics accurately, the AIMSUN vehicle parameters should be tailored for each vehicle type (Madi, 2016). Discrete dynamic parameters such as acceleration, deceleration and speed limited acceptance, for each vehicle type, result in the possibility of different fleet compositions producing markedly different average simulated second-by-second vehicle trajectories and therefore modelled rates of emission. For example, as the average rate of acceleration of the bus and HGV vehicle types is significantly slower than that for cars, an increasing percentage of these larger vehicles in a network could be expected to have a retarding influence on the average rate of acceleration of all traffic in the network, as cars travelling behind these larger vehicles are limited to their acceleration rates. The resultant slower rate of acceleration for a car in this network would reduce the car's power output from its maximum potential, were it able to accelerate at its optimum rate, changing the reference point on the vehicle's power-emission map and altering the rate of pollutant emission. An accurate representation of the vehicle fleet in AIMSUN is required to ensure that these interactions between vehicle types are captured to the correct degree within the simulation.

General fleet composition data for urban areas (outside London) are available from DEFRA's National Atmospheric Emissions Inventory (NAEI) (DEFRA, 2014). However as the "Base 2013 Fleet Composition Data" provides only an aggregated national fleet average based on vehicle kilometres travelled (VKM), it is considered unlikely to provide an accurate measure of the vehicle fleet in the Headingley test area. These aggregate figures are designed for regional analysis, however, micro-scale simulation necessitates a higher spatial resolution (Liu et al., 2011).

The NAEI figures also lack sufficient detail to inform the diurnal analysis of fleet composition, required by this study. As the aim of this research is to develop network simulations that represent the traffic conditions in the separate AM, IP, PM, EV and NI periods, it is necessary to

have a detailed fleet distribution specific to each time period. Research conducted by Palmgren et al. (1999) showed how fleet composition varies over a 24-hour period, highlighting that the ratios between vehicle types are not constant. This further reinforces the fact that individual vehicle fleet compositions are required for each of the simulated time periods.

6.2.1 Vehicle Fleet Data Collection

In order to determine the operational vehicle fleet proportions through the Headingley network, an Automatic Number Plate Recognition (ANPR) survey was undertaken on Monday 9th February 2015 on the A660, by Nationwide Data Collection on behalf of Leeds City Council and the ITS. The survey was conducted using ANPR cameras positioned on the A660, Headingley Lane, at 53.816552N, 1.567555W (see Figure 6.2) and captured the northbound and southbound traffic flows over a continuous 24-hour period from midnight to midnight. The survey was carried out in overcast but dry conditions. Traffic was considered representative of the location, with no occurrence of disruption or incidents that could have caused uncharacteristic results.

Figure 6.2: Headingley Lane ANPR Survey Site
(©Copyright Google™ 2015)

The ANPR cameras recorded the number plate (Vehicle Registration Mark, VRM) on each occasion a vehicle passed through the survey point. These cameras positioned facing the oncoming traffic, used infra-red to capture the VRM data both during daylight hours and when dark. Vehicles may be incorrectly recorded, however, in instances where the plate is very dirty or the number plate is illegal. Motorcycles were not captured by the survey as motorcycle number plates are most often mounted at the back of the vehicle, so cannot be read by the front facing ANPR cameras. Table 6.1 presents the total number of vehicles (excluding motorbikes) observed by the camera and the number of vehicles where the ANPR technology was able to

read the VRM data. The high success rate indicates that the survey captured a large majority of the vehicle fleet (94.86%).

Table 6.1: Headingley Lane ANPR Survey – VRM Capture Rate

Site	ANPR Total Vehicles	ANPR Collected Plates	Success Rate
Headingley Lane Southbound - O4	9711	9213	94.87%
Headingley Lane Northbound - D8	7219	6847	94.85%
TOTAL	**16930**	**16060**	**94.86%**

The reported 16,930 vehicles is in good agreement with past survey work on the A660. An Automated Traffic Count survey commissioned by Leeds City Council conducted between Wednesday 3rd December 2008 and Tuesday 9th December 2008 on the A660 at 53.817197N, 1.570687W, measured an average 24-hour weekday traffic flow of 10,310 southbound and 8,099 northbound vehicles, with the Monday flows lower than the weekly average at 9,760 southbound and 7,654 northbound vehicles over the 24 hours (data from Leeds City Council, Highways and Transportation, personal communication, November 2014).

The ANPR survey traffic count is 11.7% lower than the DfT Annual Average Daily Flow (AADF), calculated for the A660 in 2014 (DfT, 2015e). However this disparity is likely accounted for by the difference in chosen survey site, as the DfT site at 53.810467N, 1.556066W is 0.8 miles south of the ANPR site used in this research; sites which are separated by three major junctions. As the DfT presents an annual daily average, there may also be seasonal or weekly traffic flow patterns which cause the observed discrepancy between the traffic count figures. Figure 6.3 displays the DfT calculated AADF data for the A660 and shows a relatively consistent flow over the past 10 years.

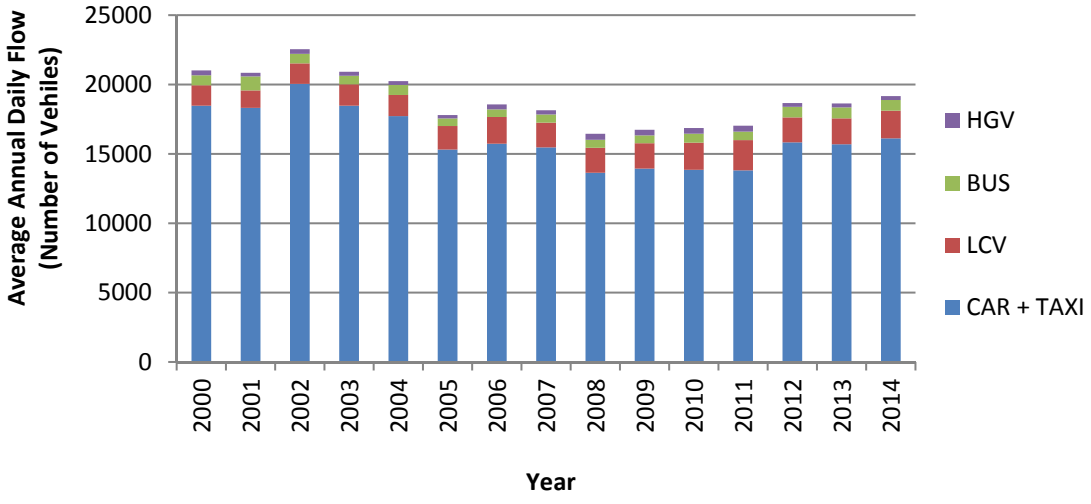

Figure 6.3: Annual Average Daily Flow for A660 by Year and Vehicle Type

To obtain detailed metadata for each vehicle passing through the survey area, the VRM database of 16,060 records was passed to CarwebUK Ltd (www.carweb.co.uk) who cross-referenced it with their vehicle database, matching each number plate to specific information about that vehicle. The VRM data recorded in the Headingley network comprised 10,999 unique number plates as there were multiple recordings of the same vehicle, e.g. scheduled bus services repeatedly passing on their route. CarwebUK's vehicle database is a construct of the Driver and Vehicle Licensing Agency (DVLA) Vehicles Database (DATA.GOV.UK), which holds more than 80 million records for all licensed and unlicensed vehicles in the UK and additional supplemental vehicle specification information from manufacturers. The output from CarwebUK's vehicle database comprised 94 information fields, including vehicle make / model, vehicle specifications, Euro emission standard and pollutant emission performance. Not all information fields were populated for each recorded vehicle as some fields were only relevant for particular vehicle types and in some cases relevant data were missing / unavailable. Table 6.2 shows a summary of the fields available for each vehicle.

Table 6.2: Overview of the Information Fields for the CarwebUK Vehicle Database

Vehicle details	Engine Details / Transmission	Performance	Environmental Details
VRM	*Fuel Type*	*Maximum Power (kW)*	*Fuel Consumption - Extra Urban / Urban Cold / Combined (mpg)*
Date First Registered	*Euro Emission Standard*	*Maximum Power (BHP)*	
DVLA Make / Model	*Transmission (Manual /Auto)*	*Maximum Power (@rpm)*	*CO_2 (g/km)*
Length / Width / Height (mm)	*Engine Capacity*	*Maximum Torque (Nm)*	*HC (g/km)*
Gross / Kerb / Unladen Weight (kg)	*Number of Forward Gears*	*Maximum Torque (@rpm)*	*NO_X (g/km)*
Mass in Service (kg)	*Number of Drive Axles*	*0 to 100 km/h (s)*	*Particulates (g/km)*
Market Segment	*Number Of Cylinders*	*Maximum Speed (km/h) & (mph)*	*Sound Level – Stationary / Drive By / Engine Speed*

The VRM database was also cross-referenced against the Leeds taxi licence register for March 2015 (data from Leeds City Council, Highways and Transportation, personal communication, April 2015). This facilitated identification of the taxi fleet component of the observed Headingley vehicle fleet.

6.2.2 Vehicle Fleet Data Processing

Initial inspection of the Headingley vehicle fleet database (each VRM with the cross-referenced vehicle information and taxi data) revealed that 3,715 of the 16,060 records (23.13%) were missing the Euro emission standard data required for the fleet composition analysis. However,

1,431 of the 3,715 had vehicle make, model and date of first registration data, which could be cross-referenced against similar vehicles in the fleet to provide the Euro emission standard. Utilising the National Tyres' website tyre search (http://www.national.co.uk), the DVLA's Vehicle Enquiry tool (https://www.gov.uk/get-vehicle-information-from-dvla) and the Parkers' Free Valuation Tool and vehicle specification database (http://www.parkers.co.uk) it was possible to identify and assign a Euro emission standard to all but 215 of the 16,060 records (1.34%). Of the 215 unknown vehicles, 14 were identified as either, a motorcycle, moped, street cleaner or digger. As these vehicle types do not form part of the simulation they were discounted from the analysis. The other unknown vehicles either lacked sufficient information to be classified or could not be found, likely due to ANPR misread of the number plate or the number plate being illegal. The overall success rate of the ANPR survey was therefore 93.59% (15,845 of 16,930 VRM records). With such a high capture rate the ANPR survey fleet is considered representative of the entire fleet.

6.2.3 Vehicle Fleet Data Analysis

The comprehensive vehicle registration information allows a detailed evaluation of the vehicle fleet on the A660 Headingley Lane. Figure 6.4 presents the observed vehicle fleet proportions over the 24 hours recorded by the ANPR Cameras on Headingley Lane. Dividing the fleet by basic vehicle type, passenger cars form the major fraction, with 70.48% of the valid fleet data, followed by Light Commercial Vehicles (12.04%), Taxis (9.51%), Buses, including coaches (4.97%) and Heavy Goods Vehicles (3.00%).

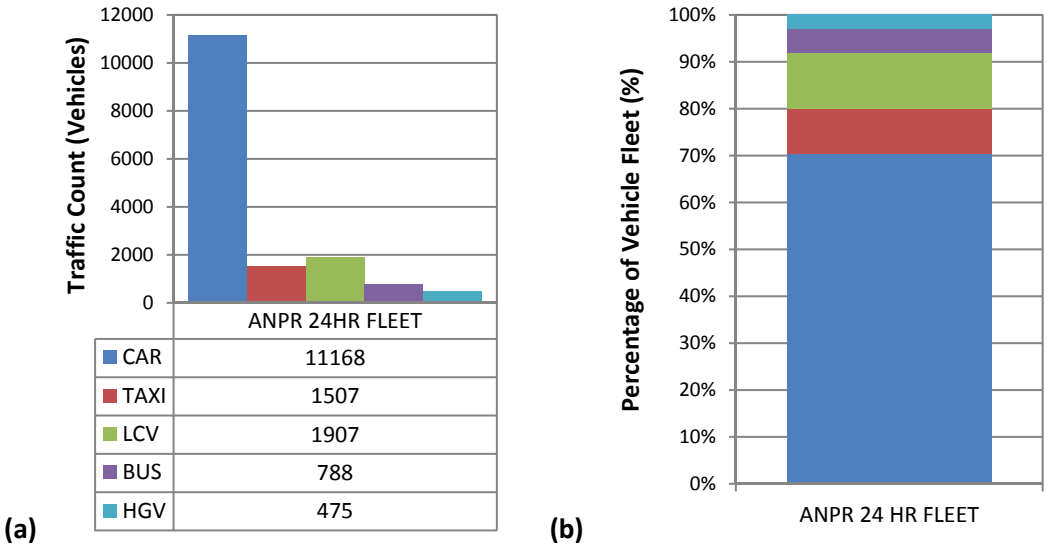

Figure 6.4: Headingley ANPR Survey 24 hr Vehicle Fleet Composition by (a) Count and (b) Percentage

Further analysis of the vehicle categories makes it possible to compare the Headingley 24-hour fleet with the NAEI's Base 2013 Fleet Composition Data (DEFRA, 2014). Table 6.3 shows the ANPR fleet arranged by vehicle type, as well as and by fuel for cars and LCVs, and by chassis type (Rigid and Articulated) for HGVs. Rigid HGVs describe an HGV with a single chassis, Articulated HGVs are HGVs where a tractor unit is attached to a separate semi-trailer (GOV.UK, 2013). The Headingley fleet composition is shown alongside the NAEI fleet projections for urban traffic conditions in England (outside London) for the years 2014, 2015 and 2016. The NAEI data are based on the DfT's traffic forecast projection from actual 2011 road traffic statistics (DfT, 2013), with projections for each vehicle type as the proportion of vehicle kilometres travelled, rather than as percentages of the vehicle stock (DEFRA, 2014).

Table 6.3: Comparison of the Headingley ANPR Survey 24 Hour Vehicle Fleet with the NAEI Base 2013 England (Outside London) Urban Fleet Composition for 2014, 2015 and 2016

	Headingley 24 hr ANPR Survey		NAEI Base 2013 Fleet Composition - England (outside London); Urban					
			NAEI 2014 Fleet		NAEI 2015 Fleet		NAEI 2016 Fleet	
	Vehicle Count	Proportion by Count	Proportion by VKM	Difference to ANPR	Proportion by VKM	Difference to ANPR	Proportion by VKM	Difference to ANPR
Electric car	4	0.03%	0.05%	-0.02%	0.07%	-0.04%	0.10%	-0.07%
Petrol car	6692	42.23%	46.70%	-4.46%	44.82%	-2.58%	43.09%	-0.85%
Diesel car	5979	37.73%	36.43%	1.31%	38.26%	-0.53%	39.85%	-2.12%
Electric LCV	4	0.03%	0.05%	-0.02%	0.08%	-0.06%	0.13%	-0.10%
Petrol LCV	19	0.12%	0.35%	-0.23%	0.31%	-0.19%	0.29%	-0.17%
Diesel LCV	1884	11.89%	12.88%	-0.99%	12.87%	-0.98%	13.01%	-1.12%
Rigid (HGV)	406	2.56%	1.71%	0.85%	1.75%	0.81%	1.73%	0.83%
Artic (HGV)	69	0.44%	0.41%	0.03%	0.41%	0.03%	0.40%	0.03%
Bus	788	4.97%	1.43%	3.54%	1.42%	3.55%	1.40%	3.57%
TOTAL	**15845**	**100.00%**	**100.00%**	**MAE = 1.27%**	**100.00%**	**MAE = 0.98%**	**100.00%**	**MAE = 0.99%**

The Mean Absolute Error (MAE) calculations comparing the Headingley Fleet proportions with the NAEI basic fleet projections reveal their compositions to be very similar. Whilst the Bus and Rigid HGV fractions are consistently greater in the Headingley fleet than accounted for by the NAEI fleets, the proportions of electric, petrol and diesel cars and LCVs are a good match. The high fraction of buses is likely due to the A660 being atypical of the average urban road, as it is the busiest and most crowded bus corridor into and out of Leeds (S.D.G., 2014a), with many bus stops and number of high frequency bus services, >5 buses per hour (TfL, 2015), covering routes from the city centre to the northern suburbs. Likewise, the Rigid HGV fraction is likely greater than a typical urban road as the A660 arterial corridor provides a direct route to and from the city to the northern section of the Leeds outer ring road (A6120).

Table 6.4 presents an analysis of the petrol / diesel fraction of the Headingley ANPR car fleet. The proportion of petrol to diesel vehicles in the observed Headingley fleet is close to parity,

with only marginally more petrol cars (52.81%) recorded than diesel (47.19%). The NAEI year-on-year change in the petrol / diesel ratio from 2014 to 2016 reflects the trend in dieselisation of the UK fleet (Ramli and Graham, 2014; Bonilla, 2009; Tate, 2013) due to policies encouraging the uptake of diesel vehicles because of their lower rate of CO_2 emission versus petrol vehicles of similar engine size. The Headingley fleet petrol / diesel split is shown to be between the NAEI 2015 and 2016 figures. Alongside the results from Table 6.4, the petrol / diesel split suggests that the recorded vehicle category distribution from the Headingley ANPR survey is in close agreement with the NAEI 2015 projected fleet composition.

Table 6.4: Comparison of Car Petrol / Diesel Fraction in the Headingley ANPR Survey with the NAEI Base 2013 England (Outside London) Urban Data for 2014, 2015 and 2016

	Headingley 24 hr ANPR Survey		NAEI Base 2013 Fleet Composition - England (outside London); Urban					
			NAEI 2014 Fleet		NAEI 2015 Fleet		NAEI 2016 Fleet	
	Vehicle Count	Proportion by Count	Proportion by VKM	Difference to ANPR	Proportion by VKM	Difference to ANPR	Proportion by VKM	Difference to ANPR
Petrol car	6692	52.81%	56.18%	-3.36%	53.95%	-1.13%	51.95%	0.86%
Diesel car	5979	47.19%	43.82%	3.36%	46.05%	1.13%	48.05%	-0.86%
TOTAL	**12671**	**100.00%**	**100.00%**		**100.00%**		**100.00%**	

6.2.4 Vehicle Fleet Analysis: Cars

The DEFRA NAEI vehicle fleet composition also provides individual year-on-year composition projections for each category as the proportion of kilometres travelled by vehicles from each defined Euro emission standard. Over time, the fleet compositions show a gradual phasing out of the older Euro standards as new vehicles, which meet the more modern Euro standards, are purchased and older vehicles are scrapped (DEFRA, 2014). Understanding the composition of the Headingley fleet by vehicle age (for which Euro emission is a proxy indicator) is very important as the EU legislation on CO_2 emission, along with other pollutants, has seen technological developments to the vehicles that influence the rate of pollutant emission. Therefore the overall fleet average pollutant emission will be directly related to the age composition of the vehicle fleet being observed.

Figure 6.5 shows the observed on-road petrol and diesel car fleets (including taxis) from the Headingley Lane ANPR survey, separated by Euro emission standard. The petrol and diesel fleets include both the conventional engines and the hybrid technologies (full hybrid and plug-in-hybrid) that use those fuels. The ANPR survey results reveal that the greatest fraction of the observed petrol car fleet was Euro 4 classified. The lowest MAE value, comparing the NAEI petrol car fleet Euro standard distributions to the Headingley fleet, was calculated for the 2013

NAEI Fleet composition. This suggests that the petrol car fleet travelling on A660 may be slightly older than the national average as there were fewer Euro 5 and Euro 6 vehicles than would be predicted from the NAEI 2014 and 2015 petrol car fleet distributions. A majority of the recorded diesel fleet were found to be Euro 5 vehicles and for the Euro 5 standard, more diesel cars (2,867) were observed than petrol cars (1989), reflecting the trend in dieselisation of the UK passenger car fleet. The MAE values for the diesel car fleet are similar for all NAEI years, as the observed distribution has a smaller proportion of Euro 3 vehicles than suggested by the NAEI fleets but a greater fraction of Euro 4 vehicles for all years. The MAE values suggest that the on-road diesel car fleet is marginally closer to the NAEI 2014 distribution than either the 2013 or 2015 fleet compositions. Overall 78.5% of the ANPR recorded car fleet met Euro 4, Euro 5 or Euro 6 emission standards.

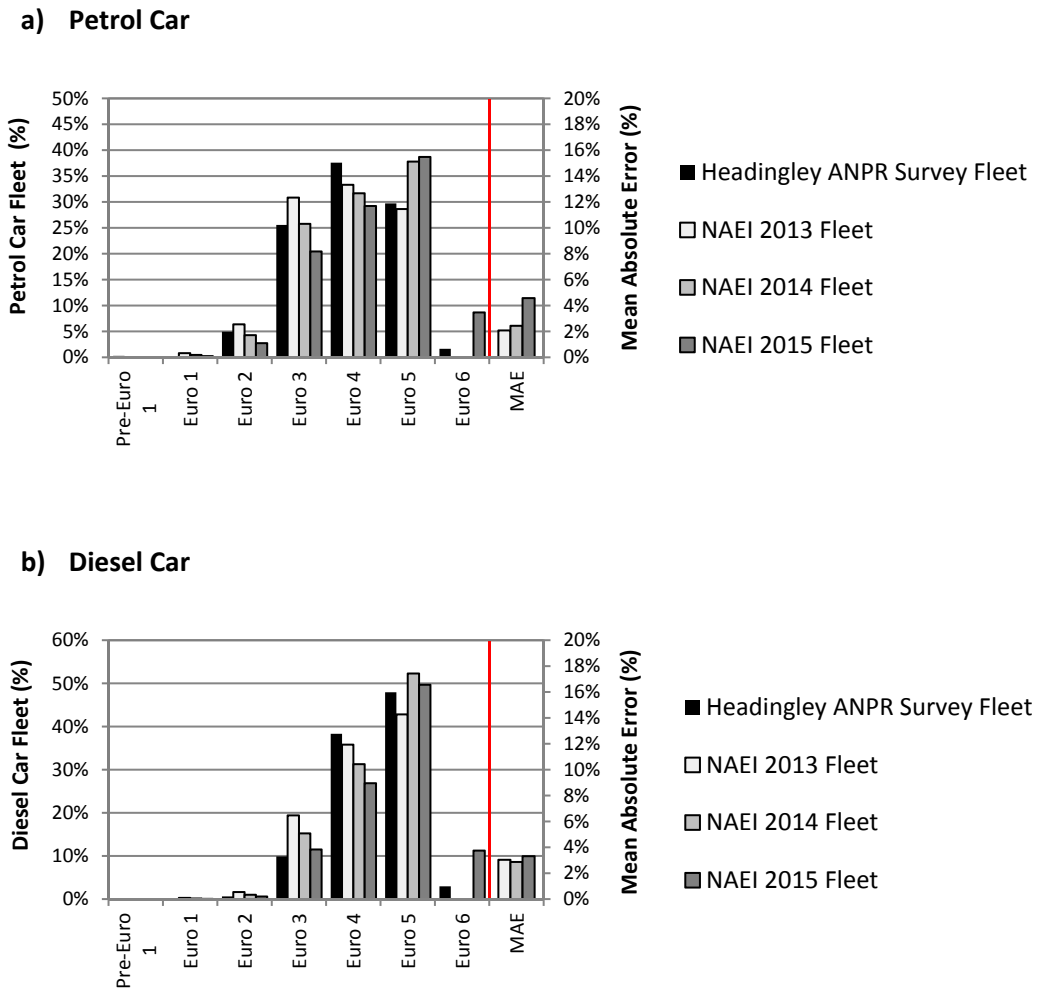

Figure 6.5: Car Euro Emission Standard Distributions in the Headingley ANPR Survey and NAEI 2013, 2014 and 2015 Vehicle Fleets: (a) Petrol and (b) Diesel

6.2.4.1 Hybrid Vehicles

The ANPR survey captured 5 VRMs for diesel/electric hybrids, recorded from four vehicles (one Range Rover, two Mercedes E-Class and a Peugeot Allure), all with a Euro 5 emission standard. Diesel/electric hybrids, therefore, make up only 0.17% of the vehicles in the on-road Euro 5 diesel car fraction and 0.08% of the total diesel car fleet. This is lower than in the NAEI fleet composition for 2015 which suggests the national average fraction for diesel/electric hybrids in the 2015 diesel car fleet to be 0.22% (DEFRA, 2014).

There were a total of 166 petrol/electric hybrid observations (from 105 vehicles) in the ANPR survey, comprising twelve Euro 4 vehicles, 151 Euro 5 and three Euro 6. Petrol/electric vehicles, therefore, account for 0.48% of the observed Euro 4 petrol car fraction, 7.59% of the Euro 5 and 2.73% of the Euro 6. Overall 2.48% of the petrol car fleet (166 of 6,692) observed by ANPR survey were petrol/electric hybrids, which is greater than the NAEI 2015 fleet national average of 1.61% (DEFRA, 2014). Toyota was the main manufacturer of petrol/electric hybrids recorded in the survey with 70 of the 105 petrol/electric vehicles. The most popular Toyota make was the Prius with 47 vehicles, followed by the Auris with 15 and the Yaris with 7. The other manufacturers were; Lexus with 20 vehicles (8 CT, 7 RX, 3 IS, 2 NX); Honda with 8 (3 Civic, 3 Insight, 2 CR-Z); Mitsubishi with 4 (Outlander); Vauxhall with 2 (Ampera) and Chevrolet with 1 (Volt).

The reason for the greater popularity of hybrid petrol electric vehicles in the observed on-road fleet than predicted by the NAEI fleet projection can at least in part be attributed to their uptake by Leeds taxi firms. Description of the observed A660 taxi fleet is presented in Table 6.5. Whilst 87.9% (1,324 of 1,507) of the observed taxi fleet is diesel powered vehicles, 52 of the observed 183 (28.3%) petrol taxis are petrol/electric hybrids. For Euro 5 petrol taxis, 48 of 70 (68.6%) of the observed vehicles in this category were petrol/electric hybrids. This suggests that in the past few years where taxi firms have chosen not to purchase conventional diesel vehicles (the traditional choice due to greater fuel efficiency and lower running costs) these firms have invested in hybrid petrol/electric vehicles. In Leeds, these petrol/electric hybrids are likely to be attractive to taxi companies looking to reduce their expenditure on fuel, especially if they can match reported fuel economy benefits in urban driving conditions, where fuel economy improvements of between 40% to 60% for some popular vehicle makes have been measured (Fontaras et al., 2008; Holmen and Sentoff, 2015).

Table 6.5: ANPR Recorded Headingley Taxi Fleet Composition

		Headingley 24 hr ANPR Survey			
Category	**Euro Standard**	**All Taxis Count**	**Proportion by Count**	**Hybrid Taxi Count**	**% Hybrids**
Petrol Taxi (conventional + hybrids)	Pre-Euro 1	0	0.00%	0	0.0%
	Euro 1	0	0.00%	0	0.0%
	Euro 2	0	0.00%	0	0.0%
	Euro 3	22	12.02%	0	0.0%
	Euro 4	91	49.73%	4	4.4%
	Euro 5	70	38.25%	48	68.6%
	Euro 6	0	0.00%	0	0.00%
	TOTAL	**183**	**100.00%**	**52**	**28.3%**
Diesel Taxi (conventional + hybrids)	Pre-Euro 1	0	0.00%	0	0.00%
	Euro 1	0	0.00%	0	0.00%
	Euro 2	0	0.00%	0	0.00%
	Euro 3	39	2.95%	0	0.00%
	Euro 4	746	56.34%	0	0.00%
	Euro 5	539	40.71%	0	0.00%
	Euro 6	0	0.00%	0	0.00%
	TOTAL	**1324**	**100.00%**	**0**	**0%**

The PHEM model has a hybrid-electric powertrain emission simulation package available for individual vehicles but this is not currently available for PHEM Advance which is used for calculating fleet emission (Luz and Hausberger, 2015). As a result hybrid vehicles in the study are modelled purely as either diesel or petrol depending on the source of fuel for the hybrid vehicle. Given the small percentage of hybrid vehicles in the observed Headingley vehicle fleet, this should have minimal impact on the current fleet emission estimate, however, a method for calculating hybrid emissions will need to be included in future work as the proportion of hybrid-electric vehicles is predicted to increase significantly (DEFRA, 2014).

6.2.4.2 Electric Vehicles

The Headingley fleet displays the relatively low current uptake of electric vehicles, with only four electric vehicles (one BMW i3, two Nissan Leafs and one Renault Kangoo ZE) recorded during the 24-hour survey. These four vehicles passed through the survey cameras a total of eight times. As electric vehicles currently form a negligible fraction of the vehicle fleet they have been excluded from the modelling. As the number of electric vehicles on UK roads is expected to increase significantly in the coming years, future studies will need to incorporate them as a proportion of the fleet. However, these vehicles will be very straightforward to model from an emission perspective as they contribute zero tailpipe emission.

6.2.5 Vehicle Fleet Analysis: Light Commercial Vehicles

The ANPR survey captured only 19 petrol LCV vehicles over the 24-hour recording period, compared to 1,884 diesel LCVs. A vast majority of this vehicle type have diesel powered engines. A sample size of only 19 makes it impossible to state whether the recorded distribution of petrol LCVs is really representative of that category in the real-world Headingley fleet and explains the relatively large MAE values, however, for those vehicles captured, the largest proportion were Euro 3. The age distribution of the diesel LCV category, illustrated in Figure 6.6, follows a similar pattern to the NAEI distributions for LCVs, with the MAE indicating that the Headingley diesel LCV fleet is best matched with the 2014 NAEI fleet.

a) Petrol LCV

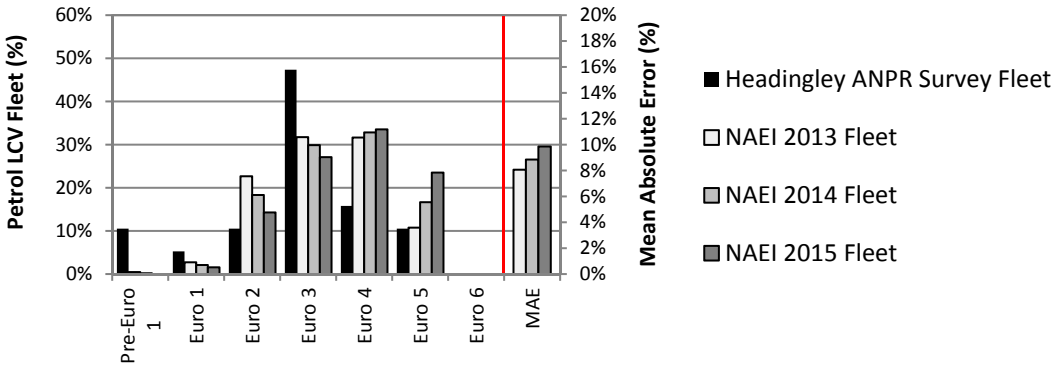

b) Diesel LCV

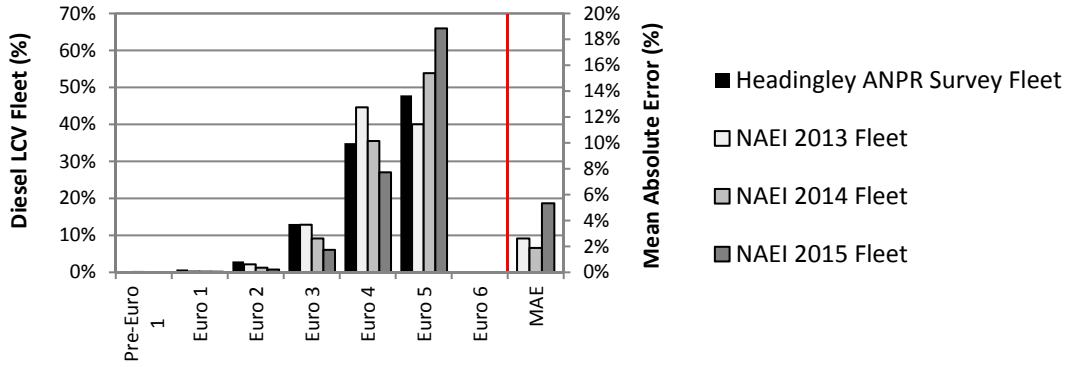

Figure 6.6: LCV Euro Emission Standard Distributions in the Headingley ANPR Survey and NAEI 2013, 2014 and 2015 Vehicle Fleets: (a) Petrol and (b) Diesel

The NAEI also provides a fraction of fleet estimate for each of the LCV weight classes, which is assumed by the NAEI to be the same split over all years. From the data in Table 6.6, the distribution of LCV weights for the vehicles recorded on the A660 is similar to the NAEI split, but with a marginally smaller fraction of lighter vehicles.

Table 6.6: LCV Fraction of Fleet by Weight Class

	Headingley 24 hr ANPR Survey		NAEI Fleet	
LCV EU Emission Standard Category	**Vehicle Count**	**Proportion by Count**	**Proportion by VKM**	**Difference**
N_1 (Class I) ≤ 1305 kg	201	10.54%	6.18%	4.36%
N_1 (Class II) 1305 - 1760 kg	444	23.28%	25.74%	-2.46%
N_1 (Class III) 1760 – 3500 kg	1262	66.18%	68.08%	-1.91%
TOTAL	**1907**	**100.00%**	**100.00%**	**MAE = 2.91%**

6.2.6 Vehicle Fleet Analysis: Heavy Goods Vehicles

6.2.6.1 Rigid HGVs

The ANPR survey recorded 406 Rigid HGVs over the 24 hours, with 249 2-Axle HGVs and 157 ≥3-Axles. Figure 6.7 shows the composition of the ANPR recorded A660 HGV fleet over the 24 survey by emission standard. The MAE indicates that the composition is closest to the NAEI HGV 2013 fleet composition, as the percentage of Euro 6 HGVs is much lower than predicted by either the 2014 or 2015 fleet. This again suggests that the A660 fleet may on average be slightly older than the national fleet.

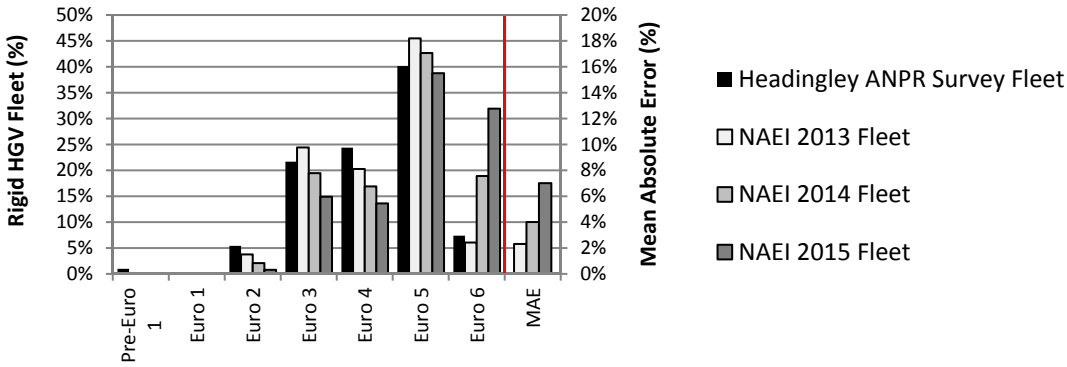

Figure 6.7: HGV Euro Emission Standard Distribution in the Headingley ANPR Survey and NAEI 2013, 2014 and 2015 Vehicle Fleets

The NAEI also provides the composition of the rigid HGV vehicle fleet by weight. Table 6.7 presents this composition for the 2015 fleet (N.B. the NAEI has assumed the same distribution since 2011) against the HGV fleet weight distribution from the 406 rigid HGVs recorded by the ANPR survey. Although there appears to be a slightly greater percentage of lighter vehicles than suggested by the NAEI fleet and there are noticeably fewer vehicles in the 26 – 28 t category recorded on the A660, the survey data, in general, seem to be a good fit for the NAEI fleet weight distribution.

Table 6.7: Composition of Rigid HGV Fleet by Weight

	Headingley 24 hr ANPR Survey		NAEI 2015 Fleet	
Weight Limit	**Vehicle Count**	**Proportion by Count**	**Proportion by VKM**	**Difference**
3.5-7.5 t	167	41.13%	33.41%	7.72%
7.5-12 t	5	1.23%	6.07%	-4.83%
12-14 t	6	1.48%	2.43%	-0.95%
14-20 t	57	14.04%	11.57%	2.47%
20-26 t	74	18.23%	15.86%	2.37%
26-28 t	3	0.74%	8.76%	-8.02%
28-32 t	61	15.02%	17.52%	-2.50%
>32 t	33	8.13%	4.38%	3.75%
TOTAL	**406**	**100.00%**	**100.00%**	**MAE = 4.08%**

Analysis of CarwebUK's vehicle database for the ANPR recorded HGV vehicles in the 3.5 t– 7.5 t category revealed that 51 of these vehicles were in the range 3.5 – 5.0 t. All of these vehicles were found to be large vans, Euro classification N_2, with Gross Vehicle Weight (GVW) greater than the 3.5 t maximum for the N_1 Class III LCV classification. Such vehicles included the Mercedes-Benz Sprinter 519, the Volkswagen Crafter CR50 and the Ford Transit 430. In the PHEM model, the rigid HGV vehicle type is sub-divided into two groups, 2-axle (GVW 12 t) and 3-axle (GVW 26 t). The 2-axle 12 t HGV category is unlikely to provide a good emission estimate for the N_2 large vans as this HGV classification describes significantly heavier vehicles. All of the 51 of large vans recorded by the ANPR survey had the same engine as a lighter N_1 LCV made by the same manufacturer. The LCV vehicle type in PHEM has three weight classes corresponding to the European Commission definitions of LCV N_1 vehicles. The heaviest of these classes (Class III) is for vehicles weighing between 1.76 t and 3.5 t. It was decided that as the 51 vehicles between 3.5 t and 5.0 t were from the same manufacturer ranges as many of the Class III vehicles, and had the same engines as that category, they were more likely to have emission maps similar to the Class III vehicles than the 12 t HGV. Therefore a fourth class of LCV was created in PHEM for these larger vehicles, using the Class III engine maps but with average weights and engine sizes derived from the 51 larger 3.5 t – 5.0 t vehicles.

6.2.6.2 Articulated HGVs

A total of 69 articulated HGV vehicles were recorded on the A660, during the 24-hour ANPR survey. Figure 6.8 present the Euro emission standard distribution recorded for each of the recorded articulated HGVs. The figure highlights a substantial difference between the articulated HGV compositions suggested by the NAEI and the observed Headingley distribution. The on-road fleet was shown to include a much greater proportion of older Euro 2, Euro 3 and Euro 4 emission standard vehicles than the NAEI fleets and a far smaller proportion of Euro 6

HGVs. The sample size of 69 is relatively small so may not give a true indication of the articulated HGV vehicle fleet, however, it does suggest that the fleet for this category on the A660 is older than the national average.

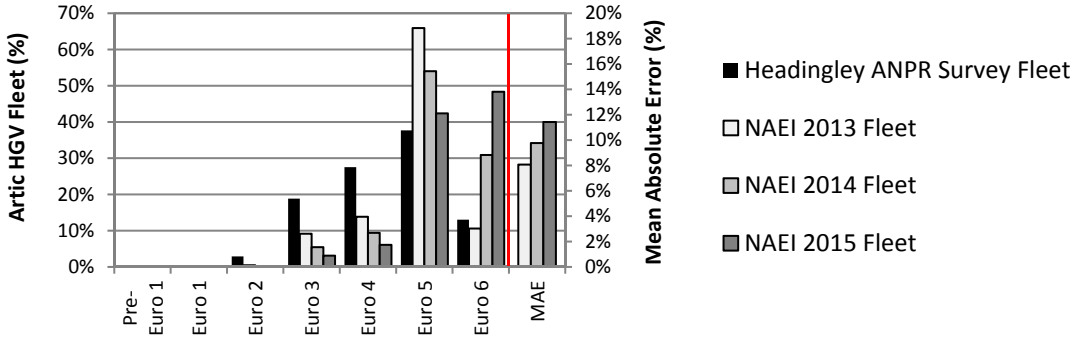

Figure 6.8: Articulated HGV Euro Emission Standard Distribution in the Headingley ANPR Survey and NAEI 2013, 2014 and 2015 Vehicle Fleets

The emission characteristics of all Euro 4 and Euro 5 HGVs and buses are also dependent on the proportion of these vehicles using Exhaust Gas Recirculation (EGR) or Selective Catalytic Reduction (SCR) as emission reduction strategies. The Euro 5 split for calculation of emission in PHEM was split 75% SCR, 25% EGR as suggested by the NAEI (DEFRA, 2014). The Euro 4 split was characterised using the PHEM default of 75% EGR, 25% SCR (Luz and Hausberger, 2015).

6.2.7 Vehicle Fleet Analysis: Buses and Coaches

As described in Chapter 6.3.6, the A660 has a number of high frequency bus services which run from the city centre to the northern suburbs and is the busiest and most crowded bus corridor into and out of Leeds (S.D.G., 2014a). Buses and coaches were recorded passing through the ANPR survey site a total of 788 times over the 24-hour recording period. A vast majority of the recorded vehicles (767) were buses operated by either First Leeds (www.firstgroup.com/leeds) or Yorkshire Tiger (www.yorkshiretiger.co.uk) which operate the scheduled bus fleet on the A660. Of the scheduled bus fleet, 40 were single-deck, 671 were double-deck, and 56 were articulated "bendy" buses. Figure 6.9 displays the Euro emission standard distribution for the A660 bus fleet against the NAEI fleet compositions. Clearly, the observed A660 bus fleet is considerably older than the NAEI fleets. Cross referencing the bus VRM data with the CarwebUK's vehicle database suggests that 95.3% of the observed bus fleet was Euro 3 emission standard or earlier.

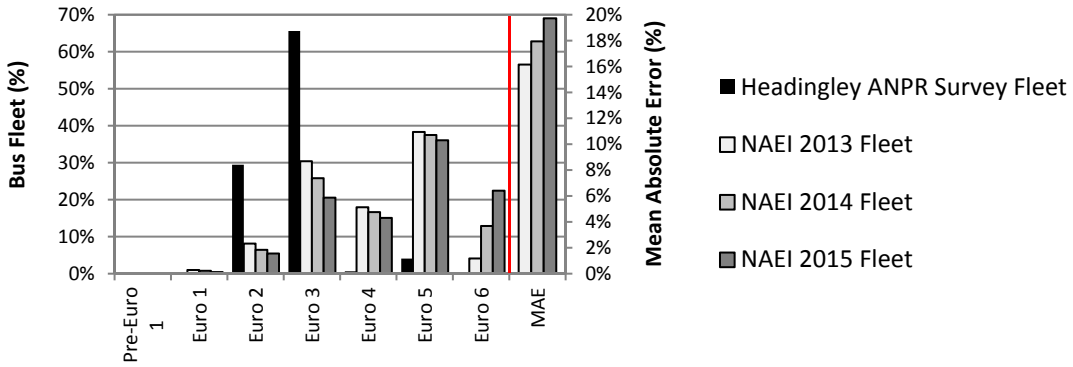

Figure 6.9: Bus Euro Emission Standard Distribution in the Headingley ANPR Survey and NAEI 2013, 2014 and 2015 Vehicle Fleets

6.2.8 Diurnal Variation in Traffic Flow Composition

The diurnal variation in traffic flow of the combined northbound and southbound directions on the A660, recorded by the ANPR survey for weekday traffic conditions, is illustrated in Figure 6.10. For each hour in the 24-hour survey period, the number of vehicles captured by the ANPR cameras is presented and this total flow is described by the fraction from each vehicle type.

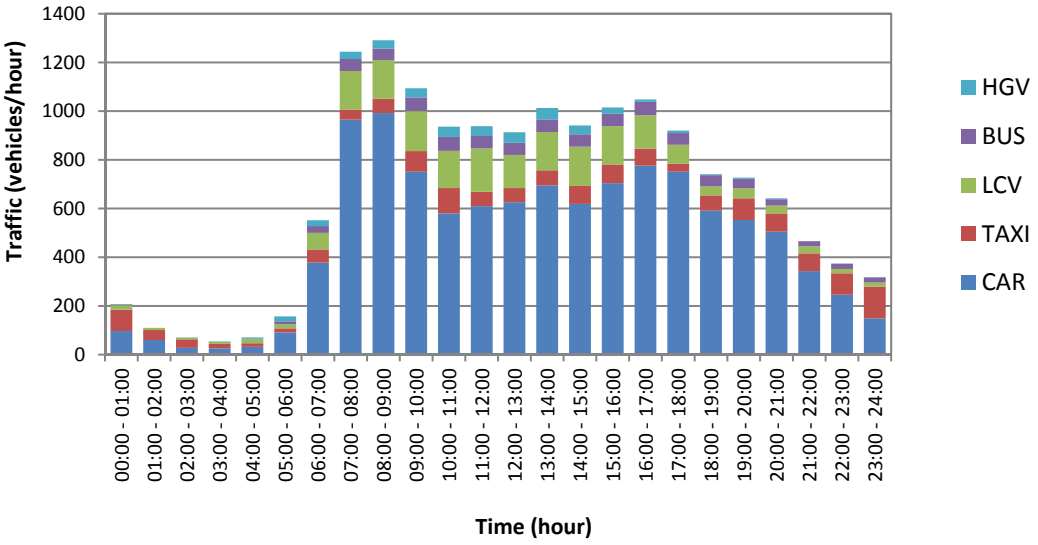

Figure 6.10: Diurnal Variation in Traffic Flow on the A660 by Vehicle Type

The weekday variation in traffic flow reveals a clear morning peak in traffic flow on the A660 between 07:00 and 09:00, as the morning rush hour traffic enters Leeds and a less distinct afternoon peak between 15:00 and 18:00. The observed traffic flow in the afternoon peak is lower than the morning peak as the capacity of the northbound A660 is lower than the southbound A660 at the location of the ANPR survey. In the afternoon peak, as traffic leaves the centre of Leeds at the end of the working day, the traffic flow of the northbound A660 is often greater than the capacity of the road, resulting in substantial delays to the northbound

traffic. These delays limit the traffic flow possible on the northbound A660. This pattern is observed in the analysis of Section 1 and Section 8 average speeds, described in Chapter 3.5.

Whilst the total flow varies throughout the day, so too does the composition of the vehicle fleet. Figure 6.11 illustrates the diurnal change in vehicle fleet composition over the 24-hour Headingley survey. During daylight hours passenger cars form a bulk of the vehicle fleet, whilst the proportion of taxis increases substantially during the evening and night hours. The figure shows a substantial fraction of HGV vehicles during the morning peak and inter-peak hours, however, that fraction decreases before the afternoon peak, as commercial drivers presumably try to avoid the delay associated with the very congested afternoon rush hour.

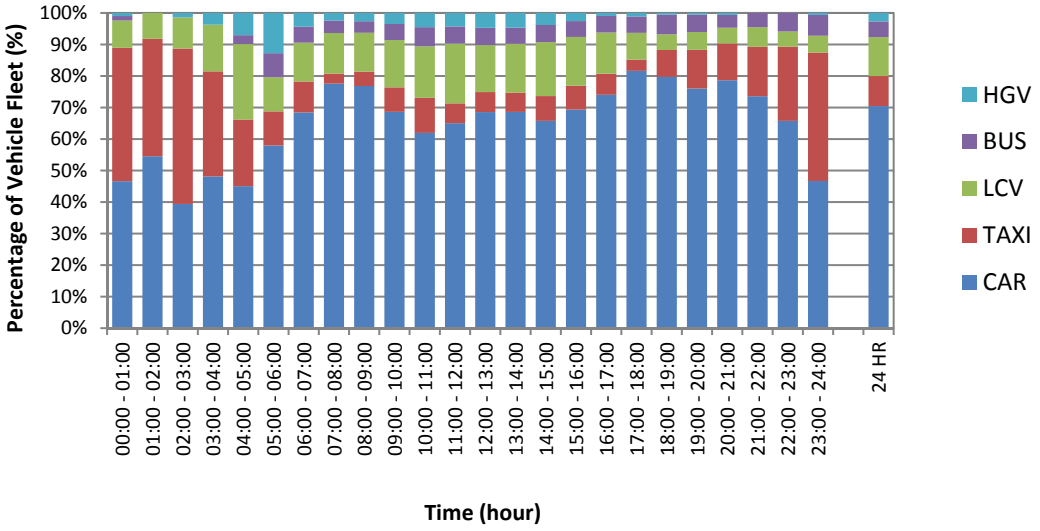

Figure 6.11: Diurnal Variation in Fleet Composition on the A660 by Vehicle Type

Figure 6.11 also presents the 24-hour aggregated vehicle fleet composition. It is clear from the figure that diurnal variations cause significant differences in the vehicle composition and that the 24-hour aggregate distribution of vehicle types would be unrepresentative of a majority of the individual hour fleet compositions. In order to quantify fleet emission during specific time periods during the day, it is not sufficient to assume that a 24-hour aggregate fleet composition (such as those provided by the NAEI) will be suitably representative of the on-road fleet. Whilst this may not be so important for CO_2 modelling which is usually assessed over longer time periods, it is vital for the modelling of other pollutants such as nitrogen dioxide (NO_2) which have urban air quality standards that are averaged hourly (EC, 2015b). Therefore, in order to accurately model vehicle fleet emission over short time periods, both the traffic flow and fleet composition for that time period must be correctly described.

In order to describe an accurate real-world vehicle fleet for each of the time periods modelled in AIMSUN and for the fleet emission calculations using PHEM, the ANPR data were analysed

individually for each time period with the traffic flow and composition calculated for each of the five, two and a half hour, time periods that represent the AM, IP, PM, EV and NI. Figure 6.12 presents both the number of vehicles recorded during each time period and the vehicle fleet composition. For AIMSUN, the HGV category was further divided into HGV Rigid and HGV Articulated fleet percentages and the Bus category was split into Articulated, Double and Single (for the scheduled bus fleet) and Bus Extra (which provides the percentage of buses and coaches that are not part of the scheduled fleet). For the PHEM .FLT file, all vehicle types are also classified by Euro emission standard; Cars, Taxis and LCV vehicles are split by fuel type and LCV and HGV Rigid are separated by weight category.

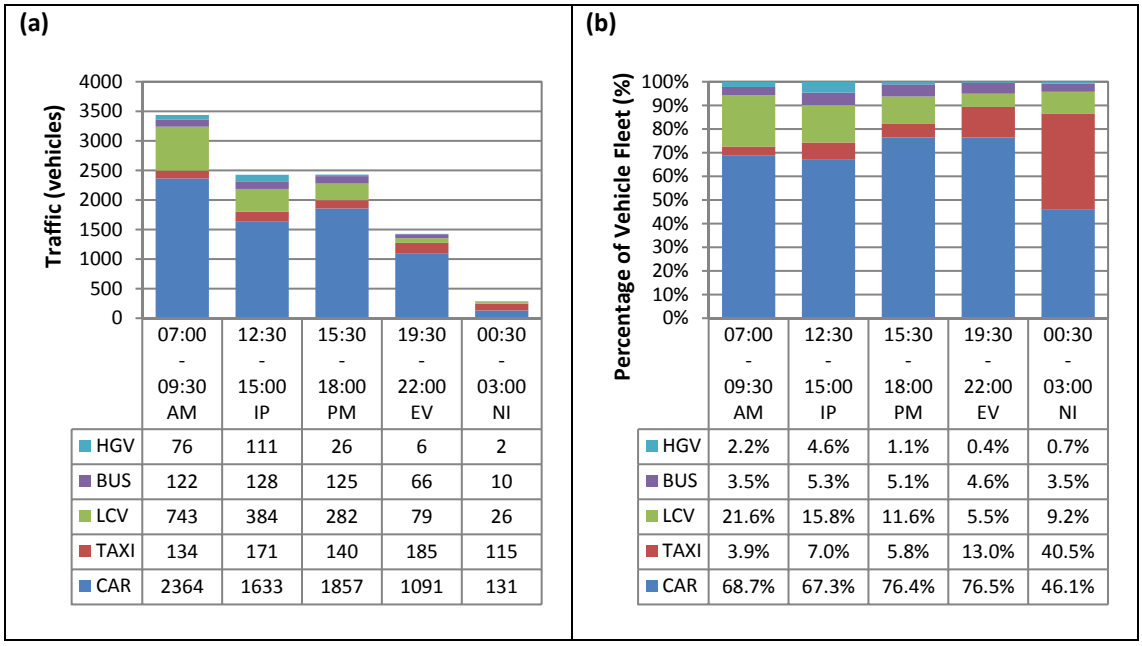

	07:00 - 09:30 AM	12:30 - 15:00 IP	15:30 - 18:00 PM	19:30 - 22:00 EV	00:30 - 03:00 NI
HGV	76	111	26	6	2
BUS	122	128	125	66	10
LCV	743	384	282	79	26
TAXI	134	171	140	185	115
CAR	2364	1633	1857	1091	131

	07:00 - 09:30 AM	12:30 - 15:00 IP	15:30 - 18:00 PM	19:30 - 22:00 EV	00:30 - 03:00 NI
HGV	2.2%	4.6%	1.1%	0.4%	0.7%
BUS	3.5%	5.3%	5.1%	4.6%	3.5%
LCV	21.6%	15.8%	11.6%	5.5%	9.2%
TAXI	3.9%	7.0%	5.8%	13.0%	40.5%
CAR	68.7%	67.3%	76.4%	76.5%	46.1%

Figure 6.12: Variation in Traffic Count (a) and Vehicle Type Fleet Composition (b) for the Five Test Periods (AM, IP, PM, EV and NI)

Confidence in the representativeness of the recorded weekday fleet composition could be strengthened with further ANPR data as this analysis is reliant on only one recorded 24 hour period. The difficulty with obtaining such data is that commissioning such surveys entails substantial cost as does obtaining the vehicle specific data for many thousands of vehicles from CarwebUK's vehicle database. However, accepting the limited sample size, unlike many traffic modelling and emission modelling projects which assess only AM and PM peak periods, the level of detail provided by the ANPR survey in this research facilitated vital characterisation of how the fleet composition changes throughout the day in the test network. The high capture rate of ANPR survey method, with access to CarwebUK's vehicle database, gives great confidence that the observed vehicle fleet captured the real-world fleet composition and provides a wealth of vehicle metadata that improves the vehicle type descriptions in PHEM.

6.3 TRAFFIC MICRO-SIMULATION IN AIMSUN

To generate the required second-by-second output for emission modelling in PHEM the AIMSUN Microscopic Simulator was employed in this research. AIMSUN continuously models each vehicle as they travel through a network. The movement of the vehicle within the network is controlled by behavioural models (e.g. car following, lane changing). Whilst some elements of the model are updated at each simulation step, such as vehicle position and detector counts, some elements are coded to change only at discrete points in simulation time, for example, traffic signals. The simulator is able to prove a highly detailed traffic network model (TSS, 2013b).

The parameters within the model must accurately reflect the real-world conditions of the modelled area. Traffic simulation requires the specification of a large number of factors including network layout, traffic demand data, traffic control plans and public transport plans (TSS, 2013b). The initial state of the traffic, at the start of each simulation, must also be defined, without such definition the model would start with the network empty, which is unlikely to accurately reflect the level of congestion at the start of the simulation period.

One of the AIMSUN outputs is a continuous animated graphical representation of the network whilst the simulation is running. Once the simulation is complete, a detailed statistical output is supplied, which includes information about flows, speed, journey times, delay and stops (TSS, 2013b). The data from AIMSUN for use with the PHEM model are gathered at each 0.5 second simulation step by a bespoke API which records the individual vehicle ID, road section / junction number, vehicle type ID, vehicle speed, position and road grade, for each vehicle in the network.

6.3.1 Extent of the Headingley A660 AIMSUN Model

The Headingley network AIMSUN (version 8.0.0) model was developed in this research to simulate a 3.8 km section of A660 from the junction of the A660 Woodhouse Lane and Clarendon Road to the junction of A660 Otley Road and Weetwood Road. The model comprises 145 junctions and 374 road sections with an average length of 81.6 m (Figure 6.13). The network was created using geo-referenced aerial photography downloaded from the Landmap Kaia service hosted at MIMAS (Millin-Chalabi et al., 2011), which provided a spatially accurate representation of the Headingley road network. The model describes all possible turning movements at each junction. The AIMSUN model encompasses the Headingley test lap and sections described in Chapter 3.2.1 and Chapter 3.4.

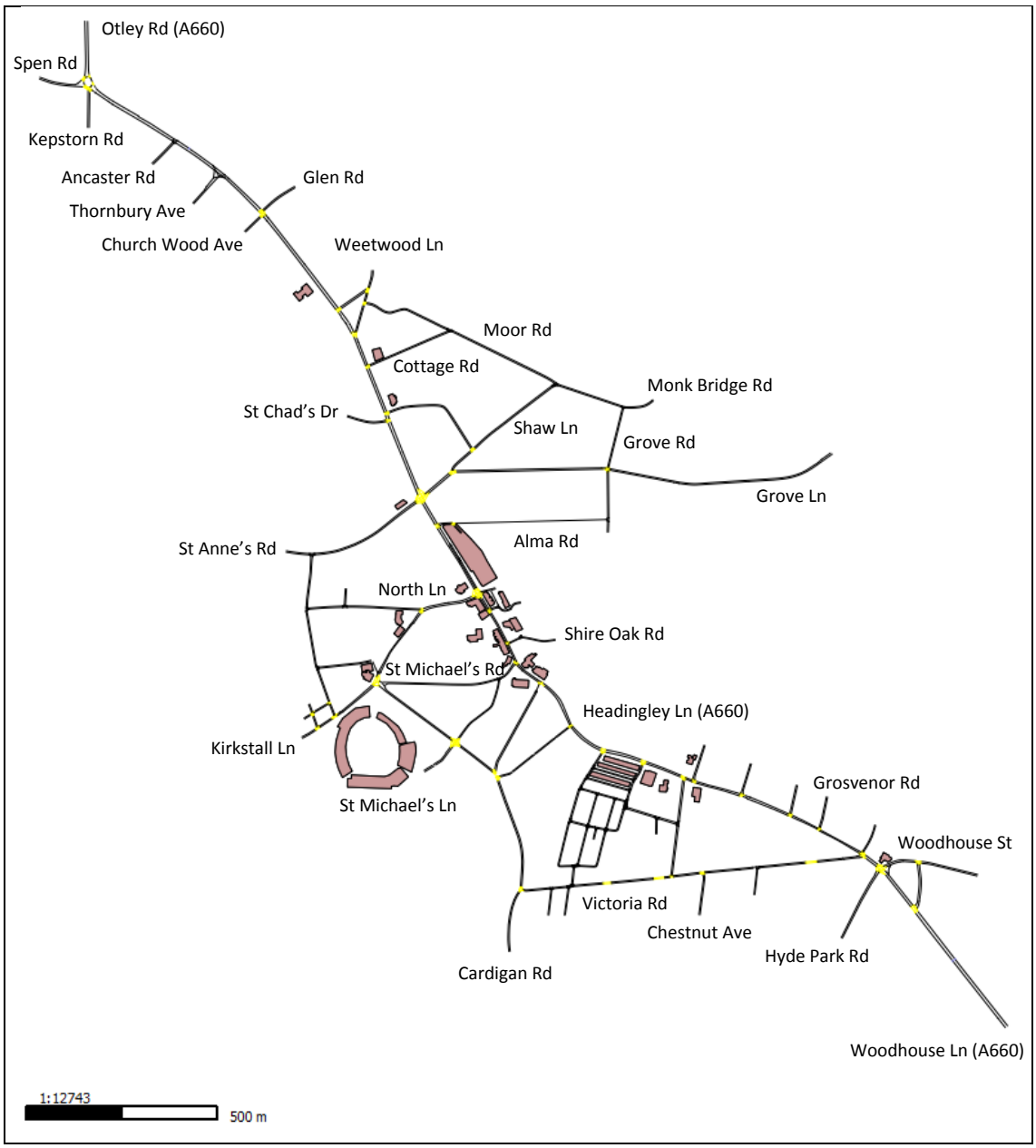

Figure 6.13: Extent of the Headingley A660 AIMSUN Model

6.3.2 AIMSUN Model Road Section Gradient

AIMSUN has the functionality to generate a road grade ("slope percentage") for each road section. For each of the 374 road sections in the Headingley A660 AIMSUN model, the latitude and longitude of start and end point were identified and were collated in an Excel .csv file. Using the ArcGIS software described in Chapter 5.4, the road section start and end points were mapped over the Bluesky 5 m resolution DTM (Bluesky, 2013) and the altitude at each coordinate was extracted. For each road section in AIMSUN, the extracted DTM altitude values, at the start point and end point, were then manually entered into the AIMSUN section detail. AIMSUN automatically calculates a road grade from these altitude values and assigns it to the road section.

6.3.3 Road Section Characteristics

Figure 6.14 displays the speed limit values assigned to the road sections in the Headingley Network. All road section maximum speed limits have been set equal to the signed speed limit in 2015 with the exception of Cardigan Road. Cardigan road was changed to a 20 mph zone (32 km/h) in 2013, however, as a majority of the traffic flow data used to calibrate the model was collected pre-2013 and Cardigan Road attracts a relatively high volume of traffic, the simulation was conducted with Cardigan Road assigned the old 30 mph limit (48 km/h).

The road section inputs including, number of lanes, bus stop locations, stop lines, junction turns were coded as accurately as possible, using tools such as Google Maps Street View (www.google.co.uk/maps) where the aerial photography was unclear.

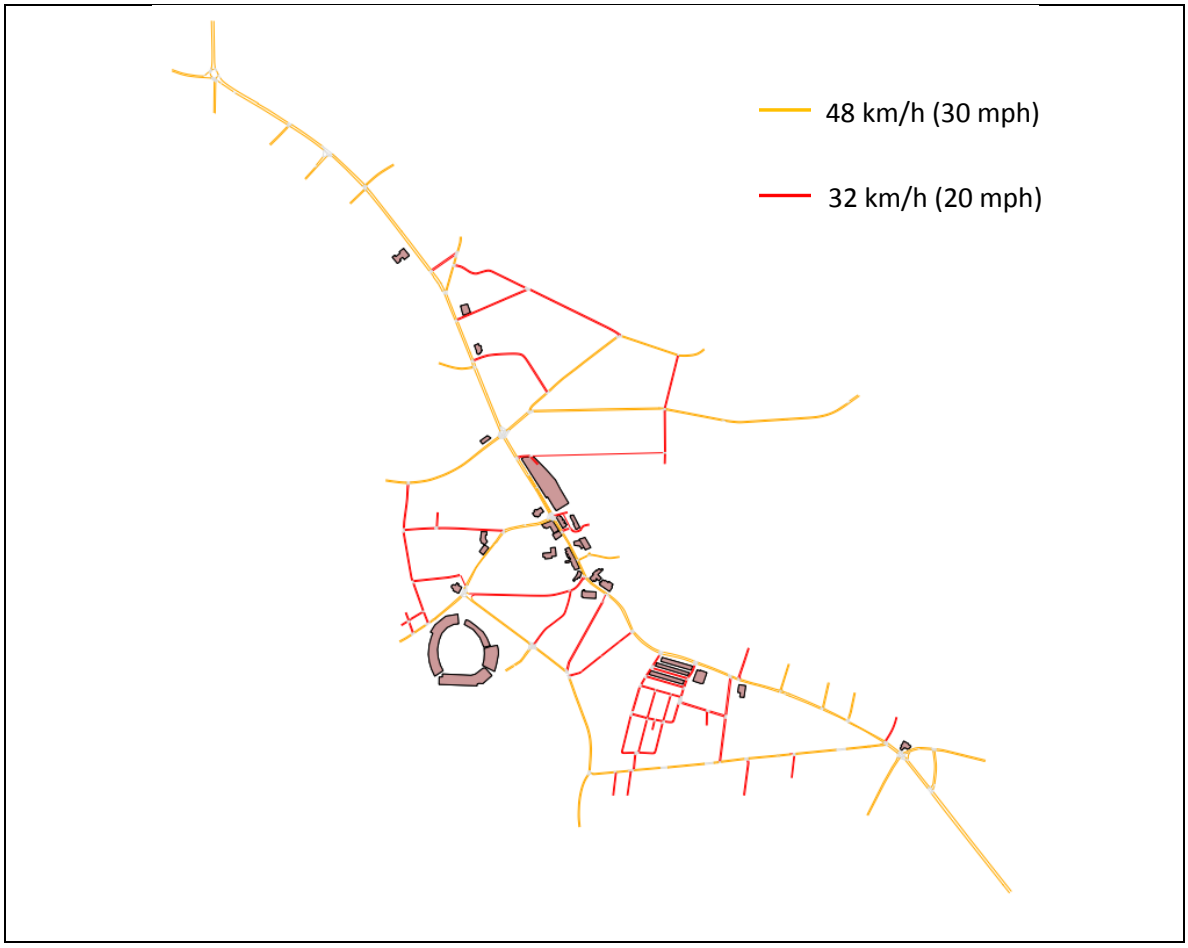

Figure 6.14: Headingley A660 AIMSUN Model Speed Limits

6.3.4 Traffic Demand

Traffic demand data for the network were calculated from observed traffic count data provided by the LCC Highways and Transportation Department. All available MCC and ATC data recorded in the Headingley network (as of November 2014) were collected from a LCC GIS database. MCC surveys are conducted by trained enumerators, who count traffic by vehicle type, commonly over the 12 hour period between 07:00 hours and 19:00 hours (DfT, 2015d). MCC data are predominantly reported in 30 minute intervals and are recorded at multiple survey points around a junction, in order to quantify vehicle turning percentages.

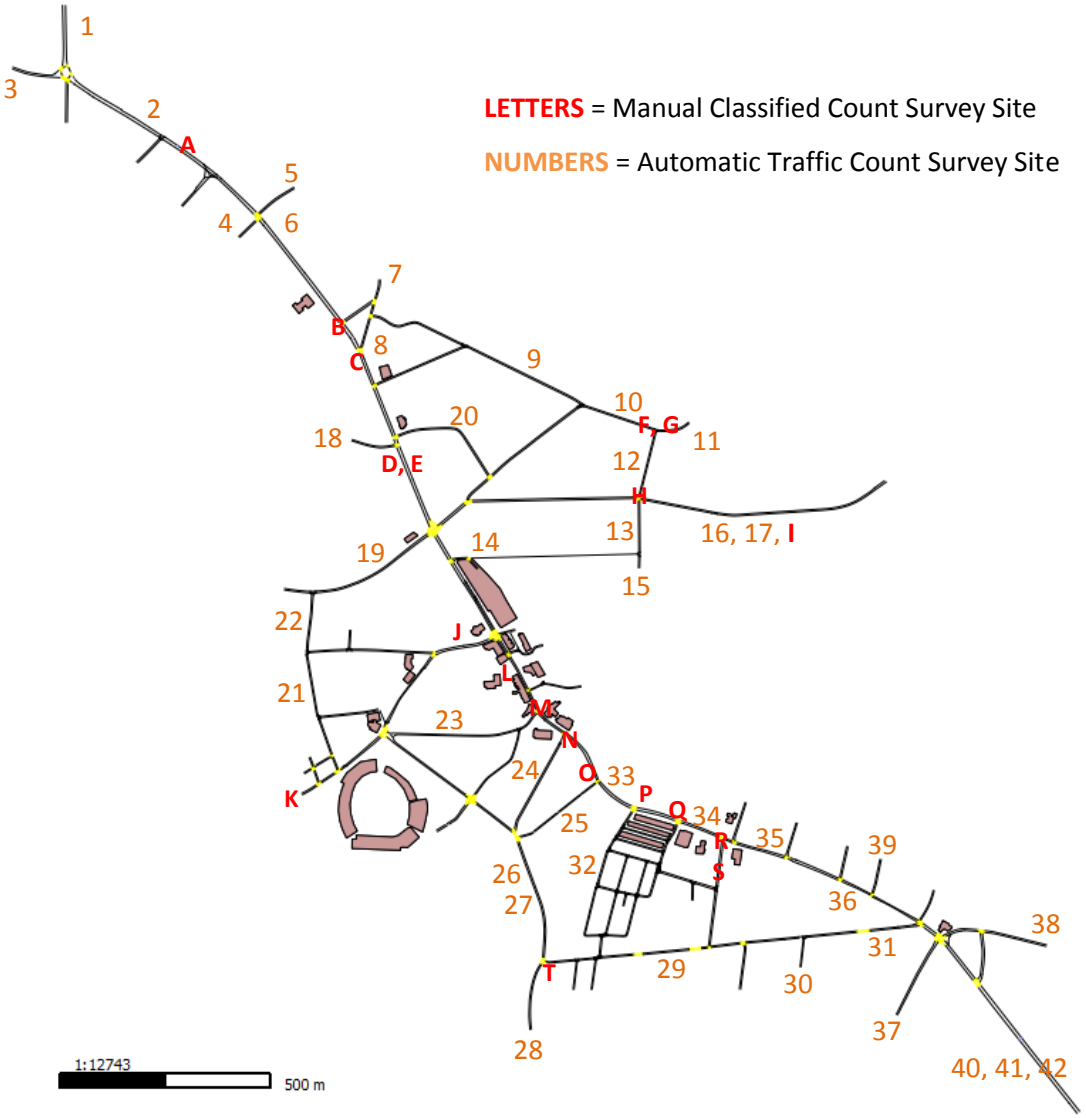

Figure 6.15: Location of ATC and MCC Survey Sites in the Headingley Network

The ATC data used in this research provided a record of vehicle flow, reported at hourly intervals. The LCC ATC data were collected 24 hours a day, usually over a 3 to 7 day period, by temporary pneumatic tube counters laid across the road. Figure 6.15 displays the location of each LCC MCC and ATC survey site in the Headingley modelled area. In total, there were 42 ATC surveys and 20 MCC surveys available for calibration of traffic flows in the network, collected between March 2006 and July 2014, with a majority recorded post-2008. Wherever possible the most recent data were used to construct the model and data recorded between September and November were given priority in an effort to minimise any seasonal disparities.

Ideally, to alleviate calibration issues resulting from weekly and seasonal variations in traffic flow, all input data for the model should have been collected at one time. The cost of such a comprehensive survey was beyond the scope of this research. The ATC and MCC data provide only a snapshot of the traffic conditions at the time of the survey. From field assessment of the network, the seasonal traffic flow conditions can vary considerably through Headingley as two university campuses are located in close proximity to the A660, causing a strong link between traffic volume and the university semesters.

Input flows, in vehicles per hour, were determined at each major input section (entrance to the network) from the ATC data (except Kirkstall Road, which used a MCC). The input flows in the model describe the traffic for an average weekday. Flow data were not available for all minor input sections, such as residential cul-de-sac side roads, so in such instances, the input flow from a similar capacity side road was used. In total there are 36 input sections to the model, of which 16 can be considered major sources of traffic flow and 20 are smaller side roads.

The input flow data for each simulated time period are defined in 30 minute 'traffic states' which designate the input flow (vehicles/hour) for each of the 36 input sections, over half hour intervals. Each time period (e.g. AM, IP, PM, EV and NI) is described by five traffic states for each vehicle type; one describes a half-hour warm-up period, to ensure that the starting traffic conditions for the recorded simulation were suitably defined, and four describe the input flows for the duration of the recorded simulation. The traffic states are vehicle type specific describing the input flow of each vehicle type separately. The AIMSUN model is set up for nine vehicle types; these are described in Table 6.8. Input traffic states for the 'Car', 'Taxi', 'HGV Rigid', 'LCV', 'Tractor Trailer' (Articulated HGV) and 'Bus' define the input flows of these vehicle types. The 'Articulated', 'Single' and 'Double' vehicle types are bus categories that exclusively describe buses which are part of the scheduled bus fleet. These three bus categories do not need to be defined by input flow because they are separately coded into the model at intervals described

by the bus fleet 'Public Transport Line' timetables. The 'Bus' vehicle category defines all non-scheduled buses in the network.

Table 6.8: Vehicle Types Coded in AIMSUN Headingley Network Model

Vehicle Type	Vehicle Type Information	PHEM Vehicle Type ID
Car	All Private Cars – Diesel / Petrol - All Euro Standards	100
Taxi	All Taxi Cars – Diesel / Petrol - All Euro Standards	101
HGV Rigid	Two Weight Categories – Only Diesel – All Euro Standards	200
LCV	Four Weight Categories – Diesel / Petrol – All Euro Standards	300
Tractor Trailer	Articulated HGV – Only Diesel – All Euro Standards	400
Bus	All Unscheduled Buses in the Network – Three Size Categories City Bus / Double / Single – Diesel – All Euro Standards	500
Articulated	Only for Scheduled Bus Fleet – Diesel – All Euro Standards	501
Double	Only for Scheduled Bus Fleet – Diesel – All Euro Standards	502
Single	Only for Scheduled Bus Fleet – Diesel – All Euro Standards	503

The ATC data used to create the traffic states, recorded only total vehicle flow. In order to calculate the separate input flows for the Car, Taxi, HGV Rigid, LCV, Articulated HGV and Bus categories, the total vehicle flow was multiplied by the respective fleet composition percentages for each of the vehicle types (as determined by the ANPR survey). The fleet compositions are specific to the simulated time period (AM, IP, PM, NI and EV). The fleet percentages shown in Table 6.9 only differ slightly from those displayed in Figure 6.12 (b) due to the redefinition of a number of smaller Rigid HGV to a Class IV LCV (described in Chapter 6.2.6.1), the fact that the HGV type has been split into two categories (Rigid and Articulated) and because the scheduled bus fleet has been removed from the fleet composition, as their entry into the model is not defined by the input flow matrices and they are coded separately as Public Transport Lines (see Chapter 6.3.6).

Table 6.9: Fleet Composition for AIMSUN Input Flows by Model Time Period

Vehicle Type	Fleet Compositions for AIMSUN Input Flow Calculations (%)				
	AM	IP	PM	EV	NI
Car	71.1	70.8	80.3	79.6	47.6
Taxi	4.0	7.4	6.1	13.5	41.8
HGV Rigid	2.0	4.0	1.0	0.2	0.7
LCV	22.3	16.6	12.2	5.8	9.5
Tractor Trailer	0.3	0.8	0.2	0.2	0.0
Bus	0.3	0.4	0.3	0.7	0.4

Therefore, for each half-hour in the two-hour simulation period, the input flows of Cars, Taxi, LCV, Rigid HGV, Articulated HGV and unscheduled buses are defined by the total flow recorded by ATC and the fleet percentage defined by the A660 ANPR survey. Both the input flows and fleet composition are calculated to be specific to each of the five model time periods. The arrival of vehicles into the AIMSUN network can be modelled by a number of distribution functions, which determine the interval between the entries of consecutive vehicles. The input flow

options available in AIMSUN are 'exponential', 'uniform', 'normal', 'constant' and 'ASAP'. The exponential distribution was found by the previous Headingley study (Tate, 2011) to best represent the real-world entry of vehicles into the network, so was retained for the new model.

Whilst the fleet compositions in Table 6.9 reflect the real-world Headingley fleet on the A660, it should be noted that the traffic on the A660 may not reflect the distribution of vehicle types on other roads within the network. For example, as the A660 is a main arterial corridor into and out of Leeds, it could reasonably be hypothesised that the percentage of HGV vehicles travelling on the A660 is likely to be greater than for smaller roads in the network. Further ANPR survey work within the network would improve confidence in the assigned fleet distributions.

6.3.5 Traffic Signals

The network contains six traffic signal controlled junctions, which have been coded to accurately reflect the on-street situation at each time period. These are listed in Table 6.10 along with pedestrian crossings in the network. The four A660 junctions were modelled using the Headingley beta simulation (Tate, 2011) coding. The stages, green times and intergreen times have been ratified by direct field observation. The Cardigan Road traffic signal timings have been modelled according to controller specifications supplied by the LCC Urban Traffic Management and Control department. These junctions were also checked by direct observation. There are twelve pedestrian crossings within the network area. Detailed information could not be found regarding the frequency of use and timing duration of these crossings, so these have been estimated from limited field observations at each location. A more rigorous survey would improve the quality of this element of the AIMSUN simulation.

Table 6.10: Traffic Signal Controlled Junctions and Pedestrian Crossings

Pedestrian Crossings		Signal Controlled Junctions
Victoria Road (before junction with A660)		A660 Woodhouse Lane / Woodhouse Street / Hyde Park Road / A660 Headingley Lane
Victoria Road (west of Ash Grove)		
A660 Headingley Lane (south of North Hill Road)		A660 Otley Road / North Lane / Wood Lane
A660 Otley Road (south of St Michael's Road)		
A660 Otley Road (Arndale Centre)		A660 Otley Road / St Anne's Road / Shaw Lane
B1657 North Lane		
B6157 Kirkstall Lane (south of Cardigan Road junction)		A660 Otley Road / Thornbury Avenue
Cardigan Road (Spring Road junction)		
Grove Lane (west of Grove Road Junction)		B6157 Kirkstall Lane / Cardigan Road
A660 Otley Road (north of Weetwood Lane junction)		
A660 Otley Road (south of Church Wood Avenue junction)		Cardigan Road / St Michael's Lane
A660 Otley Road (south of Kepstorn Road junction)		

6.3.6 Public Transport Lines

There are a total of 53 bus stops in the modelled area. The bus stop locations and type (whether a bus bay, where the bus pulls off the road, or a normal stop where the bus stops on the road) have been modelled from the geo-referenced aerial photography (Millin-Chalabi et al., 2011) and Google Maps (www.google.co.uk/maps) using the AIMSUN 'Public Transport Lines' tool. From timetable and routing information available at Metro (Metro, 2014) and via their real-time bus information tool (Metro, 2015) the bus services in Table 6.11 were identified as the regular services passing through the Headingley network (Figure 6.16). The simulation has been developed to include the university term time bus services operated by Yorkshire Tiger.

Table 6.11: Headingley Bus Routes and Service Operators

Service	Between	Operator
1	Holt Park – Beeston	First Leeds
6	Holt Park – Leeds	First Leeds
19/19A	Tinshill & Ireland Wood - Garforth	First Leeds
28	Adel – Clarence Dock	First Leeds
38	Gledhow – White Rose Centre	First Leeds
56	Moor Grange - Whinmoor	First Leeds
91	Halton Moor - Pudsey	First Leeds
92	Opal Halls – Headingley Campus	Yorkshire Tiger *term times only
93	Clarence Dock – Headingley Campus	Yorkshire Tiger *term times only
97	Guiseley - Leeds	First Leeds
X84	Skipton – Leeds	First Leeds

Figure 6.16: Headingley Bus Network Map (First, 2015)

The bus services were modelled using the AIMSUN 'Public Transport Line' tool, with fixed departure times corresponding to the timetables as of the 22nd September 2014. A possible deviation of up to 1 minute around the departure times was incorporated in the model to reflect the real-world variation, however, there has been no direct study of the timeliness of the Headingley bus service. Dwell times at each bus stop on the A660 were informed by a study conducted for the New Generation Transport proposal in Leeds, which conducted research into dwell times as part of the project appraisal process (S.D.G., 2014b).

The bus vehicle types for the scheduled bus fleet, shown in Table 6.8, comprised articulated buses, double-deck buses and single-deck buses. By cross-referencing the recorded bus number plates from the ANPR survey with the Sheffield Omnibus Enthusiast Society (SOES) fleet list (SOES, 2015) and the scheduled bus timetable for the A660 services, it was possible to determine the number of scheduled buses and the type of bus, used at each time period on the A660, and field observation identified which bus type is used for which service. The correct bus type was then coded for each service in the correct proportion at each time period.

The reserved bus and taxi lanes on the A660 were included in the AIMSUN Headingley simulation. The first runs southbound from the Otley Road (A660) input section to the Junction of the A660 Otley Road with St Anne's Road and Shaw Lane. The second runs northbound from the Woodhouse Lane (A660) input section to the junction of A660 Woodhouse Lane / Woodhouse Street / Hyde Park Road / A660 Headingley Lane.

6.3.7 Modelled Time Periods

Five versions of the model were separately calibrated and validated to represent the typical traffic conditions in the network for the following time periods:

- AM Peak Period: 07:00 to 09:30
- Inter-Peak Period: 12:30 to 15:00
- PM Peak Period: 15:30 to 18:00
- Evening Period: 19:30 to 22:00
- Night Period: 00:30 to 03:00

The initial half hour for each period acted solely as a 'warm-up' for the simulation. Network vehicle data were collected only during last two hours of each simulation period. The warm-up period was included in the model to ensure that at the start of the data collection period there

were a typical number of vehicles already in the simulation and therefore a representative level of congestion within the network.

The modelled year was 2015 as the ANPR vehicle fleet data described in Chapter 6.3 was collected on the 9th of February 2015 and the traffic signal timings are correct for 2015. However, given the nature of the modelling and the amount of data required, it was not feasible to garner the requisite input data purely from 2015. The bus routes and timetables coded into AIMSUN (Chapter 6.3.6) were released on the 22nd of September 2014, the input flows were recorded between March 2006 and July 2014 and the speed limit on Cardigan Road reflects the 30 mph value at which it was set before its change to 20 mph in 2013.

6.3.8 Model Calibration

Before calibration, during the development stage of the modelling process, the simulation was verified to ensure that it operated as expected. The AIMSUN 'Check and Fix Network' tool was used to identify any errors within the model coding. The animation facility in AIMSUN which runs a 2D representation of vehicle movement within the network as the simulation runs, highlighted any unexpected bottlenecks within the model. All network description errors were corrected during development.

In order to ascertain that the Headingley network AIMSUN simulations, for each of the five test periods, adequately model driver behaviour and network activity in the real-world, the adjustable model parameters must initially be calibrated to achieve outputs which are sufficiently representative of observed real-world data.

Dowling et al. (2004) suggest that one of the major challenges of the traffic micro-simulation process is optimising and adjusting the numerous parameters contained within the traffic simulation models. Several studies have documented that the default parameters used in AIMSUN fail to produce simulations with characteristics that represent observed real-world behaviours (Swidan, 2011; Tate, 2011; Anya et al., 2014; Madi, 2016) and require adjustment.

The Headingley beta model (Tate, 2011), calibrated for the Headingley network, made a number of alterations to the default parameters that affect vehicle behaviour within the model, such as amending the look-ahead distances which control lane changing movement, increasing the minimum distance between stopped vehicles and increasing the potential give way times at junctions. These adjustments were made to better represent the specific behaviour of vehicles

in the Headingley network. The Headingley beta model amendments to vehicle, local and global parameters were also adopted in the new Headingley AIMSUN model for this study.

Research by Anya et al. (2014) identified the importance of adjusting parameters in AIMSUN to calibrate the simulated vehicle speed trajectories (and therefore engine power output estimates) with real-world vehicle behaviour, highlighting the AIMSUN vehicle type attribute parameters 'Maximum desired speed', 'Maximum desired acceleration' and 'Normal deceleration'. These parameters influence the Gipps car following model (Gipps, 1981) which controls the acceleration and deceleration of vehicles in the simulation. The study by Anya et al. demonstrated that adjusting the vehicle type attributes, replacing the default values with values calculated from PEMS recorded field data (from within the study area), generated simulated speed profiles more representative of the real-world vehicle behaviour in the test network than are produced when using the AIMSUN default values.

Therefore, to better represent real-world vehicle movement in the Headingley network, the PEMS data set from Chapter 3 was used to generate vehicle type attribute parameter estimates for cars and taxis. The rate of change of velocity (i.e. acceleration and deceleration) value for each second of PEMS data, were calculated for each recorded Headingley test lap, enabling assessment of the 'Maximum acceleration', 'Normal deceleration' and 'Maximum deceleration'. Separate parameter estimates were calculated for each time period (i.e. AM, IP, PM, and EV) in order to incorporate the impact that varying levels of congestion may have on vehicle behaviour. The PEMS lap data were grouped by the time period in which the test lap was recorded and each time period group was then processed separately. The vehicle type attributes for each time period were calculated as follows: 'Maximum acceleration' was calculated as the 97.5^{th} percentile acceleration value from the PEMS data (to exclude outliers), 'Normal deceleration' was calculated as the mean deceleration value and 'Max deceleration' was calculated as the maximum deceleration value. The distribution of each of the parameter values was evaluated by comparing the parameter values generated for each individual test lap. The same three parameters were also calculated for the LCV vehicle category from PEMS data recorded through Headingley as part of a previous study (Wyatt et al., 2013). The LCV data set however only contained three test runs on the A660 so it was not possible to calculate bespoke values for each time period. As there were no second-by-second trajectory data available for Buses or HGVs in the Headingley network, estimates of the real-world acceleration and deceleration rates were taken from a New Generation Transport appraisal for a trolley bus scheme on the A660 which quotes typical public transport vehicle peak acceleration at 1.1 m/s^2 and deceleration at 0.9 m/s^2 (S.D.G., 2014b). The 'Maximum acceleration', 'Normal deceleration' and 'Maximum

deceleration' for each vehicle type and time period, where applicable, are set out below in Tables 6.12, 6.13, 6.14 respectively. The collection of further PEMS data in the network and sensitivity testing to establish a best practice methodology for generating vehicle type attribute parameters would greatly strengthen the AIMSUN modelling process and will be a significant area for future work.

Table 6.12: Maximum Acceleration Rates for Each Vehicle Type in the Headingley AIMSUN Network

Vehicle Type	Maximum Acceleration Rates (m/s^2)			
	Mean	Standard Deviation	Minimum	Maximum
Car / Taxi - AM	1.63	0.10	1.51	1.88
Car / Taxi - IP	1.69	0.10	1.54	1.85
Car / Taxi - PM	1.53	0.10	1.27	1.62
Car - EV	1.72	0.15	1.54	1.99
Car - NI	*No PEMS data so set to the same values as Car - EV			
LCV – ALL	1.45	0.05	1.4	1.5
HGV, BUS – ALL	1.10	0.25	0.7	1.3

Table 6.13: Normal Deceleration Rates for Each Vehicle Type in the Headingley AIMSUN Network

Vehicle Type	Normal Deceleration Rates (m/s^2)			
	Mean	Standard Deviation	Minimum	Maximum
Car / Taxi - AM	0.49	0.05	0.41	0.58
Car / Taxi - IP	0.51	0.07	0.42	0.63
Car / Taxi - PM	0.45	0.04	0.39	0.53
Car - EV	0.56	0.03	0.51	0.61
Car - NI	*No PEMS data so set to the same values as Car - EV			
LCV – ALL	0.42	0.05	0.37	0.45
HGV, BUS – ALL	0.90	0.05	0.80	1.00

Table 6.14: Maximum Deceleration Rates for Each Vehicle Type in the Headingley AIMSUN Network

Vehicle Type	Maximum Deceleration Rates (m/s^2)			
	Mean	Standard Deviation	Minimum	Maximum
Car / Taxi - AM	2.66	0.46	2.23	4.17
Car / Taxi - IP	2.97	0.49	2.17	3.93
Car / Taxi - PM	2.44	0.22	2.20	2.83
Car - EV	2.43	0.05	2.36	2.50
Car - NI	*No PEMS data so set to the same values as Car - EV			
LCV – ALL	2.38	0.08	2.29	2.44
HGV, BUS – ALL	*No data so set to the same as AM-car			

As the model was developed using input traffic flows, the movement of vehicles within the network is controlled by defining the turning proportion at each junction. The turning proportions define the percentage of the traffic flow on a particular road section assigned to each potential exit from that section. Separate turning proportions values can be defined for each vehicle type. Like the input flows, the turning proportions for all junctions in the network

are defined in the 30 minute 'traffic states', allowing the turning proportions to be re-calibrated at half hourly intervals to ensure that traffic flows are directed around the network in the correct proportions.

Initial set-up of the model utilised the turning proportions described in the Headingley beta model (Tate, 2011), however, because the new Headingley AIMSUN model was extended and the input flows were updated, considerable recalibration of the junction turning percentages was required. The Headingley beta model was also only calibrated for one AM peak and inter-peak hour. Therefore, for the IP, EV and NI simulations, the junction turning percentages had to be derived (where possible) from the MCC turning data at the locations shown in Figure 6.15. Where no real-world data existed, the percentages from AM peak were input as a starting point for the calibration and then adjusted until an acceptable level of calibration was achieved.

The calibration process adopted for the new Headingley AIMSUN simulation was similar to that used in the development of the beta model, however, significantly more calibration points were added. In-line with 'best practice' (Dowling et al., 2004) calibration was conducted using the comparison of real-world observed and model simulated flows as the 'measure of performance'. A total of 26 virtual detectors are included within the Headingley network AIMSUN model (Figure 6.17) at sites where real-world traffic count data were available (Figure 6.15). The detectors are located at points independent of the input flows, with 10 placed at exits of the model and 8 at points within the Headingley network which record bi-directional flows (16 detectors in total). These detectors record the simulated vehicle per hour flow (over the road section on which they are located) every 30 simulation minutes, as well as the average vehicles per hour flow over the two-hour simulation period. The simulated model flows were compared to the real-world flows (defined by the traffic count data) at each of the 26 detector sites using the GEH statistic (Dowling et al., 2004; DfT, 2014). The GEH statistic is a goodness of fit test used to compare two sets of traffic data. The GEH statistic formula is:

Equation 6.1:

$$\mathrm{GEH} = \sqrt{\frac{2(\mathrm{M} - \mathrm{C})^2}{\mathrm{M} + \mathrm{C}}}$$

Where M is the hourly 'modelled' traffic flow and C is the 'observed' real-world count.

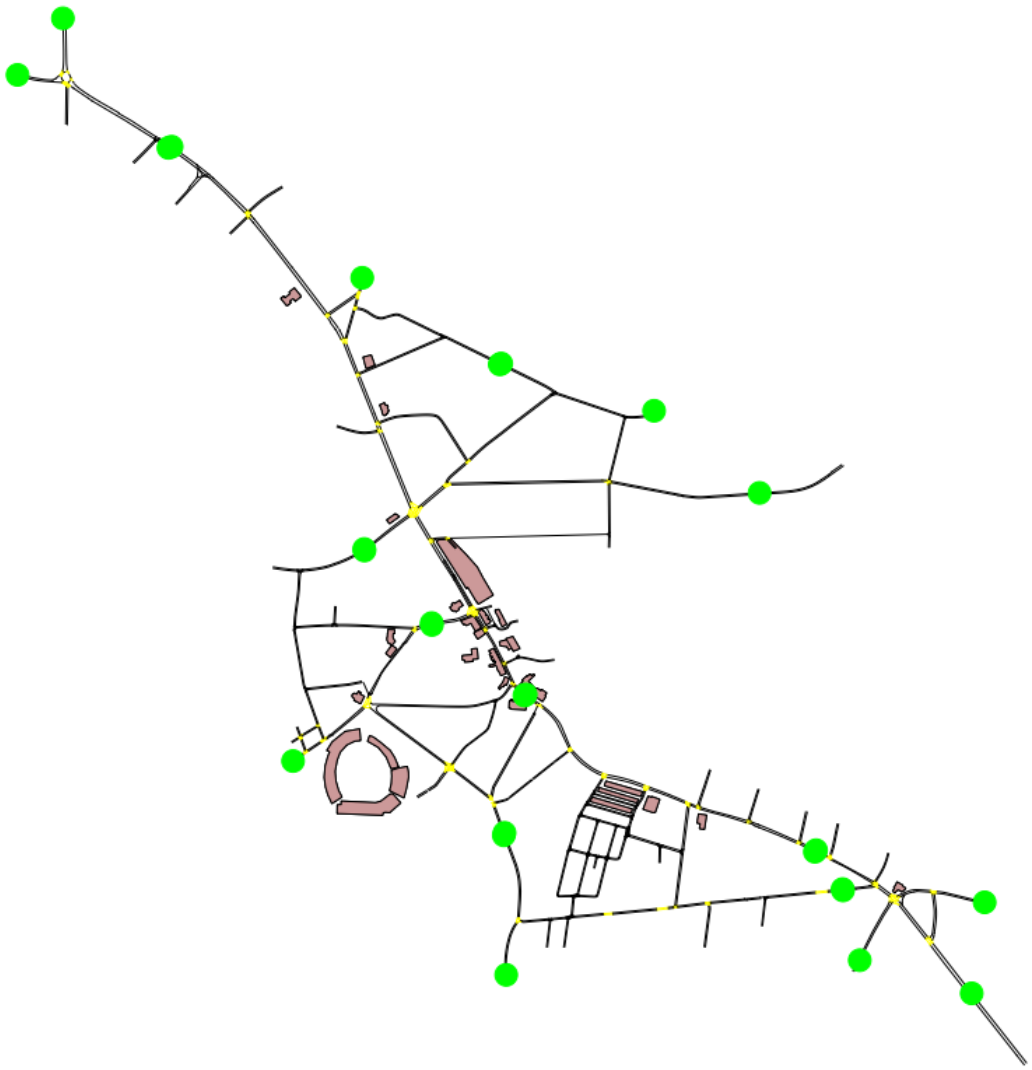

Figure 6.17: Detector Locations in the Headingley AIMSUN Network

The DfT Transport Analysis Guidelines (TAG) set out the criteria for link flow validation (DfT, 2014) as given in Table 6.15.

Table 6.15: Link Flow Validation Criteria and Acceptability Guidelines (DfT, 2014)

Description of Criteria	Acceptability Guidelines
Individual flows within 100 veh/h counts for flows less than 700 veh/h	>85% of cases
Individual flows within 15% of counts for flows from 700 to 2700 veh/h	
Individual flows within 400 veh/h of counts for flows more than 2700 veh/h	
Individual flows with a GEH statistic < 5	

The initial calibration phase of model development was considered complete when all 26 individual flows in the simulation had a GEH < 3 for each of the 30 minute traffic states and for the overall two-hour simulation, and the flow count criteria were met in 100% of cases.

6.3.9 Model Validation

To determine whether the model is an accurate representation of the observed network and to account for stochastic variability in the micro-simulation process 10 simulations (called replications in AIMSUN) of the model were run for each time period (AM, IP, PM, EV and NI), each with a unique 'random seed' ensuring different vehicle entry times and paths for each simulation. The simulated vehicle flows for each replication were validated according to the criteria in Table 6.15. All simulations were validated over all time periods and were completed with no more than 1 in 26 of the individual flows having a GEH statistic greater than 5.

In order to conform to the WebTag guidelines for model validation (DfT, 2014) analysis should be conducted to assess the difference between simulated and real-world journey time through the network. However at the time of validation, routinely collected journey time data were not available for the network, so the validation was performed using only modelled and observed traffic flows. A limited comparison of simulated and real-world journey times was made (Chapter 6.5.1) as part of a new coupled model calibration / validation methodology developed in this research, which along with an analysis of journey time and emission also includes a novel method for assessing simulated vehicle engine power output against real-world values. An important element of future work with the simulation will be to improve the robustness of the AIMSUN model validation by performing a more rigorous analysis of journey time.

6.4 PHEM EMISSION ESTIMATES FROM SIMULATED VEHICLES

As described in Chapter 6.1, in order to produce vehicle emission estimates from PHEM an .ADV job file must be prepared that incorporates three primary input files which are the .FZP drive cycle file, the .FLT fleet data file and the route section .STR files. These are described in Chapter 6.4.1, 6.4.2 and 6.4.3 respectively.

6.4.1 Simulated Drive Cycles (.FZP)

The drive cycle data for PHEM were supplied from each of the 10 validated AIMSUN simulations in each time period, which provide second-by-second vehicle activity for each vehicle in the simulated network over the 2 hour simulation periods. As described earlier in the chapter, whilst the AIMSUN network model simulation is in operation, an API records, for each vehicle in the network, the individual vehicle ID, road section / junction number, PHEM vehicle type ID (Table 6.8), vehicle speed, position and road grade, at every 0.5 second simulation step. The open

source software 'R' (R-CoreTeam, 2014) is then used to process the AIMSUN output data into a 1 Hz drive cycle .FZP file format for use in PHEM.

6.4.2 Fleet Data File (.FLT)

As discussed in Chapter 4.6.4.2, the .FLT file describes percentage of each vehicle type that is in each specific category defined by fuel type, Euro emission standard, and (where applicable) vehicle weight. Table 6.16 and Table 6.17 show the Car (PHEM vehicle type 100) and Taxi (PHEM vehicle type 101) fleet compositions by fuel type and Euro emission standard for each time period. The fleet compositions were calculated from analysis of the ANPR data described in Chapter 6.2. For each time period, the fleet compositions for each vehicle type have to be described in the .FLT file. The composition of the other vehicle types is available in Appendix 2.

Table 6.16: Car Fleet Composition by Fuel Type and Euro Emission Standard

Vehicle Type 100	Fuel	Euro Standard	AM FLEET	IP FLEET	PM FLEET	EV FLEET	NI FLEET
Car	Diesel	E0	0%	0%	0%	0%	0%
		E1	0.04%	0.12%	0.05%	0.18%	0%
		E2	0.34%	0.49%	0.27%	0.37%	0%
		E3	4.44%	5.39%	4.36%	5.50%	5.34%
		E4	13.41%	13.04%	14.11%	12.10%	12.98%
		E5	21.28%	22.41%	20.52%	17.69%	21.37%
		E6	1.73%	2.02%	1.67%	0.55%	0.76%
	Petrol	E0	0.13%	0.06%	0.22%	0.09%	0.76%
		E1	0.25%	0.12%	0.11%	0%	0%
		E2	2.24%	3.31%	2.85%	4.22%	6.11%
		E3	13.20%	14.39%	14.97%	17.42%	25.19%
		E4	22.55%	21.07%	22.46%	24.93%	18.32%
		E5	19.29%	16.53%	17.50%	16.22%	9.16%
		E6	1.10%	1.04%	0.92%	0.73%	0%
		SUM	100.00%	100.00%	100.00%	100.00%	100.00%

Table 6.17: Taxi Fleet Composition by Fuel Type and Euro Emission Standard

Vehicle Type 101	Fuel	Euro Standard	AM FLEET	IP FLEET	PM FLEET	EV FLEET	NI FLEET
Taxi	Diesel	E0	0%	0%	0%	0%	0%
		E1	0%	0%	0%	0%	0%
		E2	0%	0%	0%	0%	0%
		E3	2.99%	2.34%	2.14%	4.86%	2.61%
		E4	37.31%	49.71%	47.14%	51.35%	51.30%
		E5	43.28%	38.01%	37.86%	29.19%	39.13%
		E6	0%	0%	0%	0%	0%
	Petrol	E0	0%	0%	0%	0%	0%
		E1	0%	0%	0%	0%	0%
		E2	0%	0%	0%	0%	0%
		E3	0.75%	0%	2.14%	2.16%	0%
		E4	6.72%	5.26%	9.29%	8.65%	6.09%
		E5	8.96%	4.68%	1.43%	3.78%	0.87%
		E6	0%	0%	0%	0%	0%
		SUM	100.00%	100.00%	100.00%	100.00%	100.00%

6.4.3 Network Section Files (.STR)

These files describe each section and junction with an identification number which corresponds to the Section ID in the .FZP files. The .STR files enable calculation of total emission on each separate road section and junction. A total of 519 .STR files were created for the coupled traffic micro-simulation and instantaneous emission model, for each junction and road section in the Headingley simulation.

6.4.4 Calibrating Vehicle (.VEH) Files

As discussed in the introduction to this chapter, the default .VEH files in PHEM were amended to better represent the average vehicle in each specific vehicle type category. The data in Table 6.18 were calculated from the ANPR derived metadata from CarwebUK's vehicle database. The data tables for the other vehicle types are presented in Appendix 2.

Table 6.18: Average Vehicle Specification for Headingley

Vehicle Type	Fuel	Euro Standard	Vehicles in 24 hr ANPR Survey	Rated Engine Power (kW)	Maximum Power at RPM	Mass in Service (kg)	Loading (kg)
Car	Diesel	E0	2	55	4010	1260	50
		E1	10	60	4010	1300	50
		E2	38	73	4161	1525	50
		E3	554	85	4037	1495	50
		E4	1545	98	3949	1539	50
		E5	2328	105	3949	1565	50
		E6	178	128	3844	1615	50
	Petrol	E0	19	60	5400	1180	50
		E1	15	66	5723	1200	50
		E2	332	69	5603	1154	50
		E3	1689	72	5686	1234	50
		E4	2425	76	5752	1198	50
		E5	1919	78	5654	1201	50
		E6	110	113	5296	1303	50
Taxi	Diesel	E0	0	55	4010	1260	50
		E1	0	60	4010	1300	50
		E2	0	73	4010	1350	50
		E3	39	88	3874	1627	50
		E4	746	86	3926	1498	50
		E5	539	85	4093	1476	50
		E6	0	101	4014	1525	50
	Petrol	E0	0	60	5400	1180	50
		E1	0	66	5723	1200	50
		E2	0	68	5723	1230	50
		E3	22	99	6000	1435	50
		E4	91	96	5904	1390	50
		E5	70	91	5347	1449	50
		E6	0	84	5247	1200	50

6.4.5 Generation of PHEM Emission Estimates from AIMSUN Simulation Data

The emission estimates from the Headingley network AIMSUN-PHEM coupled model were generated by the PHEM emission model using the PHEM ADVANCE mode editor tool. The PHEM ADVANCE tool creates one job file for each AIMSUN replication, integrating the simulated vehicle activity data generated by the AIMSUN Headingley network for an individual replication (.FZP file), with data describing the AIMSUN Headingley network simulated road links and junctions (.STR files) and the Headingley network vehicle fleet composition for the designated time period (.FLT file).

A .FZP file contains the second-by-second drive cycle data for every simulated vehicle through the AIMSUN Headingley network during a replication. Each of these simulated vehicles (and respective activity data) is labelled with a PHEM vehicle type ID that corresponds to the vehicle type. The vehicle types and corresponding PHEM vehicle type IDs are shown in Table 6.8. Whilst the modelled fleet composition, by vehicle type, is determined in AIMSUN through the input flow traffic states (see Chapter 6.3.4), further classification of the fleet into vehicle type sub-categories is controlled by the .FLT file in PHEM. The drive cycle data for each simulated vehicle have a vehicle type ID which acts as a reference to the correct vehicle category in the .FLT file. The .FLT file distributes all simulated vehicles to sub-categories of their respective vehicle types (classified by fuel type, Euro standard, and weight). For any individual simulated vehicle, the sub-category assigned by PHEM is random, however, the final fleet composition in the PHEM output file must match the fleet composition described in the .FLT file.

The PHEM model data for each individual vehicle sub-category are organised in PHEM by a .GEN file that determines the input files used in the emission calculation, including the relevant engine map (.MEP and .MAP) and vehicle specifications (.VEH). For this study, the .VEH files contain the Headingley network average vehicle parameters.

The PHEM simulation of each AIMSUN replication generates three types of output file: a .mod file for each vehicle type, which gives the second-by-second emission estimates for each vehicle in g/h for FC, NO_x, CO, HC, PM, and NO; a .vehicle.sum file which presents the aggregate total emission estimate for each simulated vehicle in (g/h), along with time in the simulation (s), distance travelled (km) and average speed (km/h), and .segment.sum files which present g/km FC and pollutant emissions, for each road section in the network, along with the number of vehicles passing through the section, the total distance covered in the section (km) and the total time spent by vehicles on the section (hours).

6.5 COUPLED TRAFFIC MICRO-SIMULATION AND INSTANTANEOUS EMISSION MODEL RESULTS

For each of the 2 hour time periods (AM, PM, IP, EV and NI) the simulated drive cycle data from the 10 validated AIMSUN replications were simulated by PHEM to generate second-by-second emission estimates for each simulated vehicle. The coupled AIMSUN-PHEM model produced emission estimates for 377,062 simulated vehicles over the 50 simulation runs, generating a total of 33,111 hours of vehicle emission data, whilst travelling a total of 690,420 km.

The nature of the PHEM output enables these emission data to be analysed at a variety of scales; ranging from analysis of one individually selected vehicle trip to the calculation of the entire aggregate fleet emission. As each second of data is also labelled with details of the specific vehicle related to the emission, and its location within the network, the emission contributions from each vehicle type and Euro standard can be evaluated, along with emission analysis of specific road links.

6.5.1 Comparison of Simulated Model Journeys to Real-World Data

Although a robust validation of journey times within the model was not possible due to a lack of journey time data for the network, a comparison of the simulated car and taxi journey times with the PEMS real-world data, analysed in Chapter 3, was conducted. The PEMS data from the 1.5 km 'northbound' and 'southbound' A660 sections (see Figure 3.30) described in the analysis of the diurnal variation in CO_2 emission in Chapter 3.5 were compared to the AIMSUN-PHEM generated data for each car and taxi completing the simulated northbound and southbound sections. The instrumented vehicle completed these sections 15 times in the AM peak period, 14 times in the Inter-Peak period, 11 times in the PM peak period and 6 times in the EV period. There were no test runs during the NI time period. The links in the AIMSUN simulation which make up the northbound and southbound sections were identified and the drive cycle data for all simulated cars and taxis completing the 1.5 km sections were extracted. In order to assess the accuracy of the simulated drive cycle CO_2 emission estimates from PHEM, the northbound and southbound simulated car and taxi drive cycles (including the link road grades from the AIMSUN model) were processed in PHEM using the .FLT and .VEH files set up to represent the instrumented Euro 4 vehicle in Chapter 4.6.4.4. By means of the simulated car / taxi drive cycles, CO_2 emission estimates were generated, which could then be evaluated against the real-world PEMS measured CO_2 emissions from the instrumented vehicle in Chapter 3.

Figure 6.18 plots three different estimates of the Euro 4 test vehicle gCO_2/km emission rate over the AM model southbound section against the time taken to complete the journey. The red points indicate the 15 PEMS gCO_2/km values recorded between 07:00 and 09:30 on the southbound section in the Headingley network (Chapter 3.5). The green points describe the 15 $PHEM_G$ (PHEM with LiDAR-GIS road grade) estimates of the gCO_2/km emission from the recorded PEMS vehicle speed data (Chapter 5.7.1). The blue points present the gCO_2/km emission generated from the AIMSUN-PHEM AM model simulated drive cycles from cars and taxis completing the southbound section. From the 10 replications of the AM model, 4,722 cars and taxis completed the southbound section and the API extracted drive cycles from these vehicles were then processed in PHEM using the Euro 4 vehicle specifications developed in Chapter 4.6.

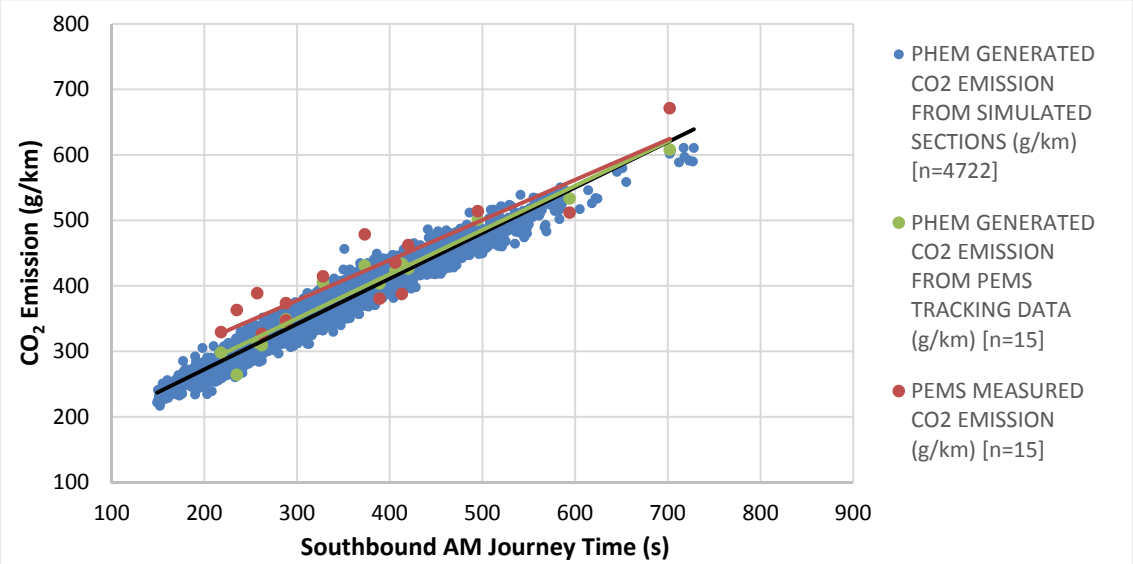

Figure 6.18: Southbound AM: PEMS, $PHEM_G$ and AIMSUN-PHEM Model CO_2 Emission Factors

Although ideally, the AIMSUN-PHEM simulated vehicle data should generate the same emission factors as the PEMS real-world recorded emission values, it is, in fact, more important to assess the ability of the AIMSUN-PHEM model output to reproduce the $PHEM_G$ emission values, because the $PHEM_G$ emission estimates were made from the PEMS on-road GPS tracking data. The closer the AIMSUN-PHEM CO_2 emission estimates are to the $PHEM_G$ values, the more likely it is the AIMSUN simulated second-by-second drive cycle data are a good approximation of the PEMS recorded real-world second-by-second vehicle speed data.

The simulated southbound journey times generated by the AIMSUN AM model cover the entire observed range of PEMS recorded journey times, which indicates that the model captures the range of real-world congestion for this section of the network. The average journey time from the 15 PEMS recorded runs was 378 s, with a range from 218 s to 702 s. The average journey

time of the 4,722 simulated journeys is slightly faster than the real-world average at 333 s and has a slightly greater range from 149 s to 728 s. A further data set from Trafficmaster (www.teletrac.co.uk) was made available by LCC with average times to complete set road links on the A660 for the AM and PM peak traffic. Analysis of this data set of approximately 1,500 observations suggests an average AM journey time on the southbound section of 303 s.

In order to meet the DfT's WebTag journey time validation criterion, journey times across greater than 85% of routes must have modelled journey times within 15% of surveyed times, or within ±1 minute if ±15% of the journey time is less than one minute (DfT, 2014). As journey time data were only available for the described northbound and southbound routes, a robust analysis cannot be conducted, however, taking the Trafficmaster average journey time of 303 s as the surveyed time, the model average of 333 s is within the one minute limit and 54.6% of the 4,722 simulated journeys were within ±1 minute of the surveyed average. The PEMS measured average of 378 s is greater than the one minute validation criterion, which perhaps indicates that the PEMS sample size is too small to treat the average journey time as a reliable surveyed travel time.

In order to assess the accuracy of the AIMSUN-PHEM model CO_2 emission per km estimates at each journey time, lines of best fit were calculated through the journey time and emission plots from the AIMSUN-PHEM model, the $PHEM_G$ and PEMS measured emission estimates. The average difference between these lines of best fit was then calculated between the range of PEMS observed journey times. The average difference (in the range 149 s to 728 s) between the AIMSUN-PHEM model CO_2 emission estimate and PEMS measured CO_2 emission was found to be -4.9% and the average difference between the AIMSUN-PHEM model and the $PHEM_G$ CO_2 estimates, -1.2%. This suggests that the AIMSUN simulated vehicle trajectory data produce emission estimates from PHEM which are on average within 1.2% of the PHEM estimates made with the actual GPS tracking data, which indicates that the AIMSUN model is well calibrated for the southbound section in the AM model.

Figure 6.19 presents the PEMS, $PHEM_G$ and AIMSUN-PHEM AM model CO_2 emission estimates by journey time to complete the northbound section. The 10 AM model replications generated 3,582 simulated car and taxi drive cycles over the northbound section. The simulated northbound journey times (133 to 540 s) do not completely cover the range of PEMS measured journey times with the instrumented vehicle (171 s to 680 s), with a couple of the PEMS journeys considerably longer than the simulated times. The Trafficmaster data average journey time of 272 s is, however, closer to the simulated average of 244 s than to the PEMS observed average

journey time of 374 s. It is possible that the congestion during the PEMS testing week on the northbound section was greater than the average network congestion at this time of day. The simulated average journey time is within the one minute DfT validation criterion and 62.5% of the 3,582 simulated journeys were within ±1 minute of the surveyed average.

Evaluating the accuracy of the AM model northbound CO_2 emission estimates over the range 171 s to 680 s, the AIMSUN-PHEM model CO_2 emission estimate line of best fit is 9.0% lower than the PEMS measured CO_2 emission but the difference between the AIMSUN-PHEM model and the $PHEM_G$ CO_2 estimates is calculated at an average of -0.2%. This again suggests that a simulated journey from the AM model generates a similar rate of CO_2 emission in PHEM as a PEMS recorded vehicle speed profile of the same journey time.

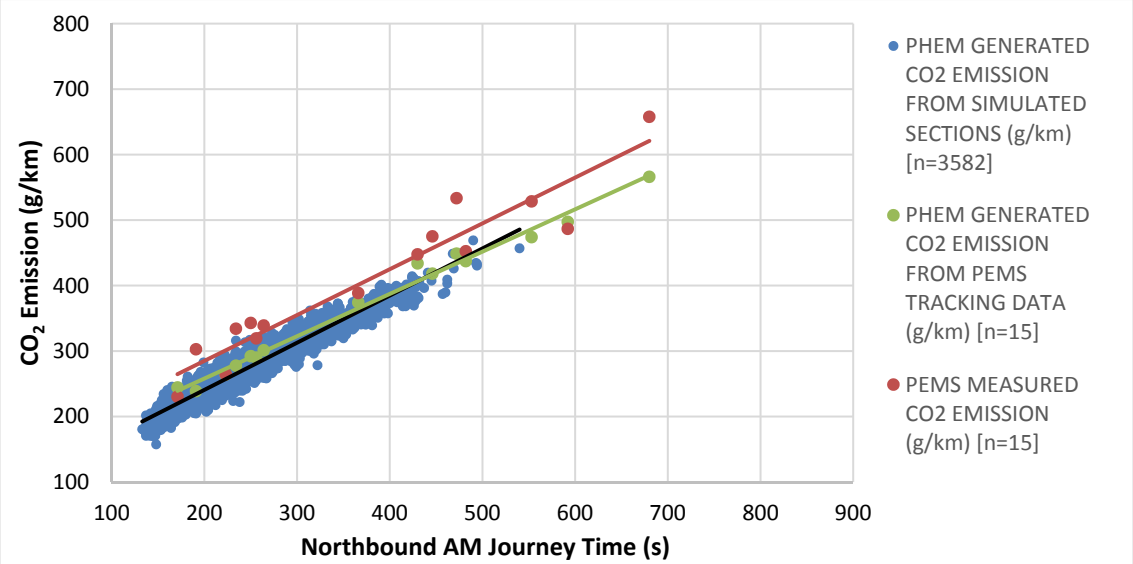

Figure 6.19: Northbound AM: PEMS, $PHEM_G$ and AIMSUN-PHEM Model CO_2 Emission Factors

The same analysis was conducted for the IP period, however, no Trafficmaster data were available for this time period. Figure 6.20 and Figure 6.21 plot the PEMS, $PHEM_G$ and AIMSUN-PHEM IP model CO_2 emission estimates by journey time on the southbound and northbound sections respectively. When compared to Figure 6.18 and Figure 6.19, it is clear that the IP simulation was relatively uncongested with a much shorter average journey times than during the AM peak. The PEMS measured average journey time on the southbound section is 268 s with a range from 194 s to 381 s, which, when compared to the AIMSUN simulated average journey time of 191 s (range 126 s to 319 s), indicates that the simulation in AIMSUN may be underestimating the average journey time. The average PEMS measured journey time on the northbound section of 327 s is similarly considerably longer than the simulated journey time average of 193 s. This is possibly the result of the inability of the Headingley AIMSUN simulation

to account for factors such as interaction with pedestrians and cyclists or may be related to increased use of pedestrian crossings on the route, for which there were no detailed survey data. The test routes used in this analysis pass through the centre of Headingley which is busy with pedestrians during the day. The route also has two large bus bays outside a large shopping centre and with the bus service at peak frequency during the IP hours, it is conceivable that there is some interaction between the bus bays and the traffic network which is not accounted for in the simulation. Further data are required to assess whether the PEMS journey times provide a fair reflection of the normal journey times and the AIMSUN model may require some improvement to better reflect the network conditions in the IP period.

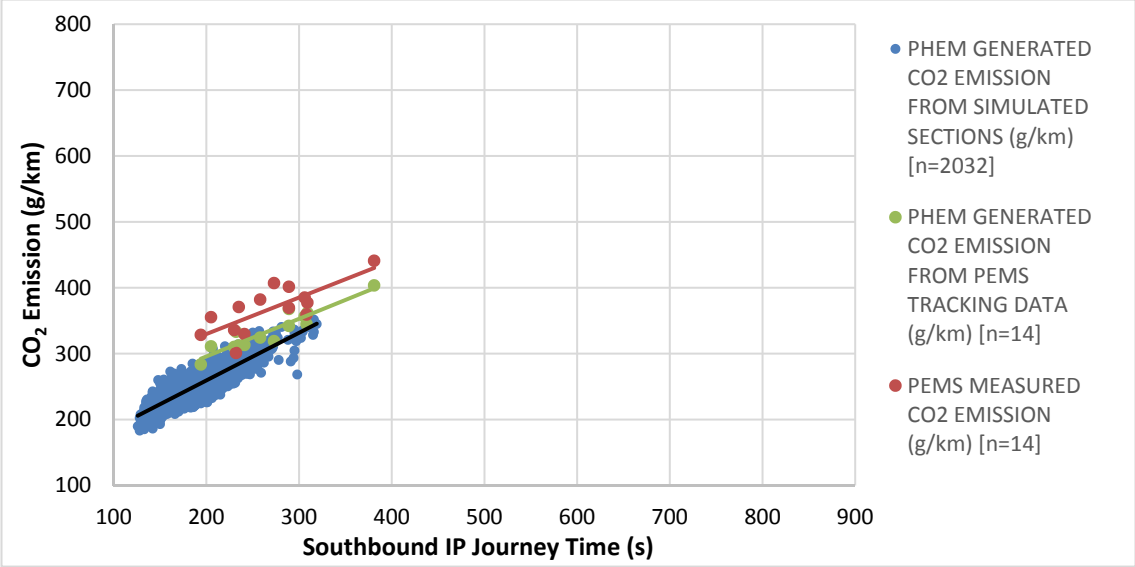

Figure 6.20: Southbound IP: PEMS, $PHEM_G$ and AIMSUN-PHEM Model CO_2 Emission Factors

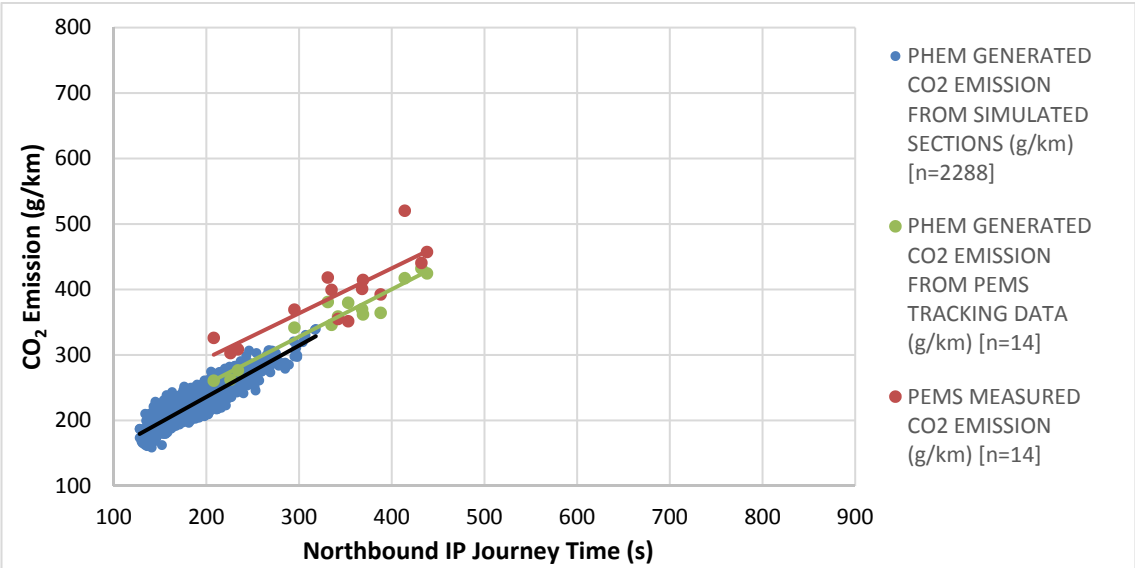

Figure 6.21: Northbound IP: PEMS, $PHEM_G$ and AIMSUN-PHEM Model CO_2 Emission Factors

The difference between the line of best fit for AIMSUN-PHEM IP model CO_2 emission rate and the $PHEM_G$ CO_2 estimates for the southbound section over the range 194 s to 381 s was -6.7% and on the northbound section over the range 208 s to 438 s was -3.5%. Despite potential issues with the average journey time in the IP AIMSUN model, the simulated second-by-second vehicle data still provide good CO_2 emission estimates from PHEM for like-for-like journey times.

The average journey time for the 3,571 simulated PM peak southbound journeys was 352 s, which is greater than both the PEMS average journey time of 302 s and the Trafficmaster average journey time of 288 s. In contrast to the IP simulation, the PM peak southbound journey times indicate that the simulation models a greater degree of congestion than found in reality. At 64 s, the difference in the average simulated journey time and the surveyed time is only slightly greater than would be acceptable for DfT WebTag validation. It is possible that small adjustments in AIMSUN could be made to reduce the southbound journey time. The northbound section experiences frequent traffic jams in the PM peak, as cars head from the city centre to the outer suburbs. As a result, vehicles which exit the southbound section to small side roads on the right-hand side often experience delays in the simulation waiting for the traffic jam to clear. As these are single lane roads, vehicles behind the turning vehicle experience a delay. Adjustment to reduce the percentage of these type of turning movements would likely therefore shorten the average southbound PM peak journey time.

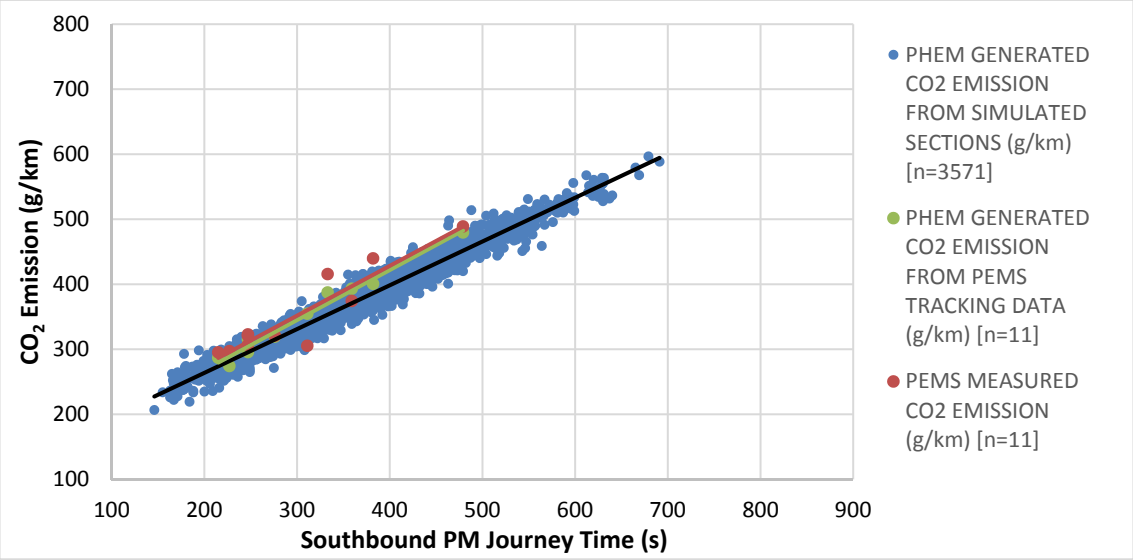

Figure 6.22: Southbound PM: PEMS, $PHEM_G$ and AIMSUN-PHEM Model CO_2 Emission Factors

Comparing the lines of best fit through the AIMSUN-PHEM PM model and the $PHEM_G$ estimates, the CO_2 emission estimate from the simulated data was on average 5.8% less than the $PHEM_G$ estimates generated from the PEMS tracking data in the range from 215 s to 479 s.

The PM peak has a much greater range of journey times in northbound section than other time periods and this range appears to have been well captured by the AIMSUN-PHEM PM model. The average simulated journey time was 540 s which is very close to the Trafficmaster average time of 535 s. The PEMS recorded journey time average was 627 s. The AIMSUN-PHEM PM model simulated CO_2 emission estimate on the northbound section was on average 0.7% greater than the $PHEM_G$ estimate.

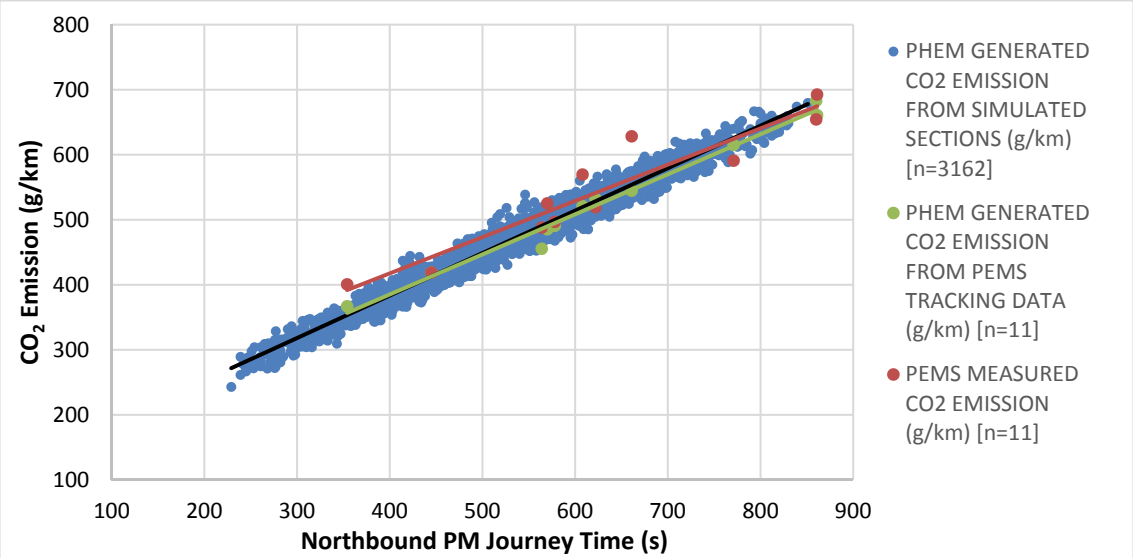

Figure 6.23: Northbound PM: PEMS, $PHEM_G$ and AIMSUN-PHEM Model CO_2 Emission Factors

Figure 6.24 and Figure 6.25 display the AIMSUN-PHEM EV model CO_2 emission estimates by journey time on the southbound and northbound sections respectively. A total of 6 journeys in the instrumented vehicle were conducted in the EV period between 20:00 and 22:00 and the PEMS measured CO_2 values are presented along with the $PHEM_G$ estimates from the PEMS 1 Hz transient vehicle data. The short journey times and a small range of PEMS and simulated values shown in the figures highlight the free flowing conditions experienced in the evening period. The PEMS and simulated average journey times are very similar, with the southbound average PEMS journey time 193 s and the simulated journey time 192 s. The northbound average PEMS recorded journey time was 199 s and the simulated journey time 193 s. 98.0% and 95.5% of the southbound and northbound journey times were with ± 1 minute of the respective PEMS average journey times.

Comparison of the lines of best fit in the southbound section shows the simulated data to be on average 6.1% less than $PHEM_G$ data in the range 147 s to 239 s. The northbound section simulated data trend line is on average 8.2% less than the $PHEM_G$ trend line in the range 153 s to 231 s. Whilst these differences are amongst the largest calculated, with such a limited PEMS sample of only six vehicle journeys, the line of best fit may not be truly representative of EV

journey CO_2 emission. A larger sample of tracking data in the EV period from which PEMS estimates could be calculated would help to clarify the trend.

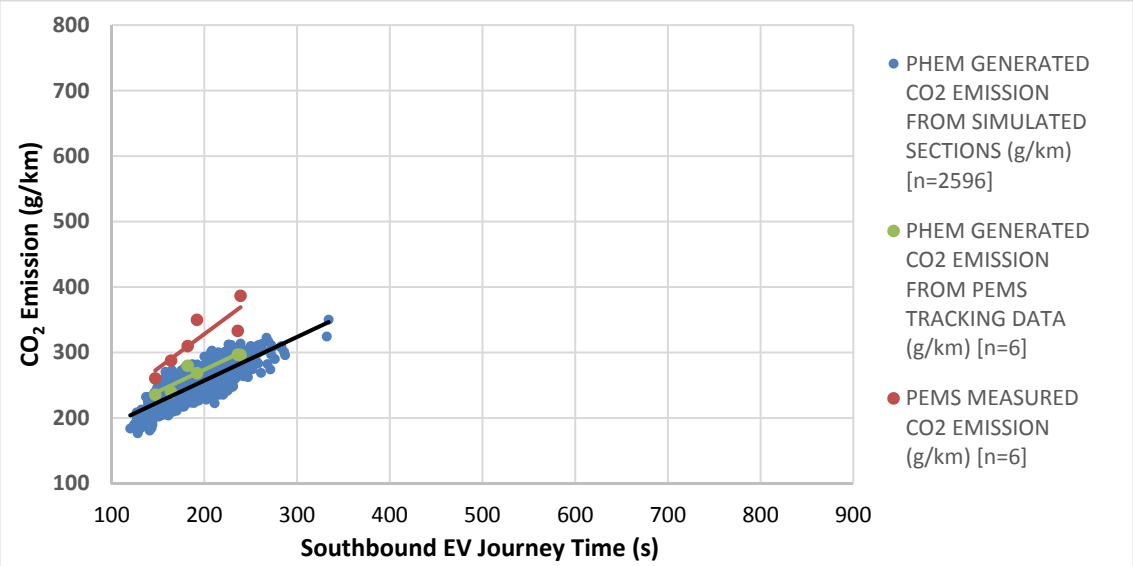

Figure 6.24: Southbound EV: PEMS, $PHEM_G$ and AIMSUN-PHEM Model CO_2 Emission Factors

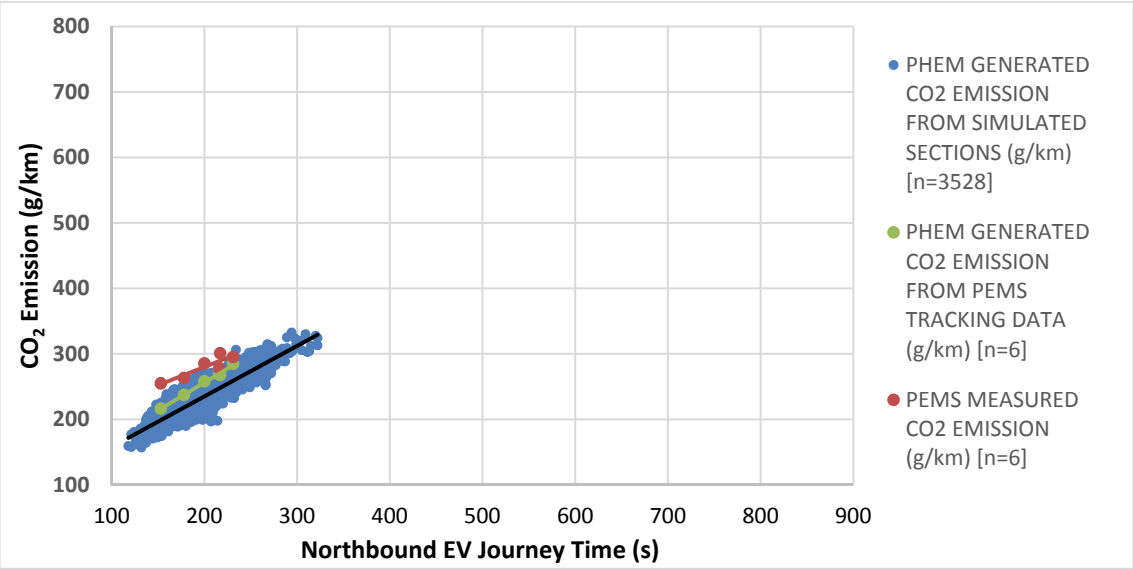

Figure 6.25: Northbound EV: PEMS, $PHEM_G$ and AIMSUN-PHEM Model CO_2 Emission Factors

Figure 6.26 and Figure 6.27 show, respectively, the southbound and northbound gCO_2/km emission factors by journey time for the AIMSUN-PHEM NI model. Unfortunately, there are no PEMS data available to check the accuracy of the PHEM estimates of CO_2 emission from these simulated drive cycles. The graphs indicate that between 01:00 and 02:00, there is no congestion, both sections are completed in under 200 s a majority of the time. The fastest time through the south section was 115 s which corresponds to an average speed of 47 km/h, which is very close to the maximum speed limit (48 km/h).

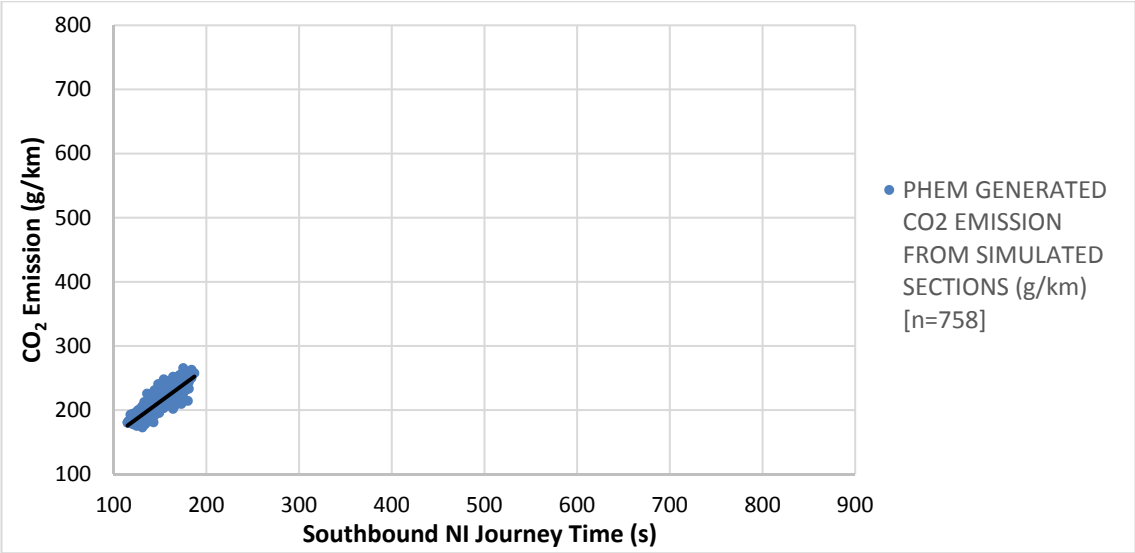

Figure 6.26: Southbound NI: AIMSUN-PHEM Model CO_2 Emission Factors

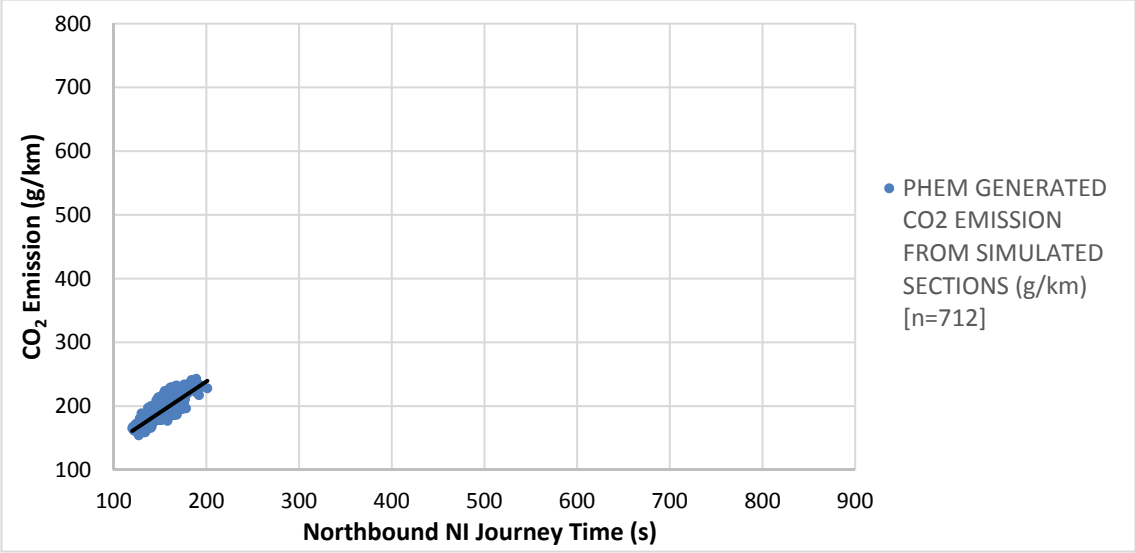

Figure 6.27: Northbound NI: AIMSUN-PHEM Model CO_2 Emission Factors

Aside from the IP period, in which the journey times are quicker than the PEMS recorded journey times, the other simulated time periods, in general, seem to capture the correct range of journey times and have approximately the same average. The line of best fit for the simulated CO_2 emission is very close to that of the $PHEM_G$ generated emission estimates, suggesting that the simulated second-by-second data are a close match for the real-world tracking data.

In order to check that the simulated second-by-second data are similar to the real-world data, it is also necessary to confirm that the VSP profile of the simulated data is comparable to the VSP profile of the PEMS recorded tracking data. Figure 4.10 in Chapter 4 plots the expected emission of CO_2 at each integer value of VSP, highlighting the near linear increase in CO_2 emission with increase in VSP. For VSP values of zero or lower the emission is a stable low idle level. Unless the comparability of the VSP distributions is carefully examined, it is possible that the simulated

vehicle journeys could have different power distributions to vehicles driven in the real-world but still derive similar CO_2 emission estimates. This is because the average positive VSP over the journey could be similar. Whilst this would result in reasonable CO_2 emission estimates, due to the linear relationship between CO_2 emission and power, for other pollutant species where the relationship is not linear, differences in VSP distribution may cause large emission estimation errors.

To assess the simulated and real-world VSP distributions of journeys of a similar duration, the following novel methodology was developed in this research. 'Time segments' describing a range of journey durations (approximately a 20 s range) were specified which included at least three completed PEMS journeys and approximately 200 simulated journeys, over the northbound or southbound 1.5 km road sections described in Chapter 3.5. Figure 6.28 compares the VSP distribution of 208 simulated southbound section journeys between 237 s and 257 s in duration, with the VSP distribution of five PEMS recorded southbound section journey times of 241 s, 247 s, 247 s, 247 s and 251 s. The simulated data are presented as boxplots of the maximum, minimum, interquartile range (IQR) and median for the percentage of each simulated journey in that VSP value. Over the 208 journeys, the average journey VSP distribution has 52.2% of the journey at a VSP <0, but one of the journeys had a very high percentage (59.9%) of the journey at VSP <0 and one had a very low percentage (34.7%) at VSP <0. The coloured points in the figure mark the actual distribution of the PEMS recorded journeys. In the example of the 241 s real-world journey, the VSP distribution had 57.9% of VSP values at VSP<0, 3.2% were in the VSP 0-1 bin, 4.9% were in the VSP 2-3 bin, etc.

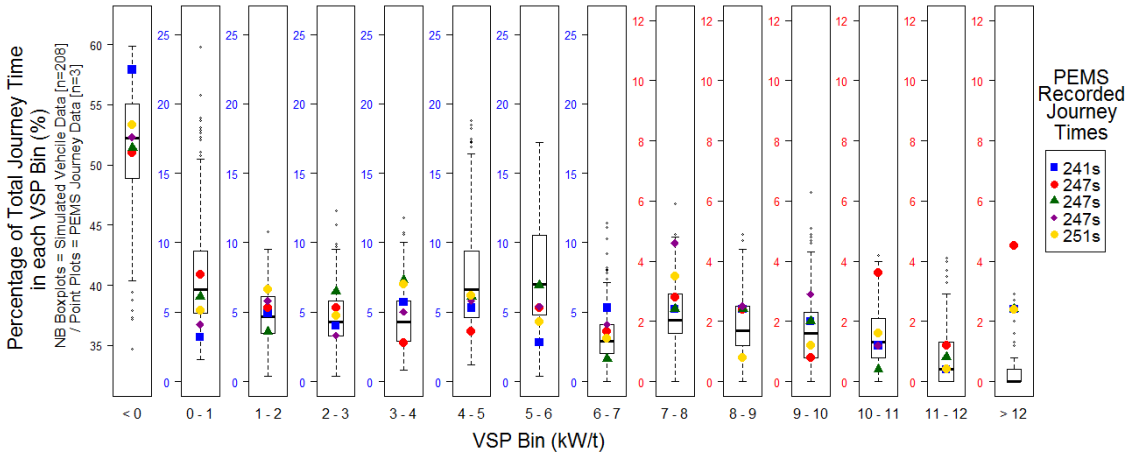

Figure 6.28: Comparison of Simulated and PEMS 1 Hz VSP Distributions: Southbound 237-257 s

The simulated distributions, in this case, look to be a good fit with the real-world data, with a large number of the VSP bins having IQR (the middle 50% of the data) which overlap with the real-world values.

Figure 6.29 compares the VSP distributions of 287 simulated southbound section journeys between 373 s and 389 s in length, with four PEMS recorded southbound journeys of 373 s, 381 s, 382 s and 389 s. The simulated VSP distributions seem to be a good match with the data again. For the 382 s journey, the VSP 6-7 bin percentage is much greater than the IQR suggested by the simulated data but it is within the range of simulated values.

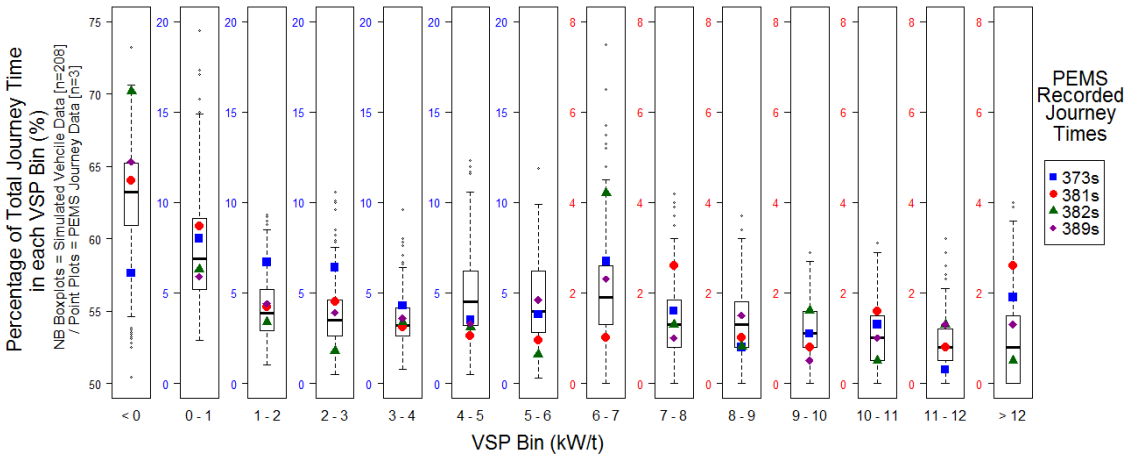

Figure 6.29: Comparison of Simulated and PEMS 1 Hz VSP Distributions: Southbound 373-389 s

Figure 6.30 is a comparison of the VSP distributions of 344 simulated northbound journeys between 208 and 217 s in length with three PEMS recorded journeys of 208 s, 216 s and 217 s in length. There appears to be a slight anomaly with the VSP 1-2 bin, which has a significant number of simulated journeys recording a large percentage of their journey VSP values in the VSP 1-2 bin. This is not reflected the PEMS distributions. The simulation also seems to underestimate the percentage of VSP values in VSP 6-7 and VSP 7-8 bins.

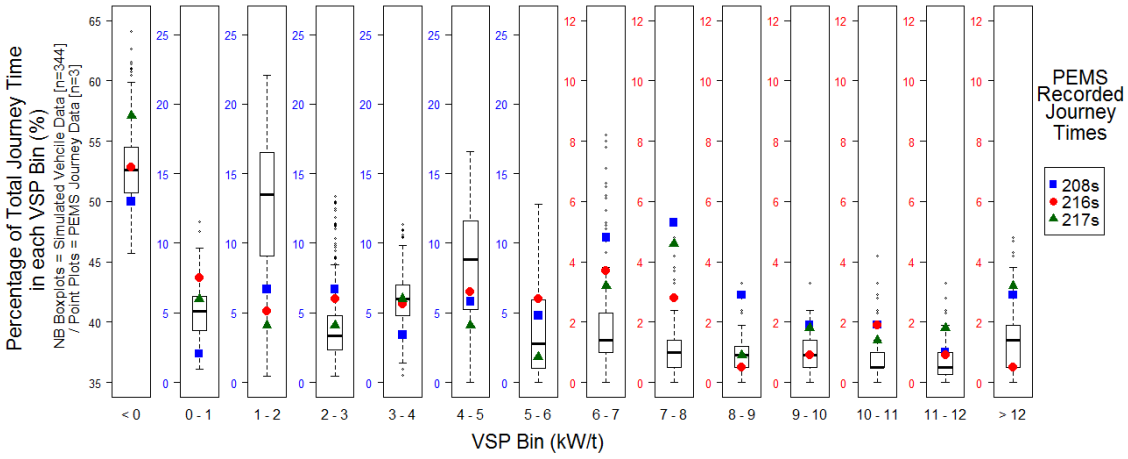

Figure 6.30: Comparison of Simulated and PEMS 1 Hz VSP Distributions: Northbound 208-217 s

Figure 6.31 compares the VSP distributions of 226 simulated northbound section journeys between 560 s and 580 s in length, with the VSP distributions of three PEMS recorded

northbound journeys of 564 s, 570 s and 578 s. The simulated and real-world distributions appear a close fit with the only discrepancy being the difference between the simulated and real-world distribution of values in the VSP <0 bin and the VSP 0-1 bin. As these bins represent very low CO_2 emission, this would likely have little impact on the emission estimate. The comparative journey times are relatively slow through the section, representative of congestion in the section. The anomaly perhaps suggests that in congested traffic the simulated vehicles are likely to come to a stationary position, whereas in the real-world drivers might approach very slowly (crawl along) rather than stopping.

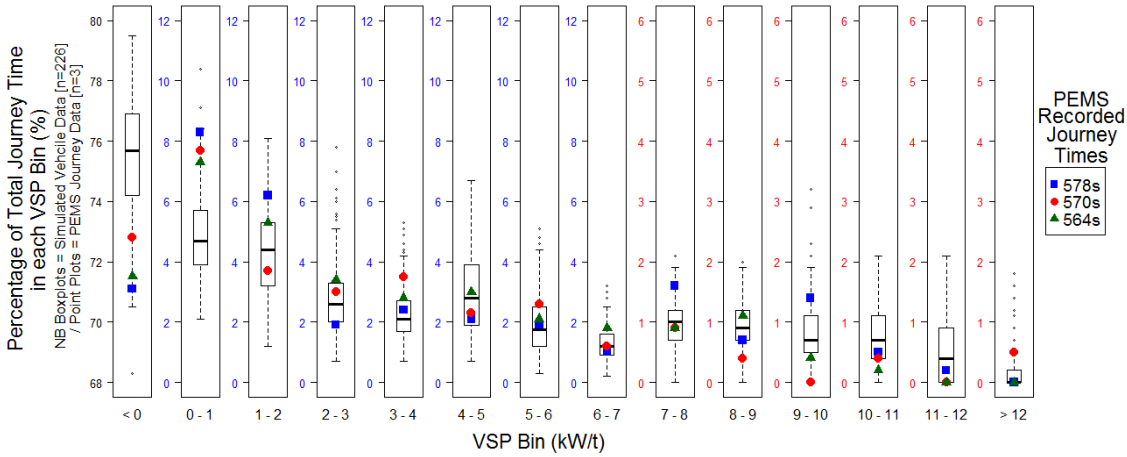

Figure 6.31: Comparison of Simulated and PEMS 1 Hz VSP Distributions: Northbound 560-580 s

The analysis of simulated and PEMS distributions, for vehicles completing similar length journeys, demonstrates that the calibrated AIMSUN simulation produces second-by-second transient vehicle data that are representative of real-world driving. However, anomalies such as found in Figure 6.30 indicate further calibration work may be required since differences in the distributions may cause more significant errors for other emission species. Sensitivity testing of the AIMSUN simulation vehicle dynamics may reveal ways to improve the match between the VSP distributions. The novel methodology demonstrated in this section (Chapter 6.5.1), which enables evaluation of the capability of coupled traffic simulation and emission model to produce real-world estimates for emission and engine power output, is in the process of being written up as a paper for peer review publication.

6.5.2 Network CO_2 Emission

The greatest strength of this coupled micro-simulation and instantaneous emission model methodology is the ability to generate high resolution emission estimates at a road network scale. This section presents an analysis of the AIMSUN-PHEM model output for each of the five simulated time periods.

Aggregating the AIMSUN-PHEM CO_2 emission estimates from all simulated vehicles in the network for each of the simulation time periods reveals that the greatest rate of CO_2 emission is generated by the vehicle fleet during the PM peak with a total of 5,594 $kgCO_2$ in the 2-hour simulation period. The PM had the greatest average flow of vehicles through the network, with 5,604 vehicles per hour and the greatest average vehicle kilometres travelled in the network at 10,137 km travelled per hour. The total average CO_2 emission over the other time periods was 5,021 kg, 4,328 kg, 2,425 kg and 416 kg, for AM, IP, EV and NI respectively. The average gCO_2/km values per vehicle (aggregated over all vehicles categories) in the network for the AM, IP, PM, EV and NI periods were 265.1, 276.6, 275.9, 205.1 and 177.0 respectively; with the surprisingly high IP emission rate the result of a greater proportion of HGV vehicles during the IP, as can be seen in Figure 6.12b. As described in Chapter 4.6.4.4, CO_2 emission is not calculated directly in PHEM. The AIMSUN-PHEM CO_2 emission estimates are derived from PHEM estimated fuel consumption, which is converted to CO_2 emission using the 2016 UK Government conversion factors for GHG reporting for diesel and petrol (standard forecourt fuel from UK filling stations). Under this guidance, one tonne of average biofuel blend diesel converts to 3,083 $kgCO_2$, whilst one tonne of average biofuel blend petrol converts to 2,929 $kgCO_2$ (GOV.UK, 2016c).

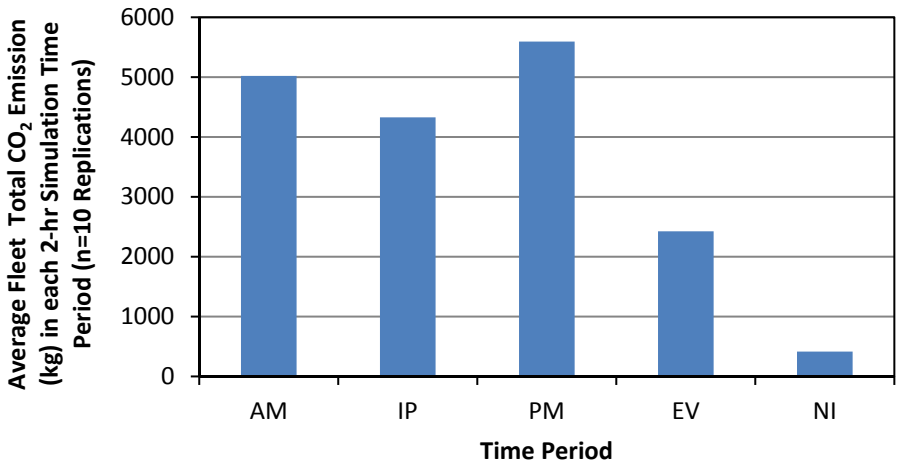

Figure 6.32: Total CO_2 Emission in Each 2-hour Time Period

The high resolution nature of the coupled AIMSUN-PHEM model allows results like those presented above to be disaggregated into much smaller constituent elements. Figure 6.33 presents the same data, but sub-divided into the contribution from each vehicle type, revealing petrol passenger cars as the leading source of CO_2 emission for all periods except at night when the primarily diesel taxi fleet becomes a significant fraction of the overall traffic fleet (40.5% - Figure 6.12b).

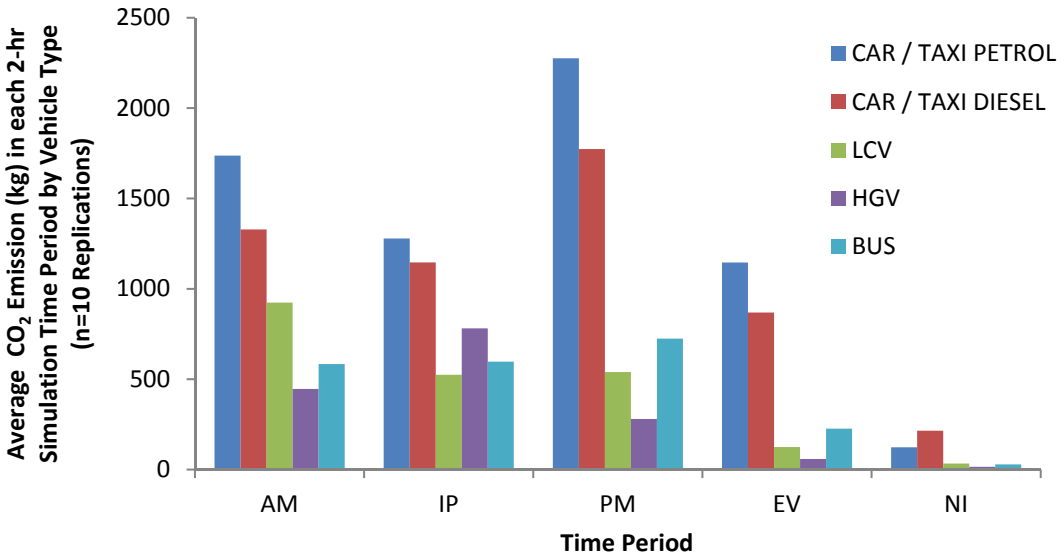

Figure 6.33: Total CO_2 Emission in Each 2-hour Time Period by Vehicle Type

The average on-road CO_2 emission factors in the simulated Headingley network from the passenger car / taxi fleet (including both petrol and diesel vehicles) were calculated by the AIMSUN-PHEM model as 219.6, 204.0, 234.7, 184.6 and 161.5 gCO_2/km for the AM, IP, PM, EV and NI periods respectively. The daytime simulation period CO_2 emission factors are substantially greater than the SMMT 2014 UK car fleet average rated CO_2 emission, which was calculated from registration data to be 156.6 gCO_2/km (SMMT, 2015b). The simulation AM, IP, and PM period results were also larger than the CO_2 emission factors calculated by DEFRA, which suggest an average emission for a petrol car in the UK fleet of 190.7 gCO_2/km and 180.6 gCO_2/km for a diesel car (DEFRA, 2015b). Only in relatively free flowing EV and NI conditions are the Headingley network emission factors for passenger cars lower than, or as low as, the suggested CO_2 emission factors from these two sources. However, the AIMSUN-PHEM emission factors for passenger cars in the Headingley network are similar to an 2008 NAEI calculation for hot exhaust emission on urban roads, which proposed emission factors of 223.9 gCO_2/km for petrol cars and 215.0 gCO_2/km for diesel (NAEI, 2011).

Figure 6.34 presents the CO_2 g/km emission factors for passenger cars separated by fuel type and emission standard. The ability to analyse at this sub-category level is one of the major advantages of the coupled model methodology. The illustrated increase in CO_2 emission from Euro 2 to Euro 4 for both petrol and diesel passenger cars is perhaps counter-intuitive, as the trend might be expected to show an improvement in efficiency and therefore in fuel consumption and CO_2 emission; the increase in emission is, however, a reflection of the increase in average rated engine power that can be seen in Table 6.18. In contrast, the drop in Euro 5 emission may be the result of the introduction of the EU's New Car CO_2 Regulation in 2009 which

forced manufacturers to reduce the CO_2 emission from their vehicle fleets (EC, 2009b). The emission factors for Euro 6 show a significant rise from Euro 5 but this is from a very limited sample size of these new vehicles (≈300) and the average engine size of the early introduction Euro 6 vehicle observed by the ANPR survey was considerably larger than for previous emission standards (Table 6.18).

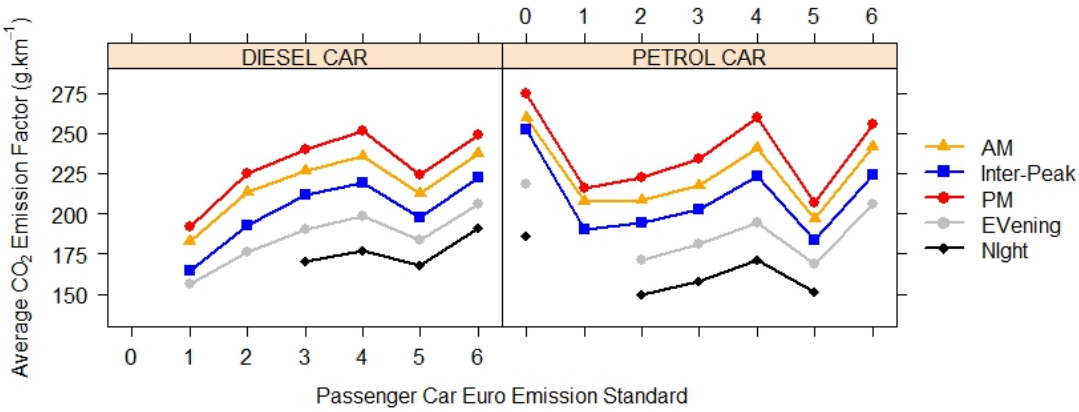

Figure 6.34: AIMSUN-PHEM CO_2 Emission Factors for Diesel and Petrol Passenger Cars

The figures reveal a clear trend in increased average CO_2 emission factor with congestion. In congested PM peak conditions, the average CO_2 emission rate per km in the simulated Headingley network is 47.1% greater for petrol passenger cars and 37.4% greater for diesel passenger cars than during free flowing NI conditions.

Figure 6.35 presents the CO_2 g/km emission factors for taxis separated by fuel type and emission standard. The same pattern of emission by time period is evident in the simulated taxi fleet, with congested stop-start conditions and lower average network speeds during the PM peak resulting in the highest rate of CO_2 emission. The diesel taxi CO_2 emission factors are lower than those of the diesel passenger car fleet. This is unsurprising given that vehicle fuel economy will have an important bearing on profit for the industry.

The metadata from the ANPR survey reveals a decrease in engine size in taxis from Euro 3 to Euro 5 (see Table 6.18), which is contrary to the trend in passenger cars and is probably the result of an effort to reduce costs in the face of increasing fuel prices. The generated average CO_2 emission factors for diesel taxis were 185.7 gCO_2/km for the AM model, 182.0 gCO_2/km in the IP, 206.8 gCO_2/km in the PM, 171.9 gCO_2/km in the EV and 153.4 gCO_2/km in the NI model.

The petrol taxi fleet's average CO_2 emission factors (N.B. from a small sample size see Table 6.5) are noticeably greater than those of the diesel taxis. As diesel engines offer better like-for-like

fuel consumption than similar sized petrol engines this difference is not unexpected. The gap is widened further by the fact that the average engine size of the petrol taxis in the Headingley fleet is larger than the diesel taxis.

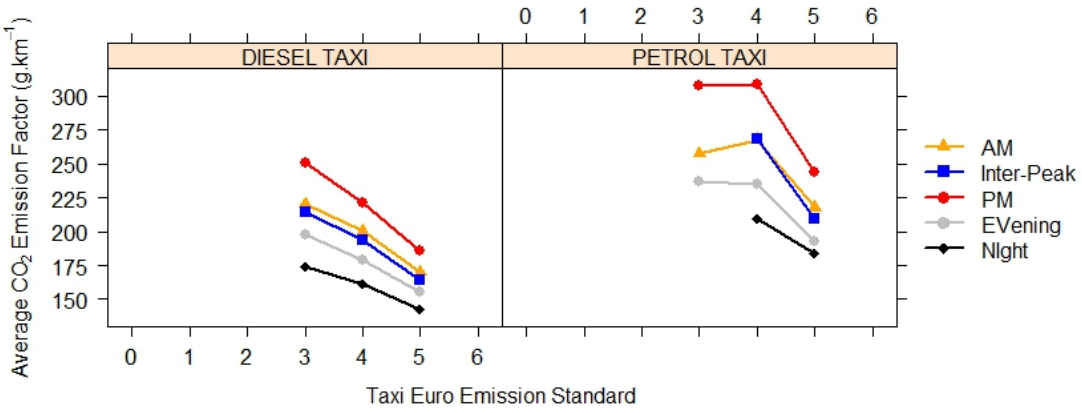

Figure 6.35: AIMSUN-PHEM CO_2 Emission Factors for Diesel and Petrol Taxis

It should be noted, however, that the Euro 5 petrol taxi CO_2 emission rates are probably an overestimation of the actual real-world emission rate. As discussed in Chapter 6.2.4.1, of the 72 Euro 5 petrol taxis observed in the Headingley fleet on the A660, 48 were hybrid vehicles. As there is currently no provision in PHEM for hybrid vehicles these vehicles had to be described in the simulation as standard petrol vehicles. The power supplied by the electric motor in the hybrid engine and the resultant reduction in CO_2 emission is therefore incorrectly modelled in the simulation and may be an overestimate in CO_2 emission, for this limited number of vehicles, by up to 60% (Fontaras et al., 2008; Holmen and Sentoff, 2015).The magnitude of the differences in taxi CO_2 emission rates between congested and free flowing conditions within the Headingley network are similar to those observed from the passenger car fleet. The average difference in the taxi gCO_2/km emission rates between the NI (free flow) and PM (congested) simulations was an increase in emission of 34.8% for diesel taxis and an increase of 47.2% for petrol taxis.

Figure 6.36 presents the average AIMSUN-PHEM Headingley network CO_2 emission factors by Euro emission standard for four sizes of LCV including the additional N_2 category between 3.5 – 5 t (identified in the graph as DIESEL IV) which is discussed in Chapter 6.2.6.1. Although this category is technically classified as HGV all N_2 category vehicles observed by the ANPR survey had the same engines as the lighter N_1 Class III LCVs. Relatively few LCVs were observed by the ANPR survey on the A660 in the EV and NI periods resulting in gaps in the graphs where there are no data to report. The trend of increased CO_2 emission during congested periods is once again clear, with the NI periods reporting the lowest values and the PM the greatest. For the Class III diesel (1.76 to 3.5 t), which travelled 66.2% of the LCV VKM in the simulations, the range

of the AIMSUN-PHEM simulated average CO_2 emission rates across the five time periods is from 195.1 gCO_2/km in the NI simulations to 263.7 gCO_2/km in the PM simulations, an increase in CO_2 emission rate of 35.2% in congested network conditions.

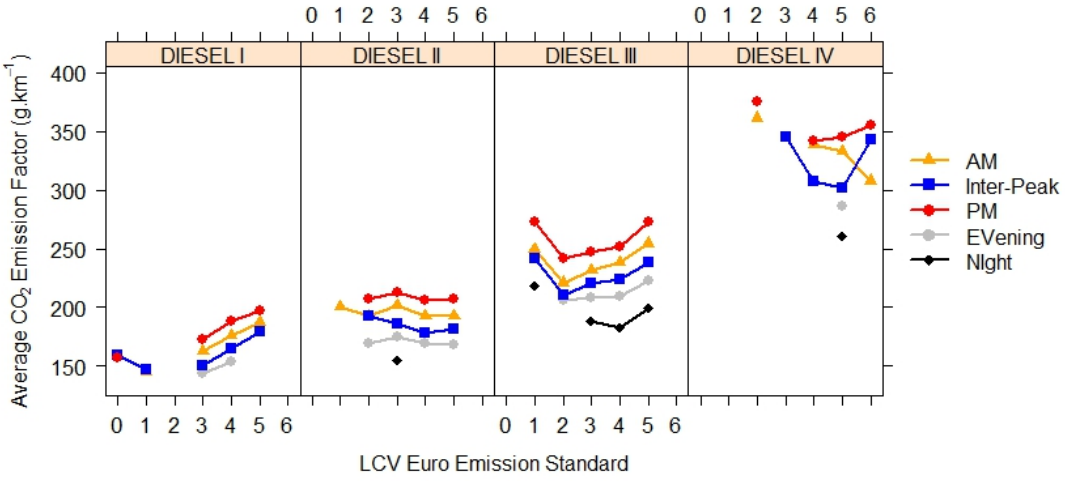

Figure 6.36: AIMSUN-PHEM CO_2 Emission Factors for Diesel LCVs by Weight Class

For each LCV vehicle class, the emission factors at each Euro standard tend to follow the trend in observed average engine size calculated from the ANPR A660 survey metadata and reported in Appendix 2. For example, the Class II LCVs were found to have only a slight increase in average rated engine power and any resultant CO_2 emission increase is offset by a trend in reduced vehicle mass, leaving the modelled CO_2 emission factors from this category relatively stable. However, for the observed Headingley LCV Classes I and III, the data reveal increasing average engine size and vehicle mass in service from Euro 2 to Euro 5, resulting in the observed increase in average modelled CO_2 emission factors. The data set for the N_2 Class IV vehicles was small with fewer than 5 observed vehicles in all but the Euro 5 emission standard category, making it difficult to draw any conclusions.

The AIMSUN-PHEM modelled CO_2 emission factors presented in Figure 6.37 show the gCO_2/km emissions for 12 t Rigid (2-Axle) HGVs, 26 t Rigid (3-Axle) HGVs and Articulated HGVs. As would be expected, the greater weight and engine sizes of these vehicle types lead to significantly greater average emission factors than those of the LCV categories. The increase of emission with network congestion is once again clear but, due to the scarcity of HGV vehicles in the EV and NI model, it is not possible to properly assess the rate of emission for all HGV categories in free flowing traffic conditions. However, for the 12 t Rigid HGV category during the congested PM simulation, the average CO_2 emission factor was 31.5% higher than in the relatively free flowing EV period, increasing from 550.1 gCO_2/km to 723.2 gCO_2/km.

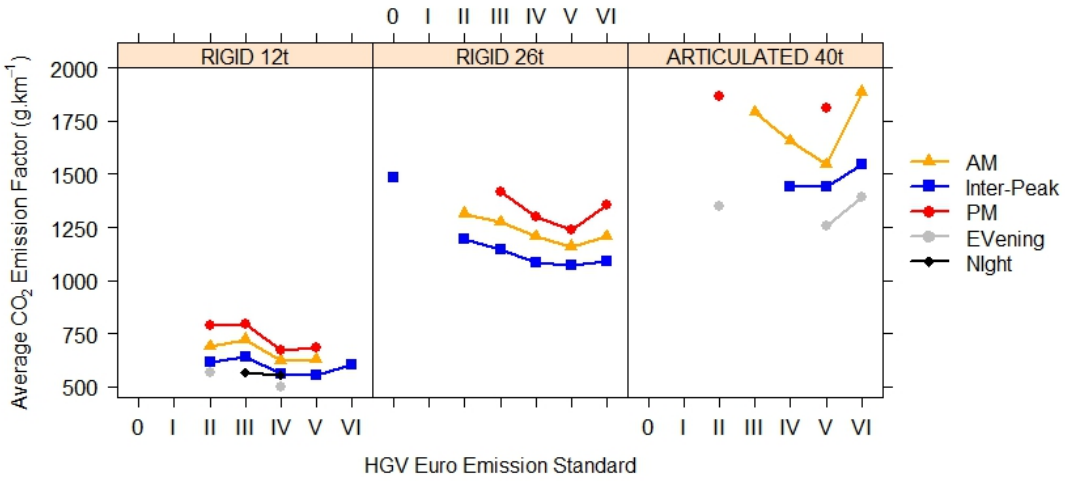

Figure 6.37: AIMSUN-PHEM CO_2 Emission Factors for Articulated and Rigid HGVs

Figure 6.38 displays the simulated Headingley bus fleet CO_2 emission per km at each Euro standard. The observed Headingley bus fleet, described in Chapter 6.2.7, was found to comprise of almost exclusively Euro 2 and Euro 3 vehicles, with 87% of the fleet being double-deck buses. As the night time bus service on the A660 is run with single-deck buses there is no double-deck CO_2 emission factor at this time for comparison. The average PM peak CO_2 emission factor calculated from the simulation data for double-deck buses is 38.6% greater than the emission factor during the EV period, at 1,284.8 gCO_2/km in the EV and 1,780.2 gCO_2/km in the PM. In reality, the difference may be greater than this as a constant loading was applied in the model throughout all time periods. For double-deck and articulated buses loading was set at 1,293 kg (19.2 passengers) and for single-deck buses it was set at 771 kg (10.9 passengers) these figures were informed by a 2008 survey (AECOM, 2008). It is likely that the loading would be significantly greater in the peak travel periods which could have been accounted for within the Headingley model had a more detailed bus occupancy survey in the network been available.

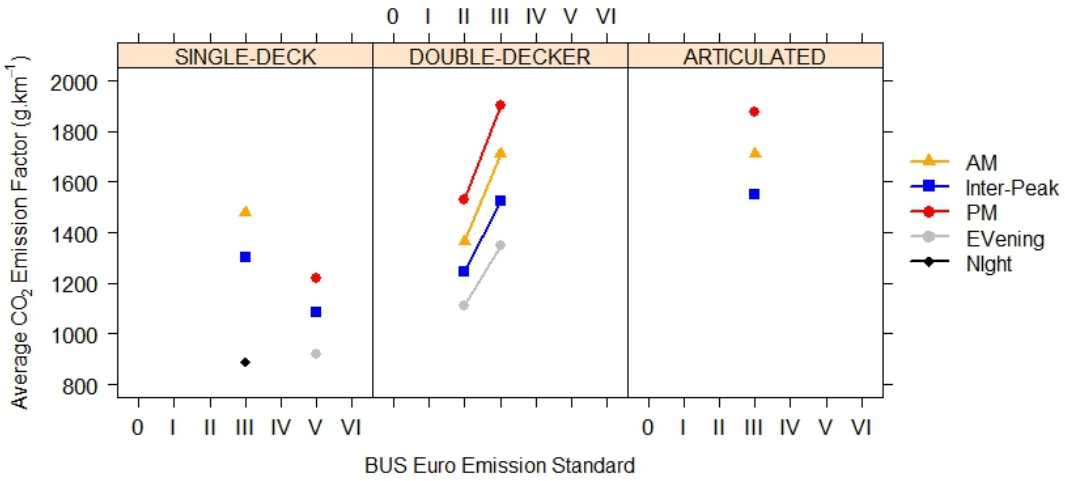

Figure 6.38: AIMSUN-PHEM CO_2 Emission Factors for Articulated, Double and Single-Deck Buses

6.5.3 Diurnal Variation in Network CO_2 Emission

The figures presented in the previous section reveal the range of average emission factors for each vehicle type and Euro standard across the different time periods in the day. These emission factors reflect the variations between congested and free flowing traffic conditions that result from diurnal changes in traffic demand in the Headingley network. Aggregating the simulated vehicle emission data into the vehicle categories described in Figure 6.33 reveals the varying degree to which the traffic conditions in each time period affect the CO_2 exhaust emission of the different vehicle types.

Figure 6.39 presents the average Headingley network gCO_2/km emission factors for all petrol cars (N.B. this comprises petrol passenger cars and petrol taxis) calculated by the AIMSUN-PHEM model for each time period. The composition of the modelled fleet for each time period reflects the real-world fleet recorded by the ANPR survey (as described in Chapter 6.2). Traffic congestion within the Headingley network in the modelled PM peak period results in the highest rate of average petrol car emission at 236.9 gCO_2/km, which is 43.5% greater than the average petrol car emission in the free flowing network during the NI period (165.1 gCO_2/km).

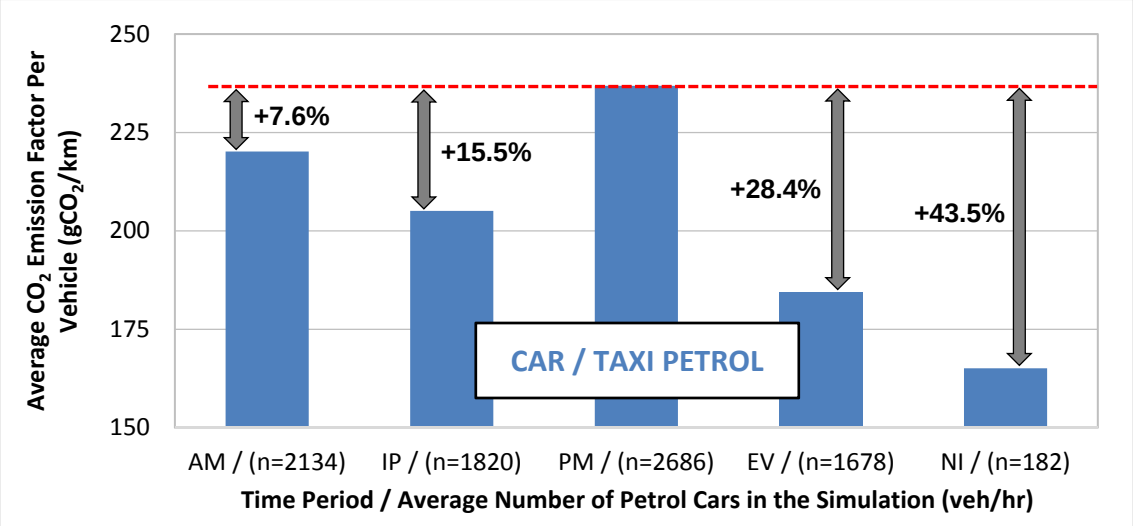

Figure 6.39: AIMSUN-PHEM Emission Factors for Petrol Cars by Simulation Time Period

It should be noted that some of the variation in emission rate between the time periods results from the different age compositions of the respective car fleets in each of the simulation time periods. However, the Headingley ANPR survey analysis, presented in Table 6.16, Table 6.17 and Appendix 2, shows that the age distribution (by Euro emission standard) of the vehicles does not vary greatly across the time periods, with the EV and NI periods having only a marginally

older vehicle fleet. The greatest influence on the change in CO_2 emission factor is the level of congestion in the simulated network.

The corresponding data for all diesel passenger vehicles (cars and taxis) are presented in Figure 6.40. The pattern is very similar to that of petrol cars and taxis, with a 45.5% increase in CO_2 emission between free-flowing NI conditions and heavily congested PM peak network conditions. The CO_2 emission factors for the other time periods reflect the level of congestion in the network at those times.

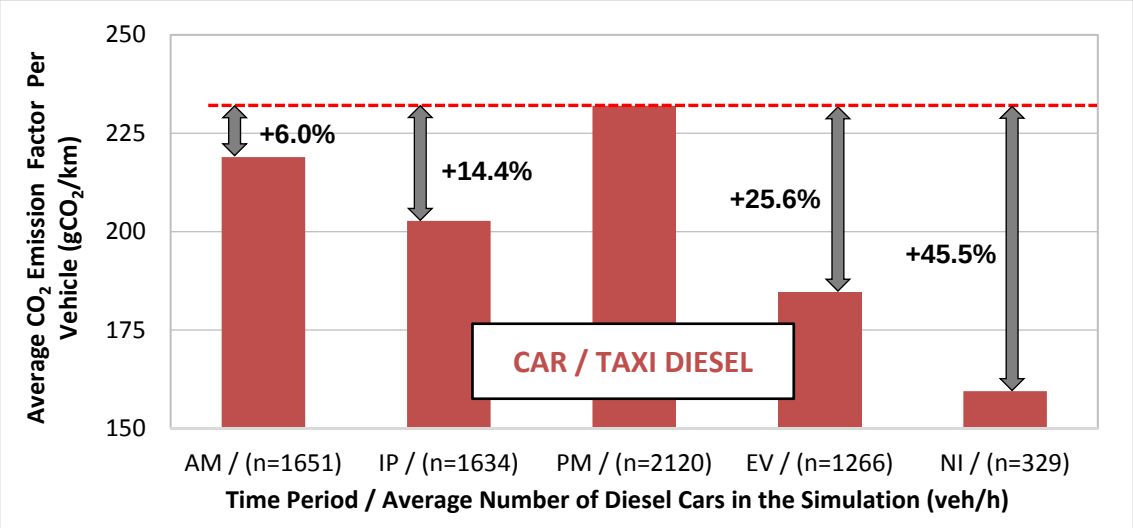

Figure 6.40: AIMSUN-PHEM Emission Factors for Diesel Cars by Simulation Time Period

Again it is notable that the diesel passenger vehicle CO_2 emission factors are very similar to the corresponding petrol CO_2 emission factors in each time period. Whilst diesel engines are more efficient than petrol and therefore have lower CO_2 emission for similar sized engines, the ANPR recorded metadata in Table 6.18 show that the average diesel car in the network is considerably heavier, with a more powerful engine than the average petrol car of the same Euro standard. Any potential CO_2 saving in the network from a large proportion of diesel vehicles in the fleet is therefore offset by the larger average diesel car.

Figure 6.41 shows the average CO_2 emission factors for LCVs in each simulation time period and displays a similar pattern of variation of average CO_2 emission with congestion in the network. The emission factors are for the entire LCV fleet including both petrol and diesel vehicles, however, a vast majority (99.0%) of the simulated LCVs have diesel engines, reflecting the same real-world proportion observed by the ANPR survey (see Table 6.3). What would appear a slight anomaly is the magnitude of the change in emission between the NI period and the PM period, with a difference of only 23.6% between the CO_2 emission factors compared to approximately

45% for the car and taxi vehicle category. The reason for the smaller difference in emission factors is the composition of the LCV vehicle fleet (see Appendix 2.1). The NI period has a substantially greater proportion (19.2%) of the heaviest N_2 (Class IV) category LCVs in its fleet than during any of the other simulated time periods. The greater average CO_2 emission from this LCV N_2 class results in the higher than expected NI average LCV CO_2 emission.

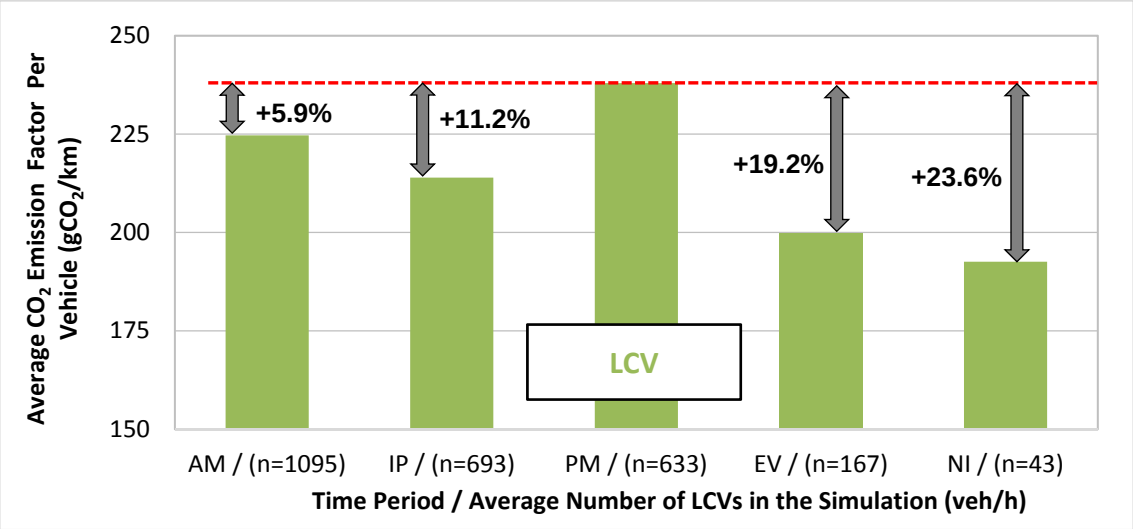

Figure 6.41: AIMSUN-PHEM Emission Factors for LCVs by Simulation Time Period

Figure 6.42 presents the average CO_2 emission factor for each HGV vehicle during the five simulation time periods. The model suggests a very similar average rate of CO_2 emission for HGVs during the AM, IP and PM simulation time periods (close to 895 gCO_2/km). This result is explained by a combination of the composition of the respective HGV fleets in each time period and the influence of congestion. The modelled HGV fleet comprises three vehicle categories Rigid 12 t (2 axle), Rigid 26 t (3+ axle) and Articulated. Figure 6.37 compares the simulated emission factors for each of these categories and presents the same pattern of increased emission with congestion as shown with other vehicle types. Whilst the PM time period has the greatest congestion and therefore would be expected to have the highest average CO_2 emission factor, the fraction of Rigid 12 t vehicles (lower CO_2 emission) in the PM HGV fleet (53.5%) is greater than in the AM (34.4%) and IP (42.9%) fleets, with a resultant reduction in the average PM emission factor. Similarly, in the relatively free flowing IP period, the average HGV CO_2 emission factor would be expected to be lower than the AM and PM periods. In practice, the greater percentage of Articulated HGVs (higher CO_2 emission) in the IP HGV fleet (16.5%), compared to the AM (5.7%) and PM (13.8%), results in a higher than expected IP CO_2 emission factor. Likewise the reason for the very large difference between the NI HGV CO_2 emission factor and the emission factors for the other time periods is the fact that none of the simulated HGVs in the NI period were the largest Rigid 26 t HGVs, which reflects the findings of the ANPR

real-world traffic survey (Appendices 6.2 and 6.3). From this survey, it can be determined HGV drivers tend to avoid the Headingley network during peak congestion periods (see Chapter 6.2.8), with a majority of HGVs travelling through the network during the IP period. At the other end of the spectrum, very few HGVs were recorded in the EV and NI periods.

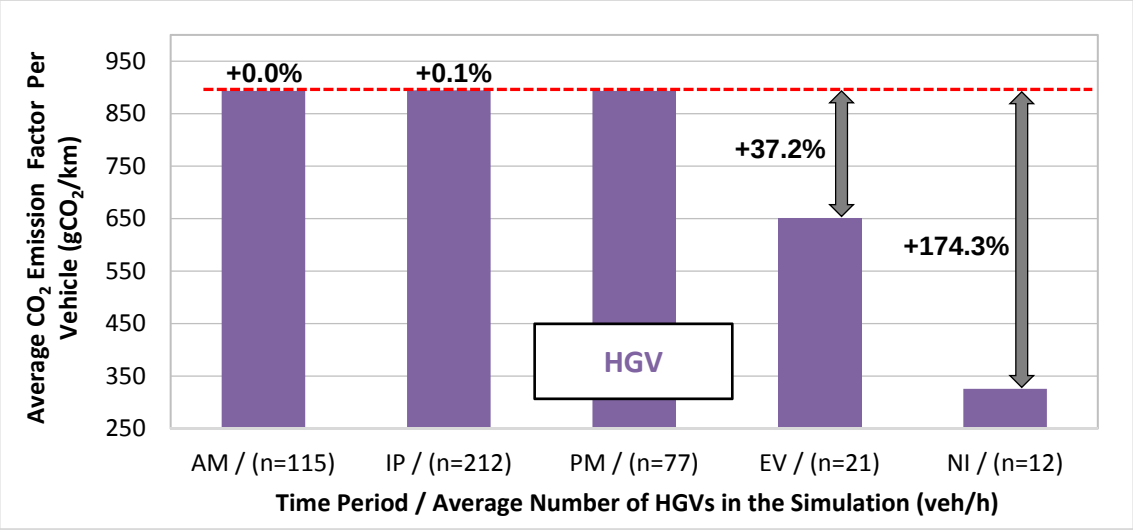

Figure 6.42: AIMSUN-PHEM Emission Factors for HGVs by Simulation Time Period

Figure 6.43 shows the average CO_2 emission factors for buses in Headingley network for each for each simulated time period. Like the HGV emission factors, these bus CO_2 emission factors are influenced by the composition of the bus fleet. The varying fractions of coaches, single-deck, double-deck and articulated buses in the simulated bus fleet for each time period are presented in Table 6.19.

Table 6.19: Composition of the Bus Fleet for each Simulation Time Period

BUS FLEET	AM	IP	PM	EV	NI
Single-Deck	16.2%	19.4%	21.7%	12.1%	100.0%
Double-Deck	77.4%	74.0%	72.9%	87.9%	0.0%
Articulated	5.7%	4.9%	5.4%	0.0%	0.0%
Coach	0.7%	1.7%	0.0%	0.0%	0.0%

The bus fleet compositions for the AM, IP and PM simulations are relatively similar (there is a slightly greater percentage of double-deck and articulated buses in the AM period) so the primary cause of the disparity between these CO_2 emission factors is likely to be due to congestion in the network. The NI bus service however comprises of only the relatively low emission single-deck buses so the 90.7% increase in average CO_2 emission factor from the NI simulation to the PM simulation reflects not only the difference in traffic flow conditions but also the absence of the higher emission buses (see Figure 6.38) from the NI bus fleet.

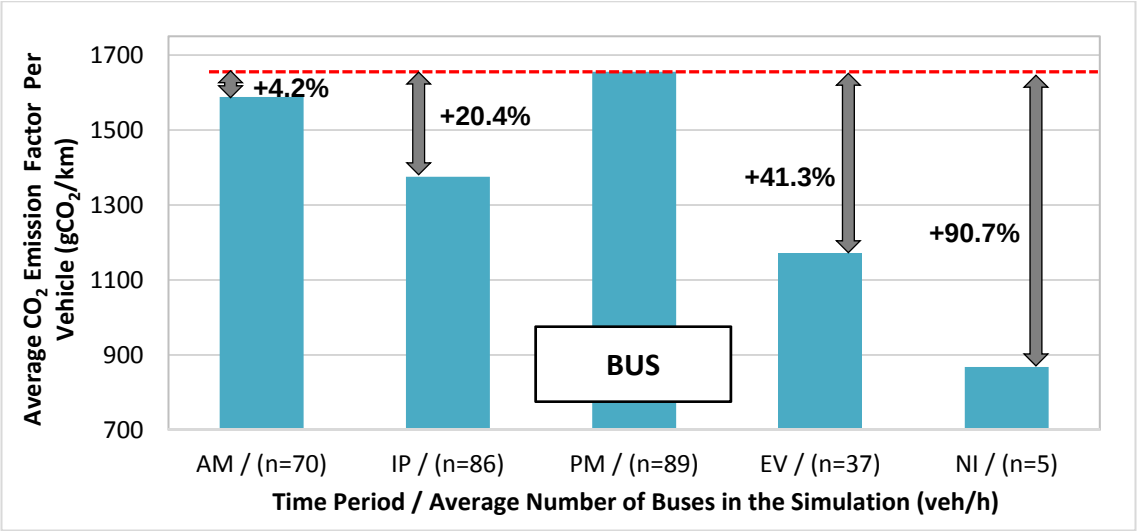

Figure 6.43: AIMSUN-PHEM Emission Factors for Buses by Simulation Time Period

Figure 6.44 presents the Headingley fleet average gCO_2/km emission factor per vehicle for each of the five simulated time periods. The average CO_2 emission factor per vehicle is 55.9% greater in the most congested PM simulation (275.9 gCO_2/km) than in the most free-flowing NI conditions (177.0 gCO_2/km). The most surprising outcome from the model is that the average IP CO_2 emission factor is greater than that of the PM period, despite the fact that there are fewer vehicles in the network during the IP simulations. As was the case for discrepancies in the bus and HGV emission figures, this peculiarity results from differences in the composition of the vehicle fleets during the respective time periods. As can be seen in Figure 6.12(b), HGVs form a much larger fraction of the IP fleet than during any other time period. The bus fraction in the IP fleet is also high and the car fraction relatively low. The greater proportion of high emission vehicles in the IP fleet results in the IP having the highest average rate of CO_2 emission per vehicle even though the traffic conditions are relatively free flowing.

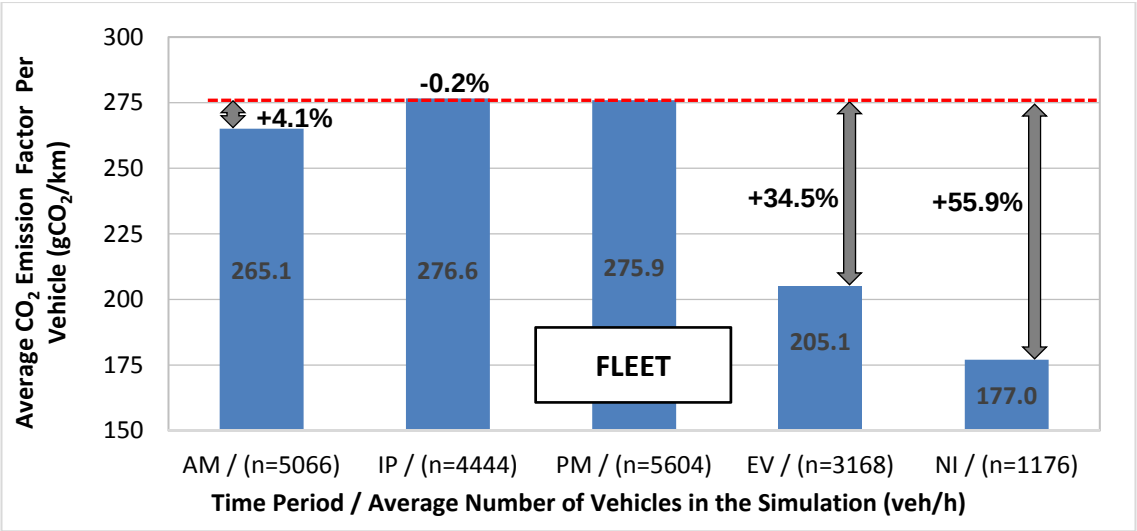

Figure 6.44: AIMSUN-PHEM Emission Factors for the Vehicle Fleet by Simulation Time Period

6.5.4 24-hour Average Emission Factors

As the five 2-hour simulated time periods cover only ten hours of the day, to produce daily average emission factors it is necessary to calculate emission estimates for the un-simulated hours. Each hour of the day was classified by the most appropriate of the five time periods (i.e. either NI, AM, IP, PM and EV). Figure 6.45 presents the classification; with 00:00 to 06:00 the Night period; 06:00 to 10:00 the AM peak; 10:00 to 15:00 the Inter-Peak; 15:00 to 18:00 the PM peak and 18:00 to 24:00 the Evening. The expected emission levels (in kg) for each hour were determined by calculating the ratio between the ANPR observed total traffic flow during each hour (veh/h) to the classification time period's ANPR observed traffic flow (veh/h). This ratio was then multiplied by the average kg/h emission factor calculated for the relevant simulation time period.

For example, the EV simulation which runs between 20:00 and 22:00 generated an emission estimate of 547 $kgCO_2/h$ from petrol cars. In order to calculate the expected emission in the un-simulated hour between 18:00 and 19:00, the hourly EV CO_2 simulated emission rate must be weighted by the difference in observed vehicle flow. The average traffic flow observed by the ANPR survey during the EV simulation period (20:00 – 22:00) was 571.5 veh/h whilst the observed traffic flow between 18:00 and 19:00 was 756.2 veh/h. The ratio of these two flows is 1.32. Multiplying the EV petrol cars emission rate (547 $kgCO_2/h$) by this ratio (1.32) gives an emission rate in the period between 18:00 and 19:00 of 723 $kgCO_2/h$. The weighted emission rate for CO_2 was calculated for each hour and for each vehicle type.

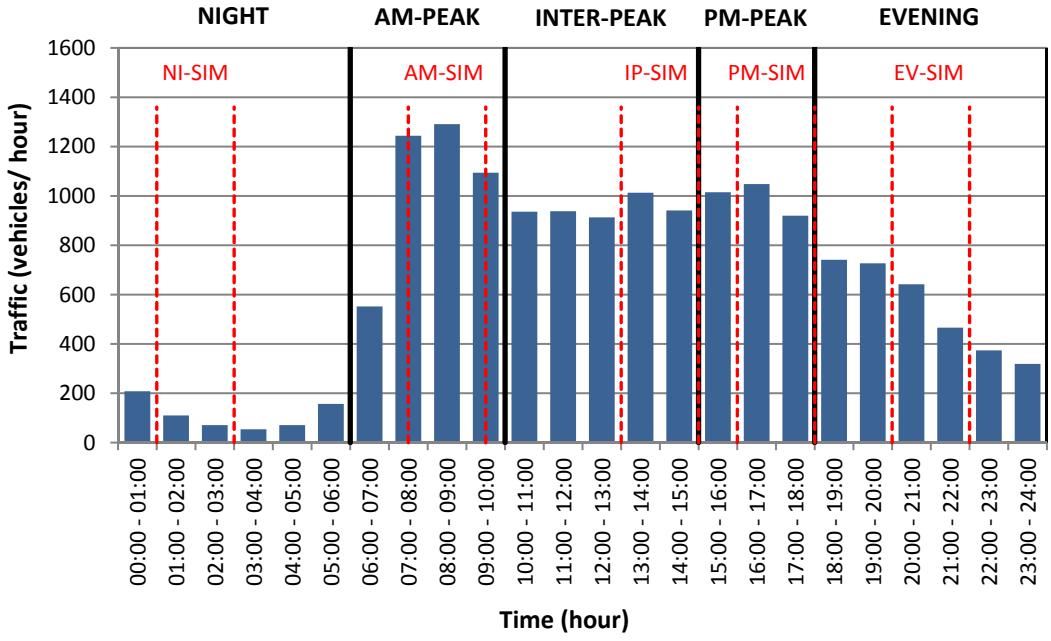

Figure 6.45: ANPR Recorded A660 Variation in Traffic Flow, with Marked Simulation Periods

Further to the analysis of CO_2 emission, the observed flow weighting methodology was used to calculate a 24-hour estimate of the NO_x emission rates, the total vehicle km travelled each hour and the total number of vehicles in the network each hour.

Table 6.20 displays the calculated average number of vehicles from each vehicle type in the simulated network during a 24-hour period and the fleet composition by percentage. This is presented alongside the ANPR vehicle fleet survey data recorded on the A660 which was analysed in Chapter 6.2. Although the network vehicle numbers in the un-simulated hours are estimated, the table shows that the simulated network fleet displays a similar vehicle type distribution to the recorded 24-hour ANPR fleet on the A660.

The greater fleet percentage of buses in the ANPR data is due to the scheduled bus services which are correct in the AIMSUN network as they were modelled using the AIMSUN 'Public Transport Line' tool, rather than as a percentage of the input traffic flow. Whilst the A660 has many bus routes, the average percentage of buses across the network is much lower than observed on the A660. It should be noted that the 3.5 – 5 t N_2 vans, which (as described in Chapter 6.2.6.1) are over the LCV maximum weight, and were processed in PHEM using LCV size III engine maps, are included in this table with the HGV fraction.

Table 6.20: Comparison of 24-Hour Simulated Network Fleet to ANPR Recorded Vehicle Fleet

24 HR	SIMULATION NETWORK VEHICLES	SIMULATION NETWORK FLEET %	ANPR A660 VEHICLES	ANPR A660 FLEET %
CAR-Petrol	34349	43.9%	6466	40.8%
CAR-Diesel	23186	29.6%	4702	29.7%
Taxi	7470	9.5%	1507	9.5%
LCV	10201	13.0%	1907	12.0%
HGV	1849	2.4%	475	3.0%
BUS	1172	1.5%	788	5.0%
TOTAL	78226	100.0%	15845	100.0%

Given the detailed analysis of the observed ANPR vehicle fleet (presented in Chapter 6.2), which found the recorded Headingley network fleet (with the exception of the bus fleet) to be broadly similar to DEFRA's NAEI fleet distributions (DEFRA, 2014), it is possible to make comparison between the 24-hour emission factors produced by the Headingley network AIMSUN-PHEM coupled model and DEFRA's fleet weighted road transport emission factors. Table 6.21 compares the daily average Headingley network CO_2 emission factors with the DEFRA CO_2 conversion factors for company reporting from their Greenhouse Gas Conversion Factor Repository (DEFRA, 2015b).

Table 6.21: Comparison of 24-Hour Simulated Network and DEFRA CO_2 Emission Factors

24 HR	SIMULATED AVERAGE 24 HR NETWORK VKM (km)	SIMULATED AVERAGE 24 HR NETWORK CO_2 EMISSION (kg)	SIMULATED AVERAGE 24 HR EMISSION RATE (gCO_2/km)	DEFRA GHG CONVERSION FACTORS (2015) (gCO_2/km)	DIFFERENCE (%)
CAR-Petrol	62115	12853	206.9	190.7	**8.5**
CAR-Diesel	41760	8852	212.0	180.6	**17.4**
Taxi	12484	2177	174.4	243.0	**-28.2**
LCV	18677	4111	220.1	248.2	**-11.3**
HGV	3863	3288	851.3	904.4	**-5.9**
BUS	3019	4288	1420.3	1167.5	**21.7**

Whilst it may appear anomalous that the simulated petrol car emission factor of 206.9 gCO_2/km is at the low end of the range of emission factors generated in the analysis in Chapter 6.5.1, it is important to note that in Chapter 6.5.1 the study was conducted using vehicle specification data describing the test vehicle and therefore used only the Euro 4 Petrol PHEM emission map (previously described in Chapter 3.2.2). The simulated network emission average is the average for all vehicles in a given vehicle type, representing all emission standards in proportion to the observed data and averaged over the entire network. The analysis in Chapter 6.5.1 was also conducted on a section of the A660 which has much more severe congestion than other parts of the network during peak periods, with consequent larger than network average gCO_2/km emission values.

The DEFRA emission factors for petrol and diesel passenger cars are generated from an SMMT data set which provides NEDC gCO_2/km type-approval factors for new cars registered between 1998 and 2014. In order to account for the age distribution of the UK car fleet the SMMT data are weighted by DfT ANPR recorded fleet composition data to generate average emission factors. From purely the NEDC emission values, the average petrol car on UK road should emit 166.9 gCO_2/km and the average diesel car 151.3 gCO_2/km, however due to the acknowledged limitations of the NEDC test cycle in generating real-world emission estimates (previously discussed in Chapter 2.7) an "uplift factor" of +15% over the NEDC based gCO_2/km is applied to account for real-world effects on fuel consumption not captured by the drive cycle (DEFRA, 2015a). With this uplift factor, the DEFRA gCO_2/km emission rises to 190.7 and 180.6 gCO_2/km for petrol and diesel cars respectively (DEFRA, 2015b). The simulated CO_2 emission factors from the AIMSUN-PHEM model are 8.5% and 17.4% greater than the DEFRA factors at 206.9 gCO_2/km for petrol cars and 212.0 gCO_2/km for diesel cars. The scale of this difference is not implausible and could be the result of a number of factors including:

- An under-estimation in the DEFRA uplift factor. The research by Mock et al. (2015) discussed in Chapter 2.7 suggests that the average divergence between the NEDC type-approval and real-world CO_2 emission has been greater than 15% since 2008 and greater than 25% since 2010. Comparing the Headingley network simulated CO_2 emission factors to the raw NEDC emission factors from the SMMT data (without the applied uplift factor), the AIMSUN-PHEM emission factors for the Headingley network are 24% greater for petrol cars and 40% greater for diesel cars than the respective average NEDC type-approval CO_2 emission factors for the UK. The scale of these discrepancies is consistent with the divergence between real-world and type-approval CO_2 emission reported by the ICCT (Mock et al., 2015; ICCT, 2015) as presented in Figure 2.15.
- The Headingley car fleet composition is slightly atypical of the UK national fleet. Figure 6.5 shows a slightly higher proportion of Euro 4 vehicles than the NAEI national fleet average and Figure 6.34 shows Euro 4 passenger cars have a significantly greater emission than Euro 5, before the introduction of the EU's New Car CO_2 Regulation in 2009 (EC, 2009b).
- The Headingley network leads to greater average emission than a typical road, either as a result of greater than average congestion, road topography and/or junction design.

The simulated Headingley network CO_2 emission factor for taxis was calculated to be 174.4 gCO_2/km, 28.2% lower than the DEFRA factor of 243 gCO_2/km. The DEFRA factor is estimated from NEDC type-approval CO_2 factors for large and medium passenger cars with a 40% uplift based on TfL testing and an average passenger occupancy of 1.4 (DEFRA, 2015a). Again this discrepancy is not unrealistic and there are a number of potential explanations for the magnitude of the difference:

- The 40% uplift employed by the DfT may be too great as it is based on a TfL study for black cabs using London Taxi test cycles which may not be appropriate for Leeds.
- The DEFRA value assumes an extra loading of 1.4 passengers, but the .VEH file in PHEM described in Table 6.18 was set at the default loading for a passenger car. The effect of this parameter could be easily assessed by rerunning the model with various loading values.
- The Leeds taxi fleet is potentially very different from London one. The DEFRA figures give only one emission factor for a 'regular taxi'. This value would be dependent on such

factors as the ratio of diesel to petrol vehicles, the average engine size and the age distribution of the fleet, which is not discussed in the literature methodology.

- An important factor, which may not have been considered in the DEFRA emission factor is the time at which the majority of taxi journeys are made and the likely traffic conditions at that time. In the Headingley network, 59% of the total taxi kilometres travelled during the 24-hours were travelled during the EV and NI periods. The emission factors for these time periods, of 171.9 and 153.4 gCO_2/km, reflect the free flowing traffic conditions experienced at that time. With fewer taxi journeys in the more congested AM (185.7 gCO_2/km), IP (182.0 gCO_2/km) and PM (206.8 gCO_2/km) the average 24-hour emission factor tends toward the lower value.

As the average engine size from the ANPR observed fleet for Euro 4 and Euro 5 diesel taxi was considerably smaller than the average engine size for Euro 4 and Euro 5 passenger cars (see Table 6.18), it seems reasonable that the CO_2 emission factor should be lower. In order to assess the accuracy of the simulated taxi emission factor estimates, a real-world survey of taxi fuel consumption data could be obtained from local taxi firms.

The CO_2 emission factor for LCV vehicles calculated from the simulation was also smaller than the DEFRA emission factor. The simulated emission factor of 220.1 gCO_2/km was 11.3% lower than the DEFRA emission factor of 248.2 gCO_2/km (this is the diesel LCV figure). The LCV emission factor is based on the NEDC type-approval figure for each LCV N_1 size, weighted by the NAEI fleet distribution by vehicle km travelled. A 15% uplift is then applied to the factor. The magnitude of the uplift is based on real-world vs type-approval car data analysis as DEFRA report that there is no similar data set for LCVs (DEFRA, 2015a). The simulated LCV CO_2 emission factor is close to the DEFRA figure but, given the car emission factors were found to be greater than the DEFRA values, it might be expected that the LCV figure should be as well. Possible reasons that this isn't the case include:

- As the uplift to represent real-world emission is based on a car data set rather than analysis of real-world LCV emission the +15% value may not be appropriate. Kadijk et al. (2015) performed real-world CO_2 emission tests on 8 Euro 5 commercial LCVs finding a range from 7% to 52% greater CO_2 emission per km than the type-approval figure, with an average increase of 23%. More work needs to be done to confirm the average uplift value over the LCV fleet.

- Vehicle loading is likely to have a significant influence on the rate of overall LCV emission. The loading of each LCV Class can be adjusted in the PHEM .VEH files to reflect the average weight of cargo carried. A DfT funded CO_2 emission study on LCVs (DfT, 2010a) indicates that the average loading for all vans is 305 kg. As the PHEM loading default values are close to this value (Class I 275 kg, Class II 285 kg, Class III 360 kg – see Appendix 2) the emission modelling was conducted employing the PHEM defaults. However, the average loading values used in the calculation of the DEFRA emission factors vary slightly from these values with suggested average payloads of 240 kg for Class I, 260 kg for Class II and 530 kg for Class III (DEFRA, 2015a). The most important of these is likely to be the 170 kg difference for Class III LCVs as 66.2% of the vehicle km travelled by the LCV vehicle category were by vehicles in this class and the extra load weight will likely increase the average emission. The .VEH files in PHEM can be adjusted to reflect these loading values and the PHEM emission estimates re-run to assess the effect of this change.

The average CO_2 emission factor for all HGV vehicles is listed in the DEFRA conversion factors as 904.4 gCO_2/km with an average loading. The AIMSUN-PHEM simulated 24-hour average emission rate for all HGVs was calculated to be 851.3 gCO_2/km, 5.9% less than the DEFRA emission factor. The DEFRA HGV factors were calculated from a DfT survey of HGV fuel consumption which was converted into gCO_2/km and combined with data from the European ARTEMIS projects to calculate emission factors at different levels of loading (DEFRA, 2015a). Although the simulated and DEFRA CO_2 emission factors are close in value, there are differences in the simulation and DEFRA methodologies that require some explanation and further investigation in future work.

- HGV vehicle type is made up of four different vehicle types in PHEM; these are the LCV Class N_2 (3,500 kg < GVW ≤ 5,000 kg); HGV Rigid 12 t; HGV Rigid 26 t and HGV Articulated. The PHEM loading values for the LCV were calculated from the PHEM default values adjusted by DfT average loading factors (DfT, 2015a). The PHEM loading values used in the simulation were 1,092 kg, 2,366 kg, 6,559 kg and 14,521 kg for the LCV Class N_2, 12 t Rigid, 26 t Rigid and Articulated HGV respectively. The new DEFRA HGV emission factor calculations suggest 1,010 kg, 2,060 kg, 5,080 kg and 11,310 kg respectively for these vehicle categories. This can be adjusted in the PHEM .VEH files and re-run to assess the impact on the emission factors.
- The average simulated emission for Articulated HGVs is considerably higher, at 1,499.9 gCO_2/km, than the DEFRA expected emission factor of 986.7 gCO_2/km, this is likely the

result of the greater loading value in the PHEM simulation, but may also be related to the fleet age distribution shown in Figure 6.8, which highlights a much greater proportion of Euro 3 and 4 and a lower proportion of Euro 5 and 6 Articulated HGVs in the observed vehicle fleet than are expected in the NAEI average UK Fleet.

- The average simulated CO_2 emission for Rigid HGVs of 752.1 gCO_2/km is 8.7% lower than the DEFRA emission factor of 824.1 gCO_2/km. This is the result of a greater number of 3.5 -7.5 t HGVs in the observed Headingley fleet than in the NAEI UK average rigid HGV fleet, as presented in Table 6.7.

The DEFRA methodology paper (DEFRA, 2015a) for emission factors calculates the emission factor for an average local bus at 1,167.5 gCO_2/km which is 21.7% lower than the AIMSUN-PHEM simulated weekday average emission of 1,420.3 gCO_2/km. Little detail is given on the DEFRA calculation of bus emission factors, and the emission factors reported are limited to 'Local bus'; 'Local London bus'; 'Average Local' bus and 'Coach'. The bus emission factors are calculated through fuel consumption data recorded as part of the bus service operators grant (which provides financial support per unit of fuel consumed) and DfT bus vehicle km and passenger km statistics (DEFRA, 2015a). The difference between the DEFRA and simulated emission factors can be explained by a number of factors:

- The vehicle detailed data for each bus observed in the Headingley network derived from the ANPR survey described in Chapter 6.2.1 suggests that the vast majority of the current bus fleet passing through the network is either Euro 2 or 3 emission standard. The NAEI average UK fleet composition (shown in Figure 6.1) specifies a much higher percentage of Euro 4, 5 and 6 buses than found in the observed Headingley fleet. If more modern buses are more efficient than the older models, it is likely that the average emission from the NAEI fleet would be lower than the simulated network. Collaboration with local bus companies to establish the fuel consumption for buses passing through the network would confirm if the simulated emission factor is reasonable.
- The modelled bus fleet describes single-deck, double-deck and articulated buses which comprise the observed network fleet. The DEFRA average emission factor gives no indication of whether different bus types were considered in their calculation or in what percentage proportion. Of the ANPR recorded scheduled buses, 87% of the fleet was double-deck, 5% single-deck and 7% articulated buses. If the percentage of double-deck buses in the fleet is greater than the national average, it is likely that the average emission factor will be greater in the simulated network.

- The average bus loading has an important bearing on the average CO_2 emission factor generated by the simulation-emission model, with greater weight increasing fuel consumption. The DEFRA emission factor suggests an average occupancy of 9.5 passengers on local buses but gives no detail of the average loading in kg. The bus occupancy and loading in the PHEM model was estimated from a bus occupancy survey carried out in 2008 for New Generation Transport (AECOM, 2008) and from information gained from personal communication with DfT. The loading in PHEM for double-deck and articulated buses was set at 1,293 kg (19.2 passengers) and at 771 kg (10.9 passengers) for single-deck buses. A detailed occupancy survey in the network would improve this estimate and enable amendments to reflect variation in passengers.
- The bus emission factors are also highly dependent on the specific details of the bus route over which it is travelling, with factors such as the distance between stops, the number of times the bus has to stop, and the road grade of the route likely to have a significant impact on fuel consumption and exhaust emission. It is possible that the difference between the DEFRA and AIMSUN-PHEM bus CO_2 emission rates reflects dissimilarities between the routes used in the derivation of the emission factors.

When comparing the AIMSUN-PHEM simulated CO_2 emission factors to the DEFRA CO_2 emission factors differences should be expected given that the DEFRA figures reflect a national average, whilst the coupled model figures are specific to the Headingley network. The difference between the emission factor values are justifiable and, given the ill-defined 15% uplift factor employed in the calculation of a number of the DEFRA emission factors, it is likely that the AIMSUN-PHEM model delivers a more accurate estimate of real-world CO_2 emission. In addition, the AIMSUN-PHEM model has the capacity to be fine-tuned to the vehicle specifications of an observed vehicle fleet. Future collaboration with local taxi, bus and freight firms to obtain accurate real-world fuel consumption values would also help to validate the simulated CO_2 emission factors for the network.

6.5.5 Emission Contributions

Figure 6.46 presents the 24-hour CO_2 emission contributions in the simulated Headingley network from each vehicle type. The width of each bar (x-axis) is proportional to the share of the total simulated VKM completed by each vehicle type in the network. For example, petrol cars covered 43.8% of the vehicle kilometres driven in the network and emitted 36.1% of the CO_2 emission whilst the buses in the network drove only 2.1% of the VKM but were responsible for 12.1% of the CO_2 emission.

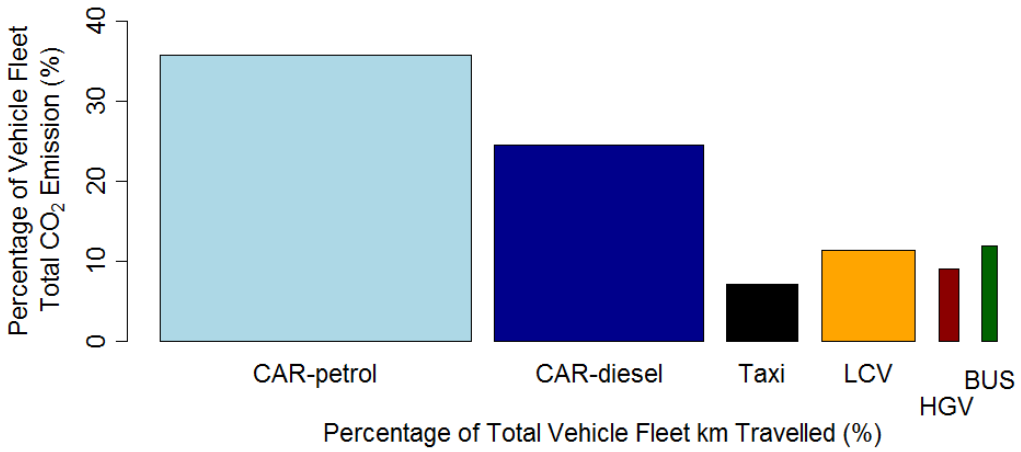

Figure 6.46: Total CO_2 Emission Contributions from Each Vehicle Type

The AIMSUN-PHEM model generates emission estimates for a number of other pollutants including Nitrogen Oxides (NO_x), Carbon Monoxide (CO), Hydrocarbons (HC), Particulate Mass (PM), and Nitrogen Monoxide (NO) each of which is likely to be of interest in investigations of air quality. Further work needs to be carried out to confirm the validity of the simulation output for these pollutants, but, as an example, Figure 6.47 presents the estimated 24-hour NO_x emission contributions in the simulated network from each vehicle type.

The modelled data suggests that although its share of vehicle kilometres driven is relatively small (2.1%) the Headingley bus fleet is responsible for 37.8% of the daily exhaust emission of NO_x in the network. The diesel car fleet is the next most polluting vehicle type, with 23.2% of the NO_x emission from 29.6% of the VKM driven. This type of analysis could be very useful for policymakers in the identification of areas to target in order to deliver substantial exhaust pollution emission reductions and should be a focus area for future work.

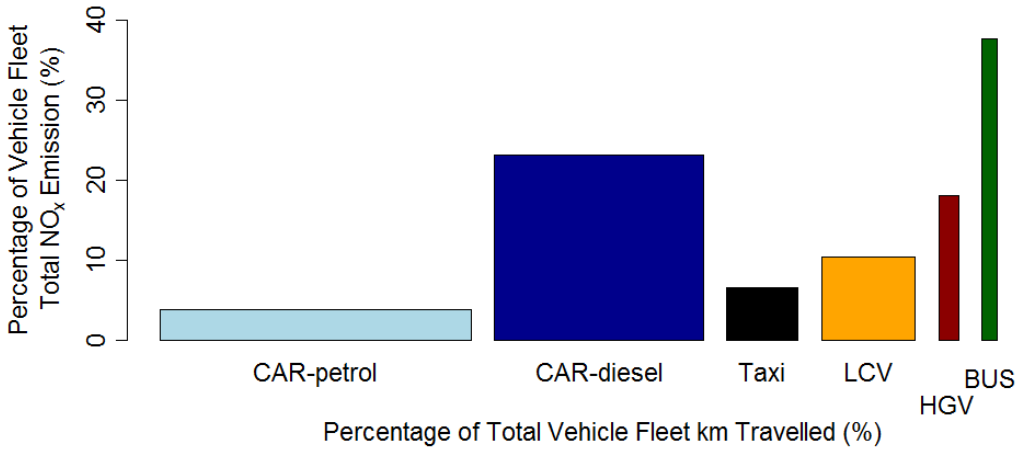

Figure 6.47: Total NO_x Emission Contributions from Each Vehicle Type

6.5.6 Effect of Road Grade on Simulated Network Emissions

The work reported in Chapter 5 demonstrated the necessity of incorporating road grade into simulation models to generate accurate micro-scale real-world emission estimates. In order to determine the importance of road grade to emission estimates at a network level, ten simulations were run of the AM Headingley model, both with and without road grade.

To create a flat version of the AM Headingley model, the slope percentage on all links (described in Chapter 6.3.2) was set to zero, whilst all other elements of the AM simulation were unchanged. The same replication random seeds were re-run to ensure that the vehicle flow entry timing into the flat model was identical to that in the AM model simulations with road grade. The ten flat AM model simulations were validated in the same manner as reported for the other models. The AIMSUN simulated vehicle data extracted by the API were processed through PHEM with the same .VEH file specifications and .FLT file fleet distributions as used in the AM model.

Table 6.22 presents the change in the average CO_2 and NO_x g/km emission rates for each vehicle type, from the ten AM model simulations without road grade and the ten AM model simulations run with road grade.

Table 6.22: Comparison of Average Emission Factors by Vehicle Type for the AM Headingley Model With and Without Road Grade

VEHICLE TYPE	NETWORK AM VKM (%)	CO_2 (g/km)			NO_x (g/km)		
		AM FLAT	AM GRADE	DIFF	AM FLAT	AM GRADE	DIFF
CAR PETROL	**41.02**	210.3	219.9	4.5%	0.07	0.07	2.2%
CAR DIESEL	**28.78**	212.6	222.7	4.8%	0.63	0.68	6.9%
TAXI PETROL	**0.64**	231.8	240.5	3.8%	0.04	0.05	2.4%
TAXI DIESEL	**3.27**	177.9	185.7	4.3%	0.64	0.68	5.9%
LCV CLASS I PETROL	**0.16**	181.4	188.5	3.9%	0.17	0.20	17.8%
LCV CLASS I DIESEL	**2.80**	165.9	173.9	4.8%	0.55	0.60	9.5%
LCV CLASS II DIESEL	**4.74**	184.5	193.7	5.0%	0.53	0.58	8.4%
LCV CLASS III DIESEL	**14.01**	234.4	245.7	4.8%	0.65	0.70	8.6%
LCV N_2 (IV) DIESEL	**0.63**	317.3	334.2	5.3%	0.66	0.72	8.7%
HGV 12 t	**0.68**	593.1	663.0	11.8%	5.10	5.44	6.6%
HGV 26 t	**1.16**	1125.1	1225.5	8.9%	7.79	8.22	5.6%
HGV ARTIC	**0.17**	1520.4	1631.4	7.3%	8.03	8.58	6.8%
BUS EXTRA	**0.04**	977.2	990.1	1.3%	9.89	10.00	1.1%
BUS SINGLE	**0.19**	1470.6	1479.1	0.6%	15.05	15.14	0.6%
BUS DOUBLE	**1.57**	1562.3	1603.1	2.6%	16.42	16.95	3.2%
BUS ARTIC	**0.15**	1610.6	1710.6	6.2%	16.06	17.03	6.0%
VKM WEIGHTED AVERAGE EMISSION		252.9	265.1	4.8%	0.82	0.86	5.4%

It is worth noting that, for all vehicle types, the inclusion of road grade increased the emission of both CO_2 and NO_x, however, the magnitude of this increase varied between vehicle types. Weighting the emission factors by the percentage of the total network VKM travelled by each vehicle category during the AM period, with the inclusion of road grade, the average vehicle CO_2 emission factor rose from 252.9 to 265.1 gCO_2/km an increase of 4.8%, whilst the average NO_x emission factor increased by 5.4% from 0.82 to 0.86 gNO_x/km.

6.6 LIMITATIONS OF THE AIMSUN-PHEM COUPLED MODEL

The Oxford English Dictionary defines a model as *"A simplified or idealised description or conception of a particular system, situation, or process, often in mathematical terms, that is put forward as a basis for theoretical or empirical understanding, or for calculations, predictions, etc."*. It is an accepted limitation when modelling any complex dynamic system that the model produced can only, at best, be a simplified approximation of the real world. Despite the AIMSUN package being amongst the most advanced traffic simulation software currently available, the dynamic movement and the interactions of vehicles within a network are described by mathematical equations which are inevitably going to fail to perfectly mimic, in all circumstances, the complex human behaviour which in reality controls the vehicles. In addition, the modelling process is limited by restrictions on the scope of the model as it is impossible to simulate all influences on real-world vehicle emission in their spatial and temporal entirety, so the emission factor outputs of the coupled AIMSUN-PHEM model are particular to the geographical location the model describes, are specific to the time period over which the input data were recorded and are accuracy limited by some necessary simplification of real-world influences on exhaust emission.

6.6.1 Limitations from AIMSUN

Like any model, the accuracy of the coupled AIMSUN-PHEM model is restricted by the availability and quality of the data required for its development, calibration and validation. Some parameters which define the Headingley network in AIMSUN such as the physical road network layout (e.g. link length, road width, number of lanes, turning movement etc.), the description of traffic control measures within the network and the definition of speed limits for each road link are relatively straightforward to set up. Other parameters such traffic demand, vehicle dynamics (e.g. factors that control the modelling of vehicle acceleration and braking), the vehicle turning movements and the description of the vehicle fleet composition in the network require significant volumes of input data in order to model the movement of all vehicles in the network

accurately. Whilst every effort has been made in this study to obtain the best available input data, the realistic scope of a PhD research project places obvious financial and time constraints on the research and limits the capture of new traffic data within the network. Consequently, there are therefore a number of parameters which influence the transit of vehicles within the AIMSUN-PHEM coupled model that could be strengthened by further comprehensive traffic and vehicle surveys within the network. These include:

- **AIMSUN Model Global Parameters**

As described in Chapter 6.1 and Chapter 6.3.8, the AIMSUN simulation package allows adjustment of a number of global parameters within the model such as; vehicle reaction times; look-ahead distances (which control lane changing behaviours); minimum distance allowed between stopped vehicles; and maximum give way times at junctions, which have an impact on operational algorithms that influence the speed profiles of vehicles in the network. Limited study was made of these factors during this research and the global parameters in the AIMSUN-PHEM coupled model rely to a substantial degree on the AIMSUN defaults alongside adjustments which were made to the parameters in the previous Headingley beta model (Tate, 2011). Further real-world study of these parameters could help to ascertain and improve their accuracy in the Headingley network model. Collaboration both with AIMSUN developers and with other AIMSUN users, to develop a firmer basis for employing the default values alongside a more robust methodology for any required parameter adjustment, would help to strengthen confidence in the overall modelling process. The development of the coupled AIMSUN-PHEM model will facilitate future sensitivity analysis of the impact on emission of each of the global parameters.

- **Traffic Demand**

The A660 and the Headingley network have been of considerable interest to Leeds City Council for many years and have therefore been the subject of numerous MCC and ATC surveys which have attempted to quantify traffic flow in the network. However, as described in Chapter 6.3.4, these surveys have been conducted at different times of the year and over a protracted number of years. The input data for the AIMSUN network simulation would ideally have been collected at one time, in order to alleviate errors in the simulation caused by weekly and seasonal variations in the traffic demand data recorded over multiple surveys.

A comprehensive survey of the Headingley network would entail 24-hour monitoring of traffic movement at each of the 36 input sections. A survey of this magnitude is unlikely to be feasible

for any university or local government body due to the considerable amount of equipment and the number people required, together with the time and cost involved. A more feasible project would comprise a concurrent set of ATC surveys at all the major input sections into the model, to improve the accuracy of the AIMSUN simulation. It is not inconceivable that automated real-time traffic flow monitoring will become much more commonplace in future as intelligent transportation systems are developed to keep traffic moving in congested urban areas (Bottino et al., 2016). The availability of such data sets would greatly enhance the field of traffic simulation modelling and result in improved emission estimates from coupled emission models.

- **ANPR Vehicle Fleet Survey**

The ANPR survey described in detail in Chapter 6.2 provides one of the strengths of the AIMSUN-PHEM model in that it captured in great detail the vehicle fleet travelling through the Headingley network. It should be noted however that as the survey was positioned only at one point in the network on the A660, an assumption was made that the vehicle fleet recorded at this point is representative of the fleet in the network as a whole. Whilst this is likely true, as a majority of traffic in the network travels on the A660, further ANPR surveys in other locations in the network could clarify whether the vehicle fleet proportions should be the same at all input sections, with special focus on HGVs where potentially the percentage might be higher on the A660 than on other roads in the Headingley network.

The ANPR survey was also conducted over only one 24-hour period. As there are weekly and seasonal variations in traffic flow in the Headingley network, further ANPR surveys could establish whether the fleet proportions of each vehicle type vary significantly on different days of the week and between seasons.

- **Junction Turning Movements**

As described in Chapter 6.3.8, the movement of traffic within the Headingley network model is controlled by defining the turning proportions at each junction, with a percentage of the traffic flow at the end of every road link directed toward each potential exit. The initial set up for the Headingley network in the coupled model utilised the turning proportions from the Headingley beta model (Tate, 2011) and then substantial adjustments were made to those proportions, using vehicle turning information gathered by Leeds City Council ATC and MCC surveys, in order to calibrate the five different time periods.

Whilst the calibration ensured that the vehicle flows within each model corresponded to the observed real-world traffic flows, only very limited data were available for smaller junctions in the network. During calibration of the model it was found that the turning movements at smaller uncontrolled junctions on the A660 could have an important influence on the movement of traffic around the network, especially at times of substantial congestion when vehicles needed to make a right turn through queuing traffic. At such junctions, it took an iterative process of adjusting the percentages which describe the turning movements in order to correctly calibrate the traffic flows. Conducting a number of surveys on the A660 to record the turning proportions at smaller uncontrolled junctions would ensure that the modelled turning proportions are a reasonable representation of the real world.

- **Vehicle Dynamics**

In order to generate simulated speed trajectories that accurately represent real-world vehicle activity in the network, AIMSUN allows the user to calibrate a number of parameters which describe vehicle dynamics. As discussed in Chapter 6.3.8, research by Anya et al. (2014) identified 'Maximum desired speed', 'Maximum desired acceleration' and 'Normal deceleration' as the three most important parameters in AIMSUN for calibrating simulated speed trajectories. Using the PEMS data set recorded in Chapter 3, the acceleration and deceleration parameters for the Car and Taxi categories in the AIMSUN vehicle fleet were adjusted to reflect the values for those parameters recorded by the instrumented vehicle driven in the Headingley network (for each of the five time periods). In an attempt to represent conditions in the Headingley network better, the assumption was made that the parameters recorded by the instrumented vehicle in the network were appropriate to describe all cars and taxis in the vehicle fleet. The LCV acceleration and deceleration parameters were assessed using another PEMS data set recorded through Headingley, whilst the parameters for the Bus and HGV categories were garnered from desktop research as there were no available vehicle tracking data recorded in the Headingley network for these categories.

Although a degree of variability is incorporated into these parameters (as the particular parameter values in AIMSUN are stochastically allotted from a normal distribution around the mean parameter value) further work to understand and develop best practice for amending vehicle dynamics parameter inputs, perhaps in collaboration with other AIMSUN users, to develop more accurate default values for different traffic scenarios, would greatly strengthen the modelling process. Whilst the Headingley network model was successfully calibrated and validated with the amended acceleration parameters, indicating that the parameters used in the

coupled model did not result in erroneous vehicle flows and journey times (see Chapter 6.5.1), drawing these parameter values from only a single vehicle with one driver is an obvious oversimplification of reality. Further research into the mean value and the variance of the acceleration parameters within low speed urban road networks, for each modelled vehicle type, would undoubtedly improve the accuracy of the Headingley AIMSUN-PHEM model.

A further limit to the accuracy of the model is the decision to model all passenger cars as one vehicle category "Car" in the AIMSUN simulation. In reality, the range of different engine sizes, body shapes and vehicle weights which make up the UK car fleet mean the range of performance (especially vehicle acceleration) can vary widely. The effect on vehicle speed profiles as a result of this difference in performance may be muted in the Headingley network due to the 30 mph speed limit on the A660 and the impact of other traffic in the network limiting vehicles to below their optimum performance, though it is likely, especially in free flowing conditions, that the acceleration performance of cars in the simulation is less varied than in the real world. However, as detailed tracking data were not available across the spectrum of models, the real-world vehicle dynamics data from the instrumented vehicle described in Chapter 3.2.2, a car fairly typical of the UK fleet, were utilised. In the future, processing of telematics data from GPS tracking devices fitted in vehicles for insurance purposes (Pellecuer et al., 2016) may enable a more accurate appraisal of the vehicle dynamics of a wide range of vehicles, which would facilitate the segregation of the modelled 'Cars' vehicle group into smaller more specific car categories.

- **Bus Dwell Times**

AIMSUN has a separate coding tool enabling input of detailed public transport infrastructure timetables. As detailed in Chapter 3.2.1 the A660 through Headingley features frequent bus stops and has a number of high frequency bus services. These bus routes contribute approximately 50 buses per hour, during weekday travel, to the combined traffic flow during peak hours. As a number of the bus stops do not have bus bays into which buses can pull off the road, traffic can be held up behind buses during passenger boarding. The dwell time (the stationary time a bus spends at a scheduled stop) can, therefore, have an important bearing on overall vehicle flow in the network. Whilst the Headingley network AIMSUN model was informed by a study conducted for a Next Generation Transport proposal in Leeds (S.D.G., 2014b), there was no direct study as part of this research into the timeliness of the Headingley bus services. A detailed survey of the Headingley bus network, over the different modelled time periods, which records the average dwell times, the likelihood of buses needing to stop at each

bus stop and the passenger numbers, would help to improve the accuracy of the model. It should also be noted that the bus timetable coded into AIMSUN describes the weekday timetable. In order to calculate weekend emission factors, the AIMSUN bus timetable would need to be adjusted to reflect the Saturday and Sunday bus service.

- **Pedestrian Crossings**

There are a total of twelve pedestrian crossings in the network. No detailed information could be found on the frequency of use of the crossings or their signal timings. The modelling of these crossings in AIMSUN was coded from limited field observations at each site. As these crossings stop traffic at several points on the A660, they can have an important influence on congestion within the network, especially during peak periods when there are likely to be a larger number of pedestrians. As noted in Chapter 6.3.5 a more rigorous survey of pedestrian crossing use in the Headingley network would improve the quality of this element of the AIMSUN simulation.

- **Road Grade Applied to Existing Network**

As demonstrated in Chapter 5, road grade can have a significant influence on vehicle exhaust emission. As PHEM generates emission estimates using both a vehicle speed profile and gradient data (for each second of the speed profile) it was considered vital to include a road grade estimate with the simulated speed profiles from AIMSUN. The Headingley network AIMSUN model incorporated a measure of road grade, described in Chapter 6.3.2, which assigns a gradient ("slope percentage") to each road section. Just as the simulated speed is recorded every half second simulation step in AIMSUN to create a speed profile, the link on which the vehicle is travelling, and therefore the road grade, is recorded at each simulation step. These data can then be used to inform PHEM.

The limitation of the AIMSUN method for assigning grade is that the grade for each road section is an average grade over the length of the section. Therefore, the simulated grade profile does not present a road grade estimate for each individual point at which the simulation step was recorded (the average grade of the section in which the point is located is referenced, not the grade at the point itself). It should be noted that the initial set-up of the Headingley network model was designed to reflect the road network, with road sections simply connecting to junctions with the result that the start and end points of the road sections do not necessarily reflect changes in topography. The average grade over a section may therefore not be representative of the true road grades in that section, especially over longer links which could have stretches of both positive and negative road grade. Future work to investigate the

sensitivity of emission estimates to the average grade simplification could be conducted by redrawing the network to ensure where possible road sections start and end at local topographic maxima and minima, though this would need to be balanced against making road sections so short that they could create potential problems for the algorithms which control vehicle behaviour in AIMSUN.

- **Journey Time Data for Calibration and Validation**

In order to meet the DfT's WebTag guidelines (DfT, 2014) for model validation, along with the link flow and turning movement validation which was conducted for the Headingley network, the duration of vehicle journey times through the network also needed to be validated, by comparing the percentage difference between modelled and observed journey times. However, as noted in Chapter 6.3.9, at the time of validation there were insufficient observed journey time data available from the network to perform a robust validation of this element of the model.

In practice, only a limited validation was possible, the difference between observed and modelled journey times through a section of the A660 is reported in Chapter 6.5.1. This compared the simulated journey times to both the journey times recorded by the instrumented vehicle in the PEMS survey and a further journey time data set from Trafficmaster (www.teletrac.co.uk) made available by Leeds City Council (which provided data only for the AM and PM periods). Aside from the IP period, in which the simulated journey times were quicker than those recorded by the instrumented vehicle, the Headingley AIMSUN network model simulations captured the correct range of journey times and had approximately the same average journey time as the observed journey times in each time period. Nevertheless, further analysis needs to be completed, that will require the sourcing of more observed journey time data for a number of routes in the network, to provide a comprehensive validation of the model.

It should also be noted that the WebTag guidelines may be difficult to apply to some time periods in the Headingley network due to fluctuation between congested and free-flow conditions. A wide discrepancy in average speed in the network between these two traffic states may lead to a bimodal distribution of journey times in a time period, with a congested mean journey time and a free flowing mean journey time (Aguiléra and Tordeux, 2014), which may not be compatible with the DfT guidelines, in which a normal distribution of journey times around the mean is assumed. A careful consideration of this effect should be assessed in the next phase of validation.

6.6.2 Limitations from PHEM

PHEM is one of the most comprehensive instantaneous exhaust emission models (Pijoan et al., 2017). When compared to other detailed instantaneous emission models, PHEM has by far the largest database for individual vehicles (Luz and Hausberger, 2015). Based on extensive measurements of vehicle tailpipe emission from a number of large scale national and international European research projects, PHEM is able to accurately model the tailpipe emission from a wide variety of vehicles in the European vehicle fleet. However, it is important to note that a number of assumptions are made in the use of PHEM which influence its accuracy in the estimation of network fleet emission.

- **Engine Maps**

As described in Chapter 4.6, the generation of the PHEM emission estimates stem from engine maps specific to vehicle type, Euro standard and vehicle fuel, which have been derived by testing a number of vehicles in each category. Whilst an ideal model would have specific engine emission maps from every manufacturer, for each vehicle model and engine size produced, the required scale and cost of a project to record these emission data makes the collection of such a data set infeasible. The PHEM emission model therefore utilises an average engine emission map for each vehicle category in the model, by fuel type and Euro standard (see Table 6.16, Table 6.17 and Appendix 2). This simplification, where calculated engine emissions reflect the average vehicle in each vehicle category, is common to all emission models as high resolution exhaust emission data are unavailable for a vast majority of vehicles. As a result, the PHEM simulated emission factor estimates cannot describe the array of emission factors that are possible from the spectrum of vehicles categorised within an individual vehicle category. For example, a Euro 5 Diesel Car would generate the same average CO_2 emission estimate from PHEM were that vehicle a small vehicle or a large multi-purpose vehicle, despite significant potential differences in vehicle engine size, body shape and vehicle weight.

This limitation is being addressed at the TU-Graz, which is continuing to expand the functionality of the PHEM model, as further emission data become available. As the number of defined vehicle categories offered by PHEM increases, the AIMSUN-PHEM coupled model can be adapted to incorporate these new categories. This can be achieved both through the description of additional vehicle types in AIMSUN (where further vehicle dynamics data for each vehicle type are also available) and also through analysis of ANPR recorded vehicle fleet data to determine the correct fleet percentages for each vehicle category (taking into account newly defined categories).

- **Emission from Hybrid Vehicles and Motorcycles**

As noted in Chapter 6.2.4.1, at the time of development of the coupled model, PHEM lacks the capability to estimate exhaust emission for hybrid vehicles within the modelled vehicle fleet. As only 171 of the 11,168 passenger cars (1.53%) observed by the ANPR survey in the Headingley vehicle fleet were hybrids, the lack of a hybrid element in PHEM is likely to have only a small impact on the current Headingley network fleet emission factor estimates. However, a method for estimating emissions from hybrid vehicles will need to be included in future work if the proportion of hybrid-electric vehicles in the vehicle fleet increases significantly.

Likewise, for networks with a high proportion of motorbikes in the fleet, this vehicle category will need to be considered in the continued development of a coupled model. The Headingley network model did not incorporate motorcycles as PHEM does not include emission maps for motorbikes and there were insufficient data for the Headingley network to code the vehicle type into AIMSUN. The simulation of the transit of motorbikes within a network is highly complex as they are not limited to lane-based overtaking and therefore, unlike other vehicle categories, can to a certain degree pass more easily through congested traffic. A great deal of relevant empirical data would be necessary to assess the accuracy of simulated drive cycles for motorcycles.

- **Vehicle Loading**

As described in Chapter 4.6.3, the PHEM calculation of engine load (and the resultant emission estimates) requires the average weight of the vehicle, for each specific vehicle category, as input into the model. As demonstrated in Chapter 4.6.4.4, amendment of the .VEH file in PHEM to better represent a test vehicle (or average vehicle in each category) is an important step in ensuring accurate estimation of vehicle emission, which includes adjustment of vehicle weight, rated power and vehicle loading. Whilst estimates of the average vehicle mass in service and the rated engine power for each vehicle type were calculated (see Chapter 6.4.4), no data were available to determine particular loading values, for each vehicle type, that relate specifically to the modelled Headingley network. The loading values employed in the Headingley network model (as described in Chapter 6.5.4) came from a combination of DEFRA and DfT suggested loading values and, where no UK data were available, the PHEM default loading values were used. If further relevant loading data were to become available from sources such as weigh-in-motion systems (Batterman et al., 2015) these figures could be easily amended within the model. Of particular value to the Headingley network model would be a bus occupancy survey (see Chapter 6.5.2) to assess the average number of people riding the bus at different time periods during the day. Such data could then be used to quantify the change in bus weight due

to variation in passenger numbers. A more detailed understanding of average LCV and HGV loading in urban areas would greatly improve the estimate of total vehicle weight for these vehicle categories. The development of the Headingley network AIMSUN-PHEM coupled model provides a unique capability to conduct a detailed sensitivity analysis of this variable, and future study could investigate the impact that loading has on the emission of a plethora of simulated vehicles in the network.

6.6.3 Limitations from Parameters outside the Scope of the Model

For any traffic emission model there is a trade-off between the complexity of the model and its predictive accuracy (Smit et al., 2007; Smit et al., 2010; Grote et al., 2016). Ideally all influences on on-road vehicle exhaust emission would be incorporated within an AIMSUN-PHEM model but, in practice, the complexity of any model is restricted by factors such as, the availability of relevant data and the volume of data required (versus the expense of obtaining such data); the physical time constraints on the recording, preparing, processing and analysis of large quantities of data; limits on the computational power available to run the models; and the infeasibility of investigating an impossibly large number of potential on-road vehicle emission scenarios. It is therefore necessary to define the scope of a model both temporally and spatially and identify the most important parameters that are likely to have a significant influence on real-world vehicle emission. There are considered to be three significant factors that influence vehicle emission which are outside the scope of developed Headingley model, namely: the influence of cold start emissions, the effect of ambient weather conditions on vehicle emission and the impact of non-motorised transportation on traffic flow in the network.

- **Cold Start**

As discussed in Chapter 4.2, cold-start which occurs at the beginning of each journey, whilst a vehicle's engine and exhaust warm-up to their normal operating temperature, can have a considerable impact on the exhaust emission of certain emission species (Khalfan et al., 2015; Li et al., 2008a; Li et al., 2008c). As no data were available to assess the number of vehicles starting from cold within the network during any simulated time period, the Headingley network coupled model was constructed with the assumption that all vehicles were at operating temperature as they entered the network. Therefore all the CO_2 emission factors generated by the model are hot exhaust emission factors. This assumption is likely to lead to an underestimate of the total vehicle fleet emission as in reality a number of vehicles in the network will have started from cold. Should data become available to quantify the percentage of cold start vehicles in the network the effect on network emission could be assessed utilising the PHEM cold start sub-

model (Luz and Hausberger, 2015). In addition, the development of the model enables the significance of the hot exhaust emission assumption on network emissions to be tested by varying the proportion of cold-start vehicles in the modelled fleet at each time period.

- **Weather**

Variation in weather conditions is not accounted for within the Headingley network model, although, in the real-world, the weather could have a significant impact on vehicle exhaust emission. For instance, the ambient temperature will influence factors such as vehicle cold start warm-up time and the use of air conditioning or heating systems and even the density of the air through which the vehicles are moving. These factors will impact fuel consumption to some degree and therefore vehicle tailpipe emissions, including CO_2 emission. The direction and speed of wind within the network can also have an impact on fuel consumption, as wind could potentially act as a force that either decelerates (a headwind) or accelerates (a tailwind) the vehicle, which affects the engine power required to move the vehicle. Other types of weather such as precipitation (rain, sleet, snow), fog and ice, would influence how vehicles are driven in the network, due to effects on visibility and tyre traction on the road surface. Such conditions will affect the acceleration and deceleration rates of vehicles and potentially reduce the desired speed of vehicles to below the maximum speed limits for each road section. Different weather conditions could, therefore, lead to markedly different average exhaust emission rates within the network. In order to incorporate these into the model, it would be necessary to quantify the range of potential weather conditions within the simulated area and determine the impact of those conditions on the model input parameters. An undertaking of this scale was beyond the scope of this research. Consequently, the CO_2 emission factors generated in the Headingley AIMSUN-PHEM model are representative of emission factors in optimal UK weather conditions for driving i.e. mild, calm, clear, and dry.

- **Impact of Non-Motorised Transportation**

The AIMSUN simulated traffic flows in the Headingley network were calibrated to reflect recorded real-world motorised vehicle traffic flows. However, the model does not realistically reflect the potential impact of non-motorised transportation on traffic flows in the road network. In urban environments, pedestrians and cyclists can have a significant influence on the movement of motorised traffic. As noted in Chapter 6.3.5, the effect of pedestrians in the modelled network is limited to the simulation of pedestrian crossings. In busy urban environments, especially in busy shopping areas, the interaction between pedestrians and motorised road users is unlikely to be restricted solely to pedestrian crossings, with drivers

perhaps likely to be more wary of their speed where there are large numbers of pedestrians. The journey time analysis, presented in Chapter 6.5.1, of the Inter-Peak period journey times within the network showed the simulated times to be faster than the limited number of real-world journeys recorded. As this journey time analysis was conducted over a road segment through the centre of Headingley it was hypothesised that the journey time discrepancy may be in part due to the inability of the AIMSUN Headingley network simulation to properly account for the interaction between pedestrians and traffic in the network.

The Headingley AIMSUN traffic simulation also does not include the movement of bicycles in the network. In the absence of separate cycle routes, cyclists share the road with motorised vehicles and are therefore likely to have some impact upon on traffic flow, especially where the lane width is insufficient to allow vehicles to safely overtake cyclists without entering the opposite lane for oncoming traffic. This facet of network simulation could not be incorporated into the Headingley network model due to a lack of relevant cycle activity data. As was mentioned in the case of motorbikes earlier in this section, for networks with large numbers of cyclists, a method of incorporating this vehicle category would need to be considered in the further development of a coupled AIMSUN-PHEM model. The addition of bicycles to the AIMSUN micro-simulation model is possible utilising another software tool called Legion (TSS, 2013b; TSS, 2013a).

- **Others**

Further to these three areas of simplification in the model, there are a number of additional possible influences on exhaust emission in the network which are not explicitly incorporated into the model developed in this research. Traffic flows in the network could, for instance, be hampered by illegal parking in the network, for example by taxis stopping to collect passengers from pavements; by accidents; by improper use of bus bays; by deterioration in the quality of the road surface or by roadworks. For any simulated network, an assessment needs to be made on the degree to which such scenarios influence the normal traffic flow in the network. Further work on the Headingley coupled model could look to quantify the impact of such factors by adjusting the input parameters in AIMSUN and PHEM to reflect such scenarios. Further areas which could influence vehicle emission within a modelled network but which were not directly considered in the development of the Headingley network model include variations in diesel and petrol fuel specifications; the effect on exhaust emission of aging vehicles / engines; the effects of varying tyre legislation (e.g. regulation of the use of summer and winter tyres in the EU) and national variations in servicing and maintenance of vehicles. These factors may need further consideration depending on the location of the modelled network.

6.7 ADVANTAGES OF THE AIMSUN-PHEM COUPLED MODEL

Despite the weaknesses inherent in any modelling process, exhaust emission simulation by models such as the AIMSUN-PHEM coupled model, offer the only practical way to generate high resolution network scale emission estimates. As mentioned noted in Chapter 6.5 the Headingley network model produced over 33,000 hours of emission data from some 377,062 simulated vehicles. To put that into context, the PEMS study that formed the basis of the research in Chapter 3 recorded 63,941 seconds (less than 18 hours) of real-world emission data from one vehicle over a week-long testing period. A week-long PEMS survey is a significant and costly undertaking, requiring not only the relevant PEMS equipment and a test vehicle but also the man-hours for equipment set-up and calibration, real-world measurement, data processing and analysis. To scale-up such a PEMS survey to multiple test vehicles running concurrently over longer measurement time periods would quickly make such projects unfeasible. Network scale exhaust emission quantification is essentially impossible by real-world measurement.

PEMS testing yields a significant snapshot of how exhaust emission varies for a test vehicle in a variety of traffic flow conditions within a network, however, the validity of the results is always limited to the test vehicle chosen, the number of test runs conducted, and the specific traffic conditions incurred during each test run. The AIMSUN-PHEM coupled model offers the capacity to simulate thousands of journeys through a test network and generate exhaust emission estimates for the range of vehicle types found in the local vehicle fleet. Whilst the essential simplifications necessary in the construction of the coupled model mean that there will always be discrepancies between measured real-world emission (recorded over a PEMS equipped journey through the network) and the exhaust emission estimates of a simulated vehicle, a well calibrated simulation combined with PHEM can deliver emission estimates for an average vehicle, in each vehicle category, that are representative of the real world.

The bottom-up approach of the AIMSUN-PHEM coupled model, generating accurate second-by-second emission estimates for each vehicle in the network, enables analysis to be conducted at a wide variety of scales, from that of a single vehicle journey, to the emission from individual vehicle types, building through to the emission of the total vehicle fleet. This can be achieved at different spatial scales. At the highest resolution, emission levels can be calculated for each road link and junction or can be evaluated in aggregate on a single road or across the total network. The coupled model also enables cumulative emission levels to be assessed at any desired time interval down to second-by-second.

A significant strength of this coupled model for network emission estimation is that calculated exhaust emission is derived from instantaneous engine power output which incorporates variables like vehicle acceleration and road grade. As demonstrated by Figure 4.11 engine power has a much clearer relationship with exhaust CO_2 emission than vehicle speed. The common methodology for estimating network emission has traditionally been to employ average speed based models (Panis et al., 2006). As discussed in Chapter 4.1, this methodology entails huge simplifications which to a large extent ignore the physical processes that result in exhaust emission, through allotting a single CO_2 emission factor at each speed. This neglects the fact that the same average speed over a section of road can be obtained from a wide range of transient speed and acceleration profiles. The shapes of the average speed emission functions utilised in these models are entirely dependent on the test over which they were generated and cannot be representative of real-world emission in all locations and in all traffic conditions. A further issue with average speed emission models is that these models are only considered valid above a certain speed. COPERT, for instance, is only valid for average speeds above 10 km/h (Ntziachristos and Samaras, 2014), which makes it impossible to assess emission in congested urban networks where average speeds can be considerably lower than this value. Such limitations are removed through the use of the AIMSUN-PHEM coupled model methodology developed in this research.

Rather than relying on NAEI Base Fleet Composition Data (DEFRA, 2014), which describes the average UK vehicle fleet, this research utilised an ANPR survey within the test network to deliver a comprehensive description of the local vehicle fleet (see Chapter 6.2). The survey data were used to inform the composition of the simulated vehicle fleet in AIMSUN (Chapter 6.3.4) and a more detailed categorisation of the fleet in PHEM i.e. by vehicle type, fuel type, Euro emission standard and vehicle size (Chapter 6.4.2). The ANPR survey also provided extensive metadata for each vehicle recorded in the network which enabled amendment of the PHEM default vehicle specifications to better characterise average vehicles in the Headingley fleet (Chapter 6.4.4). This process leads to a more accurate calculation of bespoke emission factors for the test network. An extensive collection of traffic demand data was made available for this research through the assistance of Leeds City Council Highways and Transportation Department, who provided access to their database of traffic count data recorded in the Headingley network (Chapter 6.3.4). As a 24-hour record was available for both the ANPR data and the traffic demand data, this facilitated the development of separate simulation time periods representing different traffic conditions in the network and enabled in-depth investigation into diurnal trends in CO_2 emission (Chapter 6.3.7).

As shown in Chapter 5.3 and Chapter 5.7, the importance of road grade in generating accurate exhaust emission estimates should not be underestimated due to the influence it can have on required engine power output. Whilst most average speed emission models offer individual emission factors at different road grades, these are limited to discrete road grade classes (e.g. COPERT and HBEFA offer emission factors only at -6%, -4%, -2%, 0%, 2%, 4%, 6%). AIMSUN however, has the functionality to add a "slope percentage" to each road section (see Chapter 6.3.2) from a continuous range (i.e. road grade for each road section can be set to any value). Despite the limitations to the AIMSUN method for assigning road grade discussed earlier in this section, AIMSUN is able to assign a more accurate road grade over a much wider range of values than is possible when using an average speed model. The road grade from AIMSUN populates each second of simulated data (see Chapter 6.1) and directly informs the power output equation used to generate emission estimates in PHEM.

As discussed in Chapter 6.1, to ensure that movements of vehicles in the simulated network reflect the real-world movements of vehicles in a test network, AIMSUN allows adjustment of the input parameters that inform the operational algorithms which control simulated vehicle behaviours within the model. A number of previous studies had identified that the default parameters provided in AIMSUN require adjustment, as the simulated vehicle trajectories generated from the default values are not consistent with observed real-world behaviours (Swidan, 2011; Anya et al., 2014; Madi, 2016). As a consequence, data from PEMS study within the Headingley network was used to calibrate the maximum acceleration, normal deceleration and maximum deceleration rates of passenger cars, taxis and LCVs in the Headingley AIMSUN model. As highlighted in Chapter 6.6.1, the Headingley network model vehicle dynamics parameters were drawn from a relatively small PEMS data set. Further on-road measurement and a more detailed appraisal to identify suitable real-world values for the AIMSUN acceleration and deceleration parameters would increase confidence in the model. The capacity to define accurate vehicle dynamic parameters for all vehicle types contributes to a significant strength of the AIMSUN model in that the interaction between different vehicle types in the network can be captured. This reflects the reality that, for instance, buses hinder traffic flow in the network when decelerating to stop at bus stops or accelerating to leave them and that slow accelerating HGVs on a road limit the behaviour of following vehicles.

In order to calculate accurate exhaust emission estimates, any simulated vehicle journey must generate a VSP profile akin to a real-world journey of the same duration, traversing the same part of the network. This research presented a new approach for assessing the similarity of simulated and real-world engine power output distributions. The VSP analysis in Chapter 6.5.1

suggests that the calibrated AIMSUN model produces second-by-second transient vehicle data which are representative of real-world driving, with a caveat that further sensitivity testing of the AIMSUN vehicle dynamics parameters may help to improve the match between the simulation and reality even further. The ability to assess in great detail micro-scale simulated journeys against real-world measurements should give confidence in the accuracy of the aggregate network emission factors generated by the AIMSUN-PHEM coupled model developed in this research.

Chapter 6.5.4 demonstrated a method by which 24-hour average emission in the network could be assessed by means of weighting the simulation period emission factors by observed vehicle flow. The high resolution outputs generated by the AIMSUN-PHEM coupled model facilitate detailed comparison of the modelled emission factors with the UK Government's official vehicle emission factors for GHG reporting (DEFRA, 2015b). A thorough evaluation of the modelled CO_2 emission factors is presented and it was possible to justify the scale of the differences between the model and NAEI CO_2 emission factors for all vehicle types. Of interesting note is the finding that the AIMSUN-PHEM model average 24-hour CO_2 emission factors for petrol and diesel passenger cars were 24% and 40% greater respectively than the NEDC based SMMT petrol and diesel average car CO_2 emission factors. These discrepancies, which likely reflect real-world effects on fuel consumption that are accounted for in the coupled model but not in the NEDC factors, are in line with the magnitude of the differences found between the "official" (NEDC) and real-world CO_2 emission factors (see Chapter 2.7) as reported by the ICCT (Mock et al., 2015). The relatively good agreement of the modelled network CO_2 emission factors to proposed real-world CO_2 emission factors recorded in the literature, would suggest that the AIMSUN-PHEM model is capable of producing realistic real-world CO_2 emission estimates at all disaggregate micro-scale levels (as shown in Chapter 6.5.1) and, unlike average speed models, the coupled model emission factors are not contingent on NEDC generated emission factors (which are unrepresentative of real-world driving emission) with their ambiguous uplift factors.

A significant strength of the model methodology is that as better network data become available the input parameters within the model can be updated, improving the accuracy of emission estimates. For example, further PEMS data recorded in the network could be used to inform the vehicle dynamic parameters within AIMSUN and the recorded emission could be used to validate the PHEM emission estimates. A bus occupancy survey or detailed analysis of the use of pedestrian crossing in the network could both generate useful data that could be incorporated into the model. New ATC and ANPR surveys in the network could improve the accuracy of the simulation input flows and better describe the simulated vehicle fleet. Whilst

vehicle fleet data have historically been expensive to collect, a number of recent developments, for instance, the use of telematics data from GPS tracking devices for insurance purposes (Pellecuer et al., 2016) and the increased deployment of ANPR cameras in urban areas for the monitoring of low emission zones, congestion charging, speed enforcement and traffic monitoring, should make the traffic data necessary for the calibration and validation of this coupled model more readily available. Alongside improvements to the model input data, both the AIMSUN software and the PHEM emission model are under development and new features continue to be added. As the functionality of the AIMSUN package is upgraded and the PHEM emission maps are updated and expanded to further vehicle categories, the quality of the coupled model outputs will be enhanced.

As described in Chapter 6.1, the .mod output files from the AIMSUN-PHEM coupled model, alongside generating second-by-second fuel consumption estimates (used to calculate CO_2 emission), also provide second-by-second emission estimates for the exhaust pollutants NO_x, NO, CO, HC, and PM. As the tailpipe emission of NO_x and PM can be extremely detrimental to human health (Skeete, 2017; Font and Fuller, 2016) the ability to generate link level micro-scale emission factors for these exhaust emission species should be of considerable interest to those modelling air quality through microscopic dispersion models. The work which has been done in this thesis to ensure that the AIMSUN-PHEM model produces second-by-second fuel consumption (CO_2 emission) and engine power output values that reflect real-world driving, should give confidence that the coupled model can generate appropriate emission values for the other emission species. However, a great deal of further work is required, including validation against real-world emission data, to evaluate the accuracy of the AIMSUN-PHEM model's emission predictions for these pollutants from simulated speed profiles.

Development of an AIMSUN-PHEM coupled model enables in-depth study of exhaust emission in a test network to a degree that would not be possible through direct real-world measurement. This research has demonstrated the ability of the model to generate accurate emission estimates for individual vehicles, for the network, for each vehicle type and for sub-categories of each vehicle type. Emission data can be evaluated on a second-by-second basis or emission can be analysed at any longer desired interval. The format of the model output permits access to every second of emission from the thousands of vehicles simulated in the network over 2-hour time periods. This wealth of data enables the user to develop an extremely detailed understanding of vehicle emission in the network. As discussed in Chapter 2, the on-road vehicle fleet makes a significant contribution to the UK's total national emission of CO_2. To evaluate the progress being made in reducing the level of CO_2 emission from the vehicle fleet

(which is necessary to meet the UK's legally binding CO_2 emission targets), it is important that the real-world CO_2 emission of the vehicle fleet can be accurately assessed. Given the increasing divergence between the NEDC type-approval CO_2 emission of vehicles and their on-road CO_2 emission (Dings, 2013; ICCT, 2015; Mock et al., 2015), and the difficulty of conducting large scale on-road emission studies, coupled simulation emission models may offer the only practical way of establishing the magnitude and detail of real-world network CO_2 emission. Further development of an AIMSUN-PHEM coupled model would enable towns and cities in the UK to calculate their own network emission factors rather than relying on average UK vehicle emission factors.

Development of a base model with the current input parameters allows an assessment to be made of the potential impact on vehicle emission from changes to the network. This could take the form of sensitivity analysis to understand the influence of each parameter on CO_2 emission in the network, for example by adjusting the speed limits or varying traffic demand. Alternatively, the model could be used to test the emission impact of scenarios within the network, such as altering signal timings or junction design; adding a bus lane; excluding certain vehicle types from the network; or modelling future vehicle fleets. Each of these scenarios may require further qualified decisions to be made about the potential impact of the change on other parameters within the model, such as the effect it could have on traffic demand and turning movements. Parameters within the model can be changed to reflect the scenario and the simulations rerun with the changes in order to generate new emission factors for the network. These emission factors can then be evaluated against the base model emission factors to quantify the change in emission as a result of the particular scenario.

The ability to use an AIMSUN-PHEM model to quantify the change in emission as a result of particular planning decisions could be of huge benefit to both the environmental assessment of transport planning projects and also to cost-benefit analysis of strategies to reduce on-road emission. Where the cost associated with a prospective project is known, it would be possible to use AIMSUN-PHEM to calculate the potential emission reduction from the project (potentially for multiple pollutants) and the cost per tonne emission reduction could be calculated and used to evaluate the prospective project against other possible emission reduction plans. The AIMSUN-PHEM model could be used to provide evidence for policymakers who are working to reduce CO_2 emission from the vehicle fleet and/or improve air quality in urban environments.

6.7.1 Summary: Novelty of the AIMSUN-PHEM Coupled Model Methodology

The research reported in this thesis demonstrates how two advanced software packages, AIMSUN and PHEM, can be coupled to produce a powerful exhaust emission simulation package in which:

- Emission is based on second-by-second engine power output and not average speed.
- Emission outputs are valid for all vehicle speeds.
- An accurate representation of the real-world vehicle fleet (both in AIMSUN and PHEM) is achieved through an ANPR survey method that enables a detailed description of an average vehicle (e.g. engine size, vehicle weight) for each PHEM vehicle category.
- PEMS recorded transient data has been used to inform AIMSUN vehicle dynamics for Car and LCV categories.
- Road grade values from AIMSUN have been incorporated into the PHEM calculation of second-by-second exhaust emission, through a Leeds University ITS AIMSUN API.
- A novel coupled-model calibration validation methodology, developed in this study, can be used to assess the VSP distributions and emission rates of simulated trips against real-world data to confirm that modelled vehicles operate in the network in a way that reflects reality.

This results in:

- A methodology which delivers high resolution micro-scale emission estimates that capture individual vehicle behaviour within a network and the interaction between that vehicle and the rest of the vehicle fleet, with emission estimates generated for every second of each individual vehicle's transit through the model.
- Simulated 1 Hz exhaust emission which can be aggregated over desired spatial and temporal scales and can be used to evaluate specific areas within the simulated network.
- CO_2 emission factors which can be generated for each separate vehicle sub-category as described by vehicle type, Euro emission standard and fuel type (and weight class for LCV and HGV vehicles) in PHEM.
- The CO_2 emission from each vehicle trip in the Headingley model which can be aggregated to calculate the resultant CO_2 emission factors for each vehicle type (i.e. Car, Taxi, LCV, HGV and Bus) along with the total network emission.

- The capacity to simulate traffic movement in the test network over different time periods, which can quantify the variation in vehicle exhaust emission as a function of different traffic flow conditions.
- Calculation of the average 24-hour network CO_2 emission factors for each vehicle type which can be compared to the DEFRA CO_2 emission factors for GHG reporting. The scale of the differences can be assessed for each individual vehicle category.
- A model that can be employed to generate high resolution emission estimates for the pollutants NO_x, NO, CO, HC, and PM, which are of greater relevance for local air quality (though further work will be required to evaluate the accuracy of the AIMSUN-PHEM real-world emission estimates for these pollutants).

The development of the AIMSUN-PHEM coupled model enables it to be employed to:

1. Develop a better understanding of vehicle exhaust emission within the network with the current model input parameters.
2. Test the effect on exhaust emission from potential changes within the network, e.g. in different junction design and signal timings; in the introduction of bus lanes; increased traffic demand in the network and changes in vehicle fleet composition.
3. Aid the decision making process for transport planners by providing a quantification of the potential emission reduction of proposed schemes, which can be utilised to evaluate the cost-benefit value of different emission reduction strategies and to justify expenditure.

As better quality input, calibration and validation data become available and as the AIMSUN and PHEM software packages continue to be developed, the power of an AIMSUN-PHEM coupled model to generate accurate micro-scale and network emission estimates will continue to improve. Despite the limitations to the accuracy of AIMSUN-PHEM model reported in Chapter 6.6, the scale and definition of the AIMSUN Headingley network (incorporating a detailed vehicle fleet, road grade and estimate for network specific vehicle dynamic parameters), with the work done to calibrate and validate the model (including demonstration of a novel method for assessing simulated and real-world vehicle engine power output), coupled with the quality of the AIMSUN software and the PHEM model, mean that the Headingley network AIMSUN-PHEM model developed and demonstrated in this thesis, can be considered the best specified coupled traffic simulation and vehicle emission model in current published literature.

6.8 SUMMARY

This chapter has presented the development and application of an AIMSUN-PHEM coupled traffic micro-simulation and instantaneous emission model for an urban road network around a 3.8 km section of one of the main arterial corridors into and out of Leeds, UK. Five separately calibrated and validated versions of the model were created to represent five time periods; AM peak, Inter-Peak, PM peak, Evening and Night to investigate the diurnal variation in vehicle fleet CO_2 emission rates which result from changes in traffic demand and fleet composition over a typical 24-hour weekday.

A 24-hour ANPR survey was undertaken to provide an accurate composition of the Headingley vehicle fleet, both for modelling the fleet in AIMSUN and describing the correct proportion of vehicles by vehicle type, Euro emission standard and fuel type in PHEM. This survey method was demonstrated to deliver a high capture rate (94.86%) giving confidence that the ANPR observed fleet is representative of the real-world fleet. The ANPR survey also provided a large quantity of metadata for each recorded VRM, which was used to update the background vehicle specification files in PHEM, making the average vehicle data representative of the Headingley fleet rather than relying on the PHEM default settings.

As with any model, the AIMSUN-PHEM Headingley simulations could be improved with better input data, such as a comprehensive traffic count conducted simultaneously across the network to mitigate the effect of seasonal influences on traffic flow, a longer ANPR survey to ensure the observed fleet represents the real-world fleet and a greater quantity of instrumented vehicle PEMS data to assess the accuracy of the simulated CO_2 emission estimates and inform the vehicle dynamics parameters within AIMSUN. In reality, such detailed data collection exercises are outside of the scope and budget of a study such as this. However, every effort was made to identify, obtain and utilise the highest quality and most appropriate, data sources available. Including a road grade estimate for each road link and utilising PEMS data recorded within the network to inform the AIMSUN vehicle dynamics parameters likely improved the ability of the AIMSUN-PHEM model to generate trajectory data comparable to on-road vehicle movements in the real world.

Comparing the AIMSUN-PHEM simulated CO_2 emission rates to the PHEM CO_2 emission estimates calculated from the PEMS trajectory data, by journey time (Chapter 6.5.1), suggests that in general, the 1 Hz simulated vehicle data from AIMSUN generated very similar results to the PEMS 1 Hz data, indicating that simulated data can be used to generate real-world CO_2

emission estimates. In a further check of the AIMSUN-PHEM method, analysis was conducted to compare the distribution of second-by-second VSP calculated from AIMSUN simulated journey data with the VSP distribution from PEMS real-world trajectories, for cars completing a 1.5 km road section in similar journey times. This showed the simulated data to have similar VSP distributions to the PEMS real-world data. However, a number of anomalies suggest that further calibration work may be required to improve the simulated values, as differences in distribution may have a more significance for other emission species.

The coupled model facilitated evaluation of CO_2 emission in the network at a variety of scales, from total network emission factors to individual vehicle type emission factors by fuel type and emission standard, demonstrating the ability of this method to provide both aggregated and highly disaggregated emission factors. The Headingley AIMSUN-PHEM model displayed significant diurnal variation in emission factor. For example, the average network CO_2/km emission rate under congested traffic conditions was found to be 43.5% greater for petrol passenger vehicles (cars and taxis) and 45.5% greater for diesel passenger vehicles than in free flowing conditions observed in the network.

Whilst the calculated CO_2 emission factors in this study are specific to the Headingley test area, this research advances the development, calibration and validation of the AIMSUN-PHEM coupled traffic micro-simulation and instantaneous emission model method. The study demonstrated the relative ease with which AIMSUN can be coupled to PHEM, and although the modelling process requires a large amount of detailed input data, this type of data are increasingly available. As more AIMSUN networks are developed to model traffic flows for traffic management purposes, as long as the parameters within AIMSUN are representative of the real-world network and the model is well calibrated, then a coupled AIMSUN-PHEM model can be utilised to provide improved assessment of the environmental impact of traffic networks. The coupled model offers the possibility to generate current emission factors within networks as well as assess the potential emission impact of changes to the network such as different junction designs, speed limit reductions, the addition of bus lanes and different fleet mixes. As PHEM is able to generate emission estimates for a number of exhaust emission species, the tool also enables assessment of the fleet emission of vehicle exhaust pollutants which have a greater influence on local air quality such as NO_x.

CHAPTER 7: SUMMARY AND CONCLUSION

7.1 INTRODUCTION

This chapter presents a summary of the work in this thesis, highlighting the main findings of each chapter. Each of the research questions from the Chapter 1 aims and objectives are addressed, followed by conclusions from the study and recommendations for future work.

7.2 SUMMARY OF CHAPTERS

The following subsections summarise the finding of each chapter in the thesis.

7.2.1 CHAPTER 1: Introduction

Chapter 1 introduced the thesis research topic. It discussed the background and rationale behind the study and presented the research questions, scope and objectives for the research. The objectives set out in the chapter were:

i. To provide an accurate quantification of real-world micro-scale CO_2 emission factors from a passenger car over a full range of traffic conditions in an urban traffic network.

ii. To assess the ability of different emission model methodologies to estimate real-world on-road exhaust CO_2 emission factors over the spectrum of traffic conditions likely in an urban network.

iii. To evaluate the importance of road grade in the accurate appraisal of real-world CO_2 emission and establish a practical method for incorporating road grade into the second-by-second modelling of on-road CO_2 emission.

iv. To create a calibrated and validated, coupled traffic simulation and vehicle emission model and demonstrate the ability of the model to produce high resolution CO_2 emission factor estimates for a UK network, identifying the relative contribution of different vehicle types and sub-categories.

The rationale for focusing this research on the emission of CO_2 was explained:

- The on-road vehicle fleet makes a significant contribution to the total UK national emission of CO_2, which needs to be addressed in order to meet commitments to legally binding emission targets by 2020 and 2050.

- There is an increasing disparity between real-world vehicle CO_2 emission and test cycle type-approval emission factors, which necessitates the development of simulation tools that provide realistic vehicle emission factors that are not reliant on test procedure generated emission factors.

- There is a need for accurate micro-simulation emission tools for transport planning purposes both in the development of the transport network (e.g. optimised traffic signals, junction design and bus lane evaluation) and in providing an instrument for policy-makers which enables more detailed appraisal of measures to lower vehicle emission (e.g. the uptake of low emission vehicles, increased car sharing and limiting certain vehicle types).

7.2.2 CHAPTER 2: Road Transport and CO_2 Emission

This chapter presented the latest findings of the climate science community with regard to observed global warming and outlined the potential consequences of a continuation of the current high rates of anthropogenic GHG emission. The Climate Change Act commits the UK to reducing its GHG emissions to 80% of the 1990 baseline by 2050 (Legislation.gov.uk, 2008). To meet this target, there will likely need to be an almost complete decarbonisation of road transport by 2040 (DECC, 2011), a sector which currently contributes some 22% of the UK's total domestic CO_2 emission (CCC, 2015).

A combination of low CO_2 technological innovation, increased dieselisation, economic incentives and disincentives through government policy and legislation, along with increased public awareness of the issues around climate change has seen the average type-approval CO_2 emission rating of new cars purchased in the UK fall dramatically from an average 177.8 gCO_2/km in 2001 to 124.8 gCO_2/km in 2014 (GOV.UK, 2015d). The 2014 UK new car average type-approval CO_2 emission rating was below the target set by the EU for 2015.

However, several studies have revealed that under real-world driving conditions on-road vehicle emission substantially exceeds the type-approval emission factors generated by the New European Driving Cycle (NEDC), the EU benchmark test for vehicle exhaust CO_2 emission (EC,

2009b; ICCT, 2015). These reports have demonstrated the increasing divergence between real-world and test cycle measured CO_2 emission, with the gap widening from approximately 8% in 2001 to 40% in 2014. As a result, the NEDC test is an increasingly poor proxy measure for real-world driving emission (Dings, 2013).

The smooth profile of acceleration and deceleration, used in the NEDC, tests only a small portion of a vehicle's operating range and fails to adequately represent the expected engine power outputs employed in on-road driving. The reason for the widening gap between real-world and the NEDC CO_2 emission factors is not, however, the result of the unrepresentative nature of the test cycle. The growing difference can be attributed to manufacturers manipulating the test procedure to minimise CO_2 emission during certification (Mock et al., 2015), with increasing exploitation of flexibilities and loopholes within the type-approval testing framework.

Therefore, whilst the year-on-year reduction in new car CO_2 emission would seem to suggest a significant reduction in UK vehicle fleet's on-road CO_2 emission, in reality, it is likely that the real-world reduction in CO_2 emission is considerably smaller. As the NEDC type-approval CO_2 emission figures do not accurately represent real-world vehicle exhaust CO_2 emission, tools which are able to generate better estimates of on-road emission are required.

7.2.3 CHAPTER 3: Real-World Vehicle Emission

In order to garner reliable values of on-road micro-scale CO_2 emission, Chapter 3 analysed a PEMS measured real-world CO_2 emission data set. The analysis presented in the chapter provided a quantification of on-road CO_2 exhaust emission factors and the likely variance in these emission rates associated with the variety of driving conditions that can be experienced in an urban traffic network.

The data came from a PEMS instrumented vehicle study conducted in Headingley, Leeds in 2007. During the study, on-road exhaust emission readings were measured over a 4.6 km test lap, on mainly single lane urban commuter roads. The test lap was repeated a total of 48 times by the same driver in the same instrumented vehicle during a week-long testing period, with test runs occurring between the hours of 07:30 and 21:00 in order to capture the full range of traffic conditions for this road network. A new analysis of this PEMS data revealed substantial spatial and temporal variability in CO_2 exhaust emission within the network, with a range of measured CO_2 emission factors, across the 48 test laps, from 313 gCO_2/km to 586 gCO_2/km. Micro-scale CO_2 exhaust emission estimates were calculated from the test lap data by dividing the lap into

eight short sections (Figure 3.10). The measured exhaust CO_2 emission through the short sections ranged from 219 gCO_2/km to 1,359 gCO_2/km. These PEMS measured section CO_2 emission figures were compared to the measured type-approval CO_2 emission values of the test vehicle, a 2005 Euro 4 petrol Ford Mondeo. Every one of the PEMS generated CO_2 emission factors, for each of the 384 test sections, was found to be greater than the 175 gCO_2/km NEDC type-approval emission rate. As discussed in Chapter 2.6, the NEDC test comprises a phase of urban driving and a phase of extra-urban driving. As the Headingley lap testing was conducted entirely on urban roads, the PEMS CO_2 emission figures were also compared to the 253 gCO_2/km emission figure generated by the urban driving portion of the NEDC test. Only 16 of the 384 short section CO_2 emission estimates were lower than the urban test cycle values, with the recorded PEMS CO_2 emission for each section, on average, 77.9% greater than the NEDC certified urban emission rate.

Chapter 3.5 assessed changes in the average rate of CO_2 emission from the test vehicle as a result of variation in traffic conditions. A 1.5 km section of the Headingley test lap was selected for the analysis. The CO_2 emission rate and vehicle average speed over the 'northbound' and 'southbound' lanes of this 1.5 km section were assessed for each of the 48 test runs. The PEMS measured section data were grouped into four time periods (AM peak, Inter-Peak, PM peak and Evening) determined by the time at which each test was run. The analysis (Figure 3.32) highlights considerable variation in traffic conditions within the network, with frequent severe congestion on the northbound section during PM peak traffic and congestion over the southbound section during AM peak traffic, leading to low average speeds through the sections and high gCO_2/km rates of emission. Conversely, in the predominantly free flowing traffic of the Evening period, the average speed of the test vehicle was high and that average gCO_2/km rate of emission low.

The analysis of the PEMS data presented in this chapter is used in subsequent chapters to assess the accuracy of modelled micro-scale emission estimates of real-world CO_2 emission.

7.2.4 CHAPTER 4: Modelled Vehicle Emission

Chapter Four presented an assessment of the capability of four popular emission models to replicate the real-world micro-scale emission quantified in Chapter 3. The four models used in the study were; DEFRA's Emissions Factors Toolkit, an average speed emission model; the HandBook on Emission FActors for road transport, a 'traffic situation' model; the US EPAs Motor Vehicle Emission Simulator, a 'modal' emission model; and the TU-Graz's Passenger car and

Heavy duty Emission Model, an instantaneous emission model. The chapter included a discussion on the background to each model and the methodologies employed to generate estimates of on-road exhaust emission.

The instrumented vehicle GPS recorded second-by-second transient speed profiles from the Headingley test laps were used as the input for each of four emission models. The four models calculated CO_2 emission factor estimates for each of the 48 test laps and 384 micro-scale road sections. These modelled estimates were then compared to the test vehicle's PEMS measured real-world CO_2 emission rates.

The EFT and HBEFA emission models were both found to substantially underestimate the real-world CO_2 emission rates of the test lap and micro-scale sections, calculating CO_2 emission factors which were on average around 40% lower than the PEMS measured emission rate. Therefore neither the average speed emission factor methodology nor the traffic situation technique was found to be appropriate for micro-scale emission estimation in this instance.

The MOVES and PHEM models, in contrast, were both shown to generate good estimates of the real-world CO_2 emission recorded during the PEMS testing. The mean model percentage estimate of the PEMS measured CO_2 emission was found to be between 90% to 95% for both MOVES and PHEM. The mean average percentage error (MAPE) for both models was calculated to be around 10%. In general, MOVES was found to be slightly the more accurate of the two models, but PHEM was found to have the greater precision.

The chapter concluded that a decision on which of the two models, MOVES or PHEM, is most appropriate for a particular study is likely to come down to the location of that research. PHEM was developed using measured emission predominantly from European vehicles and MOVES was created using vehicle emission data from the American vehicle fleet. Although both models provided good estimates of the Headingley recorded on-road CO_2 emission, the accuracy of the MOVES output was largely due to the coincidence that the test vehicle employed in the PEMS survey happened to be a good match with the average 2005 petrol passenger car in the MOVES model. Apart from the age of the vehicle and the year of its manufacture, it was not possible to further describe the test vehicle in MOVES, with the result that whatever the weight and engine size of the test vehicle the same CO_2 emission estimate would have been generated. The PHEM estimates, however, were accurate because the vehicle parameters for the model could be specified. The importance of this characteristic of the PHEM model was demonstrated through comparison of the PHEM CO_2 emission estimates calculated with the vehicle parameters set to

describe the test vehicle against the PHEM CO_2 emission estimates calculated with the default Euro 4, petrol passenger car specification. For the PHEM model with the default Euro 4 setting the MAPE was 25.3% compared to 12.3% for the PHEM model entered with the test vehicle specification data (Chapter 4.6.4.4).

It was noted in the chapter that there was significant section-by-section variance in the accuracy of both the MOVES and PHEM estimates of CO_2 emission. This was especially clear in Section 1 and Section 8, which are the opposite traffic flows over the same road link. It was hypothesised that this discrepancy was due to the impact of gradient, as this part of the Headingley test lap has the steepest road grade, with Section 1 being primarily downhill and Section 8 primarily uphill.

7.2.5 CHAPTER 5: Road Grade and Micro-Scale Emission Modelling

Having identified, in Chapter 4, the potential influence of road grade on the MOVES and PHEM road section emission estimates, this chapter investigated the impact of road grade on the micro-scale estimation of CO_2 emission.

Using the equation for VSP (Chapter 4.5.2) to calculate values of engine power output, the chapter presented a sensitivity analysis of road grade and CO_2 emission, utilising a CO_2 emission and VSP binning methodology. Hypothetical VSP values were calculated over the likely range of speeds in the Headingley network (from 0 km/h to 50 km/h), under three acceleration scenarios (acceleration, cruise and deceleration) at six set road grades (-6%, -3%, 0%, 3% and 6%). An estimate of the gCO_2/s emission was then calculated for each hypothetical VSP value using CO_2 emission bins (Table 5.1). Comparison of the estimated CO_2 emission values, from the hypothetical VSP values for each road grade, demonstrated that, under all three acceleration scenarios, failure to account for road grade could lead to a substantial error in the estimation of CO_2 emission. Even though the road grades assessed in this study were relatively modest, when travelling at 30 mph (48 km/h) the inclusion of positive road grade resulted in gCO_2/s exhaust emission rates between 1.3 and 2.9 times greater than on a flat road. Likewise on downhill sections, at this speed when the vehicle was accelerating (0.5 m/s^2) or cruising (0 m/s^2) the inclusion of negative road grade led to a gCO_2/s emission rate 40% to 70% of that on a flat road.

To accurately account for road grade in the estimate of real-world exhaust emission, this chapter presented the development and application of a novel LiDAR-GIS based methodology for calculating a 1 Hz road grade, utilising real-world PEMS survey measured speed, location and

CO_2 emission data. The addition of the LiDAR-GIS road grade values was shown to significantly improve the linearity of the relationship between positive VSP and CO_2 emission, when compared to VSP calculated without road grade, increasing the average R^2 value from 0.65 to 0.73.

This chapter presented a re-analysis of the MOVES and PHEM generated estimates of real-world CO_2 emission generated in Chapter 4.5.4 and Chapter 4.6.4.4 with the inclusion of a LiDAR-GIS generated road grade. Both MOVES and PHEM models have the facility to specify a road grade value for each second of the recorded speed profile, which should theoretically improve the modelled estimate of the instantaneous engine power output and therefore the estimate of the resultant CO_2 emission.

In this case, the addition of the LiDAR-GIS data to the modelling in PHEM (denoted $PHEM_G$) did not greatly improve the accuracy of Headingley lap CO_2 emission estimates, compared to the estimates without grade (denoted $PHEM_0$). The median model estimate of the PEMS CO_2 emission increased slightly, from 90.1% with $PHEM_0$ to 91.0% with $PHEM_G$. However, the LiDAR-GIS grade was shown to improve the stability of the PHEM estimate of Headingley section CO_2 emission. The $PHEM_G$ median estimates of the total PEMS CO_2 section emission (excluding the short turning sections) were between 91.5% and 94.3%, compared to a range of 79.0% to 97.8% for the $PHEM_0$ section estimates. Rather than showing the variability associated with overestimation of CO_2 emissions on downhill sections and underestimation of CO_2 emissions on uphill sections, the addition of the LiDAR-GIS road grade led to a consistent $PHEM_G$ estimates of the micro-scale real-world emission, albeit an underestimates, with a MAPE of 9.0% for the 288 longer road sections.

The LiDAR-GIS road grade data were also shown to improve the MOVES section estimates of the PEMS measured CO_2 emission. The median model estimate of the PEMS measured Headingley lap CO_2 emission actually marginally decreased, from 95.9% with $MOVES_0$ to 95.4% with $MOVES_G$. However, the $MOVES_G$ median estimates of the PEMS longer section CO_2 emission were between 92.4% and 101.3%, a significant improvement on the $MOVES_0$ estimates which had a range between 80.5% and 107.6%.

This chapter demonstrated that the incorporation of accurate road grade removed a significant degree of the section-to-section variability in estimate accuracy when compared to that determined under $MOVES_0$ and $PHEM_0$. This improvement was most obvious in Sections 1 and 8, which had the steepest average gradient of the sections in the Headingley survey (≈ ± 1.6%).

Analysis of the $PHEM_G$ modelled CO_2 estimates revealed a degree of variance in the accuracy of the longer section CO_2 emission estimates, with 90% of these estimates between 79.5% and 109.7% (for $MOVES_G$ the range was 83.0% to 113.0%). These discrepancies from the real-world emission levels are likely to be due to factors not incorporated in the engine power modelling used in either MOVES or PHEM. These influences include possible error in the PEMS CO_2 data as a result of the 'pulse effect' exhaust flow adjustment and factors affecting vehicle fuel consumption, such as day-to-day variation in ambient temperature, starter battery state of charge and use of the vehicle's air-conditioning / heating systems. The vehicle weight estimate may also have been incorrect in PHEM, as no direct measurement was made.

The on-road micro-scale CO_2 emission prediction capability of both $MOVES_G$ and $PHEM_G$ were shown to be remarkably similar, given the two different methodologies. $MOVES_G$ was shown to be marginally more accurate in its median section CO_2 emission estimate (excluding turning sections), which was 95.8% versus 93.4% for $PHEM_G$. However, $PHEM_G$ was slightly more consistent in its emission estimates, with an IQR in its estimates of 9.7% compared to 11.8% for $MOVES_G$. This research suggests that both MOVES and PHEM can be considered appropriate for the micro-scale CO_2 emission modelling of this test vehicle, however, the flexibility of PHEM in allowing adjustment to represent other test vehicles, and the fact that its default settings were developed for the European vehicle fleet, made PHEM the more appropriate choice for the coupled model.

The chapter presented a further assessment of the effect of road grade on CO_2 emission. Using the PHEM model, a sensitivity analysis was conducted employing five road grade scenarios. The scenarios were formed by multiplying the LiDAR-GIS calculated road grade for each second of data by five coefficients 0, 0.5, 1, 2 and 3. The results indicate that road grade can have a significant impact on the modelled vehicle emission. The assessment was also conducted for NO_x emission which was found to be more sensitive to road grade than CO_2, with a greater percentage increase in emission at the higher road grade coefficients. The analysis demonstrated that for road sections over which the average road grade is zero, but where there is some change in elevation, it is incorrect to assume that increased emission in uphill sections is offset by decreased emission in downhill sections. The PHEM modelling indicated that for such road sections, total emission increase with increasing steepness of road grade in the sections.

This chapter established that to generate accurate vehicle exhaust emission estimates at a micro-scale in real-world conditions, it is important to include a representative road grade for

each second of the test data. The novel LiDAR-GIS method proposed in this study provided a simple methodology for calculating 1 Hz road grade and was shown to improve the modelling of CO_2 emission for this data set. This research demonstrates that using the PHEM instantaneous emission model with inclusion of LiDAR-GIS calculated road grade estimates is a viable method for generating accurate real-world micro-scale CO_2 emission estimates from GPS transient speed profiles recorded by an instrumented vehicle survey.

7.2.6 CHAPTER 6: Emission Modelling using a Coupled Traffic Simulation (AIMSUN) and Instantaneous Emission Model (PHEM)

Whilst Chapter 5 demonstrated that using PHEM with PEMS recorded speed profiles and road grade can provide an accurate estimate of CO_2 emission for one specific vehicle driving through a network, the work reported in Chapter 6 evaluated whether it is possible to use a simulated network (including road grade) to generate 1 Hz vehicle speed data from all vehicles in the network, which is sufficiently similar to the real-world vehicle second-by-second speed data, to allow accurate estimates of real-world CO_2 emission to be made from a coupled traffic simulation and instantaneous emission model.

This chapter presented the development and utilisation of a coupled traffic simulation and instantaneous emission model to produce high resolution estimates of exhaust CO_2 emission from the vehicle fleet in an urban network. This study used the AIMSUN microscopic traffic simulation tool, to generate a model of the Headingley network which encompasses a 3.8 km section of the A660, one of the main arterial corridors into and out of Leeds, UK. The AIMSUN Headingley model includes a comprehensive depiction of the network (e.g. road layout; traffic control signals; junction turning movements; road section speed limits and road grade), a detailed description of vehicles within the network (e.g. traffic demand data, vehicle fleet composition and public transport lines) and defined values for controllable parameters within the model which reflect observations from the real world. Whilst an AIMSUN network simulation is in operation, data from the network model is extracted by an API, written at the University of Leeds ITS, which records the simulated movement of each vehicle in the network. The open source software 'R' is then used to process the AIMSUN API output data into a second-by-second drive cycle format for use in the instantaneous emission model PHEM. The simulated trajectory data along with a comprehensive description of the vehicle fleet (by vehicle type sub-category) and detail about each road section, enables PHEM to generate fuel consumption and pollutant emission estimates for each vehicle and road section in the simulated network.

This research aimed to deliver high-quality specification of all input parameters to the model in order to increase confidence in the accuracy of its emission estimate outputs. Methodologies for obtaining the necessary input data for the AIMSUN model were outlined in the chapter. In order to gather traffic fleet data of sufficient definition for the AIMSUN-PHEM coupled model a 24-hour ANPR survey was conducted within the network (Chapter 6.2). The extent of the model was captured by geo-referenced aerial photography (Chapter 6.3.1). Road section gradient was derived from a 5 m resolution DTM (Chapter 6.3.2). Traffic demand data were defined by a comprehensive database of MCC and ATC real-world data recorded throughout the network (Chapter 6.3.4). Traffic signal data were input from controller specifications supplied by LCC and the Headingley 'beta' model and confirmed by direct observation (Chapter 6.3.5). The public transport bus fleet was described in the simulation with timings from the official bus timetables (Chapter 6.3.6). Global parameters in the model (e.g. simulation step, reaction time and look-ahead distance) were employed from the previously calibrated Headingley beta AIMSUN model. To ensure that the movement of vehicles in the simulation reflected the real Headingley network, the AIMSUN model parameters which control vehicle movement were adjusted, default values being replaced with parameter estimates calculated directly from the instrumented vehicle GPS transient vehicle data from Chapter 3.

The emission modelling process in PHEM utilised a very detailed description of the Headingley vehicle fleet, with the proportion of each vehicle type in the fleet further sub-categorised by fuel type, Euro standard and weight. This detailed fleet description was informed by the vehicle data gathered by the ANPR survey on the A660. The definition by sub-category ensured the correct proportion of vehicles was allotted to each specific engine emission map in PHEM (Chapter 6.4.2). Processing the ANPR recorded number plate data through a vehicle information database also enabled the vehicle specification data for each vehicle sub-category to be updated to better represent vehicles travelling in the Headingley network (Chapter 6.4.4).

Chapter 6.3.8 and 6.3.9 describe the calibration and validation methodology respectively, with five time periods of the AIMSUN Headingley network model separately calibrated and validated, following the DfT transport analysis guidelines for link flow validation (DfT, 2014). For each time period, 10 replications were analysed. The traffic flow rates at 26 detector sites were validated at 30 minute intervals, ensuring the model conformed to the guidelines. Further to the AIMSUN calibration, a novel method for calibrating the coupled AIMSUN-PHEM model outputs with observed real-world data was developed and presented in Chapter 6.5.1. This method assessed both CO_2 emission by journey time and journey VSP power distributions for simulated and real-world data. This analysis concluded that although further sensitivity analysis of the vehicle

dynamic parameters could be conducted, which would likely improve the model, the calibrated Headingley network AIMSUN model produces second-by-second transient vehicle data which are closely representative of real-world driving. Furthermore, since the work reported in Chapter 5 demonstrated the ability of PHEM to generate accurate estimates of on-road emission using transient vehicle data, the coupled AIMSUN-PHEM model emission estimates can therefore be considered representative of real-world CO_2 exhaust emission.

The strength of the coupled model, enabling CO_2 emission estimates from the network to be calculated at a variety of scales, was demonstrated. The ability of this method to provide both aggregated and highly disaggregated emission factors has been shown from the calculation of individual vehicle type emission factors (by fuel type and emission standard) through to the calculation of total network CO_2 emission factors (Chapter 6.5.2).

The calibration of five separate time periods facilitates the use of the Headingley AIMSUN-PHEM model to estimate the diurnal variation of CO_2 emission in the network for each vehicle type, revealing significant differences between average CO_2 emission factors in the most congested PM peak traffic and in the least congested NI period (Chapter 6.5.3). From time period CO_2 emission estimates, 24-hour average emission factors were calculated for the vehicle type groups: 'Car-Petrol', 'Car-Diesel', 'Taxi', 'LCV', 'HGV' and 'Bus', which were compared directly to DEFRA's CO_2 conversion factors for company reporting (DEFRA, 2015b). This evaluation was valid due to the detailed comparison of the Headingley vehicle fleet with the DEFRA's NAEI base fleet composition data (Chapter 6.2). This ensured that any differences in the composition of the respective fleets were identified. The differences between the AIMSUN-PHEM model and DEFRAs CO_2 emission factors for each vehicle group were quantified and the magnitude of each difference was found to be justifiable (Chapter 6.5.4). The research highlighted, for example, that the DEFRA reported CO_2 emission factors for passenger car, which are based on NEDC type-approval CO_2 emission figures with a 15% uplift factor, may still be underestimates of real-world CO_2 emission. The average 24-hour AIMSUN-PHEM CO_2 emission factors for petrol and diesel passenger cars were respectively 24% and 40% greater than the NEDC generated average type-approval figures for those vehicle categories, which is in line with the scale of discrepancy reported between real-world and type-approval emission factors (Mock et al., 2015; Dings, 2013; ICCT, 2015).

Going further, the coupled model emission estimates were used to calculate the emission contribution to total fleet emission from the different vehicle groups, for both CO_2 and NO_x (which because of its impact on local air quality is an important area for future study). The

impact of incorporating road grade into the Headingley network model was analysed. The Headingley network AM simulation emission estimates were reprocessed in PHEM with road grade set to zero and then compared to the AM simulations with grade. When averaged over the entire network, the AM CO_2 emission factor was 4.8% greater when modelled with road grade than without, though as previously demonstrated in Chapter 5.8, over individual micro-scale road sections this difference is likely to be substantially greater.

The chapter concluded with a detailed evaluation of the strengths and limitations of the coupled AIMSUN-PHEM model methodology. As is the case for any model, a degree of simplification of the real-world was required, which limits the accuracy of both the AIMSUN simulation and the emission estimates of the PHEM model. These simplifications, therefore, influence the overall accuracy of the coupled model. Similarly, the quality and quantity of available data for input into the model have an important bearing on calibration and validation of the model and consequently the reliability of the modelled emission output. Throughout this research, every attempt was made to identify, obtain and utilise the most appropriate and highest quality data sources available, within the scope of a PhD research project. However, should better input data become available, these data can be incorporated into the existing Headingley AIMSUN-PHEM model to improve the calibration and validation and, ultimately, the accuracy of its real-world emission estimates. The bottom-up approach of the AIMSUN-PHEM model, generating second-by-second emission estimates for each simulated vehicle in the network from a calculated engine power output, enables analysis to be conducted at a wide variety of scales, from the emission of a single vehicle journey through to the combined emission of the entire vehicle fleet.

The development of an AIMSUN-PHEM coupled model enables a more accurate and detailed understanding of vehicle exhaust emission rates within a modelled network than is possible using commonly applied average speed emission tools. Calibration to reflect the different traffic flow time periods allows quantification of the impact that traffic demand has on on-road emission factors. The creation of base models with current input parameters allows an assessment to be made of the impact on exhaust emission that would occur as a result of potential changes to the network. The coupled model enables this kind of assessment both through parameter sensitivity analysis and scenario testing. The creation of an AIMSUN-PHEM coupled model for a given network could greatly improve the ability of transport planners to perform environmental assessments of potential schemes designed, for instance, to improve traffic flow in a network; to limit certain high emission vehicles, or to replace a proportion of the vehicle fleet with low emission vehicles.

The capability of the PHEM instantaneous emission model to generate estimates for NO_x, NO, CO, HC, and PM offers the potential to expand the scope of the coupled model from CO_2 to other exhaust pollutants which are likely to be of more interest from a local air quality perspective, due to their impact on human health. Further work to evaluate the accuracy of the real-world estimates of these pollutants is required, however, the work completed in this research to establish the accuracy of the AIMSUN-PHEM coupled model's ability to generate real-world estimates of CO_2 (through fuel consumption) and engine power output, is a very significant step towards modelling these other pollutants.

7.3 FULFILMENT OF THE AIMS AND OBJECTIVES OF THE RESEARCH

This section addresses the six research objectives set out in Chapter 1.2

1. Can the New European Driving Cycle (NEDC) vehicle type-approval CO_2 emission factors be considered good indicators of vehicle CO_2 emission in real-world driving?

The EU employs the New European Driving Cycle (NEDC) as the benchmark test for vehicle CO_2 type-approval emission, as part of the EU mandatory CO_2 regulations (EC, 2009b; ICCT, 2015). However several studies have revealed that real-world vehicle emission substantially exceeds the NEDC measured emission. These reports demonstrate an increasing divergence between real-world and test cycle measured CO_2 emission, with the gap widening from approximately 8% in 2001 to 40% in 2014. The NEDC was found to be a poor representation of real-world driving conditions (Dings, 2013) with a very smooth profile of acceleration and deceleration utilising only a small portion of a vehicles operating range. The greatest reason for the increasing gap in real-world and NEDC can be attributed to the increasing exploitation of flexibilities and loopholes within the road-load determination and type-approval testing, with manufacturers manipulating the test procedure to minimise CO_2 emission during the certification (Mock et al., 2015). So whilst the year-on-year reduction in new car CO_2 emission would seem to be reducing the UK vehicle fleet's GHG emission, in reality, it is likely that the real-world reduction in CO_2 emission is considerably smaller. The outcome is that NEDC type-approval CO_2 emission factors are becoming increasingly unrepresentative of real-world CO_2 emission.

The PEMS analysis, reported in Chapter 3, demonstrates the discrepancy between a test vehicle's type-approval NEDC CO_2 emission factor and its recorded levels of exhaust CO_2

emission in real-world driving conditions. The PEMS generated real-world CO_2 emission factors, over a 4.6 km route in an urban network (313 – 568 gCO_2/km), were found to be considerably greater than the test vehicle's NEDC test recorded CO_2 emission value (175 gCO_2/km). Furthermore, the real-world factors display significant variance depending on prevailing traffic conditions in the network. A single NEDC CO_2 emission factor is therefore highly unlikely to provide a good indication of a vehicle's CO_2 emission rate in real-world driving conditions. An accurate estimate for a vehicle's real-world CO_2 exhaust emission can only be achieved by models that have the capability to reflect the variability in CO_2 emission induced by on-road driving conditions.

2. How does micro-scale CO_2 emission vary in on-road driving conditions?

The variation in CO_2 emission associated with real-world driving has been demonstrated in this work through the micro-scale analysis of a PEMS data set (in Chapter 3). The research identified large spatial and temporal variability in CO_2 emission within the network, with a range of calculated CO_2 emission factors from 313 gCO_2/km to 586 gCO_2/km over 48 'identical' test laps. Each test lap was divided into 8 short micro-scale sections, from 175 m to 781 m in length, over which the CO_2 emission factors ranged from 219 gCO_2/km to 1,359 gCO_2/km. Over the 384 test section runs, 95.8% of real-world CO_2 emission factors over short sections were found to be greater than the certified urban test cycle emission of 253 gCO_2/km for the test vehicle and all the real-world emission factors were greater than the NEDC type-approval rated emission of 175 gCO_2/km for the vehicle.

Given the substantial variability in on-road exhaust CO_2 emission factors it is clear that, to generate an accurate estimate of the real-world CO_2 emission from a vehicle over short road sections, a micro-scale modelling process is required which can incorporate significant detail to describe both the on-road traffic conditions in the test network and the test vehicle itself.

3. How good are current emission models at estimating real-world micro-scale vehicle CO_2 emission?

In Chapter 4, the recorded second-by-second transient speed profiles, measured over the 48 Headingley test laps (described in Chapter 3), were used as input to four emission models, which employ different methodologies to generate emission estimates. Of these four models, MOVES and PHEM were shown to generate good estimates of the real-world CO_2 emission as measured

during the PEMS testing, whilst the EFT and HBEFA models were found to produce a significant underestimate of the on-road emission (on average approximately -40%).

The mean model percentage estimate of the PEMS measured CO_2 emission for each of the 48 test laps was found to be 95.7% for MOVES and 90.7% for PHEM. The accuracy decreased slightly, with percentage estimates of 93.8% and 89.6% for MOVES and PHEM respectively, when the test laps were divided into 384 micro-scale road sections (i.e. 8 sections in each of the 48 test laps). Analysis of each of the micro-scale sections revealed that PHEM, and to a lesser degree MOVES, performed relatively poorly when trying to assess the emission on the two short 'turning sections' (175 and 325 metres in length). It was hypothesised that the stop-start nature of these turning sections may have led to atypically high emission levels which don't reflect normal transient vehicle real-world drive cycles. Excluding these turning sections from the analysis, the mean model percentage estimate of the PEMS measured CO_2 emission for each of the 288 longer micro-scale sections (between 523 and 781 metres in length) was 94.7% for MOVES and 91.8% for PHEM.

In Chapter 5 the development of a LiDAR-GIS method for evaluating the road grade for each second of transient vehicle data enabled the MOVES and PHEM modelling of the lap and section data to be repeated with the inclusion of road grade as a parameter. The Chapter 4 analysis of modelled MOVES and PHEM CO_2 emission generated estimates assuming a flat network (i.e. 0 grade). The inclusion of road grade improved the mean model percentage estimate of the PEMS measured CO_2 emission for the 288 longer section to 95.8% for MOVES and 93.4% for PHEM. Both models had a similar MAPE values of 8.4% and 9.0% for MOVES and PHEM respectively, which describe the average error between the model and real-world emission values for each section. The main difference in the models, which can be best seen by comparing Figure 5.29 with Figure 5.31, is that whilst the PHEM model with road grade produces a constant CO_2 emission underestimate of around -6.5% over each of the sections, the MOVES model with grade estimates range from an overestimate of 1.3% to an underestimate of 7.6%. Therefore, whilst MOVES, in this instance, generated a more accurate average estimate of real-world micro-scale vehicle CO_2 emission, the PHEM CO_2 emission estimates were more consistent.

The accuracy of the MOVES model must largely be attributed to the fact that the test vehicle employed in the Headingley PEMS survey happened, coincidently, to be a good match with the American average 2005 petrol passenger car CO_2 emission factors within the MOVES model. The accuracy of the PHEM however, was the result of adjustment of the vehicle parameters in the PHEM model to specifically describe the test vehicle. The importance of this faculty of PHEM

model was demonstrated through comparison of the PHEM modelled CO_2 emission generated with the coded test vehicle parameters alongside the estimates from PHEM using only the default Euro 4, petrol, passenger car specification. The average percentage estimate of the PEMS measured CO_2 emission using the default PHEM Euro 4 vehicle was 74.6%, over the 384 test sections (without modelled road grade). In contrast, the PHEM model with the test vehicle specific data produced an average estimate of 89.6%. This analysis indicates that in order to represent specific vehicles or vehicle fleets in PHEM, it is important to ensure that the PHEM vehicle data are populated with average values that accurately represent each vehicle category in the modelled vehicle fleet.

The analysis in this thesis suggests that engine power based emission models like MOVES and PHEM, which are capable of producing second-by-second CO_2 emission estimates from a calculated engine power output, can be utilised to generate accurate estimates of real-world micro-scale vehicle CO_2 emission, whilst average speed emission models and traffic situation emission models cannot. However, in order to accurately generate CO_2 emission estimates, the research also demonstrated that road grade should be included with transient vehicle data and that vehicles should be accurately specified within the emission model. Although MOVES was on average marginally more accurate and was better able to model the shorter turning sections, the flexibility of PHEM to adjust the vehicle parameters and the fact that, unlike MOVES, it was developed to model the European vehicle fleet rather than the American fleet, made PHEM the most suitable choice for the coupled model.

4. To what degree does road grade influence vehicle CO_2 emission estimation at a micro-scale?

Power-based emission models such as MOVES and PHEM generate emission estimates through the derivation of second-by-second of engine power output from vehicle activity data. In order to generate accurate estimates of engine power output, the influence of road grade must be accounted for, as the combination of the gradient of the road with the force of gravity will contribute to acceleration or deceleration of the vehicle. This effect necessitates the inclusion of a road grade estimate with each second of transient vehicle data.

Chapter 5.3 demonstrated the potential importance of road grade through a sensitivity analysis. Using the VSP equation employed by the MOVES emission model (Equation 5.2), hypothetical VSP values over the range of speeds likely in the network were generated over a series of road

grades (-6%, -3%, 0%, 3% and 6%) and under three acceleration scenarios; acceleration (0.5 m/s^2), cruise (0 m/s^2) and deceleration (-0.5 m/s^2). Average real-world CO_2 emission rates for the test vehicle were calculated in 21 VSP 'bins' that described the full range of engine power outputs (Table 5.1). Using the VSP-CO_2 emission bins, estimates were generated of the expected CO_2 emission at each of the hypothetical VSP values, enabling analysis of the effect of road grade under each of the three acceleration scenarios. This research demonstrated that a failure to account for road grade could lead to a substantial error in the estimation of CO_2 emission. Even at the relatively modest road grades analysed in this study, when travelling at 30 mph (48 km/h), the expected rate of CO_2 emission was shown to be between 1.3 and 2.9 times greater with inclusion of positive road grades at +3% and +6% in the VSP calculation versus the generated emission with the road grade modelled as flat. Likewise, the exclusion of negative road grades in the calculation of VSP was shown to lead to a potential overestimation of modelled CO_2 emission of up to 60% on downhill sections. For this reason, it is essential that a road grade value is set for each second of transient vehicle data to describe the real-world topography.

The LiDAR-GIS method developed in this study and described in Chapter 5 provides a simple methodology for calculating 1 Hz road grades from PEMS recorded GPS vehicle data, which was demonstrated to improve the modelling of CO_2 emission for the Headingley PEMS data set. This was shown both through increased correlation in the linear relationship between positive VSP and CO_2 with the addition of road grade in Figure 5.27 and the improvement of PHEM and MOVES road section emission estimates in Figure 5.29 and Figure 5.31. This improvement was especially clear in Section 8 from the Headingley test lap. In this uphill section, the addition of the 1 Hz road grade improved the average PHEM modelled CO_2 estimate of the PEMS measured CO_2 emission from 80.4% without road grade to 94.0% and the MOVES estimate from 80.5% to 93.5%.

The study has demonstrated that definition of road grade for micro-scale road section emission modelling is vital. Whilst at larger scales the overestimation of emission on downhill sections, will mask the underestimation of emission on uphill sections to an extent, as demonstrated in Chapter 5.8 and 6.5.6, it is incorrect to assume that these errors completely offset each other. In a micro-scale analysis, short road sections can have very steep average road grades. If such grades are not accurately specified there will be significant error in the modelled emission estimates.

5. Can simulated vehicle activity generate CO_2 emission estimates comparable to the CO_2 emission recorded in real-world testing?

The work in Chapters 4 and 5 demonstrates that the instantaneous emission model PHEM is able to generate accurate estimates of micro-scale on-road vehicle exhaust CO_2 emission by utilising second-by-second PEMS recorded GPS transient vehicle speed data with LiDAR-GIS generated road grade values alongside adjustment to the PHEM vehicle specifications to describe the specific test vehicle.

Development of the Headingley AIMSUN network, described in Chapter 6, enabled the generation of simulated second-by-second data for all vehicles in the network. The work in Chapter 6.5.1 investigated whether AIMSUN simulated vehicle speed profiles, for passenger cars with road grade defined by road link slope percentage, were able to generate micro-scale CO_2 emission estimates from PHEM of comparable accuracy to the CO_2 emission estimates generated in PHEM using the PEMS measured tracking data and LiDAR-GIS road grade.

A summary of the analysis from Chapter 6.5.1 is presented in Table 7.1. In general, the AIMSUN-PHEM model generated average simulated vehicles journey times comparable to the PEMS recorded journey times over the northbound and southbound 1.5 km sections of the A660, for each of the time periods. The range of simulated journey times in most cases was similar to the range of recorded real-world journeys, which is significant given the substantial variance in the observed journey times during some of the time periods. The notable exception is during the IP period when the simulated journey times were significantly quicker than recorded by the PEMS instrumented vehicle. This suggests that the Headingley AIMSUN network simulation may not have correctly captured congestion on the A660 during the IP time period. Given the limited number of instrumented vehicle journeys recorded in the network, it is impossible to know without further data, whether the PEMS recorded journey times give a true reflection of the average journey times in the Headingley network. The PEMS values were collected over one week (Chapter 3.2.1) while the traffic flow in the AIMSUN Headingley network is an amalgamation of multiple MCC and ATC surveys (Chapter 6.3.4) recorded in different months and different years. It is possible that seasonal variations in traffic flow mean the PEMS recorded journeys do not reflect the average traffic demand in the Headingley network. As discussed in Chapter 6.5.1, a further average journey time data set from Trafficmaster, comprising approximately 1,500 observations, was made available by Leeds City Council, although data were only available for the AM and PM periods. As shown in Table 7.1, for the AM and PM northbound analysis, the AIMSUN simulated average journey time is significantly closer to the

Trafficmaster average journey time than the PEMS recorded value. The acquisition of further journey time data for the other time periods would help in ensuring that the model is properly calibrated.

Table 7.1: Comparison of AIMSUN-PHEM Simulated Model to PEMS and $PHEM_G$ Data

Time Period	AM	AM	IP	IP	PM	PM	EV	EV
Direction (Northbound / Southbound)	N	S	N	S	N	S	N	S
Average difference between the Simulated and $PHEM_G$ CO_2 Emission Factors (%)	-0.2 %	-1.2 %	-3.5%	-6.7 %	+ 0.7 %	-5.8 %	-8.2 %	-6.1 %
Number of PEMS Recordings	15	15	14	14	11	11	6	6
Number of Simulated Vehicles	3582	4722	2288	2032	3162	3571	3528	2596
Range of PEMS Journey Times (s)	171 - 680	218 - 702	208 - 438	194 - 381	354 - 861	215 - 479	153 - 231	147 - 239
Range of Simulated Journey Times (s)	133 - 540	149 - 728	128 - 318	126 - 319	299 - 851	146 - 691	118 - 322	120 - 334
PEMS Average Journey Time (s)	374	378	338	268	627	302	199	193
Simulated Average Journey Time (s)	244	333	193	191	540	351	193	192
Trafficmaster Average Journey Time (s)	272	303	-	-	535	288	-	-

Ideally, the AIMSUN-PHEM model should have been able to generate CO_2 emission factors very similar to those recorded directly by the PEMS real-world testing. However, as shown in Chapter 5.7.1, there was an average difference between the $PHEM_G$ section (excluding the two short turning sections) estimates of CO_2 emission and the PEMS recorded real-world CO_2 emission of between 6% to 9%. This discrepancy occurs even though the CO_2 emission estimates from $PHEM_G$ were calculated directly from real-world drive cycle data and 1 Hz LiDAR-GIS road grade. To check whether the AIMSUN simulated second-by-second vehicle speed profiles were a good approximation of the real-world GPS recorded drive cycle data, it was more important to test the ability of the AIMSUN-PHEM model to reproduce the $PHEM_G$ CO_2 emission values, rather than the PEMS measured real-world CO_2 emission figures.

To assess the accuracy of the AIMSUN-PHEM model CO_2 emission estimates, lines of best fit were calculated through the journey time and emission plots from the AIMSUN-PHEM model, and the $PHEM_G$ CO_2 emission estimates (see Figure 6.18 to Figure 6.25). The average difference between these lines of best fit was then calculated across the range of PEMS observed journey times. These differences are displayed in Table 7.1. The line of best fit for the simulated CO_2 emission generally provides a close fit to that generated for the $PHEM_G$ emission estimates. Inspection of the $PHEM_G$ results of CO_2 emission plotted by journey time, in Figures 6.18 through 6.25, show that the majority overlie simulated points of CO_2 emission from the AIMSUN-PHEM model. Although the average differences between the PHEM generated CO_2 emission estimates from the PEMS drive cycle data and those from the simulated vehicle data are relatively small,

it is likely that the limited sample of PEMS data is a factor in this observed difference, with fewer real-world emission / journey time points leading to potentially unrepresentative lines of best fit. Further instrumented vehicle GPS recorded journey data from the network would help clarify that the model is properly calibrated.

As a further check to ensure that the AIMSUN simulated second-by-second vehicle activity data were similar to the real-world data, the VSP profiles for the simulated data were compared to the VSP profiles of the PEMS recorded tracking data for similar length journeys. A poor match between the simulated and measured VSP would indicate that the acceleration parameters within the AIMSUN model are incorrect and / or road grade is incorrectly represented within the simulation. This analysis is presented in Figures 6.28 to 6.31. Failure to capture high positive engine power output properly may lead to erroneous calculations of CO_2 emission. Accurately calibrating this element of the model is likely more important for other pollutant species. This would be the case for exhaust emission species where there is an exponential increase in emission with increased positive engine power output, compared to the linear increase displayed with CO_2.

The analysis of the simulated and real-world power distributions in this study demonstrate that the calibrated AIMSUN simulations produce second-by-second transient vehicle data that are representative of real-world driving. It is worth noting that, as the vehicle dynamics parameters in AIMSUN have been calibrated using data from the test vehicle, the good fit of the model to the real-world data is likely related to that calibration and may not be wholly representative of the full range of passenger cars. Further real-world PEMS data recorded in the network, for other vehicles and vehicle types, would improve the quality of the AIMSUN parameter inputs and lead to a more accurate description of the variability in these dynamic parameters.

Although this research has established that simulated second-by-second vehicle transient data can be generated which are sufficiently accurate to generate reliable real-world estimates of second-by-second vehicle exhaust CO_2 emission, it is vital to stress that the AIMSUN simulation parameters have to be properly calibrated to ensure that the movement of simulated vehicles reflects the real world. A significant element of future work using the AIMSUN-PHEM model will be improving the calibration of the AIMSUN model input parameters with use of additional real-world data.

6. To what degree are there diurnal variations in CO_2 emission factors for different vehicle types in an urban traffic network?

The calibration of the AIMSUN-PHEM coupled model for five different time periods enabled analysis of the diurnal variation in average exhaust CO_2 emission for each of the vehicle types in the network and the overall vehicle fleet. This analysis is presented in Chapter 6.5.3.

The ANPR survey utilised in this research to provide a detailed description of the vehicle fleet in the Headingley network captured both the diurnal variation in the traffic flow on the A660 and the changes in the composition of the vehicle fleet (Chapter 6.2.8). Rather than using one homogeneous vehicle fleet to describe the simulated Headingley fleet, the ANPR survey enabled the AIMSUN-PHEM model to be separately calibrated to describe five distinct time periods (described in Chapter 6.3.7), which reflected differing traffic flow conditions in the network. For each of the 2-hour simulated time periods, the coupled model describes the period-specific traffic flows and junction turning movements; the signal timings; the vehicle fleet composition by vehicle type and by sub-category (i.e. Euro standard, fuel type, vehicle weight); the scheduled bus service; and the dynamic parameters for the passenger car vehicle category. The simulated AM, IP, PM, NI and EV periods therefore generate bespoke emission factors specific to that time period.

Chapter 6.5.3 presents the diurnal variation in the Headingley network CO_2 emission for Petrol Cars and Taxis, Diesel Cars and Taxis, LCVs, HGVs, Buses and for the aggregate vehicle fleet. The Headingley network AIMSUN-PHEM modelled CO_2 emission factors vary considerably by time period for each of the vehicle types. The average emission factor increases substantially, for each vehicle type, from the free flow conditions of the NI period to the most congested traffic in the PM period. For example for cars and taxis, which form the bulk of the vehicle fleet in each time period (>75%, Table 6.9), the average CO_2 emission factor was calculated to be 43.5% greater for petrol and 45.5% greater for diesel in the PM period than in the NI period. The strongest influence on the variability in the CO_2 emission factors is traffic flow in the network, with time periods that experience the most severe congestion having the greatest average rate of CO_2 emission. There are however noticeable discrepancies where changes in the vehicle fleet mask or exacerbate this trend. This is demonstrated in the HGV fleet CO_2 emission factors, where the PM factor is 174.3% greater than the average NI rate. The reason for this large disparity is that the modelled NI fleet (informed by the ANPR survey) contains no large HGV category Rigid 26 t vehicle. Likewise for the Bus fleet the average PM CO_2 emission rate is 90.7% greater than the NI period rate because all buses recorded in the NI period were single-deck.

Figure 6.44 displays the aggregate vehicle fleet average CO_2 emission factors, with an average emission of 265.1, 276.6, 275.9, 205.1 and 177.0 gCO_2/km for the AM, IP, PM, EV and NI periods respectively. The surprisingly high IP period average CO_2 emission is the result of a greater percentage of HGV vehicles in that time period than in any other modelled time period (Figure 6.12). The comprehensive input data necessary for construction of an AIMSUN-PHEM coupled model enables the calculation of very specific emission factors but also facilitates detailed analysis of the particular circumstances that influence the computation of each emission factor. As a result, it is a very useful tool for analysing network emission.

The AIMSUN-PHEM model revealed substantial diurnal variation in CO_2 emission factors for each of the vehicle types in the network and the entire vehicle fleet. This gives an indication of the potential impact that measures to reduce traffic congestion in a network could have on decreasing exhaust CO_2 emission.

7.4 CONCLUSIONS

The focus of this thesis was to improve the estimation of real-world CO_2 emission by developing and demonstrating a coupled traffic micro-simulation and instantaneous emission model. It would have been a relatively straightforward task to select a piece of modelling software, enter the necessary input data, run the model, and generate model outputs and make the assumption that those outputs are an accurate reflection of the real-world. The whole process could have been performed with limited consideration of the weaknesses of the input data, without an understanding the necessary simplifying assumptions incorporated into the design of the model and with limited validation of the model output against real-world data.

For example, DEFRA's Emissions Factors Toolkit provides a simple tool for UK local government authorities to fulfil their duty to evaluate the on-road vehicle emission. However, this EFT methodology incorporates a relatively simplified vehicle fleet composition, utilises an average speed emission methodology and excludes the impact of road grade. It assesses real-world CO_2 emission based on NEDC laboratory test cycle emission data, demonstrated not to reflect real-world operation (Mock et al., 2015; ICCT, 2015), and applies an uplift factor to attempt to compensate for this error (Boulter et al., 2009). The exclusion of road grade relies on an erroneous assumption (as demonstrated in Chapter 5) that underestimates of emission on uphill road sections within a network are offset by overestimates of emission on downhill sections.

Such simplified average factor methodologies largely ignore the physical processes that result in vehicle exhaust emission and, as a result, are almost certain to generate an inaccurate estimate of on-road exhaust emissions for a specific test road or network. Despite the recognised limitations, the use of average speed emission models is standard for both the management of local air quality (DEFRA, 2009) and local CO_2 emission estimation (GOV.UK, 2017b) in the UK. Of concern is the fact that the output from such models, at a network level, is largely unchallenged, as the validity of the emission estimates is difficult to verify due to the impossibility of directly measuring real-world network scale emission. The work reported in Chapter 4.3 of this thesis attempted to link the EFT emission estimates back to measured real-world CO_2 emission and confirmed that the EFT substantially underestimates the real-world on-road CO_2 emission of a test vehicle. Although this analysis tested only one passenger car, so cannot claim to represent the emission of all vehicles, the difference between the model and reality likely reflects the limitations to the average speed methodology that are reported in the literature (Panis et al., 2006; Frey et al., 2010; Barlow and Boulter, 2009).

To overcome the weakness of average speed emission factor models, the work in this thesis developed a coupled traffic simulation and vehicle emission methodology. This coupled model methodology applied a bottom-up approach, utilising a highly defined and calibrated computer simulated road network to generate accurate second-by-second engine power output estimates for every simulated vehicle within the network model. Through reference to detailed engine emission maps, the second-by-second engine power output estimates were used to calculate a CO_2 exhaust emission for each second of data, for every vehicle independently. It was demonstrated that each second of CO_2 emission data could then be aggregated to generate CO_2 emission factors at a desired spatial level, at any chosen time interval, for an individual vehicle, or a vehicle type, through to emission factors for the entire fleet. Further, it was demonstrated that every simulated vehicle journey could be validated against real-world data (where PEMS survey data exist) to confirm that the modelled vehicle moves in the network in a way that reflects reality and that the simulated emission estimate reflects real-world driving emission. This level of validation gives a high level of confidence that the aggregate vehicle fleet network emission factors are an accurate reflection of the real-world emission.

At each stage of the work in this thesis, the goal has been to ensure that the modelled micro-scale exhaust CO_2 emission is as accurate an estimate of the real-world on-road emission as possible. Chapter 2 set the context for the work, explaining the importance of limiting anthropogenic CO_2 emission due to its role as a driver of global climate change; highlighting the significant contribution road transportation makes to the UK's CO_2 emission; discussing efforts

made in the EU to reduce CO_2 emission from the vehicle fleet and identifying the widening discrepancy between the manufacturers' CO_2 emission figures for vehicles from type-approval testing and the real-world emission of CO_2 of vehicles when being driven on-road. As a result of the unreliability of the type-approval figures as indicators of real-world CO_2 emission, Chapter 3 presented a new detailed analysis of a PEMS data set recorded in the Headingley network, generating gCO_2/km emission factors over a test lap and micro-scale road sections. This real-world on-road CO_2 emission data were used in Chapter 4 to test the capability of four different emission model methodologies to estimate real-world exhaust CO_2 emission. It was identified that the engine power based emission models, MOVES and PHEM, produced a substantially more accurate micro-scale CO_2 emission estimates than the average-speed emission models EFT and HBEFA. However, the study also revealed significant section-by-section variability in the accuracy of the MOVES and PHEM CO_2 emission estimates, which was hypothesised to be due to the impact of road grade. The work reported in Chapter 5 demonstrated the influence of road grade on vehicle CO_2 emission and devised a novel LiDAR-GIS method for discerning a second-by-second road grade estimate, from GPS recorded position data, which was shown to largely resolve the section-by-section variability of the MOVES and PHEM CO_2 emission estimates reported in Chapter 4. As a result of the analysis in Chapters 4 and 5, PHEM was chosen as the most appropriate emission model for incorporation into the coupled model methodology as it produced more consistent real-world CO_2 emission estimates than MOVES, its default settings were developed for the EU vehicle fleet and it has the flexibility to allow adjustment to the vehicle specifications. Chapter 6, building on the work of the previous chapters, reports the development of a coupled traffic simulation and vehicle emission model, using the microscopic traffic simulator software AIMSUN and the instantaneous emission model PHEM. A model was built in AIMSUN to describe the Headingley network with input data to describe five different time periods, which defined different levels of congestion in the network. Every effort was made, within the realistic scope of PhD research, to obtain the best available input data, which included a detailed description of the Headingley vehicle fleet, road grade for each section, traffic demand data from a comprehensive database of MCC and ATC surveys and vehicle dynamic parameters from real-world data. The AIMSUN model traffic flows were calibrated and validated at 26 points in the network, with ten AIMSUN simulation runs for each time period. An API written in the ITS, at the University of Leeds, extracted vehicle speed and road grade data for all vehicles in each simulation from the AIMSUN Headingley network, which was converted using the open source software 'R' into a drive cycle format for use in PHEM. This simulated drive cycle data informed the calculation of instantaneous engine power output for each second and, along with a detailed description of the vehicle fleet, enabled PHEM to generate fuel consumption and pollutant emission estimates for each vehicle and road section

in the simulated network. The fuel consumption figures were converted into CO_2 emission estimates using the 2016 UK Government conversion factors for GHG reporting for diesel and petrol. A novel method for validating coupled emission models was demonstrated in Chapter 6.5.1 with a comparison of simulated model journeys and the real-world data, evaluating both the CO_2 emission by journey time and the VSP distributions for similar duration journeys. Overall, although further calibration work could be done to improve the model, the AIMSUN simulation was found to produce second-by-second transient vehicle data representative of real-world driving and the simulated emission estimates were found to be consistent with the on-road PEMS measured values. The ability of the coupled model to produce aggregated and highly disaggregated emission factors was demonstrated with emission factors in gCO_2/km calculated for the fleet, down to individual vehicle sub-categories, by Euro standard and fuel type. The calibration of the model for five separate time periods enabled evaluation of the diurnal variation in CO_2 emission factor in the Headingley network, highlighting the considerable increase in gCO_2/km from free flowing traffic to the most congested traffic conditions. From the five time period models, daily average gCO_2/km emission factors were calculated and compared to the DEFRA's NAEI emission factors, finding explainable differences for each vehicle type. Chapter 6.6 presented a thorough review of the limitations of the coupled model developed in this thesis but even recognising these limitations, the work done to develop, calibrate and validate the coupled model, mean that this Headingley network AIMSUN-PHEM model should be considered the best specified coupled traffic simulation and vehicle emission model in published literature. As discussed in Chapter 6.1, the coupled model presented in this research is of a scale and definition not found in previous studies, combining one of the world's most sophisticated traffic simulation tools with Europe's most comprehensive instantaneous exhaust emission model.

The coupled model methodology enables an extremely detailed understanding of emission within the network, permitting analysis of the emission contribution from each of the elements within the model. It also allows for scenario testing, in which any change to the network which can be modelled in AIMSUN (e.g. changes to signal timings; changes to the fleet composition; the addition of new roads to the network; the introduction of a bus lane) and then processed in PHEM to generate new emission estimates. These can be assessed against the base model to evaluate the potential effect of the proposed change(s) on exhaust emission in the network.

How does the coupled model relate back to the discussion in Chapter 2 of the UK's target of lowering its GHG emission to 80% of the 1990 baseline by 2050? Since there is no panacea that will totally eliminate CO_2 emission from road transport in the near future, it is likely that there

will be an evolution to a near zero on-road CO_2 emission vehicle fleet with a gradual, hopefully accelerating, transition from the current dominance of internal combustion engine powered vehicles to a potentially all-electric future vehicle fleet. There will be many technological, infrastructural and economic difficulties to overcome, coupled with a time delay associated with fleet turnover, before the UK will deliver a complete decarbonisation of the sector.

The coupled model methodology developed in this thesis could significantly aid efforts to reduce CO_2 emission in the interim. The transition to zero-emission vehicles necessitates investment both in new infrastructure and grants to reduce the price paid by consumers for being early adopters of a new technology. These costs are likely to be significant. An accurate appraisal of the possible reduction in CO_2 as a result of these policies is important in justifying the expense of such projects. For example, scenario testing through the coupled methodology could allow the potential emission reduction to be calculated for replacement of a diesel bus fleet with an electric bus fleet. The coupled model would also incorporate the improved acceleration of electric vehicles that might influence the entire flow of traffic in the network, potentially reducing congestion and emission. Similarly, the CO_2 emission of a network vehicle fleet could be calculated with a hypothetical percentage of electric vehicles to map out how emission in the network might be changed with varying degrees of incentivisation of the uptake of electric vehicles.

Although a complete behavioural and technology change is necessary to decarbonise the road vehicle fleet by 2050, in the interim period, as demonstrated by the diurnal variation in emission calculated for the Headingley network in Chapter 6.5.3, efforts to reduce congestion could lead to significant reductions in CO_2 emission. Scenario testing of proposals to improve traffic flow in a network employing a coupled model would give an accurate estimate of the probable CO_2 emission reduction. The estimates can be used to provide the necessary evidence for planners and policymakers to properly appraise the environmental impact of changes to the network and enable rigorous cost-benefit analysis to be conducted.

Whilst the Headingley AIMSUN-PHEM model was developed for estimation of on-road CO_2 emission, possibly of greater importance, in future, could be its ability to generate pollutant emission estimates for other exhaust emission species which have a detrimental impact on human health through their impact on local air quality. Further calibration and validation work, with appraisal against real-world PEMS emission data, is necessary to verify the accuracy of the AIMSUN-PHEM model estimates of other exhaust pollutant species (i.e. NO_x, NO, CO, HC and PM). However, accurate micro-scale analysis of the emission of these pollutants for road

sections and junctions, and the ability to generate hourly emission factors for input into air quality microscopic dispersion models, could greatly enhance the ability of local authorities to put in place effective and efficient policies to manage local air quality at points where the EU pollution level limits are frequently exceeded.

In the past average speed emission models provided the only viable means of generating network scale emission estimates. It is only relatively recently that a coupled traffic simulation and vehicle emission model methodology has become feasible on the back of increased computing power, the development of traffic network modelling tools like AIMSUN and the extensive collection of fleet-wide vehicle emission measurements in PHEM. A limiting factor for the coupled model methodology described in this research is the substantial volume of input data required to create a modelled network of sufficient detail and accuracy that the simulated movement of vehicles reflects the behaviour of vehicles in the real-world. However, the increasing availability of detailed traffic data, outside of the traditional ATC and MCC survey data, through sources such as automated real-time traffic flow monitoring, has seen a growing number of developers creating detailed AIMSUN network models to improve traffic management in and around cities, with AIMSUN reporting "thousands of licensed users in government agencies, consultancies and universities all over the world" (AIMSUN, 2017). This research demonstrated that, if these AIMSUN models are properly calibrated and validated, so that the simulated drive cycle data and road grade result in engine power outputs which are representative of the real world, that it is relatively straightforward to couple the simulation to a powerful instantaneous emission model and generate very accurate estimates of emission for each simulated vehicle. As Chapter 6.6 highlighted, there are many ways in which the Headingley AIMSUN-PHEM model and any future coupled model could be improved. However, the AIMSUN-PHEM model framework presented in this thesis marks a significant step forward in the modelling of on-road transport emission, which should eventually see the replacement of average speed emission factors models with second-by-second power based coupled traffic simulation and vehicle emission models for micro-scale and network emission estimation.

7.5 FUTURE WORK

As highlighted in the thesis, there are a number of areas that would benefit from further investigation to improve calibration and validation. The development of the LiDAR-GIS road grade estimation method and the coupled AIMSUN-PHEM simulated traffic emission model have also enabled a number of possible avenues for further research.

7.5.1 Development of the LiDAR-GIS method for 1 Hz Road Grade Estimation

With recognised deficiencies in accurately assessing on-road vehicle emission using the laboratory based NEDC type-approval emission procedures, on-road PEMS analysis of exhaust emission, which will be incorporated into future type-approval measurement through the EC's Real Driving Emissions (RDE) legislation (EC, 2016), is set to become increasingly important. As demonstrated in Chapters 3, 4 and 5 to fully understand on-road emission measurements from PEMS testing, it is vital to have a detailed appreciation of the road grade on which a test vehicle was travelling. Further development of the LiDAR-GIS method for calculating second-by-second road grade could improve the technique and validate its use in determining on-road emission rates both for CO_2 and other exhaust pollutant species. As shown in the thesis, a highly accurate tool for road 1 Hz road grade estimation significantly improves the analysis of PEMS data. A speed profile in combination with road grade enables calculation of the instantaneous power output of a vehicle, which has a demonstrable relationship to fuel consumption and vehicle emissions. Thus further work could include:

- Writing the code to automate the procedure in ArcGIS for obtaining altitude data from a DTM for each second of GPS recorded transient vehicle data.
- Testing of the LiDAR-GIS generated altitude values against direct land survey measurements, to calibrate the look ahead and look behind smoothing distances and to verify the accuracy of this method of road grade determination.
- Testing the accuracy of the LiDAR-GIS grade estimates against the stipulated EC RDE method, which relies on, and is potentially limited by, the smoothing of GPS measured altitude.
- Using the LiDAR-GIS method and PHEM to generate on-road exhaust emission estimates for other vehicle types and other exhaust pollutants (e.g. NO_X and PM) and to test the accuracy of such estimates against real-world PEMS survey data.

7.5.2 Improvement of the AIMSUN-PHEM Coupled Model

As licensed commercial software, both AIMSUN and PHEM continue to be developed by TSS and the TU-Graz, respectively, so as the functionality of these models is upgraded, the accuracy of the coupled model emission estimates should be enhanced. As an example, an important area of development for PHEM will be the inclusion of engine maps to represent the emissions from hybrid-electric vehicles. Whilst the observed number of hybrid vehicles in the Headingley survey was low, this segment of the vehicle fleet is projected to increase significantly with tightening vehicle CO_2 emission legislation across Europe. Although various elements of the coupled

model, such as upgrades to the vehicle behavioural models in AIMSUN and expansion of vehicle type engine emission maps in PHEM, are under the direct control of their respective developers, there remain a significant number of opportunities to improve the Headingley network AIMSUN-PHEM model beyond these. Chapter 6.6 provided a detailed description of the limitations of the coupled model. Theoretically, each of these areas of limitation could be improved with further work, which mainly would entail obtaining better data sets for the definition of parameters within the model. However, the most important elements to address are:

- **AIMSUN model journey time validation.** As described in Chapter 6.3.9, in order to meet the WebTag guidelines (DfT, 2014) for model validation, an evaluation of simulated and real-world journey times in the network should be completed. Although Chapter 6.5.1 presented comparison between the simulated journeys generated by the Headingley network model and the PEMS instrumented vehicle journeys, the small sample size of the PEMS data set limits the significance of this analysis. The AM and PM simulated journeys were assessed against a larger 'Trafficmaster' journey time data set (average data for ≈ 1,500 vehicles) made available by Leeds City Council, which mostly proved to be a better match to the AIMSUN simulated average journey time than was the case for the relatively small sample of PEMS data (see Table 7.1). However, these Trafficmaster data was not available for all modelled time periods at the time of model validation. Future work should acquire further recorded vehicle journey time data for roads within the network, especially for the IP, EV and NI periods. This would enable a more robust validation of the model, although some consideration of the appropriateness of the WebTag guidelines for the Headingley network, which stipulate that modelled journey times must be within ±15% or 1 minute (whichever is the larger) of observed average time for > 85% of routes, may be necessary given the wide range of observed journey times in the congested time periods.

- **Description of vehicle dynamic parameters.** A number of studies noted that the default parameters which control vehicle movement in AIMSUN resulted in vehicle behaviour that was not representative of observed real-world behaviours. The vehicle parameters in the AIMSUN Headingly network model were, therefore, amended using GPS data recorded in the network to inform the movement of the car, taxi and LCV vehicle categories. Although the comparison of simulated and real-world journeys, reported in Chapter 6.5.1, showed the simulated vehicle behaviour to be a relatively good fit for the real-world data, the new parameter values were drawn from a very small sample of PEMS data, with one driver, and it was limited to only a few vehicle categories. Future study is required to develop this area of the model. The collection of further real-world GPS movement data for all vehicle types

and additional work to identify the appropriate methodology for determining the acceleration parameters from such real-world data would improve the ability of the model to generate simulated vehicle behaviour which is a close approximation to that of vehicles in the real world. A possible avenue to explore is the acquisition of telematics data from GPS tracking devices fitted in vehicles for insurance purposes (Pellecuer et al., 2016). A large second-by-second vehicle tracking data set would enable a more accurate appraisal of the vehicle dynamics for a wide range of vehicles and multiple drivers. This could also facilitate the segregation of the modelled 'Cars' vehicle group into smaller more specific car categories. It would also be valuable to explore the possibility of collaboration with other AIMSUN users to discuss all parameter inputs, in order to establish a best practice methodology for selecting or generating parameter values to replace the AIMSUN defaults, perhaps establishing a shared database of input values for particular traffic network settings. The collection of further GPS data is also vital for the continued development of the calibration and validation methodology described in Chapter 6.5.1, in which real-world and simulated vehicle VSP profiles were compared over similar journey times.

- **Collection of further PEMS data for calibration and validation of the model.** Along with further GPS tracking data for improving the vehicle behaviour parameters in AIMSUN, further PEMS exhaust emission surveys within the network should be conducted, using a range of vehicle types, to provide a greater body of evidence that the PHEM model outputs are representative of real-world emission. The PEMS surveys should incorporate the measurement of as wide a range of exhaust emission species as feasible, however, NO_x should be given special consideration due to its impact on human health. Such data would help confirm that the coupled AIMSUN-PHEM model is capable of generating micro-scale estimates of emission for a range of emission species and not only CO_2.

- **Description of the network vehicle fleet composition.** Whilst the ANPR data described in Chapter 6.2 provided a very detailed description of the Headingley vehicle fleet, the ANPR survey was recorded over only one weekday. In order to identify if the data recorded was typical of the network vehicle fleet on other days of the week, and potentially at different times of the year, a larger scale ANPR survey should be conducted.

- **Updating the AIMSUN network traffic input flows.** MCC and ATC survey data collected by Leeds City Council provided the traffic flow data for the network. However, as mentioned in Chapter 6.3.4, these data, from 62 surveys, were collected over an 8 year time interval. Ideally, all the input data would have been collected at one time. Cost permitting, a large

traffic survey conducted simultaneously, counting vehicle flow across the multiple entry points into the network, would help to alleviate calibration issues resulting from weekly and seasonal variations in traffic flow. In future, automated real-time traffic flow monitoring may become much more commonplace (Bottino et al., 2016). The availability of such data sets, from the continuous monitoring of traffic flows in a network, could greatly enhance the field of traffic simulation modelling and result in improved emission estimates from coupled emission models.

- **Conducting a survey of pedestrian crossings.** The Headingley network model contained a total of twelve pedestrian crossings. Detailed information regarding the frequency of use and the signal time duration was not available during the construction of the AIMSUN network. As a result, the pedestrian crossings were coded from limited field observation at each location. As Headingley is an urban network with a significant number of pedestrians throughout the day, especially at the peak AM and PM time periods, the frequency with which pedestrian crossings halt traffic flow necessitates further study. A more robust survey of the crossings in the network would greatly improve the accuracy of this element of the AIMSUN simulation by better describing the interaction of pedestrians and vehicles in the network.

7.5.3 Future Study using the AIMSUN-PHEM Model

The development of the coupled AIMSUN-PHEM traffic simulation and emission model in this research, and the bottom-up approach it employs, enables analysis of network emission at a resolution which is simply impossible for any other network emission model. The ability to analyse the model output at different spatial scales, at any desired time interval, and at levels from a single vehicle, to that of a specific vehicle type, through to that of the entire fleet, with sub-category assessment by Euro emission standard and fuel type, makes the coupled model a highly dexterous tool for both understanding current vehicle exhaust emission with the network and assessing the effect on exhaust emission of changes to the network. Potential avenues for future study include:

- **Sensitivity analysis of model parameters.** Development of the base Headingley network model in this research, allows a detailed assessment to be made of the influence on exhaust emission from each of the AIMSUN input parameters, including vehicle acceleration, road grade and speed limits. Varying each of the model parameters and analysing the impact this has on the modelled emission estimates would highlight the most important parameters for emission and indicate where further data are required to ensure that parameter estimates

are accurate. Sensitivity analysis would also help to define the likely range of error for the model emission estimates.

- **Expansion of the model to other exhaust emission species.** Road transport is one of the main reasons why many EU cities are currently in breach of air pollution limits. With 70,000 premature deaths a year in the EU linked to NO_2, exhaust emissions from road transport are of major concern to the EC which is leading substantial efforts to reduce the emission of pollutants that affect air quality (EC, 2017). Along with CO_2 emission (derived from fuel consumption), the AIMSUN-PHEM model can be employed to generate high resolution emission estimates for the pollutants NO_x, NO, CO, HC and PM. Further work needs to be conducted to evaluate the accuracy of the simulated emission estimates for these pollutants against real-world measurements. The work performed in this thesis confirmed that the model generated VSP profiles, and therefore the CO_2 emission estimates, reflected real-world values. This should give some confidence in the accuracy of the model estimates for these further exhaust emission species, where the emission of these species is also proportional to the instantaneous engine power output.

- **Scenario Testing.** The AIMSUN-PHEM coupled model methodology should be of great interest to transport planners and policymakers performing environmental assessment of on-road emission, as it will enable quantification of not only network emissions, but the contribution to those emissions from each vehicle type and sub-category within the vehicle fleet. It can then be used to identify the best areas to target in order to deliver effective exhaust pollution emission reduction strategies. The coupled model facilitates a significant further step in such evaluations, as it could also be used to test hypothetical changes to the network. When evaluated against a base model the effect on pollutant emission across the network as a result of a specific action could be estimated. Where the expected cost of potential alterations is known, this can be used to calculate a cost per tonne emission reduction which could then be evaluated as part of a cost-benefit analysis against other emission reduction proposals. This is the kind of evidence necessary to justify the potentially large cost of such projects, especially given the current climate of austerity and the restrictions that have been placed on Government spending. Scenarios for reducing on-road vehicle emission in the Headingley network that could be analysed as part of future study include:

- **The exclusion of certain vehicle types from the Headingley fleet.** This could be the result of the introduction of a low emission zone or of incentives to remove older vehicles from the fleet such as via a scrappage scheme.

- **Electrification of the local bus fleet, replacing the current diesel fleet.** This could form part of a larger project on evaluating bus emission in the network. Liaising with the local operators could confirm that the Headingley base model bus fuel consumption estimates are consistent with the real-world fuel consumption figures and ensure that the vehicle specifications (i.e. bus weight, Euro standard, engine size) are correctly described in the model. A survey of bus occupancy could be conducted to confirm both the bus loading figures and also to give a clearer understanding of bus dwell times at each stop in the network.

- **Potential schemes to improve traffic flow in the network.** These could include congestion charging, optimised traffic signal timings at junctions, the construction of new roads in the network and/or changes to speed limits in the network.

- **Emission rate analysis for future vehicle fleet scenarios.** Amending the fleet descriptions in the AIMSUN-PHEM model to describe what the composition of the vehicle fleet could look like in 5 years, 10 years and 15 years, would help to clarify how emissions in the network are likely to change as a result of fleet turnover and to assess the potential progress made toward decarbonising road transport and improving air quality. Such scenarios could reflect for example a greater fraction of electric vehicles in the fleet and a decreasing diesel passenger car fraction. As electric vehicle performance is likely to differ from the performance of traditional combustion engine vehicles (with potentially a greater rate of acceleration for electric vehicles) this could be described in the model through the vehicle parameters. The effect of electric vehicle performance could influence the overall flow of vehicles in the network, which through using the AIMSUN-PHEM methodology could be incorporated and evaluated.

- **Comparison of AIMSUN-PHEM network emission estimates against the EFT.** DEFRA's Emissions Factors Toolkit (see Chapter 4.3) is used in the UK by local government authorities to conduct 'review and assessment' of local air quality as part of their obligations under the Environmental Act 1995 (DEFRA, 2009). The EFT is used to generate road vehicle pollutant estimates for CO_2, NO_x and PM for a specified year, road type, vehicle speed and fleet composition. This is part of the methodology for the assessment of Clean Air Zone's which

form part of the UK strategy to comply with EU emission limit values (DEFRA, 2016). The EFT could be used to calculate emission estimates for the Headingley network, which could be compared to the AIMSUN-PHEM model emission estimates. Analysis of any disparity between the emission estimates might reveal whether the AIMSUN-PHEM model offers a more robust methodology for local government to review local air quality.

- **AIMSUN-PHEM coupled models emission estimation for other networks.** Further work with the AIMSUN-PHEM model could look to generate emission estimates using the same methodology in other traffic networks. Of special interest might be assessing vehicle fleet emission over a motorway section analysing the impact on emission from the introduction of smart motorway technologies, which are designed to reduce congestion (GOV.UK, 2017a). Future research using this methodology is likely to involve collaboration with existing AIMSUN users who have created network model simulations for traffic management but need to add the capacity to generate highly accurate emission estimates. Working with such AIMSUN users to couple their models with PHEM, ensuring that the model is properly calibrated and validated, could enable a more widespread use of this extremely promising methodology.

BIBLIOGRAPHY

"model, n. and adj." [Online]. Oxford English Dictionary: Oxford University Press. Available: http://www.oed.com/view/Entry/120577?rskey=8MTC4O&result=1.

AECOM. 2008. *Appendix 3 - Data and Traffic Surveys Documents: Appendix 13 - Bus Occupancy Profiles* [Online]. New Generation Transport. Available: http://www.ngtmetro.com/Documents/Appendices/Appendix-3---Data-and-Traffic-Surveys-Documents/.

AGUILÉRA, V. & TORDEUX, A. 2014. A new kind of fundamental diagram with an application to road traffic emission modeling. *Journal of Advanced Transportation,* 48**,** 165-184.

AHN, K., KRONPRASERT, N. & RAKHA, H. 2009. Energy and environmental assessment of high-speed roundabouts. *Transportation Research Record: Journal of the Transportation Research Board***,** 54-65.

AIMSUN. 2017. *Aimsun: the integrated tool for transportation modelling applications* [Online]. Available: https://www.aimsun.com/aimsun/ [Accessed 18/10 2017].

ANDERSSON, J., MAY, J., FAVRE, C., BOSTEELS, D., DE VRIES, S., HEANEY, M., KEENAN, M. & MANSELL, J. 2014. On-Road and Chassis Dynamometer Evaluations of Emissions from Two Euro 6 Diesel Vehicles. *SAE Int. J. Fuels Lubr.,* 7**,** 919-934.

ANYA, A., ROUPHAIL, N., FREY, H. & SCHROEDER, B. 2014. Application of AIMSUN Microsimulation Model to Estimate Emissions on Signalized Arterial Corridors. *Transportation Research Record: Journal of the Transportation Research Board***,** 75-86.

BARCELÓ, J., CODINA, E., CASAS, J., FERRER, J. L. & GARCÍA, D. 2005. Microscopic traffic simulation: A tool for the design, analysis and evaluation of intelligent transport systems. *Journal of Intelligent and Robotic Systems,* 41**,** 173-203.

BARLOW, T. J. & BOULTER, P. G. 2009. Emission factors 2009: Report 2 - a review of the average-speed approach for estimating hot exhaust emissions version: 3. *In:* LIMITED, T. (ed.) *Published Project Report PPR355.* Department For Transport.

BARTH, M. & BORIBOONSOMSIN, K. 2008. Real-World Carbon Dioxide Impacts of Traffic Congestion. *Transportation Research Record***,** 163-171.

BATTERMAN, S., COOK, R. & JUSTIN, T. 2015. Temporal variation of traffic on highways and the development of accurate temporal allocation factors for air pollution analyses. *Atmospheric Environment,* 107**,** 351-363.

BERNSTEIN, L., BOSCH, P., CANZIANI, O., CHEN, Z., CHRIST, R., DAVIDSON, O., HARE, W., HUQ, S., KAROLY, D. & KATTSOV, V. 2007a. Climate change 2007: Synthesis report. Contribution of Working Groups I, II and III to the fourth assessment report of the Intergovernmental Panel on Climate Change. *IPCC: Geneva, Switzerland*.

BERNSTEIN, L., BOSCH, P., CANZIANI, O., CHEN, Z., RENATE CHRIST, O. D., WILLIAM HARE, SALEEMUL, HUQ, D. K., VLADIMIR KATTSOV, ZBIGNIEW KUNDZEWICZ, JIAN LIU, ULRIKE LOHMANN, MARTIN MANNING, TAROH MATSUNO,, BETTINA MENNE, B. M., MONIRUL MIRZA, NEVILLE NICHOLLS, LEONARD NURSE, RAJENDRA PACHAURI, JEAN PALUTIKOF, MARTIN, PARRY, D. Q., NIJAVALLI RAVINDRANATH, ANDY REISINGER, JIAWEN REN, KEYWAN RIAHI, CYNTHIA ROSENZWEIG, MATILDE, RUSTICUCCI, S. S., YOUBA SOKONA, SUSAN SOLOMON, PETER STOTT, RONALD STOUFFER, TAISHI SUGIYAMA, ROB SWART, & DENNIS TIRPAK, C. V., GARY YOHE 2007b. Summary for Policymakers. *Climate Change 2007: Synthesis Report.* Intergovernmental Panel on Climate Change.

BLUESKY. 2013. *LiDAR Height Data* [Online]. Available: http://www.bluesky-world.com/products/lidar/ [Accessed 05/11/2013 2013].

BONILLA, D. 2009. Fuel demand on UK roads and dieselisation of fuel economy. *Energy Policy,* 37**,** 3769-3778.

BORGE, R., DE MIGUEL, I., DE LA PAZ, D., LUMBRERAS, J., PEREZ, J. & RODRIGUEZ, E. 2012. Comparison of road traffic emission models in Madrid (Spain). *Atmospheric Environment,* 62**,** 461-471.

BORIBOONSOMSIN, K. & BARTH, M. 2009. Impacts of Road Grade on Fuel Consumption and Carbon Dioxide Emissions Evidenced by Use of Advanced Navigation Systems. *Transportation Research Record*, 21-30.

BOROUJENI, B. Y. & FREY, H. C. 2014. Road grade quantification based on global positioning system data obtained from real-world vehicle fuel use and emissions measurements. *Atmospheric Environment,* 85, 179-186.

BOROUJENI, B. Y., FREY, H. C. & SANDHU, G. S. 2013. Road Grade Measurement Using In-Vehicle, Stand-Alone GPS with Barometric Altimeter. *Journal of Transportation Engineering-Asce,* 139, 605-611.

BOTTINO, A., GARBO, A., LOIACONO, C. & QUER, S. 2016. Street viewer: an autonomous vision based traffic tracking system. *Sensors,* 16, 813.

BOULTER, P., BARLOW, T. J. & MCCRAE, I. S. 2009. Emission factors 2009: Report 3-exhaust emission factors for road vehicles in the United Kingdom. *TRL Published Project Report*.

BOULTER, P., MCCRAE, I. S. & BARLOW, T. J. 2007. *A review of instantaneous emission models for road vehicles*, TRL Limited.

CCC. 2015. *Meeting Carbon Budgets - Progress in reducing the UK's emissions: 2015 Report to Parliament* [Online]. The Committee on Climate Change. Available: https://d2kjx2p8nxa8ft.cloudfront.net/wp-content/uploads/2015/06/6.737_CCC-BOOK_WEB_030715_RFS.pdf [Accessed 17/11 2015].

CHEN, Y. C. & BORKEN-KLEEFELD, J. 2014. Real-driving emissions from cars and light commercial vehicles Results from 13 years remote sensing at Zurich/CH. *Atmospheric Environment,* 88, 157-164.

CLOKE, J., BOULTER, P., DAVIES, G. P., HICKMAN, A. J., LAYELD, R. E., MCCRAE, I. S. & NELSON, P. M. 1998. Traffic management and air quality research programme. *Report 327*.

COELHO, M. C., FREY, H. C., ROUPHAIL, N. M., ZHAI, H. & PELKMANS, L. 2009. Assessing methods for comparing emissions from gasoline and diesel light-duty vehicles based on microscale measurements. *Transportation Research Part D-Transport and Environment,* 14, 91-99.

COLBERG, C. A., TONA, B., CATONE, G., SANGIORGIO, C., STAHEL, W. A., STURM, P. & STAEHELIN, J. 2005. Statistical analysis of the vehicle pollutant emissions derived from several European road tunnel studies. *Atmospheric Environment,* 39, 2499-2511.

COLLINS, M., KNUTTI, R., ARBLASTER, J., DUFRESNE, J.-L., FICHEFET, T., FRIEDLINGSTEIN, P., GAO, X., GUTOWSKI, W., JOHNS, T. & KRINNER, G. 2013. Long-term climate change: projections, commitments and irreversibility.

DAHAM, B., ANDREWS, G. E., LI, H., BALLESTEROS, R., BELL, M. C., TATE, J. & ROPKINS, K. 2005. Application of a Portable FTIR for Measuring On-road Emissions. SAE International.

DATA.GOV.UK. 2017. *DVLA Vehicles Database (Unpublished)* [Online]. Available: https://data.gov.uk/dataset/dvla-vehicles-database.

DECC. 2011. *The Carbon Plan: Delivering our Low Carbon Future* [Online]. Departmenet of Energy and Climate Change. Available: http://www.decc.gov.uk/assets/decc/11/tackling-climate-change/carbon-plan/3702-the-carbon-plan-delivering-our-low-carbon-future.pdf.

DECC. 2012. *Digest of United Kingdom Energy Statistics 2012* [Online]. Department of Energy and Climate Change. Available: https://www.gov.uk/government/uploads/system/uploads/attachment_data/file/65881/5949-dukes-2012-exc-cover.pdf [Accessed 14/01 2013].

DECC. 2015. *Monthly and annual prices of road fuels and petroleum products* [Online]. Department of Energy & Climate Change. Available: https://www.gov.uk/government/statistical-data-sets/oil-and-petroleum-products-monthly-statistics [Accessed 29/12 2015].

DEFRA. 2009. *Emission Factors Toolkit for Vehicle Emissions* [Online]. Department for Environment, Food and Rural Affairs. Available: http://laqm.defra.gov.uk/review-and-assessment/tools/emissions-factors-toolkit.html [Accessed 11/10 2013].

DEFRA. 2014. *National Atmospheric Emissions Inventory: Vehicle fleet composition projections (Base 2013)* [Online]. Available: http://naei.defra.gov.uk/data/ef-transport [Accessed 05/11 2015].
DEFRA. 2015a. *2015 Government GHG Conversion Factors for Company Reporting: Methodology Paper for Emission Factors Final Report* [Online]. Department for Environment, Food and Rural Affairs. Available: http://www.ukconversionfactorscarbonsmart.co.uk/Documents/Emission%20Factor%20Methodology%20Paper%20-%202015.pdf.
DEFRA. 2015b. *Greenhouse Gas Conversion Factor Repository* [Online]. Department for Environment Food & Rural Affairs. Available: http://www.ukconversionfactorscarbonsmart.co.uk/.
DEFRA. 2016. *Emissions Factors Toolkit v7.0 User Guide* [Online]. Department for Environment, Food and Rural Affairs. Available: https://laqm.defra.gov.uk/documents/EFTv7.0-user-guide-v2.0.pdf [Accessed 15/10 2017].
DELPHI. 2013. Worldwide Emission Standards: Passenger Cars and Light Duty Vehicles 2013/2014. Available: http://delphi.com/docs/default-source/catalogs/delphi-worldwide-emissions-standards-pc-ldv-15-16.pdf?sfvrsn=2 [Accessed 24/01/2014].
DFT. 2009a. *Road vehicle emission factors 2009* [Online]. Available: http://www.dft.gov.uk/publications/road-vehicle-emission-factors-2009 [Accessed 24/08/2012.
DFT. 2009b. *Low Carbon Transport: A Greener Future* [Online]. Available: http://www.decc.gov.uk/en/content/cms/what_we_do/lc_uk/lc_trans_plan/lc_trans_plan.aspx.
DFT 2010a. Light Goods Vehicle – CO2 Emissions Study: Final report. *In:* TRANSPORT, D. F. (ed.).
DFT. 2010b. *Office for Low Emission Vehicles* [Online]. Department for Transport. Available: http://www.dft.gov.uk/pgr/sustainable/olev/ [Accessed 13/12 2010].
DFT. 2013. *Road transport forecasts 2013* [Online]. Department for Transport. Available: https://www.gov.uk/government/publications/road-transport-forecasts-2013.
DFT. 2014. *Transport Analysis Guidance (TAG) Unit M3.1 Highway Assignment Modelling* [Online]. Department for Transport. Available: https://www.gov.uk/government/uploads/system/uploads/attachment_data/file/427124/webtag-tag-unit-m3-1-highway-assignment-modelling.pdf 2015].
DFT. 2015a. *Percentage empty running and loading factors by type and weight of vehicle: Table RFS0117* [Online]. Department for Transport. Available: https://www.gov.uk/government/statistical-data-sets/rfs01-goods-lifted-and-distance-hauled.
DFT. 2015b. *Statistical data set: All licensed vehicles and new registrations (VEH01). Table VEH0102. Licensed vehicles by body type, Great Britain, annually: 1994 to 2014* [Online]. Department for Transport. Available: https://www.gov.uk/government/statistical-data-sets/veh01-vehicles-registered-for-the-first-time [Accessed 29/12 2015].
DFT. 2015c. *Statistical data set Traffic volume - kilometres (TRA02): Table TRA0201 Road traffic (vehicle kilometres) by vehicle type in Great Britain* [Online]. Department for Transport. Available: https://www.gov.uk/government/statistical-data-sets/tra02-traffic-by-road-class-and-region-kms [Accessed 29/12 2015].
DFT. 2015d. *Traffic Statistics Methodology Review: Moving Britain Ahead* [Online]. Department for Transport. Available: https://www.gov.uk/government/uploads/system/uploads/attachment_data/file/453274/traffic-statistics-methodology-review.pdf [Accessed 02/01 2016].
DFT 2015e. GB Road Traffic Counts: AADF Data - major roads. www.data.gov.uk/dataset/gb-road-traffic-counts: Department for Transport DATA.GOV.UK
DFT. 2015f. *Statistical data set: All licensed vehicles and new registrations (VEH01). Table VEH0103. Licensed vehicles by tax class, Great Britain, annually from 1909* [Online].

Department for Transport. Available: https://www.gov.uk/government/statistical-data-sets/veh01-vehicles-registered-for-the-first-time [Accessed 29/12 2015].
DFT. 2015g. *Statistical Data Set: Table ENV0202, Carbon dioxide emissions by transport mode: United Kingdom* [Online]. Department for Transport. Available: https://www.gov.uk/government/statistical-data-sets/tsgb03 [Accessed 29/12 2015].
DFT. 2015h. *Statistical Data Set: Table ENV0201, Greenhouse gas emissions by transport mode: United Kingdom* [Online]. Department for Transport. Available: https://www.gov.uk/government/statistical-data-sets/tsgb03 [Accessed 29/12 2015].
DFT 2015i. Vehicle Licensing Statistics: Quarter 4 (Oct - Dec) 2014. https://www.gov.uk/government/uploads/system/uploads/attachment_data/file/421337/vls-2014.pdf: Department for Transport.
DIA, H., GONDWE, W. & PANWAI, S. A traffic simulation approach to evaluating the benefits of incident management programs. AUSTRALASIAN TRANSPORT RESEARCH FORUM (ATRF), 29TH, 2006, GOLD COAST, QUEENSLAND, AUSTRALIA, VOL 29, 2006.
DINGS, J. 2013. Mind the Gap! Why official car fuel economy figures don't match up to reality. *Transport and Environment*.
DOUCETTE, R. T. & MCCULLOCH, M. D. 2011. Modeling the CO2 emissions from battery electric vehicles given the power generation mixes of different countries. *Energy Policy,* 39**,** 803-811.
DOWLING, R., SKABARDONIS, A., HALKIAS, J., MCHALE, G. & ZAMMIT, G. 2004. Guidelines for calibration of microsimulation models: framework and applications. *Transportation Research Record: Journal of the Transportation Research Board***,** 1-9.
EC. 2008. *CO2 Emissions from New Passenger Cars: Monitoring* [Online]. Available: http://eur-lex.europa.eu/legal-content/EN/TXT/HTML/?uri=LEGISSUM:l28055&from=EN [Accessed 09/03 2017].
EC 2009a. Setting emission performance standards for new light commercial vehicles as part of the Community's integrated approach to reduce CO2 emissions from light-duty vehicles. *Regulation of the European Parliament and of the Council.* Commission of the European Communities.
EC 2009b. Regulation (EC) No. 443/2009 of the European Parliament and of the Council of 23 April 2009 Setting Emission Performance Standards for New Passenger Cars as Part of the Community's Integrated Approach to Reduce CO2 Emissions from Light-duty Vehicles, Official Journal of the European Union, L140/1. 443/2009/EC. European Commission.
EC 2011. Roadmap for Moving to a Low-Carbon Economy in 2050. *In:* COMMISSION, E. (ed.).
EC. 2015a. *Climate Action: Paris Agreement* [Online]. European Commission Available: http://ec.europa.eu/clima/policies/international/negotiations/future/index_en.htm [Accessed 28/12 2015].
EC. 2015b. *European Commission: Environment: Air Quality Standards* [Online]. European Commission. Available: http://ec.europa.eu/environment/air/quality/standards.htm [Accessed 20/12 2015].
EC. 2015c. *Commission welcomes Member States' agreement on robust testing of air pollution emissions by cars* [Online]. European Commission. Available: http://europa.eu/rapid/press-release_IP-15-5945_en.htm [Accessed 30/12 2015].
EC 2016. Commission Regulation (EU) 2016/646 of 20 April 2016 amending Regulation (EC) No 692/2008 as regards emissions from light passenger and commercial vehicles (Euro 6). European Commission.
EC. 2017. *EU Action to Curb Air Pollution by Cars* [Online]. European Commission. Available: http://europa.eu/rapid/press-release_MEMO-17-2821_en.htm [Accessed 14/10 2017].
EHSANI, M., GAO, Y. & EMADI, A. 2009. *Modern electric, hybrid electric, and fuel cell vehicles : fundamentals, theory, and design,* Boca Raton, Fla., CRC ; London : Taylor & Francis [distributor].

ELKAFOURY, A., NEGM, A., ALY, M., BADY, M. & ICHIMURA, T. 2015. Develop dynamic model for predicting traffic CO emissions in urban areas. *Environmental Science and Pollution Research*, 1-12.

ELS, P. 2015. *The real world of emissions testing* [Online]. http://writingaboutcars.com. Available: http://writingaboutcars.com/the-real-world-of-emissions-testing/ [Accessed 23/10 2017].

EPA. 2012a. *Modeling and Inventories: MOVES (Motor Vehicle Emission Simulator)* [Online]. U.S. Environmental Protection Agency. Available: http://www.epa.gov/otaq/models/moves/index.htm

EPA 2012b. User guide for moves2010b. Technical report, United States Environmental Protection Agency.

FIELD, C. B. & VAN AALST, M. 2014. *Climate change 2014: impacts, adaptation, and vulnerability*, IPCC.

FIRST. 2015. *Leeds Network Map* [Online]. First Group Leeds. Available: http://www.firstgroup.com/leeds/routes-and-maps/network-maps [Accessed 23/12 2015].

FONT, A. & FULLER, G. W. 2016. Did policies to abate atmospheric emissions from traffic have a positive effect in London? *Environmental Pollution,* 218**,** 463-474.

FONTARAS, G., FRANCO, V., DILARA, P., MARTINI, G. & MANFREDI, U. 2014. Development and review of Euro 5 passenger car emission factors based on experimental results over various driving cycles. *Science of the Total Environment,* 468**,** 1034-1042.

FONTARAS, G., PISTIKOPOULOS, P. & SAMARAS, Z. 2008. Experimental evaluation of hybrid vehicle fuel economy and pollutant emissions over real-world simulation driving cycles. *Atmospheric Environment,* 42**,** 4023-4035.

FORD 2005. Ford Motor Company Limited. The New Ford Mondeo. Brochure. Published by Ford Motor Company Limited, Brentwood, Essex, England; May 2005.

FREY, H. C., UNAL, A., ROUPHAIL, N. M. & COLYAR, J. D. 2003. On-road measurement of vehicle tailpipe emissions using a portable instrument. *Journal of the Air & Waste Management Association,* 53**,** 992-1002.

FREY, H. C., ZHANG, K. & ROUPHAIL, N. M. 2010. Vehicle-Specific Emissions Modeling Based upon on-Road Measurements. *Environmental Science & Technology,* 44**,** 3594-3600.

FREY, H. C., ZHANG, K. S. & ROUPHAIL, N. M. 2008. Fuel use and emissions comparisons for alternative routes, time of day, road grade, and vehicles based on in-use measurements. *Environmental Science & Technology,* 42**,** 2483-2489.

GIPPS, P. G. 1981. A behavioural car-following model for computer simulation. *Transportation Research Part B: Methodological,* 15**,** 105-111.

GOV.UK. 2009. *Road vehicle emission factors 2009: regulated* [Online]. Department for Transport. Available: https://www.gov.uk/government/publications/road-vehicle-emission-factors-2009 [Accessed 24/10 2013].

GOV.UK. 2013. *A Simplified Guide to Lorry Types and Weights* [Online]. Available: https://www.gov.uk/government/publications/guide-to-lorry-types-and-weights.

GOV.UK. 2015a. *Statistical data set: Cars (VEH02) Table VEH0253: Cars registered for the first time by propulsion / fuel type, Great Britain, annually from 2001* [Online]. GOV.UK. Available: https://www.gov.uk/government/statistical-data-sets/veh02-licensed-cars#table-veh0253 [Accessed 29/12 2015].

GOV.UK. 2015b. *Vehicle tax rate tables* [Online]. GOV.UK. Available: https://www.gov.uk/vehicle-tax-rate-tables/overview [Accessed 29/12 2015].

GOV.UK. 2015c. *Tax on shopping and services: 7. Fuel Duty* [Online]. GOV.UK. Available: https://www.gov.uk/tax-on-shopping/fuel-duty [Accessed 29/12 2015].

GOV.UK. 2015d. *Statistical data set: Cars (VEH02) Table VEH0256: Cars registered for the first time by CO2 emission band, Great Britain, annually from 2001* [Online]. GOV.UK. Available: https://www.gov.uk/government/statistical-data-sets/veh02-licensed-cars#table-veh0253 [Accessed 29/12 2015].

GOV.UK. 2016a. *Statistical data set: Cars (VEH02) Table VEH0205: Cars licensed by engine capacity (all fuel types): Great Britain and United Kingdom* [Online]. GOV.UK. Available: https://www.gov.uk/government/statistical-data-sets/veh02-licensed-cars [Accessed 13/02 2017].

GOV.UK. 2016b. *Statistical data set: Cars (VEH02) Table VEH0211: Licensed cars by years since first registration: Great Britain and United Kingdom* [Online]. GOV.UK. Available: https://www.gov.uk/government/statistical-data-sets/veh02-licensed-cars [Accessed 13/02 2017].

GOV.UK. 2016c. *Greenhouse gas reporting - Conversion factors 2016* [Online]. GOV.UK. Available: https://www.gov.uk/government/publications/greenhouse-gas-reporting-conversion-factors-2016 [Accessed 26/03 2017].

GOV.UK. 2016d. *Statistical data set: Cars (VEH02) Table VEH0220: Licensed cars by make, model and engine capacity: Great Britain and United Kingdom* [Online]. GOV.UK. Available: https://www.gov.uk/government/statistical-data-sets/veh02-licensed-cars [Accessed 13/02 2017].

GOV.UK. 2017a. *Smart Motorways Programme* [Online]. Available: http://www.highways.gov.uk/smart-motorways-programme/ [Accessed 15/10 2017].

GOV.UK. 2017b. *2005 to 2015 UK local and regional CO2 emissions technical report* [Online]. Available: https://www.gov.uk/government/uploads/system/uploads/attachment_data/file/623020/2005_to_2015_UK_local_and_regional_CO2_emissions_technical_report.pdf [Accessed 17/10 2017].

GRANELL, J., GUENSLER, R. & BACHMAN, W. Using Locality-Specific Fleet Distribution in Emissions Inventories: Current Practice, Problems and Alternatives. In Proceedings of the 81st Annual Meeting of the Transportation Research Board, Washington, D.C. , 2002.

GROTE, M., WILLIAMS, I., PRESTON, J. & KEMP, S. 2016. Including congestion effects in urban road traffic CO2 emissions modelling: Do Local Government Authorities have the right options? *Transportation Research Part D: Transport and Environment,* 43**,** 95-106.

HARRISON, R. M., BRUNEKREEF, B., KEUKEN, M., DENIER VAN DER GON, H. & QUEROL, X. 2014. New directions: cleaning the air–will the European Commission's clean air policy package of December 2013 deliver. *Atmos Environ,* 91**,** 172-174.

HAUSBERGER, S. 2003. *Simulation of Real World Vehicle Exhaust Emissions*, VKM-THD Mitteilungen; Heft/Vol 82; Verlag der Technischen Universitat Graz 2003, ISBN 3-901351-74-4.

HAUSBERGER, S., REXEIS, M., ZALLINGER, M. & LUZ, R. 2009. Emission factors from the model PHEM for the HBEFA version 3. Report Nr. I-20/2009 Haus-Em 33/08/679 from 07.12.

HEISLER, H. 2002. *Advanced vehicle technology,* Oxford, Butterworth-Heinemann.

HOLDER, J. 2015. *VW emissions scandal: Nine VW vehicles have false CO2 ratings* [Online]. autocar.co.uk. Available: http://www.autocar.co.uk/car-news/industry/vw-emissions-scandal-nine-vw-vehicles-have-false-co2-ratings [Accessed 30/12 2015].

HOLMEN, B. A. & SENTOFF, K. M. 2015. Hybrid-Electric Passenger Car Carbon Dioxide and Fuel Consumption Benefits Based on Real-World Driving. *Environmental Science & Technology,* 49**,** 10199-10208.

HÜLSMANN, F., GERIKE, R. & KETZEL, M. 2014. Modelling traffic and air pollution in an integrated approach – the case of Munich. *Urban Climate,* 10, Part 4**,** 732-744.

ICCT. 2015. *Quantifying the impact of real-world driving on total CO2 emissions from UK cars and vans* [Online]. The Committee on Climate Change. Available: https://www.theccc.org.uk/wp-content/uploads/2015/09/Impact-of-real-world-driving-emissions-for-UK-cars-and-vans.pdf [Accessed 20/11 2015].

IEA. 2012. *CO2 Emissions from Fuel Combustion. Beyond 2020 Online Database. 2012 Edition.* [Online]. International Energy Agency. Available: Available at: http://www.iea.org/statistics/onlinedataservice/.

IEA 2014. Policy Pathways: A Tale of Renewed Cities. International Energy Agency.

JACKSON, E. & AULTMAN-HALL, L. 2010. Analysis of Real-World Lead Vehicle Operation for Modal Emissions and Traffic Simulation Models. *Transportation Research Record*, 44-53.

JIMENEZ-PALACIOS, J. 1999. Understanding and quantifying motor vehicle emissions with vehicle specific power and TILDAS remote sensing. . Doctoral Dissertation, Department of Mechanical Engineering, Massachusetts Institute of Technology, Cambridge, MA.

KADIJK, G., LIGTERINK, N. & SPREEN, J. 2015. On-road NOx and CO2 investigations of Euro 5 light commercial vehicles. *TNO report*, R10192.

KHALFAN, A., LI, H. & ANDREWS, G. 2015. Cold Start SI Passenger Car Emissions from Real World Urban Congested Traffic. SAE International.

KOUPAL, J., NAM, E., GIANNELLI, B. & BAILEY, C. 2004. The MOVES Approach to Modal Emission Modeling. *Presented at the 14th CRC On-Road Vehicle Emissions Workshop, San Diego, CA.*

KRASCHL-HIRSCHMANN, K., ZALLINGER, M., LUZ, R., FELLENDORF, M. & HAUSBERGER, S. A method for emission estimation for microscopic traffic flow simulation. Integrated and Sustainable Transportation System (FISTS), 2011 IEEE Forum on, 2011. IEEE, 300-305.

KWON, J., ROUSSEAU, A. & SHARER, P. 2007. Analyzing the Uncertainty in the Fuel Economy Prediction for the EPA MOVES Binning Methodology. SAE International.

LCC 2015. Site Allocations Plan and Aire Valley Leeds Area Action Plan: Infrastructure Background Paper. *Leeds Local Development Framework Development Plan Document.* Leeds City Council.

LEGISLATION.GOV.UK. 2008. *Climate Change Act* [Online]. Available: http://www.legislation.gov.uk/ukpga/2008/27/contents.

LENTON, T. M., HELD, H., KRIEGLER, E., HALL, J. W., LUCHT, W., RAHMSTORF, S. & SCHELLNHUBER, H. J. 2008. Tipping elements in the Earth's climate system. *Proceedings of the National Academy of Sciences of the United States of America,* 105, 1786-1793.

LI, H., ANDREWS, G. E., SAVVIDIS, D., DAHAM, B., ROPKINS, K., BELL, M. & TATE, J. 2008a. Study of Thermal Characteristics and Emissions during Cold Start using an on-board Measuring Method for Modern SI Car Real World Urban Driving. *SAE Int. J. Engines,* 1, 804-819.

LI, H., ANDREWS, G. E., SAVVIDIS, D., DAHAM, B., ROPKINS, K., BELL, M. & TATE, J. 2008b. Comparisons of the Exhaust Emission for Different Generations of SI Cars under Real World Urban Driving Conditions. *SAE TECHNICAL PAPERS*.

LI, H., ANDREWS, G. E., SAVVIDIS, D., ROPKINS, K., TATE, J. & BELL, M. 2008c. Investigation of Regulated and Non-Regulated Cold Start Emissions using a EURO3 SI Car as a Probe Vehicle under Real World Urban Driving Conditions. SAE International.

LIU, B. & FREY, H. C. Development and Evaluation of a Simplified Version of MOVES for Coupling with a Traffic Simulation Model. 105th Annual Meeting of the Air & Waste Management Association 2012 San Antonio, Texas.

LIU, H., TOK, Y. C. A. & RITCHIE, S. G. 2011. Development of A Real-Time On-Road Emissions Estimation and Monitoring System. *2011 14th International Ieee Conference on Intelligent Transportation Systems (Itsc)*, 1821-1826.

LIU, H. A., BARTH, M., SCORA, G., DAVIS, N. & LENTS, J. 2010. Using Portable Emission Measurement Systems for Transportation Emissions Studies Comparison with Laboratory Methods. *Transportation Research Record*, 54-60.

LUZ, R. & HAUSBERGER, S. 2015. PHEM User Guide for Version 11. Technische Universitat Graz.

MADI, M. Y. 2016. Investigating and Calibrating the Dynamics of Vehicles in Traffic Micro-simulations Models. *Transportation Research Procedia,* 14, 1782-1791.

MALCOLM, C., YOUNGLOVE, T., BARTH, M. & DAVIS, N. 2003. Mobile-source emissions - Analysis of spatial variability in vehicle activity patterns and vehicle fleet distributions. *Energy, Air Quality, and Fuels 2003*, 91-98.

MAY, J., BOSTEELS, D. & FAVRE, C. 2014. An Assessment of Emissions from Light-Duty Vehicles using PEMS and Chassis Dynamometer Testing. *SAE Int. J. Engines,* 7, 1326-1335.

MEINSHAUSEN, M., SMITH, S. J., CALVIN, K., DANIEL, J. S., KAINUMA, M. L. T., LAMARQUE, J. F., MATSUMOTO, K., MONTZKA, S. A., RAPER, S. C. B., RIAHI, K., THOMSON, A., VELDERS, G. J. M. & VAN VUUREN, D. P. P. 2011. The RCP greenhouse gas concentrations and their extensions from 1765 to 2300. *Climatic Change,* 109**,** 213-241.

METRO. 2014. *Metro Transport for West Yorkshire: Bus Timetables* [Online]. Metro. Available: http://www.wymetro.com/BusTravel/bustimetables/ [Accessed 04/09 2014].

METRO. 2015. *Your Next Bus: Bus stops and real-time bus information* [Online]. 2015].

MILLIN-CHALABI, G., SCHUMM, J., GUPTA, B., TUN, Y., KANDEH, J. & KITMITTO, K. 2011. The Landmap Service: Reaching New Horizons in Data Management and E-Learning. *RSPSoc Annual Conference 2011, Bournemouth University, UK*.

MOCK, P., GERMAN, J., BANDIVADEKAR, A. & RIEMERSMA, I. 2012. Discrepancies between type-approval and "real-world" fuel-consumption and CO2 values. *Assessment for 2001-2011 European passenger cars. ICCT Working Paper; April 2012. Paper no 2012-2.*

MOCK, P., TIETGE, U., ZACHAROF, N., FRANCO, V., GERMAN, J., BANDIVADEKAR, A., LIGTERINK, N. & LAMBRECHT, U. 2015. *From Laboratory to Road: A 2015 update of official and "real-world" fuel consumption and CO2 values for passenger cars in Europe* [Online]. ICCT White Paper. Available: http://www.theicct.org/sites/default/files/publications/ICCT_LaboratoryToRoad_2015_Report_English.pdf [Accessed 22/11 2015].

MOSS, R. H., BABIKER, M., BRINKMAN, S., CALVO, E., CARTER, T., EDMONDS, J. A., ELGIZOULI, I., EMORI, S., LIN, E. & HIBBARD, K. 2008. Towards new scenarios for analysis of emissions, climate change, impacts, and response strategies. Pacific Northwest National Laboratory (PNNL), Richland, WA (US).

NAEI. 2011. *Road transport emission factors from 2008 NAEI* [Online]. UK National Atmospheric Emission Inventory. Available: http://naei.defra.gov.uk/resources/3_9_307_130573_roadtransportefs_naei08_v1.xls.

NAKAMURA, H., KIHARA, N., ADACHI, M. & ISHIDA, K. 2002. Development of a Wet-based NDIR and Its Application to On-board Emission Measurement System. SAE International.

NGT. 2014. *Information Paper B8: Transport Case – Road use and congestion* [Online]. New Generation Transport - Metro. Available: http://www.ngtmetro.com/uploadedFiles/Content/About/B8%20-%20Congestion.pdf [Accessed 13/11 2015].

NRC 2000. Modeling Mobile Source Emissions. National Acadamy Press, Washington, DC.: National Research Council.

NTZIACHRISTOS, L. & SAMARAS, Z. 2014. *EMEP/EEA air pollutant emission inventory guidebook - 2013: Exhaust emissions from road transport* [Online]. COPERT IV. Available: file:///C:/Users/pmdww/Downloads/1.A.3.b%20Road%20transport%20GB2013%20update%20Sept2014%20(1).pdf [Accessed 02/12 2015].

ONS. 2012. *Census result shows increase in population of Yorkshire and the Humber* [Online]. Office for National Statistics. Available: http://www.ons.gov.uk/ons/rel/mro/news-release/census-result-shows-increase-in-population-of-yorkshire-and-the-humber/censusyorkandhumbernr0712.html [Accessed 15/11 2015].

PACHAURI, R. K., ALLEN, M., BARROS, V., BROOME, J., CRAMER, W., CHRIST, R., CHURCH, J., CLARKE, L., DAHE, Q. & DASGUPTA, P. 2014. Climate Change 2014: Synthesis Report. Contribution of Working Groups I, II and III to the Fifth Assessment Report of the Intergovernmental Panel on Climate Change.

PALMGREN, F., BERKOWICZ, R., ZIV, A. & HERTEL, O. 1999. Actual car fleet emissions estimated from urban air quality measurements and street pollution models. *Science of the Total Environment,* 235**,** 101-109.

PANIS, L. I., BROEKX, S. & LIU, R. H. 2006. Modelling instantaneous traffic emission and the influence of traffic speed limits. *Science of the Total Environment,* 371**,** 270-285.

PANWAI, S. & DIA, H. 2005. Comparative evaluation of microscopic car-following behavior. *Intelligent Transportation Systems, IEEE Transactions on,* 6**,** 314-325.

PELKMANS, L. & DEBAL, P. 2006. Comparison of on-road emissions with emissions measured on chassis dynamometer test cycles. *Transport Research Part D,* 11**,** pp. 233-241.
PELLECUER, L., TATE, J. & CHAPMAN, S. 2016. How do traffic flow and the emissions they produce vary through the day, week, season and year: evidence from big telematics data. *21st International Transport and Air Pollution Conference.* Lyon, France.
PIJOAN, A., ORIBE-GARCIA, I., KAMARA-ESTEBAN, O., GENIKOMSAKIS, K. N., BORGES, C. E. & ALONSO-VICARIO, A. 2017. Regression based emission models for vehicle contribution to climate change. *Intelligent Transport Systems and Travel Behaviour.* Springer.
PTV 2004. VISSIM User Manual Version 3.70. PTV Group - www.http://vision-traffic.ptvgroup.com/.
QUADSTONE 2005. Quadstone Paramics V5.0: Modeller Reference Manual. Quadstone - http://www.paramics-online.com/.
R-CORETEAM. 2014. *R: A Language and Environment for Statistical Computing. R Foundation for Statistical Computing. Vienna, Austria* [Online]. R Development Core Team. Available: http://www.R-project.org.
RACELOGIC. 2008. *VBOX II Lite 5Hz GPS Data Logger User Guide* [Online]. Available: http://www.racelogic.co.uk/_downloads/vbox/Manuals/Data_Loggers/RLVB2L_Manual.pdf [Accessed 30/06/2014.
RAMLI, A. R. & GRAHAM, D. J. 2014. The demand for road transport diesel fuel in the UK: Empirical evidence from static and dynamic cointegration techniques. *Transportation Research Part D-Transport and Environment,* 26**,** 60-66.
ROPKINS, K., QUINN, R., BEEBE, J., LI, H., DAHAM, B., TATE, J., BELL, M. & ANDREWS, G. 2007. Real-world comparison of probe vehicle emissions and fuel consumption using diesel and 5% biodiesel (B5) blend. *Science of the Total Environment,* 376**,** 267-284.
ROPKINS, K., TATE, J. E., LI, H., ANDREWS, G. E., HAWLEY, G. & BELL, M. C. 2008. Chassis Dynamometer Evaluation of On-board Exhaust Emission Measurement System Performance in SI Car under Transient Operating Conditions. SAE International.
S.D.G. 2014a. *Leeds NGT Review of Technology Alternatives* [Online]. Steer Davis Gleave for Metro - Leeds New Generation Transport. Available: file:///C:/Users/pmdww/Downloads/C-1-1%20NGT%20Alternatives%20Review%20Report.pdf.
S.D.G. 2014b. *Runtime Assessment: New Generation Transport: Technical note: January 2014. C-1-13 Runtime Assessment Note* [Online]. Steer Davies Gleave for Metro. Available: http://www.ngtmetro.com/Site/Templates/Pages/Content.aspx?pageid=4294968197 [Accessed 15/10 2014].
SAHLHOLM, P. & JOHANSSON, K. H. 2010. Road grade estimation for look-ahead vehicle control using multiple measurement runs. *Control Engineering Practice,* 18**,** 1328-1341.
SCHMIED, M. 2014. *The European Handbook of Emission Factor for Road Transport (HBEFA)* [Online]. Available: http://transport-namas.org/wp-content/uploads/2014/07/D2_1_HBEFA_Schmied.pdf [Accessed 25/11 2015].
SIMS, R., R. SCHAEFFER, F. CREUTZIG, X. CRUZ-NÚÑEZ, M. D'AGOSTO, D. DIMITRIU, M.J. FIGUEROA MEZA, L. FULTON, S. KOBAYASHI, O. LAH, A., MCKINNON, P. NEWMAN, M. OUYANG, J.J. SCHAUER, D. SPERLING & TIWARI, G. 2014. Transport. In: Climate Change 2014: Mitigation of Climate Change. Contribution of Working Group III to the Fifth Assessment Report of the Intergovernmental Panel on Climate Change. Cambridge University Press, Cambridge, United Kingdom and New York, NY, USA.
SKEETE, J.-P. 2017. Examining the role of policy design and policy interaction in EU automotive emissions performance gaps. *Energy Policy,* 104**,** 373-381.
SMIT, R., NTZIACHRISTOS, L. & BOULTER, P. 2010. Validation of road vehicle and traffic emission models - A review and meta-analysis. *Atmospheric Environment,* 44**,** 2943-2953.
SMIT, R., SMOKERS, R. & RABE, E. 2007. A new modelling approach for road traffic emissions: VERSIT+. *Transportation Research Part D-Transport and Environment,* 12**,** 414-422.

SMMT. 2012. *New Car CO2 Report 2012: 11th Report* [Online]. The Society of Motor Manufacturers and Traders. Available: http://www.smmt.co.uk/wp-content/uploads/SMMT-New-Car-CO2-Report-2012.pdf [Accessed 25/08 2012].

SMMT 2015a. New UK Registrations for 2010 – 2015. Purchased from the SMMT: The Society of Motor Manufacturers and Traders Limited.

SMMT. 2015b. *New Car CO2 Report 2015: The 14th Report* [Online]. The Society of Motor Manufacturers and Traders Limited. Available: http://www.smmt.co.uk/wp-content/uploads/sites/2/101924_SMMT-CO2-Report-FINAL-270415.pdf [Accessed 17/11 2015].

SOES. 2015. *SOES Fleet Lists* [Online]. Sheffield Omnibus Enthusiasts Society Available: http://www.soes.pwp.blueyonder.co.uk/fleets.html 2015].

SONG, G., YU, L. & TU, Z. 2012a. Distribution Characteristics of Vehicle-Specific Power on Urban Restricted-Access Roadways. *Journal of Transportation Engineering,* 138**,** 202-209.

SONG, G., YU, L. & ZHANG, Y. 2012b. Applicability of traffic microsimulation models in vehicle emissions estimates: case study of VISSIM. *Transportation Research Record: Journal of the Transportation Research Board***,** 132-141.

SONG, G. H. & YU, L. 2009. Estimation of Fuel Efficiency of Road Traffic by Characterization of Vehicle-Specific Power and Speed Based on Floating Car Data. *Transportation Research Record***,** 11-20.

STERN, N. 2006. *The Economics of Climate Change: The Stern Review,* New York, Cambridge University Press.

STOCKER, T., QIN, D., PLATTNER, G.-K., ALEXANDER, L., ALLEN, S., BINDOFF, N., BRÉON, F.-M., CHURCH, J., CUBASCH, U. & EMORI, S. 2013a. Technical summary. *Climate Change 2013: The Physical Science Basis. Contribution of Working Group I to the Fifth Assessment Report of the Intergovernmental Panel on Climate Change.* Cambridge University Press.

STOCKER, T., QIN, D., PLATTNER, G., TIGNOR, M., ALLEN, S. & BOSCHUNG, J. 2013b. IPCC, 2013: summary for policymakers in climate change 2013: the physical science basis, contribution of working group I to the fifth assessment report of the intergovernmental panel on climate change. Cambridge University Press, Cambridge, New York, USA.

SWIDAN, H. 2011. Integrating AIMSUN Micro Simulation Model with Portable Emissions Measurement System (PEMS): Calibration and Validation Case Study.

TATE, J. E. 2011. Improved assessment of Environmental Traffic Management Policies - Headingley - Leeds City Council. Institute For Transport Studies, University of Leeds.

TATE, J. E. 2013. Vehicle Emission Measurement and Analysis - Cambridge City Council. Draft document version 1.0: 28th November 2013: University of Leeds.

TATE, J. E. 2015. Wakefield Modelling of Action Plan Measures - Vehicle Emission Modelling. Institute For Transport Studies, University of Leeds.

TFL. 2015. *Bus routes & borough reports* [Online]. Transport for London. Available: https://tfl.gov.uk/forms/14144.aspx [Accessed 10/11 2015].

TSS 2013a. Aimsun Version 8 User's Manual July 2013 © 2005-2013 TSS-Transport Simulation Systems. Transport Simulation Systems, Barcelona, Spain, www.aimsun.com.

TSS 2013b. Aimsun 8 Dynamic Simulators Users' Manual July 2013 © 1997-2013 TSS-Transport Simulation Systems. Transport Simulation Systems, Barcelona, Spain, 2013 www.aimsun.com.

UNFCCC. 2010. *Report of the Conference of the Parties on its fifteenth session, held in Copenhagen from 7 to 19 December 2009. Addendum. Part Two: Action taken by the Conference of the Parties at its fifteenth session.* [Online]. United Nations Framework Convention on Climate Change. Available: http://unfccc.int/resource/docs/2009/cop15/eng/11a01.pdf#page=4.

VALLAMSUNDAR, S. & LIN, J. 2011. MOVES Versus MOBILE Comparison of Greenhouse Gas and Criterion Pollutant Emissions. *Transportation Research Record***,** 27-35.

VELOVIEWER. 2013. *The Climbs of Stage 2 of the 2014 Tour de France – Part 2* [Online]. Veloviewer. Available: http://blog.veloviewer.com/the-climbs-of-stage-2-of-the-2014-tour-de-france-part-2/ [Accessed 28/02 2017].

WANG, H. & MCGLINCHY, I. Review of vehicle emission modelling and the issues for New Zealand. Proceedings of the 32nd Australasian Transport Research Forum, 2009.

WANG, H. K. & FU, L. X. 2010. Developing a High-Resolution Vehicular Emission Inventory by Integrating an Emission Model and a Traffic Model: Part 1-Modeling Fuel Consumption and Emissions Based on Speed and Vehicle-Specific Power. *Journal of the Air & Waste Management Association,* 60**,** 1463-1470.

WEISS, M., BONNEL, P., HUMMEL, R., MANFREDI, U., COLOMBO, R., LANAPPE, G., LE LIJOUR, P. & SCULATI, M. 2011a. Analyzing on-road emissions of light-duty vehicles with Portable Emission Measurement Systems (PEMS). European Commission Joint Research Centre: Institute for Energy. European Commission.

WEISS, M., BONNEL, P., HUMMEL, R., PROVENZA, A. & MANFREDI, U. 2011b. On-Road Emissions of Light-Duty Vehicles in Europe. *Environmental Science & Technology,* 45**,** 8575-8581.

WEISS, M., BONNEL, P., KUHLWEIN, J., PROVENZA, A., LAMBRECHT, U., ALESSANDRINI, S., CARRIERO, M., COLOMBO, R., FORNI, F., LANAPPE, G., LE LIJOUR, P., MANFREDI, U., MONTIGNY, F. & SCULATI, M. 2012. Will Euro 6 reduce the NOx emissions of new diesel cars? - Insights from on-road tests with Portable Emissions Measurement Systems (PEMS). *Atmospheric Environment,* 62**,** 657-665.

WYATT, D. W., LI, H. & TATE, J. 2013. Examining the Influence of Road Grade on Vehicle Specific Power (VSP) and Carbon Dioxide (CO2) Emission over a Real-World Driving Cycle. SAE International.

WYATT, D. W., LI, H. & TATE, J. E. 2014. The impact of road grade on carbon dioxide (CO2) emission of a passenger vehicle in real-world driving. *Transportation Research Part D-Transport and Environment,* 32**,** 160-170.

XU, Y. F., YU, L. & SONG, G. H. 2010. Improved Vehicle-Specific Power Bins for Light-Duty Vehicles in Estimation of Carbon Dioxide Emissions in Beijing. *Transportation Research Record***,** 158-165.

XUE, H., JIANG, S. & LIANG, B. 2013. A Study on the Model of Traffic Flow and Vehicle Exhaust Emission. *Mathematical Problems in Engineering*.

YU, Q., LI, T. & LI, H. 2016. Improving urban bus emission and fuel consumption modeling by incorporating passenger load factor for real world driving. *Applied Energy,* 161**,** 101-111.

ZACHARIADIS, T. & SAMARAS, Z. 1997. Comparative assessment of European tools to estimate traffic emissions. *International Journal of Vehicle Design,* 18**,** 312-325.

ZALLINGER, M., J., T. & HAUSBERGER, S. An Instantaneous Emission Model For The Passenger Car Fleet. 6th International Transport and Air Pollution Congress, 2008 Graz, Austria

ZALLINGER, M., TATE, J., HAUSBERGER, S. & GOODMAN, P. 2009. Evaluation of a Coupled Micro-scopic Traffic Simulator and Instantaneous Emission Model. *Air Quality Conference.* Istanbul.

ZHAI, H. B., FREY, H. C. & ROUPHAIL, N. M. 2008. A Vehicle-Specific Power Approach to Speed- and Facility-Specific Emissions Estimates for Diesel Transit Buses. *Environmental Science & Technology,* 42**,** 7985-7991.

ZHANG, K. S. & FREY, H. C. 2006. Road grade estimation for on-road vehicle emissions modeling using light detection and ranging data. *Journal of the Air & Waste Management Association,* 56**,** 777-788.

APPENDIX 1 Summary Table of the 48 Headingley Test Laps

LAP	TYPE	DATE	SURVEY TIME	PERIOD	TIME (s)	DISTANCE (m)	AVE SPEED (km/h)	CO_2 EMISSION (g)	CO_2 (g/km)
1.1	A	01_03_2007	1159_1241	Inter-Peak (IP)	1223	4587	13.5	2106.7	459
1.2	B	01_03_2007	1159_1241	Inter-Peak (IP)	950	4574	17.3	1867.4	408
2.1	A	01_03_2007	1250_1402	Inter-Peak (IP)	999	4584	16.5	1768.2	386
2.2	B	01_03_2007	1250_1402	Inter-Peak (IP)	1030	4571	16.0	1969.8	431
2.3	A	01_03_2007	1250_1402	Inter-Peak (IP)	973	4580	16.9	2004.3	438
2.4	B	01_03_2007	1250_1402	Inter-Peak (IP)	856	4584	19.3	1878.1	410
3.1	A	01_03_2007	1627_1726	PM Peak (PM)	1575	4578	10.5	2319.3	507
3.2	B	01_03_2007	1627_1726	PM Peak (PM)	1530	4561	10.7	2412.7	529
4.1	A	01_03_2007	1731_1826	PM Peak (PM)	1384	4582	11.9	2062.4	450
4.2	B	01_03_2007	1731_1826	PM Peak (PM)	1471	4565	11.2	1979.5	434
5.1	A	02_03_2007	0734_0829	AM Peak (AM)	819	4575	20.1	1685.7	368
5.2	B	02_03_2007	0734_0829	AM Peak (AM)	1042	4561	15.7	1676.9	368
5.3	A	02_03_2007	0734_0829	AM Peak (AM)	1107	4575	14.9	1625.0	355
6.1	A	02_03_2007	0838_0937	AM Peak (AM)	1370	4581	12.0	2344.7	512
6.2	B	02_03_2007	0838_0937	AM Peak (AM)	1059	4564	15.5	2110.3	462
6.3	B	02_03_2007	0838_0937	AM Peak (AM)	738	4566	22.3	1756.4	385
7.1	A	05_03_2007	1855_1959		1045	4585	15.8	1993.2	435
7.2	B	05_03_2007	1855_1959		770	4565	21.3	1677.5	367
7.3	A	05_03_2007	1855_1959	Evening (EV)	786	4577	21.0	1736.9	379
7.4	B	05_03_2007	1855_1959	Evening (EV)	760	4566	21.6	1774.4	389
8.1	A	05_03_2007	2007_2100	Evening (EV)	818	4578	20.1	1605.6	351
8.2	B	05_03_2007	2007_2100	Evening (EV)	638	4559	25.7	1443.6	317
8.3	A	05_03_2007	2007_2100	Evening (EV)	614	4574	26.8	1439.9	315
8.4	B	05_03_2007	2007_2100	Evening (EV)	631	4560	26.0	1488.8	326
9.1	A	26_02_2007	1204_1250	Inter-Peak (IP)	1167	4595	14.2	2149.2	468
9.2	B	26_02_2007	1204_1250	Inter-Peak (IP)	1326	4574	12.4	2532.3	554
10.1	A	26_02_2007	1256_1409	Inter-Peak (IP)	1468	4801	11.8	2354.4	490
10.2	B	26_02_2007	1256_1409	Inter-Peak (IP)	1120	4574	14.7	2125.0	465
11.1	A	26_02_2007	1635_1721	PM Peak (PM)	1250	4576	13.2	2017.8	441
11.2	B	26_02_2007	1635_1721	PM Peak (PM)	1173	4572	14.0	1955.6	428
12.1	A	26_02_2007	1728_1840	PM Peak (PM)	1407	4581	11.7	2272.9	496
12.2	B	26_02_2007	1728_1840	PM Peak (PM)	1365	4567	12.0	2149.4	471
13.1	A	27_02_2007	0733_0810	AM Peak (AM)	806	4614	20.6	1709.4	370
13.2	B	27_02_2007	0733_0810	Inter-Peak (IP)	1047	4556	15.7	1925.5	423
14.1	A	27_02_2007	0819_0919	AM Peak (AM)	1717	4583	9.6	2692.1	587
14.2	B	27_02_2007	0819_0919	AM Peak (AM)	1559	4563	10.5	2488.9	545
15.1	A	27_02_2007	1159_1259	Inter-Peak (IP)	1536	4591	10.8	2343.2	510
15.2	B	27_02_2007	1159_1259	Inter-Peak (IP)	1699	4572	9.7	2315.7	507
16.1	A	27_02_2007	1307_1407	Inter-Peak (IP)	1656	4586	10.0	2376.3	518
16.2	B	27_02_2007	1307_1407	Inter-Peak (IP)	1685	4574	9.8	2464.4	539
17.1	A	28_02_2007	0731_0817	AM Peak (AM)	921	4584	17.9	1780.2	388
17.2	B	28_02_2007	0731_0817	AM Peak (AM)	1480	4560	11.1	2171.7	476
18.1	A	28_02_2007	0826_0936	AM Peak (AM)	1550	4585	10.6	2277.1	497
18.2	B	28_02_2007	0826_0936	AM Peak (AM)	1186	4563	13.9	1979.9	434
18.3	A	28_02_2007	0826_0936	AM Peak (AM)	972	4586	17.0	1764.8	385
19.1	A	28_02_2007	1631_1723	PM Peak (PM)	1517	4582	10.9	2239.8	489
20.1	B	28_02_2007	1732_1830	PM Peak (PM)	1587	4565	10.4	2268.7	497
20.2	A	28_02_2007	1732_1830	PM Peak (PM)	1604	4578	10.3	2193.4	479
TOTAL					56986	219832		97275.2	

APPENDIX 2 Composition by Fuel Type, Euro Emission Standard and Vehicle Weight

A2.1 - LCV Fleet

Vehicle Type 300	Fuel	Euro Standard	AM FLEET	IP FLEET	PM FLEET	EV FLEET	NI FLEET
LCV N_1 Class I RW ≤1305 kg	Diesel	E0	0%	0.26%	0.35%	0%	0%
		E1	0.40%	0.52%	0%	0%	0%
		E2	0%	0%	0%	0%	0%
		E3	2.96%	1.56%	2.48%	6.33%	0%
		E4	5.79%	3.13%	5.67%	3.80%	0%
		E5	2.96%	2.08%	3.19%	0%	0%
		E6	0%	0%	0%	0%	0%
	Petrol	E0	0%	0%	0%	0%	0%
		E1	0%	0%	0%	0%	0%
		E2	0.40%	0%	0.35%	0%	0%
		E3	0%	0%	0.35%	2.53%	0%
		E4	0.27%	0%	0%	0%	0%
		E5	0%	0%	0%	0%	0%
		E6	0%	0%	0%	0%	0%
LCV N_1 Class II 1305 kg < RW ≤1760 kg	Diesel	E0	0%	0%	0%	0%	0%
		E1	0.13%	0%	0%	0%	0%
		E2	0.67%	0.52%	1.06%	1.27%	0%
		E3	2.29%	2.34%	2.48%	6.33%	3.85%
		E4	7.94%	6.51%	9.57%	2.53%	0%
		E5	10.90%	12.76%	14.18%	5.06%	0%
		E6	0%	0%	0%	0%	0%
	Petrol	E0	0%	0%	0%	0%	0%
		E1	0%	0%	0.35%	0%	0%
		E2	0%	0%	0%	0%	0%
		E3	0%	0%	0%	0%	0%
		E4	0%	0%	0%	0%	0%
		E5	0%	0%	0%	0%	0%
		E6	0%	0%	0%	0%	0%
LCV N_1 Class III RW > 1760 kg N_1 GVW < 3500 kg	Diesel	E0	0%	0%	0%	0%	0%
		E1	0.27%	0.26%	1.42%	0%	3.85%
		E2	1.62%	1.56%	1.42%	3.80%	0%
		E3	5.52%	7.03%	7.80%	10.13%	3.85%
		E4	23.01%	24.74%	13.12%	15.19%	26.92%
		E5	32.30%	33.85%	32.98%	35.44%	42.31%
		E6	0%	0%	0%	0%	0%
	Petrol	E0	0%	0%	0%	0%	0%
		E1	0%	0%	0%	0%	0%
		E2	0%	0%	0%	0%	0%
		E3	0%	0.26%	0%	1.27%	0%
		E4	0%	0%	0%	0%	0%
		E5	0%	0%	0%	0%	0%
		E6	0%	0%	0%	0%	0%
LCV N_2 Class IV 3500 kg < GVW ≤ 5000 kg	Diesel	E0	0%	0%	0%	0%	0%
		E1	0%	0%	0%	0%	0%
		E2	0.13%	0%	0.35%	0%	0%
		E3	0%	0.26%	0%	0%	0%
		E4	0.54%	0.78%	0.71%	0%	0%
		E5	1.62%	1.30%	1.77%	6.33%	19.23%
		E6	0.27%	0.26%	0.35%	0%	0%
		SUM	100.00%	100.00%	100.00%	100.00%	100.00%

APPENDIX 2 Composition by Fuel Type, Euro Emission Standard and Vehicle Weight

A2.2 -Rigid HGV Fleet

Vehicle Type 200	Fuel	Euro Standard	AM FLEET	IP FLEET	PM FLEET	EV FLEET	NI FLEET
HGV Rigid 12t (2 Axle)	Diesel	E0	0%	0%	0%	0%	0%
		E1	0%	0%	0%	0%	0%
		E2	3.03%	3.23%	9.09%	66.67%	0%
		E3	12.12%	8.60%	18.18%	0%	50.00%
		E4 - EGR	9.09%	11.29%	17.05%	25.00%	37.50%
		E4 - SCR	3.03%	3.76%	5.68%	8.33%	12.50%
		E5 - EGR	2.65%	5.38%	3.41%	0%	0%
		E5 - SCR	7.96%	16.13%	10.23%	0%	0%
		E6	0%	3.23%	0%	0%	0%
HGV Rigid 26t (3+ Axle)	Diesel	E0	0%	1.08%	0%	0%	0%
		E1	0%	0%	0%	0%	0%
		E2	1.52%	2.15%	0%	0%	0%
		E3	22.73%	16.13%	9.09%	0%	0%
		E4 - EGR	12.50%	7.26%	10.23%	0%	0%
		E4 - SCR	4.17%	2.42%	3.41%	0%	0%
		E5 - EGR	3.41%	3.23%	2.27%	0%	0%
		E5 - SCR	10.23%	9.68%	6.82%	0%	0%
		E6	7.58%	6.45%	4.55%	0%	0%
		SUM	100.00%	100.00%	100.00%	100.00%	100.00%

A2.3 - Articulated HGV (Tractor Trailer) Fleet

Vehicle Type 400	Fuel	Euro Standard	AM FLEET	IP FLEET	PM FLEET	EV FLEET	NI FLEET
HGV Articulated	Diesel	E0	0%	0%	0%	0%	0%
		E1	0%	0%	0%	0%	0%
		E2	0%	0%	25.00%	33.33%	0%
		E3	10.00%	0%	0%	0%	0%
		E4 - EGR	7.50%	45.83%	0%	0%	0%
		E4 - SCR	2.50%	15.28%	0%	0%	0%
		E5 - EGR	17.50%	4.17%	18.75%	8.33%	0%
		E5 - SCR	52.50%	12.50%	56.25%	25.00%	0%
		E6	10.00%	22.22%	0%	33.33%	0%
		SUM	100.00%	100.00%	100.00%	100.00%	

APPENDIX 2 Composition by Fuel Type, Euro Emission Standard and Vehicle Weight

A2.4 - Unscheduled Bus Fleet

Vehicle Type 500 Extra Bus (not on Bus Schedule)	Fuel	Euro Standard	AM FLEET	IP FLEET	PM FLEET	EV FLEET	NI FLEET
Bus Extra - Single-Deck	Diesel	E0	0%	0%	0%	0%	0%
		E1	0%	0%	0%	0%	0%
		E2	0%	0%	14.29%	0%	0%
		E3	0%	0%	14.29%	0%	0%
		E4 - EGR	0%	9.38%	0%	0%	0%
		E4 - SCR	0%	3.13%	0%	0%	0%
		E5 - EGR	0%	0%	0%	0%	0%
		E5 - SCR	0%	0%	0%	0%	100.00%
		E6	0%	0%	0%	0%	0%
Bus Extra - Double-Deck	Diesel	E0	0%	0%	14.29%	0%	0%
		E1	0%	12.50%	0%	0%	0%
		E2	0%	0%	0%	0%	0%
		E3	42.86%	62.50%	57.14%	100.00%	0%
		E4 - EGR	0%	0%	0%	0%	0%
		E4 - SCR	0%	0%	0%	0%	0%
		E5 - EGR	0%	0%	0%	0%	0%
		E5 - SCR	0%	0%	0%	0%	0%
		E6	0%	0%	0%	0%	0%
Bus Extra - City Bus PHEM Default	Diesel	E0	0%	0%	0%	0%	0%
		E1	0%	0%	0%	0%	0%
		E2	14.29%	0%	0%	0%	0%
		E3	28.57%	12.50%	0%	0%	0%
		E4 - EGR	0%	0%	0%	0%	0%
		E4 - SCR	0%	0%	0%	0%	0%
		E5 - EGR	0%	0%	0%	0%	0%
		E5 - SCR	14.28%	0%	0%	0%	0%
		E6	0%	0%	0%	0%	0%
		SUM	100.00%	100.00%	100.00%	100.00%	100.00%

APPENDIX 2 Composition by Fuel Type, Euro Emission Standard and Vehicle Weight

A2.5 - Double-Deck Bus Fleet

Vehicle Type 501	Fuel	Euro Standard	AM FLEET	IP FLEET	PM FLEET	EV FLEET	NI FLEET
Bus Double-Deck	Diesel	E0	0%	0%	0%	0%	0%
		E1	0%	0%	0%	0%	0%
		E2	27.00%	31.07%	29.29%	29.03%	0%
		E3	73.00%	68.93%	70.71%	70.97%	0%
		E4 - EGR	0%	0%	0%	0%	0%
		E4 - SCR	0%	0%	0%	0%	0%
		E5 - EGR	0%	0%	0%	0%	0%
		E5 - SCR	0%	0%	0%	0%	0%
		E6	0%	0%	0%	0%	0%
		SUM	100.00%	100.00%	100.00%	100.00%	

A2.6 - Single-Deck Bus Fleet

Vehicle Type 502	Fuel	Euro Standard	AM FLEET	IP FLEET	PM FLEET	EV FLEET	NI FLEET
Bus Single-Deck	Diesel	E0	0%	0%	0%	0%	0%
		E1	0%	0%	0%	0%	0%
		E2	0%	0%	0%	0%	0%
		E3	100.00%	42.86%	0%	0%	100.00%
		E4 - EGR	0%	0%	0%	0%	0%
		E4 - SCR	0%	0%	0%	0%	0%
		E5 - EGR	0%	0%	0%	0%	0%
		E5 - SCR	0%	57.14%	100.00%	100.00%	0%
		E6	0%	0%	0%	0%	0%
		SUM	100.00%	100.00%	100.00%	100.00%	100.00%

A2.7 - Articulated Bus Fleet

Vehicle Type 503	Fuel	Euro Standard	AM FLEET	IP FLEET	PM FLEET	EV FLEET	NI FLEET
Bus Articulated	Diesel	E0	0%	0%	0%	0%	0%
		E1	0%	0%	0%	0%	0%
		E2	0%	0%	0%	0%	0%
		E3	100.00%	100.00%	100.00%	100.00%	0%
		E4 - EGR	0%	0%	0%	0%	0%
		E4 - SCR	0%	0%	0%	0%	0%
		E5 - EGR	0%	0%	0%	0%	0%
		E5 - SCR	0%	0%	0%	0%	0%
		E6	0%	0%	0%	0%	0%
		SUM	100.00%	100.00%	100.00%	100.00%	

APPENDIX 2 Average Vehicle Specification for Headingley

A2.8 - HGV Fleet

Vehicle Type	Fuel	Euro Standard	Vehicles in 24 hr ANPR Survey	Rated Engine Power (kW)	Maximum Power at RPM	Mass in Service (kg)	Loading (kg)
HGV Rigid 12t (2 Axle)	Diesel	E0	3	150	2639	6821	2366
		E1	0	153	2639	6821	2366
		E2	17	164	2507	6821	2366
		E3	37	140	2451	6821	2366
		E4	50	142	2478	6821	2366
		E5	83	146	2579	6821	2366
		E6	8	182	2507	6821	2366
HGV Rigid 26t (3+ Axle)	Diesel	E0	1	247	2132	12143	6559
		E1	0	253	2132	12143	6559
		E2	3	271	2025	12143	6559
		E3	50	247	2015	12143	6559
		E4	41	278	1931	12143	6559
		E5	45	257	1982	12143	6559
		E6	17	301	2025	12143	6559
HGV Articulated	Diesel	E0	0	262	2000	14502	14521
		E1	0	268	2000	14502	14521
		E2	2	287	1900	14502	14521
		E3	13	295	1900	14502	14521
		E4	19	301	1900	14502	14521
		E5	26	326	1848	14502	14521
		E6	9	319	1900	14502	14521

APPENDIX 2 Average Vehicle Specification for Headingley

A2.9 - LCV Fleet

Vehicle Type	Fuel	Euro Standard	Vehicles in 24 hr ANPR Survey	Rated Engine Power (kW)	Maximum Power at RPM	Mass in Service (kg)	Loading (kg)
LCV N_1 Class I RW ≤1305 kg	Diesel	E0	3	50	3500	1025	275
		E1	5	50	3500	1100	275
		E2	0	50	3500	1100	275
		E3	50	55	4363	1280	275
		E4	88	61	4003	1295	275
		E5	42	67	4205	1382	275
		E6	0	64	3500	1100	275
	Petrol	E0	0	50	5400	1000	228
		E1	0	50	5723	1000	228
		E2	2	50	5723	1090	228
		E3	6	51	5723	1060	228
		E4	3	55	5565	1100	228
		E5	2	55	5565	1100	228
		E6	0	55	5565	1100	228
LCV N_1 Class II 1305 kg < RW ≤1760 kg	Diesel	E0	0	62	3500	1500	285
		E1	2	65	3500	1500	285
		E2	12	65	3500	1500	285
		E3	55	65	3936	1571	285
		E4	155	63	3867	1513	285
		E5	213	68	4030	1492	285
		E6	0	74	3500	1500	285
	Petrol	E0	2	70	5400	1400	229
		E1	1	70	5723	1475	229
		E2	0	70	5723	1400	229
		E3	0	73	5723	1310	229
		E4	0	65	5565	1300	229
		E5	0	65	5565	1300	229
		E6	0	65	5565	1225	229
LCV N_1 Class III RW > 1760 kg N_1 GVW < 3500 kg	Diesel	E0	0	68	3500	2100	360
		E1	8	70	3500	2050	360
		E2	43	71	3726	1699	360
		E3	147	76	3731	1811	360
		E4	425	82	3591	1872	360
		E5	636	89	3627	2008	360
		E6	0	90	3500	2050	360
	Petrol	E0	0	85	5400	1685	340
		E1	0	85	5723	1790	340
		E2	0	90	5723	1820	340
		E3	3	95	5723	1840	340
		E4	0	95	5565	1910	340
		E5	0	95	5565	1910	340
		E6	0	95	5565	1910	340
LCV N_2 Class IV 3500 kg < GVW ≤ 5000 kg	Diesel	E0	0				
		E1	0				
		E2	2	110	3675	2488	1092
		E3	1	110	3675	2488	1092
		E4	8	110	3675	2488	1092
		E5	35	110	3675	2488	1092
		E6	5	110	3675	2488	1092

RW = Reference Mass; the mass of the vehicle in running order less the mass of the driver (75 kg) plus a uniform 100 kg

APPENDIX 2 Average Vehicle Specification for Headingley

A2.10 - Bus Fleet

Vehicle Type	Fuel	Euro Standard	Vehicles in 24 hr ANPR Survey	Rated Engine Power (kW)	Maximum Power at RPM	Mass in Service (kg)	Loading (kg)
Bus Double-Deck	Diesel	E0	0	228	1979	12360	1293.2
		E1	0	228	1979	12360	1293.2
		E2	173	173	2200	12360	1293
		E3	497	247	1900	12360	1293
		E4	0	228	1912	12360	1293
		E5	1	166	2000	11665	1293
		E6	0	228	1979	12360	1293
Bus Single-Deck	Diesel	E0	0	198	2113	10400	771
		E1	0	198	2113	10400	771
		E2	0	198	2113	10400	771
		E3	13	169	1900	11845	771
		E4	27	198	2113	10400	771
		E5	0	210	2200	10400	771
		E6	0	198	2113	10400	771
Bus Articulated	Diesel	E0	0	202	2200	15660	1293
		E1	0	202	2200	15660	1293
		E2	0	202	2200	15660	1293
		E3	56	202	2200	15660	1293
		E4	0	202	2200	15660	1293
		E5	0	202	2200	15660	1293
		E6	0	202	2200	15660	1293
Bus Unscheduled	Diesel	E0	0	162	2418	8348	3042
		E1	2	165	2418	8348	3042
		E2	3	177	2297	8348	3042
		E3	7	182	2297	8348	3042
		E4	5	185	2297	8348	3042
		E5	4	189	2297	8348	3042
		E6	0	197	2297	8348	3042